

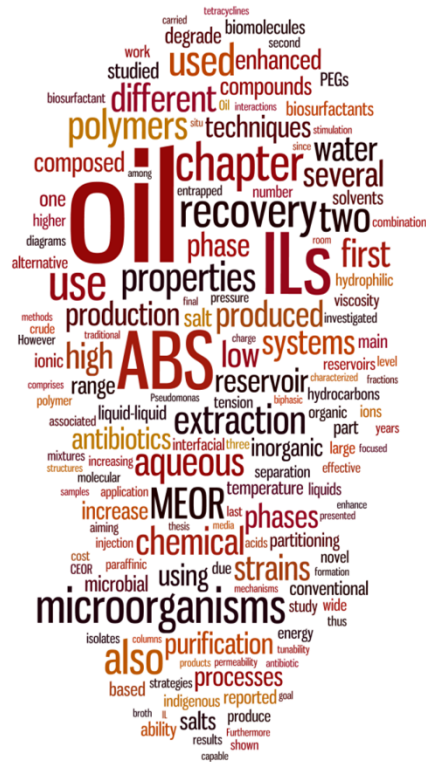


Universidade de Aveiro Departamento de Química
2013

JORGE FERNANDO
BRANDÃO PEREIRA

UM CONTO DE DOIS BIOPROCESSOS

A TALE OF TWO BIOPROCESSES





**JORGE FERNANDO
BRANDÃO PEREIRA**

UM CONTO DE DOIS BIOPROCESSOS

A TALE OF TWO BIOPROCESSES

Tese apresentada à Universidade de Aveiro para cumprimento dos requisitos necessários à obtenção do grau de Doutor no Programa Doutoral em Engenharia Química, realizada sob a orientação científica do Professor Doutor João Manuel da Costa Araújo Pereira Coutinho, Professor Associado com Agregação do Departamento de Química da Universidade de Aveiro e da Doutora Mara Guadalupe Freire Martins aluna de Pós-Doutoramento do Instituto de Tecnologia Química e Biológica, ITQB2, Universidade Nova de Lisboa.

Apoio financeiro do POCTI no âmbito do III Quadro Comunitário de Apoio.

O doutorando agradece o apoio financeiro da FCT no âmbito do III Quadro Comunitário de Apoio (SFRH/BD/60228/2009).



A todos que contribuíram para a minha formação pessoal e profissional.

o júri

presidente

Prof. Doutor Luís Filipe Pinheiro de Castro
Professor Catedrático da Universidade de Aveiro

Prof. Doutor José António Couto Teixeira
Professor Catedrático da Universidade do Minho

João Manuel da Costa e Araújo Pereira Coutinho
Professor Associado com Agregação da Universidade de Aveiro

Prof. Doutor Adalberto Pessoa Júnior
Professor Titular da Faculdade de Ciências Farmacêuticas da Universidade de São Paulo, Brasil

Prof. Doutora Lúcia Raquel Marona Rodrigues
Professora Auxiliar da Universidade do Minho

Doutora Mara Guadalupe Freire Martins
Estagiária de Pós-Doutoramento do Instituto de Tecnologia Química e Biológica, ITQB2,
Universidade Nova de Lisboa

Doutora Sónia Patrícia Marques Ventura
Estagiária de Pós-Doutoramento da Universidade de Aveiro

agradecimentos

Os meus sinceros agradecimentos aos meus orientadores Prof. João Coutinho e Dr^a. Mara Freire os quais contribuíram significativamente no desenvolvimento de todo o trabalho ao longo destes últimos quatro anos. Agradeço-lhes toda a paciência e tempo disponibilizado, e a forma como sempre me transmitiram os conhecimentos permitindo desse modo toda a minha evolução como profissional.

Em segundo lugar gostaria de agradecer aos colaboradores da Universidade do Minho, Prof. José Teixeira, Prof.^a Lúcia Rodrigues e Dr. Eduardo Gudiña, pela colaboração e ajuda no desenvolvimento do projecto MEOR.

Queria agradecer ao Prof. Adalberto Pessoa Jr. e respectivo grupo pela oportunidade de desenvolver trabalho durante dois meses na Universidade de São Paulo. Gostaria de destacar a apoio especial dos meus grandes amigos André e da Valéria.

Agradeço à Prof.^a Rosário Domingues e ao Prof. Rui Vitorino pela ajuda na caracterização estrutural dos biosurfactantes, bem como pela disponibilização dos equipamentos de espectrometria de massa.

Agradeço também ao Prof. Robin Rogers da Universidade do Alabama, pela colaboração e experiência transmitida no âmbito do trabalho dos ABS com polímeros e líquidos iónicos. Gostaria principalmente de agradecer-lhe a possibilidade de realizar o pós-doutoramento no seu grupo, e desse modo poder continuar a evoluir como investigador.

Gostaria de agradecer ainda a todos os outros Professores e respectivos grupos que directa ou indirectamente colaboraram no desenvolvimento do trabalho compilado neste documento, apesar de não os frisar individualmente são de igual modo importantes.

Não posso deixar de agradecer de uma forma especial a todos o meus colegas desta grande “família” que é o grupo “PATH”. Agradeço a todos sem excepção, mas é como sabem somos tantos que é impossível agradecer-lhes individualmente. No entanto, e sem querer ferir susceptibilidades quero enaltecer o apoio da Sónia, que além de colega foi uma Grande Amiga, aturando tudo o que calha em sorte às pessoas realmente importantes. Engrandeço também a ajuda dos alunos, e colegas que trabalharam comigo: Jorge, Filipa, Maria João, Soraia, Rita Costa, Teresa e Xica.

A nível pessoal agradeço a todos os meus amigos, desde Vale de Cambra, Aveiro, Coimbra, Braga, até São Paulo, sem excepção. Vocês sabem o quanto me ajudaram, e apoiaram nos melhores momentos mas mais importante, nos piores.

Agradeço especialmente a toda a minha família, em particular aos meus pais, irmão e avós, por acreditarem que eu conseguiria passar mais esta etapa, e acima de tudo, pela ajuda retribuída em todos os momentos da minha vida.

Finalmente agradeço à Fundação para a Ciência e Tecnologia pela bolsa de doutoramento atribuída, e a empresa PARTEX pela bolsa de investigação. A ambas instituições agradeço os subsídios para participação em conferências, e financiamentos atribuídos para o desenvolvimento dos trabalhos experimentais.

palavras-chave

Bioprocessos, microrganismos, recuperação avançada de petróleo com microrganismos, *Pseudomonas aeruginosa*, *Bacillus subtilis*, biosurfactantes, biodegradação, sistemas de duas fases aquosas, biomoléculas, líquidos iónicos, polímeros, antibióticos.

resumo

Os bioprocessos utilizam microrganismos ou células de forma a produzir e/ou obter determinados produtos. Nos dias de hoje estes bioprocessos assumem uma posição fundamental como alternativa aos processos químicos tradicionais. Entre as diversas vantagens associadas ao seu uso pelas indústrias químicas, petrolíferas e farmacêuticas destacam-se o seu baixo custo, facilidade de “scale-up” e menor impacto ambiental. Este trabalho reporta dois exemplos de bioprocessos utilizados como alternativa aos processos químicos utilizados pelas indústrias petrolífera e farmacêutica.

Na primeira parte deste trabalho foi estudado um bioprocessos alternativo recorrendo ao uso de microrganismos para a recuperação avançada de petróleo. Actualmente, devido aos elevados preços do petróleo e à sua escassez, as técnicas de recuperação avançada de petróleo tornaram-se muito atractivas. Entre as várias técnicas tem-se destacado o uso da recuperação avançada de petróleo com microrganismos (MEOR), técnica que se fundamenta na estimulação de microrganismos indígenas ou injeção de consórcios de microrganismos de forma a produzir metabólitos específicos e consequentemente aumentar a quantidade de óleo recuperado. Nos primeiros capítulos deste trabalho descreve-se o isolamento de diversos microrganismos de um óleo parafínico brasileiro e a caracterização das suas propriedades tensioactivas e de biodegradação. Posteriormente caracterizaram-se as estruturas químicas dos biosurfactantes produzidos. No final desta primeira parte foi avaliada ainda a capacidade de algumas das bactérias isoladas na recuperação do óleo parafínico brasileiro aprisionado em colunas de areia.

Na segunda parte deste trabalho apresenta-se um exemplo da utilização de sistemas de duas fases aquosas ou sistemas bifásicos aquosos (ABS) para a extracção de antibióticos directamente do meio fermentativo no qual foram produzidos. Neste contexto foram estudados pela primeira vez sistemas de duas fases aquosas constituídos por líquidos iónicos (LIs) e polímeros e onde se determinaram os respectivos diagramas de fase. Os novos ABS surgem como uma metodologia eficaz e economicamente viável para a extracção de diversas biomoléculas e/ou produtos biológicos. Assim, e tendo como objectivo final a extracção de antibióticos de um meio fermentativo, foi estudada a influência de uma vasta gama de líquidos iónicos e polímeros na formação destes sistemas, bem como o seu efeito na partição de diferentes moléculas-tipo, como aminoácidos, alcalóides e corantes. Como capítulo final apresenta-se a capacidade destes novos sistemas de duas fases aquosas para extrair o antibiótico tetraciclina directamente do meio fermentativo de *Streptomyces aureofaciens*.

keywords

Bioprocesses, microorganisms, microbial enhanced oil recovery, *Pseudomonas aeruginosa*, *Bacillus subtilis*, biosurfactants, biodegradation, aqueous two-phase systems, aqueous biphasic systems, biomolecules, ionic liquids, polymers, antibiotics.

abstract

Bioprocesses use microorganisms or cells in order to produce and/or obtain some desired products. Nowadays these strategies appear as a fundamental alternative to the traditional chemical processes. Amongst the many advantages associated to their use in the chemical, oil or pharmaceutical industries, their low cost, easily scale-up and low environmental impact should be highlighted. This work reports two examples of bioprocesses as alternatives to traditional chemical processes used by the oil and pharmaceutical industries. In the first part of this work it was studied an example of a bioprocess based on the use of microorganisms in enhanced oil recovery. Currently, due to high costs of oil and its scarcity, the enhanced oil recovery techniques become very attractive. Between the available techniques the use of microbial enhanced oil recovery (MEOR) has been highlighted. This process is based on the stimulation of indigenous microorganisms or by the injection of microorganism consortia to produce specific metabolites and hence increase the amount of oil recovered. In the first chapters of this work the isolation of several microorganisms from samples of paraffinic Brazilian oils is described, and their tensioactive and biodegradability properties are presented. Furthermore, the chemical structures of the biosurfactants produced by those isolates were also characterized. In the final chapter of the first part, the capabilities of some isolated bacteria to enhance the oil recovery of paraffinic Brazilian oils entrapped in sand-pack columns were evaluated.

In the second part of this work it was investigated aqueous two-phase systems or aqueous biphasic systems (ABS) as extractive strategies for antibiotics directly from the fermented broth in which they are produced. To this goal, several aqueous two-phase systems composed of ionic liquids (ILs) and polymers were studied for the first time and their phase diagrams were determined. The novel ATPS appear as effective and economic methods to extract different biomolecules or/and biological products. Thus, aiming the initial antibiotics extraction purpose it was studied the influence of a wide range of ILs and polymers in the aqueous two-phase formation ability, as well as their influence in the partitioning of several type-molecules, such as amino acids, alkaloids and dyes. As a final chapter it is presented the capacity of these novel systems to extract the antibiotic tetracycline directly from the fermented broth of *Streptomyces aureofaciens*.

CONTENTS

Contents	i
Notation	v
List of Figures	xiii
List of Tables	xix
Document Organization	xxii
PART A – Microbial Enhanced Oil Recovery	1
1. INTRODUCTION	3
1.1. General Context	5
1.2. Enhancement of Oil Production and Recovery	5
1.3. Microbial Enhanced Oil Recovery	6
1.4. Work Aims and Motivation	8
1.5. References	11
2. PAPER 1- Isolation and Study of Microorganisms from Oil Samples for Application in Microbial Enhanced Oil Recovery	15
3. PAPER 2 - Characterization by Electrospray Ionization and Tandem Mass Spectrometry of Rhamnolipids Produced by Two <i>Pseudomonas aeruginosa</i> Strains Isolated from Brazilian Crude Oil	41
4. PAPER 3 - Optimization and Characterization of Biosurfactant Production by <i>Bacillus subtilis</i> Isolates Towards Microbial Enhanced Oil Recovery Applications	57
5. PAPER 4 - Biosurfactant Producing Microorganisms and its Application to Enhance Oil Recovery at Lab Scale	83
6. PAPER 5 - Biosurfactant-Producing and Oil-Degrading <i>Bacillus subtilis</i> Strains Enhance Oil Recovery in Laboratory Sand-Pack Columns	97
7. CONCLUSIONS AND FUTURE WORK	117

PART B – Antibiotics Purification Using Aqueous Biphasic Systems	
Composed of Ionic Liquids and Polymers	121
8. INTRODUCTION	123
8.1. General Context	125
8.2. Antibiotics	126
8.3. Aqueous Biphasic Systems	126
8.4. Ionic Liquids	127
8.5. Work Aims and Motivation	130
8.6. References	137
9. PAPER 6 - Ionic Liquids as Adjuvants for the Tailored Extraction of Biomolecules in Aqueous Biphasic Systems	139
10. PAPER 7 - Insights into the Interactions that Control the Phase Behavior of Novel Aqueous Biphasic Systems Composed of Polyethylene Glycols and Ionic Liquids	165
11. PAPER 8 - “Washing-out” in Polyethylene Glycol + Ionic Liquid Mixtures to form Aqueous Biphasic Systems	189
12. PAPER 9 - Combining Ionic Liquids and Polyethylene Glycols to Boost the Hydrophobic-Hydrophilic Range of Aqueous Biphasic Systems	205
13. PAPER 10 - Aqueous Biphasic Systems composed of Ionic Liquids and Polymers: A Platform for the Purification of Biomolecules	217
14. PAPER 11 - Biocompatible Aqueous Biphasic Systems Composed of Polyethylene Glycol and Cholinium-based Ionic Liquids: Towards the Understanding of Their Formation Ability	237
15. PAPER 12 - Extraction of Tetracycline from Fermentation Broth using Aqueous Two-Phase Systems Composed of Polyethylene Glycol and Cholinium-based Salts	257
16. CONCLUSIONS AND FUTURE WORK	275

17. LIST OF PUBLICATIONS	281
18. SUPPORTING INFORMATION	285

NOTATION

List of Symbols

$\Delta_{tr}G_m^0$	standard molar Gibbs free energy of transfer ($\text{kJ}\cdot\text{mol}^{-1}$)
$\Delta_{tr}H_m^0$	standard molar enthalpy of transfer ($\text{kJ}\cdot\text{mol}^{-1}$)
$\Delta_{tr}S_m^0$	standard molar entropy of transfer ($\text{J}\cdot\text{mol}^{-1}\cdot\text{K}^{-1}$)
% <i>EE</i>	percentage extraction efficiency
α'	ratio between the top and the total mass of the mixture
[Biomass]	biomass concentration ($\text{g}\cdot\text{L}^{-1}$)
[P _{BSA}]	protein concentration ($\text{g}\cdot\text{L}^{-1}$)
[surfactin]	surfactin concentration ($\text{g}\cdot\text{L}^{-1}$)
[TP]	total protein concentration ($\text{g}\cdot\text{L}^{-1}$)
ΔG_{hyd}	Gibbs free energy of hydration
A	Merchuck correlation constant
B	Merchuck correlation constant
C	Merchuck correlation constant
<i>cmc</i>	Critical micelle concentration ($\text{g}\cdot\text{L}^{-1}$)
E_{24}	emulsification index (%)
G^E	excess free Gibbs energy ($\text{kJ}\cdot\text{mol}^{-1}$)
H^E	excess enthalpy ($\text{kJ}\cdot\text{mol}^{-1}$)
IFT	interfacial tension ($\text{mN}\cdot\text{m}^{-1}$)
K	partition coefficient
K_{ow}	octanol-water partition coefficient
m/z	mass-to-charge ratio
pK_a	acid constant dissociation
R	universal gas constant ($\text{J}\cdot\text{K}^{-1}\cdot\text{mol}^{-1}$)

S	selectivity
ST	surface tension ($\text{mN}\cdot\text{m}^{-1}$)
ST^{-2}	lower surface tension ($\text{mN}\cdot\text{m}^{-1}$)
T	temperature ($^{\circ}\text{C}$, K)
TLL	tie-line length
X	PEG weight percentage
Y	PEG weight percentage
δ	chemical shifts deviations (ppm)
η	dynamic viscosity ($\text{mPa}\cdot\text{s}$)
ρ	density ($\text{g}\cdot\text{cm}^{-3}$)

List of Abbreviations

[amim]Cl	1-allyl-3-methylimidazolium chloride
[C ₁ mim]Cl or [mim]Cl	1-methylimidazolium chloride
[C ₁ mim]Cl	1,3-dimethylimidazolium chloride
[C ₂ mim][$(\text{CH}_3)_2\text{PO}_4$] or [C ₂ mim][DMP]	1-ethyl-3-methylimidazolium dimethylphosphate
[C ₂ mim][CH ₃ CO ₂]	1-ethyl-3-methylimidazolium acetate
[C ₂ mim][CH ₃ SO ₃]	1-ethyl-3-methylimidazolium methanesulfonate
[C ₂ mim][HSO ₄]	1-ethyl-3-methylimidazolium hydrogen sulfate
[C ₂ mim]Cl	1-ethyl-3-methylimidazolium chloride
[C ₄ C ₁ mim]Cl	1-butyl-2,3-dimethylimidazolium chloride
[C ₄ mim][CF ₃ SO ₃]	1-butyl-3-methylimidazolium trifluoromethanesulfonate
[C ₄ mim][CH ₃ CO ₂]	1-butyl-3-methylimidazolium acetate
[C ₄ mim][CH ₃ SO ₃]	1-butyl-3-methylimidazolium methanesulfonate
[C ₄ mim][HSO ₄]	1-butyl-3-methylimidazolium hydrogenosulfate
[C ₄ mim][MeSO ₄]	1-butyl-3-methylimidazolium methylsulfate
[C ₄ mim]Br	1-butyl-3-methylimidazolium bromide
[C ₄ mim]Cl	1-butyl-3-methylimidazolium chloride
[C ₄ mpip]Cl	1-butyl-1-methylpiperidinium chloride
[C ₄ mpy]Cl	1-butyl-3-methylpyridinium chloride
[C ₄ mpyr]Cl	1-butyl-1-methylpyrrolidinium chloride
[C ₆ mim]Cl	1-hexyl-3-methylimidazolium chloride
[C ₇ H ₇ mim]Cl	1-benzyl-3-methylimidazolium chloride
[C ₈ mim]Cl	1-methyl-3-octylimidazolium chloride
[im]Cl	imidazolium chloride
[OHC ₂ mim]Cl	1-hydroxyethyl-3-methylimidazolium chloride

[Ch]Ac	cholinium acetate
[Ch]Bic	cholinium bicarbonate
[Ch]But	cholinium butanoate
[Ch]Cl	cholinium chloride
[Ch]DHcit	cholinium dihydrogencitrate
[Ch]DHph	cholinium dihydrogenphosphate
[Ch]Gly	cholinium glycolate
[Ch]Lac	cholinium lactate
[Ch]Pro	cholinium propanoate
[P ₄₄₄₄]Cl	tetrabutylphosphonium chloride
¹³ C NMR	carbon nuclear magnetic resonance
¹ H NMR	proton nuclear magnetic resonance
ABS	aqueous biphasic systems
AC	sodium acetate
AC	ammonium citrate
ACN	acetonitrile
alk	alkaloid
AN	ammonium nitrate
ANP	Agência Nacional de Petróleo
AOR	Additional Oil Recovery
AS	ammonium sulfate
ATR	attenuated total reflection
<i>B. licheniformis</i>	<i>Bacillus licheniformis</i>
<i>B. subtilis</i>	<i>Bacillus subtilis</i>
BCA	bicinchoninic acid method
BMSM	basal mineral salt medium

BSA	bovine Serum Albumin
CA	chloranilic Acid
caf	caffeine
CCC	countercurrent chromatography
CEOR	chemical enhanced oil recovery
CI	sodium citrate
COSMO-RS	COnductor-like Screening MOdel for Real Solvents
EDTA	ethylenediamine tetraacetic acid
EOR	enhanced oil recovery
ESI	electrospray
ESI-MS	mass spectrometry coupled with electrospray
FID	flame ionization detector
FRU	fructose
FTIR	Fourier transform infrared spectroscopy
GC	gas chromatography
GLU	glucose
GLY	glycerol
HEX	<i>n</i> -hexadecane
IB	indigo blue
IC	indigo carmine
IL	ionic liquid
ILs	ionic liquids
LAC	lactose
L-Asp	L-asparaginase
LB	Luria-Bertani
LC	liquid chromatography

L-Glu	L-glutamic acid
L-Leu	L-leucine
L-Val	L-valine
MALDI	matrix-assisted laser desorption/ionization
MALDI-TOF	matrix-assisted laser desorption ionization-time of flight mass spectrometry
MD	molecular dynamics
ME	meat extract
MEOR	microbial enhanced oil recovery
MS	mass spectrometry
MS/MS	Tandem mass spectrometry
MSM	mineral salt medium
MSS	mineral salt solution
MSSH	mineral salt solution with <i>n</i> -hexadecane
NCBI	National Center for Biotechnology Information
nic	nicotine
OD	optical density
OOIP	original oil in place
<i>P. aeruginosa</i>	<i>Pseudomonas aeruginosa</i>
PAR	paraffin
PBS	phosphate buffered saline
PCR	polymerase chain reaction
PEG	polyethylene glycol
PPG	polypropylene glycol
PV	pore volume
RDFs	radial distribution functions

Rha-	mono-rhamnose
Rha-Rha	di-rhamnose
rRNA	ribosomal ribonucleic acid
<i>S. aureofaciens</i>	<i>Streptomyces aureofaciens</i>
SDS	sodium dodecyl sulphate
SN	sodium nitrate
S_{oi}	initial oil saturation
S_{or}	residual oil saturation
S_{ormf}	oil recovered after microbial flooding
S_{orwf}	oil recovered after water flooding
SQL	squalane
SUC	sucrose
S_{wi}	initial water saturation
TC	tetracycline
TCA	methanolic trichloroacetic acid
TEG	tetraethylene glycol
TFA	trifluoroacetic acid
TL	Tie-line
TLL	Tie-line length
TMS	tetramethylsilane
Trp	L-tryptophan
TRY	tryptone
U	urea
xant	xanthine
YE	yeast extract

LIST OF FIGURES

- Figure 2.1.** Variation of relative weight fraction of *n*-alkanes present in paraffinic mixture A after incubation with bacterial isolates, for 4 days at 40°C and aerobic conditions as compared to the control. (SQL: squalane). 31
- Figure 2.2.** Variation of relative weight fraction of *n*-alkanes present in paraffinic mixture A after incubation with bacterial isolates, for 15 days at 40°C and anaerobic conditions as compared to the control. 31
- Figure 2.3.** Variation of relative weight fraction of *n*-alkanes present in paraffinic mixture B after incubation with bacterial isolates for 15 days, at 40°C and anaerobic conditions as compared to the control. 33
- Figure 3.1** ESI-MS spectra obtained using an electrospray Q TOF mass spectrometer in positive mode of #111 and #902 biosurfactants. Y-axis: Relative abundance considering the highest abundant ion as 100%; X-axis: *m/z* for each ion. ESI- MS spectra were acquired in the positive mode. 48
- Figure 3.2 a)** ESI – MS/MS spectrum of the $[M+Na]^+$ ion at *m/z* 555.3 corresponding to mono-rhamnolipid Rha-C10:0/C12:0 obtained in ESI-QTOF. **b)** Molecular structure of Rha-C10:0/C12:0 with the main cleavages correspondent to the fragmentation observed in the MS/MS spectrum of $[M+Na]^+$ ion. **c)** Molecular structure of the ions originated from the fragmentation of $[M+Na]^+$ ion. 51
- Figure 3.3 a)** ESI – MS/MS spectrum of the $[M+Na]^+$ ion at *m/z* 673.3 corresponding to di-rhamnolipid Rha-Rha-10:0/10:0 obtained in ESI-Q TOF. **b)** Molecular structure of Rha-Rha-10:0/10:0 with the main cleavages correspondent to the fragmentation observed in the MS/MS spectrum of $[M+Na]^+$ ion at *m/z* 673.3. **c)** Molecular structure of the ions originated from the fragmentation of $[M+Na]^+$ ion at *m/z* 673.3. 52
- Figure 4.1** FTIR-ATR spectra for biosurfactant extracts produced by isolates #309 (a), #311 (b) and #573 (c). 71
- Figure 4.2** ¹H NMR spectra for biosurfactant extracts produced by *B. subtilis* isolates #309 (a), #311 (b) and #573 (c). 72
- Figure 4.3** MALDI-TOF spectra for surfactin-like extracts produced by *B. subtilis* isolates #309 (a), #311 (b) and #573 (c). 74
- Figure 4.4** Structure of surfactin. 75
- Figure 4.5** Interfacial tension values (IFT, mN.m⁻¹) versus logarithm of biosurfactant concentration (g.L⁻¹) for each biosurfactant extract from *B. subtilis* isolates #309 (a), #311 (b) and #573 (c). 76

Figure 5.1 Illustration of the sand-pack column model used to evaluate the mobilization of residual oil by microorganisms. Adapted from Suthar et al. ⁹ .	89
Figure 5.2 Values of anaerobic degradation of 0.1% and 1% (w/w) solid paraffin by bacterial isolates after 15 days of incubation at 40°C and 150 rpm.	92
Figure 5.3 Variation of relative weight fraction of <i>n</i> -alkanes present in solid paraffinic mixture after incubation with isolate #309, for 15 days at 40°C and anaerobic conditions as compared to the control (error bars show the average error).	93
Figure 6.1 Schematic representation of the sand-pack column process.	102
Figure 6.2 Variation of relative weight fraction of <i>n</i> -alkanes present in the different oil samples (Heating oil, Arabian Light Oil and Heavy Crude Oil) after <i>B. subtilis</i> isolates #309, #311 and #573 incubation for 14 days at 40°C in sand-pack columns. Results are compared to control columns and error bars represent the average error of three independent assays.	108
Figure 8.1 Chemical structure of tetracyclines.	126
Figure 8.2 Common chemical structures of ionic liquids.	129
Figure 9.1 Chemical structures of the studied ILs: (i) [im]Cl; (ii) [C ₁ im]Cl; (iii) [C ₂ mim]Cl; (iv) [C ₄ mim]Cl; (v) [C ₄ C ₁ mim]Cl; (vi) [OHC ₂ mim]Cl; (vii) [amim]Cl; (viii) [C ₇ H ₇ mim]Cl; (ix) [C ₄ mim][CH ₃ CO ₂]; (x) [C ₄ mim][MeSO ₄]; (xi) [C ₄ mim][HSO ₄].	143
Figure 9.2 Phase diagrams for the imidazolium-based quaternary systems composed of PEG 600 + Na ₂ SO ₄ + H ₂ O + 5 wt% IL at 298 K: (—) no IL; (●) [im]Cl; (○) [C ₁ im]Cl; (■) [C ₂ mim]Cl; (Δ) [C ₄ mim]Cl; (▲) [C ₄ C ₁ mim][Cl].	147
Figure 9.3 Phase diagrams for the imidazolium-based quaternary systems composed of PEG 600 + Na ₂ SO ₄ + H ₂ O + 5 wt% IL at 298 K: (—) no IL; (Δ) [C ₄ mim]Cl; (■) [OHC ₂ mim]Cl; (○) [amim]Cl; (●) [C ₇ H ₇ mim]Cl.	147
Figure 9.4 Phase diagrams for the imidazolium-based quaternary systems composed of PEG 600 + Na ₂ SO ₄ + H ₂ O + 5 wt% IL at 298 K: (—) no IL; (■) [C ₄ mim]Cl; (●) [C ₄ mim][CH ₃ CO ₂]; (○) [C ₄ mim][MeSO ₄]; (Δ) [C ₄ mim][HSO ₄].	148
Figure 9.5 Phase diagram for the PEG 600 + Na ₂ SO ₄ + H ₂ O + 5 wt% [C ₂ mim]Cl quaternary system at 298 K: (■) binodal curve data; (-) binodal adjusted curve; (□) TL data.	151
Figure 9.6 Partition coefficients of L-tryptophan (K_{Trp}) (light grey) and of each IL (K_{IL}) (dark grey), and pH of both top (black squares) and bottom phases (grey circles) for the chloride-based systems composed by 40 wt% PEG 600 + 5 wt% Na ₂ SO ₄ + H ₂ O + 5wt % IL, at 298.15 K.	155

Figure 9.7 Partition coefficients of L-tryptophan (K_{Trp}) (light grey) and of each IL (K_{IL}) (dark grey), and pH of both top (black squares) and bottom (grey circles) phases, for the [C₄mim]-based systems composed by 40 wt% PEG 600 + 5wt % Na₂SO₄ + H₂O + 5wt % IL, at 298.15 K. 156

Figure 9.8 Partition coefficients of L-tryptophan (K_{Trp}) at different temperatures. 158

Figure 9.9 Partition coefficients of L-tryptophan as a function of PEG 600 and Na₂SO₄ concentrations at 298.15 K: no IL (A); 5 wt% of [im]Cl (B); 5 wt% [C₇H₇mim]Cl (C). 161

Figure 10.1 Chemical structures of the studied ILs: a) [im]Cl; b) [mim]Cl; c) [C_nmim]Cl (where *n* stands for the number of carbon atoms in the alkyl chain (R); *n* = 1, 2, 4, 6, or 8); d) [amim]Cl; e) [HOC₂mim]Cl; f) [C₄mpy]Cl; g) [C₄mpip]Cl; h) [C₄mpyr]Cl; i) [P₄₄₄₄]Cl; j) [C₄mim][CF₃SO₃]; k) [C_nmim][CH₃CO₂] (*n* = 2 or 4); l) [C_nmim][CH₃SO₃] (*n* = 2 or 4); m) [C₄mim]Br; n) [C₂mim][HSO₄]; o) [C₂mim][(CH₃)₂PO₄]. 171

Figure 10.2 Experimental solubility data for PEG/IL ABS at 298 K to analyze the effect of the IL anion: PEG 2000/[C₄mim][CF₃SO₃] (●), PEG 2000/[C₄mim]Br (◆), PEG 2000/[C₄mim]Cl (○), PEG 2000/[C₄mim][CH₃SO₃] (▲), and PEG 2000/[C₄mim][CH₃CO₂] (◇). The lines correspond to the respective correlations using Equation 10.1. 172

Figure 10.3 Experimental solubility data for PEG/IL ABS, at 298 K to analyze the effect of the IL anion: PEG 2000/[C₂mim]Cl (○), PEG 2000/[C₂mim][HSO₄] (◆), PEG 2000/[C₂mim][CH₃SO₃] (▲), PEG 2000/[C₂mim][CH₃CO₂] (◇), and PEG 2000/[C₂mim][(CH₃)₂PO₄] (△). The lines correspond to the respective correlations using Equation 10.1. 174

Figure 10.4 Experimental solubility data for PEG/IL ABS at 298 K to analyze the effect of the IL cation core: PEG 2000/[C₄mim]Cl (●), PEG 2000/[C₄mpy]Cl (△), PEG 2000/[C₄mpyr]Cl (◆), PEG 2000/[C₄mpip]Cl (○), and PEG 2000/[P₄₄₄₄]Cl (▲). The lines correspond to the respective correlations using Equation 10.1. 175

Figure 10.5 Experimental solubility data for PEG/IL ABS at 298 K to analyze the effect of the length and number of the alkyl substituents in the ionic liquid cation: PEG 2000/[im]Cl (●), PEG 2000/[mim]Cl (△), PEG 2000/[C₁mim]Cl (*), PEG 2000/[C₂mim]Cl (◆), PEG 2000/[C₄mim]Cl (○), PEG 2000/[C₆mim]Cl (▲), and PEG 2000/[C₈mim]Cl (◇). The lines correspond to the respective correlations using Equation 10.1. 177

Figure 10.6 Experimental solubility data for PEG/IL ABS at 298 K to analyze the effect of the functionalization of the alkyl substituent in the ionic liquid cation: PEG 2000/[amim]Cl (●), PEG 2000/[HOC₂mim]Cl (◇), PEG 2000/[C₂mim]Cl (◆), and PEG 2000/[C₄mim]Cl (○). The lines correspond to the respective correlations using Equation 10.1. 179

Figure 10.7 Experimental solubility data for PEG/IL ABS at 298 K to analyze the effect of the molecular weight of the PEG: PEG 1000/[C ₄ mim]Cl (□), PEG 2000/[C ₄ mim]Cl (▲), PEG 3400/[C ₄ mim]Cl (◇), and PEG 4000/[C ₄ mim]Cl (■). The lines correspond to the respective correlations using Equation 10.1.	181
Figure 10.8 Experimental solubility data for PEG 2000/[C ₂ mim]Cl ABS, at 298 K (○), 308 K (◆), and 323 K (▲). The lines correspond to the respective correlations using Equation 10.1.	182
Figure 10.9 Experimental solubility data for PEG 2000/[C ₂ mim][CH ₃ CO ₂] ABS at 298 K (○), 308 K (◆), and 323 K (▲). The lines correspond to the respective correlations using Equation 10.1.	183
Figure 11.1 Experimental solubility data for the PEG 1500/[C ₄ mim]Cl ABS at 323.15 K (red dots) and 334.15 K (black squares).	194
Figure 11.2 Structure and atom labeling of (i) TEG and (ii) [C ₄ mim] ⁺ . Ctb stands for the terminal carbon atoms of the butyl side chain of the IL cation, while CB _x (x = 1, 2, 3) is used to denote the other carbon atoms of the same alkyl chain. Ctm stands for the carbon atom of the methyl side chain of the IL cation. Hydrogen atoms of the molecules, omitted for clarity, are labeled with the number of the carbon atoms to which they are attached to.	195
Figure 11.3 Radial distribution functions for the interactions of the (a) IL anion and (b) the H2 atom, (c) the H4 atom and (d) the terminal carbon atom of the alkyl chain of the IL cation with selected atoms of TEG for the ([C ₄ mim]Cl+water) binary system and for ([C ₄ mim]Cl + TEG + water) ternary mixtures at three different concentrations.	197
Figure 12.1 Experimental solubility data for IL-PEG 1500 ABS at 323 K and atmospheric pressure: (■) [C ₄ mpip]Cl; (●) [C ₄ mpyr]Cl; (◆) [C ₂ mim]Cl; (▲) [C ₄ mim]Cl.	209
Figure 12.2 Logarithm of the partition coefficients of CA, log <i>K</i> , in several IL-based ABS at 323 K: neutral CA and charged CA; and of neutral CA in conventional PEG 4000/Dextran 40000- and PEG 1500/Na ₂ SO ₄ -based ABS.	211
Figure 12.3 Visual aspect of the migration pattern of neutral CA in the studied ABS at 323 K.	211
Figure 12.4 Logarithm of the partition coefficients of neutral IB and charged IC, log <i>K</i> , in several IL-based ABS at 323 K and in the conventional PEG 1500/Na ₂ SO ₄ -based ABS.	213
Figure 12.5 Visual aspect of the migration pattern of IB and IC in the studied ABS at 323 K.	213
Figure 13.1 Chemical structure and respective abbreviation name of all the ILs investigated.	222
Figure 13.2 Chemical structure of the three alkaloids investigated.	223

- Figure 13.3** Logarithm of the alkaloids partition coefficients ($\log K_{alk}$) in the ABS composed of PEG 2000 (≈ 53 wt%) + chloride-based ILs (≈ 27 wt%) and at 323 K. The pH values of the top and bottom phases are also displayed. 226
- Figure 13.4** Logarithm of the alkaloids partition coefficients ($\log K_{alk}$) in the ABS composed of PEG 2000 (≈ 53 wt%) + [C₂mim]-based ILs (≈ 27 wt%) and at 323 K. The pH values of the top and bottom phases are also displayed. 228
- Figure 13.5** Selectivity parameters for: **A**) xanthine/caffeine ($S_{xant/caf}$) and nicotine/caffeine ($S_{nic/caf}$) pairs considering all PEG 2000-ILs-based ABS tested and **B**) nicotine/caffeine ($S_{nic/caf}$) pair considering the PEG 2000-[C₂mim]Cl-based ABS and different temperatures of extraction. 229
- Figure 13.6 A**) Spectra of the diluted aqueous solutions of nicotine, caffeine and a mixture containing nicotine + caffeine ; **B**) Spectra of the diluted IL- and PEG-rich phases of the ABS composed of PEG 2000 (≈ 53 wt%) + [OHC₂mim]Cl (≈ 27 wt%) containing both alkaloids at (323 ± 1) K. 230
- Figure 13.7** Logarithm of the alkaloids partition coefficients ($\log K_{alk}$) in the ABS composed of PEG 2000 (≈ 53 wt%) + [C₂mim]Cl (≈ 27 wt%) and different temperatures. 231
- Figure 14.1** Experimental solubility data for ABS composed of PEG 600 + [Ch]-based ILs at 298 K: (Δ) [Ch]DHph; (\blacktriangle) [Ch]Bit; (\blacksquare) [Ch]Bic; (\circ) [Ch]DHcit; (\diamond) [Ch]Lac; (\square) [Ch]Gly; (\bullet) [Ch]Ac; (\blacklozenge) [Ch]Cl. 244
- Figure 14.2** Ternary phase diagram of the ABS composed of [Ch]Cl and PEG at 298 K: (\blacklozenge) binodal curve data; (-) binodal adjusted curve; (\square) TL data. 245
- Figure 14.3** Experimental water activities data at 298 K: (\bullet) PEG 600; (\circ) [Ch]DHcit; (\blacktriangle) [Ch]Bit; (Δ) [Ch]DHph; (\blacksquare) [Ch]Bic; (\bullet) [Ch]Ac; (\blacklozenge) [Ch]Cl. The data shown for the ILs was adapted from Khan et al²⁹. 247
- Figure 14.4** Excess enthalpies of mixing between PEG 600 and the IL anion predicted by COSMO-RS as a function of the polymer mole fraction: (Δ) [Ch]DHph; (\blacktriangle) [Ch]Bit; (\circ) [Ch]DHcit; (\blacksquare) [Ch]Bic; (\diamond) [Ch]Lac; (\square) [Ch]Gly; (\bullet) [Ch]Ac; (\blacklozenge) [Ch]Cl. 249
- Figure 14.5** Experimental solubility data for ABS composed of PEG + [Ch]-based ILs at 298 K: (\diamond) PEG 1000/[Ch]DHph; (\circ) PEG 600/[Ch]DHph; (Δ) PEG 400/[Ch]DHph; (\blacklozenge) PEG 1000/[Ch]Cl; (\bullet) PEG 600/[Ch]Cl; (\blacktriangle) PEG 400/[Ch]Cl. 250
- Figure 14.6** Experimental solubility data for ABS composed of PEG 600 + [Ch]-based ILs: (\circ) PEG 600/[Ch]DHph at 323K; (Δ) PEG 600/[Ch]DHph at 298K; (\blacklozenge) PEG 600/[Ch]Cl at 298K; (\bullet) PEG 600/[Ch]Cl at 323K. 252
- Figure 15.1** Logarithm of K_{TC} versus TLL, at 25°C, for the systems composed of PEG 600 + [Ch]-based salt + water: (\blacklozenge) [Ch]Bic; (\blacksquare) [Ch]Ac; (\bullet) [Ch]DHph; (\circ) [Ch]DHcit; (\blacktriangle) [Ch]Cl. 267

Figure 15.2 Logarithm of K_{TC} (■) and $\%EE_{TC}$ (-●-) obtained in several ABS formed with the fermented broth.

272

LIST OF TABLES

- Table 2.1** Number of isolates obtained from the different oil samples at different temperatures and results obtained regarding biosurfactant production from the screening process under aerobic and anaerobic conditions. 24
- Table 2.2** Surface tension values ($\text{mN}\cdot\text{m}^{-1}$), emulsification indexes (E_{24} , %) and biomass concentrations ($\text{g}\cdot\text{L}^{-1}$) obtained with the different isolates grown aerobically and anaerobically in LB medium at 40°C . Surface tension (ST) values were determined at room temperature (20°C). Emulsification indexes were calculated at 25°C . Biomass concentration was calculated as the dry weight (105°C , 48 h). Results represent the average of three independent experiments \pm standard deviation. 26
- Table 2.3** Surface tension values ($\text{mN}\cdot\text{m}^{-1}$), emulsification indexes (E_{24} , %) and biomass concentrations ($\text{g}\cdot\text{L}^{-1}$) obtained with the different isolates grown in different media for 120 h at 40°C and 120 rpm under anaerobic conditions. Surface tension (ST) values were determined six times at room temperature (20°C). Emulsification indexes were calculated three times at 25°C . Biomass concentration was calculated as the dry weight (105°C , 48 h). Results represent the average of three independent experiments \pm standard deviation. 29
- Table 2.4** Surface tension values (ST, $\text{mN}\cdot\text{m}^{-1}$), emulsification indexes (E_{24} , %) and critical micelle concentrations (cmc , $\text{g}\cdot\text{L}^{-1}$), obtained with freeze-dried biosurfactants from the different isolates dissolved in PBS (pH 7.0). Samples were prepared with a concentration of $1\text{ g}\cdot\text{L}^{-1}$ for *B. subtilis* isolates and $5\text{ g}\cdot\text{L}^{-1}$ for *P. aeruginosa* isolates. Surface tension values were determined six times at room temperature (20°C). Emulsification indexes were calculated three times at 25°C . Results represent the average of three independent experiments \pm standard deviation. 34
- Table 2.5** Effect of NaCl concentration on the surface activity. Surface tension values (ST, $\text{mN}\cdot\text{m}^{-1}$) obtained with culture broth supernatants at different NaCl concentrations ($10\text{-}200\text{ g}\cdot\text{L}^{-1}$). Surface tension values were determined six times at room temperature (20°C). Results are expressed as average \pm standard deviations of three independent measurements. 35
- Table 2.6** Effect of pH on surface activity. Surface tension values (ST, $\text{mN}\cdot\text{m}^{-1}$) obtained with culture broth supernatants at different pH values. Surface tension values were determined six times at room temperature (20°C). Results are expressed as the average \pm standard deviations of three independent experiments. 36
- Table 2.7** Surface tension values (ST, $\text{mN}\cdot\text{m}^{-1}$) and emulsification indexes (E_{24} , %) obtained with culture broth supernatants from the different isolates before and after exposure to 121°C for 20 min. Surface tension values were determined six times at room temperature (20°C). Results are expressed as average \pm standard deviations of values from triplicate experiments. 37

Table 3.1 ¹ H NMR spectroscopy data from rhamnolipids (δ values, ppm) produced by two different strains of <i>Pseudomonas aeruginosa</i> (#111 and #902).	47
Table 3.2 Identification of [M+Na] ⁺ and [M+K] ⁺ ions observed in the ESI-MS spectra corresponding to mono and di-rhamnolipids present in the total sample (extract).	49
Table 4.1 Surface tension values (ST, mN.m ⁻¹), emulsifying indexes (E_{24} , %), biomass concentrations (g dry weight <i>per</i> L) and surfactin concentrations (mg.L ⁻¹) obtained for the three <i>Bacillus subtilis</i> isolates grown in MSS with different carbon sources (10 g.L ⁻¹) at 40°C for 120 h. Results represent the average of three independent experiments \pm standard deviation.	66
Table 4.2 Surface tension values (ST, mN.m ⁻¹), emulsifying indexes (E_{24} , %), biomass concentrations (g dry weight <i>per</i> L) and surfactin concentrations (mg.L ⁻¹) obtained for the three <i>Bacillus subtilis</i> isolates grown in MSS with different nitrogen sources (2 g.L ⁻¹) at 40°C for 120 h. Results represent the average of three independent experiments \pm standard deviation.	67
Table 4.3 Percentages of oil recovered by the different biosurfactants and chemical surfactants at a concentration of 1 g.L ⁻¹ . Results represent the average of three independent experiments \pm standard deviation.	78
Table 5.1 Surface tension values (ST, mN.m ⁻¹) and emulsifying indexes (E_{24} , %) obtained with the different isolates grown in MSS and MSSH for 120 h at 40°C and 120 rpm under anaerobic conditions.	91
Table 5.2 Oil recovery in sand-pack columns using isolates #309, #311 and #573.	94
Table 5.3 Results of additional oil recovery from sand-pack column assays using different <i>Bacillus</i> isolates.	95
Table 6.1 Properties of the hydrocarbon mixtures: viscosity (η), density (ρ), API gravity (API) and <i>n</i> -alkanes range. Viscosity and density values were measured at 40°C.	100
Table 6.2 Summary of the results obtained in the MEOR sand-pack experiments using <i>B. subtilis</i> isolates #309, #311 and #573 and different hydrocarbon mixtures. Results represent the average of three independent experiments \pm standard deviation.	105
Table 6.3 Additional oil recoveries obtained with sand-pack column or core assays using different <i>Bacillus</i> isolates reported in the literature.	107
Table 6.4 Relative viscosities variation ($\Delta\eta$) (at 50°C) of heavy crude oil recovered from sand-pack column assays using <i>B. subtilis</i> isolates #309, #311 and #573 relatively to the control (the associated errors are lower than 6%).	111
Table 6.5 Biosurfactant concentrations (mg.L ⁻¹) obtained in the mini-sand-pack column assays performed with the different isolates and hydrocarbon mixtures. Results represent the average of three independent experiments \pm standard deviation.	112

Table 9.1 Correlation parameters used in equation 9.1 to describe the binodal curves (and respective standard deviations, σ) for the PEG 600 + Na ₂ SO ₄ + H ₂ O + 5 wt% IL quaternary systems at 298 K.	149
Table 9.2 Initial mass fraction compositions for the TLs and TLLs determination, and compositions of the respective top (<i>T</i>) and bottom (<i>B</i>) phases at 298 K.	150
Table 9.3 Partition coefficients of each IL (K_{IL}) and mass fraction compositions of the quaternary systems at 298.15 K	152
Table 9.4 Partition coefficients of L-tryptophan (K_{Trp}) and mass fraction compositions of the quaternary systems at 298.15 K	154
Table 9.5 Partition coefficients of L-tryptophan (K_{Trp}) and mass fraction compositions of the quaternary systems at different temperatures.	157
Table 9.6 Standard molar thermodynamic functions of transfer of L-tryptophan at 298.15 K	159
Table 9.7 Partition coefficients of L-tryptophan (K_{Trp}) and IL (K_{IL}) dependence on the IL concentration at 298.15 K	162
Table 11.1 Interaction energies for some complexes fully optimized at the M06/aug-cc-pVDZ level of theory. ^a	200
Table 11.2 Energies calculated for the reaction $[ClTEG]^- + (H_2O)_n \rightarrow TEG + [Cl(H_2O)_n]^-$ with $n = 1 - 4$.	200
Table 13.1 Partition coefficients of nicotine (K_{nic}) and caffeine (K_{caf}), and selectivity parameters for the nicotine + caffeine ($S_{nic/caf}$) pair in the ABS composed of PEG 2000 (≈ 53 wt%) + [OHC ₂ mim]Cl (≈ 27 wt%) at 323 (± 1) K.	230
Table 13.2 Standard molar thermodynamic functions of transfer for nicotine and caffeine at 323 K.	232
Table 14.1 Chemical structure of the studied cholinium-based salts and respective octanol-water partition coefficients (K_{ow}) ²⁶ .	243
Table 14.2 Solubilities of several [Ch]-based ILs in PEG 600 (expressed in molality) at 298 K and atmospheric pressure.	248
Table 15.1 Chemical structures of the studied cholinium-based salts.	261
Table 15.2 Weight fraction composition of the initial mixture, TLL, pH value of each phase and partition coefficient of TC at 25°C.	266
Table 15.3 Weight fraction composition of the initial mixture, TLL, pH value of each phase and partition coefficient of TC at 25°C in the conventional systems.	270
Table 15.4 pH value of each phase, % EE_{TC} and partition coefficient of TC from the fermented broth at 25°C.	271

DOCUMENT ORGANIZATION

During the past four years I developed research work in two different fields, namely in Microbial Enhanced Oil Recovery and in Antibiotics Purification Using Aqueous Two-Phase Systems Composed of Ionic Liquids and Polymers. The obtained research data was published in a significant amount of different international scientific journals. Thus, this thesis is presented by different chapters, each one corresponding to a different published manuscript. Each chapter was adapted and compiled in each one of the two parts of the thesis according to their research field. In addition, the respective introductions of each paper were reduced to avoid common repetitions along the thesis and all the chapters have their own bibliographic references.

PART A

Microbial Enhanced Oil Recovery

1. INTRODUCTION

1.1. General Context

Nowadays there is an increasing attention given to the increment of oil production through enhanced oil recovery (EOR) techniques. The interest on these techniques results from the oil prices rising and their scarcity. Amongst the main EOR techniques, the microbial enhanced oil recovery (MEOR) has been experiencing a growing exploitation. The MEOR can be based on the indigenous microorganism's stimulation or on the injection of microbial consortia into the reservoir to produce specific metabolites, aiming at increasing the oil recovery. The first part of this thesis aims at the study of different indigenous microorganisms with abilities to degrade hydrocarbons, to produce biocompounds with tensioactive and emulsifying properties, and their application in MEOR.

1.2. Enhancement of Oil Production and Recovery

The world population is expected to grow about 45% in the next 3 decades. This increase, coupled with higher energy consumption *per* person, is bound to lead to an energy demand that will suffer a steady increase over the next years¹. This poses the question: How will we meet this increased energy needs?² Broadly, more than 80% of the world's energy comes from the fossil fuels, half of which being obtained from oil³. Actually the use of alternative energies (such as solar, hydric and wind) are increasing. However, these are expected to meet only 10% of the world's population needs², so that we will remain dependent on fossil energies in the near future.

Among the fossil energies, the oil appears as the essential source of energy and one of the main factors driving the economic development of the World. Its recovery comprises a primary phase, where oil and gas are produced using the natural pressure drive of the reservoir; and a secondary phase, which involves the stimulation of the oil wells by the injection of fluids to improve the flow of oil and gas to the well-head⁴. While primary recovery produces 5-10% of the original oil in place, recovery efficiencies in the secondary stage range from 10% to 40%⁵. Therefore, the remaining crude oil in the reservoirs, after the conventional oil recovery operations, makes up to two-thirds of the total oil reserves⁶⁻⁸. The main factors responsible for the poor oil recovery from producing wells are the low permeability of some reservoirs, the high viscosity of the oil and the high interfacial tension between the hydrocarbon and

aqueous phases, which result in high capillary forces that entrap oil in small pores within the reservoir^{5, 6}. As the price of petroleum increases and petroleum reserves shrink, exploitation of oil resources in mature reservoirs is essential for meeting future energy demands. In the last years, more attention has been focused on tertiary recovery techniques, known as Chemical Enhanced Oil Recovery (CEOR), to mobilize entrapped oil^{5, 6, 9}.

The EOR processes have been applied successfully in several countries, such as USA, Canada, China and Middle East, among others⁴. Traditionally, the chemical methods include the use of surfactants, polymers, acids, gases and solvents⁴. Surfactants reduce the interfacial tension between the oil-water and oil-rock interfaces decreasing thus the capillary forces that prevent the oil movement through the rock pores; they also alter the wettability of the reservoir rock. Polymers are used to increase the viscosity of water in water-flooding operations and also enhance the effectiveness of the process. Furthermore, polymers plug oil-depleted zones, directing the water-flood to oil-rich channels to release residual oil. Acids are used to increase the permeability through the porous network. Gases and solvents decrease oil viscosity and promote its flow; gases also increase the pressure in the reservoir. It is generally accepted that about 30% of the oil contained in the reservoirs can be recovered using current CEOR technology¹⁰. In spite of its efficacy, these methods increase the oil production costs, and also present several environmental hazards such as the high discharge of undesirable residues in aquatic environments.

1.3. Microbial Enhanced Oil Recovery

Microbial Enhanced Oil Recovery (MEOR) is an important tertiary oil recovery technology that represents a cost-effective and eco-friendly alternative to CEOR. In MEOR, selected microbial strains are used to synthesize compounds analogous to those used in CEOR processes to increase the recovery of oil from depleted and marginal reservoirs, thereby extending their life. MEOR has a potential to be a less expensive process when compared with CEOR because microorganisms can synthesize useful products by fermenting low-cost substrates or raw materials. Furthermore, microbial products are biodegradable and have low toxicity^{4, 7, 11}.

The microorganisms can promote the enhanced oil recovery using different mechanisms: CO₂ production that lead to an increase of the reservoir pressure and a reduction of the oil viscosity; production of acids that dissolve certain rocks, increasing therefore the reservoir permeability; blocking of reservoir channels through the biopolymers and biomass produced, which favours the oil displacement; *in situ* or *ex situ* biosurfactants and/or emulsifiers production that allow the reduction of oil/water/rock interfacial tension and the oil emulsification; and reduction of the oil viscosity by the biodegradation of the heavier saturated hydrocarbons fractions¹². Although all these processes can be useful to MEOR applications, their relative efficiencies depend on each reservoir characteristics, being the microorganism strains, nutrients media and injection processes relevant in every case². The common microorganisms with higher potential to be applied in MEOR are the following species: *Clostridium acetobutylicum*¹³, *Pseudomonas aeruginosa*¹⁴, *Bacillus*¹⁵, *Brevibacillus*, *Rhizobium* e *Nocardia*¹⁶. The use of these strains can be done by two different approaches: the injection and inoculation of these strains in the reservoir; and the nutritional stimulation *in situ* of the indigenous strains naturally present in the reservoirs¹⁷.

Among the several MEOR techniques, biosurfactant MEOR represents one of the most promising methods to recover a substantial proportion of the residual oil from mature oil fields^{11, 18}. Biosurfactants are a heterogeneous group of surface-active molecules produced by microorganisms, with both hydrophilic and hydrophobic domains, and which allow them to partition at the interface between the fluid phases with different degrees of polarity, such as oil-water or air-water interfaces. Due to these properties, biosurfactants reduce the surface and interfacial tension and form stable emulsions where hydrocarbons can be dispersed in water^{7, 11, 19, 20}. Biosurfactants produced by some microorganisms are capable of generating a low interfacial tension between the hydrocarbon and the aqueous phases required to mobilize entrapped oil^{8, 18, 21}. These compounds are good candidates for application in MEOR processes and can efficiently replace synthetic surfactants due to their specific activity, low toxicity, high biodegradability and effectiveness at extreme conditions of temperature, pressure, pH and salinity^{10, 22-25}. Similarly to other MEOR mechanisms, there are also two strategies that can be adopted for the use of biosurfactants in enhanced oil recovery. Biosurfactants can be produced *ex-situ* and subsequently injected into the reservoir; or

they can be produced *in situ* by indigenous or injected microorganisms, stimulated by the addition of selected nutrients into the well. The first approach is expensive due to the capital required for the bioreactors operation, product purification and introduction into oil-containing rocks. The second option is more favourable from an economic point of view, but requires the use of microorganisms capable of producing sufficient amounts of biosurfactant within the reservoir^{4, 11}.

Another important mechanism of MEOR is the use of microorganisms to degrade heavy oil fractions. As a result, the oil viscosity decreases and it becomes more fluid, lighter and more valuable. In some cases, combining multiple mechanisms by using consortia of microorganisms with different properties (ability to degrade heavy oil fractions and biosurfactant production) may be an effective strategy for enhanced oil recovery²⁶. There are a number of microorganisms able to degrade hydrocarbons using them as carbon sources²⁷. During the last decade interesting results for the microbial *n*-alkane degradation have been reported²⁸⁻³². In particular, strains of *Gordonia amicalis* have shown ability to degrade large *n*-alkanes under aerobic and anaerobic conditions³³; *Pseudomonas fluorescens* are capable of degrading hydrocarbons with chain lengths between C12 and C32³⁴; heavier *n*-alkanes (C36 to C40) can be degraded by *Pseudomonas aeruginosa* strains³⁵; and a thermophilic *Bacillus* strain that degraded long-chain (C15-C36) but not short-chain (C8-C14) *n*-alkanes³⁶ has also been reported. The use of biosurfactant-producing indigenous *Bacillus* strains to degrade the higher fractions of crude oil and enhance its flow characteristics has been also studied in a petroleum reservoir in the Daqing Oilfield³⁷.

Several scientific and technical reports have demonstrated the MEOR successful applicability in oil reservoirs³⁸, being estimated that until 2015 up to one third of the EOR may be based in microbial processes⁵.

1.4. Work aims and Motivation

In the past few years Brazil has achieved its highest rate of oil production. However, according to the Oil Production report from *Agência Nacional de Petróleo (ANP)*³⁹ only 8% of it are light oil, being 39% of the crude oil produced considered heavy oil. Thus, in our work, we have been aiming at the study of the application of MEOR processes to a paraffinic heavier oil in collaboration with the Biological Engineering Department

(University of Minho), and the reservoir operator PARTEX Oil and Gas. For that purpose, four different oil samples, with high pour point and gravity of 25° API, and with very low solution gas, were supplied by the operator. The samples were obtained from reservoirs consisting of sands with an average porosity of 25% and a permeability of 50 mD. Initially, on chapter 2, we will show the isolation of several microorganisms directly from oil samples, and the study of their ability to produce compounds with surface-active and emulsifying properties and to degrade the higher *n*-alkanes fractions. To this end it was studied the isolation and growth in aerobic and anaerobic conditions, the biosurfactant production by those isolates, and the degradation of wax paraffinic mixtures by the isolates with higher biosurfactant-production rates. By the isolation of several strains, *Bacillus subtilis* and two strains of *Pseudomonas aeruginosa* were identified. On chapter 3 and 4, the chemical characterization of the biosurfactants produced by the strains *P. aeruginosa* and *B. subtilis* is then presented. In chapter 3 two mixtures of rhamnolipids produced by two different strains of *P.aeruginosa* are characterized using Nuclear Magnetic Resonance (¹H NMR) and Mass Spectrometry (MS). On chapter 4 three different surfactant mixtures produced by three *B. subtilis* isolates were also characterized using ¹H NMR, MS and Fourier Transform Infrared Spectroscopy (FTIR). The optimization of the nitrogen and carbon sources in order to maximize the biosurfactant production and the study of the biosurfactants ability to influence the interfacial tension of water/oil systems were also evaluated. After the characterization and study of the biosurfactants production, chapter 5 is focused on the study of the capacities of five different strains to produce compounds with emulsifying and surface-active properties, in a medium supplemented with hydrocarbons, and also on their abilities to degrade paraffinic mixtures and to mobilize liquid paraffin entrapped in sand-pack columns increasing its recovery. Finally and having in mind the main goal of this first part of the thesis, chapter 6 is focused on the MEOR laboratory studies using sand-pack columns applying three *B. subtilis* strains previously isolated. It was investigated the effect of these isolates on the mobilization of four different hydrocarbon mixtures (heating oil, viscous paraffin, Arabian light crude oil, and heavy crude oil) entrapped in sand-pack columns, and on the degradation of the oils recovered after the microbial treatment.

As mentioned above this work was developed in collaboration with the Biological Engineering Department of University of Minho, Portugal. In the Chemistry

Department of University of Aveiro, the biodegradation assays, oil densities and viscosities analysis, chemical characterization of the biosurfactants, and part of the sand-pack enhanced oil recovery tests (these tests were performed by both research groups) were carried out.

1.5. References

1. Hall, C.T., P., Hallock, J. Cleveland, C., Jefferson, M., Hydrocarbons and the evolution of human culture. *Nature*, 2002. **426**: p. 318-322.
2. Youssef, N., Elshahed, M.S., McInerney, M.J., Allen I. Laskin, S.S., and Geoffrey, M.G., Chapter 6 Microbial Processes in Oil Fields: Culprits, Problems, and Opportunities, in *Advances in Applied Microbiology*, 2009, Academic Press. p. 141-251.
3. Available from: http://scimaps.org/maps/map/the_oil_age_world_oi_73/detail/.
4. Lazar, I., Petrisor, I.G., and Yen, T.E., Microbial enhanced oil recovery (MEOR). *Petroleum Science and Technology*, 2007. **25**(11-12): p. 1353-1366.
5. Sen, R., Biotechnology in petroleum recovery: The microbial EOR. *Progress in Energy and Combustion Science*, 2008. **34**(6): p. 714-724.
6. Brown, L.R., Microbial enhanced oil recovery (MEOR). *Current Opinion in Microbiology*, 2010. **13**(3): p. 316-320.
7. Suthar, H., Hingurao, K., Desai, A., and Nerurkar, A., Evaluation of bioemulsifier mediated Microbial Enhanced Oil Recovery using sand pack column. *Journal of Microbiological Methods*, 2008. **75**(2): p. 225-230.
8. Youssef, N., Simpson, D.R., Duncan, K.E., McInerney, M.J., Folmsbee, M., Fincher, T., and Knapp, R.M., In situ biosurfactant production by *Bacillus* strains injected into a limestone petroleum reservoir. *Applied and Environmental Microbiology*, 2007. **73**(4): p. 1239-1247.
9. Youssef, N., Elshahed, M.S., and McInerney, M.J., Microbial processes in oil fields: culprits, problems, and opportunities. *Advances in Applied Microbiology*, Vol 66, 2009. **66**: p. 141-251.
10. Bordoloi, N.K. and Konwar, B.K., Microbial surfactant-enhanced mineral oil recovery under laboratory conditions. *Colloids and Surfaces B-Biointerfaces*, 2008. **63**(1): p. 73-82.
11. Banat, I.M., Franzetti, A., Gandolfi, I., Bestetti, G., Martinotti, M.G., Fracchia, L., Smyth, T.J., and Marchant, R., Microbial biosurfactants production, applications and future potential. *Applied Microbiology and Biotechnology*, 2010. **87**(2): p. 427-444.
12. Zhang Y., X.Z., Ji P., Hou W., Microbial EOR Laboratory Studies and Application Results in Daqing Oilfield. Society of Petroleum Engineers Inc., 1999.
13. Behlulgil, K. and Mehmetoglu, M.T., Bacteria for improvement of oil recovery: A laboratory study. *Energy Sources*, 2002. **24**(5): p. 413-421.
14. Li, Q.X., Kang, C.B., Wang, H., Liu, C.D., and Zhang, C.K., Application of microbial enhanced oil recovery technique to Daqing Oilfield. *Biochemical Engineering Journal*, 2002. **11**(2-3): p.197-199
15. Rauf, M.A., Ikram, M., and Tabassum, N., Enhanced oil recovery through microbial treatment. *Journal of Trace and Microprobe Techniques*, 2003. **21**(3): p. 533-541.
16. Wang, J., Ma, T., Zhao, L.X., Lv, J.H., Li, G.Q., Zhang, H., Zhao, B., Liang, F.L., and Liu, R.L., Monitoring exogenous and indigenous bacteria by PCR-DGGE technology during the process of microbial enhanced oil recovery. *Journal of Industrial Microbiology & Biotechnology*, 2008. **35**(6): p. 619-628.
17. Sayyoub M.H., A.B.M.S., Hemeida A. M., Possible Applications of MEOR to the Arab Oil Fields. *Eng. Sci.*, 1993. **5**: p. 533-541.
18. Simpson, D.R., Natraj, N.R., McInerney, M.J., and Duncan, K.E., Biosurfactant-producing *Bacillus* are present in produced brines from Oklahoma oil reservoirs with a wide range of salinities. *Applied Microbiology and Biotechnology*, 2011. **91**(4): p. 1083-1093.
19. Jenneman, G.E., Mcinerney, M.J., Knapp, R.M., Clark, J.B., Feero, J.M., Revus, D.E., and Menzie, D.E., A Halotolerant, biosurfactant-producing *Bacillus* species potentially useful for enhanced oil-recovery. *Developments in Industrial Microbiology*, 1983. **24**: p. 485-492.

20. Yakimov, M.M., Timmis, K.N., Wray, V., and Fredrickson, H.L., Characterization of a new lipopeptide surfactant produced by thermotolerant and halotolerant subsurface *Bacillus licheniformis* Bas50. *Applied and Environmental Microbiology*, 1995. **61**(5): p. 1706-1713.
21. Yakimov, M.M., Amro, M.M., Bock, M., Boseker, K., Fredrickson, H.L., Kessel, D.G., and Timmis, K.N., The potential of *Bacillus licheniformis* strains for in situ enhanced oil recovery. *Journal of Petroleum Science and Engineering*, 1997. **18**(1-2): p. 147-160.
22. Abdel-Mawgoud, A., Aboulwafa, M., and Hassouna, N.-H., Characterization of Surfactin Produced by *Bacillus subtilis* Isolate BS5. *Applied Biochemistry and Biotechnology*, 2008. **150**(3): p. 289-303.
23. Nitschke, M. and Pastore, G.M., Production and properties of a surfactant obtained from *Bacillus subtilis* grown on cassava wastewater. *Bioresource Technology*, 2006. **97**(2): p. 336-341.
24. Pornsunthorntawe, O., Arttaweeporn, N., Paisanjit, S., Somboonthanate, P., Abe, M., Rujiravanit, R., and Chavadej, S., Isolation and comparison of biosurfactants produced by *Bacillus subtilis* PT2 and *Pseudomonas aeruginosa* SP4 for microbial surfactant-enhanced oil recovery. *Biochemical Engineering Journal*, 2008. **42**(2): p. 172-179.
25. Lotfabad, T.B., Shourian, M., Roostaazad, R., Najafabadi, A.R., Adelzadeh, M.R., and Noghabi, K.A., An efficient biosurfactant-producing bacterium *Pseudomonas aeruginosa* MR01, isolated from oil excavation areas in south of Iran. *Colloids and Surfaces B: Biointerfaces*, 2009. **69**(2): p. 183-193.
26. Jinfeng, L., Lijun, M., Bozhong, M., Rulin, L., Fangtian, N., and Jiayi, Z., The field pilot of microbial enhanced oil recovery in a high temperature petroleum reservoir. *Journal of Petroleum Science and Engineering*, 2005. **48**(3-4): p. 265-271.
27. Wentzel, A., Ellingsen, T.E., Kotlar, H.K., Zotchev, S.B., and Throne-Holst, M., Bacterial metabolism of long-chain *n*-alkanes. *Applied Microbiology and Biotechnology*, 2007. **76**(6): p. 1209-1221.
28. Binazadeh, M., Karimi, I.A., and Li, Z., Fast biodegradation of long chain *n*-alkanes and crude oil at high concentrations with *Rhodococcus* sp. Moj-3449. *Enzyme and Microbial Technology*, 2009. **45**(3): p. 195-202.
29. Etoumi, A., Microbial treatment of waxy crude oils for mitigation of wax precipitation. *Journal of Petroleum Science and Engineering*, 2007. **55**(1-2): p. 111-121.
30. Grishchenkov, V.G., Townsend, R.T., McDonald, T.J., Autenrieth, R.L., Bonner, J.S., and Boronin, A.M., Degradation of petroleum hydrocarbons by facultative anaerobic bacteria under aerobic and anaerobic conditions. *Process Biochemistry*, 2000. **35**(9): p. 889-896.
31. Li, Q., Kang, C., Wang, H., Liu, C., and Zhang, C., Application of microbial enhanced oil recovery technique to Daqing Oilfield. *Biochemical Engineering Journal*, 2002. **11**(2-3): p. 197-199.
32. Sabirova, J.S., Ferrer, M., Regenhart, D., Timmis, K.N., and Golyshin, P.N., Proteomic insights into metabolic adaptations in *Alcanivorax borkumensis* induced by alkane utilization. *Journal of Bacteriology*, 2006. **188**(11): p. 3763-3773.
33. Hao, D.H., Lin, J.Q., Song, X., Su, Y.J., and Qu, Y.B., Isolation, identification, and performance studies of a novel paraffin-degrading bacterium of *Gordonia amicalis* LH3. *Biotechnology and Bioprocess Engineering*, 2008. **13**(1): p. 61-68.
34. Banat, I.M., Biosurfactants production and possible uses in microbial enhanced oil recovery and oil pollution remediation: A review. *Bioresource Technology*, 1995. **51**(1): p. 1-12.
35. Hasanuzzaman, M., Ueno, A., Ito, H., Ito, Y., Yamamoto, Y., Yumoto, I., and Okuyama, H., Degradation of long-chain *n*-alkanes (C 36 and C 40) by *Pseudomonas aeruginosa* strain WatG. *International Biodeterioration and Biodegradation*, 2007. **59**(1): p. 40-43.
36. Wang, L., Tang, Y., Wang, S., Liu, R.L., Liu, M.Z., Zhang, Y., Liang, F.L., and Feng, L., Isolation and characterization of a novel thermophilic *Bacillus* strain degrading long-chain *n*-alkanes. *Extremophiles*, 2006. **10**(4): p. 347-356.
37. She, Y.H., Zhang, F., Xia, J.J., Kong, S.Q., Wang, Z.L., Shu, F.C., and Hu, J.M., Investigation of biosurfactant-producing Indigenous microorganisms that enhance residue oil recovery in

an oil reservoir after polymer flooding. *Applied Biochemistry and Biotechnology*, 2011. **163**(2): p. 223-234.

38. Maudgalya, S., Knapp, R. M., McInerney, Microbial Enhanced Oil Recovery, A review of the Past, Present and Future, in *Proceedings of the SPE/DOE Improved Oil Recovery Symposium*, 2007, Society of Petroleum Engineers: Richardson, Texas.

39. Agência Nacional do Petróleo, G.N.e.B., *Boletim da Produção de Petróleo e Gás Natural*, in *Superintendência de Desenvolvimento e Produção – SDP2011*: Brazil.

2. PAPER 1

Isolation and Study of Microorganisms from Oil Samples for Application in Microbial Enhanced Oil Recovery

International Biodeterioration & Biodegradation (2012) 68, 56-64.

2.1. Abstract

Microbial Enhanced Oil Recovery (MEOR) is potentially useful to increment oil recovery from a reservoir beyond primary and secondary recovery operations using microorganisms and their metabolites. Stimulation of bacterial growth for biosurfactant production and degradation of heavy oil fractions by indigenous microorganisms can enhance the fluidity and reduce the capillary forces that retain the oil into the reservoir. MEOR offers major advantages over conventional EOR techniques, namely low energy consumption and independence of the price of crude oil. In this work, the isolation and identification of microorganisms capable of producing biosurfactants and promote degradation of long-chain *n*-alkanes under conditions existent in oil reservoirs was addressed. Among the isolated microorganisms, five *Bacillus* strains were able to produce extracellular biosurfactants at 40°C under anaerobic conditions in a medium supplemented with hydrocarbons. Three isolates were selected as the higher biosurfactant producers. The obtained biosurfactants reduced the surface tension of water from 72 to 30 mN.m⁻¹, exhibited emulsifying activity and were not affected by their exposure to high temperatures (121°C). These characteristics make them good candidates for use at conditions usually existing in oil reservoirs. Furthermore, it was here shown, for the first time, that *Bacillus* strains were able to degrade large alkyl chains and to reduce the viscosity of hydrocarbon mixtures under anaerobic conditions. The results obtained show that the isolated microorganisms are promising candidates for the development of enhanced oil recovery processes.

Keywords: MEOR; Biosurfactant; Hydrocarbon; Degradation; *Bacillus*, Microbial Enhanced Oil Recovery.

2.2. Introduction

As described in Chapter 1, fossil oil is an essential source of energy and one of the main factors driving the economic development of the World, whereas its recovery comprises three different phases (primary, secondary and tertiary). The remaining crude oil in the reservoirs after conventional oil recovery operations makes up to two-thirds of the total oil reserves¹⁻³. In the last years the tertiary recovery techniques have received a huge attention and this chapter considers the Microbial Enhanced Oil Recovery (MEOR)

applicability aiming at mobilizing the entrapped oil and enhancing the oil productivity^{1, 4, 5}.

Among the several techniques applied in MEOR, the use of microorganisms with ability to produce biosurfactants and/or to degrade the heavy oil fractions are two of the most promising platforms to increase the production of the residual oil from mature oil fields^{6, 7}. The first can be carried out by two main strategies: 1) Biosurfactants can be produced *ex-situ* and subsequently injected into the reservoir; 2) Biosurfactants can be produced *in situ* by indigenous or injected microorganisms stimulated by the addition of selected nutrients into the well. From the two strategies, the *in situ* approach is more favourable from an economical point of view; however, dependent on a sufficient biosurfactant productivity^{6, 8}. The second technique consists in the use of microorganisms with biodegradation ability in order to decrease the oil viscosity turning it more fluid, lighter and more valuable. Oftentimes, the combination of the multiple mechanisms by using consortia of microorganisms with different properties (ability to degrade heavy oil fractions and biosurfactant production) may be an effective strategy for enhanced oil recovery⁹. Recently, a combination of both techniques, with the use of biosurfactant-producing indigenous *Bacillus* strains able to degrade the higher fractions of crude oil, was studied with a petroleum reservoir in the Daqing Oilfield¹⁰ aiming the enhancement of its flow characteristics.

The main drawback of MEOR is the difficulty of isolating microorganisms that can grow and produce the desired metabolic products under the environmental conditions that usually exist in oil reservoirs; many reservoirs are anaerobic and have high salinities and temperatures. Since few environmental parameters of the reservoirs can be manipulated, this also limits the number of reservoirs where microorganisms can be used for *in situ* treatment. *Bacillus subtilis* and *Bacillus licheniformis* strains have been isolated repeatedly from oil reservoirs meaning that they are able to tolerate the reservoir conditions^{5, 7, 11-14}.

In this work, several microorganisms were isolated from crude oil samples and screened for anaerobic growth, biosurfactant production and ability to degrade heavy oil fractions, in order to obtain suitable candidates for application in MEOR.

2.3. Materials and Methods

2.3.1. Isolation of Microorganisms from Oil Samples

Crude oil samples obtained from four wells (PTX-3, PTX-8, PTX-9 and PTX-11) of a Brazilian oil field were collected in sterile bottles. The temperature of the reservoir is about 40°C. Samples were stored at room temperature until use. For isolation of microorganisms, two different methods were used. Direct isolation was performed by serially diluting crude oil samples, that were plated on agar solidified Bushnell-Hass medium and Raymond medium (containing 1% (v/v) *n*-hexadecane as the sole carbon source), as well as Luria-Bertani (LB) medium. Plates were incubated both in aerobic and anaerobic conditions at different temperatures. Enrichment cultures were prepared in 500 mL glass bottles containing 250 mL of mineral media (Bushnell-Hass medium and Raymond medium) supplemented with 1% (v/v) *n*-hexadecane as the sole carbon source. Crude oil samples (5 mL) were transferred to the bottles and incubated at 37, 42 and 50°C for one month. To isolate bacterial strains, samples (200 µL) of the enrichment cultures were periodically spread on agar plates that were incubated at 37, 42 and 50°C under aerobic and anaerobic conditions. After incubation, morphologically distinct colonies were re-isolated by transfer to fresh agar plates, at least three times, to obtain pure cultures. Isolate purity was verified through microscopic observation of Gram stained cultures. Pure cultures were stored at -80°C in LB medium containing 20% (v/v) of a glycerol aqueous solution.

The composition of Raymond medium was as follows (g.L⁻¹): NaCl 50.0; Na₂HPO₄ 3.0; NH₄NO₃ 2.0; KH₂PO₄ 2.0; yeast extract 0.5; MgSO₄·7H₂O 0.2; Na₂CO₃ 0.1; MnSO₄·4H₂O 0.02; CaCl₂ 0.01; FeSO₄ 0.01; supplemented with 1% (v/v) *n*-hexadecane. The composition of Bushnell-Hass medium was (g.L⁻¹): KH₂PO₄ 1.0; K₂HPO₄ 1.0; NH₄NO₃ 1.0; MgSO₄·7H₂O 0.2; FeCl₃ 0.05; CaCl₂ 0.02; supplemented with 1% (v/v) *n*-hexadecane. The composition of the LB medium was (g.L⁻¹): NaCl 10.0; tryptone 10.0; yeast extract 5.0. All the media were adjusted to pH 7.0.

2.3.2. Screening of Biosurfactant-producing Strains

LB medium was used to study biosurfactant production by the different bacterial isolates. A single colony of each isolate was taken from the plate and transferred to 30 mL of LB liquid medium; cultures were incubated at 40°C and 120 rpm. Growth and

biosurfactant production were examined under aerobic and anaerobic conditions. Anaerobic cultures were prepared removing oxygen by aseptically bubbling oxygen-free nitrogen into the flasks, which were sealed with rubber stoppers.

Samples were taken at different time points during the fermentation to determine biomass concentration and biosurfactant production. Bacterial growth was determined by measuring the optical density at 600 nm. Afterwards, the samples were centrifuged (10000 x g, 20 min, 10°C) and cell-free supernatants were used to measure surface tension and emulsifying activity. At the end of the fermentation, cells were harvested by centrifugation and the cell dry weight ($\text{g}\cdot\text{L}^{-1}$) was determined (48 h at 105°C).

2.3.3. Growth and Biosurfactant Production in Mineral Media

The bacterial strains were grown in 30 mL of different mineral media (medium E and Mineral Salt Solution with and without *n*-hexadecane (1%, v/v)) at 40°C. The composition of Medium E was ($\text{g}\cdot\text{L}^{-1}$): NaCl 50.0; K_2HPO_4 10.6; sucrose 10.0; KH_2PO_4 5.3; $(\text{NH}_4)_2\text{SO}_4$ 1.0; $\text{MgSO}_4\cdot 7\text{H}_2\text{O}$ 0.25; supplemented with 1% (v/v) of trace salt solution. The trace salt solution contained ($\text{g}\cdot\text{L}^{-1}$): $\text{MnSO}_4\cdot 4\text{H}_2\text{O}$ 3.0; EDTA 1.0; $\text{FeSO}_4\cdot 7\text{H}_2\text{O}$ 0.1; $\text{CaCl}_2\cdot 2\text{H}_2\text{O}$ 0.1; $\text{CoCl}_2\cdot 6\text{H}_2\text{O}$ 0.1; $\text{ZnSO}_4\cdot 7\text{H}_2\text{O}$ 0.1; $\text{CuSO}_4\cdot 5\text{H}_2\text{O}$ 0.01; $\text{AlK}(\text{SO}_4)_2\cdot 12\text{H}_2\text{O}$ 0.01; H_3BO_3 0.01; $\text{Na}_2\text{MoO}_4\cdot 2\text{H}_2\text{O}$ 0.01. The Mineral Salt Solution consisted of ($\text{g}\cdot\text{L}^{-1}$): NaCl 10.0; sucrose 10.0; Na_2HPO_4 5.0; NH_4NO_3 2.0; KH_2PO_4 2.0; $\text{MgSO}_4\cdot 4\text{H}_2\text{O}$ 0.2. Both media were adjusted to pH 7.0.

2.3.4. Biosurfactant Production and Isolation

Biosurfactant production was carried out in shake flasks containing 500 mL of LB medium. Each flask was inoculated with 5 mL of a pre-culture that was prepared using the same culture medium and incubated overnight at the optimum conditions established for each isolate. The flasks were then incubated at the same conditions until the stationary phase was reached. At the end of the fermentation, cells were harvested by centrifugation ($10,000 \times g$, 20 min, 10°C) and the cell dry weight ($\text{g}\cdot\text{L}^{-1}$) was determined (48 h at 105 °C). To recover the biosurfactant, the cell free supernatant was subjected to acid precipitation. Briefly, the supernatant was adjusted to pH 2.0 with HCl 6 M and left overnight at 4°C. Afterwards, the precipitate was collected by centrifugation ($10000 \times g$, 20 min, 4°C) and washed twice with acidified water (pH 2.0). The crude biosurfactant was dissolved in a minimal amount of demineralised water and the pH was adjusted to

7.0 using NaOH 1 M. Finally, the crude biosurfactant solution was freeze-dried and stored at -20°C for further use.

2.3.5. Surface-activity Determination

Surface tension measurements of culture broth supernatants and biosurfactant solutions were performed according to the Du Noüy ring method described elsewhere¹⁵. A KRÜSS K6 Tensiometer (KRÜSS GmbH, Hamburg, Germany) equipped with a 1.9 cm Du Noüy platinum ring was used. To increase the accuracy of the surface tension measurements, an average of triplicate determinations was conducted. All the measurements were performed at room temperature (20°C). Isolates which reduced the culture broth surface tension, below 40 mN.m⁻¹, were considered biosurfactant producers.

2.3.6. Emulsifying Activity Determination

Emulsifying activity was determined by the addition of 2 mL of *n*-hexadecane to the same volume of cell-free culture broth supernatant or biosurfactant solution in glass test tubes. The tubes were vortex mixed at high speed for 2 min and then incubated at 25°C for 24 h. The stability of the emulsion was determined after 24 h, and the emulsification index (E_{24}) was calculated as the percentage of the height of the emulsified layer (mm) divided by the total height of the liquid column (mm). Emulsions formed by the different isolates were compared with those formed by a 1% (w/v) solution of the synthetic surfactant sodium dodecyl sulphate (SDS) in demineralised water, as proposed by Das et al.¹⁶. All emulsification indexes were performed in triplicate.

2.3.7. Critical Micelle Concentration (*cmc*)

Critical micelle concentration is the concentration of an amphiphilic component in solution at which the formation of micelles is initiated. Concentrations ranging from 0.001 to 5 g.L⁻¹ of the crude biosurfactants recovered from the different isolates were prepared in PBS (10 mM KH₂PO₄/K₂HPO₄ and 150 mM NaCl with pH adjusted to 7.0) and the surface tension of each sample was determined by the Du Noüy ring method at room temperature (20°C) as previously described. The *cmc* was determined by plotting the surface tension as a function of the logarithm of biosurfactant concentration and it

was found at the point of intersection between the two lines that best fit through the pre- and post-*cmc* data. All measurements were done in triplicate.

2.3.8. Identification of the Isolates

Bacterial isolates that displayed high biosurfactant production were selected and identified by partial 16S rRNA sequencing. The 16S rRNA gene was amplified by PCR using primers 341F and 907R. The resulting sequences were compared with sequences in the GenBank database of the National Center for Biotechnology Information (NCBI) (<http://www.ncbi.nlm.nih.gov>) using the nucleotide-nucleotide blast (BLASTn) network service, to determine their phylogenetic affiliations.

2.3.9. Stability Studies

The effect of several environmental parameters on the activity of biosurfactants produced by the different isolates was determined. Stability studies were performed using the cell-free broth obtained by centrifuging the cultures at $10,000 \times g$ for 20 min. In order to assess the effect of salinity on biosurfactant activity, the culture broth supernatants were supplemented with different NaCl concentrations (from 10 to 200 g.L^{-1}) and the surface tension was measured as described above. To evaluate the stability of the biosurfactants to high temperatures, broth samples were incubated at 121°C for 20 min and allowed to cool to room temperature. Surface tension and emulsification indexes were measured and compared to the corresponding values before heat treatment. The pH stability was studied by adjusting the cell-free broth to different pH values (2.0-13.0) using HCl or NaOH solutions, and then surface tension values were measured as described above. All the experiments were carried out in triplicate.

2.3.10. Growth at Different Temperatures and Salinities

In addition to the lack of oxygen, temperature and salinity appear to be the most important environmental factors that influence bacterial growth in the reservoir. Therefore, media containing different NaCl concentrations ($0\text{-}200 \text{ g.L}^{-1}$) were used to grow the isolated bacteria and cultures were incubated at temperatures ranging from 40°C to 60°C for different time intervals.

2.3.11. Hydrocarbon Degradation Determination

The ability of the isolated microorganisms to degrade paraffinic mixtures under aerobic and anaerobic conditions was evaluated using two different experimental conditions. In the first experimental condition used, YP medium supplemented with a paraffinic mixture A (containing *n*-alkanes between C14-C24) was used. In the second condition, Mineral salt Medium (MSM) and a heavier paraffinic mixture B (containing *n*-alkanes between C20-C30) were used. The mixture A was prepared in order to make a preliminary assessment of the degradation ability of 5 different strains. The mixture B was prepared in order to evaluate the ability of 6 different strains to degrade heavier *n*-alkanes chains under anaerobic conditions, aiming the possibility of application on Microbial Enhanced Oil Recovery.

The composition of YP medium was (g.L⁻¹): peptone 20.0; yeast extract 10.0. The MSM contained (g.L⁻¹): KH₂PO₄ 4.7; KNO₃ 4.0; MgSO₄·4H₂O 1.0; Na₂HPO₄ 0.119; FeSO₄·7H₂O 0.015; CaCl₂·2H₂O 0.01; MnCl₂·4H₂O 0.01. MSM was used to evaluate the degradation of *n*-alkanes by the different isolates in medium without additional carbon sources, since YP medium contains peptone and yeast extract, which can be used as carbon sources by the microorganisms.

Flasks containing 50 mL of each culture media supplemented with 10% (w/v) of the respective sterile paraffinic mixture were prepared. The flasks were sealed with rubber stoppers. Anaerobic cultures were prepared removing oxygen by aseptically bubbling oxygen-free nitrogen into the flasks. The paraffinic mixture A was composed by a ratio of 3:1 of two synthetic liquid paraffins, RT20 and RT31, obtained from Rubitherm (Rubitherm GmbH, Berlin, Germany). Culture media were supplemented with 1% (w/v) of squalane (Sigma-Aldrich Co., St. Louis, USA), in order to evaluate the ability of the strains to degrade ramified hydrocarbons. The mixture B was prepared with 23% (w/w) of solid paraffin wax with a melting point of 50-52°C (purchased from Sigma-Aldrich), dissolved in dodecane (99% of purity, also from Sigma-Aldrich). Cultures were performed at 40°C and 150 rpm during 4 days under aerobic conditions, and during 15 days in anaerobic conditions. Control flasks were incubated at the same conditions without addition of microorganisms.

After the incubation time, the organic phase was separated and diluted (20 mg.mL⁻¹) in dichloromethane for gas chromatography (GC) analysis. The GC analysis of each sample was performed with a CP 3800 Varian gas Chromatograph equipped with an on-column injection, FID detector, and DB-5HT capillary column (30 m × 0.32 mm i.d., 0.1 µm thickness) (J&W Scientific Inc., California, USA). Helium was used as gas carrier and a constant flow rate of 2 mL.min⁻¹ was set. The injector and detector temperatures were 350°C and 370°C, respectively. The oven temperature was set at 50°C during 1 min, raised to 350°C at the rate of 10°C.min⁻¹, and at last kept at 370°C during 1 min. All the samples were analyzed in triplicate.

2.4. Results and Discussion

2.4.1. Isolation of Microorganisms from Oil Samples

When petroleum samples were spread on agar plates and incubated at different temperatures, no isolates were obtained, neither under aerobic nor anaerobic conditions. However, using the enrichment method, a total of fifty-eight bacterial strains were recovered. The results obtained are summarized in Table 2.1.

Table 2.1 Number of isolates obtained from the different oil samples at different temperatures and results obtained regarding biosurfactant production from the screening process under aerobic and anaerobic conditions.

Sample	Number of isolates				Biosurfactant production	
	37°C	42°C	50°C	Total	Aerobic	Anaerobic
PTX-3	3	3	14	20	8	2
PTX-8	3	11	7	21	12	0
PTX-9	2	3	3	8	2	0
PTX-11	2	1	6	9	8	3
Total	10	18	30	58	30	5

2.4.2. Screening of Biosurfactant-producing Strains

The different isolates were screened for extracellular biosurfactant production in LB medium under aerobic and anaerobic conditions at 40°C. To evaluate biosurfactant production, both the surface tension and emulsifying activity were taken into account. However, only those isolates that reduced surface tension were found to exhibit

emulsifying activity (no bioemulsifier production was detected). Under aerobic conditions, thirty of the fifty-eight isolates reduced the culture medium surface tension below $40 \text{ mN}\cdot\text{m}^{-1}$, and therefore were considered biosurfactant producers. From these, only five isolates produced biosurfactants also under anaerobic conditions (Table 2.1). The most relevant results obtained are shown in Table 2.2.

Biosurfactants produced by isolates #111 and #902 showed the highest emulsifying activity against *n*-hexadecane, similar to the one obtained with the synthetic surfactant SDS. However, surface tension values obtained with those isolates were not as low as the obtained with other isolates. Furthermore, although isolates #111 and #902 grew at anaerobic conditions, no surface tension reduction or emulsifying activity could be observed, which hampers their application in MEOR processes *in situ*, since most oil reservoirs are anaerobic. The other isolates described in Table 2.2 produced biosurfactants under aerobic and anaerobic conditions. However, biomass and biosurfactant production were higher under aerobic conditions for all the isolates, which is in agreement with the results obtained by other authors^{12-14, 17}. Isolates #309, #311 and #573 showed the highest surface activity, reducing the surface tension of the culture broth from $51.3 \text{ mN}\cdot\text{m}^{-1}$ to values around $30 \text{ mN}\cdot\text{m}^{-1}$, and emulsified *n*-hexadecane similarly to SDS. Isolates #309 and #311 were identified as the best biosurfactant producers under anaerobic conditions. In addition, emulsions formed by supernatants obtained from isolates #111, #309, #311, #573 and #902 remained stable for two weeks at 25°C .

Table 2.2 Surface tension values ($\text{mN}\cdot\text{m}^{-1}$), emulsification indexes (E_{24} , %) and biomass concentrations ($\text{g}\cdot\text{L}^{-1}$) obtained with the different isolates grown aerobically and anaerobically in LB medium at 40°C . Surface tension (ST) values were determined at room temperature (20°C). Emulsification indexes were calculated at 25°C . Biomass concentration was calculated as the dry weight (105°C , 48 h). Results represent the average of three independent experiments \pm standard deviation.

Strain	Aerobic			Anaerobic		
	ST / ($\text{mN}\cdot\text{m}^{-1}$)	E_{24} / (%)	[Biomass] / ($\text{g}\cdot\text{L}^{-1}$)	ST / ($\text{mN}\cdot\text{m}^{-1}$)	E_{24} / (%)	[Biomass] / ($\text{g}\cdot\text{L}^{-1}$)
#111	34.1 ± 0.6	56.5 ± 0.0	1.315 ± 0.346	53.7 ± 4.9	0.0 ± 0.0	0.363 ± 0.138
#191	31.0 ± 1.1	52.3 ± 2.4	1.364 ± 0.467	35.7 ± 1.5	2.6 ± 4.1	0.195 ± 0.050
#309	29.9 ± 0.1	51.6 ± 1.4	0.709 ± 0.252	31.0 ± 1.3	22.9 ± 11.7	0.218 ± 0.097
#311	30.1 ± 0.4	50.8 ± 0.0	0.365 ± 0.110	31.0 ± 1.3	22.7 ± 9.4	0.246 ± 0.041
#552	32.0 ± 0.2	46.1 ± 12.3	1.373 ± 0.379	35.4 ± 1.3	3.0 ± 3.7	0.207 ± 0.060
#573	30.5 ± 0.5	52.3 ± 1.5	1.686 ± 0.648	36.0 ± 2.4	2.2 ± 3.5	0.178 ± 0.041
#902	36.1 ± 0.6	56.5 ± 0.0	1.328 ± 0.011	56.0 ± 3.6	0.0 ± 0.0	0.413 ± 0.144
LB	51.3 ± 0.5	0.0 ± 0.0	----	51.3 ± 0.5	0.0 ± 0.0	----
SDS 1%	39.9 ± 0.4	55.0 ± 1.7	----	39.9 ± 0.4	55.0 ± 1.6	----

2.4.3. Identification of the Isolates

The isolates described in Table 2.2 were identified according to the partial sequence obtained from their 16S rRNA genes. The sequences obtained were compared with those described in databases. The partial sequence of 16S rRNA genes from isolates #111 and #902 showed 100% similarity with *P. aeruginosa*. The partial sequence of 16S rRNA genes of the remaining isolates showed 100% similarity with *B. subtilis*. The sequences were deposited in the GenBank database under accession numbers JQ281104–JQ281110.

2.4.4. Study of Biosurfactant Production in Mineral Media

The isolates presenting the best results regarding biosurfactant production in LB medium were then evaluated under anaerobic conditions using Mineral Salt Solution (MSS), Mineral Salt Solution supplemented with 1% (v/v) *n*-hexadecane (MSSH) and medium E. The results obtained are gathered in Table 2.3. As can be seen from these results, the MSS (with and without *n*-hexadecane) offered better results than medium E for all the isolates. Addition of *n*-hexadecane to the culture broth was found to promote a higher biosurfactant production by some isolates and had no effect on the others. None of the isolates was able to grow or produce biosurfactants in MSS using *n*-hexadecane as the sole carbon source (*data not shown*). The lowest surface tension values (around 30 mN.m⁻¹) were obtained by isolates #309, #311 and #573, with emulsifying indexes between 24% and 34%.

Several *P. aeruginosa* strains have been recovered from petroleum samples and oil contaminated places, and their biosurfactants exhibit good characteristics for application in MEOR, as demonstrated by simulations performed in sand-pack columns¹⁸⁻²⁰. However, those isolates were studied under aerobic conditions and the biosurfactants were produced *ex-situ*. Therefore, although the authors suggested their possible use in MEOR, these strains are not appropriate for use in oil reservoirs. Most of the microorganisms that are potentially useful for application in MEOR *in situ* belong to the genus *Bacillus*. *Bacillus mojavensis* JF-2, a thermotolerant and halotolerant strain isolated from an oil field by Jenneman and collaborators¹¹, grows and produces similar amounts of a lipopeptide biosurfactant under both aerobic and anaerobic conditions, reducing the surface tension of the medium below 30 mN.m⁻¹, and additionally it is not

inhibited by crude oil^{11, 21}. Other strains isolated from oil fields and which applicability in MEOR has been demonstrated are *B. licheniformis* BAS50^{12, 17}, *B. licheniformis* ACO1¹³ and *B. subtilis* PTCC1696¹⁴. Biosurfactants produced by those microorganisms recovered 22-60% of the residual oil entrapped in sand-packed columns^{2, 13, 17, 20}. Furthermore, Youssef et al.³ demonstrated that inoculation of oil wells with *Bacillus* strains and nutrients is possible, and that biosurfactants can be produced *in situ* at concentrations that are sufficient to mobilize significant amount of residual oil. Taking into account these data and the results obtained with isolates #309, #311 and #573 regarding biosurfactant production, they can be considered good candidates for application in MEOR.

Table 2.3 Surface tension values ($\text{mN}\cdot\text{m}^{-1}$), emulsification indexes (E_{24} , %) and biomass concentrations ($\text{g}\cdot\text{L}^{-1}$) obtained with the different isolates grown in different media for 120 h at 40°C and 120 rpm under anaerobic conditions. Surface tension (ST) values were determined six times at room temperature (20°C). Emulsification indexes were calculated three times at 25°C. Biomass concentration was calculated as the dry weight (105°C, 48 h). Results represent the average of three independent experiments \pm standard deviation.

Strain	MSS			MSSH			Medium E		
	ST / ($\text{mN}\cdot\text{m}^{-1}$)	E_{24} / (%)	[Biomass] / ($\text{g}\cdot\text{L}^{-1}$)	ST / ($\text{mN}\cdot\text{m}^{-1}$)	E_{24} / (%)	[Biomass] / ($\text{g}\cdot\text{L}^{-1}$)	ST / ($\text{mN}\cdot\text{m}^{-1}$)	E_{24} / (%)	[Biomass] / ($\text{g}\cdot\text{L}^{-1}$)
#191	41.7 \pm 1.2	14.6 \pm 1.9	0.194 \pm 0.062	40.0 \pm 2.0	13.3 \pm 5.9	0.176 \pm 0.055	50.5 \pm 1.9	11.7 \pm 2.1	0.188 \pm 0.071
#309	31.4 \pm 1.3	25.9 \pm 4.2	0.221 \pm 0.050	31.4 \pm 0.5	24.6 \pm 5.3	0.196 \pm 0.068	32.2 \pm 1.5	28.9 \pm 2.7	0.193 \pm 0.033
#311	30.5 \pm 0.1	8.5 \pm 4.0	0.245 \pm 0.076	31.0 \pm 0.6	34.2 \pm 3.9	0.191 \pm 0.042	36.4 \pm 1.3	8.0 \pm 2.8	0.175 \pm 0.035
#552	48.6 \pm 1.7	13.4 \pm 1.6	0.263 \pm 0.087	41.5 \pm 1.9	14.1 \pm 5.6	0.238 \pm 0.008	56.3 \pm 0.9	10.2 \pm 4.8	0.160 \pm 0.051
#573	31.5 \pm 0.4	24.9 \pm 2.3	0.284 \pm 0.057	33.7 \pm 1.4	19.4 \pm 5.6	0.217 \pm 0.073	43.2 \pm 1.2	16.9 \pm 7.5	0.230 \pm 0.071
Control	66.4 \pm 1.5	0.0 \pm 0.0	----	63.3 \pm 0.9	0.0 \pm 0.0	----	65.6 \pm 0.8	0.0 \pm 0.0	----
SDS 1%	39.9 \pm 0.4	55.0 \pm 1.7	----	39.9 \pm 0.4	55.0 \pm 1.7	----	39.9 \pm 0.4	55.0 \pm 1.7	----

2.4.5. Growth at Different Temperatures and Salinities

The growth at several temperatures and salinities was evaluated for the different isolates in solid and liquid medium. *B. subtilis* isolates (#191, #309, #311, #552 and #573) were able to grow at temperatures between 40 and 55°C in solid medium. At 45°C they grew at NaCl concentrations up to 100 g.L⁻¹. Isolates #309 and #311 grew at 50°C in liquid medium, and biosurfactant production was similar to the obtained at 40°C. However, isolates #191, #552 and #573 were unable to grow in liquid medium at temperatures higher than 45°C. Similar results with several *Bacillus* strains have been reported by other authors^{11-14, 17, 21}. For *P. aeruginosa* isolates #111 and #902 no growth was observed at temperatures higher than 42°C neither in liquid or solid media.

2.4.6. Hydrocarbon Degradation

Although the use of *Bacillus* strains for biosurfactant production has been widely described in the literature, their use to degrade *n*-alkanes has seldom been addressed. In order to evaluate the ability of the isolated *B. subtilis* strains to degrade *n*-alkanes, two different paraffinic mixtures (A and B) were used. The mixture A was incubated with isolates #191, #551, #571, #572 and #573 under aerobic and anaerobic conditions. The respective variations of relative weight fraction of each *n*-alkane present in mixture A compared with the control sample (incubated at the same conditions without microorganisms) are illustrated in Figures 2.1 and 2.2.

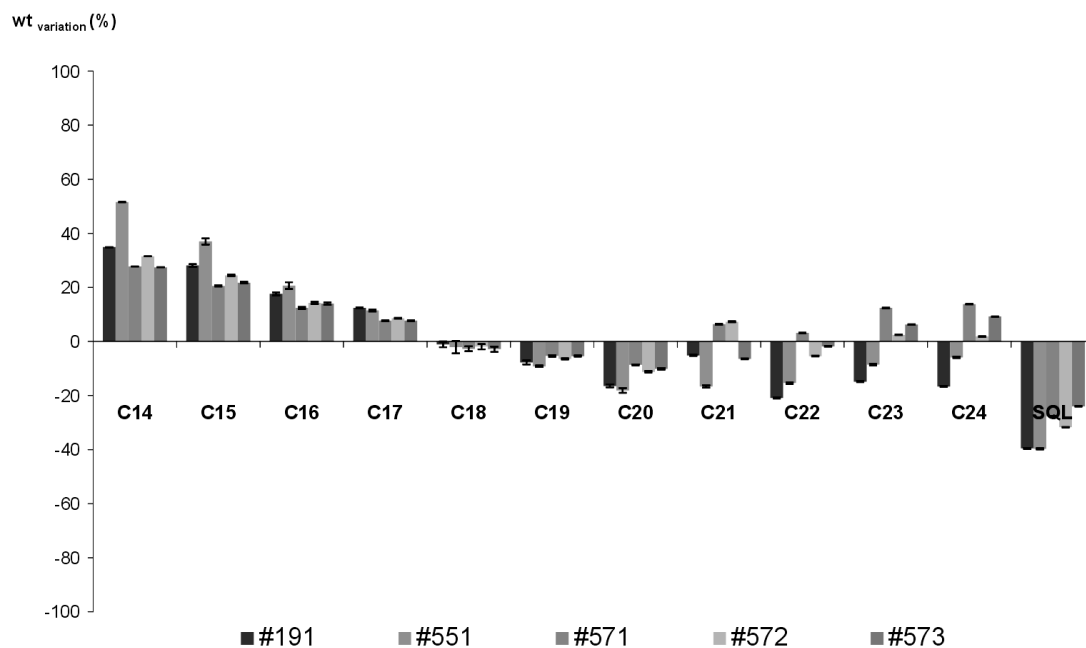


Figure 2.1 Variation of relative weight fraction of *n*-alkanes present in paraffinic mixture A after incubation with bacterial isolates, for 4 days at 40°C and aerobic conditions as compared to the control. (SQL: squalane).

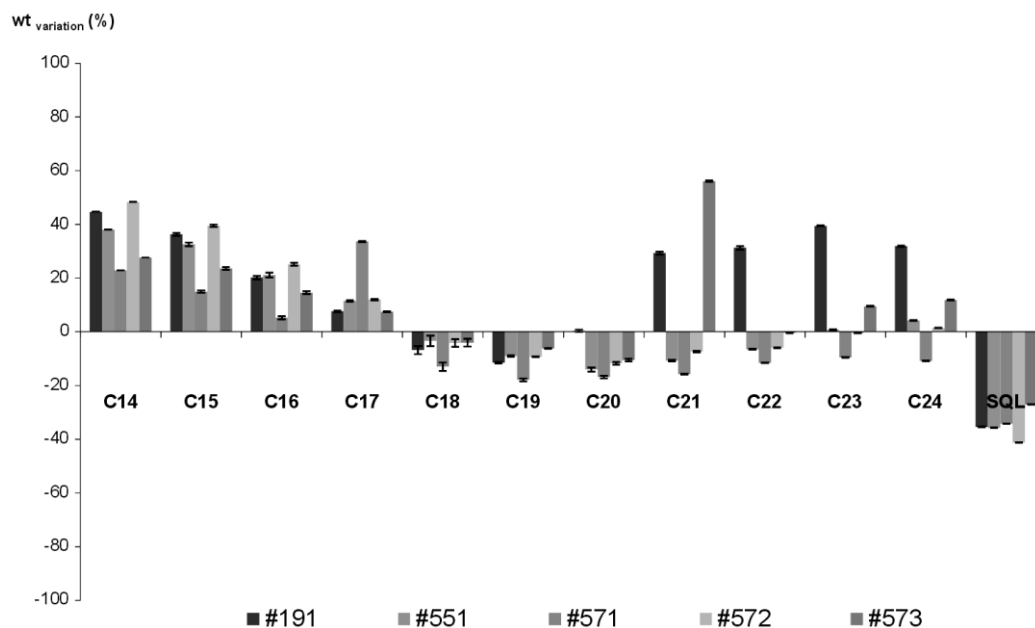


Figure 2.2 Variation of relative weight fraction of *n*-alkanes present in paraffinic mixture A after incubation with bacterial isolates, for 15 days at 40°C and anaerobic conditions as compared to the control. (SQL: squalane).

The isolates studied were found to be able to grow in YP medium supplemented with paraffinic mixture A, both under aerobic and anaerobic conditions. The increase observed in the relative weight fraction of *n*-alkanes lower than C18 and the decrease

observed in the percentage of *n*-alkanes between C18 and C20 after treatment with isolates #191, #551, #571, #572 and #573 indicates that those isolates degraded *n*-alkanes between C18 and C20 into lighter ones, both under aerobic and anaerobic conditions. In the presence of oxygen, isolates #191 and #551 were able to degrade also *n*-alkanes higher than C20. Comparing the influence of oxygen on the degradation of *n*-alkanes by the different isolates, significant differences were only observed for isolates #191 and #571. Isolate #191 showed a higher ability to degrade the long chain *n*-alkanes (C18-C24) under aerobic conditions; however, in absence of oxygen it was only able to degrade *n*-octadecane and *n*-nonadecane. On other hand, isolate #571 exhibited an opposite behaviour and better results were obtained under anaerobic conditions. For the remaining isolates, similar degradation values were obtained in both conditions. The experiments also showed that all the isolates were able to degrade ramified hydrocarbons (squalane) either with or without oxygen.

In view of the positive results obtained, the anaerobic degradation in a mineral medium where the hydrocarbons were the only available carbon source was also studied. Furthermore, aiming at extending the range of *n*-alkanes studied a new mixture B containing *n*-alkanes up to C30 was used. It was observed that *B. subtilis* isolates #191, #309, #316, #551, #552 and #572 degraded the higher *n*-alkanes (>C27) under anaerobic conditions, and the percentage of *n*-alkanes with chains containing less than 25 carbons increased relatively to the control sample (Figure 2.3). The best results were obtained with isolates #191, #309 and #552.

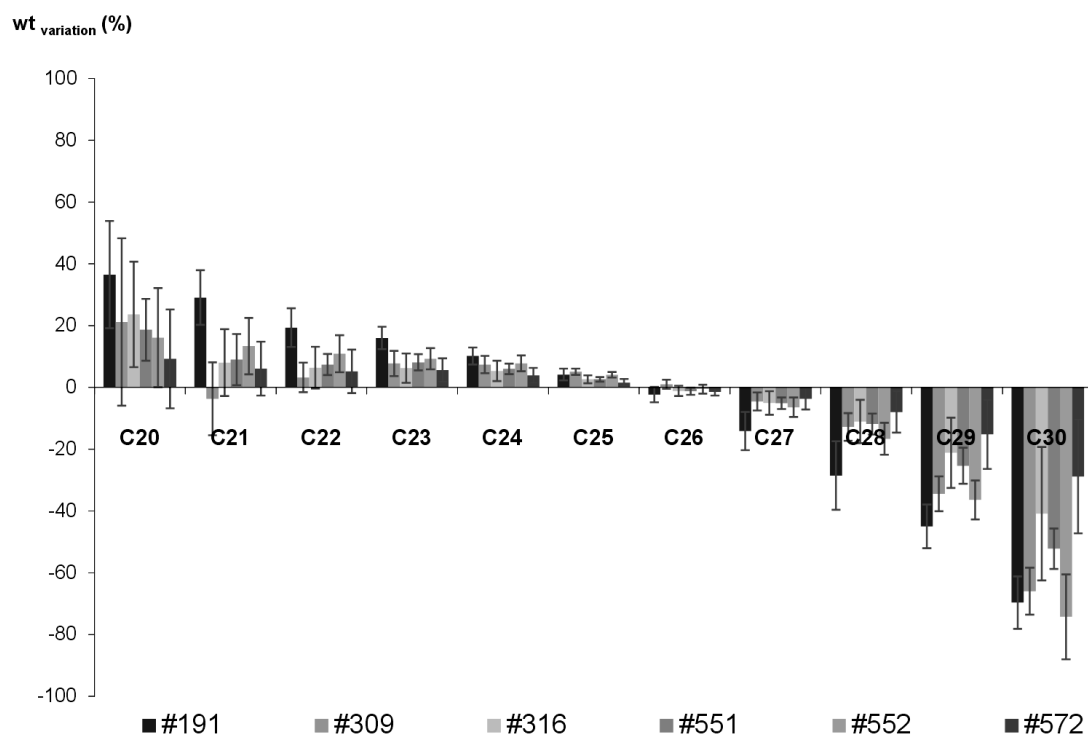


Figure 2.3 Variation of relative weight fraction of *n*-alkanes present in paraffinic mixture B after incubation with bacterial isolates for 15 days, at 40°C and anaerobic conditions as compared to the control.

The ability of a thermophilic *Bacillus* strain to degrade *n*-alkanes ranging from C15 to C36, but not those lower than C14 was observed by Wang et al.²². She et al.¹⁰ observed degradation of *n*-alkanes between C14 and C26 by three *Bacillus* strains isolated from an oil field. Kato et al.²³ isolated two *Bacillus thermoleovorans* strains from a petroleum reservoir which degraded *n*-alkanes between C12 and C30. Das and Mukherjee²⁴ also observed that *B. subtilis* DM-04 preferentially degraded crude oil *n*-alkanes between C14 and C30. However, those assays were performed in aerobic conditions. *G. amicalis* LH3 utilizes a wide range of long-chain *n*-alkanes (C18-C36), although under aerobic conditions degraded preferentially *n*-alkanes between C18 and C24, whereas under anaerobic conditions degraded higher *n*-alkanes (C34-C36)²⁵. In MEOR processes, the degradation of long-chain *n*-alkanes under anaerobic conditions is a very important tool, since most of the oil reservoirs are anaerobic. Isolates #191, #309 and #552 showed the ability of degrading *n*-alkanes with chains higher than C27 into lighter ones under anaerobic conditions, which can be applied to improve the flow properties of crude oil. Furthermore, isolates #191 and #309 additionally showed biosurfactant production

under anaerobic conditions, thus suggesting those isolates attractive candidates for application in MEOR.

2.4.7. Critical Micelle Concentration (*cmc*)

Freeze-dried biosurfactants obtained from the different isolates were dissolved in PBS (pH 7.0) at a concentration of 1 g.L⁻¹ for *B. subtilis* isolates, and 5 g.L⁻¹ for *P. aeruginosa* strains, and surface tensions, as well as their emulsifying activity, were determined. As can be seen from Table 2.4, the lowest surface tension values were obtained with isolates #309 and #311; those isolates also showed the highest emulsifying activities, except for the isolates #111 and #902 (but in this case, biosurfactant concentration was five times higher). To obtain the *cmc*, the original concentrations were serially diluted with PBS buffer and the surface tension was determined. The effective concentration of biosurfactants from *B. subtilis* isolates was found to be much lower than that of biosurfactants from *P. aeruginosa* strains, with *cmc* values 20-100 times lower. The lowest *cmc* values (0.02 g.L⁻¹) correspond to isolates #309 and #311, with a minimum surface tension value of 30 mN.m⁻¹.

Table 2.4 Surface tension values (ST, mN.m⁻¹), emulsification indexes (*E*₂₄, %) and critical micelle concentrations (*cmc*, g.L⁻¹), obtained with freeze-dried biosurfactants from the different isolates dissolved in PBS (pH 7.0). Samples were prepared with a concentration of 1 g.L⁻¹ for *B. subtilis* isolates and 5 g.L⁻¹ for *P. aeruginosa* isolates. Surface tension values were determined six times at room temperature (20°C). Emulsification indexes were calculated three times at 25°C. Results represent the average of three independent experiments ± standard deviation.

Isolate	ST / (mN.m ⁻¹)	<i>E</i> ₂₄ / (%)	<i>cmc</i> / (g.L ⁻¹)
#111	35.5 ± 0.1	53.7 ± 0.0	2.3
#191	32.8 ± 0.2	34.8 ± 1.9	0.13
#309	30.4 ± 0.2	50.8 ± 3.6	0.02
#311	30.3 ± 0.3	51.3 ± 4.1	0.02
#552	32.0 ± 0.3	31.1 ± 2.0	0.10
#573	31.2 ± 0.2	43.3 ± 1.6	0.03
#902	37.9 ± 0.1	52.3 ± 0.0	2.3

Lipopeptide biosurfactants produced by *Bacillus* strains include, among others, surfactin and lichenysin, which reduce surface tension to values around 26-36 mN.m⁻¹, with *cmc*

values from 0.01 to 0.04 g.L⁻¹, and emulsification indexes of about 60%^{12, 20, 21, 26-29}. In sand-pack column assays performed with different *Bacillus* strains, Suthar and co-workers² observed that the combination of surface and emulsifying activity resulted in higher oil recovery when compared with strains possessing merely surface activity, since emulsifiers stabilize oil-water emulsions, which facilitates oil displacement².

2.4.8. Effect of Temperature, pH and Salinity on Biosurfactant Stability

In order to assess the effect of salinity on biosurfactant activity, culture broth supernatants were supplemented with different NaCl concentrations, ranging from 10 to 200 g.L⁻¹, and surface tension was measured. Data obtained are presented in Table 2.5. The maximum surface tension reduction was reached with a NaCl concentration of 50 g.L⁻¹ for all the isolates, and at 100 g.L⁻¹ the surface tension values were still lower than the obtained at 10 g.L⁻¹, similar to the results described by other authors^{12, 13, 26-28}. NaCl concentrations above 100 g.L⁻¹ resulted in higher surface tension values.

Table 2.5 Effect of NaCl concentration on the surface activity. Surface tension values (ST, mN.m⁻¹) obtained with culture broth supernatants at different NaCl concentrations (10-200 g.L⁻¹). Surface tension values were determined six times at room temperature (20°C). Results are expressed as average ± standard deviations of three independent measurements.

Isolate	[NaCl] / (g.L ⁻¹)				
	10 g.L ⁻¹	50 g.L ⁻¹	100 g.L ⁻¹	150 g.L ⁻¹	200 g.L ⁻¹
ST / (mN.m ⁻¹)					
#191	30.8 ± 0.2	28.5 ± 0.1	29.4 ± 0.4	38.0 ± 4.1	49.5 ± 2.3
#309	29.6 ± 0.2	27.0 ± 0.0	27.8 ± 0.1	31.5 ± 1.4	37.4 ± 0.5
#311	29.8 ± 0.1	27.0 ± 0.0	27.9 ± 0.2	31.2 ± 0.2	38.8 ± 0.8
#552	31.4 ± 0.1	29.0 ± 0.1	30.6 ± 0.3	45.0 ± 3.9	51.5 ± 0.7
#573	30.6 ± 0.1	28.1 ± 0.1	30.1 ± 0.3	42.4 ± 4.4	47.7 ± 0.8

The pH of biosurfactant-containing culture media was changed from 2.0 to 13.0 and surface tension values were measured (Table 2.6). Biosurfactant activity was retained at a pH range of 5.0-11.0 with a minimum deviation in surface tension for all the isolates, showing higher stability at alkaline than acidic conditions, and the minimum surface

tension values were obtained at pH 6.0 for all the isolates, as previously described²⁶⁻²⁹. Below pH 5.0, surface tension increases due to the biosurfactant precipitation.

Table 2.6 Effect of pH on surface activity. Surface tension values (ST, mN.m⁻¹) obtained with culture broth supernatants at different pH values. Surface tension values were determined six times at room temperature (20°C). Results are expressed as the average ± standard deviations of three independent experiments.

Isolate	pH					
	2.0	3.0	4.0	5.0	6.0	7.0
	ST / (mN.m ⁻¹)					
#191	56.2 ± 2.3	49.7 ± 3.4	38.9 ± 1.6	30.8 ± 0.1	29.0 ± 0.1	30.9 ± 0.3
#309	60.0 ± 2.0	54.6 ± 1.8	43.8 ± 4.0	31.8 ± 0.1	27.5 ± 0.1	29.8 ± 0.1
#311	62.5 ± 1.2	63.4 ± 2.2	46.5 ± 5.3	31.2 ± 0.3	27.7 ± 0.1	29.8 ± 0.1
#552	60.1 ± 1.8	55.7 ± 2.5	47.3 ± 2.6	33.0 ± 0.6	29.1 ± 0.2	31.7 ± 0.2
#573	61.7 ± 1.2	56.4 ± 2.4	41.8 ± 2.7	30.3 ± 0.1	28.6 ± 0.2	30.8 ± 0.2
	8.0	9.0	10.0	11.0	12.0	13.0
	ST / (mN.m ⁻¹)					
#191	30.8 ± 0.3	31.0 ± 0.3	31.2 ± 0.2	31.3 ± 0.2	32.6 ± 0.1	35.2 ± 0.3
#309	29.9 ± 0.1	30.1 ± 0.1	30.1 ± 0.2	30.2 ± 0.1	33.0 ± 0.1	34.8 ± 0.1
#311	29.9 ± 0.1	30.4 ± 0.1	30.4 ± 0.2	30.4 ± 0.1	33.5 ± 0.1	34.4 ± 0.1
#552	31.3 ± 0.3	31.8 ± 0.2	32.0 ± 0.1	32.2 ± 0.2	34.2 ± 0.2	34.9 ± 0.2
#573	30.9 ± 0.1	31.0 ± 0.2	31.2 ± 0.1	31.3 ± 0.2	34.1 ± 0.4	35.0 ± 0.4

Usually, lipopeptide biosurfactants retain their surface active properties after incubation at 100°C for 2 h²⁸, and their stability to exposure to 121°C has been described by several authors^{13, 26, 27, 29}. To study the stability of biosurfactants at high temperatures, culture broth supernatants obtained at the end of the fermentation were incubated at 121°C for 20 min. Surface tension and emulsification activity were measured before and after heating. As can be seen from Table 2.7, the temperature increase has no negative effect in surface activity.

Table 2.7 Surface tension values (ST, mN.m⁻¹) and emulsification indexes (E_{24} , %) obtained with culture broth supernatants from the different isolates before and after exposure to 121°C for 20 min. Surface tension values were determined six times at room temperature (20°C). Results are expressed as average \pm standard deviations of values from triplicate experiments.

	Before		After	
	ST / (mN.m ⁻¹)	E_{24} / (%)	ST / (mN.m ⁻¹)	E_{24} / (%)
#191	31.8 \pm 0.1	50.8 \pm 0.0	32.6 \pm 0.1	42.4 \pm 0.0
#309	29.9 \pm 0.1	50.8 \pm 0.0	30.0 \pm 0.1	53.7 \pm 0.0
#311	29.8 \pm 0.0	50.8 \pm 0.0	30.1 \pm 0.1	53.7 \pm 0.0
#552	31.9 \pm 0.2	46.6 \pm 1.9	32.8 \pm 0.2	43.8 \pm 2.0
#573	30.6 \pm 0.3	52.3 \pm 1.9	31.1 \pm 0.1	52.3 \pm 1.9

2.5. Conclusion

In the current study, *B. subtilis* strains exhibiting desirable properties for application in MEOR were isolated from crude oil samples. Some isolates grew under anaerobic conditions in medium with NaCl concentrations up to 100 g.L⁻¹ and temperature up to 45-50°C and were not inhibited by the presence of hydrocarbons. The biosurfactants produced by those isolates have some interesting properties, including thermo- and salt-tolerance; ability to reduce the surface tension of water to 30 mN.m⁻¹; ability to emulsify hydrocarbons and critical micelle concentrations of 0.02-0.03 g.L⁻¹. Some *B. subtilis* isolates were also capable of degrading the heavier *n*-alkanes in different paraffinic mixtures, both under aerobic or anaerobic conditions at 40°C. Some isolates (#191 and #309) also exhibited simultaneously the ability for biosurfactant production and hydrocarbon degradation, making them promising candidates for MEOR. Their usefulness for MEOR applications will be further evaluated using laboratory scale sand-pack columns.

2.6. References

1. Brown, L.R., Microbial enhanced oil recovery (MEOR). *Current Opinion in Microbiology*, 2010. **13**(3): p. 316-320.
2. Suthar, H., Hingurao, K., Desai, A., and Nerurkar, A., Evaluation of bioemulsifier mediated Microbial Enhanced Oil Recovery using sand pack column. *Journal of Microbiological Methods*, 2008. **75**(2): p. 225-230.
3. Youssef, N., Simpson, D.R., Duncan, K.E., McInerney, M.J., Folmsbee, M., Fincher, T., and Knapp, R.M., In situ biosurfactant production by *Bacillus* strains injected into a limestone petroleum reservoir. *Applied and Environmental Microbiology*, 2007. **73**(4): p. 1239-1247.
4. Sen, R., Biotechnology in petroleum recovery: The microbial EOR. *Progress in Energy and Combustion Science*, 2008. **34**(6): p. 714-724.
5. Youssef, N., Elshahed, M.S., and McInerney, M.J., Microbial processes in oil fields: culprits, problems, and opportunities. *Advances in Applied Microbiology*, 2009. **66**: p. 141-251.
6. Banat, I.M., Franzetti, A., Gandolfi, I., Bestetti, G., Martinotti, M.G., Fracchia, L., Smyth, T.J., and Marchant, R., Microbial biosurfactants production, applications and future potential. *Applied Microbiology and Biotechnology*, 2010. **87**(2): p. 427-444.
7. Simpson, D.R., Natraj, N.R., McInerney, M.J., and Duncan, K.E., Biosurfactant-producing *Bacillus* are present in produced brines from Oklahoma oil reservoirs with a wide range of salinities. *Applied Microbiology and Biotechnology*, 2011. **91**(4): p. 1083-1093.
8. Lazar, I., Petrisor, I.G., and Yen, T.E., Microbial enhanced oil recovery (MEOR). *Petroleum Science and Technology*, 2007. **25**(11-12): p. 1353-1366.
9. Jinfeng, L., Lijun, M., Bozhong, M., Rulin, L., Fangtian, N., and Jiayi, Z., The field pilot of microbial enhanced oil recovery in a high temperature petroleum reservoir. *Journal of Petroleum Science and Engineering*, 2005. **48**(3-4): p. 265-271.
10. She, Y.H., Zhang, F., Xia, J.J., Kong, S.Q., Wang, Z.L., Shu, F.C., and Hu, J.M., Investigation of biosurfactant-producing Indigenous microorganisms that enhance residue oil recovery in an oil reservoir after polymer flooding. *Applied Biochemistry and Biotechnology*, 2011. **163**(2): p. 223-234.
11. Jenneman, G.E., Mcinerney, M.J., Knapp, R.M., Clark, J.B., Feero, J.M., Revus, D.E., and Menzie, D.E., A Halotolerant, biosurfactant-producing *Bacillus* species potentially useful for enhanced oil-recovery. *Developments in Industrial Microbiology*, 1983. **24**: p. 485-492.
12. Yakimov, M.M., Timmis, K.N., Wray, V., and Fredrickson, H.L., Characterization of a new lipopeptide surfactant produced by thermotolerant and halotolerant subsurface *Bacillus licheniformis* Bas50. *Applied and Environmental Microbiology*, 1995. **61**(5): p. 1706-1713.
13. Dastgheib, S.M.M., Amoozegar, M.A., Elahi, E., Asad, S., and Banat, I.M., Bioemulsifier production by a halothermophilic *Bacillus* strain with potential applications in microbially enhanced oil recovery. *Biotechnology Letters*, 2008. **30**(2): p. 263-270.
14. Ghojavand, H., Vahabzadeh, F., Mehranian, M., Radmehr, M., Shahraki, K.A., Zolfagharian, F., Emadi, M.A., and Roayaei, E., Isolation of thermotolerant, halotolerant, facultative biosurfactant-producing bacteria. *Applied Microbiology and Biotechnology*, 2008. **80**(6): p. 1073-1085.
15. Gudiña, E.J., Teixeira, J.A., and Rodrigues, L.R., Isolation and functional characterization of a biosurfactant produced by *Lactobacillus paracasei*. *Colloids and Surfaces B-Biointerfaces*, 2010. **76**(1): p. 298-304.
16. Das, M., Das, S.K., and Mukherjee, R.K., Surface active properties of the culture filtrates of a micrococcus species grown on n-alkanes and sugars. *Bioresource Technology*, 1998. **63**(3): p. 231-235.
17. Yakimov, M.M., Amro, M.M., Bock, M., Boseker, K., Fredrickson, H.L., Kessel, D.G., and Timmis, K.N., The potential of *Bacillus licheniformis* strains for in situ enhanced oil recovery. *Journal of Petroleum Science and Engineering*, 1997. **18**(1-2): p. 147-160.

18. Bordoloi, N.K. and Konwar, B.K., Microbial surfactant-enhanced mineral oil recovery under laboratory conditions. *Colloids and Surfaces B-Biointerfaces*, 2008. **63**(1): p. 73-82.
19. Lotfabad, T.B., Shourian, M., Roostaazad, R., Najafabadi, A.R., Adelzadeh, M.R., and Noghabi, K.A., An efficient biosurfactant-producing bacterium *Pseudomonas aeruginosa* MR01, isolated from oil excavation areas in south of Iran. *Colloids and Surfaces B: Biointerfaces*, 2009. **69**(2): p. 183-193.
20. Pornsunthorntawe, O., Arttaweeporn, N., Paisanjit, S., Somboonthanate, P., Abe, M., Rujiravanit, R., and Chavadej, S., Isolation and comparison of biosurfactants produced by *Bacillus subtilis* PT2 and *Pseudomonas aeruginosa* SP4 for microbial surfactant-enhanced oil recovery. *Biochemical Engineering Journal*, 2008. **42**(2): p. 172-179.
21. Javaheri, M., Jenneman, G.E., McInerney, M.J., and Knapp, R.M., Anaerobic production of a biosurfactant by *Bacillus licheniformis* JF-2. *Applied and Environmental Microbiology*, 1985. **50**(3): p. 698-700.
22. Wang, L., Tang, Y., Wang, S., Liu, R.L., Liu, M.Z., Zhang, Y., Liang, F.L., and Feng, L., Isolation and characterization of a novel thermophilic *Bacillus* strain degrading long-chain n-alkanes. *Extremophiles*, 2006. **10**(4): p. 347-356.
23. Kato, T., Haruki, M., Imanaka, T., Morikawa, M., and Kanaya, S., Isolation and characterization of long-chain-alkane degrading *Bacillus thermoleovorans* from deep subterranean petroleum reservoirs. *Journal of Bioscience and Bioengineering*, 2001. **91**(1): p. 64-70.
24. Das, K. and Mukherjee, A.K., Crude petroleum-oil biodegradation efficiency of *Bacillus subtilis* and *Pseudomonas aeruginosa* strains isolated from a petroleum-oil contaminated soil from North-East India. *Bioresource Technology*, 2007. **98**(7): p. 1339-1345.
25. Hao, D.H., Lin, J.Q., Song, X., Su, Y.J., and Qu, Y.B., Isolation, identification, and performance studies of a novel paraffin-degrading bacterium of *Gordonia amicalis* LH3. *Biotechnology and Bioprocess Engineering*, 2008. **13**(1): p. 61-68.
26. Abdel-Mawgoud, A., Aboulwafa, M., and Hassouna, N.-H., Characterization of Surfactin Produced by *Bacillus subtilis* Isolate BS5. *Applied Biochemistry and Biotechnology*, 2008. **150**(3): p. 289-303.
27. Nitschke, M. and Pastore, G.M., Production and properties of a surfactant obtained from *Bacillus subtilis* grown on cassava wastewater. *Bioresource Technology*, 2006. **97**(2): p. 336-341.
28. Ghojavand, H., Vahabzadeh, F., Roayaei, E., and Shahraki, A.K., Production and properties of a biosurfactant obtained from a member of the *Bacillus subtilis* group (PTCC 1696). *Journal of Colloid and Interface Science*, 2008. **324**(1-2): p. 172-176.
29. Vaz, D.A., Gudiña, E.J., Alameda, E.J., Teixeira, J.A., and Rodrigues, L.R., Performance of a biosurfactant produced by a *Bacillus subtilis* strain isolated from crude oil samples as compared to commercial chemical surfactants. *Colloids and Surfaces B: Biointerfaces*, 2012. **89**: p. 167-174.

3. PAPER 2

Characterization by Electrospray Ionization and Tandem Mass Spectrometry of Rhamnolipids Produced by Two *Pseudomonas aeruginosa* Strains Isolated from Brazilian Crude Oil

European Journal of Mass Spectrometry (2012) 18, 399-406.

3.1. Abstract

In this work, biosurfactants produced by two *Pseudomonas aeruginosa* strains isolated from Brazilian crude oils were identified by proton Nuclear Magnetic Resonance (^1H NMR) and further characterized by Mass Spectrometry (MS) coupled with electrospray (ESI) and MS/MS analysis in positive mode, and their surface-activities evaluated. Mono-rhamnolipids and di-rhamnolipids were identified for both isolates, but the most abundant were found to be mono-rhamnolipids. The similarity of rhamnolipids produced by the two strains was in good agreement with their surface-activities. Both biosurfactants exhibited similar aqueous solution surface tensions, high emulsification indexes, and critical micelle concentration values. The results obtained show that ESI-MS and MS/MS analysis alone provide a fast and highly specific characterization of biosurfactants produced by microbial strains.

Keywords: rhamnolipids, *Pseudomonas aeruginosa*, biosurfactants, mass spectrometry, ESI-MS.

3.2. Introduction

Surface-active agents or surfactants are amphiphilic molecules that comprise both hydrophobic and hydrophilic moieties, which are able to reduce surface and interfacial tensions, and can form and stabilize oil-in-water or water-in-oil emulsions¹. These compounds have several applications and traditionally are used in food, pharmaceutical, cosmetics and petroleum industries². Chemical surfactants are widely used in industry but the increase of environmental issues and restrictive laws led to the development of biodegradable and naturally produced surfactants, such as oleo chemical- or sugar-based and microbial surfactants³. Biosurfactants appear as a reliable alternative due to their lower toxicity, higher biodegradability and effectiveness at extreme temperature, salinity and pH conditions^{4,5}.

Several biosurfactants have been reported, but the most important groups include glycolipids and lipopeptides². Glycolipids consist of a carbohydrate moiety linked to long-chain aliphatic acids or hydroxyl aliphatic acids⁶. Among them, the most relevant are the rhamnolipids produced by *Pseudomonas* species due to their good surface-activity and emulsifying properties^{7, 8}. Rhamnolipids are composed of one or two β -hydroxy fatty acids of different chain length (C8-C22) linked to a mono-rhamnose

(Rha-) or di-rhamnose (Rha-Rha) unit^{6, 9}. The two major rhamnolipids groups are the mono-rhamnolipids and di-rhamnolipids; however, there are more than 58 rhamnolipid congeners and homologs with different combinations of saturated and unsaturated acyl chains and sugar moieties^{2, 7, 8, 10, 11}.

Mass spectrometry (MS) coupled with electrospray ionization (ESI) is a powerful analytical technique that has been commonly used for the identification and analysis of several biomolecules, such as lipids¹² and carbohydrates¹³. Using this approach, it is possible to obtain information about the structural details of the analyzed molecules. Moreover, taking into account that rhamnolipids contain both lipids and carbohydrates in their structure, these molecules are ideal to be analyzed by MS with ESI. This technique has the advantage of allowing the analysis of very small amounts of sample, even when present in mixtures and without derivatization. However, information on the analysis of rhamnolipids by MS is scarce; thus, this study constitutes an important approach to fill this necessity. Until now, the characterization of the structure of rhamnolipids using MS focused mainly in the use of ESI-MS analysis in the negative mode^{10, 14-18} and only one study reported the use of MS in positive mode, using matrix-assisted laser desorption/ionization (MALDI)¹⁹. Among these studies, only the work carried out in the negative mode suggested the use of tandem MS (MS/MS) for the identification of the structure details of these biomolecules¹⁴. Even if these works performed the study of the fragmentation by increasing the cone voltage ion of the ESI source, after MS had been coupled with liquid chromatography (LC), this is not a truly MS/MS analysis. In addition, analysis of the fragmentation pathways of rhamnolipids positive ions was not previously performed or reported. In positive mode the rhamnolipid ionized preferentially as $[M+Na]^+$ ions, as identified by Price and collaborators¹⁹. However, these authors did not confirm the structural features of the rhamnolipids identified by MS/MS. In fact, MS spectra with the identification of the $[M+Na]^+$ ions allowed the identification of the molecular weight of compounds, while the identification and confirmation of the structural features can only be achieved using MS/MS strategies.

In this work the chemical characterization of rhamnolipids produced by two different strains of *Pseudomonas aeruginosa*, isolated from Brazilian crude oils (chapter 2), was conducted using ¹H NMR and MS approach based on ESI-MS and MS/MS techniques in positive mode. Furthermore, a detailed analysis of the fragmentation pathways

observed in the MS/MS spectra of the $[M+Na]^+$ ions was performed to confirm the structural features of the glycolipids. The surface-active and emulsification properties of rhamnolipid solutions were evaluated, as well as the relation between these features and the chemical structure of the rhamnolipids.

3.3. Experimental

3.3.1. Isolation of Microorganisms from Crude Oil Samples and Biosurfactant Production and Recovery

Crude oil samples from four wells of a Brazilian oil field were collected in sterile bottles. For the isolation of microorganisms, enrichment cultures were performed as described previously²⁰. Biosurfactant production by the selected strains was carried out in shake flasks containing 500 mL of LB medium. Each flask was inoculated with 5 mL of a pre-culture that was prepared using the same culture medium and incubated overnight at 40°C and 120 rpm. The flasks were then incubated at the same conditions until the stationary phase was reached. At the end of the fermentation, the cells were harvested by centrifugation (10000×g, 20 min, 10°C) and cell dry weight (g.L⁻¹) was determined. To recover the biosurfactant, the cell free supernatant was subjected to acid precipitation. After the precipitation, the crude biosurfactant was dissolved in a minimal amount of demineralized water and the pH was adjusted to 7.0 using NaOH 1 M. Finally, the crude biosurfactant solution was freeze-dried and the product obtained was weighed and stored at -20°C for further use.

3.3.2. Identification of the Isolates

Bacterial isolates that displayed high biosurfactant production were selected and identified by partial 16S rRNA sequencing. The 16S rRNA gene was amplified by PCR using primers 341F and 907R. The resulting sequences were compared with sequences in the GenBank database of the National Center for Biotechnology Information (NCBI) (<http://www.ncbi.nlm.nih.gov>) using the nucleotide-nucleotide blast (BLASTn) network service, to determine their phylogenetic affiliations.

3.3.3. Extraction and Purification of Rhamnolipids

Rhamnolipids were extracted from cell-free supernatants, using the Folch extraction commonly used to extract lipids from biomolecules. The Folch extraction procedure

was performed as described elsewhere²², briefly by adding 2:1 chloroform/methanol mixture to the supernatant sample to achieve a final ratio of chloroform/methanol/water (8:4:3). The mixture was centrifuged (9000×g, 5 min), the organic layer was collected and the samples were evaporated to dryness under N₂ at 37°C for 30 min. Prior to MS and NMR analysis, the samples were re-dissolved in chloroform.

3.3.4. Mass Spectrometry

Analysis of rhamnolipids was carried out by MS using ESI ionization obtained in a Q-ToF 2 (Micromass, Manchester, UK). ESI conditions in electrospray Q-Tof mass spectrometer were as follows: electrospray voltage was 3 kV in the positive mode with a cone voltage of 30 V. The source temperature was 80°C and the desolvation temperature was 150°C. MS/MS spectra were performed using argon as collision gas and energy between 30-40 V. Data was acquired using a Mass Lynx data system (V4.0).

3.3.5. NMR Spectroscopy

The purified rhamnolipids were re-dissolved in deuterated chloroform (CDCl₃), and the respective ¹H NMR spectra were recorded using a BrukerAvance 300 spectrometer operating at 300.13 MHz.

3.4. Results and Discussion

3.4.1. Isolation and Identification of Biosurfactant-producing Microorganisms

Isolates #111 and #902 were identified according to the partial sequence obtained from their 16S rRNA genes. The sequences obtained were compared with those described in databases and both of them showed 100% similarity with *P. aeruginosa*. The sequences were deposited in the GenBank database under accession numbers JQ281109 and JQ281110. The sequences obtained for both isolates showed 99% similarity. This fact, together with the different morphology exhibited by both isolates growing in solid and liquid media, confirms that they are different isolates.

3.4.2. NMR Spectroscopy Analysis

The composition of the biosurfactants obtained from isolates #111 and #902 was probed by ^1H NMR analysis. The respective ^1H chemical shifts are shown in Table 3.1, and respective spectra presented in Supporting Information (Figure S3.1 and S3.2).

Table 3.1 ^1H NMR spectroscopy data from rhamnolipids (δ values, ppm) produced by two different strains of *Pseudomonas aeruginosa* (#111 and #902).

		#902	#111
Moiety	Proton location	δ (ppm)	δ (ppm)
Rhamnose(s)	C-1'	4.82	4.86
	C-2'	3.63 – 3.78	3.62 – 3.80
	C-3'	3.63 - 3.78	3.62 - 3.80
	C-4'	3.48	3.47
	C-5'	3.63 – 3.78	3.62 – 3.80
	C-6'	1.24	1.24
Hydroxy fatty acid	C-1	4.20 – 4.22	4.18 - 4.25
	C-2	2.29 - 2.61	2.15 – 2.72
	C-3	-	1.65-1.69
	COOH	-	-
	CH ₃	0.86	0.84
	C-4	5.28 – 5.38	5.28-5.46
	C-5	2.29 – 2.61	2.15 – 2.72
CH ₂	1.24 – 1.58	1.24-1.50	

The ^1H NMR spectra were in good agreement with those obtained by other authors^{6, 10, 19} showing that the purified surfactants samples presented the chemical shifts deviations characteristic of rhamnolipids homologs. The spectrum of isolate #902 showed signals related to a sugar moiety at δ 4.82 (C-1'), 3.63–3.78 (C-2', C-3', C-5'), 3.48 (C-4') and 1.24 (C-6') related to a rhamnose moiety. A similar spectrum was also obtained for isolate #111 at, respectively, δ 4.86 (C-1'), 3.62–3.80 (C-2', C-3', C-5'), 3.47 (C-4') and 1.24 (C-6'). In addition, both spectra showed the hydroxy fatty acid signals. As ^1H NMR was used, it was not possible to define the rhamnolipids structure precisely, thus these were further characterized by ESI/MS and MS-MS as described below.

3.4.3. Mass Spectrometry

The ESI-MS spectra, obtained in positive mode, of the extracts obtained for each isolate (#111 and #902) are shown in Figure 3.1. In both ESI-MS spectra, it is possible to identify several sodium adducts, $[M+Na]^+$ ions, from the rhamnolipids present in the samples. The correspondent potassium adducts, $[M+K]^+$ ions, are also observed, thus allowing the confirmation that rhamnolipid species are present. The formation of these adducts is typical of carbohydrate derivatives¹³ by ESI-MS and was also observed by other researchers during MALDI-MS analysis of rhamnolipids¹⁹.

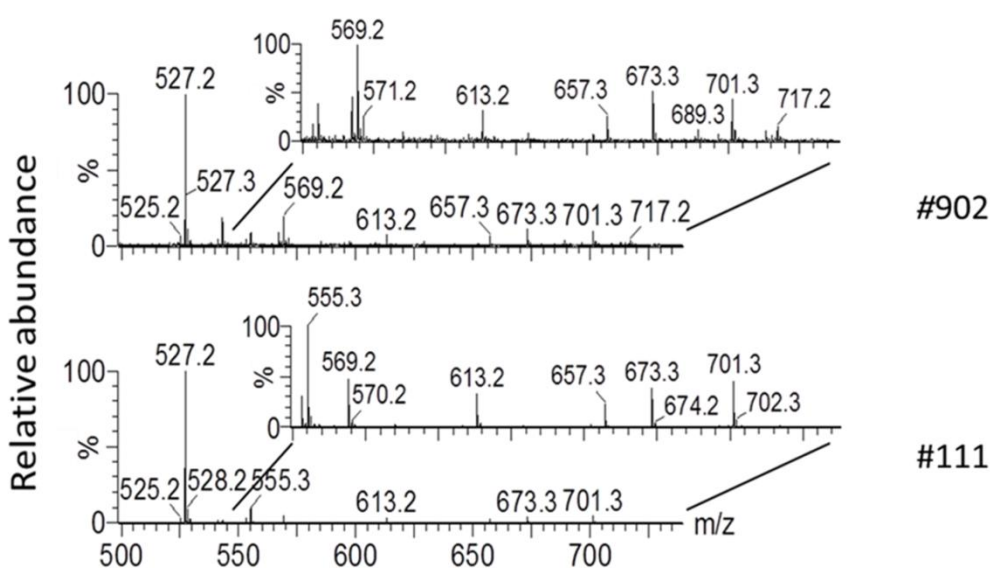


Figure 3.1 ESI-MS spectra obtained using an electrospray Q TOF mass spectrometer in positive mode of #111 and #902 biosurfactants. Y-axis: Relative abundance considering the highest abundant ion as 100%; X-axis: m/z for each ion. ESI-MS spectra were acquired in the positive mode.

The ions identified in the ESI-MS spectra (Figure 3.1) were attributed to both mono- and di-rhamnolipids with distinct fatty acyl chains as shown in Table 3.2.

The most abundant ions observed in the extracts are mono-rhamnolipids, namely Rha-C10:0/C10:0, corresponding to $[M+Na]^+$ ion at m/z 527.2, followed by Rha-C10:0/C12:0 and Rha-C10:0/C12:1, corresponding to $[M+Na]^+$ ions at m/z 555.3 and 553.3, respectively. The di-rhamnolipids found are Rha-Rha-C10:0/C10:0 and Rha-Rha-C10:0/C12:0, corresponding to $[M+Na]^+$ ions at m/z 673.3 and 701.3, respectively (Table 3.2).

Table 3.2 Identification of $[M+Na]^+$ and $[M+K]^+$ ions observed in the ESI-MS spectra corresponding to mono and di-rhamnolipids present in the total sample (extract).

	m/z $[M+K]^+$	m/z $[M+Na]^+$	Fatty acyl chains*
Mono-rhamnolipids	543.2	527.2	C10:0/C10:0
	569.2	553.3	C10:0/C12:1
	571.2	555.3	C10:0/C12:0
Di-rhamnolipids	689.3	673.3	C10:0/C10:0
	717.2	701.3	C10:0/C12:0

*The attribution of the fatty acyl chains composition of each molecular species was done accordingly with the interpretation of the correspondent MS/MS spectra; fatty acyls (Cx:y): the first value indicates x number of carbons in the fatty acid chain and the second value y represents the number of double bonds in that chain.

Few differences were found between the two samples analyzed. Although ESI-MS is a qualitative and not a quantitative method, it was possible to notice some differences in the relative abundance of di-rhamnolipids ions comparing samples from #902 and #111 isolates. Biosurfactant from isolate #111 seems to have a minor relative abundance of the Rha-Rha-C10:0/C10:0 and Rha-Rha-C10:0/C12:0 comparing to #902. Although obtained from two *P. aeruginosa* strains, apparently these two samples have a similar composition of rhamnolipids, which could be explained by their similar surface activities and emulsifying properties previously described²⁰. The large *cmc* values obtained for these biosurfactants²⁰ when compared with other rhamnolipids previously reported may be due to two factors: on one hand Mata-Sandoval *et al.*²⁶ showed that rhamnolipids with short chain fatty acids have smaller hydrophobicity and, accordingly, start to form micelles at higher biosurfactant concentrations; on the other hand, the presence of di-rhamnolipids in the mixtures of surfactants obtained from both isolates (#111 and #902) also leads to an increase in the *cmc* values. This behavior has also been observed by Haba *et al.*²⁷ that showed that higher *cmc* values are obtained due the contribution of the di-rhamnolipid.

In order to confirm the proposed structure of each species identified by ESI-MS spectra, namely the presence of rhamnose units and the identification of the fatty acyl chain composition, the ESI-MS/MS spectra of each $[M+Na]^+$ ions were conducted and analyzed. This approach allows the identification of the fatty acyl chains length, their

position in the rhamnolipid structure and the confirmation of presence of the rhamnose sugar units. Below, a detailed explanation on the typical fragmentation of a mono-rhamnolipid and a di-rhamnolipid is given. Rha-C10:0/C12:0 corresponding to $[M+Na]^+$ ion at m/z 555.3 and Rha-Rha-C10:0/C10:0 corresponding to $[M+Na]^+$ ion at m/z 673.3 are used as examples.

An MS/MS spectrum of the $[M+Na]^+$ ion of the Rha-C10:0/C12:0 (Figure 3.2a)) shows a product ion at m/z 409, formed due to the loss of the rhamnose residue (-146 Da) and ions attributed to the rhamnose residue $[Rhamnose_{res}+Na]^+$ at m/z 169 and to rhamnose unit $[Rhamnose+Na]^+$ at m/z 187 as illustrated in Figure 3.2. Other product ions are observed at m/z 357 due to the loss of the terminal fatty acyl chain (-170 Da), and also the ions corresponding to the $[hydroxy\ fatty\ acid+Na]^+$ at m/z 239, identified as the terminal fatty acid ($C_{12}H_{24}O_3$), and at m/z 211 identified as the middle fatty acid ($C_{10}H_{20}O_3$). These fragmentation pathways allow identifying the molecular weight and structure of the fatty acids that constitute the mono-rhamnolipid and their position in the initial molecule.

Moreover, the ESI-MS/MS spectrum of the $[M+Na]^+$ ion of the di-rhamnolipid, Rha-Rha-C10:0/C10:0 (Figure 3.3a)), showed product ions formed by the loss of one (-146 Da) and two rhamnose residues (2x -146 Da) with the subsequent formation of the ions at m/z 527 and m/z 381, respectively. The product ion at m/z 315, identified as $[Rhamnose_2+Na]^+$ confirms that both rhamnose units are linked together. Ions attributed to one rhamnose were identified at m/z 169 $[Rhamnose_{res}+Na]^+$ and m/z 187 $[Rhamnose+Na]^+$. In this spectrum, it is possible to see other informative ions formed by the loss of the terminal of fatty acyl chain (-170 Da- $-C_{10}H_{20}O_3$) at m/z 503, the loss of a fatty acyl and a rhamnose (-316 Da) at m/z 357 and also the ions corresponding to the fatty acyls chains at m/z 211.

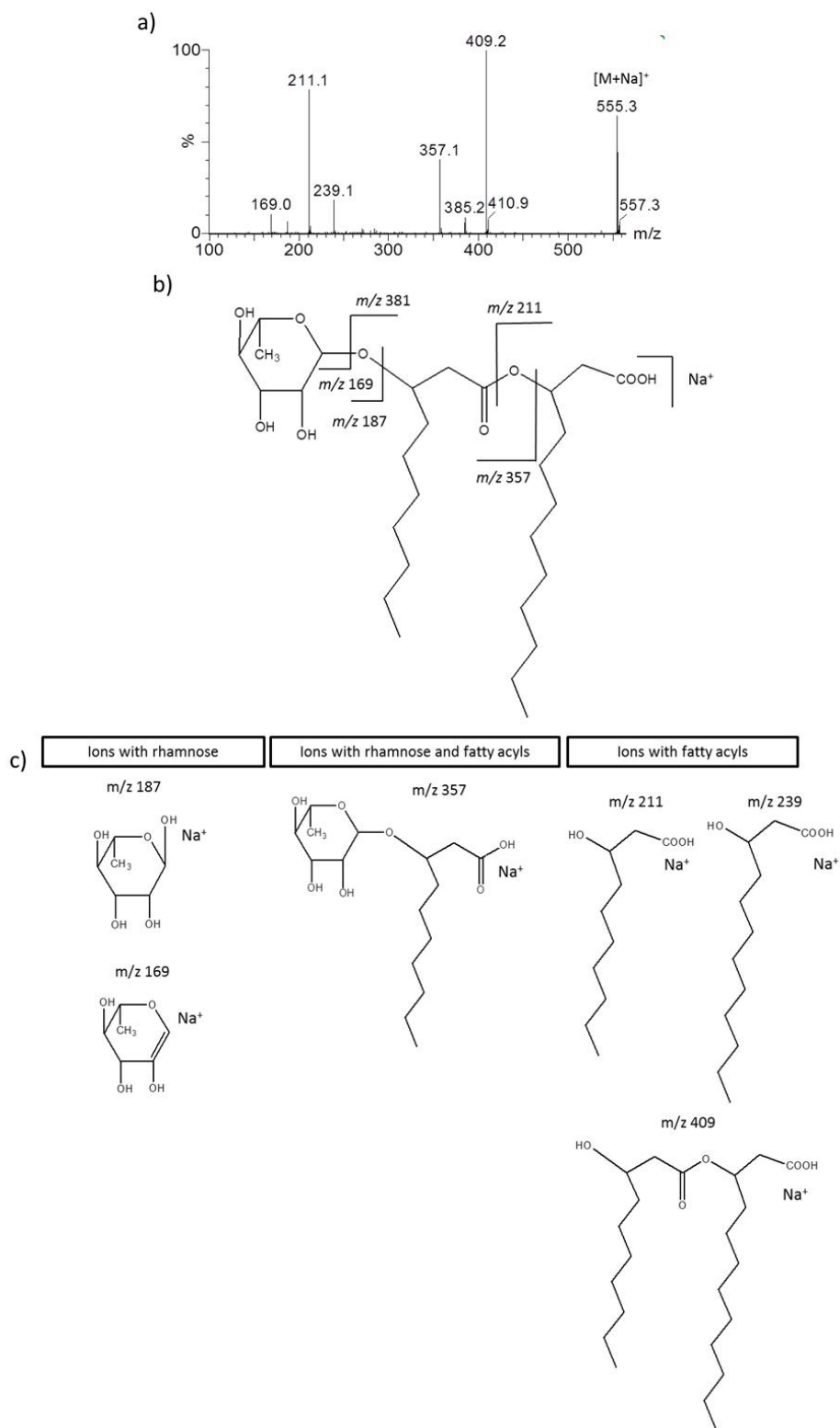


Figure 3.2 a) ESI-MS/MS spectrum of the $[M+Na]^+$ ion at m/z 555.3 corresponding to mono-rhamnolipid Rha-C10:0/C12:0 obtained in ESI-QTOF. b) Molecular structure of Rha-C10:0/C12:0 with the main cleavages correspondent to the fragmentation observed in the MS/MS spectrum of $[M+Na]^+$ ion. c) Molecular structure of the ions originated from the fragmentation of $[M+Na]^+$ ion.

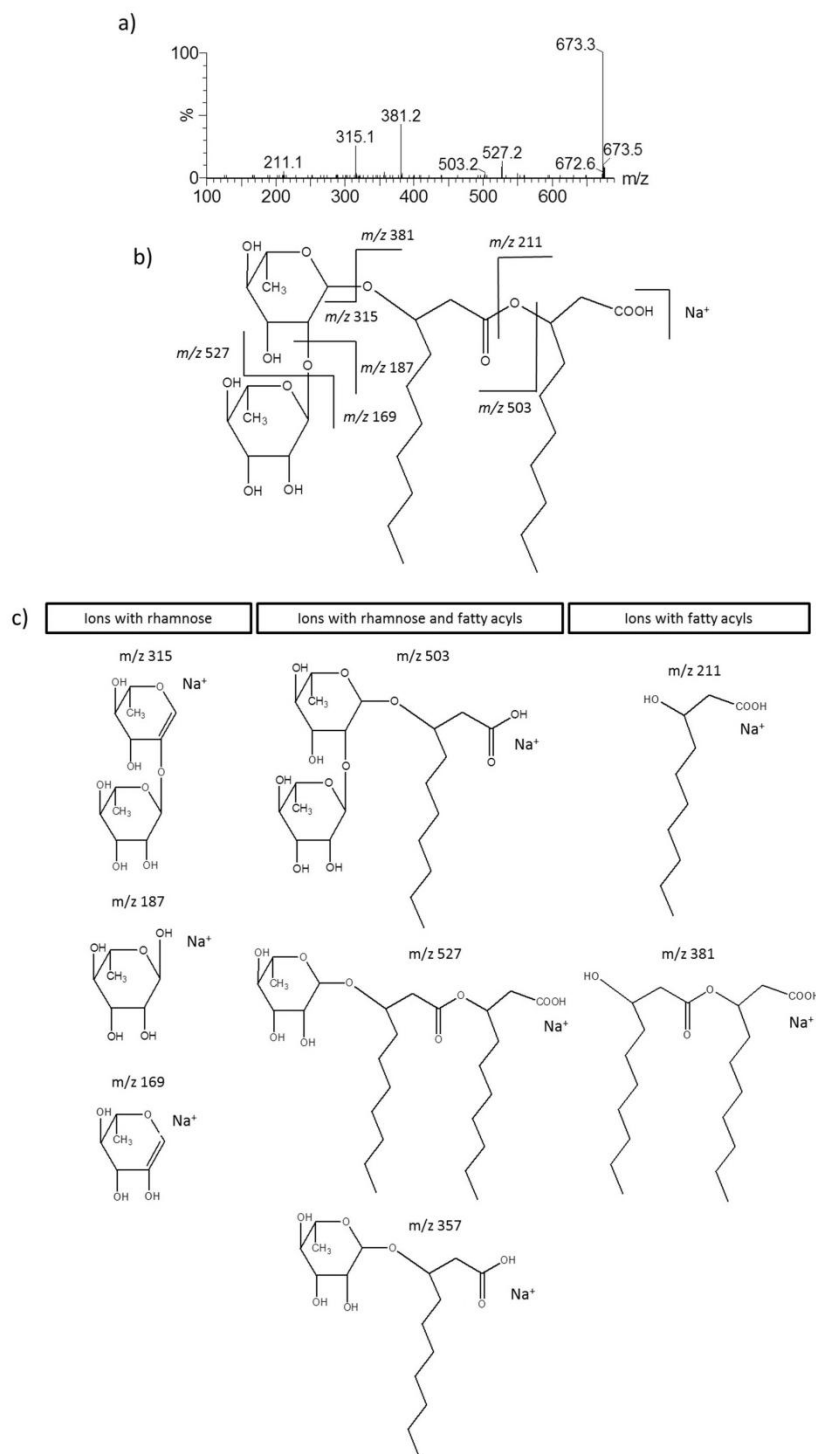


Figure 3.3 a) ESI-MS/MS spectrum of the $[M+Na]^+$ ion at m/z 673.3 corresponding to di-rhamnolipid Rha-Rha-10:0/10:0 obtained in ESI-Q TOF. b) Molecular structure of Rha-Rha-10:0/10:0 with the main cleavages correspondent to the fragmentation observed in the MS/MS spectrum of $[M+Na]^+$ ion at m/z 673.3. c) Molecular structure of the ions originated from the fragmentation of $[M+Na]^+$ ion at m/z 673.3.

This approach was used to elucidate the structure of all the rhamnolipids identified and the results are reported in Table 3.2. There are a few studies that characterize the fragmentation of rhamnolipids with MS/MS, the best known being the rupture of ester link between two alkyl chains of rhamnolipids and near sugar units in negative mode ($[M-H]^-$)^{6, 28}. In spite of this work having been carried in positive mode, with formation of $[M+Na]^+$, the fragmentations observed are similar, suggesting that they are characteristic of these molecules.

This is one of the first studies on the characterization of rhamnolipids by MS in positive mode, with formation of $[M+Na]^+$ ions^{19, 29}, and the first using electrospray ionization. The results here reported are in good agreement with Price et al¹⁹ which identified the rhamnolipids structure with MS in positive mode and MALDI ionization, observing the mono-rhamnolipids Rha-C10:0/C10:0, Rha-C10:0/C12:0 and Rha-C10:0/C12:1 and the di-rhamnolipids Rha-Rha-C10:0/C10:0 and Rha-Rha-C10:0/C12:0 with formation of $[M+Na]^+$ ions and a minor part with formation of $[M+K]^+$ ions. The results obtained herein show that ESI-MS and MS/MS analysis are powerful techniques for characterizing biosurfactants produced by microbial strains, allowing the identification and confirmation of the structural features using only MS/MS strategies, without the LC previous analysis.

3.5. Conclusion

In this work biosurfactants produced by two isolated *P. aeruginosa* strains were characterized. Their structures have been identified by ¹H NMR as being rhamnolipids and further characterized by ESI/MS and MS/MS as mixtures of mono-rhamnolipids and di-rhamnolipids. The most abundant homologs found in the extracts were the mono-rhamnolipids, Rha-C10:0/C12:0 and Rha-C10:0/C12:1 and the di-rhamnolipids Rha-Rha-C10:0/C10:0 and Rha-Rha-C10:0/C12:0. The rhamnolipid structural characterization showed that although these surfactants have been obtained from two different *P. aeruginosa* strains, they have a close composition that explains their similar behavior. The structural characterization of the biosurfactants produced by microorganisms is very important to understand their surface-active properties and formation of molecular aggregates. The development of rapid analysis, such as ESI-MS and MS/MS, which allow the characterization with high sensitivity and specificity of the surfactants present in bacterial extracts, is crucial. In conclusion, it is important to

understand biosurfactants specificities in order to increase their potential applications as, for example, in bioremediation of environments contaminated with crude oil and in tertiary recovery of crude oil from reservoirs by MEOR processes. In this context, the results herein reported show that ESI-MS and MS/MS analysis can be powerful techniques for a simple and fast structural characterization of biosurfactants produced by microbial strains.

3.6. References

1. Desai, J. D., Banat, I. M., Microbial production of surfactants and their commercial potential. *Microbiology and Molecular Biology Reviews*. **61**: 47- 64 (1997).
2. Nitschke, M., Costa, S. G. V. A. O., Contiero, J., Rhamnolipid surfactants: An update on the general aspects of these remarkable biomolecules. *Biotechnology Progress*. **21**: 1593-600 (2005).
3. Mukherjee, S., Das P., Sen R., Towards commercial production of microbial surfactants. *Trends in Biotechnology*. **24**: 509-15 (2006).
4. Van Hamme, J. D., Singh, A., Ward, O. P., Physiological aspects - Part 1 in a series of papers devoted to surfactants in microbiology and biotechnology. *Biotechnology Advances*. **24**: 604-20 (2006).
5. Singh, A., Van Hamme, J. D., Ward, O. P., Surfactants in microbiology and biotechnology: Part 2. Application aspects. *Biotechnology Advances*. **25**: 99-121 (2007).
6. Raza, Z. A., Khalid, Z. M., Banat, I. M., Characterization of rhamnolipids produced by a *Pseudomonas aeruginosa* mutant strain grown on waste oils. *Journal of Environmental Science and Health Part A*. **44**: 1367-73 (2009).
7. Mulligan, C. N., Environmental applications for biosurfactants. *Environmental Pollution*. **133**: 183-98 (2005).
8. Soberon-Chavez, G., Lepine, F., Deziel, E., Production of rhamnolipids by *Pseudomonas aeruginosa*. *Applied Microbiology and Biotechnology*. **68**: 718-25 (2005).
9. Perfumo, A., Banat, I. M., Canganella, F., Marchant, R., Rhamnolipid production by a novel thermophilic hydrocarbon-degrading *Pseudomonas aeruginosa* AP02-1. *Applied Microbiology and Biotechnology*. **72**: 132-8 (2006).
10. Monteiro, S. A., Sasaki, G. L., de Souza, L. M., Meira, J. A., de Araujo, J. M., Mitchell, D. A., Ramos, L.P., Krieger, N., Molecular and structural characterization of the biosurfactant produced by *Pseudomonas aeruginosa* DAUPE 614. *Chemistry and Physics of Lipids*. **147**: 1-13 (2007).
11. Abdel-Mawgoud, A. M., Lepine, F., Deziel, E., Rhamnolipids: diversity of structures, microbial origins and roles. *Applied Microbiology and Biotechnology*. **86**: 1323-36 (2010).
12. Milne, S., Ivanova, P., Forrester, J., Brown, H. A., Lipidomics: An analysis of cellular lipids by ESI-MS. *Methods*. **39**: 92-103 (2006).
13. Zaia, J., Mass spectrometry of oligosaccharides. *Mass Spectrometry Reviews*. **23**: 161-227 (2004).
14. Heyd, M., Kohnert, A., Tan, T. H., Nusser, M., Kirschhofer, F., Brenner-Weiss, G., Berensmeier, S., Development and trends of biosurfactant analysis and purification using rhamnolipids as an example. *Analytical and Bioanalytical Chemistry*. **391**: 1579-90 (2008).
15. Yin, H., Qiang, J., Jia, Y., Ye, J. S., Peng, H., Qin, H. M., Zhang, N., He, B., Characteristics of biosurfactant produced by *Pseudomonas aeruginosa* S6 isolated from oil-containing wastewater. *Process Biochemistry*. **44**: 302-8 (2009).
16. de Sousa, J. R., Correia, J. A. D., de Almeida, J. G. L., Rodrigues, S., Pessoa, O. D. L., Melo, V. M. M., Gonçalves, L. R. B., Evaluation of a co-product of biodiesel production as carbon source in the production of biosurfactant by *P. aeruginosa* MSIC02. *Process Biochemistry*. **46**: 1831-9 (2011).
17. Wei, Y. H., Chou, C. L., Chang, J. S., Rhamnolipid production by indigenous *Pseudomonas aeruginosa* J4 originating from petrochemical wastewater. *Biochemical Engineering Journal*. **27**: 146-54 (2005).
18. Rikalovic, M. G., Gojgic-Cvijovic, G., Vrvic, M. M., Karadzic, I., Production and characterization of rhamnolipids from *Pseudomonas aeruginosa* san-ai. *Journal of the Serbian Chemical Society*. **77**: 27-42 (2012).
19. Price, N. P. J., Ray, K. J., Vermillion, K., Kuo, T. M., MALDI-TOF mass spectrometry of naturally occurring mixtures of monorhamnolipids and dirhamnolipids. *Carbohydrate Research*. **344**: 204-9 (2009).

20. Gudiña, E. J., Pereira, J. F. B., Rodrigues, L. R., Coutinho, J. A. P., Teixeira, J. A., Isolation and study of microorganisms from oil samples for application in Microbial Enhanced Oil Recovery. *International Biodeterioration and Biodegradation*. **68**: 56-64 (2012).
21. Gudiña, E. J., Teixeira, J. A., Rodrigues, L. R., Isolation and functional characterization of a biosurfactant produced by *Lactobacillus paracasei*. *Colloids and Surfaces B: Biointerfaces*. **76**: 298-304 (2010).
22. Folch, J., Lees, M., Stanley, G. H. S., A Simple Method for the Isolation and Purification of Total Lipides from Animal Tissues. *The Journal of Biological Chemistry*. **226**: 497-509 (1957).
23. Bordoloi, N. K., Konwar B. K., Microbial surfactant-enhanced mineral oil recovery under laboratory conditions. *Colloids and Surfaces B: Biointerfaces*. **63**: 73-82 (2008).
24. Pornsunthorntawee, O., Arttaweeporn, N., Paisanjit, S., Somboonthanate, P., Abe, M., Rujiravanit, R., Chavadej, S., Isolation and comparison of biosurfactants produced by *Bacillus subtilis* PT2 and *Pseudomonas aeruginosa* SP4 for microbial surfactant-enhanced oil recovery. *Biochemical Engineering Journal*. **42**: 172-9 (2008).
25. M. Q. Nie, Yin, X. H., Ren, C. Y., Wang, Y., Xu, F., Shen, Q. R., Novel rhamnolipid biosurfactants produced by a polycyclic aromatic hydrocarbon-degrading bacterium *Pseudomonas aeruginosa* strain NY3. *Biotechnology Advances*. **28**: 635-43 (2010).
26. Mata-Sandoval, J. C., Karns, J., Torrents, A., High-performance liquid chromatography method for the characterization of rhamnolipid mixtures produced by *Pseudomonas aeruginosa* UG2 on corn oil. *Journal of Chromatography A*. **864**: 211-20 (1999).
27. Haba, E., Abalos, A., Jauregui, O., Espuny, M. J., Manresa, A., Use of liquid chromatography-mass spectroscopy for studying the composition and properties of rhamnolipids produced by different strains of *Pseudomonas aeruginosa*. *Journal of Surfactants and Detergents*. **6**: 155-61 (2003).
28. Haba, E., Pinazo, A., Jauregui, O., Espuny, M. J., Infante, M. R., Manresa, A., Physicochemical characterization and antimicrobial properties of rhamnolipids produced by *Pseudomonas aeruginosa* 47T2 NCBIM 40044. *Biotechnology and Bioengineering*. **81**: 316-22 (2003).
29. Pajarron, A. M., Dekoster, C. G., Heerma, W., Schmidt, M., Haverkamp, J., Structure Identification of Natural Rhamnolipid Mixtures by Fast-Atom-Bombardment Tandem Mass-Spectrometry. *Glycoconjugate Journal*. **10**: 219-26 (1993).

4. PAPER 3

Optimization and Characterization of Biosurfactant Production by *Bacillus subtilis* Isolates Towards Microbial Enhanced Oil Recovery Applications

Fuel (2013) Doi.org/10.1016/j.fuel.2013.04.040

4.1. Abstract

Biosurfactant production by three *Bacillus subtilis* strains (#309, #311 and #573) isolated from Brazilian crude oils was optimized based on different carbon and nitrogen sources. The lowest surface tension values were obtained using sucrose containing media for the three isolates. Biosurfactants produced by each strain were characterized by Fourier Transform Infrared Spectroscopy (FTIR), and were further characterized by proton Nuclear Magnetic Resonance (^1H NMR), and Matrix-Assisted Laser Desorption Ionization-Time of Flight mass spectrometry (MALDI-TOF). The chemical characterization showed that the three isolates produced very similar mixtures, containing C_{13} -, C_{14} - and C_{15} -surfactin, although in different proportions. The structure of surfactins produced by the three strains was shown to be in good agreement with their surface-activities. The interfacial-activities of the biosurfactants were characterized and compared with chemical surfactants. Furthermore, the application of biosurfactants and chemical surfactants in oil recovery was evaluated. The results obtained showed that these biosurfactants have better interfacial-activity and oil recovery efficiency than common chemical surfactants, thus being more attractive to be applied in Microbial Enhanced Oil Recovery.

Keywords: Surfactins; *Bacillus subtilis*; Biosurfactants; MEOR; MALDI-TOF.

4.2. Introduction

As described in chapter 3, the interest for biosurfactants is increasing mainly due to environmental issues and restrictive laws¹, and also by the fast progress of biotechnology and their interesting features, including their lower toxicity, higher biodegradability and effectiveness at extreme temperature, salinity and pH conditions^{2,3}. Furthermore, biosurfactants exhibit high surface-activities together with low critical micelle concentrations (*cmc*), being in some cases even lower than most of the traditional chemical surfactants².

Despite all these advantages, only few biosurfactants are produced at large scale for commercial applications, essentially due to their considerable low production and recovery costs⁴. In the last years, aiming a large industrial application of biosurfactants, the use of novel resources, raw materials and new microorganisms has been explored to reduce the production costs and to increase their effectiveness⁵⁻¹¹. Many biosurfactants

have been described, being glycolipids^{12, 13} and lipopeptides^{14, 15} the most common. Lipopeptides are produced, among others, by several *Bacillus* species. They are constituted by a peptide (hydrophilic moiety) linked to a fatty acid (hydrophobic component)¹⁴. Surfactin, produced by *Bacillus subtilis* strains, is the best studied lipopeptide biosurfactant. It consists of a long-chain β -hydroxy fatty acid whose two functional groups close a short peptidic moiety composed of seven amino acid residues^{16, 17}. The surfactins are classified in three different types (A, B and C) according to their amino acid sequences¹⁸. *B. subtilis* strains do not produce a unique type of surfactin, occurring a natural diversity of homologues, which differ in the length and ramification of the fatty acid chains, and isoforms, characterized by some differences in the peptidic sequence¹⁶. Different isoforms and homologues exhibit different properties and activities. As the surfactin name indicates, this biosurfactant exhibits an exceptional surface activity, and is among the most effective biosurfactants known so far, being able to decrease the surface tension of water from 72 to 27 mN.m⁻¹ at concentrations as low as 0.005%¹⁹.

Surfactins are considered powerful biosurfactants²⁰, and can be used by the petroleum industry in MEOR processes and bioremediation³, as well as by the biomedical industry as therapeutic agents^{17, 18}. Amongst the several potential applications of surfactin, its use in MEOR represents one of the most promising methods to recover substantial amounts of the residual oil entrapped in mature oil fields^{21, 22}. The replacement of conventional synthetic surfactants by these bio-compounds appears to be a good and efficient approach; however, it still depends on the strategy adopted. The use of biosurfactants in MEOR can be performed in two different ways. In the first one, biosurfactants are produced *ex situ*, and subsequently injected into the reservoir. The other option is to produce the biosurfactant *in situ* by stimulation and/or injection of indigenous microorganisms. The first approach is limited by the costs involved in the biosurfactant production and purification processes. On the other hand, the costs involved in the second approach are apparently lower; however it requires that the microorganisms used are properly stimulated and able to produce sufficient amounts of the biosurfactant²¹.

Taking into account the use of surfactins *in situ* MEOR processes, the greatest challenge is to isolate microorganisms able to grow under anaerobic conditions, high salinities, temperatures and pressures. Several reports have described the isolation of *B. subtilis* strains from oil reservoirs²²⁻²⁵, which suggest that these organisms can be successfully

used under reservoir conditions. Recently, Gudiña et al.²⁶ isolated several *B. subtilis* strains from a Brazilian oil reservoir that were able to produce different biosurfactants under aerobic and anaerobic conditions. Among them, three different strains produced biosurfactants with interesting surface-activities and emulsifying properties.

Aiming at the further use of these *B. subtilis* strains in MEOR processes, the biosurfactant production yields must be improved which can be achieved through the optimization of culture media, specifically of the carbon and nitrogen sources. In this work, biosurfactant production by the three *B. subtilis* strains previously isolated from Brazilian oil reservoirs²⁶ was optimized through a proper manipulation of the carbon and nitrogen sources. The biosurfactants produced by each strain were characterized by ¹H NMR, FTIR and MALDI-TOF, and their abilities to influence the interfacial tension of water/oil systems and enhance oil recovery were evaluated and compared with chemical surfactants.

4.3. Materials and Methods

4.3.1. Microorganisms

Three biosurfactant-producing *B. subtilis* strains (#309, #311 and #573) previously isolated from crude oil samples obtained from a Brazilian oil field²⁶ were used. Isolates were stored at -80°C in LB medium supplemented with a 20% (v/v) glycerol aqueous solution. The composition of LB medium was (g.L⁻¹): NaCl 10.0; tryptone 10.0; yeast extract 5.0. The pH was adjusted to 7.0.

4.3.2. Chemical Surfactants

Two chemical surfactants (Enordet and Petrostep) commonly used in chemical enhanced oil recovery (CEOR) were studied and their interfacial activities were compared with the biosurfactants produced by *B. subtilis* strains.

4.3.3. Effect of Carbon and Nitrogen Sources on Growth and Biosurfactant Production

Growth and biosurfactant production by the three isolates was evaluated using Mineral Salt Solution (MSS) with different carbon and nitrogen sources. The MSS consisted of (g.L⁻¹): NaCl 10.0; Na₂HPO₄ 5.0; KH₂PO₄ 2.0; MgSO₄.7H₂O 0.2. The carbon sources evaluated were: sodium acetate (AC), sodium citrate (CI), fructose (FRU), glucose

(GLU), glycerol (GLY), *n*-hexadecane (HEX), lactose (LAC), meat extract (ME), paraffin (PAR), sucrose (SUC), tryptone (TRY) and yeast extract (YE), using ammonium nitrate as the nitrogen source (2 g.L⁻¹). The different carbon sources were added to the MSS at a concentration of 10 g.L⁻¹. The nitrogen sources tested were: ammonium citrate (AC), ammonium nitrate (AN), ammonium sulfate (AS), meat extract (ME), sodium nitrate (SN), tryptone (TRY), urea (U) and yeast extract (YE), keeping sucrose as the carbon source (10 g.L⁻¹). The different nitrogen sources were added to the MSS at a concentration of 2 g.L⁻¹. All media were adjusted to pH 7.0.

Assays were performed in 100 mL flasks containing 50 mL of the different media. Each flask was inoculated with 1% of a pre-culture grown in the same medium for 24 h. Cultures were incubated at 40°C without shaking for 120 h. Samples were taken at different times during the fermentation to determine biomass concentration and biosurfactant production. Bacterial growth was determined by measuring the optical density at 600 nm. Afterwards, the samples were centrifuged (10000 × *g*, 20 min, 20°C) and the cell-free supernatants were used to measure surface tension and emulsifying activity. At the end of the fermentation, cells were harvested by centrifugation and dry cell weight (g.L⁻¹) was determined (48 h at 105°C).

To recover the biosurfactants, cell free supernatants were subjected to an acid precipitation. Briefly, the supernatants were adjusted to pH 2.0 with HCl 6 M and left overnight at 4°C. Afterwards, the precipitate was collected by centrifugation (10000 × *g*, 20 min, 4°C) and washed twice with acidified water (pH 2.0). The precipitated biosurfactants were dissolved in a minimal amount of demineralized water and the pH was adjusted to 7.0 using NaOH 1 M. Finally, the biosurfactant solutions were freeze dried and the products obtained were weighed.

4.3.4. Surface-activity Determination

Surface tension measurements of culture broth supernatants and chemical surfactant solutions were performed according to the Du Noüy ring method described elsewhere²⁷. A KRÜSS K6 Tensiometer (KRÜSS GmbH, Hamburg, Germany) equipped with a 1.9 cm Du Noüy platinum ring was used. Whenever required, the culture broth supernatants were diluted 10 times (ST⁻¹) or 100 times (ST⁻²) with PBS (10 mM KH₂PO₄/K₂HPO₄ plus 150 mM NaCl with pH adjusted to 7.0) and the surface tension was measured as

described above. The *cmc* of each chemical surfactant dissolved in demineralized water were calculated as described elsewhere²⁷. To increase the accuracy of the surface tension measurements, an average of triplicates was determined. All measurements were performed at room temperature (20°C).

4.3.5. Emulsifying Activity Determination

The emulsifying activity was determined by the addition of 2 mL of *n*-hexadecane to the same volume of cell-free culture broth supernatant in glass test tubes. The tubes were mixed with vortex at high speed for 2 min and subsequently incubated at 25°C for 24 h. The stability of the emulsion was determined after 24 h, and the emulsification index (E_{24}) was calculated as the percentage of the height of the emulsified layer (mm) divided by the total height of the liquid column (mm). All emulsification indexes were performed in triplicate.

4.3.6. Interfacial-activity Determination

Concentrations ranging from 0.001 to 0.1 g.L⁻¹ of crude biosurfactants recovered from the different isolates were prepared in brine solution (50 g.L⁻¹ NaCl with pH adjusted to 6.0). These conditions were previously established as optimal for the activity of biosurfactants under study²⁶. The chemical surfactants were dissolved in demineralized water at different concentrations up to 1 g.L⁻¹. Arabian light crude oil used in these experiments was kindly provided by GALP (Portugal). Interfacial tension of the water/oil system at different biosurfactant/chemical surfactant concentrations was measured using a Dataphysics contact angle system OCA-20. The method consisted in the analysis of the shape of a pendant drop by fitting to the Young-Laplace equation. A Hamilton DS 500/GT syringe connected to a stainless steel needle placed inside a glass chamber with the biosurfactant aqueous solution at room temperature was used to set a fixed drop oil volume ($5.00 \pm 0.15 \mu\text{L}$). For each biosurfactant concentration, at least three independent measures were conducted. For each drop, data were recorded immediately after the drop volume was reached (5 μL) and continued during 1 min (an average of 80 images was captured *per* drop). The drop shape was analyzed with the software modules SCA 20, using the gravitational acceleration ($g = 9.8018 \text{ m.s}^{-2}$) and latitude (lat = 40°) values in accordance with the assay location. The density values

required for the calculation of the interfacial tensions from the drop image data were acquired using a Viscometer-Densimeter Anton Paar (Model SVM 3000).

4.3.7. *Extraction and Purification of Biosurfactants*

Biosurfactants for chemical composition analysis were extracted from cell-free supernatants using the Folch extraction method that is commonly used to extract lipids from biomolecules. The Folch extraction procedure was performed as described elsewhere²⁸. Briefly, a chloroform/methanol mixture (2:1, v/v) was added to the supernatant sample to a final chloroform/methanol/water ratio of 8:4:3. The mixture was centrifuged ($9000 \times g$, 5 min), the organic layer was collected and the samples were evaporated to dryness under N_2 at $37^\circ C$ for 30 min. Prior to NMR spectroscopy and mass spectrometry analysis, the samples were re-dissolved in chloroform.

4.3.8. *Fourier Transform Infrared Spectroscopy*

The solid biosurfactant extracts recovered from the supernatants of the three *B. subtilis* isolates were characterized by FTIR. The FTIR spectra, with a resolution of 4 cm^{-1} , were collected from 400 to 4000 cm^{-1} wavenumbers (cm^{-1}), and is an average of 128 scans using a Tensor 27 Infrared Spectrometer operating in the attenuated total reflection (ATR) mode (equipped with a single horizontal Golden Gate ATR cell).

4.3.9. *Nuclear Magnetic Resonance Spectroscopy*

The extracted biosurfactants were re-dissolved in deuterated chloroform ($CDCl_3$) and the respective 1H NMR spectra were recorded at $25^\circ C$ using a Bruker Avance 300 spectrometer operating at 300.13 MHz. Chemical shifts (δ) are given on the ppm scale relative to tetramethylsilane (TMS) used as reference.

4.3.10. *Mass Spectrometry analysis*

The extracted biosurfactants were dissolved at a concentration of 2 g.L^{-1} in a solution composed of 50% acetonitrile (ACN), 50% water and 0.1% trifluoroacetic acid (TFA). The samples were mixed (1:1, v/v) with a matrix consisting of a saturated solution of α -cyano-4-hydroxycinnamic acid prepared in 50% acetonitrile / 0.1% TFA. An aliquot of $1 \mu\text{L}$ of each sample/matrix mixture was spotted onto the MALDI sample and slowly dried to allow matrix crystallization. Then, the extracted biosurfactants were analyzed

by mass spectrometry (MS) using a MALDI-TOF/TOF mass spectrometer (4800 Proteomics Analyzer, Applied Biosystems, Europe) in the positive ion reflector mode. Spectra were obtained in the mass range between 800 and 4500 Da with *ca.* 1500 laser shots, thus providing a mass resolution of about 18000 (FWMH) and a mass accuracy of 20–25 ppm. MS data were processed using Data Explorer 4.4 (Applied Biosystems).

4.3.11. Application of Chemical Surfactants and Biosurfactants in the Removal of Crude Oil from Sand

The applicability of biosurfactants produced by *B. subtilis* #309, #311 and #573 and the chemical surfactants Enordet and Petrostep in oil recovery was evaluated using artificially contaminated sand containing 10% (w/w) of Arabian Light oil. Samples of 40 g of sand were mixed with 4 g of crude oil in 100 mL Erlenmeyer flasks by shaking and allowed to age for 24 h. Afterwards, 40 mL of biosurfactants and commercial surfactants solutions at a concentration of 1 g.L⁻¹ were added to each flask. The flasks were incubated at 100 rpm and 40°C for 24 h. Then, the oil removed was recovered from the surface and its volume was measured. Control assays were performed using demineralized water at the same conditions. All the experiments were carried out in triplicate.

4.4. Results and Discussion

4.4.1. Effect of Carbon and Nitrogen Sources on Growth and Biosurfactant Production

To determine the optimal conditions that yield the highest biosurfactant production by *B. subtilis* #309, #311 and #573, the effect of various carbon and nitrogen sources was evaluated. The three isolates were able to grow in all the carbon sources tested, except for *n*-hexadecane. When paraffin was used as the sole carbon source, a slight growth was observed in all the isolates, however lower than the obtained with the water soluble carbon sources tested (Table 4.1). Several authors reported, with different *Bacillus* strains, that the use of hydrocarbons (including *n*-hexadecane and paraffin) as the only carbon source, inhibited bacterial growth and biosurfactant production²⁹⁻³¹, or resulted in poor growth and biosurfactant production³².

Table 4.1 Surface tension values (ST, mN.m⁻¹), emulsifying indexes (E_{24} , %), biomass concentrations (g dry weight *per* L) and surfactin concentrations (mg.L⁻¹) obtained for the three *Bacillus subtilis* isolates grown in MSS with different carbon sources (10 g.L⁻¹) at 40°C for 120 h. Results represent the average of three independent experiments ± standard deviation.

Parameter	AC	CI	FRU	GLU	GLY	HEX	LAC	ME	PAR	SUC	TRY	YE
Isolate #309												
ST (mN.m ⁻¹)	30.5 ± 0.5	31.6 ± 0.9	28.4 ± 0.4	29.2 ± 0.3	29.7 ± 0.2	68.5 ± 0.1	30.7 ± 0.2	29.9 ± 0.2	32.6 ± 0.7	28.0 ± 0.3	29.8 ± 0.4	29.7 ± 0.2
ST ⁻¹ (mN.m ⁻¹)	48.9 ± 3.2	62.7 ± 3.8	31.0 ± 0.7	32.8 ± 0.7	34.8 ± 1.4	---	54.9 ± 3.8	33.1 ± 1.1	66.4 ± 1.9	31.3 ± 0.7	33.9 ± 1.5	32.5 ± 0.5
ST ⁻² (mN.m ⁻¹)	71.2 ± 0.8	71.2 ± 0.7	46.2 ± 5.1	62.6 ± 3.6	69.0 ± 2.9	---	72.7 ± 0.1	46.2 ± 2.7	---	42.3 ± 2.1	58.8 ± 5.1	61.3 ± 3.7
E_{24} (%)	10.9 ± 2.1	12.7 ± 2.8	10.7 ± 5.3	35.3 ± 1.7	33.5 ± 2.7	0.0 ± 0.0	12.9 ± 3.0	47.8 ± 1.8	3.1 ± 0.0	39.7 ± 3.9	49.6 ± 0.7	52.7 ± 0.9
[Biomass] (g.L ⁻¹)	0.808 ± 0.083	1.012 ± 0.021	1.150 ± 0.047	0.778 ± 0.091	0.568 ± 0.011	0.0 ± 0.0	0.628 ± 0.027	0.598 ± 0.019	0.195 ± 0.034	1.066 ± 0.092	1.238 ± 0.063	0.878 ± 0.021
[Surfactin] (mg.L ⁻¹)	92.0 ± 22.1	107.1 ± 19.0	743.9 ± 129.5	325.1 ± 91.7	154.1 ± 71.3	0.0 ± 0.0	65.3 ± 5.1	744.6 ± 69.0	22.8 ± 4.7	844.1 ± 53.8	475.2 ± 131.5	410.8 ± 67.7
Isolate #311												
ST (mN.m ⁻¹)	33.3 ± 1.5	35.6 ± 0.9	28.1 ± 0.2	29.0 ± 0.0	30.1 ± 0.1	68.2 ± 0.4	31.2 ± 0.5	30.2 ± 0.1	34.7 ± 1.0	27.9 ± 0.2	30.1 ± 0.1	30.4 ± 0.1
ST ⁻¹ (mN.m ⁻¹)	66.7 ± 1.9	71.5 ± 1.0	32.7 ± 0.9	33.1 ± 1.1	37.6 ± 0.7	---	52.6 ± 4.3	36.2 ± 1.1	71.0 ± 1.2	32.5 ± 1.2	34.8 ± 0.9	36.4 ± 1.3
ST ⁻² (mN.m ⁻¹)	71.8 ± 0.9	---	56.2 ± 2.7	68.5 ± 2.5	69.9 ± 2.9	---	72.3 ± 0.2	70.8 ± 1.0	---	46.5 ± 4.9	68.1 ± 1.8	71.1 ± 0.9
E_{24} (%)	8.8 ± 3.7	9.4 ± 4.4	0.0 ± 0.0	29.8 ± 2.3	26.2 ± 0.6	0.0 ± 0.0	10.9 ± 2.2	40.3 ± 0.4	6.2 ± 0.0	37.3 ± 2.8	39.1 ± 2.2	26.8 ± 5.8
[Biomass] (g.L ⁻¹)	1.038 ± 0.056	0.705 ± 0.043	1.042 ± 0.065	0.536 ± 0.026	0.660 ± 0.029	0.0 ± 0.0	0.758 ± 0.053	0.702 ± 0.033	0.201 ± 0.046	1.002 ± 0.092	0.924 ± 0.025	0.934 ± 0.041
[Surfactin] (mg.L ⁻¹)	117.7 ± 21.4	12.4 ± 2.4	516.3 ± 68.1	233.0 ± 57.2	150.3 ± 70.5	0.0 ± 0.0	81.9 ± 24.1	141.5 ± 24.6	13.8 ± 3.1	765.8 ± 126.1	231.2 ± 30.1	135.7 ± 23.9
Isolate #573												
ST (mN.m ⁻¹)	33.2 ± 1.5	36.4 ± 2.9	29.4 ± 0.3	29.5 ± 0.4	29.9 ± 0.3	68.1 ± 0.3	32.9 ± 0.9	31.1 ± 0.4	41.5 ± 1.8	28.4 ± 0.3	31.0 ± 0.1	30.4 ± 0.2
ST ⁻¹ (mN.m ⁻¹)	62.7 ± 2.2	71.6 ± 1.1	36.6 ± 1.5	35.0 ± 1.8	35.1 ± 1.2	---	66.2 ± 1.8	39.4 ± 1.6	72.2 ± 0.2	33.0 ± 1.3	38.6 ± 1.6	35.4 ± 1.3
ST ⁻² (mN.m ⁻¹)	72.3 ± 0.7	---	70.4 ± 1.0	66.9 ± 2.9	66.1 ± 3.4	---	72.2 ± 0.9	69.7 ± 1.3	---	46.3 ± 3.0	70.8 ± 0.9	66.0 ± 3.7
E_{24} (%)	7.1 ± 1.6	4.6 ± 1.9	30.6 ± 2.6	27.1 ± 1.6	48.4 ± 2.2	0.0 ± 0.0	9.6 ± 3.1	34.0 ± 3.2	2.9 ± 0.0	38.8 ± 4.4	43.6 ± 4.3	40.3 ± 2.9
[Biomass] (g.L ⁻¹)	0.848 ± 0.032	0.762 ± 0.021	1.150 ± 0.012	0.556 ± 0.048	0.870 ± 0.033	0.0 ± 0.0	0.780 ± 0.052	0.708 ± 0.010	0.221 ± 0.067	1.030 ± 0.057	1.184 ± 0.042	1.058 ± 0.047
[Surfactin] (mg.L ⁻¹)	109.6 ± 60.5	24.8 ± 6.8	292.6 ± 47.9	725.9 ± 114.5	965.3 ± 89.3	0.0 ± 0.0	160.1 ± 40.2	323.6 ± 67.6	20.2 ± 7.3	2158.5 ± 240.2	284.0 ± 29.1	894.3 ± 110.5

Table 4.2 Surface tension values (ST, mN.m⁻¹), emulsifying indexes (E_{24} , %), biomass concentrations (g dry weight *per* L) and surfactin concentrations (mg.L⁻¹) obtained for the three *Bacillus subtilis* isolates grown in MSS with different nitrogen sources (2 g.L⁻¹) at 40°C for 120 h. Results represent the average of three independent experiments ± standard deviation.

Parameter	AC	AN	AS	ME	SN	TRY	U	YE
	Isolate #309							
ST (mN.m ⁻¹)	28.5 ± 0.5	28.0 ± 0.3	28.4 ± 0.2	29.0 ± 0.2	29.3 ± 0.2	30.2 ± 0.2	29.6 ± 0.2	28.7 ± 0.3
ST ⁻¹ (mN.m ⁻¹)	31.1 ± 0.7	31.3 ± 0.7	31.3 ± 0.2	32.0 ± 0.6	31.9 ± 0.8	39.9 ± 1.9	31.9 ± 0.9	30.8 ± 0.4
ST ⁻² (mN.m ⁻¹)	42.3 ± 5.3	42.3 ± 2.1	44.0 ± 2.7	47.8 ± 3.4	45.6 ± 5.4	70.4 ± 0.8	44.4 ± 2.4	38.3 ± 1.8
E_{24} (%)	32.3 ± 1.5	39.7 ± 3.9	11.2 ± 1.8	0.0 ± 0.0	41.0 ± 2.8	0.0 ± 0.0	31.2 ± 8.8	43.3 ± 6.7
[Biomass] (g.L ⁻¹)	1.270 ± 0.044	1.066 ± 0.092	1.184 ± 0.065	1.662 ± 0.044	1.243 ± 0.032	1.396 ± 0.074	0.997 ± 0.032	1.534 ± 0.094
[Surfactin] (mg.L ⁻¹)	789.3 ± 107.6	844.1 ± 53.8	799.6 ± 67.9	703.2 ± 85.6	758.2 ± 138.5	110.5 ± 25.0	790.7 ± 62.2	931.8 ± 42.7
Isolate #311								
ST (mN.m ⁻¹)	28.5 ± 0.4	27.9 ± 0.2	28.5 ± 0.2	28.5 ± 0.2	29.5 ± 0.3	29.1 ± 0.1	29.4 ± 0.1	28.7 ± 0.4
ST ⁻¹ (mN.m ⁻¹)	31.3 ± 0.2	32.5 ± 1.2	31.3 ± 1.8	30.6 ± 1.2	33.0 ± 0.6	31.5 ± 0.7	35.0 ± 0.7	31.2 ± 0.8
ST ⁻² (mN.m ⁻¹)	44.1 ± 4.0	46.5 ± 4.9	37.0 ± 1.7	43.2 ± 2.8	55.4 ± 4.2	54.0 ± 2.6	68.7 ± 3.3	39.2 ± 6.1
E_{24} (%)	4.7 ± 2.2	37.3 ± 2.8	0.0 ± 0.0	0.0 ± 0.0	37.2 ± 3.2	0.0 ± 0.0	25.0 ± 7.1	32.8 ± 2.2
[Biomass] (g.L ⁻¹)	1.404 ± 0.038	1.002 ± 0.092	0.934 ± 0.041	1.632 ± 0.023	1.080 ± 0.062	0.954 ± 0.032	0.874 ± 0.088	1.242 ± 0.024
[Surfactin] (mg.L ⁻¹)	828.9 ± 103.1	765.8 ± 126.1	980.7 ± 45.4	851.0 ± 73.0	537.1 ± 107.5	574.6 ± 66.2	196.6 ± 85.8	980.1 ± 46.7
Isolate #573								
ST (mN.m ⁻¹)	30.3 ± 0.9	28.4 ± 0.3	29.6 ± 0.7	30.0 ± 0.1	29.9 ± 0.6	32.7 ± 0.6	30.1 ± 0.5	29.5 ± 0.5
ST ⁻¹ (mN.m ⁻¹)	34.3 ± 2.5	33.0 ± 1.3	32.6 ± 0.3	36.3 ± 1.1	35.2 ± 2.0	53.2 ± 2.4	32.6 ± 0.5	33.6 ± 1.5
ST ⁻² (mN.m ⁻¹)	54.4 ± 5.4	46.3 ± 3.0	44.6 ± 2.7	57.9 ± 4.1	57.5 ± 5.5	71.7 ± 0.2	51.6 ± 5.1	56.7 ± 5.1
E_{24} (%)	33.3 ± 1.5	38.8 ± 4.4	35.0 ± 2.3	0.0 ± 0.0	41.7 ± 1.8	0.0 ± 0.0	27.3 ± 5.6	25.0 ± 7.1
[Biomass] (g.L ⁻¹)	1.154 ± 0.050	1.030 ± 0.057	1.466 ± 0.065	1.708 ± 0.030	1.020 ± 0.044	1.562 ± 0.015	1.500 ± 0.029	1.762 ± 0.080
[Surfactin] (mg.L ⁻¹)	1500.2 ± 251.5	2158.5 ± 240.2	2288.9 ± 210.5	1369.9 ± 169.9	1129.5 ± 266.7	157.8 ± 16.8	1853.5 ± 305.7	1496.9 ± 300.6

The highest biomass production, expressed as dry cell weight, was obtained with tryptone and fructose for isolates #309 and #573, and with fructose and sodium acetate for isolate #311 (Table 4.1). Glucose and sucrose were reported as the best carbon sources for growth using different *Bacillus* isolates^{29, 30}, although Joshi et al.³² obtained better results with fructose.

The lowest surface tension values (ST^{-2}) were obtained when sucrose was used as the sole carbon source for all the isolates. The surface tension values were between 27.9 and 28.4 $mN.m^{-1}$, and the ST^{-2} values between 46.5 and 42.3 $mN.m^{-1}$ (Table 4.1). Fructose also offered good results regarding surface tension reduction (ST^{-2}) for isolate #309. The use of lactose as carbon source resulted in high surface tension values when compared with the other carbohydrates tested.

The results obtained are in agreement with those reported by other authors with different *B.subtilis* isolates²⁹⁻³³. Several authors obtained the lowest surface tension values using glucose or sucrose²⁹⁻³³ as the sole carbon sources. Abdel-Mawgoud et al.²⁹ also found a poor biosurfactant production using lactose as the sole carbon source. On the other hand, the use of hydrocarbons as the sole carbon source usually resulted in no biosurfactant production^{29, 30, 32}. In the case of *B. subtilis* #309, #311 and #573, the combination of a water soluble carbon source (sucrose) and a hydrocarbon (*n*-hexadecane) did not have a negative effect on the biosurfactant production²⁶.

Regarding the emulsifying activity, the complex carbon sources tested (meat extract, tryptone and yeast extract) were amongst the most favorable. For isolate #309, the highest emulsifying activity was obtained with yeast extract (52.7%), and similar results were obtained with tryptone and meat extract (49.6 and 47.8%, respectively). For isolate #311, the best result was obtained with meat extract (40.3%), followed by tryptone (39.1%) and sucrose (37.3%). For isolate #573, the highest emulsifying activity was obtained with glycerol (48.4%), followed by tryptone (43.6%) and yeast extract (40.3%). Dastgheib et al.³¹ found the highest emulsifying activity using yeast extract as the carbon source, followed by sucrose, fructose and glucose, whereas the use of lactose resulted in poor emulsifying activity. For the three isolates, the highest amount of biosurfactant produced (expressed as $mg.L^{-1}$) was obtained when using sucrose as the carbon source. The amounts of crude biosurfactant produced were 844, 755 and 2158 $mg.L^{-1}$ for isolates #309, #311 and #573, respectively. The highest amount of

biosurfactant produced is in agreement with the lowest surface tension values (ST^{-2}) obtained for all the isolates, but curiously not with the highest emulsifying activities, thus suggesting that different types of biosurfactants with different properties are being synthesized depending on the carbon sources used.

Regarding the nitrogen sources, the highest biomass production was obtained using meat extract as the sole nitrogen source for isolates #309 and #311. For isolate #573, yeast extract and meat extract gave a similar result (Table 4.2).

The lowest surface tension values (ST^{-2}), which corresponded to the highest biosurfactant productions, were obtained with yeast extract for isolate #309 ($38.3\text{mN}\cdot\text{m}^{-1}$); ammonium sulfate and ammonium nitrate for isolate #573 (44.6 and $46.3\text{mN}\cdot\text{m}^{-1}$, respectively); and for the isolate #311, yeast extract and ammonium sulfate gave similar results (39.2 and $37.0\text{mN}\cdot\text{m}^{-1}$, respectively). The highest biosurfactant productions were 931 , 980 and $2288\text{mg}\cdot\text{L}^{-1}$ for isolates #309, #311 and #573, respectively. Other authors reported crude biosurfactant productions between 720 and $1120\text{mg}\cdot\text{L}^{-1}$ ^{29, 30}. Isolate #573 produced higher amounts of biosurfactant when compared with isolates #309 and #311. The critical micelle concentrations for these crude biosurfactants were determined in a previous work: $20\text{mg}\cdot\text{L}^{-1}$ for isolates #309 and #311, and $30\text{mg}\cdot\text{L}^{-1}$ for isolate #573²⁶. Therefore, biosurfactants produced by isolates #309 and #311 are more efficient than the ones produced by isolate #573, which explains why isolate #573 although producing higher amounts of biosurfactant provides similar (or higher, *i.e.* less active surfactant) surface tension values than the obtained with the other two isolates.

Abdel-Magwoud et al.²⁹ reported the highest biosurfactant production using sodium nitrate and ammonium nitrate as nitrogen sources. Other authors reported the highest biosurfactant production using urea^{30, 33}. Some *Bacillus* isolates do not use ammonium sulfate for growth or biosurfactant production, but they can use ammonium nitrate, potassium nitrate or sodium nitrate³⁰.

The highest emulsifying indexes were obtained with sodium nitrate for isolate #573 (41.7%); while for isolate #309, similar results were obtained using yeast extract and sodium nitrate (43.3 and 41.0% , respectively); and for isolate #311, the highest emulsifying indexes were obtained with ammonium nitrate and sodium nitrate (37.3 and

37.2% respectively). Dastgheib et al.³¹ reported that sodium nitrate was the best substrate for emulsifier production, followed by urea, yeast extract and peptone.

Taking into account the amounts of biosurfactant produced with the different carbon and nitrogen sources, and in order to standardize the medium for all isolates, sucrose and ammonium nitrate were selected for the production of biosurfactants to be further used in the chemical characterization experiments. Moreover, the use of sucrose and ammonium nitrate represents a good compromise between biosurfactant yields and the costs associated with their production. More complex nitrogen sources provide higher emulsification indexes; however, their cost is also higher which makes a potential application in MEOR economically unfeasible. Also, this medium was found to be adequate for the three isolates (*i.e.* could be considered as standard medium) and nitrate is crucial for microbial growth under the low oxygen concentrations present in reservoirs.

4.4.2. Chemical Characterization

4.4.2.1. FTIR-ATR

Firstly fast and direct characterizations of the biosurfactants produced by each isolate were performed using a FTIR-ATR analysis (Figure 4.1). The spectra obtained for the three isolates showed a great similarity between them. It can be clearly observed characteristic absorbance bands of peptides at 3305 cm^{-1} (NH-stretching mode); at 1643 cm^{-1} (1645 cm^{-1} for isolate #311) resulting from the stretching mode of the CO-N bond; and at 1543 cm^{-1} from the deformation mode of the N-H bond combined with C-N stretching mode. In addition, it is also clear the presence of aliphatic chains (-CH₃; -CH₂-), represented by the bands between 2957 to 2855 cm^{-1} , and 1465 to 1368 cm^{-1} . The band observed at 1734 cm^{-1} is characteristic of a carbonyl group. This first FTIR-ATR analysis indicates the presence of aliphatic hydrocarbons combined with a peptide moiety that is characteristic of lipopeptide biosurfactants, as it has been described in the literature previously^{32, 34}.

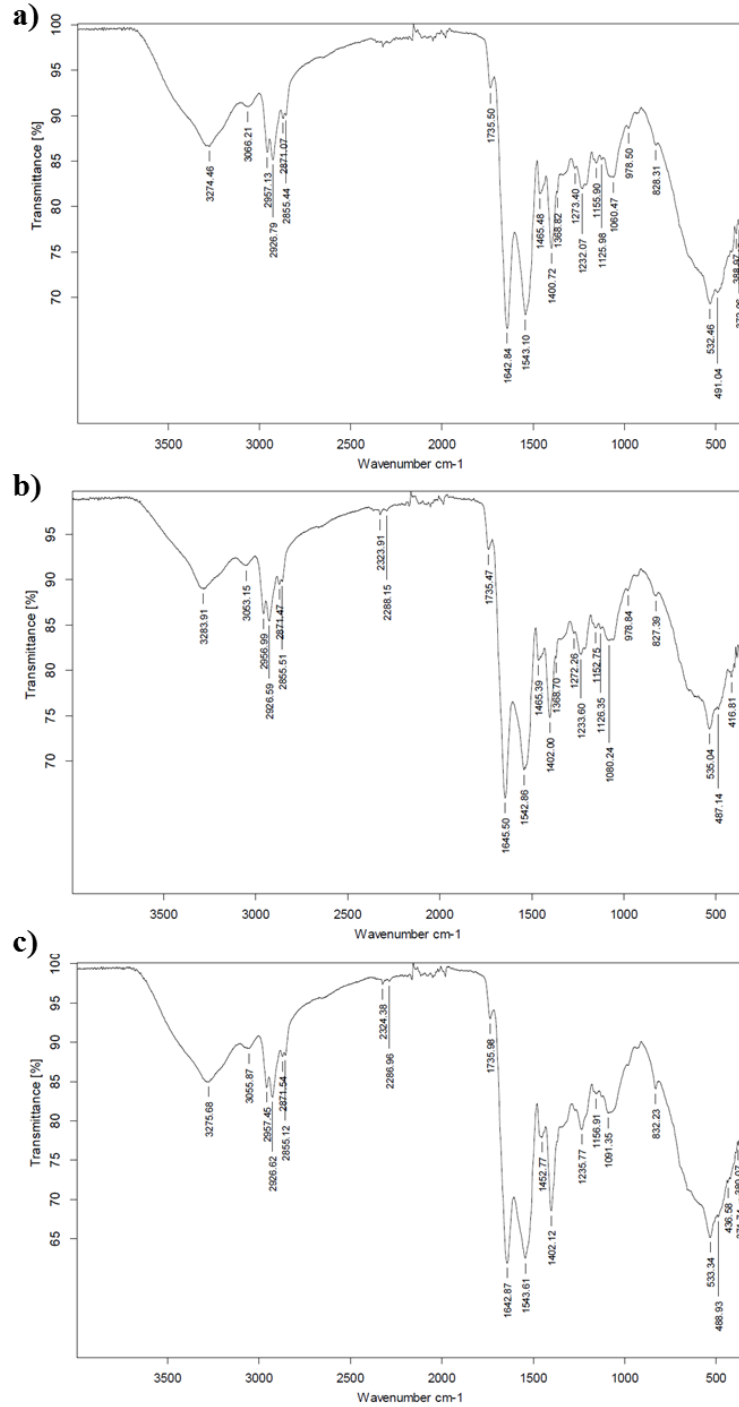


Figure 4.1 FTIR-ATR spectra for biosurfactant extracts produced by isolates #309 (a), #311 (b) and #573 (c).

4.4.2.2. ¹H NMR Spectroscopy

The characterization of the biosurfactants produced by *B. subtilis* strains using NMR spectroscopy is well described in the literature³⁵⁻³⁷. Therefore, the composition of the

biosurfactants obtained from isolates #309, #311 and #573 was probed by ^1H NMR analysis (Figure 4.2).

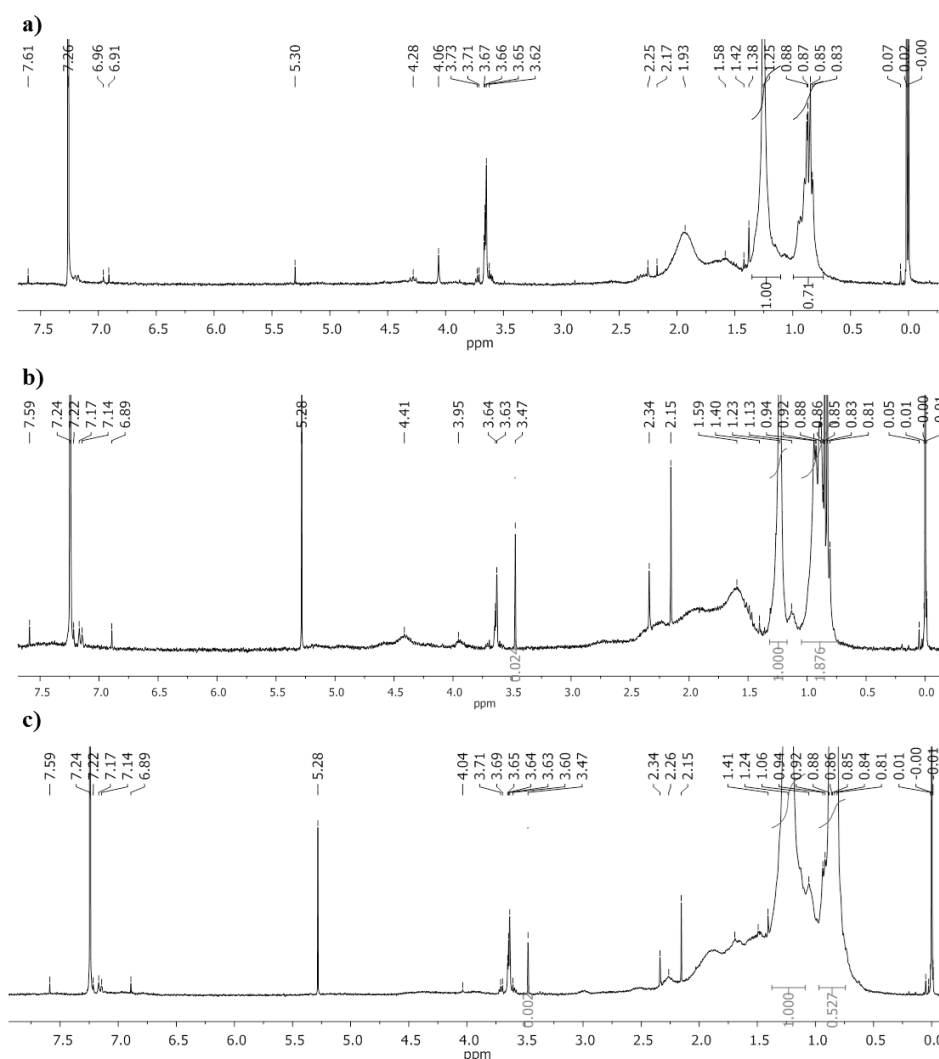


Figure 4.2 ^1H NMR spectra for biosurfactant extracts produced by *B. subtilis* isolates #309 (a), #311 (b) and #573 (c).

The three spectra showed two main regions corresponding to resonance of α -carbon protons (3.5-5.5 ppm) and side-chain protons (0.25-3.0 ppm)^{38, 39}. The differences observed in the spectra are in chemical shifts from the region correspondent to the amide protons (6.5-10 ppm), in which the NMR spectrum is less defined. All spectra showed some similarity with the standard surfactin (spectra for standard surfactin reported by Wei and Chu⁴⁰). However, it is clear the presence of distinct regions relatively to the standard molecule, as well as among the three biosurfactant extracts herein studied. The intense singlet at 3.47 ppm observed in the biosurfactants extracted from isolates #311 and #573 is similar with that observed in ^1H NMR spectra of

lipopeptide monoesters reported previously in literature³⁵⁻³⁷, thus suggesting the presence of one OCH₃ group in those biosurfactants. The presence of the methyl esters in the structure of surfactins has been related with an increase of its hydrophobicity and, consequently an increment of their surfactant powers, antifungal and hemolytic activities³⁶. On the other hand, for the three extracts, an intense singlet at 5.28 ppm (5.30 ppm for isolate #309) was observed. This resonance probably corresponds to the H-3 (terminal proton) of the fatty acid chain, which has also been previously observed by other authors^{36, 37}.

The integral relation of the two different regions of aliphatic chains (approximately 1.55 to 1.25 ppm and 0.80 to 0.90 ppm) can give an important correlation between the presence of *n*-surfactin and *iso*- or/and *anteiso*-surfactins. The results showed a higher presence of *iso* forms in the biosurfactants recovered from the supernatant of the isolate #311, and lower concentrations of those forms in the biosurfactant recovered from isolate #573. According to Youssef et al.⁴¹, the surface activity of lipopeptptides with structures analogous to surfactin increases when the ratio of *iso*- to *normal*-even-numbered fatty acids is increased. In our case, lower surface tension values (ST⁻²) and *cmc* were obtained for isolate #311 when compared with the isolate #573. However, in the case of lichenysin, iturin and mycosubtilin an opposite behavior was observed, and an increase in the percentage of branched-chain fatty acids was found to decrease the activity of the biosurfactant, whereas an increase in the percentage of straight-chains increased their surface activity³⁶. This may be due to the different amino acid composition of those biosurfactants, which can result in different properties.

The ¹H NMR analysis of the different biosurfactant extracts produced by different isolates demonstrates the presence of different surfactins mixtures, supporting the different surface activities and emulsifying properties previously discussed. Each surfactins mixture obtained with the *Bacillus* isolates herein studied was further characterized by mass spectrometry.

4.4.2.3. Mass Spectrometry

The MALDI-TOF spectra of the biosurfactants obtained from each isolate (#309, #311 and #573) are shown in Figure 4.3.

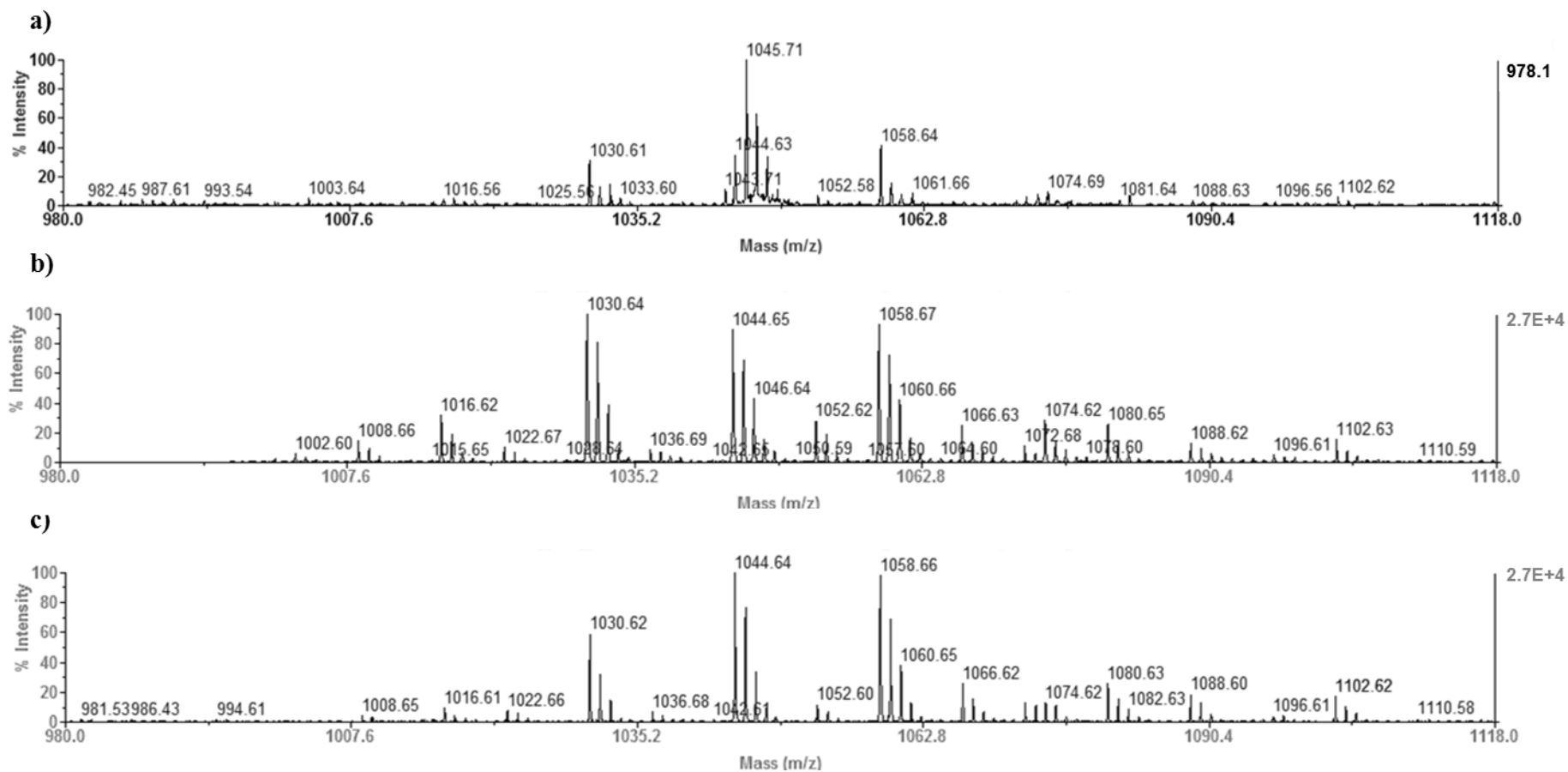


Figure 4.3 MALDI-TOF spectra for surfactin-like extracts produced by *B. subtilis* isolates #309 (a), #311 (b) and #573 (c).

The three mass spectra represented in Figure 4.3 show that there are one well-resolved group of peaks at m/z values between 1000 and 1060. This group could be attributed to the different variants of surfactins, as previously described by Vater et al.⁴² using MALDI-TOF mass spectrometry. Each surfactins mixture extracted has peaks which can be attributed to the protonated forms, with sodium adducts. Each isolate spectrum displays three $[M+Na]^+$ peaks at $m/z = 1030.6, 1044.6$ and 1058.7 , that correspond to the heptapeptide moiety (L-Glu-L-Leu-D-Leu-L-Val-L-Asp-D-Leu-L-Leu) characteristic of surfactins, linked to a C₁₃, C₁₄ or C₁₅ hydroxy fatty acid chain, respectively (Figure 4.4).

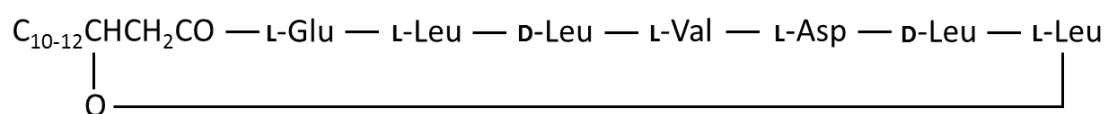


Figure 4.4 Structure of surfactin.

The spectra here reported are very similar to those obtained by Vater et al.⁴² and Leenders et al.⁴³. In addition, it is possible to observe the presence of other surfactins in the extract mixtures, although in lower amounts. These results confirm the data previously obtained by ¹H NMR spectra, where it was clearly shown the presence of some mono-methyl ester surfactins, as well as the existence of different types of biosurfactants with different properties synthesized by the three isolates studied. Furthermore, comparing the three different spectra (Figure 4.3) it is possible to found similarity between the mixtures obtained by isolate #311 and #573, as earlier also seen by ¹H NMR, in which approximate amounts of C₁₃-, C₁₄-, and C₁₅-surfactin are visible. On the other hand, the spectrum of the biosurfactant produced by the isolate #309 exhibited a more intense peak at 1045.7, corresponding to higher amounts of C₁₄-surfactin in the mixture. Youssef et al.⁴¹ showed that *iso*-C₁₄ surfactin exhibits the optimum hydrophilic-lipophilic balance required for optimum surface activity. Also, Bacon et al.⁴⁴ reported that surfactins with C-14 acyl chains possess a higher surface activity. This could explain the higher efficiency of biosurfactants produced by isolate #309 when compared with the isolate #573.

4.4.3.3. Water-Oil Interfacial Tension

To use these biosurfactants in MEOR processes it is important to first understand their interfacial properties in liquid-liquid equilibrium. Although several researchers have

studied the surface-activities at the air/water interface^{26, 29-31, 45, 46} and the oil/water/rock systems wettability (by the contact angle measurement)^{47, 48}, only few reports present information on the properties of lipopeptides at the liquid/liquid interfaces^{49, 50}. Therefore, to overcome this scarcity, the interfacial tension of a water/oil system was studied for each crude biosurfactant at different concentrations (Figure 4.5).

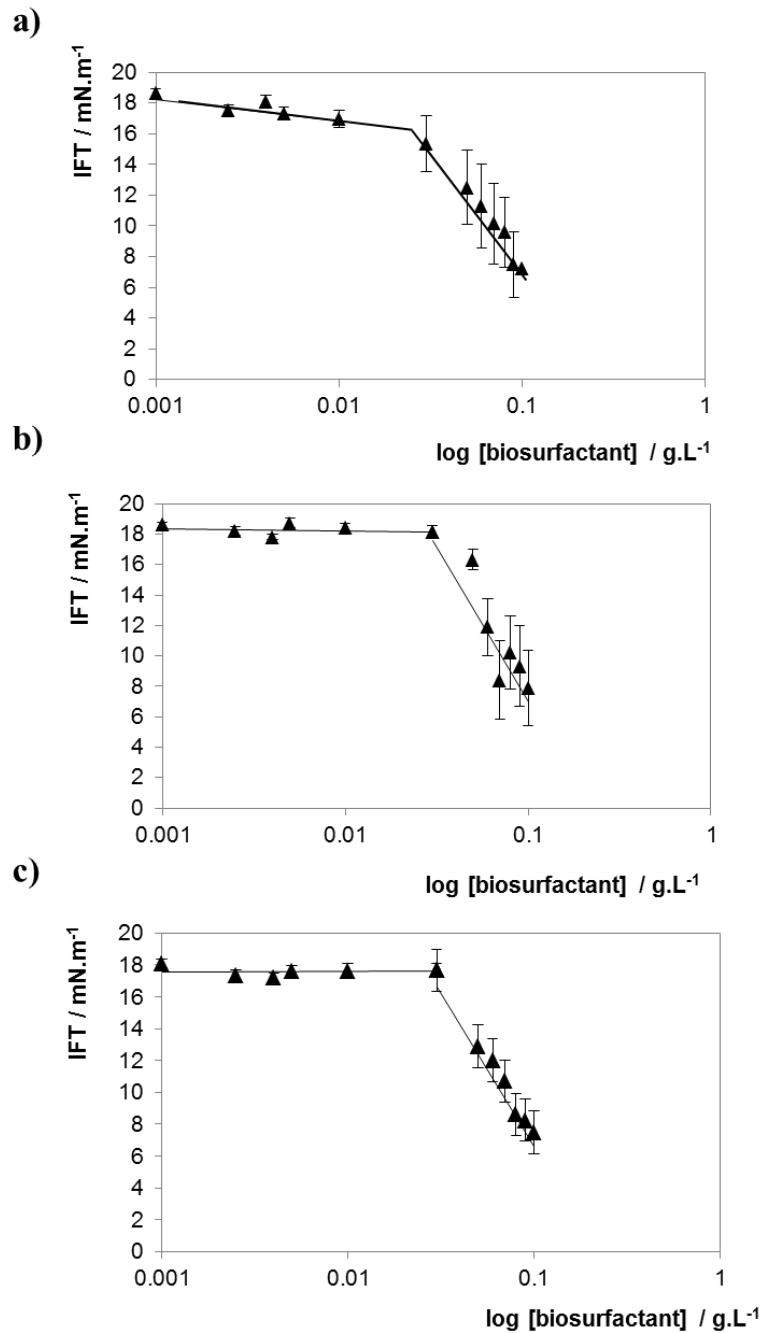


Figure 4.5 Interfacial tension values (IFT, mN.m⁻¹) versus logarithm of biosurfactant concentration (g.L⁻¹) for each biosurfactant extract from *B. subtilis* isolates #309 (a), #311 (b) and #573 (c).

The analysis of the interfacial tension values showed that the biosurfactants produced by the isolates #311 and #573 exhibit a similar ability to decrease the IFT of the Arabian light crude oil/water system. These two biosurfactant mixtures only showed surfactant activities above their *cmc* (approximately 0.02 and 0.03 g.L⁻¹, respectively, as determined in our previous work²⁶), while in the case of the biosurfactant produced by the isolate #309 it occurred a slight decrease of the IFT before the *cmc* was reached (0.02 g.L⁻¹)²⁶, being this decrease more significant afterwards. This may be due to the higher percentage of C₁₄-surfactin in the mixture of biosurfactants produced by this isolate, as discussed previously, whereas the similar interfacial-activities observed with the biosurfactants produced by #311 and #573 are in accordance with their surfactin composition, earlier characterized by ¹H NMR and mass spectrometry. The three biosurfactant mixtures were found to reduce the IFT values up to 7 mN.m⁻¹. However, higher IFT decreases were expected based on reports from the literature⁴⁹. Yet, the methodology herein used presents some limitations regarding the drop formation, since for biosurfactant concentrations above 0.1 g.L⁻¹ the drop is unstable originating the immediate drop release, thus for higher biosurfactant concentrations it was not possible to determine the IFT values. Regarding the chemical surfactants Enordet and Petrostep, their *cmcs* were found to be 1 g.L⁻¹. For a concentration of 0.1 g.L⁻¹ (the highest biosurfactant concentration tested) the IFT values were similar to those obtained with demineralized water (about 21 mN.m⁻¹), whereas for a concentration of 1 g.L⁻¹, Enordet and Petrostep reduced the IFT to 3.0 and 10.5 mN.m⁻¹, respectively. The results obtained show that biosurfactants studied in this work are more efficient than chemical surfactants. Al-Bahry et al.⁵¹ observed that surfactins produced by a *B. subtilis* strain grown on molasses reduced the IFT between water and *n*-hexadecane from 23 to 5 mN.m⁻¹ at a concentration of 2.2 g.L⁻¹. However, when higher concentrations of biosurfactant were used, the IFT was reduced up to 1 mN.m⁻¹. Deleu et al.⁴⁹ reported the reduction of the dodecane/water IFT to values around 2 mN.m⁻¹ using surfactin produced by *B. subtilis*, being this reduction higher than the observed with other biosurfactants, such as iturin A (14.94 mN.m⁻¹) and fengycin (11.63 mN.m⁻¹). Urum and Pekdemir⁵⁰ studied the ability of several biosurfactants to decrease the IFT of *Ekofisk* crude oil and reported that biosurfactants have a higher potential than the chemical surfactant SDS (7.0 mN.m⁻¹), as for example lecithin (5.0 mN.m⁻¹), rhamnolipid (4.5 mN.m⁻¹), saponin (6.0 mN.m⁻¹) and tannin (4.5 mN.m⁻¹). In summary, the reduction of IFT observed indicates the ability of the surfactin mixtures produced by the three *B.*

subtilis isolates herein studied to remove oil from reservoir. As the IFT between crude oil and water is reduced, the capillary force between the oil and the reservoir rock is also reduced. Therefore, this reduction leads to an increased mobilization of the oil in the reservoir which is of great interest to enhance oil recovery in mature reservoirs.

4.4.3.4. Application of Chemical Surfactants and Biosurfactants in the Removal of Crude Oil from Sand

The performance of biosurfactants and chemical surfactants in oil recovery was studied using crude oil contaminated sand. As can be seen from the results obtained (Table 4.3), the different biosurfactants at a concentration of 1 g.L⁻¹ recovered between 19 and 22% of oil, whereas the recoveries obtained with the chemical surfactants at the same concentration were between 9 and 12%. From the results obtained it can be concluded that these biosurfactants are more effective in oil recovery when compared with the chemical surfactants Enordet and Petrostep.

Table 4.3 Percentages of oil recovered by the different biosurfactants and chemical surfactants at a concentration of 1 g.L⁻¹. Results represent the average of three independent experiments \pm standard deviation.

Biosurfactant / Chemical Surfactant	% oil recovered
<i>B. subtilis</i> #309	22.1 \pm 2.4
<i>B. subtilis</i> #311	19.0 \pm 1.6
<i>B. subtilis</i> #573	18.8 \pm 1.1
Enordet	11.7 \pm 1.9
Petrostep	8.7 \pm 1.3
Control	8.7 \pm 1.3

4.5. Conclusion

In the current work, the biosurfactant production by three *B. subtilis* strains was optimized using different carbon and nitrogen sources. The strains were found to produce biosurfactants with better surface-activities and emulsification properties when sucrose was used as carbon source. No major differences in the biosurfactants performance could be observed when using different nitrogen sources. Crude biosurfactant mixtures were found to be mainly constituted of surfactins with a heptapeptide moiety (_L-Glu-_L-Leu-_D-Leu-_L-Val-_L-Asp-_D-Leu-_L-Leu), linked to a C₁₃, C₁₄ or C₁₅ hydroxy fatty acid chain. Although several similarities were found among the

biosurfactant mixtures produced by the different isolates, it was evident the presence of different variants of surfactins that could be implicated in the distinct emulsification and surface-active properties found. These biosurfactant mixtures were able to decrease the interfacial tension of Arabian light crude oil/water system more efficiently than chemical surfactants, and showed better results in oil recovery, thus suggesting their interest for use in MEOR processes.

4.6. References

1. Mukherjee, S., Das, P., and Sen, R., Towards commercial production of microbial surfactants. *Trends in Biotechnology*, 2006. **24**(11): p. 509-515.
2. Van Hamme, J.D., Singh, A., and Ward, O.P., Physiological aspects. Part 1 in a series of papers devoted to surfactants in microbiology and biotechnology. *Biotechnology Advances*, 2006. **24**(6): p. 604-620.
3. Singh, A., Van Hamme, J.D., and Ward, O.P., Surfactants in microbiology and biotechnology: Part 2. Application aspects. *Biotechnology Advances*, 2007. **25**(1): p. 99-121.
4. Shete, A.M., Wadhawa, G., Banat, I.M., and Chopade, B.A., Mapping of patents on bioemulsifier and biosurfactant: A review. *Journal of Scientific & Industrial Research*, 2006. **65**(2): p. 91-115.
5. Makkar, R.S., Cameotra, S.S., and Banat, I.M., Advances in utilization of renewable substrates for biosurfactant production. *AMB Express*, 2011. **1**: p. 1-5.
6. Meyer, H.P., Sustainability and biotechnology. *Organic Process Research and Development*, 2011. **15**(1): p. 180-188.
7. Fox, S.L. and Bala, G.A., Production of surfactant from *Bacillus subtilis* ATCC 21332 using potato substrates. *Bioresource Technology*, 2000. **75**(3): p. 235-240.
8. Bustos, G., de la Torre, N., Moldes, A.B., Cruz, J.M., and Domínguez, J.M., Revalorization of hemicellulosic trimming vine shoots hydrolyzates through continuous production of lactic acid and biosurfactants by *L. pentosus*. *Journal of Food Engineering*, 2007. **78**(2): p. 405-412.
9. Rodrigues, L.R., Teixeira, J.A., and Oliveira, R., Low-cost fermentative medium for biosurfactant production by probiotic bacteria. *Biochemical Engineering Journal*, 2006. **32**(3): p. 135-142.
10. Gudiña EJ, Teixeira JA, Rodrigues LR. Biosurfactant-producing lactobacilli: screening, production profiles and effect of medium composition. *Appl Environ Soil Sci* 2011. doi: 10.1155/2011/201254.
11. Rodrigues LR, Teixeira JA. Biosurfactants production from cheese whey. In: Cerdán ME, González-Siso M, Becerra M, editors. *Advances in Cheese Whey Utilization*, Kerala, India: Transworld Research Network Publishers; 2008, p. 81-104.
12. Pereira, J.F.B., Gudiña, E.J., Doria, M.L., Domingues, M.R., Rodrigues, L.R., Teixeira, J.A., and Coutinho, J.A.P., Characterization by electrospray ionization and tandem mass spectrometry of rhamnolipids produced by two *Pseudomonas aeruginosa* strains isolated from Brazilian crude oil. *European Journal of Mass Spectrometry*, 2012. **18**(4): p. 399-406.
13. Nitschke, M. and Pastore, G.M., Production and properties of a surfactant obtained from *Bacillus subtilis* grown on cassava wastewater. *Bioresource Technology*, 2006. **97**(2): p. 336-341.
14. Nitschke, M., Costa, S.G.V.A.O., and Contiero, J., Rhamnolipid surfactants: An update on the general aspects of these remarkable biomolecules. *Biotechnology Progress*, 2005. **21**(6): p. 1593-1600.
15. Vaz, D.A., Gudiña, E.J., Alameda, E.J., Teixeira, J.A., and Rodrigues, L.R., Performance of a biosurfactant produced by a *Bacillus subtilis* strain isolated from crude oil samples as compared to commercial chemical surfactants. *Colloids and Surfaces B-Biointerfaces*, 2012. **89**: p. 167-174.
16. Dufour, S., Deleu, M., Nott, K., Wathélet, B., Thonart, P., and Paquot, M., Hemolytic activity of new linear surfactin analogs in relation to their physico-chemical properties. *Biochimica Et Biophysica Acta-General Subjects*, 2005. **1726**(1): p. 87-95.
17. Seydlová, G. and Svobodová, J., Review of surfactin chemical properties and the potential biomedical applications. *Central European Journal of Medicine*, 2008. **3**(2): p. 123-133.
18. Rodrigues, L., Banat, I.M., Teixeira, J., and Oliveira, R., Biosurfactants: Potential applications in medicine. *Journal of Antimicrobial Chemotherapy*, 2006. **57**(4): p. 609-618.

19. Vollenbroich, D., Ozel, M., Vater, J., Kamp, R.M., and Pauli, G., Mechanism of inactivation of enveloped viruses by the biosurfactant surfactin from *Bacillus subtilis*. *Biologicals*, 1997. **25**(3): p. 289-297.
20. Cooper, D.G., Macdonald, C.R., Duff, S.J.B., and Kosaric, N., Enhanced production of surfactin from *Bacillus subtilis* by continuous product removal and metal cation additions. *Applied and Environmental Microbiology*, 1981. **42**(3): p. 408-412.
21. Banat, I.M., Franzetti, A., Gandolfi, I., Bestetti, G., Martinotti, M.G., Fracchia, L., Smyth, T.J., and Marchant, R., Microbial biosurfactants production, applications and future potential. *Applied Microbiology and Biotechnology*, 2010. **87**(2): p. 427-444.
22. Simpson, D.R., Natraj, N.R., McInerney, M.J., and Duncan, K.E., Biosurfactant-producing *Bacillus* are present in produced brines from Oklahoma oil reservoirs with a wide range of salinities. *Applied Microbiology and Biotechnology*, 2011. **91**(4): p. 1083-1093.
23. Youssef, N., Elshahed, M.S., and McInerney, M.J., Microbial processes in oil fields: culprits, problems, and opportunities. *Advances in Applied Microbiology*, Vol 66, 2009. **66**: p. 141-251.
24. Yakimov, M.M., Timmis, K.N., Wray, V., and Fredrickson, H.L., Characterization of a new lipopeptide surfactant produced by thermotolerant and halotolerant subsurface *Bacillus licheniformis* Bas50. *Applied and Environmental Microbiology*, 1995. **61**(5): p. 1706-1713.
25. Ghojavand, H., Vahabzadeh, F., Mehranian, M., Radmehr, M., Shahraki, K.A., Zolfagharian, F., Emadi, M.A., and Roayaei, E., Isolation of thermotolerant, halotolerant, facultative biosurfactant-producing bacteria. *Applied Microbiology and Biotechnology*, 2008. **80**(6): p. 1073-1085.
26. Gudiña, E.J., Pereira, J.F.B., Rodrigues, L.R., Coutinho, J.A.P., and Teixeira, J.A., Isolation and study of microorganisms from oil samples for application in Microbial Enhanced Oil Recovery. *International Biodeterioration & Biodegradation*, 2012. **68**(0): p. 56-64.
27. Gudiña, E.J., Teixeira, J.A., and Rodrigues, L.R., Isolation and functional characterization of a biosurfactant produced by *Lactobacillus paracasei*. *Colloids and Surfaces B-Biointerfaces*, 2010. **76**(1): p. 298-304.
28. Folch, J., Lees, M., and Stanley, G.H.S., A Simple Method for the Isolation and Purification of Total Lipides from Animal Tissues. *Journal of Biological Chemistry*, 1957. **226**(1): p. 497-509.
29. Abdel-Mawgoud, A.M., Aboulwafa, M.M., and Hassouna, N.A.H., Optimization of surfactin production by *Bacillus subtilis* isolate BS5. *Applied Biochemistry and Biotechnology*, 2008. **150**(3): p. 305-325.
30. Makkar, R.S. and Cameotra, S.S., Biosurfactant production by a thermophilic *Bacillus subtilis* strain. *Journal of Industrial Microbiology & Biotechnology*, 1997. **18**(1): p. 37-42.
31. Dastgheib, S.M.M., Amoozegar, M.A., Elahi, E., Asad, S., and Banat, I.M., Bioemulsifier production by a halothermophilic *Bacillus* strain with potential applications in microbially enhanced oil recovery. *Biotechnology Letters*, 2008. **30**(2): p. 263-270.
32. Joshi, S., Bharucha, C., and Desai, A.J., Production of biosurfactant and antifungal compound by fermented food isolate *Bacillus subtilis* 20B. *Bioresource Technology*, 2008. **99**(11): p. 4603-4608.
33. Ghribi, D. and Ellouze-Chaabouni, S., Enhancement of *Bacillus subtilis* Lipopeptide Biosurfactants Production through Optimization of Medium Composition and Adequate Control of Aeration. *Biotechnology Research International*, 2011. doi:10.4061/2011/653654.
34. de Faria, A.F., Teodoro-Martinez, D.S., de Oliveira Barbosa, G.N., Gontijo Vaz, B., Serrano Silva, Í., Garcia, J.S., Tótola, M.R., Eberlin, M.N., Grossman, M., Alves, O.L., and Regina Durrant, L., Production and structural characterization of surfactin (C14/Leu7) produced by *Bacillus subtilis* isolate LSFM-05 grown on raw glycerol from the biodiesel industry. *Process Biochemistry*, 2011. **46**(10): p. 1951-1957.
35. Tang, J.S., Gao, H., Hong, K., Yu, Y., Jiang, M.M., Lin, H.P., Ye, W.C., and Yao, X.S., Complete assignments of H-1 and C-13 NMR spectral data of nine surfactin isomers. *Magnetic Resonance in Chemistry*, 2007. **45**(9): p. 792-796.

36. Kowall, M., Vater, J., Kluge, B., Stein, T., Franke, P., and Ziessow, D., Separation and characterization of surfactin isoforms produced by *Bacillus subtilis* OKB 105. *Journal of Colloid and Interface Science*, 1998. **204**(1): p. 1-8.
37. Liu, X.Y., Yang, S.Z., and Mu, B.Z., Production and characterization of a C-15-surfactin-O-methyl ester by a lipopeptide producing strain *Bacillus subtilis* HSO121. *Process Biochemistry*, 2009. **44**(10): p. 1144-1151.
38. Peypoux, F., Bonmatin, J.-M., Labbé, H., Das, B.C., Ptak, M., and Michel, G., Isolation and characterization of a new variant of surfactin, the [Val7]surfactin. *European Journal of Biochemistry*, 1991. **202**(1): p. 101-106.
39. Chen, H.L. and Juang, R.S., Recovery and separation of surfactin from pretreated fermentation broths by physical and chemical extraction. *Biochemical Engineering Journal*, 2008. **38**(1): p. 39-46.
40. Wei, Y.-H. and Chu, I.M., Enhancement of surfactin production in iron-enriched media by *Bacillus subtilis* ATCC 21332. *Enzyme and Microbial Technology*, 1998. **22**(8): p. 724-728.
41. Youssef, N.H., Duncan, K.E., and McInerney, M.J., Importance of 3-hydroxy fatty acid composition of lipopeptides for biosurfactant activity. *Applied and Environmental Microbiology*, 2005. **71**(12): p. 7690-7695.
42. Vater, J., Kablitz, B., Wilde, C., Franke, P., Mehta, N., and Cameotra, S.S., Matrix-assisted laser desorption ionization-time of flight mass spectrometry of lipopeptide biosurfactants in whole cells and culture filtrates of *Bacillus subtilis* C-1 isolated from petroleum sludge. *Applied and Environmental Microbiology*, 2002. **68**(12): p. 6210-6219.
43. Leenders, F., Stein, T.H., Kablitz, B., Franke, P., and Vater, J., Rapid typing of *Bacillus subtilis* strains by their secondary metabolites using matrix-assisted laser desorption ionization mass spectrometry of intact cells. *Rapid Communications in Mass Spectrometry*, 1999. **13**(10): p. 943-949.
44. Bacon, C.W., Hinton, D.M., Mitchell, T.R., Snook, M.E., and Olubajo, B., Characterization of endophytic strains of *Bacillus mojavensis* and their production of surfactin isomers. *Biological Control*, 2012. **62**(1): p. 1-9.
45. Maget-Dana, R. and Ptak, M., Interfacial properties of surfactin. *Journal of Colloid and Interface Science*, 1992. **153**(1): p. 285-291.
46. Thimon, L., Peyoux, F., Maget-Dana, R., and Michel, G., Surface-active properties of antifungal lipopeptides produced by *Bacillus subtilis*. *Journal of the American Oil Chemists Society*, 1992. **69**(1): p. 92-93.
47. Karimi, M., Mahmoodi, M., Niazi, A., Al-Wahaibi, Y., and Ayatollahi, S., Investigating wettability alteration during MEOR process, a micro/macro scale analysis. *Colloids and Surfaces B-Biointerfaces*, 2012. **95**: p. 129-136.
48. Ismail, W., Al-Rowaihi, I.S., Al-Humam, A.A., Hamza, R.Y., El Nayal, A.M., and Bououdina, M., Characterization of a lipopeptide biosurfactant produced by a crude-oil-emulsifying *Bacillus* sp. I-15. *International Biodeterioration & Biodegradation*, *in press*.
49. Deleu, M., Razafindralambo, H., Popineau, Y., Jacques, P., Thonart, P., and Paquot, M., Interfacial and emulsifying properties of lipopeptides from *Bacillus subtilis*. *Colloids and Surfaces A-Physicochemical and Engineering Aspects*, 1999. **152**(1-2): p. 3-10.
50. Urum, K. and Pekdemir, T., Evaluation of biosurfactants for crude oil contaminated soil washing. *Chemosphere*, 2004. **57**(9): p. 1139-1150.
51. Al-Bahry, S.N., Al-Wahaibi, Y.M., Elshafie, A.E., Al-Bemani, A.S., Joshi, S.J., Al-Makhmari, H.S., and Al-Sulaimani, H.S., Biosurfactant production by *Bacillus subtilis* B20 using date molasses and its possible application in enhanced oil recovery. *International Biodeterioration & Biodegradation*, *in press*.

5. PAPER 4

Biosurfactant Producing Microorganisms and Its Application to Enhance Oil Recovery at Lab Scale

SPE EOR Conference at Oil and Gas West Asia (16-18 April 2012) Muscat, Oman.

5.1. Abstract

Microbial Enhanced Oil Recovery (MEOR) is a tertiary oil recovery process where microorganisms and their metabolites are used to retrieve unrecoverable oil from mature reservoirs. Stimulation of biosurfactant production by indigenous microorganisms can reduce the capillary forces that retain the oil into the reservoir. The studied reservoir is characterized by alternated oil and water sand layers, with an average porosity of 25% and a permeability of 50 mD. It's a flat structure at 450 m depth, with an initial pressure of 32.4 bars and a temperature of 42.5°C. The oil is paraffinic, with low viscosity, high pour point and a gravity of 25° API, with no gas dissolved. Due to these properties, the wells can't flow naturally and the production has to be lifted, making this reservoir a good candidate for MEOR application. This work addresses the isolation and identification of microorganisms capable of producing biosurfactants and degrading heavy oil fractions at the oil reservoir conditions. Five *Bacillus subtilis* strains isolated from oil samples were able to grow and produce extracellular biosurfactants at 40°C under anaerobic conditions in medium supplemented with hydrocarbons. In addition, some of the isolates displayed a capacity to degrade, both in aerobic and anaerobic conditions, the large alkyl chains, and reduce the viscosity of hydrocarbon mixtures. A sand-pack column model was designed to simulate the oil recovery operations and evaluate the mobilization of residual oil by microorganisms. Additional oil recovery using *B. subtilis* isolates ranged from 19.8 to 35.0%, suggesting that stimulation of biosurfactant production by these strains *in situ* can contribute to mobilize entrapped oil. The novelty of this technique, compared to the conventional EOR methods, is the application of indigenous microorganisms to increase the oil recovery.

5.2. Introduction

As explained in chapters 1 and 2, the MEOR techniques studied in this work, were focused on the biosurfactants production by microorganisms isolated from Brazilian oil reservoirs and their biodegradation ability. However, the efficiency of biodegradation of oil compounds is limited by a poor mass transfer due to their high hydrophobicity and low aqueous solubility. Surfactants and biosurfactants increase the aqueous solubility of hydrocarbons and enhance their bioavailability and degradation rates¹.

Laboratory studies on MEOR have typically used sand-pack columns, which provide a convenient bench-scale approach to evaluate oil recovery for several reasons: it is an economic model; a battery of columns can be set up simultaneously; and they simulate oil recovery operations of oil reservoirs². In this study, a sand-pack column model was used to study the effect of biosurfactant-producing and oil-degrading microorganisms isolated from crude oil samples on the mobilization of entrapped oil. For that purpose the degradation of a solid paraffin mixture was studied for different *Bacillus* species, as well as evaluated the additional recovery of liquid paraffin in the sand-pack columns by the action of three *Bacillus subtilis* species.

5.3. Materials and Methods

5.3.1. Reservoir and Fluid Characteristics

The studied reservoir is characterized by alternated oil and water sand layers, with an average porosity of 25% and a permeability of 50 mD. The reservoir is a flat structure at 450 m depth, with no natural pressure support and with an initial pressure and temperature of 32.4 bars and 42.5°C, respectively. The oil is paraffinic, with low viscosity, high pour point and a gravity of 25° API, with no gas dissolved. Due to these properties, the wells cannot flow naturally and the production has to be lifted. Based on these characteristics, the reservoir is a good candidate for MEOR application as a process to enhance the fluid flow and the ultimate recovery of the reservoir.

5.3.2. Isolation of Microorganisms from Oil Samples

Crude oil samples obtained from four different wells of the studied reservoir were collected in sterile bottles. For the isolation of microorganisms, enrichment cultures were prepared in 500 mL glass bottles containing 250 mL of Raymond medium supplemented with 1% (v/v) *n*-hexadecane as the sole carbon source. Crude oil samples (5 mL) were transferred to the bottles and incubated at 40°C for one month. To isolate bacterial strains, samples (200 µL) of the enrichment cultures were periodically spread on LB agar plates that were incubated at 40°C under aerobic and anaerobic conditions. After incubation, morphologically different colonies were re-isolated by transfer to fresh agar plates at least three times to obtain pure cultures. Isolates purity was verified through microscopic observation of Gram stained cultures. Pure cultures were stored at -80°C in LB medium supplemented with 20% (v/v) glycerol.

The composition of Raymond medium was (g.L⁻¹): NaCl 50.0; Na₂HPO₄ 3.0; NH₄NO₃ 2.0; KH₂PO₄ 2.0; yeast extract 0.5; MgSO₄.7H₂O 0.2; Na₂CO₃ 0.1; MnSO₄.4H₂O 0.02; CaCl₂ 0.01; FeSO₄ 0.01; supplemented with 1% (v/v) *n*-hexadecane. The composition of LB medium was (g.L⁻¹): NaCl 10.0; tryptone 10.0; yeast extract 5.0. Both media were adjusted to pH 7.0.

5.3.3. Screening of Biosurfactant-producing Strains in Mineral Media

The bacterial strains were grown in Mineral Salt Solution (MSS) with and without *n*-hexadecane (1%, v/v) at 40°C. The MSS consisted of (g.L⁻¹): NaCl 10.0; sucrose 10.0; Na₂HPO₄ 5.0; NH₄NO₃ 2.0; KH₂PO₄ 2.0; MgSO₄.7H₂O 0.2. The pH was adjusted to 7.0.

A single colony of each isolate was taken from the plate and transferred to 30 mL of MSS. Anaerobic cultures were prepared removing oxygen by aseptically bubbling oxygen-free nitrogen into the flasks, which were sealed with rubber stoppers. Cultures were incubated at 40°C and 120 rpm. Samples were taken at different time points during the fermentation to determine biomass concentration and biosurfactant production. Bacterial growth was determined by measuring the optical density at 600 nm. Afterwards, the samples were centrifuged (10000 × *g*, 20 min, 10°C) and the cell-free supernatants were used to measure surface tension and emulsifying activity.

5.3.4. Surface-activity Determination

Surface tension measurements of culture broth supernatants were performed according to the Ring method described elsewhere³. A KRÜSS K6 Tensiometer (KRÜSS GmbH, Hamburg, Germany) equipped with a 1.9 cm Du Noüy platinum ring was used. To increase the accuracy of the surface tension measurements, an average of triplicates was determined. All the measurements were performed at room temperature (20°C). Isolates which reduced the culture broth surface tension below 40 mN.m⁻¹ were considered biosurfactant producers.

5.3.5. Emulsifying Activity Determination

Emulsifying activity was determined by the addition of 2 mL of *n*-hexadecane to the same volume of cell-free culture broth supernatant in glass test tubes. The tubes were mixed with vortex at high speed for 2 min and then incubated at 25°C for 24 h. The

stability of the emulsion was determined after 24 h, and the emulsification index (E_{24}) was calculated as the percentage of the height of the emulsified layer (mm) divided by the total height of the liquid column (mm). Emulsions formed by the different isolates were compared with those formed by a 1% (w/v) solution of the synthetic surfactant sodium dodecyl sulphate (SDS) in demineralized water. All emulsification indexes were performed in triplicate.

5.3.6. Identification of the Isolates

Bacterial isolates that displayed high biosurfactant production were selected and identified by partial 16S rRNA sequencing. The 16S rRNA gene was amplified by PCR using the primers 341F and 907R. The resulting sequences were compared with sequences in the GenBank database of the National Center for Biotechnology Information (NCBI) (<http://www.ncbi.nlm.nih.gov>) using the nucleotide-nucleotide blast (BLASTn) network service, to determine their phylogenetic affiliations.

5.3.7. Hydrocarbon Degradation Determination

The ability of three isolated microorganisms to degrade paraffinic mixtures at anaerobic conditions was evaluated. A basal mineral salt medium (BMSM) supplemented with a paraffinic mixture containing *n*-alkanes between C20-C30 was used. The BMSM contained (g.L⁻¹): KH₂PO₄ 5.0; NaNO₃ 2.0; MgSO₄·7H₂O 0.25; K₂HPO₄·3H₂O 1.0; (NH₄)₂SO₄ 1.0; NaCl 5.0.

Flasks containing 50 mL of culture media supplemented with 0.1% or 1% (w/v) of sterile solid paraffin wax with a melting point of 50-52°C (purchased from Sigma-Aldrich Co., St. Louis, USA) were sealed with rubber stoppers. Anaerobic cultures were prepared removing oxygen by aseptically bubbling oxygen-free nitrogen into the flasks. Cultures were incubated at 40°C and 150 rpm during 15 days in anaerobic conditions along with control flasks incubated at the same conditions without addition of microorganisms.

At the end of the treatment the paraffinic mixture was quantified via the extraction of the residual solid paraffin in the culture media using an equal volume of dichloromethane, and the extract was dried and weighed accurately. The control was extracted via the same method and the percentage (w/w) of solid paraffin degradation

estimated. The organic phase extracted was then diluted (20 mg.mL^{-1}) in dichloromethane for gas chromatography (GC) analysis. GC analysis of each sample were performed with CP 3800 Varian gas Chromatograph equipped with and on-column injection, FID detector, and DB-5HT capillary column ($30 \text{ m} \times 0.32 \text{ mm i.d.}$, $0.1 \mu\text{m}$ thickness) (J&W Scientific Inc., California, USA). Helium was used as gas carrier and a constant flow rate of 2 mL.min^{-1} was set. Injector and detector temperatures were 350 and 370°C , respectively. Oven temperature was set at 50°C during 1 min , raised to 350°C at the rate of $10^\circ\text{C.min}^{-1}$, and at last kept at 370°C during 1 min . All the samples were analyzed in triplicate.

5.3.8. Sand-pack Column Assays

Sand-pack columns were designed to simulate the oil reservoir and used to evaluate the effect of microorganisms in the oil recovery (Figure 5.1). Vertically oriented acrylic columns with a volume of 250 mL were uniformly packed with acid washed dry sand. The columns were provided with a sieve and cap fixed at the bottom. After packing the sand tightly, a top sieve and cap were fixed. The caps on both the ends of the column were provided with holes for insertion of inlet and outlet tubes. Rubber ‘O’ rings surrounded the caps to hermetically seal the column.

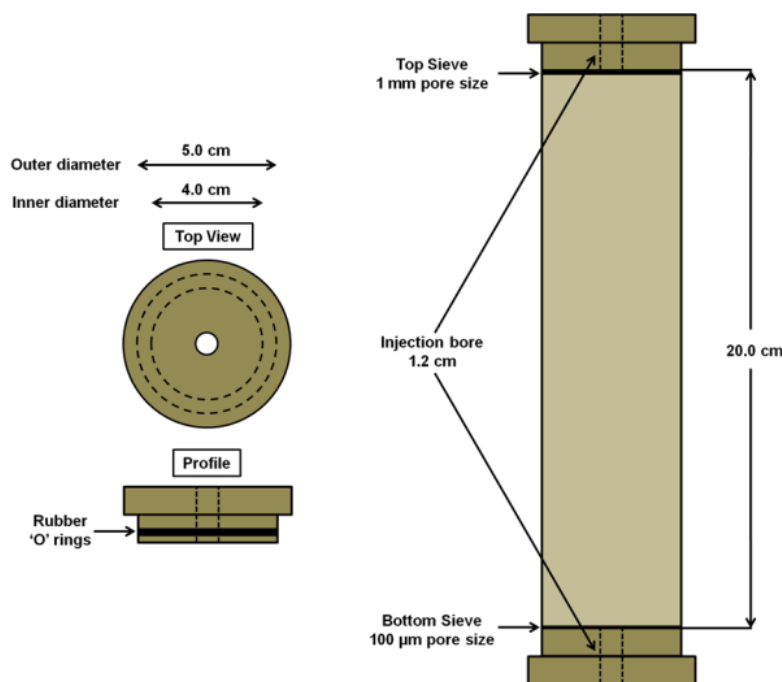


Figure 5.1 Illustration of the sand-pack column model used to evaluate the mobilization of residual oil by microorganisms. Adapted from Suthar et al.²

The experiments were carried out at 40°C. The column was first flooded with water at a constant flow rate of 3 mL.min⁻¹; the pore volume (PV, mL), defined as the empty volume of the model, was calculated by measuring the volume of water required to saturate the column. The porosity (%) of the column was calculated as the PV divided by the total volume of the column (250 mL). In the second step, liquid paraffin was injected into the column in the same way to replace water, until there was no more water coming out from the effluent. The volume of paraffin required to saturate the column was 200 mL. Original oil in place (OOIP, mL) was calculated as the volume of paraffin retained in the column. Initial oil saturation (S_{oi} , %) and initial water saturation (S_{wi} , %) were calculated as follows:

$$S_{oi}(\%) = \frac{OOIP}{PV} \times 100 \quad \text{Equation 5.1}$$

$$S_{wi}(\%) = \frac{PV-OOIP}{PV} \times 100 \quad \text{Equation 5.2}$$

The sand-pack column was incubated at 40°C for 24 h and afterwards flooded again with water to remove the excess of paraffin, until no more paraffin was observed in the effluent. The amount of paraffin recovered, so called oil recovered after water flooding (S_{orwf} , mL) was determined volumetrically. Residual oil saturation (S_{or}) was calculated as follows:

$$S_{or}(\%) = \frac{OOIP-S_{orwf}}{OOIP} \times 100 \quad \text{Equation 5.3}$$

The residual oil was subjected to microbial recovery processes. The column was inoculated with 50 mL of the different isolates in MSS ($OD_{600nm} = 0.2$), sealed and incubated for 14 days at 40°C. After incubation, the column was flooded with water and the volume of paraffin recovered (oil recovered after microbial flooding (S_{ormf} , mL)) was measured. Additional Oil Recovery (AOR, %) was calculated as follows:

$$AOR(\%) = \frac{S_{ormf}}{OOIP-S_{orwf}} \times 100 \quad \text{Equation 5.4}$$

5.4. Results and Discussion

5.4.1. Screening of Biosurfactant-Producing Strains

A total of 58 isolates were obtained from crude oil samples. Biosurfactant production was evaluated in MSS under anaerobic conditions at 40°C. Five of the isolates were found to produce biosurfactants under anaerobic conditions (Table 5.1). The surface tension values were determined six times at room temperature (20°C) and the emulsification indexes were calculated three times at 25°C (results presented in Table 5.1 represent the average of three independent experiments \pm standard deviation). Furthermore, all isolates were identified as *B. subtilis* according to the partial sequence of their 16S rRNA genes. Biosurfactant production was not negatively affected by the presence of *n*-hexadecane (MSSH) in the culture broth. The best results regarding biosurfactant production were obtained with the isolates #309, #311 and #573. Those isolates reduced the surface tension of the culture broth to values around 30 mN.m⁻¹ and exhibited emulsifying indexes from 24 to 34%.

Table 5.1 Surface tension values (ST, mN.m⁻¹) and emulsifying indexes (E_{24} , %) obtained with the different isolates grown in MSS and MSSH for 120 h at 40°C and 120 rpm under anaerobic conditions.

Strain	MSS		MSSH	
	ST / (mN.m ⁻¹)	E_{24} / (%)	ST / (mN.m ⁻¹)	E_{24} / (%)
#191	41.7 \pm 1.2	14.6 \pm 1.9	40.0 \pm 2.0	13.3 \pm 5.9
#309	31.4 \pm 1.3	25.9 \pm 4.2	31.4 \pm 0.5	24.6 \pm 5.3
#311	30.5 \pm 0.1	8.5 \pm 4.0	31.0 \pm 0.6	34.2 \pm 3.9
#551	51.6 \pm 1.5	7.1 \pm 1.6	42.2 \pm 2.4	13.6 \pm 4.2
#573	31.5 \pm 0.4	24.9 \pm 2.3	33.7 \pm 1.4	19.4 \pm 5.6
Control	66.4 \pm 1.5	0.0 \pm 0.0	63.3 \pm 0.9	0.0 \pm 0.0
SDS 1%	39.9 \pm 0.4	55.0 \pm 1.7	39.9 \pm 0.4	55.0 \pm 1.7

Most of the microorganisms potentially useful for application in MEOR *in situ* belong to the genus *Bacillus*. *Bacillus mojavensis* JF-2, a thermotolerant and halotolerant strain isolated from an oil field, grows and produces similar amounts of a lipopeptide biosurfactant under both aerobic and anaerobic conditions, reducing the surface tension of the medium below 30 mN.m⁻¹, and is not inhibited by crude oil^{4, 5}. Other strains

isolated from oil fields and which applicability in MEOR has been demonstrated are *Bacillus licheniformis* BAS50^{6, 7}, *B. licheniformis* ACO1⁸ and *B. subtilis* PTCC1696⁹. Taking into account these data and the results obtained with isolates #309, #311 and #573 regarding biosurfactant production, they can be considered good candidates for application in MEOR.

5.4.2. Hydrocarbon Degradation

In order to evaluate the ability of the isolated *B. subtilis* strains to degrade the paraffinic oil fraction, a mixture of solid paraffin was incubated with isolates #309, #191 and #551 under anaerobic conditions. The respective anaerobic degradation (% w/w) of each paraffinic mixture is illustrated in Figure 5.2 and compared with the control sample (incubated without microorganisms).

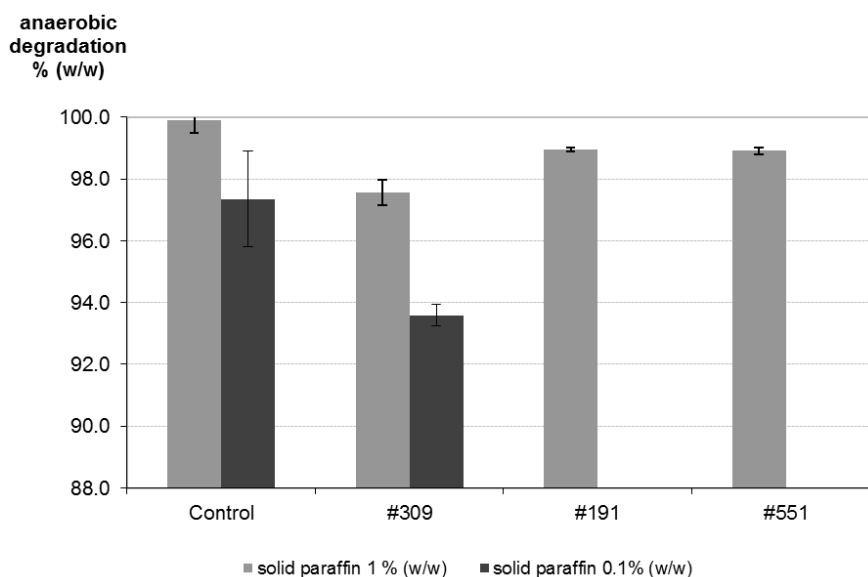


Figure 5.2 Values of anaerobic degradation of 0.1% and 1% (w/w) solid paraffin by bacterial isolates after 15 days of incubation at 40°C and 150 rpm.

The isolates studied were able to grow in BMSM medium supplemented with solid paraffinic wax, under anaerobic conditions. After the treatment with #191 and #551 bacterial isolates, the percentage of paraffin degraded was of about 1% (w/w). The highest degradation rates observed (*circa* 2.5%) were obtained for the isolate #309. Thus, the isolate #309 was selected to further study its ability to degrade a mixture with a lower concentration of solid paraffin wax (0.1%, w/w). The anaerobic degradation (% w/w) for this system and the respective control sample are also presented in Figure 5.2.

The results show that in presence of lower concentrations of paraffin, the strain #309 presents a higher capacity for anaerobic degradation, and degrades approximately 6% (w/w) of solid paraffin. These results are in good agreement with those reported by Etoumi¹⁰, which showed that microbial degradation of paraffinic hydrocarbon of crude oil was higher for lower concentrations of crude oil.

The paraffin extracted after the treatment with isolate #309 was analyzed by GC and the relative degradation of each *n*-alkane was measured. The respective variations of relative weight fraction of each *n*-alkane present in the paraffin mixture are illustrated in Figure 5.3.

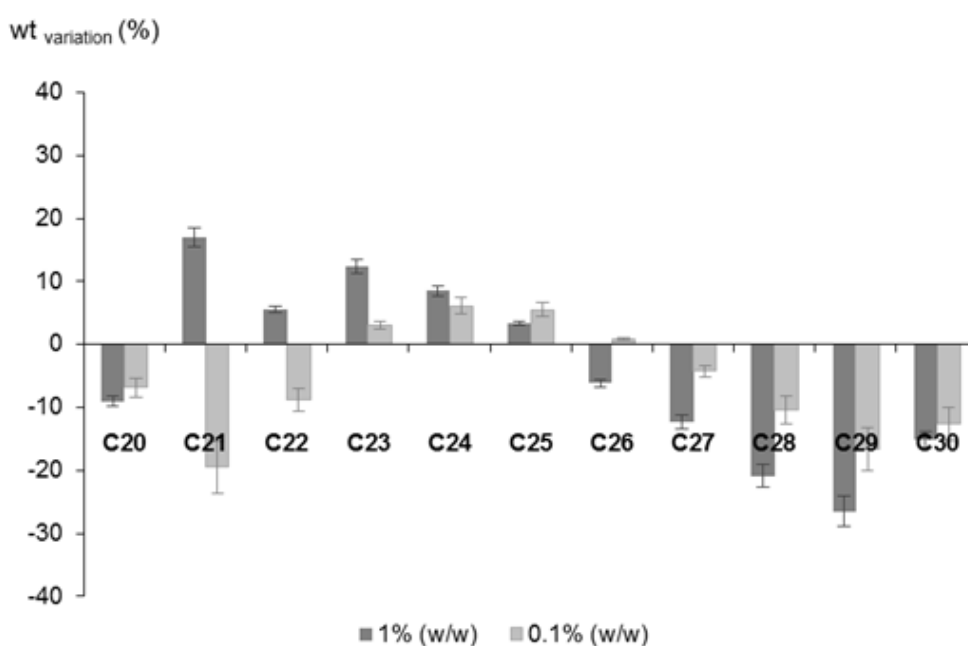


Figure 5.3 Variation of relative weight fraction of *n*-alkanes present in solid paraffinic mixture after incubation with isolate #309, for 15 days at 40°C and anaerobic conditions as compared to the control (error bars show the average error).

For both paraffin concentrations the isolate #309 led to a decrease in the alkanes higher than C26, while for the lower paraffin concentration (0.1%, w/w) a decrease in the lower alkanes was also observed suggesting a degradation of the whole range of alkanes above C20 at these conditions. The aerobic degradation of *n*-alkanes has been also reported by other authors¹⁰⁻¹⁴, however anaerobic studies using *B. subtilis* strains have not been described. One exception is our recent work¹⁵ in which it was studied the anaerobic abilities of different *B. subtilis* isolates to degrade *n*-alkanes. In that work the

same isolate (#309) showed identical *n*-alkanes degradation abilities to higher concentrations of solid paraffin.

5.4.3. Sand-pack Columns Assays

B. subtilis #309, #311 and #573 were selected to perform the oil recovery assays using sand-pack columns. The results obtained are shown in Table 5.2 (results represent the average of three independent experiments \pm standard deviation).

Table 5.2 Oil recovery in sand-pack columns using isolates #309, #311 and #573.

	#309	#311	#573	Control
PV (mL)	92.5 \pm 3.5	94.0 \pm 3.5	92.5 \pm 3.5	91.0 \pm 1.4
Porosity (%)	37.0 \pm 1.4	37.6 \pm 1.4	37.0 \pm 1.4	36.4 \pm 0.6
OOIP (mL)	88.0 \pm 2.8	89.3 \pm 3.8	87.0 \pm 4.2	87.5 \pm 3.5
S_{oi} (%)	95.1 \pm 0.6	95.0 \pm 0.7	94.0 \pm 1.0	96.1 \pm 2.4
S_{wi} (%)	4.9 \pm 0.6	5.0 \pm 0.7	6.0 \pm 1.0	3.9 \pm 2.4
S_{orwf} (mL)	43.0 \pm 0.2	42.0 \pm 1.7	44.0 \pm 0.0	43.5 \pm 2.1
OOIP-S_{orwf} (mL)	45.0 \pm 7.1	47.3 \pm 2.1	43.0 \pm 4.2	44.0 \pm 5.7
S_{or} (%)	51.0 \pm 6.4	53.0 \pm 0.3	49.4 \pm 2.5	50.2 \pm 4.5
S_{ormf} (mL)	15.8 \pm 2.5	12.3 \pm 1.1	8.5 \pm 0.0	1.8 \pm 0.4
AOR (%)	35.0 \pm 0.0	23.1 \pm 1.2	19.9 \pm 1.9	4.0 \pm 0.4

As can be seen from Table 5.2, the pore volume was in the range of 91-94 mL, and the OOIP was between 87.0 and 89.3 mL. Water flooding was able to recover about 42.0-44.0 mL of the OOIP, leaving about 50% of paraffin unrecovered in the column. When the different isolates were introduced in the column with the appropriate nutrients (MSS) and incubated for 14 days at 40°C, additional paraffin was recovered. The best result was obtained with the isolate #309, which recovered 35% of the entrapped paraffin; isolates #311 and #573 recovered 23 and 20% of paraffin, respectively. In the control columns, which were incubated in the same conditions but without microorganisms, the amount of paraffin recovered was about 4%, so it can be suggested that the remaining paraffin was recovered due the action of microorganisms. Table 5.3 compiles the recovery efficiencies obtained by other authors in sand-pack column assays *in situ* using different *Bacillus* strains isolated from oil reservoirs.

Table 5.3 Results of additional oil recovery from sand-pack column assays using different *Bacillus* isolates.

Microorganism	Substrate	AOR / (%)	Reference
<i>B. licheniformis</i> XDS1	Crude oil	4.8-6.9	She et al. ¹⁴
<i>B. licheniformis</i> XDS2			
<i>Bacillus cereus</i> XDS3			
<i>B. licheniformis</i> BNP29	Crude oil	9.3-22.1	Yakimov et al ⁷
<i>Bacillus brevis</i>	Paraffinic oil	18.0	Almeida et al ¹⁶
<i>Bacillus polymyxa</i>			
<i>B. licheniformis</i>			
<i>B. licheniformis</i> ACO1	Paraffin	22.0	Dastgheib et al ⁸

As can be seen, large additional oil recoveries were obtained with all the isolates and these were particularly important with isolate #309 which was higher than the reported in other studies. The results gathered in the current work show that the isolated microorganisms are promising candidates for application in MEOR processes.

5.5. Conclusions

In the current work some *B. subtilis* strains were isolated from crude oil samples from the target reservoir. Five isolates were able to grow and produce extracellular biosurfactants at 40°C under anaerobic conditions in a culture medium supplemented with hydrocarbons. Those isolates reduced the surface tension of the culture broth to 30 mN.m⁻¹ and were able to emulsify hydrocarbons. The isolate #309 was also capable of degrading a solid paraffinic mixture, mainly the heavier *n*-alkanes under anaerobic conditions. The simulation of the oil recovery operations using the sand-pack column showed that three isolates (#309, #311 and #573) recovered between 19.8 and 35% of the entrapped oil. These results suggest that stimulation of biosurfactant production and anaerobic degradation of heavy oil fractions *in situ* can contribute to mobilize the entrapped oil and improve the oil fluidity.

5.6. References

1. Jinfeng, L., Lijun, M., Bozhong, M., Rulin, L., Fangtian, N., and Jiayi, Z., The field pilot of microbial enhanced oil recovery in a high temperature petroleum reservoir. *Journal of Petroleum Science and Engineering*, 2005. **48**(3-4): p. 265-271.
2. Suthar, H., Hingurao, K., Desai, A., and Nerurkar, A., Evaluation of bioemulsifier mediated Microbial Enhanced Oil Recovery using sand pack column. *Journal of Microbiological Methods*, 2008. **75**(2): p. 225-230.
3. Gudiña, E.J., Teixeira, J.A., and Rodrigues, L.R., Isolation and functional characterization of a biosurfactant produced by *Lactobacillus paracasei*. *Colloids and Surfaces B-Biointerfaces*, 2010. **76**(1): p. 298-304.
4. Jenneman, G.E., McInerney, M.J., Knapp, R.M., Clark, J.B., Feero, J.M., Revus, D.E., and Menzie, D.E., A Halotolerant, biosurfactant-producing *Bacillus* species potentially useful for enhanced oil-recovery. *Developments in Industrial Microbiology*, 1983. **24**: p. 485-492.
5. Javaheri, M., Jenneman, G.E., McInerney, M.J., and Knapp, R.M., Anaerobic production of a biosurfactant by *Bacillus licheniformis* JF-2. *Applied and Environmental Microbiology*, 1985. **50**(3): p. 698-700.
6. Yakimov, M.M., Timmis, K.N., Wray, V., and Fredrickson, H.L., Characterization of a new lipopeptide surfactant produced by thermotolerant and halotolerant subsurface *Bacillus licheniformis* Bas50. *Applied and Environmental Microbiology*, 1995. **61**(5): p. 1706-1713.
7. Yakimov, M.M., Amro, M.M., Bock, M., Boseker, K., Fredrickson, H.L., Kessel, D.G., and Timmis, K.N., The potential of *Bacillus licheniformis* strains for in situ enhanced oil recovery. *Journal of Petroleum Science and Engineering*, 1997. **18**(1-2): p. 147-160.
8. Dastgheib, S.M.M., Amoozegar, M.A., Elahi, E., Asad, S., and Banat, I.M., Bioemulsifier production by a halothermophilic *Bacillus* strain with potential applications in microbially enhanced oil recovery. *Biotechnology Letters*, 2008. **30**(2): p. 263-270.
9. Ghojavand, H., Vahabzadeh, F., Mehranian, M., Radmehr, M., Shahraki, K.A., Zolfagharian, F., Emadi, M.A., and Roayaei, E., Isolation of thermotolerant, halotolerant, facultative biosurfactant-producing bacteria. *Applied Microbiology and Biotechnology*, 2008. **80**(6): p. 1073-1085.
10. Etoumi, A., Microbial treatment of waxy crude oils for mitigation of wax precipitation. *Journal of Petroleum Science and Engineering*, 2007. **55**(1-2): p. 111-121.
11. Wang, L., Tang, Y., Wang, S., Liu, R.L., Liu, M.Z., Zhang, Y., Liang, F.L., and Feng, L., Isolation and characterization of a novel thermophilic *Bacillus* strain degrading long-chain n-alkanes. *Extremophiles*, 2006. **10**(4): p. 347-356.
12. Kato, T., Haruki, M., Imanaka, T., Morikawa, M., and Kanaya, S., Isolation and characterization of long-chain-alkane degrading *Bacillus thermoleovorans* from deep subterranean petroleum reservoirs. *Journal of Bioscience and Bioengineering*, 2001. **91**(1): p. 64-70.
13. Das, K. and Mukherjee, A.K., Crude petroleum-oil biodegradation efficiency of *Bacillus subtilis* and *Pseudomonas aeruginosa* strains isolated from a petroleum-oil contaminated soil from North-East India. *Bioresource Technology*, 2007. **98**(7): p. 1339-1345.
14. She, Y.H., Zhang, F., Xia, J.J., Kong, S.Q., Wang, Z.L., Shu, F.C., and Hu, J.M., Investigation of biosurfactant-producing Indigenous microorganisms that enhance residue oil recovery in an oil reservoir after polymer flooding. *Applied Biochemistry and Biotechnology*, 2011. **163**(2): p. 223-234.
15. Gudiña, E.J., Pereira, J.F.B., Rodrigues, L.R., Coutinho, J.A.P., and Teixeira, J.A., Isolation and study of microorganisms from oil samples for application in Microbial Enhanced Oil Recovery. *International Biodeterioration and Biodegradation*, 2012. **68**: p. 56-64.
16. Almeida, P.E., Moreira, R.S., Almeida, R.C.C., Guimaraes, A.K., Carvalho, A.S., Quintella, C., Esperidia, M.C.A., and Taft, C., Selection and application of microorganisms to improve oil recovery. *Engineering in Life Sciences*, 2004. **4**(4): p. 319-325.

6. PAPER 5

Biosurfactant-producing and Oil-degrading *Bacillus subtilis* Strains Enhance Oil Recovery in Laboratory Sand-pack Columns

Journal of Hazardous Materials (2013) (submitted for publication)

6.1. Abstract

Microbial Enhanced Oil Recovery (MEOR) technology uses microorganisms and their metabolites to retrieve unrecoverable oil from mature reservoirs. *In situ* stimulation of biosurfactant-producing and oil-degrading microorganisms reduces the capillary forces retaining the oil inside the reservoir and decreases its viscosity, thus promoting the oil flow and consequently production. In this work, a sand-pack column model was designed to simulate oil recovery operations and to evaluate the mobilization of residual oil by selected microorganisms. Four different hydrocarbon mixtures and three *Bacillus subtilis* strains isolated from crude oil samples were used. Additional oil recoveries ranged from 6 to 24% depending on the hydrocarbon mixture and microorganism used. Biosurfactant production was observed with all the microorganisms and hydrocarbon mixtures studied. Furthermore, the long chain *n*-alkanes present in the oils, with the subsequent viscosity reduction, was demonstrated by the first time in sand-pack columns using *Bacillus* isolates under oxygen limiting conditions. The results obtained suggest that the stimulation of the selected *B. subtilis* strains *in situ* can contribute to the mobilization of entrapped oil in mature reservoirs.

Keywords: MEOR; *Bacillus subtilis*; biosurfactant; sand-pack column; biodegradation.

6.2. Introduction

As explained in chapter 5, laboratory studies on MEOR using sand-pack columns provide a suitable bench-scale approach to evaluate the oil recovery: it is an economic model; a battery of columns can be set up simultaneously; and they can simulate the oil recovery operations usually conducted in reservoirs¹. Thus, following the preliminary sand-pack tests performed with a liquid paraffin mixture, in this work, a sand-pack column model was used to study the effect of three different biosurfactant-producing and oil-degrading *B. subtilis* strains, previously isolated from crude oil samples (chapter 2), on the mobilization of entrapped oil. Additionally, the degradation of oil hydrocarbons was evaluated in the oils recovered after the MEOR process. Herein four different sources of hydrocarbons were used to study the degradation and oil recovery of the *Bacillus subtilis* strains isolated with best surface and emulsifying properties.

6.3. Material and Methods

6.3.1. Hydrocarbon Mixtures

Four different hydrocarbon mixtures were used: heating oil, viscous paraffin, and two different types of crude oil, Arabian Light and heavy oil. Viscous paraffin was purchased from Merck (Merck, Darmstadt, Germany). Heating oil (ZibroTM) was obtained from commercial sources. Heavy crude oil was obtained from a Brazilian oil field. Arabian Light oil was kindly provided by GALP (Portugal). The properties of each hydrocarbon mixture are presented in Table 6.1.

Table 6.1 Properties of the hydrocarbon mixtures: viscosity (η), density (ρ), API gravity (API) and *n*-alkanes range. Viscosity and density values were measured at 40°C.

Hydrocarbon mixture	η / (mPa.s)	ρ / (g.cm ⁻³)	API	<i>n</i> -alkanes range
Heating oil	1.34	0.76	-	C16 - C30
Viscous paraffin	44.64	0.85	-	*
Arabian light oil	8.33	0.86	29.7°	C11 - C24
Heavy crude oil	73.91	0.90	25.5°	C14 - C32

* Mainly composed of ramified hydrocarbons. The *n*-alkane composition was not determined.

6.3.2. Microorganisms

Three *B. subtilis* strains (#309, #311 and #573) previously isolated from crude oil samples obtained from a Brazilian oil field at depths of 300-400 m² were used. These isolates produced extracellular biosurfactants with high surface and emulsifying activities at 40°C under anaerobic conditions in medium supplemented with hydrocarbons. Furthermore, the isolates degraded the large alkyl chains of hydrocarbon mixtures under anaerobic conditions, reducing their viscosity. However, the three isolates exhibit some differences regarding the biosurfactants produced and their hydrocarbon degradation profiles^{2, 3}. These characteristics make them good candidates for application in the oil reservoir under study. The isolates were stored at -80°C in LB medium supplemented with 20% (v/v) glycerol.

6.3.3. Sand-pack Column Assays

Sand-pack columns were designed to simulate the oil reservoir and used to evaluate the effect of microorganisms in enhanced oil recovery. Vertically oriented acrylic columns with a volume of 250 mL were uniformly packed with dry sand (previously sterilized). The columns were provided with a sieve and cap fixed at the bottom. After packing the sand tightly, a top sieve and cap were fixed. The caps on both the ends of the column were provided with holes for insertion of inlet and outlet tubes. Rubber 'O' rings surrounded the caps to hermetically seal the column (Figure 5.1).

The experiments were carried out at 40°C and different hydrocarbon mixtures were used, as described above (Figure 6.2). The column was first flooded with water at a constant flow rate of 3 mL.min⁻¹. Pore volume (PV, mL), defined as the empty volume of the model, was calculated by measuring the volume of water required to saturate the column. The porosity (%) of the column was calculated as the PV divided by the total volume of the column (250 mL). In the second step, in the same way the hydrocarbon mixture (previously sterilized) was injected into the column to replace water, until there was no more water coming out from the effluent. Original oil in place (OOIP, mL) was calculated as the volume of hydrocarbon retained in the column. Initial oil saturation (S_{oi} , %) and initial water saturation (S_{wi} , %) were calculated as follows:

$$S_{oi}(\%) = \frac{OOIP}{PV} \times 100 \quad \text{Equation 6.1}$$

$$S_{wi}(\%) = \frac{PV - OOIP}{PV} \times 100 \quad \text{Equation 6.2}$$

The sand-pack column was incubated at 40°C for 24 h and afterwards flooded again with water to remove the excess of hydrocarbon mixture, until no more hydrocarbon mixture was observed in the effluent. The amount of hydrocarbon mixture recovered, so-called oil recovered after water flooding (S_{orwf} , mL) was determined volumetrically. Residual oil saturation (S_{or}) was calculated as follows:

$$S_{or}(\%) = \frac{OOIP - S_{orwf}}{OOIP} \times 100 \quad \text{Equation 6.3}$$

Further, the residual oil was subjected to microbial recovery processes. The column was inoculated with 50 mL of the different microorganisms in MSS culture medium ($OD_{600nm} = 0.2$), sealed and incubated for 14 days at 40°C. Control columns were

inoculated only with MSS and incubated at the same conditions. The MSS medium consisted of (g.L⁻¹): NaCl 10.0; Na₂HPO₄ 5.0; KH₂PO₄ 2.0; MgSO₄.7H₂O 0.2; sucrose 10.0. After incubation, the column was flooded with water and the volume of hydrocarbon mixture recovered (oil recovered after microbial flooding (S_{ormf}, mL)) was measured. Whenever required, the samples were centrifuged to break the emulsion formed. Additional Oil Recovery (AOR, %) was calculated as follows:

$$\text{AOR (\%)} = \frac{S_{ormf}}{OOIP - S_{orwf}} \times 100 \quad \text{Equation 6.4}$$

All the experiments were performed in triplicate.

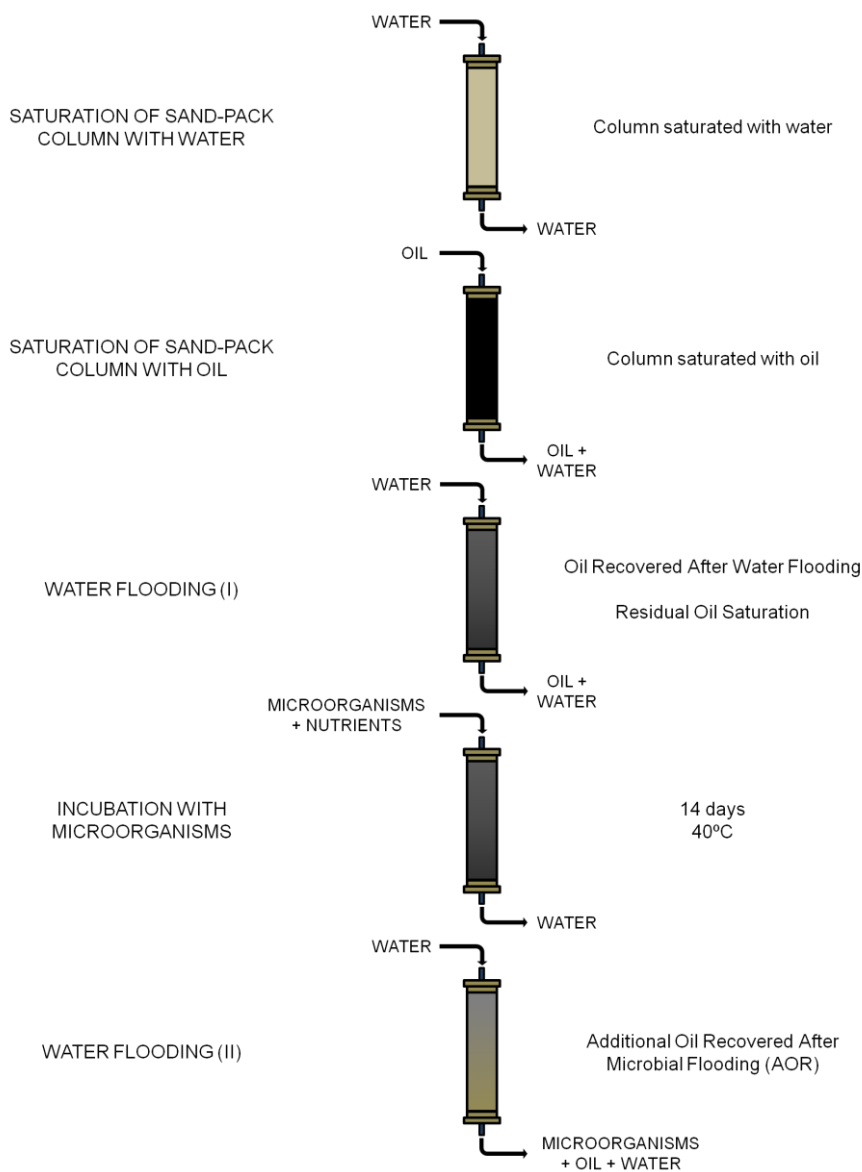


Figure 6.2 Schematic representation of the sand-pack column process.

6.3.4. Hydrocarbon Degradation

After conducting the sand-pack column assays with the different hydrocarbon mixtures and microorganisms, the *n*-alkanes degradation was evaluated. The oil recovered from the simulated MEOR experiments was diluted (20 mg.mL⁻¹) in dichloromethane for gas chromatography (GC) analysis. GC analysis of each sample was performed using a CP 3800 Varian gas Chromatograph equipped with an on-column injector, FID detector, and DB-HT-SIMDIS capillary column (5 m × 0.53 mm i.d., 0.15 μm thickness) (Agilent J&W Scientific Inc., California, USA). Helium was used as the carrier gas at a constant flow rate of 18 mL.min⁻¹. Injector and detector temperatures were 350 and 370°C, respectively. For Arabian Light and heavy crude oil samples, the oven temperature was set at 40°C during 5 min, raised to 350°C at a rate of 5°C.min⁻¹, and at last kept at 370°C during 15 min. For heating oil samples, the oven temperature was set at 40°C during 8 min, raised to 300°C at a rate of 5°C.min⁻¹, and at last kept at 300°C during 15 min. The *n*-alkanes degradation was evaluated by comparing the composition of hydrocarbons recovered after the treatment (with different microorganisms) with the hydrocarbons recovered in the abiotic control assays. All the samples were analyzed in triplicate.

6.3.5. Viscosity

The dynamic viscosity (η) measurements were carried out using an automated Anton Paar (model SVM 3000) rotational Stabinger viscosimeter-densimeter at 50°C and at atmospheric pressure (approximately 0.1 MPa). The viscosity of hydrocarbons recovered after the treatment with the different isolates was compared with the hydrocarbons recovered in the abiotic control columns. The relative uncertainty in dynamic viscosity measurements is $\pm 0.35\%$.

6.3.6. Biosurfactant Production in Sand-pack Columns

B. subtilis isolates used in this study have been previously found to produce biosurfactants both under aerobic and anaerobic conditions in the presence of different hydrocarbons in liquid medium². In order to evaluate biosurfactant production in sand-pack columns, mini-sand-pack columns were prepared in 15 mL tubes. The tubes were uniformly packed with autoclaved dry sand. After that, the corresponding hydrocarbon mixture (previously sterilized) was introduced into the mini-column to attain the same

percentage obtained in the sand-pack columns after the water flooding process. The remaining pore volume of the columns was saturated with a suspension of the corresponding microorganism in MSS medium ($OD_{600nm} = 0.2$). Afterwards, the columns were sealed and incubated at 40°C for 14 days. Control columns were prepared in the same way but without addition of microorganisms. At the end of the incubation period, the content of each column was transferred to 50 mL test tubes. 5 mL of distilled water were added and the tubes were mixed using vortex for 2 min to extract the biosurfactants. The resulting mixture was centrifuged (9000 rpm, 30 min); the remaining hydrocarbon mixture was removed and the supernatant was filtered (0.2 μ m) to remove residual hydrocarbon, sand and cells. The surface tension of the supernatants was determined according to the Ring method (as described by Gudiña et al.²) using a KRÜSS K6 Tensiometer (KRÜSS GmbH, Hamburg, Germany). These surface tension values were then used to calculate the concentration of biosurfactant using a calibration curve (surface tension *versus* biosurfactant concentration). The calibration curves were calculated for each strain using different concentrations of the corresponding crude biosurfactant (isolated as described by Gudiña et al.²) in distilled water below the critical micelle concentration (*cmc*). In this biosurfactant concentration range there is a linear relationship between biosurfactant concentration and surface tension. Therefore, whenever adequate, the supernatants obtained from the sand-pack columns were diluted to guarantee that biosurfactant concentrations were below the *cmc*.

6.4. Results and Discussion

6.4.1. Sand-pack Column Assays

B. subtilis #309, #311 and #573 were used to perform the oil recovery assays with different hydrocarbon mixtures using sand-pack columns. The results obtained are shown in Table 6.2.

Table 6.2 Summary of the results obtained in the MEOR sand-pack experiments using *B. subtilis* isolates #309, #311 and #573 and different hydrocarbon mixtures. Results represent the average of three independent experiments \pm standard deviation.

Hydrocarbon mixture				
Oil Recovery Parameters	<i>Heating Oil</i>			
	Control	#309	#311	#573
OOIP (mL)	68.5 \pm 4.9	68.2 \pm 7.3	63.0 \pm 1.7	69.0 \pm 7.9
S_{oi} (%)	90.0 \pm 5.7	76.5 \pm 5.5	82.8 \pm 0.4	90.6 \pm 7.4
OOIP-S_{orwf} (mL)	25.0 \pm 2.8	23.0 \pm 8.1	31.7 \pm 0.6	34.0 \pm 5.3
S_{or} (%)	36.4 \pm 1.6	34.9 \pm 10.1	50.3 \pm 2.3	49.4 \pm 6.7
S_{ormf} (mL)	0.0 \pm 0.0	5.0 \pm 2.2	3.2 \pm 0.3	2.3 \pm 0.3
AOR (%)	0.0 \pm 0.0	25.0 \pm 0.8	10.3 \pm 1.2	6.4 \pm 0.6
<i>Viscous Paraffin</i>				
	Control	#309	#311	#573
OOIP (mL)	87.5 \pm 3.5	86.5 \pm 4.7	89.3 \pm 3.8	87.0 \pm 4.2
S_{oi} (%)	96.1 \pm 2.4	89.1 \pm 7.1	95.0 \pm 0.7	94.0 \pm 1.0
OOIP-S_{orwf} (mL)	44.0 \pm 5.7	45.8 \pm 5.1	47.3 \pm 2.1	43.0 \pm 4.2
S_{or} (%)	50.2 \pm 4.5	52.9 \pm 4.3	53.0 \pm 0.3	49.4 \pm 2.5
S_{ormf} (mL)	1.8 \pm 0.4	11.8 \pm 4.8	13.3 \pm 4.5	8.5 \pm 0.0
AOR (%)	4.0 \pm 0.4	25.9 \pm 10.6	27.9 \pm 8.5	19.9 \pm 1.9
<i>Arabian Light Oil</i>				
	Control	#309	#311	#573
OOIP (mL)	80.0 \pm 5.1	73.0 \pm 3.6	80.5 \pm 7.7	77.3 \pm 5.9
S_{oi} (%)	69.0 \pm 3.0	77.0 \pm 3.4	79.8 \pm 3.8	77.8 \pm 3.7
OOIP-S_{orwf} (mL)	30.0 \pm 5.7	24.3 \pm 1.7	26.8 \pm 2.4	24.0 \pm 1.2
S_{or} (%)	37.7 \pm 5.6	33.3 \pm 2.8	33.3 \pm 2.6	31.1 \pm 1.1
S_{ormf} (mL)	1.3 \pm 0.4	4.2 \pm 1.5	5.3 \pm 0.6	5.4 \pm 0.8
AOR (%)	4.1 \pm 2.2	17.1 \pm 5.7	19.6 \pm 1.2	22.4 \pm 2.1
<i>Heavy Crude Oil</i>				
	Control	#309	#311	#573
OOIP (mL)	91.8 \pm 5.1	93.0 \pm 1.4	91.0 \pm 1.4	90.0 \pm 2.8
S_{oi} (%)	98.9 \pm 1.8	98.4 \pm 2.2	95.8 \pm 0.1	96.8 \pm 1.4
OOIP-S_{orwf} (mL)	55.0 \pm 5.0	52.0 \pm 2.8	55.5 \pm 0.7	54.0 \pm 1.4
S_{or} (%)	59.7 \pm 5.3	55.9 \pm 2.2	61.0 \pm 0.2	60.0 \pm 0.3
S_{ormf} (mL)	0.5 \pm 0.0	8.0 \pm 0.0	9.5 \pm 0.7	9.5 \pm 0.7
AOR (%)	0.8 \pm 0.1	15.4 \pm 0.8	17.1 \pm 1.0	17.7 \pm 1.8

The pore volume of the columns was 96.1 ± 6.3 mL and the porosity 38.3 ± 2.4 %. The OOIP values, the amount of hydrocarbon removed during the water flooding process (S_{orwf}) and the amount of entrapped hydrocarbon ($OOIP - S_{orwf}$) varied depending on the hydrocarbon mixture used (Table 6.2). These differences are most probably due to the different viscosities of the oils.

When the different isolates were incubated for 14 days at 40°C into the columns together with appropriate nutrients (MSS medium), an additional hydrocarbon recovery was observed for all cases as compared to the controls. However, different outcomes were obtained depending on the hydrocarbon mixture used (Table 6.2).

The isolate #573 was the most effective when heating oil was used as hydrocarbon (25% of additional oil recovered (AOR) after incubation with microorganisms). However, in the experiments conducted with viscous paraffin, the highest AOR values (26-28%) were obtained with isolates #309 and #311. Regarding the experiments performed with crude oil, using Arabian Light, the highest recovery was obtained with the isolate #573 (22%), whereas with heavy crude oil similar oil recoveries were obtained with the three isolates (15-17%).

As shown in Table 6.3, enhanced oil recovery has been demonstrated by several authors with different hydrocarbon mixtures in sand-pack columns or cores after growing *in situ* different *Bacillus* strains which have been reported to produce surface-active compounds. The AOR values reported were between 5 and 22%. In some cases, the strains produced also extracellular polymers, which can contribute to enhance oil recovery as they increase the efficiency of the water-flooding operation⁴.

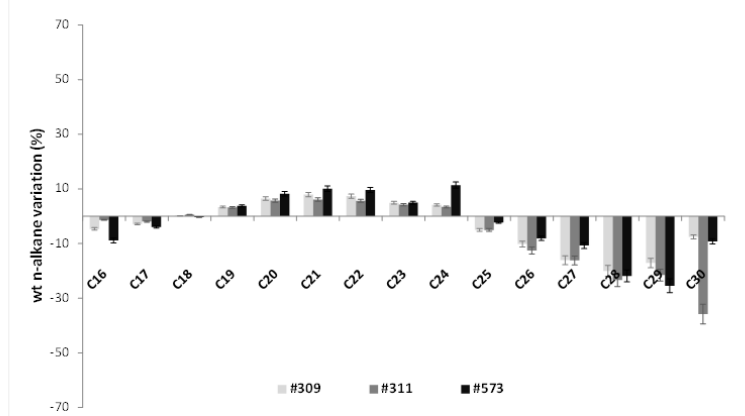
Table 6.3 Additional oil recoveries obtained with sand-pack column or core assays using different *Bacillus* isolates reported in the literature.

Microorganism	Substrate	AOR / (%)	Reference
<i>B. licheniformis</i> XDS1, XDS2 <i>Bacillus cereus</i> XDS3	Crude oil	4.8-6.9	She et al. ⁴
<i>B. licheniformis</i> BNP29 <i>Bacillus brevis</i>	Crude oil	9.3-22.1	Yakimov et al. ³
<i>Bacillus polymyxa</i> <i>B. licheniformis</i>	Paraffinic oil	18.0	Almeida et al. ⁵
<i>B. licheniformis</i> ACO1	Paraffin	21.7	Dastgheib et al. ⁶

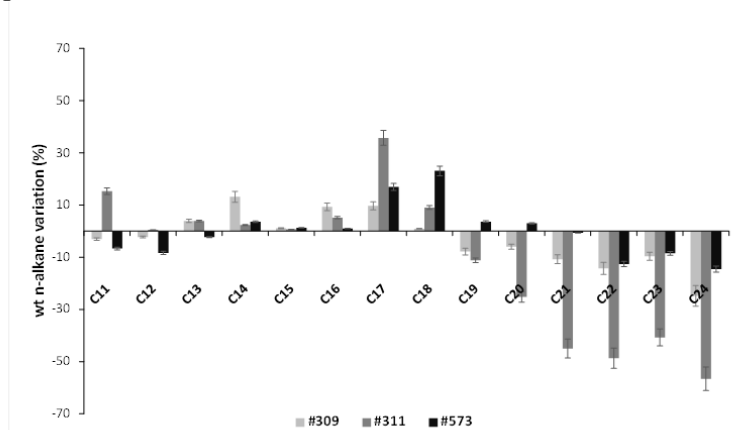
6.4.2. Evaluation of Hydrocarbon Degradation

In order to evaluate the degradation of the different hydrocarbon mixtures after being recovered from the sand-pack column assays performed with *B. subtilis* isolates #309, #311 and #573, the oils recovered were analyzed by GC and the relative degradation of each *n*-alkane was measured and compared with the oils recovered in the abiotic control columns (abiotic controls were subjected to the same incubation period and flood processes, to avoid the possible effect of the loss of hydrocarbons which may be retained in the system during the process). The oil recovered from the viscous paraffin experiments could not be analyzed by GC, since this hydrocarbon mixture was mainly composed of ramified hydrocarbons. The respective variations of relative weight fraction of each *n*-alkane present in the different oil samples, as compared with the control assays, are illustrated in Figure 6.3.

Heating Oil



Arabian Light



Heavy Crude Oil

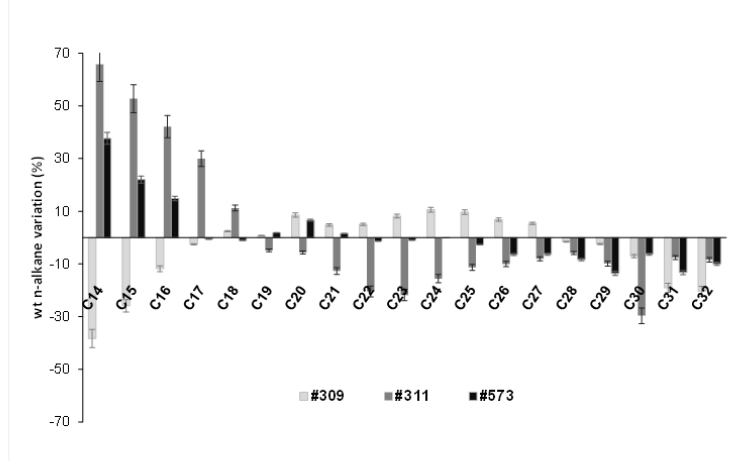


Figure 6.3 Variation of relative weight fraction of *n*-alkanes present in the different oil samples (Heating oil, Arabian Light Oil and Heavy Crude Oil) after *B. subtilis* isolates #309, #311 and #573 incubation for 14 days at 40°C in sand-pack columns. Results are compared to control columns and error bars represent the average error of three independent assays.

As observed by the GC analysis, the three hydrocarbon mixtures recovered after the treatment with the strains #309, #311 and #573 were degraded. It was also observed that all the *B. subtilis* strains preferentially degrade the higher *n*-alkane fractions of each hydrocarbon mixture.

Analyzing the results obtained with heating oil, it was found that all the isolates degraded the higher *n*-alkanes (C25-C30), causing an increase in *n*-alkanes in the C19-C24 range with respect to the original oil. The isolate #311 showed the highest degradation. The Arabian Light Oil was composed of *n*-alkanes up to C24. In this case, the oil recovered after the sand-pack column assays showed a reduction in *n*-alkanes higher than C19 for isolates #309 and #311; and higher than C21 for isolate #573. As in the case of heating oil, the highest degradation rate was obtained with the isolate #311. The GC analysis also shows an increase in the percentages of C17 and C18 *n*-alkanes when compared with the controls, perhaps due to the increase of the isoprenoids (pristane and phytane) compositions.

The study of *n*-alkanes variation of the heavy crude oil recovered shows that all the strains are able to degrade the hydrocarbon chains higher than C27. Among them, the isolate #311 exhibited the highest degradation rate with an increase in the relative weight fraction of *n*-alkanes lower than C19, and a decrease in the percentage of *n*-alkanes higher than C18. These results indicate that this isolate degraded the higher *n*-alkanes into lighter ones during the sand-pack column assays. Similarly, the isolate #573 shows the ability to degrade the long chain *n*-alkanes (>C25), thus increasing the percentage of *n*-alkanes with chains containing 20 carbons or less than 17 carbons, when compared with the control sample. On the other hand, the isolate #309 displays a different oil degradation profile, degrading the higher *n*-alkanes (>C28) as well as the lower ones (chains lower than 17 carbons).

Several microorganisms able to degrade heavy oil hydrocarbons have been described⁸, but only a few reports refer *Bacillus* species as oil degraders. *Bacillus thermoleovorans* strains with the ability of degrading *n*-alkanes up to C23 at 70°C were isolated by Kato et al.⁹. A thermophilic *Bacillus* strain that degraded long-chain (C15 to C36) rather than short-chain *n*-alkanes was isolated by Wang et al.¹⁰. *Bacillus* strains isolated from a Brazilian oil reservoir were found to degrade *n*-alkanes of Arabian Light and Marlin oil¹¹. Das and Mukherjee¹² reported that *B. subtilis* DM-04 preferentially degraded

crude oil *n*-alkanes between C14 and C30. She et al.⁵ studied three *Bacillus* strains isolated from an oil reservoir in the Daqing Oilfield (China) which degraded *n*-alkanes with chain lengths between C14 and C26. However, all these assays were performed under aerobic conditions. Recently, our group showed the ability of the three *B. subtilis* strains used in the current study to preferentially degrade the large alkyl chains of different paraffinic mixtures under anaerobic conditions². To the best of our knowledge, this is the first time that degradation of *n*-alkanes of different hydrocarbon mixtures in sand-pack columns using *Bacillus* species is demonstrated. The most common pathway, for *n*-alkanes degradation under aerobic conditions is via terminal oxidation, in which *n*-alkanes are first oxidized to the corresponding primary alcohol, which is further oxidized by alcohol and aldehyde dehydrogenases. Although the conditions existent in the sand-pack columns are not strictly anaerobic, the oxygen present must be quickly consumed by the microorganisms, so it is still not clear how the *n*-alkanes degradation can occur under oxygen limiting conditions. Several authors have reported in the last years the degradation of *n*-alkanes under anaerobic conditions using microorganisms, even strict anaerobic bacteria¹³⁻¹⁹. However, the pathways involved in this process have not yet been elucidated, although many researchers have suggested that nitrate can work as an alternative electron acceptor for hydrocarbon degradation under anaerobic conditions^{17, 19}.

The results herein obtained using different hydrocarbon mixtures (including heavy crude oil) were similar to the ones previously reported in liquid medium², thus suggesting that these isolates can be used to reduce the percentage of long chain *n*-alkanes of crude oil also in porous media (sand-pack column). The comparison between different hydrocarbons showed that even changing their *n*-alkanes composition, the different isolates maintained the ability to degrade preferentially the heavier oil fractions. Therefore, these results are very interesting in view of their application in MEOR processes in reservoirs containing heavy and paraffinic oils.

As a result of the degradation of high *n*-alkanes present in the crude oil into lighter ones, a reduction in oil viscosity is expected, with the subsequent improvement in the flow properties. The viscosity of the heavy crude oil recovered after the sand-pack column assays was measured, and the respective variation relatively to the control samples (oil recovered from the abiotic control columns) is presented in Table 6.4.

Table 6.4 Relative viscosities variation ($\Delta\eta$) (at 50°C) of heavy crude oil recovered from sand-pack column assays using *B. subtilis* isolates #309, #311 and #573 relatively to the control (the associated errors are lower than 6%).

<i>Bacillus subtilis</i> isolates			
	#309	#311	#573
$\Delta\eta$ / (%)	-21.4	-28.7	-32.0
η of the heavy crude oil (control) at 50°C / (mPa.s)	37.6		

The results presented in Table 6.4 show that the viscosity of heavy crude oil samples recovered after the sand-pack column assays was reduced when compared with the control samples. The viscosity of the crude oil decreased more than 20% in all the examples after the treatment with microorganisms, being the isolate #573 the one that promotes the highest viscosity reduction (32%).

The reduction in oil viscosity is in close agreement with the AOR values obtained for each microorganism, as a direct relationship was observed between the increase in oil recovered and the decrease of oil viscosity. These results are expectable since the reduction in oil viscosity enhances the oil fluidity in the reservoir.

6.4.3. Biosurfactant Production in Sand-pack Columns

The results obtained regarding biosurfactant production by the different microbial isolates in sand-pack columns are shown in Table 6.5. As it can be seen from those results, all the isolates produced biosurfactants in sand-pack columns with the different hydrocarbons tested. In the control columns, no biosurfactant production was observed. For all the cases evaluated, the lowest biosurfactant production was obtained with the isolate #573, whereas isolates #309 and #311 produced similar amounts of biosurfactant. Furthermore, for all isolates, the lowest biosurfactant production was obtained when using heating oil was used as hydrocarbon mixture.

Table 6.5 Biosurfactant concentrations (mg.L^{-1}) obtained in the mini-sand-pack column assays performed with the different isolates and hydrocarbon mixtures. Results represent the average of three independent experiments \pm standard deviation.

Hydrocarbon	#309	#311	#573
	Biosurfactant concentration / (mg.L^{-1})		
Heating Oil	20.1 ± 3.3	22.0 ± 1.6	8.2 ± 1.2
Viscous Paraffin	86.7 ± 1.8	85.2 ± 3.6	23.1 ± 2.7
Arabian Light Oil	82.2 ± 3.9	72.6 ± 2.9	24.7 ± 1.8
Heavy Crude Oil	85.0 ± 2.2	82.4 ± 3.1	30.7 ± 2.2

Biosurfactants, which reduce the interfacial tension between water-oil-sand and emulsify hydrocarbons, contributed to the enhanced oil recoveries observed. As reported by several authors, low biosurfactant concentrations (close to the *cmc*) are enough to mobilize entrapped oil²⁰⁻²², although their effect depends on the system studied. Even biosurfactant concentrations lower than the *cmc* can contribute to mobilize entrapped oil²³. The *cmc* values determined for the crude biosurfactants produced by isolates #309, #311 and #573 were 20, 20 and 30 mg.L^{-1} , respectively². Taking into account these values, for isolate #573 the amount of biosurfactant produced was lower than the *cmc* in all the cases (except for heavy crude oil). Likewise, biosurfactants production by isolates #309 and #311 with heating oil was below their *cmc*. However, with the other hydrocarbon mixtures, the concentration of biosurfactant produced was approximately four times the *cmc*. According to these results, it can be suggested that for all hydrocarbon mixtures evaluated, the biosurfactants produced contributed to enhance the oil recovery.

As previously mentioned, sand-pack columns provide a suitable approach to study the ability of injected microorganisms to increase oil recovery in reservoirs, because these models allow the simulation of oil recovery operations in oil fields. After the water flooding process, residual oil is trapped in the pores of the reservoir rocks. Biosurfactants produced by microorganisms reduce the interfacial tension at the oil-water-rock interface, thus reducing the capillary forces that prevent oil from moving through rock pores.

The increases in oil recovery observed in sand-pack columns can be due to several factors, and it is not straightforward to assign a percentage of recovery to a specific one. *B. subtilis* isolates used in this study produce biosurfactants which reduce surface tension and emulsify hydrocarbons, decreasing the interfacial tension at the oil-water interface. In sand-pack column assays performed with heating oil and viscous paraffin, the lowest recoveries were obtained with isolate #573. This isolate was also found to exhibit the lowest biosurfactant production with both hydrocarbons. However, with the other hydrocarbon mixtures studied, a direct relationship between biosurfactant production and the amount of oil recovered is not evident. Furthermore, the microorganisms herein used have the ability of degrading long-chain *n*-alkanes, reducing oil viscosity, which can contribute to enhance the mobilization of the hydrocarbon into the column. In sand-pack column assays performed with heavy crude oil, the highest recoveries were obtained with isolate #573, which was found to produce less biosurfactants than the other two isolates. However, this was the isolate that caused the highest reduction in crude oil viscosity. Indeed, as previously mentioned there are other factors that can contribute to the increase in oil recovery, such as the production of gases by the microbial isolates, increasing the pressure into the column; or the plugging of high permeability channels due to the accumulation of biomass, which redirects water to oil rich zones, thus increasing oil production.

In field assays, inoculation of mature oil wells with *Bacillus* strains resulted in biosurfactant production (20-90 mg.L⁻¹) and in an increase in oil production in the inoculated wells, as well as in a decrease in the water/oil ratio. These figures were maintained for a period of 40-60 days following the treatment, therefore constituting a cost effective process^{20, 24}.

6.5. Conclusion

B. subtilis isolates were evaluated for their oil-degrading and biosurfactant-production capabilities in sand-pack columns. For the first time, degradation of *n*-alkanes by *Bacillus* species in sand-pack columns under oxygen limiting conditions was demonstrated. Different hydrocarbon mixtures were studied and the isolates were able to increase the oil recovery in all cases, 6-25% for heating oil, 16-24% for viscous paraffin, 13-18% for Arabian light oil and 15-17% for heavy crude oil. *In situ* treatment of heavy and paraffinic oils with *B. subtilis* can thus contribute to improve the entrapped

oil fluidity and to reduce interfacial tension, increasing the additional oil recoveries. These isolates are good candidates for use in MEOR process and may be useful to recover residual oil from mature reservoirs.

6.6. References

1. Suthar, H., Hingurao, K., Desai, A., and Nerurkar, A., Evaluation of bioemulsifier mediated Microbial Enhanced Oil Recovery using sand pack column. *Journal of Microbiological Methods*, 2008. **75**(2): p. 225-230.
2. Gudiña, E.J., Pereira, J.F.B., Rodrigues, L.R., Coutinho, J.A.P., and Teixeira, J.A., Isolation and study of microorganisms from oil samples for application in Microbial Enhanced Oil Recovery. *International Biodeterioration & Biodegradation*, 2012. **68**: p. 56-64.
3. Pereira, J.F.B., Gudiña, E.J., Costa, R., Vitorino, R., Coutinho, J.A.P., Teixeira, J.A., and Rodrigues, L.R., Optimization and characterization of biosurfactant production by *Bacillus subtilis* isolates towards Microbial Enhanced Oil Recovery applications. *Fuel*, 2013. *in press*.
4. Yakimov, M.M., Amro, M.M., Bock, M., Boseker, K., Fredrickson, H.L., Kessel, D.G., and Timmis, K.N., The potential of *Bacillus licheniformis* strains for in situ enhanced oil recovery. *Journal of Petroleum Science and Engineering*, 1997. **18**(1-2): p. 147-160.
5. She, Y.H., Zhang, F., Xia, J.J., Kong, S.Q., Wang, Z.L., Shu, F.C., and Hu, J.M., Investigation of biosurfactant-producing Indigenous microorganisms that enhance residue oil recovery in an oil reservoir after polymer flooding. *Applied Biochemistry and Biotechnology*, 2011. **163**(2): p. 223-234.
6. Almeida, P.E., Moreira, R.S., Almeida, R.C.C., Guimarães, A.K., Carvalho, A.S., Quintella, C., Esperidia, M.C.A., and Taft, C., Selection and application of microorganisms to improve oil recovery. *Engineering in Life Sciences*, 2004. **4**(4): p. 319-325.
7. Dastgheib, S.M.M., Amoozegar, M.A., Elahi, E., Asad, S., and Banat, I.M., Bioemulsifier production by a halothermophilic *Bacillus* strain with potential applications in microbially enhanced oil recovery. *Biotechnology Letters*, 2008. **30**(2): p. 263-270.
8. Wentzel, A., Ellingsen, T.E., Kotlar, H.K., Zotchev, S.B., and Throne-Holst, M., Bacterial metabolism of long-chain n-alkanes. *Applied Microbiology and Biotechnology*, 2007. **76**(6): p. 1209-1221.
9. Kato, T., Haruki, M., Imanaka, T., Morikawa, M., and Kanaya, S., Isolation and characterization of long-chain-alkane degrading *Bacillus thermoleovorans* from deep subterranean petroleum reservoirs. *Journal of Bioscience and Bioengineering*, 2001. **91**(1): p. 64-70.
10. Wang, L., Tang, S., Wang, R.-L., Liu, M.-Z., Zangh, Y., Liang, F.-L., Feng, L., Isolation and characterization of a novel thermophilic *Bacillus* strain degrading long-chain n-alkanes. *Extremophile*, 2006. **10**: p. 347-356.
11. Cunha, C., Rosado, A., Sebastián, G., Seldin, L., and Weid, I., Oil biodegradation by *Bacillus* strains isolated from the rock of an oil reservoir located in a deep-water production basin in Brazil. *Applied Microbiology and Biotechnology*, 2006. **73**(4): p. 949-959.
12. Das, K. and Mukherjee, A.K., Crude petroleum-oil biodegradation efficiency of *Bacillus subtilis* and *Pseudomonas aeruginosa* strains isolated from a petroleum-oil contaminated soil from North-East India. *Bioresource Technology*, 2007. **98**(7): p. 1339-1345.
13. Youssef, N., Elshahed, M.S., and McInerney, M.J., Microbial processes in oil fields: culprits, problems, and opportunities. *Advances in Applied Microbiology*, 2009, **66**: p. 141-251.
14. Brown, L.R., Microbial enhanced oil recovery (MEOR). *Current Opinion in Microbiology*, 2010. **13**(3): p. 316-320.
15. Magot, M., Ollivier, B., and Patel, B.K.C., Microbiology of petroleum reservoirs. *Antonie Van Leeuwenhoek International Journal of General and Molecular Microbiology*, 2000. **77**(2): p. 103-116.
16. Aitken, C.M., Jones, D.M., and Larter, S.R., Anaerobic hydrocarbon biodegradation in deep subsurface oil reservoirs. *Nature*, 2004. **431**(7006): p. 291-294.
17. Castorena-Cortes, G., Roldan-Carrillo, T., Reyes-Avila, J., Zapata-Penasco, I., Mayol-Castillo, M., and Olguin-Lora, P., Coreflood assay using extremophile microorganisms for recovery of heavy oil in Mexican oil fields. *Journal of Bioscience and Bioengineering*, 2012. **114**(4): p. 440-445.

18. Silva, T.R., Verde, L.C.L., Santos Neto, E.V., and Oliveira, V.M., Diversity analyses of microbial communities in petroleum samples from Brazilian oil fields. *International Biodeterioration & Biodegradation*, 2012, doi:10.1016/j.ibiod.2012.05.005.
19. Zheng, C., Yu, L., Huang, L., Xiu, J., and Huang, Z., Investigation of a hydrocarbon-degrading strain, *Rhodococcus ruber* Z25, for the potential of microbial enhanced oil recovery. *Journal of Petroleum Science and Engineering*, 2012. **81**: p. 49-56.
20. Youssef, N., Simpson, D.R., Duncan, K.E., McInerney, M.J., Folmsbee, M., Fincher, T., and Knapp, R.M., In situ biosurfactant production by *Bacillus* strains injected into a limestone petroleum reservoir. *Applied and Environmental Microbiology*, 2007. **73**(4): p. 1239-1247.
21. Pornsunthorntawe, O., Arttaweeporn, N., Paisanjit, S., Somboonthanate, P., Abe, M., Rujiravanit, R., and Chavadej, S., Isolation and comparison of biosurfactants produced by *Bacillus subtilis* PT2 and *Pseudomonas aeruginosa* SP4 for microbial surfactant-enhanced oil recovery. *Biochemical Engineering Journal*, 2008. **42**(2): p. 172-179.
22. Amani, H., Sarrafzadeh, M.H., Haghghi, M., and Mehrnia, M.R., Comparative study of biosurfactant producing bacteria in MEOR applications. *Journal of Petroleum Science and Engineering*, 2010. **75**(1-2): p. 209-214.
23. Deshpande, S., Shiau, B.J., Wade, D., Sabatini, D.A., and Harwell, J.H., Surfactant selection for enhancing *ex situ* soil washing. *Water Research*, 1999. **33**(2): p. 351-360.
24. Youssef, N., Simpson, D.R., McInerney, M.J., and Duncan, K.E., In-situ lipopeptide biosurfactant production by *Bacillus* strains correlates with improved oil recovery in two oil wells approaching their economic limit of production. *International Biodeterioration & Biodegradation*, 2013, **81**: p. 127-132.

7. CONCLUSIONS AND FUTURE WORK

7.1. Conclusions

The first part of this thesis was aimed at the study of a bioprocess to be applied in petroleum industry in order to enhance the oil recovery of mature oilfields. Thus, from several isolates were obtained from 4 Brazilian crude oil samples and which were used to produce compounds with surface-emulsifying properties, as well as biodegradability properties. Several bacterial strains were recovered under aerobic and anaerobic conditions, belonging mostly to the *Bacillus subtilis* and *Pseudomonas aeruginosa* species. The biosurfactants produced by those isolates present some interesting properties, such as salt-, thermo- and pH-tolerance, and abilities to reduce the surface tension of water and to emulsify different sources of hydrocarbons. Therefore, the compounds produced by *P. aeruginosa* and *B.subtilis* isolates with best surface-activities and emulsifying properties were then characterized. The biosurfactants produced by two different *P.aeruginosa* strains were identified using MALDI-TOF and ESI-MS/MS as mixtures of mono-rhamnolipids and di-rhamnolipids. On the other hand, the chemical characterization of the compounds produced by three isolates of *Bacillus subtilis* shows that they are mainly constituted of surfactins with a heptapeptide moiety (L-Glu-L-Leu-D-Leu-L-Val-L-Asp-D-Leu-L-Leu) linked to a C₁₃, C₁₄ or C₁₅ hydroxy fatty acid chain.

The isolates with best results relatively to the biosurfactants production in the reservoir conditions (40°C and under anaerobic conditions) were *B.subtilis* #309, #311 and #573. Thus, after the optimization of these conditions in order to produce higher concentrations of biosurfactants, and higher *n*-alkanes biodegradation, some assays of MEOR in sand-pack columns were then performed using those isolates. The MEOR sand-pack columns tests were optimized with different hydrocarbon sources, and it was possible to obtain additional oil recoveries of 6-25% for heating oil, 16-24% for viscous paraffin, 13-18% for Arabian Light oil and 15-17% for heavy crude oil. In addition, those strains were able to reduce the percentage of heavier fractions of *n*-alkanes, and reduce the oils viscosities after the bacterial treatment in the sand-pack columns. In conclusion, these results, although conducted at a lab-scale, suggest that these isolates can be applied in the oil reservoirs in order to improve the entrapped oil fluidity, to reduce the interfacial water-oil-rock tension and consequently increase the recovery of residual crude oil from mature oilfields.

7.2. Future Work

The bioprocess described in part A of this thesis addresses a systematic study on the use of microorganisms as a new alternative to be applied in Enhanced Oil Recovery assays. The *B. subtilis* strains isolated and identified in this work show interesting properties at lab-scale suggesting that they can be promising strains to be used at a pilot-scale and in field pilot-studies. Besides all the studies here carried out, some new investigations should be considered and conducted in order to achieve a sustainable bioprocess at an industrial scale. In fact, some of these tests are already *in progress* and include:

- Study of consortia of several microorganisms to be applied at lab-scale tests;
- Optimization of sand-pack columns tests, using sand from the reservoir and testing heavy crude oils from other reservoirs;
- Study of MEOR tests at a pilot scale, aiming not only a scale-up, but also to simulate the reservoirs conditions, namely temperature and pressure.

Meanwhile, additional work at industrial scale must still be performed and should include:

- Study of a pilot field of MEOR in a Brazilian crude oil reservoir by an *in situ* treatment with the strains tested at lab- and pilot-scale. This study should comprise the technical design, scale-up optimization, evaluation and monitoring of its technical feasibility and the effectiveness of the isolated strains.

PART B

Antibiotics Purification Using Aqueous Biphasic Systems Composed of Ionic Liquids and Polymers

8. INTRODUCTION

8.1. General Context

The second part of this thesis aims at the development of new friendly and environmentally benign separation techniques, namely aqueous biphasic systems composed of ionic liquids and polymers, to replace the conventional liquid-liquid processes which require the use of volatile and hazardous organic solvents, to be employed in the separation and purification of antibiotics.

Antibiotics are chemical compounds that can be totally or partly synthesized by living microorganisms and that either inhibit the growth or kill other microorganisms. They are currently used worldwide for an effective control of bacteria levels in humans and animals. At a global level the antibiotic market value was of US \$42 billion (\approx 34 billion €) in 2009¹. In the past few years, a number of patents regarding the synthesis and applications of antibiotics and other drugs have expired falling into the public domain². The pharmaceutical industry is facing now the growth of generic drugs and there is a crucial need to minimize operational costs by optimizing the antibiotics' production and their purification steps. The high production cost associated to antibiotics results, to a large extent, from the downstream processing, *i.e.* from the extraction and purification steps. In this context, it is imperative to find and evaluate new extraction/purification techniques which could be cheap, reliable, and easily scaled-up by the biopharmaceutical companies.

Chromatographic techniques (particularly ion exchange chromatography), liquid-liquid or solid-liquid extractions are commonly used for the extraction and purification of antibiotics from the fermentation broth^{3,4}. Among these techniques, the most used is the liquid-liquid extraction which is typically carried out using organic solvents, namely ethyl acetate, acetonitrile and methanolic trichloroacetic acid (TCA)⁵. This type of liquid-liquid extraction is a useful technique of low cost and leads to a high purity level. However, these organics compounds present some drawbacks since they are volatile and hazardous to human health³. Aiming at developing not only cheaper, but also safer, biocompatible and sustainable extraction processes, the use of aqueous biphasic systems (ABS) can represent a viable option. ABS are liquid-liquid extraction systems, in which both phases are rich in water, and that can be used for the purification of a wide array of biomolecules by their selective partitioning between the coexisting phases.

8.2. Antibiotics

There are several classes of antibiotics, such as β -lactams, aminoglycosides, macrolides and tetracyclines (TCs). Tetracyclines are bacteriostatic antimicrobials produced by *Streptomyces aureofaciens* or *Streptomyces rimosus*. They are a broad-spectrum antibiotic since they can be used against Gram positive and Gram negative bacteria, *Coccidian*, *Trichomonas*, *Mycoplasma*, *Chlamydia* and *Rickettsia*. Tetracyclines inhibit the synthesis of bacterial proteins by binding to the small unit (30S) of bacterial ribosome while preventing the access of aminoacyl-tRNA to the acceptor site on the mRNA-ribosome complex⁶. Besides their antibiotic properties, tetracyclines also possess anti-inflammatory, anti-apoptotic and anti-neurodegenerative properties⁶. Due to all their benefits tetracyclines are currently added to animal feed in order to prevent diseases as well as a feed additive to accelerate the growth⁷. The TCs family comprises a wide range of compounds based on the naphthacene core with similar functional groups presenting only minor differences in structure (Figure 8.1). They were reported for the first time in 1948⁸.

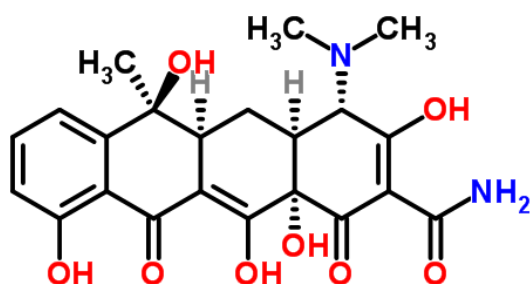


Figure 8.1 Chemical structure of tetracyclines.

8.3. Aqueous Biphasic Systems

Aqueous biphasic systems (ABS) are considered a low cost, gentler and biocompatible extraction technique since the extractive phases are mainly composed of water. In ABS, two aqueous phases coexist in equilibrium as a result of the dissolution, at appropriate concentrations, of suitable pairs of solutes (*e.g.* two polymers, or a polymer and a salt) in water. These systems have shown to be capable of maintaining the native conformation and biological activities of several biomolecules⁹⁻¹¹ and they have been satisfactorily tested, for over forty years, for the separation and purification of biological molecules, such as DNA, proteins, enzymes, alkaloids, antibiotics and blood cells,

among others¹²⁻²². These systems were also found valuable in other types of separations, such as the extraction of metal ions²³ and, on the whole, ABS strategies can be considered as a more sustainable alternative to many separations carried out by traditional volatile organic solvents.

ABS were first reported by Beijerinck in 1896, showing that the combination of gelatin, agar and water in certain proportions promoted the formation of two immiscible aqueous rich phases²⁴. Nonetheless, it was only in 1958 that Albertsson²⁵ reported the ability of ABS, formed by polyethylene glycol (PEG) and dextran, to separate biomolecules from aqueous media. PEGs are common polymers of low toxicity, negligible volatility, improved biodegradability and, unlike dextran, of low cost²⁶. Besides the polymer-polymer ABS, in 1986, Albertsson reported the possibility of forming an ABS using a polymer and an inorganic salt²⁷. Each phase of these systems becomes enriched in one of the two compounds creating thus two aqueous phases of different chemical and physical nature, which leads to the partitioning of biomolecules between them²⁸. The biomolecules partitioning among the phases results from surface dependent properties, and relies on the hydrophobicity, polarity and charge of the biomolecule, that further determines to which phase the biomolecule will preferentially migrate. More recently, other substances such as proteins, surfactants, sugars, or amino acids, have been used as solutes for ABS formation in combination with either polymers or salts²⁹⁻³³. Interestingly, the co-dissolution of two salts in water can also generate ABS³⁴⁻³⁸. In the latter case, one of the salts typically comprises one or both ions of high charge density (with water-ion interactions stronger than water-water interactions), and thus ions that are preferentially hydrated, while the other salt comprises low charge density ions (with water-ion interactions weaker than water-water interactions)^{39, 40}. The delocalization of charge in the ions of the latter salt inherently implies a lower melting temperature of the salt itself, which often fits within the category of ionic liquids. In this context, in the last decade, a large interest has been devoted to ABS composed of ionic liquids and salts, amino acids, carbohydrates or polymers, as alternative purification systems⁶⁶.

8.4. Ionic Liquids

By definition ionic liquids (ILs) are purely ionic materials with melting temperatures lower than 100 °C⁴¹. Unlike conventional solvents constituted by molecules, these are

formed by ions as typical salts; yet, a large range of ILs are liquid at room temperature allowing the mutual combination of the properties afforded by salts and organic solvents. ILs have gained a vast attention from both academia and industry since the late 1990s due to a series of interesting features that they often exhibit⁴². These interesting properties include an extremely low vapour pressure, melting temperatures around or even well below room temperature, wide liquid temperature range, good chemical and thermal stabilities, the ability to solvate a broad range of compounds, and a considerable degree of tailoring of their properties by a judicious selection of the constitutive ions^{56,57}. Therefore, ILs have been explored in several domains such as in catalysis⁴³⁻⁵⁰, analytical chemistry⁵¹, polymers technology⁵², nanotechnology⁵³, among others. However, one of the most promising areas involving ILs relies on their use as alternatives to the conventional volatile organic solvents actually used in separation and reaction processes⁵⁸⁻⁶⁰.

As stated before, the possibility of varying, in a large extent, the chemical structures of the ILs ions allows a high degree of tunability in their physical and chemical properties. Therefore, by virtue of their tunability, ILs cover essentially the whole hydrophilicity-hydrophobicity range^{61,62}. The estimated number of available anion/cation combinations is larger than one million⁶³. Between them, the most common cations are imidazolium, pyridinium, piperidinium, pyrrolidinium, ammonium, phosphonium, guanidinium and cholinium that can be further combined with a wide variety of organic or inorganic anions. In most cations the substituent groups are alkyl chains of variable size or structure that can also be functionalized. Figure 8.2 depicts some examples of the ILs chemical structures.

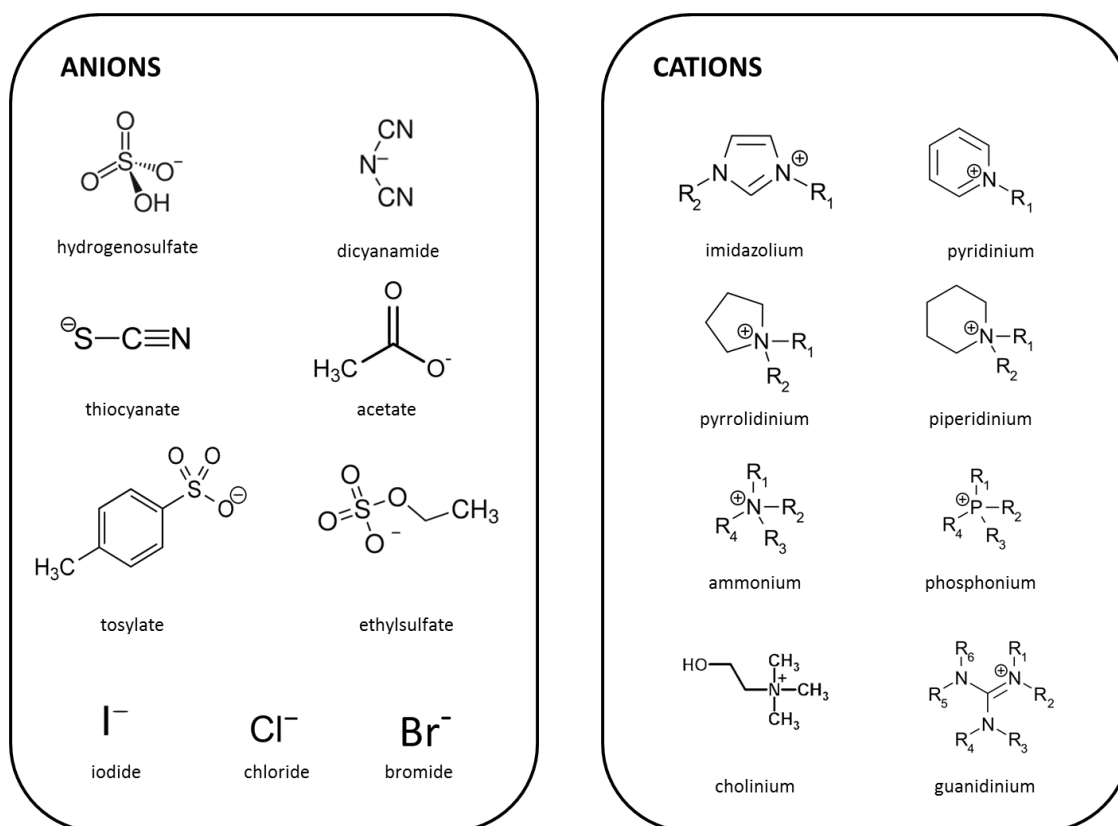


Figure 8.2 Common chemical structures of ionic liquids.

Based on the solubility of ILs in water, they can be divided into two main categories: hydrophobic (water immiscible) and hydrophilic (water miscible). In particular, the water solubility of ILs is mostly dependent on the constituting anion while the effects of the cation core, alkyl side chain length and functionalized groups have a lower impact although still significant^{40, 64-65}. The existence of hydrophilic ILs, *i.e.* ILs miscible with water in all composition range, allows their use as ABS-forming solutes. The first advances in this field were reported by Gutowski et al.³⁴ which showed that a hydrophilic IL can form an ABS when in contact with appropriate concentrations of a salting-out inorganic salt. Recently, it was further showed that a wide number of ILs, in presence of inorganic salts, could be used to prepare ABS for the extraction of added-value biomolecules^{36, 37, 66}. It was observed that, as for other applications, it is possible to control the ABS physicochemical properties by a wise combination of IL cations and/or anions, making thus possible the manipulation of the properties of the coexisting phases aiming at attaining enhanced selectivities and yields of the product recovery^{36, 37}. A number of works on the extraction of several biomolecules with IL-based ABS have

been reported within the last couple of years revealing that these novel platforms are by far more effective than the conventional polymer-polymer or polymer-salt ABS^{36,37,67-71}.

8.5. Work Aims and Motivation

A series of advantages can be associated to the use of ILs as phase forming components of ABS instead of the conventional high-melting inorganic salts. For example, salt crystallization problems can be fully avoided when using an IL which melts below room temperature. Even in the case of an IL melting above room temperature, the presence of water will largely preclude its solidification - the saturation levels of ILs in aqueous solutions are usually significantly higher than those observed with common inorganic salts^{72, 73}. Furthermore, the large number of available hydrophilic ILs may enable the customization of ABS with regard to specific separation or purification challenges.

The most critical issue associated to typical ABS composed of two polymers or a polymer and an inorganic salt is the limited range of polarities of their coexisting phases which have been preventing effective extractions, enhanced purification factors and high yields. Some approaches have been developed to overcome this limitation, such as the functionalization of polyethylene glycol (PEG)⁷⁷⁻⁸² or the inclusion of salt additives⁸³⁻⁸⁸. The first approach is focused on the modification of the chemical structure of PEGs, while the second is based on inclusion of an additional inorganic salt to manipulate the solute partitioning between the two liquid phases. Nevertheless, it should be remarked the high cost associated to the polymer functionalization limiting thus its application at an industrial scale.

The combined use of ILs in conventional polymer-based ABS can be foreseen as an alternative approach to enhance the tunability of these traditional systems⁸⁹. The first advances reporting the combination of polymers and ILs in aqueous media showed the presence of salting-in and salting-out effects of ILs over the polymer^{90, 91}. Recently, polymer-IL-based ABS were also shown, yet with a series of more hydrophobic polymers, polypropylene glycols (PPGs)⁹². However, ABS composed of ILs and less hydrophobic polymers, such as PEGs, have not been previously investigated maybe due to the difficulty in separating a more hydrophilic polymer from aqueous media.

In this work, and based on the tunability afforded by ILs, the main objective is to develop and characterize novel ABS composed of PEGs and ILs with the final goal of

applying them to the purification of antibiotics. Besides the direct application of these systems as extractive strategies, due to their novelty, they were initially characterized in terms of their formation capability and molecular level phenomena involved in the liquid-liquid demixing. As a first approach, in chapter 9, it was investigated the use of ILs as additives in typical PEG- Na_2SO_4 ABS aiming at tuning their intrinsic properties and extraction performance. For this purpose, it was studied the effect of several ILs through the ternary phase diagrams behaviour and on the extraction of L-tryptophan (used here as a model biomolecule). Then, in chapter 10, novel phase diagrams composed of PEGs and ILs were studied for the first time to replace the inorganic salts typically used. Distinct pairs of PEGs and ILs were addressed to better understand the liquid-liquid demixing phenomenon at a molecular level. In chapter 11, it is clear demonstrated the molecular level phenomena that regulate the phase separation in PEG-IL-based ABS by the experimental determination of the complete ternary phase diagrams at two temperatures coupled with molecular dynamics (MD) simulation calculations. In chapter 12, to properly confirm the vast hydrophobic-hydrophilic range afforded by IL-based ABS, it is shown the partitioning behaviour of three dyes used as molecular probes. In chapter 13, it was investigated the aptitude of PEG-IL-based ABS to be employed as extractive platforms making use of three alkaloids of different polarity (caffeine, nicotine and xhantine), in order to demonstrate that ILs are able to control the partitioning of different biomolecules.

Having in mind the final goal, the extraction of antibiotics from the fermentation broth, a new class of ABS composed of polymers and more benign and biocompatible cholinium-based ILs was finally studied - chapter 14. In this chapter the novel ternary phase diagrams composed of PEG, cholinium-based ILs and water are presented. To gather additional insights into the main mechanisms which rule the phase behaviour of PEG-IL-based ABS additional experiments were carried out, namely the solubility of ILs in PEGs, together with CONductor-like Screening MOdel for Real Solvents (COSMO-RS) prediction results. Finally, in the last chapter (chapter 15) it was carried out the extraction of tetracycline directly from a fermentation broth of *Streptomyces aureofaciens* employing ABS constituted by PEG 600 and cholinium-based salts.

The second part of this thesis was mainly developed in the Chemistry Department of University of Aveiro. I have been involved in the determination of all the experimental

data, with the exception of MD simulation calculations (in chapter 11) and COSMO-RS prediction data (shown in chapter 14).

8.6. References

1. Hamad, B., The antibiotics market. *Nature Reviews Drug Discovery*, 2010. **9**(9): p. 675-676.
2. Chandon, P., Innovative Marketing Strategies after Patent Expiry: The Case of GSK's Antibiotic Clamoxyl in France. *International Journal of Medical Marketing*, 2004. **4**(1): p. 65-73.
3. Fedeniuk, R.W., and Shand, P.J., Theory and methodology of antibiotic extraction from biomatrices. *Journal of Chromatography A*, 198. **812**(1-2): p. 3-15.
4. Ratledge, C. and Kristiansen, B., *Basic Biotechnology*. 2nd ed 2001: Cambridge University.
5. Anderson, C.R., Rupp, H.S., and Wu, W.-H., Complexities in tetracycline analysis—chemistry, matrix extraction, cleanup, and liquid chromatography. *Journal of Chromatography A*, 2005. **1075**(1-2): p. 23-32.
6. Griffin, M.O., Fricovsky, E., Ceballos, G., and Villarreal, F., Tetracyclines: a pleiotropic family of compounds with promising therapeutic properties. Review of the literature. *American Journal of Physiology - Cell Physiology*, 2010. **299**(3): p. C539-C548.
7. Ma, C.H., Wang, L., Yan, Y.S., Che, G.B., Yin, Y.S., Wang, R.Z., and Li, D.Y., Extraction of Tetracycline via Ionic Liquid Two-phase System. *Chemical Research in Chinese Universities*, 2009. **25**(6): p. 832-835.
8. Nelson, M.L. and Levy, S.B., The history of the tetracyclines. *Annals of the New York Academy of Sciences*, 2011. **1241**(1): p. 17-32.
9. Freire, M.G., Pereira, J.F.B., Francisco, M., Rodríguez, H., Rebelo, L.P.N., Rogers, R.D., and Coutinho, J.A.P., Insight into the Interactions That Control the Phase Behaviour of New Aqueous Biphasic Systems Composed of Polyethylene Glycol Polymers and Ionic Liquids. *Chemistry – A European Journal*, 2012. **18**(6): p. 1831-1839.
10. Liu, C.-Z., Wang, F., Stiles, A.R., and Guo, C., Ionic liquids for biofuel production: Opportunities and challenges. *Applied Energy*, 2012. **92**: p. 406-414.
11. Ventura, S.P.M., Sousa, S.G., Serafim, L.S., Lima, Á.S., Freire, M.G., and Coutinho, J.A.P., Ionic Liquid Based Aqueous Biphasic Systems with Controlled pH: The Ionic Liquid Cation Effect. *Journal of Chemical & Engineering Data*, 2011. **56**(11): p. 4253-4260.
12. Li, S.H., He, C.Y., Gao, F., Li, D.B., Chen, Z., Liu, H.W., Li, K., and Liu, F., Extraction and determination of morphine in compound liquorice using an aqueous two-phase system of poly(ethylene glycol)/K₂HPO₄ coupled with HPLC. *Talanta*, 2007. **71**(2): p. 784-789.
13. Bora, M.M., Borthakur, S., Rao, P.C., and Dutta, N.N., Aqueous two-phase partitioning of cephalosporin antibiotics: effect of solute chemical nature. *Separation and Purification Technology*, 2005. **45**(2): p. 153-156.
14. Chen, X.C., Xu, G.M., Li, X., Li, Z.J., and Ying, H.J., Purification of an alpha-amylase inhibitor in a polyethylene glycol fructose-1,6-bisphosphate trisodium salt aqueous two-phase system. *Process Biochemistry*, 2008. **43**(7): p. 765-768.
15. Bolognese, B., Nerli, B., and Pico, G.N., Application of the aqueous two-phase systems of ethylene and propylene oxide copolymer-maltodextrin for protein purification. *Journal of Chromatography B-Analytical Technologies in the Biomedical and Life Sciences*, 2005. **814**(2): p. 347-353.
16. Shanbhag, V.P. and Johansson, G., Specific Extraction of Human-Serum Albumin by Partition in Aqueous Biphasic Systems Containing Poly(Ethylene Glycol) Bound Ligand. *Biochemical and Biophysical Research Communications*, 1974. **61**(4): p. 1141-1146.
17. Johansson, G., Partition of Proteins and Microorganisms in Aqueous Biphasic Systems. *Molecular and Cellular Biochemistry*, 1974. **4**(3): p. 169-180.
18. Johansson, G., Comparison of 2 Aqueous Biphasic Systems Used for Partition of Biological-Material. *Journal of Chromatography*, 1978. **150**(1): p. 63-71.

19. Shanbhag, V.P. and Johansson, G., Interaction of Human-Serum Albumin with Fatty-Acids - Role of Anionic Group Studied by Affinity Partition. *European Journal of Biochemistry*, 1979. **93**(2): p. 363-367.
20. Backman, L., Binding of human carbonic anhydrase to human hemoglobin. *European Journal of Biochemistry*, 1981. **120**(2): p. 257-61.
21. Kessel, D., Some Determinants of Partitioning Behavior of Lymphoblasts in Aqueous Biphasic Systems. *Biochimica Et Biophysica Acta*, 1981. **678**(2): p. 245-249.
22. Welton, T., Ionic liquids in catalysis. *Coordination Chemistry Reviews*, 2004. **248**(21-24): p. 2459-2477.
23. Rogers, R.D., Bond, A.H., and Bauer, C.B., Metal-Ion Separations in Polyethylene Glycol-Based Aqueous Biphasic Systems. *Separation Science and Technology*, 1993. **28**(5): p. 1091-1126.
24. Beijerinck, M.W., *Centr-BI f. Bakter u. Parasitenk.* 1896. **2**: p. 698-699.
25. Albertsson, P.-Å., Partitioning of Proteins in Liquid Polymer-Polymer Two-Phase Systems. *Nature*, 1958. **182**: p. 709-711.
26. Pereira, J.F.B., Lima, A.S., Freire, M.G., and Coutinho, J.A.P., Ionic liquids as adjuvants for the tailored extraction of biomolecules in aqueous biphasic systems. *Green Chemistry*, 2010. **12**(9).
27. Albertsson, P.-Å., Partition of cell particles and macromolecules : separation and purification of biomolecules, cell organelles, membranes, and cells in aqueous polymer two-phase systems and their use in biochemical analysis and biotechnology. 3rd ed 1986, New York: Wiley. 346 p.
28. Alves, J.G.L.F., Chumpitaz, L.D.A., da Silva, L.H.M., Franco, T.T., and Meirelles, A.J.A., Partitioning of whey proteins, bovine serum albumin and porcine insulin in aqueous two-phase systems. *Journal of Chromatography B-Analytical Technologies in the Biomedical and Life Sciences*, 2000. **743**(1-2): p. 235-239.
29. Zeng, X., Quaye, J., and Osseo-Asare, K., Partition of hematite in the Triton X-100/Dextran aqueous biphasic system. *Colloids and Surfaces a-Physicochemical and Engineering Aspects*, 2004. **246**(1-3): p. 135-145.
30. Chen, Y., Zhang, S., Zhang, J., Zhang, Y., New type ionic-liquid-sugar aqueous biphasic system, 2006.
31. Franzreb, M., Becker, J.S., and Thomas, O.R.T., Protein separation with magnetic adsorbents in micellar aqueous two-phase systems. *Separation and Purification Technology*, 2009. **65**(1): p. 46-53.
32. Spyropoulos, F., Portschi, A., and Norton, I.T., Effect of sucrose on the phase and flow behaviour of polysaccharide/protein aqueous two-phase systems. *Food Hydrocolloids*, 2010. **24**(2-3): p. 217-226.
33. Coutinho, J.A.P., Dominguez-Perez, M., Tome, L.I.N., Freire, M.G., Marrucho, I.M., and Cabeza, O., (Extraction of biomolecules using) aqueous biphasic systems formed by ionic liquids and aminoacids. *Separation and Purification Technology*, 2010. **72**(1): p. 85-91.
34. Gutowski, K.E., Broker, G.A., Willauer, H.D., Huddleston, J.G., Swatloski, R.P., Holbrey, J.D., and Rogers, R.D., Controlling the aqueous miscibility of ionic liquids: Aqueous biphasic systems of water-miscible ionic liquids and water-structuring salts for recycle, metathesis, and separations. *Journal of the American Chemical Society*, 2003. **125**(22): p. 6632-6633.
35. Bridges, N.J., Gutowski, K.E., and Rogers, R.D., Investigation of aqueous biphasic systems formed from solutions of chaotropic salts with kosmotropic salts (salt-salt ABS). *Green Chemistry*, 2007. **9**(2): p. 177-183.
36. Neves, C.M.S.S., Ventura, S.P.M., Freire, M.G., Marrucho, I.M., and Coutinho, J.A.P., Evaluation of Cation Influence on the Formation and Extraction Capability of Ionic-Liquid-Based Aqueous Biphasic Systems. *Journal of Physical Chemistry B*, 2009. **113**(15): p. 5194-5199.

37. Ventura, S.P.M., Neves, C.M.S.S., Freire, M.G., Marrucho, I.M., Oliveira, J., and Coutinho, J.A.P., Evaluation of Anion Influence on the Formation and Extraction Capacity of Ionic-Liquid-Based Aqueous Biphasic Systems. *Journal of Physical Chemistry B*, 2009. **113**(27): p. 9304-9310.
38. Coutinho, J.A.P., Louros, C.L.S., Claudio, A.F.M., Neves, C.M.S.S., Freire, M.G., Marrucho, I.M., and Pauly, J., Extraction of Biomolecules Using Phosphonium-Based Ionic Liquids + K(3)PO(4) Aqueous Biphasic Systems. *International Journal of Molecular Sciences*, 2010. **11**(4): p. 1777-1791.
39. Coutinho, J.A.P., Freire, M.G., Neves, C.M.S.S., Silva, A.M.S., Santos, L.M.N.B.F., Marrucho, I.M., Rebelo, L.P.N., Shah, J.K., and Maginn, E.J., (1)H NMR and Molecular Dynamics Evidence for an Unexpected Interaction on the Origin of Salting-In/Salting-Out Phenomena. *Journal of Physical Chemistry B*, 2010. **114**(5): p. 2004-2014.
40. Coutinho, J.A.P., Freire, M.G., Carvalho, P.J., Silva, A.M.S., Santos, L.M.N.B.F., Rebelo, L.P.N., and Marrucho, I.M., Ion Specific Effects on the Mutual Solubilities of Water and Hydrophobic Ionic Liquids. *Journal of Physical Chemistry B*, 2009. **113**(1): p. 202-211.
41. Wilkes, J.S., A short history of ionic liquids - from molten salts to neoteric solvents. *Green Chemistry*, 2002. **4**(2): p. 73-80.
42. Afonso, C.A.M., Kulkarni, P.S., Branco, L.C., Crespo, J.G., Nunes, M.C., and Raymundo, A., Comparison of physicochemical properties of new ionic liquids based on imidazolium, quaternary ammonium, and guanidinium cations. *Chemistry-a European Journal*, 2007. **13**(30): p. 8478-8488.
43. Dupont, J., de Souza, R.F., and Suarez, P.A.Z., Ionic Liquid (Molten Salt) Phase Organometallic Catalysis. *Chemical Reviews*, 2002. **102**(10): p. 3667-3692.
44. Earle, M.J. and Seddon, K.R., Ionic liquids. Green solvents for the future. *Pure Appl. Chem.*, 2000. **72**: p. 1391-1398.
45. Gordon, C.M., New developments in catalysis using ionic liquids. *Applied Catalysis A: General*, 2001. **222**(1-2): p. 101-117.
46. Olivier-Bourbigou, H. and Magna, L., Ionic liquids: perspectives for organic and catalytic reactions. *J. Mol. Catal. A Chem*, 2002. **182**: p. 419-437.
47. Seddon, K.R., Ionic Liquids for Clean Technology. *Journal of Chemical Technology & Biotechnology*, 1997. **68**(4): p. 351-356.
48. Sheldon, R., Catalytic reactions in ionic liquids. *Chem. Commun.*, 2001: p. 2399-2407.
49. Welton, T., Room-temperature ionic liquids. Solvents for synthesis and catalysis. *Chem. Rev.*, 1999. **99**: p. 2071-2083.
50. Zhao, D., Wu, M., Kou, Y., and Min, E., Ionic liquids: applications in catalysis. *Catalysis Today*, 2002. **74**(1-2): p. 157-189.
51. Koel, M., Ionic Liquids in Chemical Analysis. *Critical Reviews in Analytical Chemistry*, 2005. **35**(3): p. 177 - 192.
52. Kubisa, P., Ionic liquids in the synthesis and modification of polymers. *Journal of Polymer Science Part A: Polymer Chemistry*, 2005. **43**(20): p. 4675-4683.
53. Antonietti, M., Kuang, D., Smarsly, B., and Zhou, Y., Ionic Liquids for the Convenient Synthesis of Functional Nanoparticles and Other Inorganic Nanostructures. *Angewandte Chemie International Edition*, 2004. **43**(38): p. 4988-4992.
54. Dietz, M.L., Ionic Liquids as Extraction Solvents: Where do we Stand? *Sep. Sci. Technol.*, 2006. **41**: p. 2047-2063.
55. Han, D. and Row, K.H., Recent Applications of Ionic Liquids in Separation Technology Molecules, 2010. **15**: p. 2405-2426.
56. Earle, M.J. and Seddon, K.R., Ionic liquids. Green solvents for the future. *Pure and Applied Chemistry*, 2000. **72**(7): p. 1391-1398.
57. Brennecke, J.F. and Maginn, E.J., Ionic liquids: Innovative fluids for chemical processing. *Aiche Journal*, 2001. **47**(11): p. 2384-2389.

58. Handy, S.T., Greener solvents: Room temperature ionic liquids from biorenewable sources. *Chemistry-a European Journal*, 2003. **9**(13): p. 2938-2944.
59. Herrmann, W.A. and Bohm, V.P.W., Coordination chemistry and mechanisms of metal-catalyzed C-C coupling reactions, part 12 - Nonaqueous ionic liquids: Superior reaction media for the catalytic Heck-vinylation of chloroarenes. *Chemistry-a European Journal*, 2000. **6**(6): p. 1017-1025.
60. Welton, T., Room-temperature ionic liquids. *Solvents for synthesis and catalysis*. *Chemical Reviews*, 1999. **99**(8): p. 2071-2083.
61. Huddleston, J.G., Visser, A.E., Reichert, W.M., Willauer, H.D., Broker, G.A., and Rogers, R.D., Characterization and comparison of hydrophilic and hydrophobic room temperature ionic liquids incorporating the imidazolium cation. *Green Chemistry*, 2001. **3**(4): p. 156-164.
62. Freemantle, M., *An Introduction to ionic liquids* 2010, Cambridge, UK: RSC Pub. xiv, 281 p.
63. Holbrey, J.D., Reichert, W.M., Swatloski, R.P., Broker, G.A., Pitner, W.R., Seddon, K.R., and Rogers, R.D., Efficient, halide free synthesis of new, low cost ionic liquids: 1,3-dialkylimidazolium salts containing methyl- and ethyl-sulfate anions. *Green Chem.*, 2002. **4**(407-413).
64. Freire, M. G., Neves, C.M.S.S., Ventura, S.P.M., Pratas, M.J., Marrucho, I. M., Oliveira, J., Coutinho, J.A.P. and Fernandes, A.M., Solubility of non-aromatic ionic liquids in water and correlation using a QSPR approach. *Fluid Phase Equilibria*, 2010. **294**(1-2): p. 234-240.
65. Freire, M.G., Neves, C.M.S.S., Shimizu, K., Bernardes, C.E.S., Marrucho, I.M., Coutinho, J.A.P., Canongia Lopes, J.N., and Rebelo, L.P.N., Mutual Solubility of Water and Structural/Positional Isomers of N-Alkylpyridinium-Based Ionic Liquids. *Journal of Physical Chemistry B*, 2010. **114** (48): p. 15925-15934.
66. Freire, M.G., Cláudio, A.F.M., Araújo, J.M.M., Coutinho, J.A.P., Marrucho, I.M., Canongia Lopes, J.N., and Rebelo, L.P.N., Aqueous Biphasic Systems: A boost brought about by using ionic liquids. *Chemical Society Reviews*, 2012. **41**(14): p. 4966-4995.
67. Dreyer, S. and Kragl, U., Ionic liquids for aqueous two-phase extraction and stabilization of enzymes. *Biotechnology and Bioengineering*, 2008. **99**(6): p. 1416-1424.
68. Li, S., He, C., Liu, H., Li, K., and Liu, F., Ionic liquid-based aqueous two-phase system, a sample pretreatment procedure prior to high-performance liquid chromatography of opium alkaloids. *Journal of Chromatography B*, 2005. **826**(1-2): p. 58-62.
69. He, C., Li, S., Liu, H., Li, K., and Liu, F., Extraction of testosterone and epitestosterone in human urine using aqueous two-phase systems of ionic liquid and salt. *Journal of Chromatography A*, 2005. **1082**(2): p. 143-149.
70. Najdanovic-Visak, V., Rodriguez, A., Visak, Z.P., Rosa, J.N., Afonso, C.A.M., da Ponte, M.N., and Rebelo, L.P.N., Co-solvent effects in LLE of 1-hydroxyethyl-3-methylimidazolium based ionic liquids plus 2-propanol plus dichloromethane or 1,2-dichloroethane. *Fluid Phase Equilibria*, 2007. **254**(1-2): p. 35-41.
71. Soto, A., Arce, A., and Khoshkbarchi, M.K., Partitioning of antibiotics in a two-liquid phase system formed by water and a room temperature ionic liquid. *Separation and Purification Technology*, 2005. **44**(3): p. 242-246.
72. Domanska, U., Krolkowski, M., Pobudkowska, A., and Letcher, T.M., Phase Equilibria Study of the Binary Systems (N-Butyl-4-methylpyridinium Tosylate Ionic Liquid plus Organic Solvent, or Water). *Journal of Chemical and Engineering Data*, 2009. **54**(5): p. 1435-1441.
73. Domanska, U., Physico-Chemical Properties and Phase Behaviour of Pyrrolidinium-Based Ionic Liquids. *International Journal of Molecular Sciences*, 2010. **11**(4): p. 1825-1841.
74. Mei, L.H., Lin, D.Q., Zhu, Z.Q., and Han, Z.X., Densities and Viscosities of Polyethylene-Glycol Plus Salt Plus Water-Systems at 20 Degrees-C. *Journal of Chemical and Engineering Data*, 1995. **40**(6): p. 1168-1171.
75. Perumalsamy, M. and Murugesan, T., Phase Compositions, Molar Mass, and Temperature Effect on Densities, Viscosities, and Liquid-Liquid Equilibrium of Polyethylene Glycol and Salt-Based Aqueous Two-Phase Systems. *Journal of Chemical and Engineering Data*, 2009. **54**(4): p. 1359-1366.

76. Coutinho, J.A.P., Claudio, A.F.M., Freire, M.G., Freire, C.S.R., and Silvestre, A.J.D., Extraction of vanillin using ionic-liquid-based aqueous two-phase systems. *Separation and Purification Technology*, 2010. **75**(1): p. 39-47.
77. Rosa, P.A.J., Azevedo, A.M., Ferreira, I.F., de Vries, J., Korporaal, R., Verhoef, H.J., Visser, T.J., and Aires-Barros, M.R., Affinity partitioning of human antibodies in aqueous two-phase systems. *Journal of Chromatography A*, 2007. **1162**(1): p. 103-113.
78. Zalipsky, S., Functionalized Poly(Ethylene Glycol) for Preparation of Biologically Relevant Conjugates. *Bioconjugate Chemistry*, 1995. **6**(2): p. 150-165.
79. Li, J. and Kao, W.J., Synthesis of polyethylene glycol (PEG) derivatives and PEGylated-peptide block copolymer conjugates. *Biomacromolecules*, 2003. **4**(4): p. 1055-1067.
80. Azevedo, A.M., Rosa, P.A.J., Ferreira, I.F., Pisco, A.M.M.O., de Vries, J., Korporaal, R., Visser, T.J., and Aires-Barros, M.R., Affinity-enhanced purification of human antibodies by aqueous two-phase extraction. *Separation and Purification Technology*, 2009. **65**(1): p. 31-39.
81. Jiang, Y.Y., Xia, H.S., Yu, J., Guo, C., and Liu, H.Z., Hydrophobic ionic liquids-assisted polymer recovery during penicillin extraction in aqueous two-phase system. *Chemical Engineering Journal*, 2009. **147**(1): p. 22-26.
82. Wu, C., Peng, J.J., Li, J.Y., Bai, Y., Hu, Y.Q., and Lai, G.Q., Synthesis of poly(ethylene glycol) (PEG) functionalized ionic liquids and the application to hydrosilylation. *Catalysis Communications*, 2008. **10**(2): p. 248-250.
83. Hachem, F., Andrews, B.A., and Asenjo, J.A., Hydrophobic partitioning of proteins in aqueous two-phase systems. *Enzyme and Microbial Technology*, 1996. **19**(7): p. 507-517.
84. Ferreira, L.A. and Teixeira, J.A., Salt effect on the (polyethylene glycol 8000+sodium sulfate) aqueous two-phase system: Relative hydrophobicity of the equilibrium phases. *Journal of Chemical Thermodynamics*, 2011. **43**(8): p. 1299-1304.
85. Marcos, J.C., Trindade, I.P., Diogo, M.M., and Prazeres, D.M.F., Purification of plasmid DNA vectors by aqueous two-phase extraction and hydrophobic interaction chromatography. *Journal of Chromatography A*, 2005. **1082**(2): p. 176-184.
86. Aires-Barros, M.R., Azevedo, A.M., Rosa, P.A.J., and Ferreira, I.F., Optimisation of aqueous two-phase extraction of human antibodies. *Journal of Biotechnology*, 2007. **132**(2): p. 209-217.
87. Aires-Barros, M.R., Rosa, P.A.J., Azevedo, A.M., Sommerfeld, S., Mutter, M., and Backer, W., Application of aqueous two-phase systems to antibody purification: A multi-stage approach. *Journal of Biotechnology*, 2009. **139**(4): p. 306-313.
88. Aires-Barros, M.R., Rosa, P.A.J., and Azevedo, A.M., Application of central composite design to the optimisation of aqueous two-phase extraction of human antibodies. *Journal of Chromatography A*, 2007. **1141**(1): p. 50-60.
89. Rogers, R.D. and Rodriguez, H., Liquid mixtures of ionic liquids and polymers as solvent systems. *Fluid Phase Equilibria*, 2010. **294**(1-2): p. 7-14.
90. Lopes, J.N.C., Visak, Z.P., and Rebelo, L.P.N., Ionic liquids in polyethylene glycol aqueous solutions: Salting-in and salting-out effects. *Monatshefte Fur Chemie*, 2007. **138**(11): p. 1153-1157.
91. Lopes, J.N.C. and Rebelo, L.P.N., Salting effects in ionic liquid aqueous solutions - From aqueous biphasic system formation to salting agent precipitation. *Chimica Oggi-Chemistry Today*, 2007. **25**(6): p. 37-39.
92. Wang, J.J., Wu, C.Z., Pei, Y.C., Wang, H.Y., and Li, Z.Y., Salting-Out Effect of Ionic Liquids on Poly(propylene glycol) (PPG): Formation of PPG plus Ionic Liquid Aqueous Two-Phase Systems. *Journal of Chemical and Engineering Data*, 2010. **55**(11): p. 5004-5008.

9. PAPER 6

Ionic Liquids as Adjuvants for the Tailored Extraction of Biomolecules in Aqueous Biphasic Systems

Green Chemistry, 12 (2010) 1661-1669.

9.1. Abstract

The potential use of ionic liquids (ILs) as adjuvants in typical polymer-salt aqueous systems for the separation and purification of vital biomolecules is investigated. An innovative study involving the addition of various imidazolium-based ILs to conventional polyethylene glycol (PEG)/inorganic salt aqueous biphasic systems (ABS), aiming at controlling their phase behaviour and extraction capability for L-tryptophan, is carried out here. For this purpose, phase diagrams and respective tie-lines for PEG 600/ Na_2SO_4 ABS with the addition of small quantities of IL were established. In addition, the partition coefficients of L-tryptophan were determined in those systems. The results obtained indicate that the addition of small amounts of IL to the typical PEG/inorganic salt aqueous systems could largely control the extraction efficiency for L-tryptophan, and that efficiency depends on the IL employed. Salting-in inducing ILs enhance the partition coefficient of L-tryptophan for the PEG-rich phase while salting-out inducing ILs decrease the partitioning of the amino acid. These results are an interesting advance in biotechnological separation processes regarding the extraction of biomolecules that could be used instead of the usual approach of PEG functionalization.

Keywords: Ionic Liquids; Aqueous Biphasic Systems; L-tryptophan; Phase Diagrams; Partition Coefficients.

9.2. Introduction

Polyethylene glycols (PEGs) are a class of polymers widely used in industrial processes, especially due to their high biodegradability, low toxicity, low volatility, low melting temperature, large water solubility and low cost. These attractive properties have prompted the use of PEGs in various processes, one of the most interesting being their use as phase forming components of aqueous biphasic systems (ABS)¹.

ABS typically formed by polymer and inorganic salt solutions have several advantages over conventional polymer-polymer counterparts², such as low interfacial tension, lower viscosity, fast and high phase separation rates and low cost, which makes them more viable for downstream processing. However, the hydrophilic nature of PEG limits the applicability of this technique when the goal is to extract hydrophobic biomolecules. To overcome this limitation one possible approach used by some researchers has been the functionalization of PEG^{3, 4}. Rosa et al.⁵ and Azevedo et al.⁶ applied the

functionalization of PEG to the purification of human immunoglobulin while Jiang *et al.*⁷ have used an ionic liquid functionalized PEG for the extraction of penicillin. This last approach⁷ allowed the modification of the polymer-rich phase hydrophilicity enhancing the recovery of penicillin. Moreover, Wu *et al.*⁸ have recently shown that PEG can be functionalized with ionic liquids for enhanced extraction and polymer recovery. In summary, these works⁵⁻⁸ aimed at tuning the properties of PEG through the modification of its chemical structure.

Aimed at developing an alternative technique for the modification of the PEG-rich phase characteristics, a new approach making use of ILs is here proposed. Instead of the PEG functionalization, the IL is used here as a promoter or adjuvant of ABS formation aimed at tuning the intrinsic properties of the aqueous phases. The formation of PEG-sodium sulphate ABS, and their phase behaviour, in the presence of various ILs, is investigated. Moreover, the effect of adding distinct ILs as adjuvants for the extraction ability of archetypal ABS is evaluated here using L-tryptophan as a model biomolecule. Influences of the IL and inorganic salt concentrations, temperature, and pH of the medium were discussed throughout the partition coefficients obtained.

9.3. Experimental Section

9.3.1. Materials

Na₂SO₄ was purchased from LabSolve (purity > 99.8 wt%), and L-tryptophan (purity > 99.0 wt%) and polyethylene glycol 600 (PEG 600) were provided by Fluka. All reagents were of analytical grade. The following ionic liquids (ILs) were acquired at Iolitec: imidazolium chloride, [im]Cl; 1-methylimidazolium chloride, [C₁im]Cl; 1-ethyl-3-methylimidazolium chloride, [C₂mim]Cl; 1-butyl-3-methylimidazolium chloride, [C₄mim]Cl; 1-butyl-2,3-dimethylimidazolium chloride, [C₄C₁mim]Cl; 1-hydroxyethyl-3-methylimidazolium chloride, [OHC₂mim]Cl; 1-allyl-3-methylimidazolium chloride, [amim]Cl; 1-benzyl-3-methylimidazolium chloride, [C₇H₇mim]Cl; 1-butyl-3-methylimidazolium acetate, [C₄mim][CH₃CO₂]; 1-butyl-3-methylimidazolium methylsulphate, [C₄mim][MeSO₄]; 1-butyl-3-methylimidazolium hydrogensulphate, [C₄mim][HSO₄]. Figure 9.1 shows the chemical structure of the studied ILs. The ILs were dried under constant agitation at vacuum and moderate temperature (353 K), for a minimum of 48 h, to reduce the content of water and volatile compounds to negligible

values. After this procedure, the purity of the ILs was further checked by ^1H and ^{13}C NMR spectra. A weight fraction purity above 99 % was observed for all IL samples. The water used was double distilled, passed across a reverse osmosis system and further treated with a Milli-Q plus 185 water purification apparatus.

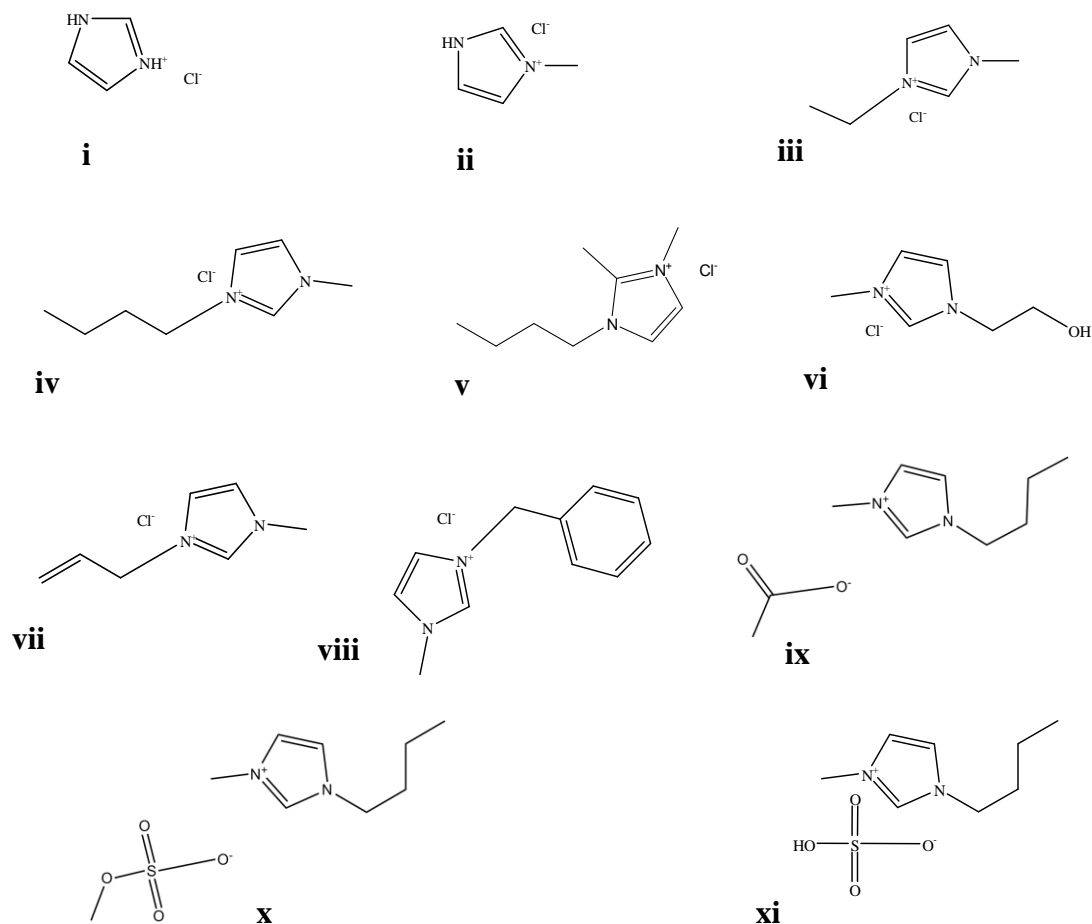


Figure 9.1 Chemical structures of the studied ILs: **(i)** [im]Cl; **(ii)** [C₁im]Cl; **(iii)** [C₂mim]Cl; **(iv)** [C₄mim]Cl; **(v)** [C₄C₁mim]Cl; **(vi)** [OHC₂mim]Cl; **(vii)** [amim]Cl; **(viii)** [C₇H₇mim]Cl; **(ix)** [C₄mim][CH₃CO₂]; **(x)** [C₄mim][MeSO₄]; **(xi)** [C₄mim][HSO₄].

9.3.2. Methods

9.3.2.1. Phase Diagrams and Tie-Lines

Aqueous solutions of Na₂SO₄ at 20 wt% + 5 wt% of each IL, aqueous solutions of PEG 600 at 40 wt% + 5 wt% of the same IL, and aqueous solutions of 5 wt% of IL were prepared and used for the determination of the binodal curves. The phase diagrams were determined through the cloud point titration method at 298 (± 1) K and atmospheric

pressure. The experimental procedure adopted is described in detail elsewhere^{9, 10}. The systems composition was determined by the weight quantification of all components added within an uncertainty of $\pm 10^{-5}$ g.

The tie-lines were determined by a gravimetric method described by Merchuck et al.³⁵. For the TLs' determination a mixture at the biphasic region was prepared, vigorously stirred and allowed to reach equilibrium, by the separation of both phases, for 12 h at 298 K using small ampoules (*ca.* 10 cm³) especially designed for the purpose^{9, 10}. After the equilibration step, the top and bottom phases were separated, recovered and weighed. Each individual TL was determined by the application of the lever arm rule to the relationship between the top mass phase composition and the overall system composition. For that purpose the experimental binodal curves were correlated using equation 9.1¹¹.

$$Y = A \exp\left[\left(BX^{0.5}\right) - \left(CX^3\right)\right] \quad \text{Equation 9.1}$$

where Y and X are, respectively, the PEG and inorganic salt weight percentages, and A , B and C are constants obtained by the regression of the experimental data.

The determination of the TLs was accomplished by solving the following system of four equations (equations. (9.2) to (9.5)) for the unknown values of Y_T , Y_B , X_T and X_B .

$$Y_T = A \exp\left[\left(BX_T^{0.5}\right) - \left(CX_T^3\right)\right] \quad \text{Equation 9.2}$$

$$Y_B = A \exp\left[\left(BX_B^{0.5}\right) - \left(CX_B^3\right)\right] \quad \text{Equation 9.3}$$

$$X_T = \frac{Y_M}{\alpha'} - \left(\frac{1 - \alpha'}{\alpha'}\right) Y_B \quad \text{Equation 9.4}$$

$$X_B = \frac{X_M}{\alpha'} - \left(\frac{1 - \alpha'}{\alpha'}\right) X_B \quad \text{Equation 9.5}$$

where Y and X are respectively, the PEG and inorganic salt weight percentages, and the subscript letters T , B and M represent the top, the bottom and the mixture phase, respectively. The parameter α' is the ratio between the top and the total mass of the mixture.

The tie-lines length (TLL) was determined accordingly to equation 9.6:

$$\text{TLL} = \sqrt{(X_T - X_B)^2 + (Y_T - Y_B)^2} \quad \text{Equation 9.6}$$

9.3.2.2. *Partitioning of L-tryptophan and ILs*

A mixture point into the biphasic region was selected and used to evaluate the L-tryptophan partitioning. An aqueous solution of L-tryptophan at 2.34 g.dm^{-3} was used in the water content composition. After 5 min of gently stirring, the biphasic system was allowed to equilibrate for 12 h immersed in a refrigerated water bath, Julabo F34, at each temperature of interest (278.15 K, 288.15 K, 298.15 K, 308.15 K and 318.15 K) within an uncertainty of $\pm 0.01 \text{ K}$. After that period of equilibration the phases were clear and the interface well defined. The phases were thus carefully separated for further quantification of the amino acid and IL.

9.3.2.3. *Amino acid and ILs Quantification*

The L-tryptophan and IL concentrations, in the top and bottom phases, were determined using an UV spectrophotometer (SHIMADZU UV-1700), at a wavelength of 279 nm and 211 nm, respectively. Calibration curves were established for each compound. Possible interferences of the PEG 600, IL and Na_2SO_4 in the L-tryptophan analytical method were taken into account and found to be of no significance at the dilutions carried out. Particularly for the aromatic ILs, the maximum peak of absorbance for the studied imidazolium-based ILs is at *ca.* 211 nm and, given the dilutions carried out in all phases, there was no contribution of the ILs to the absorbance at 279 nm.

9.3.2.4. *pH measurements*

After the partition of L-tryptophan and phases separation, the pH of each phase was determined using a pH Meter (Hanna Instruments, Model 9321) at 298 K.

9.4. Results and Discussion

9.4.1. Phase Diagrams and Tie-Lines

The chemical structures of the studied imidazolium-based ILs are depicted in Figure 9.1. We have focused on the subgroup of imidazolium halides to evaluate the impact of IL cation on the separations, and on the 1-butyl-3-methylimidazolium cation, $[\text{C}_4\text{mim}]^+$, combined with a variety of anions, to analyze their influence on the liquid-liquid phase diagrams and L-tryptophan extraction ability.

Figures 9.2 to 9.4 present the experimental phase diagrams at 298 K, and atmospheric pressure, for each PEG 600 + Na_2SO_4 + H_2O + 5 wt% IL system (*cf.* Supporting Information with experimental weight fraction data, Table S9.1 to S9.6). It should be pointed out that the IL concentration was kept constant in all phase diagrams. The binodal curves are reported in molality units for an enhanced understanding on the impact of distinct ILs in the formation of ABS. Figure 9.2 shows the influence of the IL cation alkyl chain length, as well as the number of alkyl substitutions at the cation, in the binodal curves using different ILs, namely $[\text{im}]\text{Cl}$, $[\text{C}_1\text{im}]\text{Cl}$, $[\text{C}_2\text{mim}]\text{Cl}$, $[\text{C}_4\text{mim}]\text{Cl}$ and $[\text{C}_4\text{C}_1\text{mim}]\text{Cl}$. Figure 9.3 describes the effect of the presence of diverse functional groups at the IL cation through the binodal curves, with results for $[\text{OHC}_2\text{mim}]\text{Cl}$, $[\text{amim}]\text{Cl}$ and $[\text{C}_7\text{H}_7\text{mim}]\text{Cl}$. Finally, Figure 9.4 evaluates the influence of the IL anion nature in the phase diagrams, where results for $[\text{C}_4\text{mim}]\text{Cl}$, $[\text{C}_4\text{mim}][\text{CH}_3\text{CO}_2]$, $[\text{C}_4\text{mim}][\text{MeSO}_4]$ and $[\text{C}_4\text{mim}][\text{HSO}_4]$ are depicted. In all figures the binodal curve for the control system without IL is further represented for comparison issues.

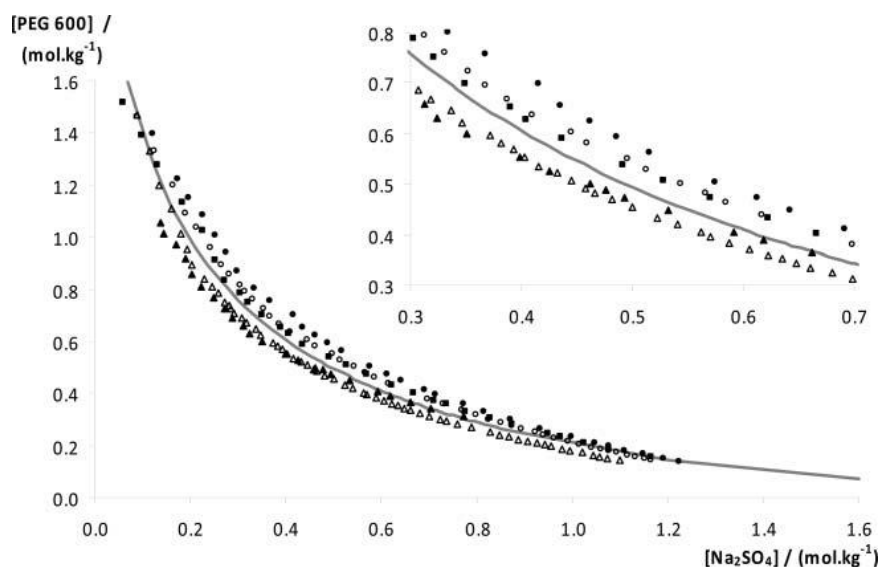


Figure 9.2 Phase diagrams for the imidazolium-based quaternary systems composed of PEG 600 + Na₂SO₄ + H₂O + 5 wt% IL at 298 K: (—) no IL; (●) [im]Cl ; (○) [C₁im]Cl; (■) [C₂mim]Cl; (Δ) [C₄mim]Cl; (▲) [C₄C₁mim][Cl].

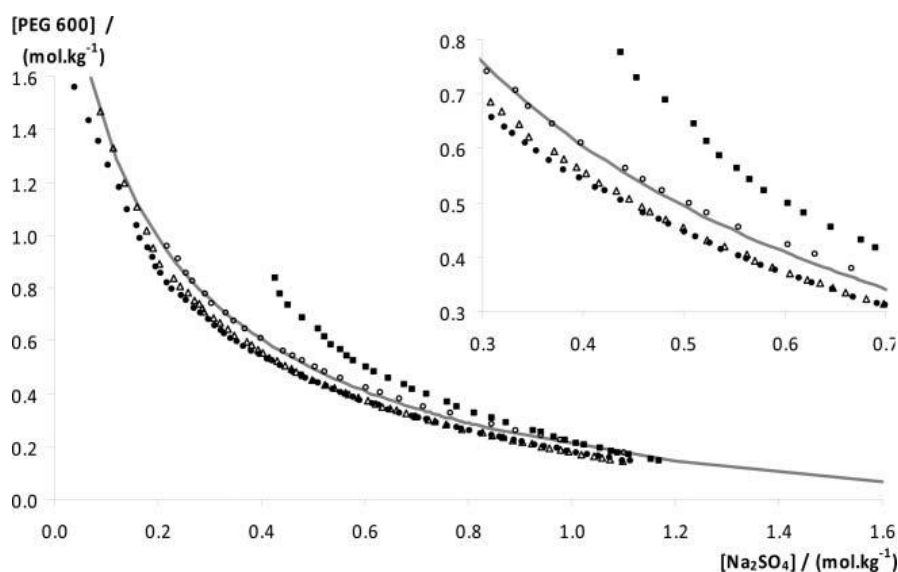


Figure 9.3 Phase diagrams for the imidazolium-based quaternary systems composed of PEG 600 + Na₂SO₄ + H₂O + 5 wt% IL at 298 K: (—) no IL; (Δ) [C₄mim]Cl; (■) [OHC₂mim]Cl ; (○) [amim]Cl; (●) [C₇H₇mim]Cl.

It is known that an increase of the ILs hydrophobic nature leads to a lower affinity for water¹¹⁻¹³, and consequently, to an enhanced phase separation in IL-based ABS¹⁴. Figure 9.2 shows how an increase in the cation alkyl chain length from [C₂mim]Cl to [C₄mim]Cl, and the presence of more alkyl substitutions at the cation, reduces the phases' miscibility. In contrast, in Figure 9.3 it is shown that the introduction of a terminal hydroxyl group or a double bond at the alkyl chain confers a polar character to

the IL, reducing the degree of phase separation. The effect of the IL on the binodal curves reported in Figures 9.2 and 9.3 thus follows a trend imposed by the IL hydrophobicity. The increase in the cation chain length and number of alkyl substitutions leads to a larger immiscibility, although only ILs larger than [C₄mim]Cl present two-phase regions larger than that observed for the ABS with no IL.

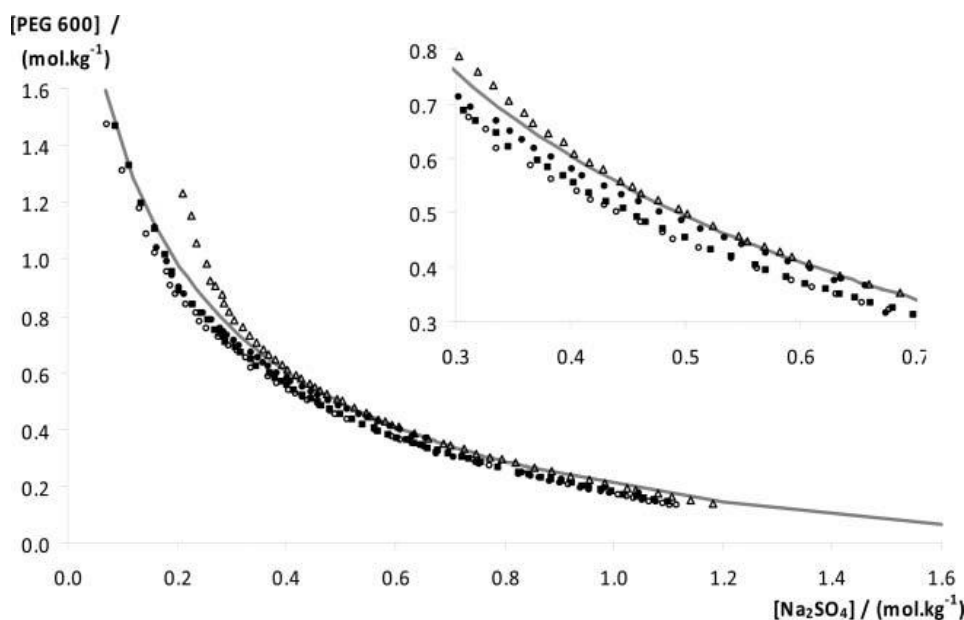


Figure 9.4 Phase diagrams for the imidazolium-based quaternary systems composed of PEG 600 + Na₂SO₄ + H₂O + 5 wt% IL at 298 K: (—) no IL; (■) [C₄mim]Cl; (●) [C₄mim][CH₃CO₂]; (○) [C₄mim][MeSO₄]; (Δ) [C₄mim][HSO₄].

The results for the [C₄mim]-based ILs, sketched in Figure 9.4, show the impact of the IL anion on the ABS formation. Only the IL [C₄mim][HSO₄] increases the phases' miscibility when compared to the system with no IL. All the other ILs induced a larger phase separation. The trend of the anion increasing immiscibility between the two phases is identical to that previously reported by Ventura et al.¹⁰ for IL-based ABS formation. There is a decrease on the ABS formation ability with the increase of the IL anion affinity for water, following the trend of the anion hydrogen bond acidity¹⁰. As observed for the IL cations, the hydrophobicity of the IL anion also controls the ABS formation ability.

The experimental binodal curves were correlated using the empirical relationship described by equation 9.1¹¹. The fitted parameters, and respective standard deviations, are summarized in Table 9.1. The experimental tie-lines (TLs) measured for each system along with the respective tie-line lengths (TLLs) are reported in Table 9.2. An

example of the TLs measured in this work is provided in Figure 9.5 along with the binodal curve for the system PEG 600 + Na₂SO₄ + H₂O + 5 wt% [C₂mim]Cl.

Table 9.1 Correlation parameters used in equation 9.1 to describe the binodal curves (and respective standard deviations, σ) for the PEG 600 + Na₂SO₄ + H₂O + 5 wt% IL quaternary systems at 298 K.

Quaternary System	($A \pm \sigma$)	($B \pm \sigma$)	$10^5(C \pm \sigma)$
no IL	81.8 ± 0.6	-0.471 ± 0.004	20.0 ± 0.6
[im]Cl	79.1 ± 1.2	-0.405 ± 0.008	20.0 ± 0.9
[C ₁ im]Cl	75.7 ± 0.8	-0.405 ± 0.006	30.0 ± 0.7
[C ₂ mim]Cl	70.8 ± 1.7	-0.381 ± 0.014	30.0 ± 2.3
[C ₄ mim]Cl	83.3 ± 0.5	-0.506 ± 0.003	20.0 ± 0.5
[C ₄ C ₁ mim]Cl	73.2 ± 1.1	-0.457 ± 0.009	10.0 ± 2.2
[OHC ₂ mim]Cl	155.8 ± 6.4	-0.645 ± 0.018	20.0 ± 1.3
[amim]Cl	84.4 ± 1.1	-0.485 ± 0.006	10.0 ± 0.7
[C ₇ H ₇ mim]Cl	72.4 ± 0.8	-0.448 ± 0.006	20.0 ± 1.1
[C ₄ mim][CH ₃ CO ₂]	76.4 ± 1.4	-0.452 ± 0.100	20.0 ± 1.7
[C ₄ mim][MeSO ₄]	77.1 ± 0.5	-0.476 ± 0.004	20.0 ± 0.5
[C ₄ mim][HSO ₄]	105.5 ± 1.6	-0.576 ± 0.007	10.0 ± 0.7

Table 9.2 Initial mass fraction compositions for the TLs and TLLs determination, and compositions of the respective top (*T*) and bottom (*B*) phases at 298 K.

Quaternary System	Mass Fraction Composition / (wt%)		Y_T	X_T	Y_B	X_B	TLL
	PEG 600	Na ₂ SO ₄					
	no IL	40.00					
	39.94	7.04	50.56	1.04	0.04	29.58	58.02
[im]Cl	40.04	5.02	44.53	2.00	0.01	31.85	53.60
	40.30	6.97	48.39	1.47	0.00	34.38	58.51
[C ₁ im]Cl	39.96	7.04	48.64	1.19	0.00	34.00	58.67
	39.97	5.10	44.52	1.48	0.00	36.90	56.89
[C ₂ mim]Cl	39.95	6.04	45.83	1.30	0.00	38.27	58.88
	40.09	7.01	46.54	1.21	0.00	43.03	62.56
[C ₄ mim][Cl]	40.15	5.01	45.14	1.46	0.00	33.50	55.36
	40.18	6.00	46.64	1.31	0.00	35.10	57.60
[C ₄ C ₁ mim]Cl	39.93	5.02	44.70	1.17	0.02	37.24	57.42
	39.97	6.04	45.31	1.10	0.00	42.96	61.68
[OHC ₂ mim]Cl	40.04	5.07	44.67	3.70	6.56	14.98	39.75
	40.07	6.99	49.93	3.08	0.74	22.55	52.90
[amim]Cl	40.13	5.99	44.00	1.80	0.00	49.49	64.88
	40.13	7.00	45.09	1.67	0.00	50.10	66.17
[C ₇ H ₇ mim]Cl	39.94	5.03	45.52	1.07	0.00	33.40	55.83
	40.03	7.00	49.19	0.74	0.00	34.32	59.56
[C ₄ mim][CH ₃ CO ₂]	39.93	6.10	47.14	1.14	0.00	33.60	57.23
	39.95	7.03	47.84	1.07	0.00	37.20	59.95
[C ₄ mim][MeSO ₄]	39.98	5.01	44.47	1.34	0.00	37.71	57.45
[C ₄ mim][HSO ₄]	39.99	5.06	44.78	2.21	0.45	28.72	51.64
	40.10	7.13	48.10	1.86	0.09	33.52	57.51

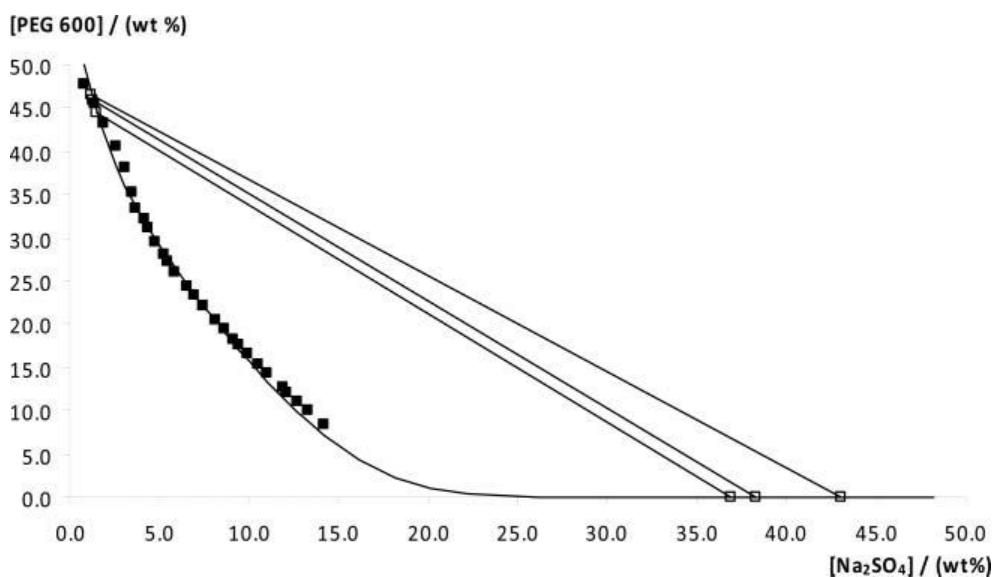


Figure 9.5 Phase diagram for the PEG 600 + Na₂SO₄ + H₂O + 5 wt% [C₂mim]Cl quaternary system at 298 K: (■) binodal curve data; (-) binodal adjusted curve; (□) TL data.

9.4.2. Partitioning of the ILs in the ABS

As could be expected, the ILs added to the ABS also partition themselves between the two phases according to their physical and chemical nature. For a better understanding of their impact on the phase separation and on the extraction ability of the ABS, the ILs distribution between the two aqueous phases was also evaluated. The partition coefficient of each IL, K_{IL} , is defined as the ratio of the IL concentration in the PEG 600 and that in the Na₂SO₄-rich phase, as described by equation 9.7:

$$K_{IL} = \frac{[IL]_{PEG600}}{[IL]_{Na_2SO_4}} \quad \text{Equation 9.7}$$

where $[IL]_{PEG600}$ and $[IL]_{Na_2SO_4}$ are the concentrations of IL in the polymer and in the inorganic salt aqueous phases, respectively.

The partition coefficients of each IL at 298.15 K are reported in Table 9.3. In addition, the mass fraction compositions of each component at which the partition coefficients were determined are also presented in Table 9.3. With the exception of [im]Cl, all ILs present partition coefficients larger than 1, indicating thus that ILs will partition preferentially for the PEG-rich phase. Certainly, [im]Cl is the strongest salting-out inducing IL evaluated, and thus preferentially partitions for the inorganic-salt-rich phase, while the intensity on the partitioning of the IL is proportional to the IL salting-

in/-out ability. Salting-out inducing ions (high charge density ions) have a greater tendency to form hydration complexes when compared to salting-in inducing ions (low charge density ions). Therefore, the ions' aptitude to form hydration complexes, and thus affinity for aqueous environments, will define the phase for which the IL ions mainly migrate¹⁵. This IL migration for a particular phase will naturally change the chemical and physical properties of such phase, and as will be shown below, such IL partitioning is responsible for the enhanced extraction ability of L-tryptophan observed in several ABS. Although outside the scope of this work it is interesting to notice that these results suggest the possibility of using PEG-based ABS to remove hydrophilic ILs from aqueous solutions, providing an interesting approach to the treatment of aqueous effluents contaminated with ILs.

Table 9.3 Partition coefficients of each IL (K_{IL}) and mass fraction compositions of the quaternary systems at 298.15 K

Quaternary System	Mass Fraction Composition / (wt%)			K_{IL}
	PEG 600	Na ₂ SO ₄	IL	
[im]Cl	39.96	5.00	5.08	0.48
[C ₁ mim]Cl	40.12	5.00	5.00	2.23
[C ₂ mim]Cl	39.98	5.01	5.03	4.80
[C ₄ mim]Cl	40.02	5.00	5.01	7.04
[C ₇ H ₇ mim]Cl	39.94	5.06	5.00	15.02
[C ₄ C ₁ mim]Cl	42.98	4.76	4.81	13.80
[amim]Cl	39.98	5.04	4.99	2.91
[OHC ₂ mim]Cl	39.97	5.02	5.01	2.21
[C ₄ mim][HSO ₄]	39.99	5.04	5.06	6.64
[C ₄ mim][CH ₃ CO ₂]	39.98	5.08	5.06	7.34
[C ₄ mim][MeSO ₄]	39.98	5.01	5.00	8.74

A comparison between the ILs' partition coefficients reported in Table 9.3 and the binodal curves sketched in Figures 9.2 to 9.4 indicate that the addition of 5 wt% of IL to ABS enlarges the biphasic region of the PEG 600 + Na₂SO₄ + H₂O system when the IL displays a $K_{IL} > 7.0$, while an opposite result is obtained when $K_{IL} < 7.0$.

9.4.3. Partitioning of L-tryptophan in the ABS

Tryptophan ($C_{11}H_{12}N_2O_2$) is an essential amino acid that has to be supplied through the feed, since its synthesis cannot be achieved by animals. The body uses tryptophan to produce niacin and serotonin¹⁶. Its chemical structure is formed by an indole group that confers the hydrophobic characteristics to the amino acid. Even so, L-tryptophan was used in this work as a model biomolecule and as a proof of principle to the proposed technique. In this context, these novel systems can be further explored through their selective extraction capability with a wide range of biomolecules of interest.

The partition coefficient of L-tryptophan, K_{Trp} , is here defined as the ratio of the concentration of L-tryptophan in the polymer and salt-rich phases and as described by equation 9.8:

$$K_{Trp} = \frac{[Trp]_{PEG\ 600}}{[Trp]_{Na_2SO_4}} \quad \text{Equation 9.8}$$

where $[Trp]_{PEG\ 600}$ and $[Trp]_{Na_2SO_4}$ are the concentration of L-tryptophan in the PEG 600 and Na_2SO_4 aqueous-rich phases, respectively.

The partition coefficients of biomolecules in ABS are dependent on hydrophobic type interactions, electrostatic forces, molecular size, solubility, and affinity for both phases, and their magnitudes further depend on the two-phase compositions and on the nature of the biomolecules¹⁷⁻¹⁹. The partition coefficients of L-tryptophan (K_{Trp}) at 298.15 K in the studied ABS, and respective systems composition, are reported in Table 9.4. The reproducibility of the measurements was evaluated with the PEG 600 + Na_2SO_4 + water system without IL addition, and the average uncertainty associated to the L-tryptophan partition coefficients is within $\pm 5\%$. The K_{Trp} dependence on the IL cation and anion, at 298.15 K, is displayed in Figures 9.6 and 9.7. For all cases, K_{Trp} is larger than 1.0, denoting the amino acid's preferential partitioning for the PEG-rich phase (hydrophobic phase). Typical solute-solvent interactions are likely to involve van der Waals forces, electrostatic interactions, hydrogen-bonding and $\pi \cdots \pi$ stacking. The presence of the IL enhances this type of interactions allowing the manipulation of the characteristics and the extraction ability by the polymer-rich phase. Moreover, the protons of the imidazolium ring can act as proton donors while the counterions are typically proton accepting anions.

Table 9.4 Partition coefficients of L-tryptophan (K_{Trp}) and mass fraction compositions of the quaternary systems at 298.15 K

Quaternary System	Mass Fraction Composition / (wt %)			K_{Trp}
	PEG 600	Na ₂ SO ₄	IL	
no IL	40.00	5.04		14.93
	39.96	6.04		16.72
	39.94	7.04		20.54
[im]Cl	40.04	5.02	5.04	4.82
	39.84	6.06	5.26	5.28
	40.30	6.97	5.04	7.27
[C ₁ im]Cl	40.01	5.01	5.04	4.69
	40.08	6.01	5.00	5.55
	39.96	7.04	5.07	6.01
[C ₂ mim]Cl	39.97	5.10	5.01	7.63
	39.95	6.04	5.29	8.69
	40.09	7.01	5.04	9.11
[C ₄ mim]Cl	40.15	5.01	4.98	21.84
	40.18	6.00	5.05	29.43
	40.01	7.00	5.00	37.03
[C ₄ C ₁ mim]Cl	39.93	5.02	5.14	28.62
	39.97	6.04	5.00	31.21
	40.21	6.97	5.05	32.11
[OHC ₂ mim]Cl	40.04	5.07	5.00	4.72
	40.15	6.04	5.06	5.51
	40.07	6.99	5.20	5.71
[amim]Cl	39.93	5.01	5.08	11.88
	40.13	5.99	5.00	14.85
	40.13	7.00	5.07	13.06
[C ₇ H ₇ mim]Cl	39.94	5.03	5.00	23.46
	40.04	6.00	5.03	29.57
	40.03	7.00	5.11	42.47
[C ₄ mim][CH ₃ CO ₂]	39.97	5.01	4.96	19.24
	39.93	6.10	5.04	29.83
	39.95	7.03	4.96	34.81
[C ₄ mim][MeSO ₄]	39.98	5.01	5.03	20.76
	40.08	5.99	5.00	25.76
	40.04	7.01	5.00	32.64
[C ₄ mim][HSO ₄]	39.99	5.06	5.02	17.08
	40.16	5.99	5.15	21.28
	40.10	7.13	5.03	36.28

The K_{Trp} observed for the systems using ILs with salting-out inducing characteristics were smaller than those obtained for the ABS reference system without IL, but it showed a strong increase with the alkyl-chain size of the cation (*e.g.* from 4.82 with [im]Cl to 21.84 with [C₄mim]Cl in the system using 40 wt% PEG 600 + 5 wt% Na₂SO₄ + 5 wt% IL). This trend follows the IL salting-in/-out inducing ability. While salting-out ILs such as [im]Cl, [C₁im]Cl, [C₂mim]Cl, [OHC₂mim]Cl and [amim]Cl reduce K_{Trp} , the

remaining ILs increase the partitioning of the amino acid (salting-in inducing ILs). In addition, removing the most acidic hydrogen at the C₂ position of the IL by increasing the number of alkyl chains substitutions, as in [C₄C₁mim]Cl, leads to a higher K_{Trp} when compared to [C₄mim]Cl.

It seems that it is mainly the IL partition to the PEG-rich phase that improves the partitioning of L-tryptophan. Indeed, it can be seen in Figure 9.6 that there is a close agreement between K_{Trp} and K_{IL} , meaning that it is the presence of the IL on the PEG-rich phase that enhances the partitioning of the amino acid. Moreover, the presence of benzyl groups or double bonds at the IL cation also enhances the ability of the PEG-rich phase for extracting the amino acid. Remarkable are the results obtained for [C₇H₇mim]Cl where K_{Trp} takes the value 23.46 for the system composed by 40 wt% PEG 600 + 5 wt% Na₂SO₄ + 5 wt% IL, or 42.27 for the system containing 40 wt% PEG 600 + 7 wt% Na₂SO₄ + 5 wt% IL. In this particular case, it appears that the additional contributions of $\pi \cdots \pi$ interactions of a second aromatic ring are responsible for the increase in the K_{Trp} values.

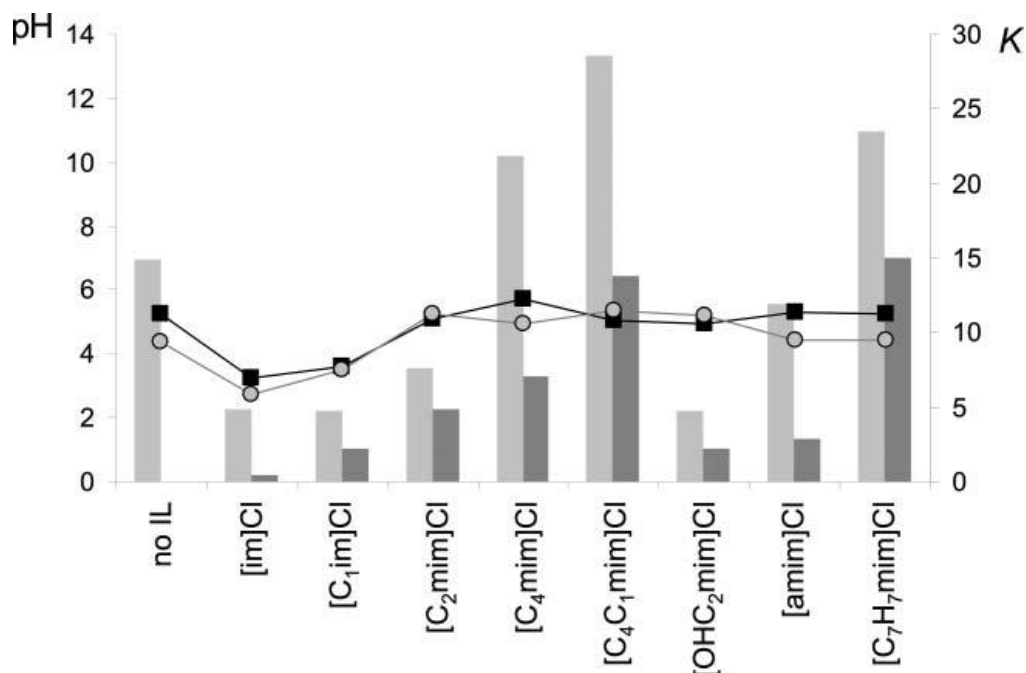


Figure 9.6 Partition coefficients of L-tryptophan (K_{Trp}) (light grey) and of each IL (K_{IL}) (dark grey), and pH of both top (black squares) and bottom phases (grey circles) for the chloride-based systems composed by 40 wt% PEG 600 + 5 wt% Na₂SO₄ + H₂O + 5wt % IL, at 298.15 K.

The observed influence of the IL anion follows the anion hydrophobicity¹⁰ but it is minor when compared with the influence of the IL cation. The K_{Trp} observed for the various [C₄mim]-based ILs studied are similar to those observed for [C₄mim]Cl. Therefore, the IL cation plays a major role in controlling the PEG-rich phase extraction ability for L-tryptophan. This effect is identical to what was observed for IL-based ABS previously studied by us^{9,10}.

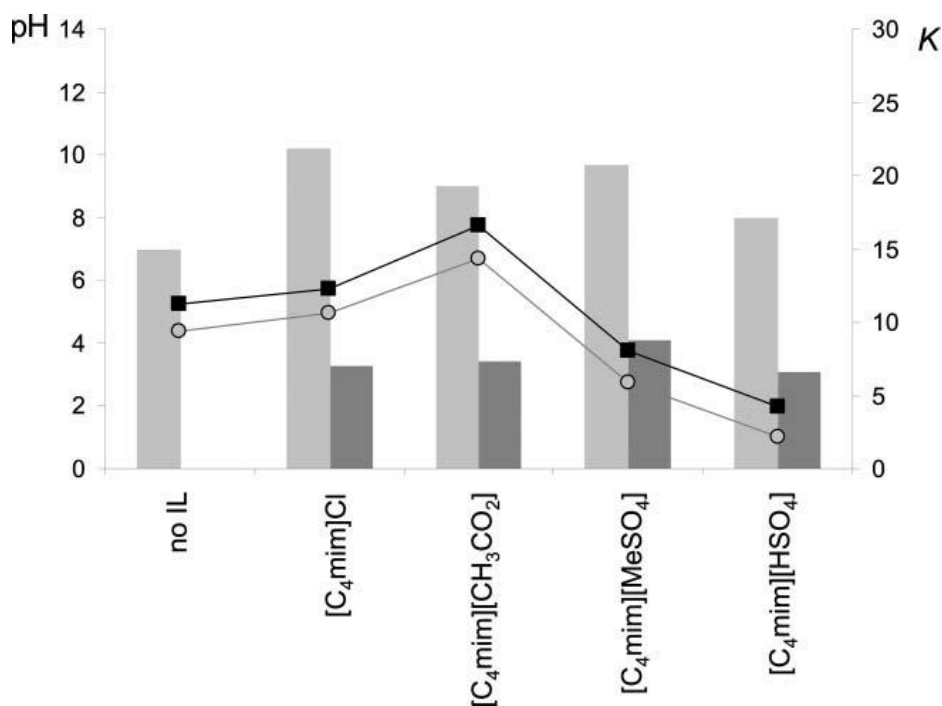


Figure 9.7 Partition coefficients of L-tryptophan (K_{Trp}) (light grey) and of each IL (K_{IL}) (dark grey), and pH of both top (black squares) and bottom (grey circles) phases, for the [C₄mim]-based systems composed by 40 wt% PEG 600 + 5wt % Na₂SO₄ + H₂O + 5wt % IL, at 298.15 K.

Previously, Pei et al.²⁰ reported that the temperature significantly influences the extraction efficiency of proteins. Therefore, aiming at evaluating the temperature influence in the extraction of L-tryptophan four systems were selected (those containing no IL, [C₄mim]Cl, [C₇H₇mim]Cl and [C₄mim][CH₃CO₂]). K_{Trp} was determined at the following temperatures: 278.15, 288.15, 298.15, 308.15 and 318.15 K. These systems allowed us to study the temperature effect upon the separation, in combination with different cations and anions. The data gathered, and accurate mass fraction compositions for each system, are displayed in Table 9.5. The associated uncertainty to the experimental measurements was determined with the 40 wt% PEG 600 + 5 wt% Na₂SO₄ + 5 wt% [C₄mim]Cl system (3 independent equilibration samples for each temperature) and shown to be inferior to 5%. The K_{Trp} dependence on temperature is

displayed in Figure 9.8. The four systems, and at all temperatures, present a K_{Trp} larger than 1.0. The results indicate that the temperature has a significant effect in the amino acid partitioning. Indeed, for the system without IL there is a maximum in K_{Trp} at temperatures close to 298.15 K, while for the systems containing IL, this maximum is observed at 288.15 K. Both IL cation and anion contribute for the differences observed in the partition coefficients and their dependence on temperature. Since electrostatic contributions are rather independent on temperature, the main deviations in K_{Trp} as a function of temperature should be a consequence of dispersive forces and H-bonding interactions taking place in those systems.

Table 9.5 Partition coefficients of L-tryptophan (K_{Trp}) and mass fraction compositions of the quaternary systems at different temperatures.

Quaternary System	T / K	Mass Fraction Composition / (wt %)			K_{Trp}
		PEG 600	Na_2SO_4	IL	
no IL	278.15	40.07	5.18		4.62
	288.15	39.89	5.16		10.87
	298.15	40.00	5.04		14.93
	308.15	39.97	5.06		11.60
	318.15	39.92	5.08		7.45
[C ₄ mim]Cl	278.15	40.04	5.08	5.12	7.24
	288.15	39.91	5.06	5.05	26.77
	298.15	40.15	5.01	4.98	21.84
	308.15	40.16	5.03	4.99	16.96
	318.15	40.24	5.01	5.03	9.74
[C ₇ H ₇ mim]Cl	278.15	39.88	5.00	5.07	5.33
	288.15	39.95	5.01	5.12	25.90
	298.15	39.94	5.03	5.00	23.46
	308.15	39.95	5.12	5.08	20.41
	318.15	40.25	5.04	5.06	15.52
[C ₄ mim][CH ₃ CO ₂]	278.15	39.92	5.02	4.98	4.11
	288.15	39.73	4.99	5.28	20.52
	298.15	39.97	5.01	4.96	19.24
	308.15	40.01	5.05	5.31	12.76
	318.15	40.03	5.05	5.00	11.28

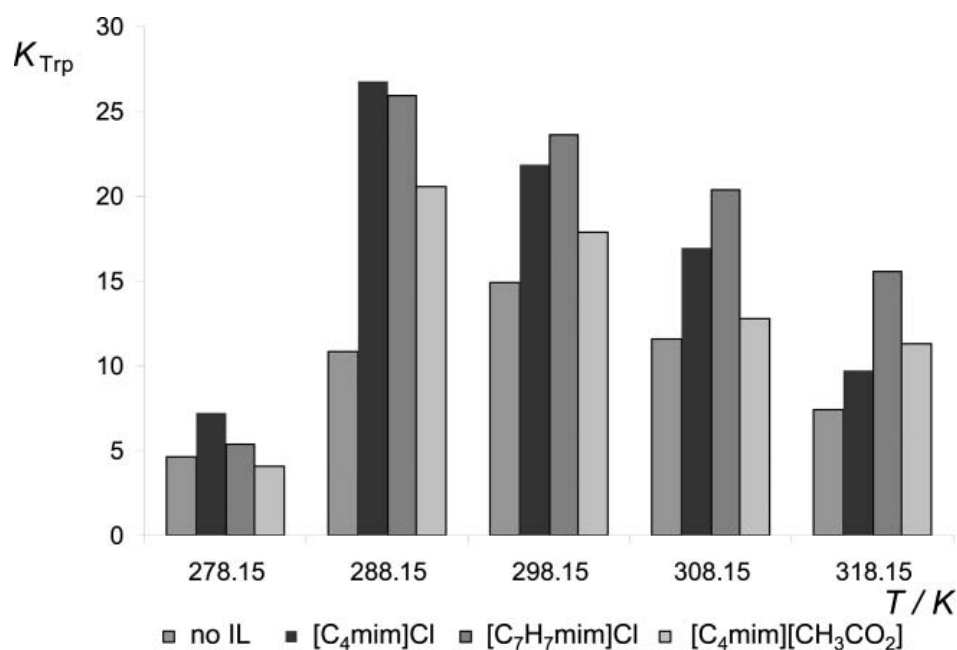


Figure 9.8 Partition coefficients of L-tryptophan (K_{Trp}) at different temperatures.

From a thermodynamics perspective, the partitioning of L-tryptophan can be regarded as a process of mass transfer from the inorganic-salt-rich phase to the PEG-rich. The amino acid thermodynamic parameters of transfer, namely the standard molar Gibbs energy ($\Delta_{\text{tr}}G_{\text{m}}^0$), the standard molar enthalpy ($\Delta_{\text{tr}}H_{\text{m}}^0$), and the standard molar entropy of transfer ($\Delta_{\text{tr}}S_{\text{m}}^0$), were determined through the application of the following equations²¹:

$$\ln(K_{\text{Trp}}) = -\frac{\Delta_{\text{tr}}H_{\text{m}}^0}{R} \times \frac{1}{T} + \frac{\Delta_{\text{tr}}S_{\text{m}}^0}{R} \quad \text{Equation 9.9}$$

$$\Delta_{\text{tr}}G_{\text{m}}^0 = \Delta_{\text{tr}}H_{\text{m}}^0 - T\Delta_{\text{tr}}S_{\text{m}}^0 \quad \text{Equation 9.10}$$

$$\Delta_{\text{tr}}G_{\text{m}}^0 = -RT \ln(K_{\text{Trp}}) \quad \text{Equation 9.11}$$

where K_{Trp} is the partition coefficient of L-tryptophan between the Na₂SO₄-rich and the PEG-rich phases, R is the universal gas constant, and T is the temperature. The enthalpic and entropic contributions can be directly deduced from the linear approximation of $\ln(K_{\text{Trp}})$ versus T^{-1} . It should be remarked that this linear function was only applied to the partition coefficient results equal to, and above, the maximum.

Table 9.6 Standard molar thermodynamic functions of transfer of L-tryptophan at 298.15 K

Quaternary System	$\frac{\Delta_{tr}H_m^0}{\text{kJ} \cdot \text{mol}^{-1}}$	$\frac{\Delta_{tr}S_m^0}{\text{J} \cdot \text{mol}^{-1} \cdot \text{K}^{-1}}$	$\frac{T \times \Delta_{tr}S_m^0}{\text{J} \cdot \text{mol}^{-1}}$	$\frac{\Delta_{tr}G_m^0}{\text{kJ} \cdot \text{mol}^{-1}}$	$\ln(K_{\text{Trp}})$
no IL	-27.34	-68.94	-20.55	-6.79	2.74
[C ₄ mim]Cl	-24.86	-58.26	-17.37	-7.49	3.02
[C ₇ H ₇ mim]Cl	-12.73	-16.76	-5.00	-7.74	3.12
[C ₄ mim][CH ₃ CO ₂]	-16.25	-31.09	-9.27	-6.99	2.82

The plots of $\ln(K_{\text{Trp}})$ versus T^{-1} exhibit linearity indicating that the molar enthalpy of transfer of L-tryptophan is temperature independent. The molar thermodynamic functions of transfer at 298.15 K, obtained by the linear least-square analysis, are summarized in Table 9.6. For all the systems studied, $\Delta_{tr}G_m^0$ is shown to be negative, which in turn reflects the spontaneous and preferential partitioning of the amino acid for the PEG-rich phase. In addition, there is an increase in the absolute values of $\Delta_{tr}G_m^0$ in the presence of IL when compared to the system with no IL. On the other hand, the $\Delta_{tr}H_m^0$ negative values reveal that the transfer of L-tryptophan between the Na₂SO₄-rich phase and the PEG-rich phase is an exothermic process, either for the system without IL and those containing 5 wt% of IL. The standard molar enthalpies of transfer largely depend on the IL cation, such as [C₇H₇mim]⁺, while the effect of changing the IL anion is mainly relevant for systems containing more complex anions, such as [CH₃CO₂]⁻. Nevertheless, it is clear that the presence of [C₇H₇mim]Cl increases the overall molar enthalpy of transfer in the system, increasing therefore the partition coefficient of the amino acid. These results suggest - and as verified before with the experimental partition coefficient values - that the partitioning process is essentially controlled by the IL cation interactions with the solute. However, the presence of anions with a stronger proton accepting ability, such as [CH₃CO₂]⁻ (compared to Cl⁻), leads to an increase in the molar enthalpy of transfer. Yet, this increase does not directly reflect an increase in K_{Trp} since, on the other hand, there is an increase of $\Delta_{tr}S_m^0$ when using such more complex anions. The inclusion of the IL strongly affects the molar entropy of the initial ternary system. In fact there is an increase in the L-tryptophan molar entropy of transfer following the rank: [C₄mim]Cl < [C₄mim][CH₃CO₂] < [C₇H₇mim]Cl.

In summary, the absolute results of $T \times \Delta_{tr} S_m^0$ are inferior to $\Delta_{tr} H_m^0$ suggesting that the enthalpic changes are the main driving forces ruling the amino acid partitioning.

The results obtained in this work suggest that the characteristics of the polymer-rich phase can be manipulated by the introduction of a small amount of an adequate IL into the system. The characteristics of the IL cation can be used to either intensify or reduce the hydrophobic character of the PEG-rich phase, or to add to it a particular type of interaction that will allow the extraction of the most diverse molecules of interest.

As shown in a previous work²², the extraction of L-tryptophan is strongly affected by the pH of the medium. To rule out pH effects on the measured partition coefficients, the pH of both top and bottom phases for all the ABS studied at 298 K were measured. The pH values are presented in Figures 9.6 and 9.7 together with the partition coefficient results. The pH values observed clearly reflect the acidic or alkaline character of the IL. For instance, lower pH values are observed for [C₄mim][HSO₄] compared to [C₄mim]Cl. In addition, no significant variations in the pH values are observed for the chloride-based series, meaning that structural and functional differences at the imidazolium cation do not alter significantly their acidic/alkaline characteristics. Although the pH value of the phases is somewhat influenced by the ILs, the pH variations are too small to affect the L-tryptophan partition. Previously²² it was shown that acidic conditions (in a pH range from 1 to 3) enhance the partition coefficient of L-tryptophan, and here it is not the most acidic or alkaline IL that induces the higher partition coefficient. Therefore, the effect of the pH of both phases in ABS on the partition coefficients can be considered negligible.

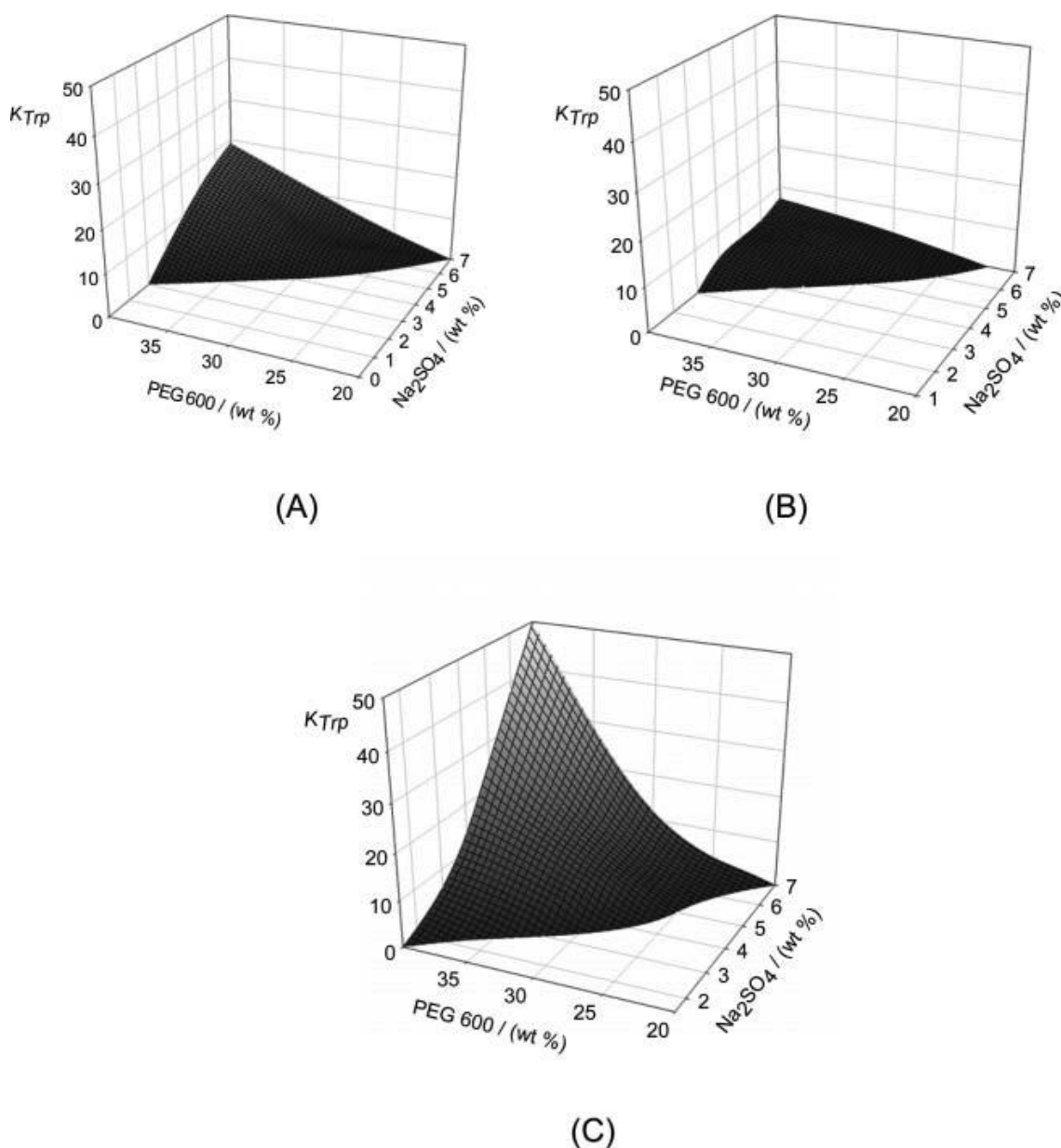


Figure 9.9 Partition coefficients of L -tryptophan as a function of PEG 600 and Na_2SO_4 concentrations at 298.15 K: no IL (A); 5 wt% of [im]Cl (B); 5 wt% [C₇H₇mim][Cl] (C).

The increase of Na_2SO_4 concentration reduces the solubility of L -tryptophan in the salt-rich phase (bottom phase), resulting in a further increase in the partitioning of amino acid to the top phase (PEG-rich phase)^{23, 24}. The effect of PEG 600 and Na_2SO_4 concentration on the ABS extraction ability was studied for the all the systems containing IL and for the control system without IL, and at 298.15 K. The results obtained are presented in Table 9.4. As main example of the results obtained for the PEG 600 and inorganic salt concentration influence, Figure 9.9 presents the K_{Trp} values for the ABS with [im]Cl or [C₇H₇mim]Cl. Figure 9.9 shows that the increase of the

polymer concentration or salt concentration leads to an increase in K_{Trp} . As expected, the influence of the inorganic salt concentration leads to more pronounced differences in the K_{Trp} values than the influence of the PEG concentration.

Table 9.7 Partition coefficients of L-tryptophan (K_{Trp}) and IL (K_{IL}) dependence on the IL concentration at 298.15 K

Quaternary System	Mass Fraction Composition / (wt%)			K_{IL}	K_{Trp}
	PEG 600	Na ₂ SO ₄	IL		
[im]Cl	40.02	4.99	2.62	1.14	6.64
	39.96	5.00	5.08	0.48	5.54
	40.00	5.02	6.03	0.46	5.32
[C ₇ H ₇ mim]Cl	40.00	5.01	2.51	14.21	21.48
	39.94	5.03	5.00	15.01	25.92

The concentration of IL added to the ABS system was also studied for the ILs [C₇H₇mim]Cl and [im]Cl, and at 298.15 K. These were chosen because they present the most extreme opposite behaviours of K_{Trp} . The results are reported in Table 9.7. When the [C₇H₇mim]Cl concentration is reduced from 5 to 2.5 wt % a decrease of only 20 % on the partition coefficient of L-tryptophan is observed. This behaviour is followed by a negligible decrease of the K_{IL} . In contrast, when using [im]Cl, both partition coefficients decrease with the increase on the IL concentration but, while the K_{IL} falls by one half, the effect on K_{Trp} is still negligible.

9.5. Conclusions

The use of ILs as adjuvants for the extraction of biomolecules using polymer-based ABS is here proposed. It is shown, using L-tryptophan as a model biomolecule, that ILs can be used to finely tune the phase behaviour and extraction capability of ABS through an appropriate choice of the IL employed. The effect of both the IL cation and anion on L-tryptophan extraction was established and the results can be extrapolated to other biomolecules of interest. The results reported suggest that the use of ILs as adjuvants to modify the characteristics of the polymer-rich phase could be an interesting alternative to the usual approach of PEG functionalization.

9.6. References

1. Bridges, N.J., Gutowski, K.E., and Rogers, R.D., Investigation of aqueous biphasic systems formed from solutions of chaotropic salts with kosmotropic salts (salt-salt ABS). *Green Chemistry*, 2007. **9**(2): p. 177-183.
2. Lin, D.Q., Wu, Y.T., Mel, L.H., Zhu, Z.Q., and Yao, S.J., Modeling the protein partitioning in aqueous polymer two-phase systems: influence of polymer concentration and molecular weight. *Chemical Engineering Science*, 2003. **58**(13): p. 2963-2972.
3. Zalipsky, S., *Functionalized Poly(Ethylene Glycol) for Preparation of Biologically Relevant Conjugates*. *Bioconjugate Chemistry*, 1995. **6**(2): p. 150-165.
4. Li, J. and Kao, W.J., Synthesis of polyethylene glycol (PEG) derivatives and PEGylated-peptide blockpolymer conjugates. *Biomacromolecules*, 2003. **4**(4): p. 1055-1067.
5. Rosa, P.A.J., Azevedo, A.M., Ferreira, I.F., de Vries, J., Korporaal, R., Verhoef, H.J., Visser, T.J., and Aires-Barros, M.R., Affinity partitioning of human antibodies in aqueous two-phase systems. *Journal of Chromatography A*, 2007. **1162**(1): p. 103-113.
6. Azevedo, A.M., Rosa, P.A.J., Ferreira, I.F., Pisco, A.M.M.O., de Vries, J., Korporaal, R., Visser, T.J., and Aires-Barros, M.R., Affinity-enhanced purification of human antibodies by aqueous two-phase extraction. *Separation and Purification Technology*, 2009. **65**(1): p. 31-39.
7. Jiang, Y.Y., Xia, H.S., Yu, J., Guo, C., and Liu, H.Z., Hydrophobic ionic liquids-assisted polymer recovery during penicillin extraction in aqueous two-phase system. *Chemical Engineering Journal*, 2009. **147**(1): p. 22-26.
8. Wu, C., Peng, J.J., Li, J.Y., Bai, Y., Hu, Y.Q., and Lai, G.Q., Synthesis of poly(ethylene glycol) (PEG) functionalized ionic liquids and the application to hydrosilylation. *Catalysis Communications*, 2008. **10**(2): p. 248-250.
9. Neves, C.M.S.S., Ventura, S.P.M., Freire, M.G., Marrucho, I.M., and Coutinho, J.A.P., Evaluation of Cation Influence on the Formation and Extraction Capability of Ionic-Liquid-Based Aqueous Biphasic Systems. *Journal of Physical Chemistry B*, 2009. **113**(15): p. 5194-5199.
10. Ventura, S.P.M., Neves, C.M.S.S., Freire, M.G., Marrucho, I.M., Oliveira, J., and Coutinho, J.A.P., Evaluation of Anion Influence on the Formation and Extraction Capacity of Ionic-Liquid-Based Aqueous Biphasic Systems. *Journal of Physical Chemistry B*, 2009. **113**(27): p. 9304-9310.
11. Merchuk, J.C., Andrews, B.A., and Asenjo, J.A., Aqueous two-phase systems for protein separation Studies on phase inversion. *Journal of Chromatography B*, 1998. **711**(1-2): p. 285-293.
12. Freire, M.G., Carvalho, P.J., Gardas, R.L., Marrucho, I.M., Santos, L.M.N.B.F., and Coutinho, J.A.P., Mutual solubilities of water and the [C(n)mim][Tf(2)N] hydrophobic ionic liquids. *Journal of Physical Chemistry B*, 2008. **112**(6): p. 1604-1610.
13. Huddleston, J.G., Visser, A.E., Reichert, W.M., Willauer, H.D., Broker, G.A., and Rogers, R.D., Characterization and comparison of hydrophilic and hydrophobic room temperature ionic liquids incorporating the imidazolium cation. *Green Chemistry*, 2001. **3**(4): p. 156-164.
14. Rito-Palomares, M., Negrete, A., Miranda, L., Flores, C., Galindo, E., and Serrano-Carreón, L., The potential application of aqueous two-phase systems for in situ recovery of 6-pentyl-proportional to-pyrone produced by *Trichoderma harzianum*. *Enzyme and Microbial Technology*, 2001. **28**(7-8): p. 625-631.
15. Freire, M.G., Neves, C.M.S.S., Silva, A.M.S., Santos, L.M.N.B.F., Marrucho, I.M., Rebelo, L.P.N., Shah, J.K., Maginn, E.J., and Coutinho, J.A.P., H-1 NMR and Molecular Dynamics Evidence for an Unexpected Interaction on the Origin of Salting-In/Salting-Out Phenomena. *Journal of Physical Chemistry B*, 2010. **114**(5): p. 2004-2014.
16. Le Floc'h, N. and Seve, B., Biological roles of tryptophan and its metabolism: Potential implications for pig feeding. *Livestock Science*, 2007. **112**(1-2): p. 23-32.
17. Albertsson, P.-Å., *Partition of Cell Particles and Macromolecules*. 3rd ed 1986: Wiley, New York.

18. Nozaki, Y. and Tanford, C., Solubility of Amino Acids and 2 Glycine Peptides in Aqueous Ethanol and Dioxane Solutions - Establishment of a Hydrophobicity Scale. *Journal of Biological Chemistry*, 1971. **246**(7): p. 2211-&.
19. Eiteman, M.A. and Gainer, J.L., Peptide Hydrophobicity and Partitioning in Poly(Ethylene Glycol)-Salt Aqueous 2-Phase Systems. *Abstracts of Papers of the American Chemical Society*, 1990. **200**: p. 116-BIOT.
20. Pei, Y.C., Wang, J.J., Wu, K., Xuan, X.P., and Lu, X.J., Ionic liquid-based aqueous two-phase extraction of selected proteins. *Separation and Purification Technology*, 2009. **64**(3): p. 288-295.
21. Sadava, D., Hillis, D.M., Heller, H.C., and Berenbaum, M., *Life: The Science of Biology* 2009: W. H. Freeman.
22. Tome, L.I.N., Catambas, V.R., Teles, A.R.R., Freire, M.G., Marrucho, I.M., and Coutinho, J.A.P., Tryptophan extraction using hydrophobic ionic liquids. *Separation and Purification Technology*, 2010. **72**(2): p. 167-173.
23. Babu, B.R., Rastogi, N.K., and Raghavarao, K.S.M.S., Liquid-liquid extraction of bromelain and polyphenol oxidase using aqueous two-phase system. *Chemical Engineering and Processing*, 2008. **47**(1): p. 83-89.
24. Kuboi, R., Tanaka, H., and Komasa, I., Effect of Salt Addition on the Hydrophobicities of the System and Proteins in Aqueous 2-Phase Extraction Systems. *Kagaku Kogaku Ronbunshu*, 1991. **17**(1): p. 67-74.

10. PAPER 7

Insights into the Interactions that Control the Phase Behavior of Novel Aqueous Biphasic Systems Composed of Polyethylene Glycols and Ionic Liquids

Chemistry – a European Journal, 18 (2012) 1831-1839.

10.1. Abstract

New polyethylene glycol (PEG)/ionic liquid aqueous biphasic systems (ABS) are presented. Distinct pairs of PEGs and ionic liquids (ILs) can induce phase separation in aqueous media when dissolved at appropriate concentrations. Phase diagrams have been determined for a large array of systems at 298, 308 and 323 K. A comparison of the binodal curves allowed the analysis of the tunable structural features of the IL (*i.e.*, anion nature, cationic core, cationic alkyl side chain length and functionalization, and number of alkyl substituents in the cation) and the influence of the molecular weight of the PEG polymer on the ability of these solutes to induce an ABS. It was observed that contrary to typical ABS based on ILs and inorganic salts, in which the phase behavior is dominated by the formation of hydration complexes of the ions, the interactions between the PEG polymers and ionic liquids control the phase demixing in the polymer-type ABS studied here. It is shown that both the ionic liquids and PEG polymers can act as the salting-out species; that is, it is an occurrence that is dependent on the structural features of the IL. For the first time, PEG/IL ABS are reported and insights into the major interactions that govern the polymer/IL phase behavior in aqueous media are provided. The use of two different non-volatile species (*i.e.*, ILs and PEG polymers) to form ABS allows the polarities of the phases to be tailored. Hence, the development of environmentally friendly separation processes that make use of these novel systems is directly envisaged.

Keywords: Biphasic systems, ionic liquid, phase diagrams, polyethylene glycol, salting-in/-out.

10.2. Introduction

As described in the previous chapter, ABS typically formed by polymer and inorganic salt aqueous solutions have several advantages over conventional polymer-polymer ABS¹. However, the hydrophilic nature of PEG limits the applicability of this technique. Derivatization of the polymer is a viable possibility to overcome this issue; still, it implies significant costs and turns their application more complex. On chapter 9, it has been shown that the use of ILs as adjuvants permits a fine tuning of the characteristics of either the salt- or the polymer-rich phases in a polymer/conventional salt ABS², allowing thus an efficient and tailored control of the partition coefficients and of the

purification efficiencies achieved within these systems. An additional advantageous aspect is that ILs can optionally be designed to have a low corrosive character³, compared to the highly corrosive aqueous solutions of conventional inorganic salts, which largely hinders their use in industrial processes. Additionally, the undesirable handling of solids in a process plant may be reduced with the replacement of the traditional inorganic salt by an IL.

Salt additives are known to strongly influence the solute partitioning in two-polymer ABS⁴. The salting-out ability of the salt-rich phase and the exclusion limit of the polymer-rich phase are the two main factors which determine the partition of biological macromolecules in polymer/salt ABS⁵. Previous studies have also shown that the addition of a neutral salt, such as NaCl, can strongly affect the extraction performance parameters⁶⁻¹⁰. The relative hydrophobicity of the coexisting phases of several polymer-salt ABS with the addition of NaCl or KCl was measured by the free energy of transfer of a methylene group ($\Delta G(\text{CH}_2)$)¹¹. The results showed that there is a linear relationship between ($\Delta G(\text{CH}_2)$) and the tie-line length (TLL) and it was established a straight correlation between the relative hydrophobicity of the phases and the ionic strength of the salt additive¹¹.

To date, the use of ILs in ABS has been mainly confined to salt/salt ABS, where one of the two salts is an IL. Nevertheless, the possibility of using ILs in ABS of the type polymer/salt has remained largely unexplored. The idea of a polymer-IL-based ABS was present in some examples from the patent literature in the mid-2000s^{12, 13}, which, however, did not include experimental support for the related claims. Approximately at the same time, salting-in and salting-out effects of ILs over polyethylene glycol (PEG) aqueous media were reported, tacitly anticipating that a proper selection of the polymer and the IL could give rise to a polymer/IL ABS^{14, 15}. Recently, polymer/IL ABS were reported with a series of hydrophobic polypropylene glycol (PPG) polymers¹⁶. Since PPG is a thermo-sensitive polymer, these novel ABS were proposed to have applications in the recycling and/or enrichment of hydrophilic ILs from aqueous media¹⁶. In spite of these preliminary efforts, no reports were found in the open literature regarding ABS composed of PEGs (less hydrophobic polymers) and hydrophilic ILs (highly polar fluids) that will allow the tailoring of the co-existing phases' polarities. Moreover, it should be remarked that the addition of PEGs to

aqueous solutions of ILs could be also advantageous in the recuperation/recycling of ILs from the most distinct approaches processed in aqueous media.

Herein, it is reported, for the first time, the formation of PEG/IL ABS. Novel insights into the influence of both the structural features of the polymer and of the IL on the aqueous phase diagrams are also provided. These gathered results allowed to infer on the main driving forces that control the liquid-liquid demixing in PEG-IL-water systems. PEG has been selected because it is non-toxic, inexpensive, biodegradable, and has been widely used in ABS formulations with inorganic salts^{17, 18}. Moreover, the molecular weight of PEG can be easily varied over a considerable range, thus enabling a certain tuning of its characteristics and of the phase diagrams of the ABS formed. In regard to the IL, a set of hydrophilic (or moderately hydrophobic) ILs was selected, thus allowing a deep examination of the effect of several structural features related to the cationic or anionic nature and the length, number, or functionalization of the cationic alkyl side chains, on the formation and characteristics of the ABS. Phase diagrams were determined at 298, 308 and 323 K and atmospheric pressure.

10.3. Experimental Section

PEG polymers of average molecular weights 1000, 2000, 3400 and 4000 g.mol⁻¹ (abbreviated as PEG 1000, PEG 2000, PEG 3400 and PEG 4000, respectively) were supplied by Fluka, and used as received.

The ILs studied were: imidazolium chloride ([im]Cl), 1-methylimidazolium chloride ([mim]Cl), 1,3-dimethylimidazolium chloride ([C₁mim]Cl), 1-ethyl-3-methylimidazolium chloride ([C₂mim]Cl), 1-butyl-3-methylimidazolium chloride ([C₄mim]Cl), 1-hexyl-3-methylimidazolium chloride ([C₆mim]Cl), 1-methyl-3-octylimidazolium chloride ([C₈mim]Cl), 1-allyl-3-methylimidazolium chloride ([amim]Cl), 1-(2-hydroxyethyl)-3-methylimidazolium chloride ([HOC₂mim]Cl), 1-butyl-3-methylpyridinium chloride ([C₄mpy]Cl), 1-butyl-1-methylpiperidinium chloride ([C₄mpip]Cl), 1-butyl-1-methylpyrrolidinium chloride ([C₄mpyr]Cl), tetrabutylphosphonium chloride ([P₄₄₄₄]Cl), 1-butyl-3-methylimidazolium bromide ([C₄mim]Br), 1-ethyl-3-methylimidazolium acetate ([C₂mim][CH₃CO₂]), 1-butyl-3-methylimidazolium acetate ([C₄mim][CH₃CO₂]), 1-ethyl-3-methylimidazolium methanesulfonate ([C₂mim][CH₃SO₃]), 1-butyl-3-methylimidazolium methanesulfonate

([C₄mim][CH₃SO₃]), 1-butyl-3-methylimidazolium trifluoromethanesulfonate ([C₄mim][CF₃SO₃]), 1-ethyl-3-methylimidazolium hydrogensulfate ([C₂mim][HSO₄]), and 1-ethyl-3-methylimidazolium dimethylphosphate ([C₂mim][(CH₃)₂PO₄]). Their chemical structures are shown in Figure 10.1. All ILs were purchased from Iolitec, with the exception of [P₄₄₄₄]Cl, which was kindly supplied by Cytec Industries, Inc. All IL samples were dried under moderate temperature (343 K) and high vacuum conditions (< 0.1 mbar), for a minimum of 48 h. The purity of the ILs was additionally checked by ¹H, ¹⁹F (whenever necessary), and ¹³C NMR spectroscopy, and found to be > 99 wt%, except for [P₄₄₄₄]Cl, which was > 97 wt%.

The water content of all ILs and all polymers was measured by Karl-Fischer titrations, and each value was individually taken into account for the calculation of the global compositions of the PEG + IL + H₂O mixtures prepared. In general, the water content in all IL samples after the drying procedure was found to be < 100 ppm, while the water content in the polymers was < 10000 ppm. Ultrapure water, doubly distilled, and passed through a reverse osmosis system, and further treated with Milli-Q plus water purification apparatus, was used.

The binodal curves in the phase diagrams were determined by means of the turbidometric titration method¹⁹ at atmospheric pressure and at the constant temperature of 298.2 ± 0.5 K. Moreover, additional phase diagrams at 308.2 K and 323.2 K were determined for selected systems within ± 0.5 K using a double jacketed cell coupled to a Julabo circulator (model F25-HD). Different ternary mixtures (*ca.* 1 g) of known total composition, located in the biphasic region, were prepared inside closed glass tubes. Upon dilution with minimal drop-wise additions of water, the test tubes were stirred for at least 12 h and allowed to settle for 24 h, which was found to be the common minimum time to reach the equilibrium in the different samples. These periods were found particularly important due to the high viscosity of higher-molecular-weight PEG polymers that could provide erroneous results if not enough time for dissolution and phase separation was allowed. This process was repeatedly carried out until a limp and monophasic solution was obtained. The additions were controlled gravimetrically, with an uncertainty of ± 10⁻⁴ g. The total amount of water added was determined, and the final mass fraction of each component was calculated.

10.4. Results and Discussion

Phase diagrams for the PEG/IL ABS were determined at 298, 308 and 323 K¹⁹, and the corresponding binodal curves were successfully correlated by means of Equation 10.1:

$$Y = A \cdot \exp(B \cdot X^{0.5} - C \cdot X^3) \quad \text{Equation 10.1}$$

where A , B and C are the correlation constants, and X and Y are the concentrations (in molality units) of ionic liquid and PEG, respectively (the fitted parameters are reported in Supporting Information, Table S10.1).

Several ILs were investigated in order to access the influence of the anionic nature, cationic core, length and functionalization of the cationic alkyl side chain, and the number of alkyl substituents on the phase diagrams behaviour. The ionic structures of these ILs are shown in Figure 10.1. A list, including the definition of their acronyms, is provided in the Experimental Section.

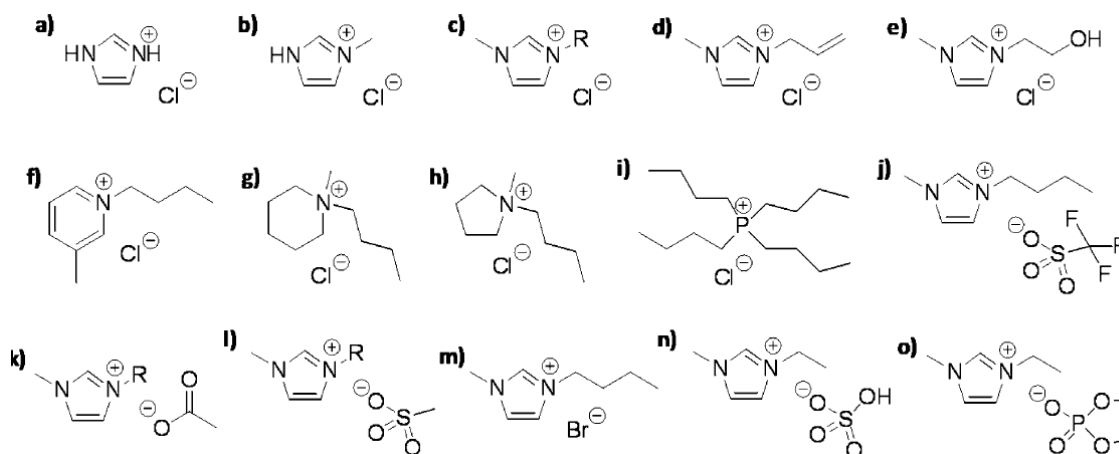


Figure 10.1 Chemical structures of the studied ILs: a) [im]Cl; b) [mim]Cl; c) [C_nmim]Cl (where n stands for the number of carbon atoms in the alkyl chain (R); $n = 1, 2, 4, 6,$ or 8); d) [amim]Cl; e) [HOC₂mim]Cl; f) [C₄mpy]Cl; g) [C₄mpip]Cl; h) [C₄mpyr]Cl; i) [P₄₄₄₄]Cl; j) [C₄mim][CF₃SO₃]; k) [C_nmim][CH₃CO₂] ($n = 2$ or 4); l) [C_nmim][CH₃SO₃] ($n = 2$ or 4); m) [C₄mim]Br; n) [C₂mim][HSO₄]; o) [C₂mim][(CH₃)₂PO₄].

PEG 1000, PEG 2000, PEG 3400 and PEG 4000 were used to investigate the influence of the polymer in the ABS.

All binodal data are shown in Figures 10.2 to 10.9 and are displayed in molality units, thus avoiding disparities in the ionic liquid-based ABS formation capability that could be a direct outcome of their distinct molecular weights (the detailed weight fraction experimental data are listed in Supporting Information, Table S10.2 to S10.9).

10.4.1. Effect of the Anion of the Ionic Liquid

In a typical PEG/inorganic salt ABS, the anion of the salt has a crucial impact on the phase behavior relative to the influence of the cation. To analyze this effect in the PEG/IL ABS studied herein, aqueous systems formed by PEG 2000 and distinct ILs with a common cation were investigated. Specifically, two sets of ILs were used: one with the $[C_4mim]^+$ cation in common ($[C_4mim]Cl$, $[C_4mim]Br$, $[C_4mim][CH_3CO_2]$, $[C_4mim][CH_3SO_3]$, and $[C_4mim][CF_3SO_3]$), and the other with the $[C_2mim]^+$ cation ($[C_2mim]Cl$, $[C_2mim][CH_3CO_2]$, $[C_2mim][CH_3SO_3]$, $[C_2mim][HSO_4]$, and $[C_2mim][(CH_3)_2PO_4]$). The corresponding experimental binodal curves at 298 K and their correlation, derived by using Equation 10.1, are shown in Figures 10.2 and 10.3.

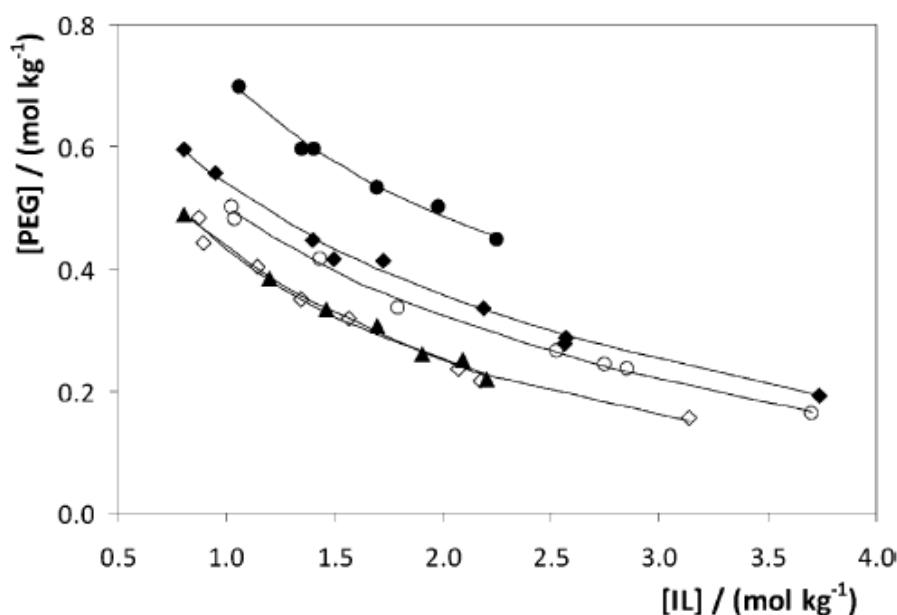


Figure 10.2 Experimental solubility data for PEG/IL ABS at 298 K to analyze the effect of the IL anion: PEG 2000/ $[C_4mim][CF_3SO_3]$ (\bullet), PEG 2000/ $[C_4mim]Br$ (\blacklozenge), PEG 2000/ $[C_4mim]Cl$ (\circ), PEG 2000/ $[C_4mim][CH_3SO_3]$ (\blacktriangle), and PEG 2000/ $[C_4mim][CH_3CO_2]$ (\diamond). The lines correspond to the respective correlations using Equation 10.1.

The ability of [C₄mim]-based ILs to induce PEG-based ABS, as measured by the minimum required combined concentrations, follows the trend: [C₄mim][CH₃CO₂] ≈ [C₄mim][CH₃SO₃] > [C₄mim]Cl > [C₄mim]Br > [C₄mim][CF₃SO₃]; whereas for the [C₂mim]-based ILs, the trend is as follows: [C₂mim][(CH₃)₂PO₄] > [C₂mim][CH₃CO₂] > [C₂mim][CH₃SO₃] > [C₂mim][HSO₄] > [C₂mim]Cl. The relative ability of an IL anion to induce the formation of a second liquid phase in PEG/IL ABS follows the opposite order to that observed for K₃PO₄/IL ABS previously reported²⁰. These reverse sequences can be rationalized taking into account the different salting-out aptitude of the distinct species solvated in aqueous media. When dealing with high charge density salts with an enhanced capacity for creating ion/water hydration complexes, such as K₃PO₄, the ability to induce ABS increases with the decrease in the affinity of the IL for water, namely, the IL is salted-out by the inorganic ions²⁰. On the contrary, in this study, when making mixtures of polymers and ILs, the stronger agents for promoting ABS are ILs that present an improved affinity for water and, hence, IL ions with a greater salting-out ability. This consequence comes directly from the PEG hydrophobic nature and the ease with which it is salted-out by charged species.

Regarding the sequence of the anions of the IL, it was verified that compounds with a better ability to form ion/water complexes are more effective in promoting PEG/IL-based ABS. Indeed, the salting-out aptitude of an ion can be directly related to its Gibbs free energy of hydration (ΔG_{hyd}). Thus, the acetate anion, with $\Delta G_{\text{hyd}} = 373 \text{ kJ}\cdot\text{mol}^{-1}$, is a stronger salting-out species, and therefore more prone to induce the liquid-liquid demixing of PEG from aqueous media than, for example, the chloride or the bromide anions ($\Delta G_{\text{hyd}} = 347$ and $321 \text{ kJ}\cdot\text{mol}^{-1}$, respectively)²¹.

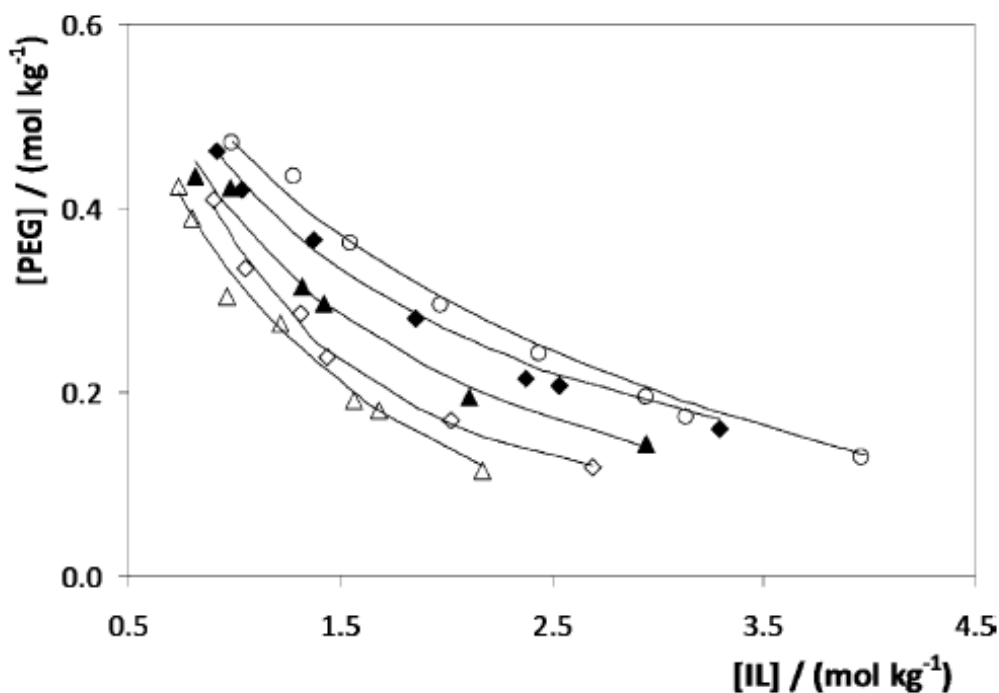


Figure 10.3 Experimental solubility data for PEG/IL ABS, at 298 K to analyze the effect of the IL anion: PEG 2000/[C₂mim]Cl (○), PEG 2000/[C₂mim][HSO₄] (◆), PEG 2000/[C₂mim][CH₃SO₃] (▲), PEG 2000/[C₂mim][CH₃CO₂] (◇), and PEG 2000/[C₂mim][(CH₃)₂PO₄] (△). The lines correspond to the respective correlations using Equation 10.1.

Interestingly, the [CF₃SO₃]-based IL, one of the ILs that is better at inducing the formation of the K₃PO₄/IL ABS²⁰, is the weakest species for salting-out the polymer when dealing with PEG-based ABS. Besides the IL/water and PEG/water interactions that govern the phase behavior in the systems presented above, we must be aware of the PEG/IL interactions that could additionally control the phase diagrams. In general, the larger the immiscibility between the IL and PEG polymer, the greater is the ability of the ionic fluid to induce the polymer separation from aqueous media. This trend correlates well with previously reported binary phase diagrams between poly(ethyl glycidyl ether) and several imidazolium-based ILs²². Watanabe and co-workers²² demonstrated that the solubility behavior is largely dependent on the anionic nature of the IL. Fluorinated anions and/or anions with lower hydrogen-bond basicity are more miscible with the polymers investigated than anions with a higher aptitude to create ion/water complexes, such as acetate²². As a consequence of this lower affinity between the acetate anion and polymers, the acetate-based IL is more efficient for the separation of the PEG aqueous phase than, for example, the [CF₃SO₃]-based (as experimentally

observed in this study). Usually, strongly basic anions tightly interact with imidazolium cations and interrupt the hydrogen-bonding interactions between the PEG and the aromatic cation of the IL, thereby lowering their miscibility.

10.4.2. Effect of the Cationic Core of the Ionic Liquid

Several PEG/IL ABS, chosen to evaluate the effect of different classes of IL cation in ABS formation, were studied. PEG 2000 was used as the common phase-forming polymer, and five different chloride-based ILs were investigated: [C₄mim]Cl, [C₄mpy]Cl, [C₄mpyr]Cl, [C₄mpip]Cl, and [P₄₄₄₄]Cl. The respective phase diagrams and the correlation of the experimental data derived by using Equation 10.1, are depicted in Figure 10.4.

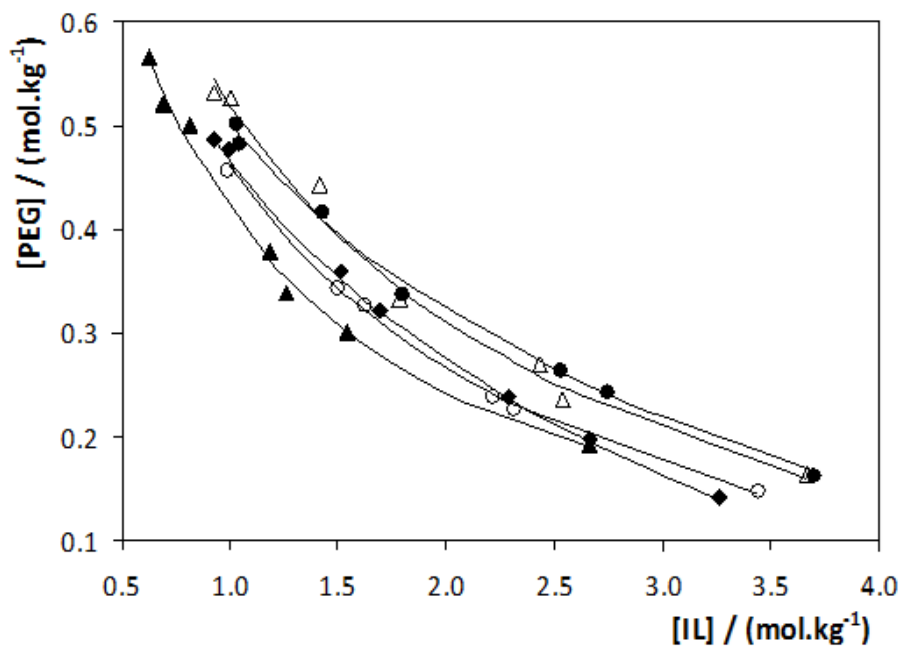


Figure 10.4 Experimental solubility data for PEG/IL ABS at 298 K to analyze the effect of the IL cation core: PEG 2000/[C₄mim]Cl (●), PEG 2000/[C₄mpy]Cl (△), PEG 2000/[C₄mpyr]Cl (◆), PEG 2000/[C₄mpip]Cl (○), and PEG 2000/[P₄₄₄₄]Cl (▲). The lines correspond to the respective correlations using Equation 10.1.

The experimental results show that the ability of ILs to induce PEG-based ABS follows the trend: [P₄₄₄₄]Cl > [C₄mpip]Cl ≈ [C₄mpyr]Cl > [C₄mpy]Cl ≈ [C₄mim]Cl. This ability correlates well with the relative hydrophobic character of the IL, with the most hydrophobic species showing cloud points at lower concentrations of IL (for a given

concentration of PEG). The higher the affinity for water and/or hydrophilic nature of the IL, the less effective such IL is in promoting the PEG phase separation. As previously reported²³, imidazolium and pyridinium cations present stronger interactions with water (as a result of their aromatic character), which results in binodal curves that are more shifted to the top/right in the phase diagram. The quaternary phosphonium-based IL (with four alkyl chains) was found to be the strongest promoter of the formation of PEG/IL ABS amongst the ILs studied as a result of the lower affinity of this compound for aqueous phases. The phosphonium IL/water miscibility essentially derives from the hydrogen-bonding interactions of water with the chloride anion. This is in stark contradiction to the trend obtained for the anions discussed above, but the cationic pattern is in good agreement with previous reports in which ABS of imidazolium-, phosphonium- and ammonium-based ILs, in the presence of common inorganic salts, were investigated^{24, 25}. This behavior occurs because the ABS formation for these systems is being driven by a different phenomenon from that discussed above for the effect of the anion of the IL. Here, the ABS formation is, as for the salt/IL ABS^{24, 25}, a direct result of the PEG salting-out aptitude over the moderate hydrophobic ILs considered. PEG is preferentially hydrated, and thus, tends to salt-out the ILs.

As for the anion-effect discussed above, the interactions that occur between the PEG polymer and ILs may also have an impact upon their phase separation. PEG is a polyether and, thus, hydrogen-bonding interactions are expected to occur with the aromatic pyridinium and imidazolium cations. The presence of π electrons in these ILs corresponds to stronger interactions with PEG. Hence, this reason could be the major factor for the lower ability of these ILs to promote the PEG-based ABS, that is, the enhanced affinity between two compounds would require a higher quantity of both solutes for liquid-liquid demixing. Reports of results on the phase behaviour of binary systems composed of polyether compounds and ILs²² corroborate the ability of the cation core to promote the PEG/aqueous phase separation observed here. Polyether compounds are more soluble in ILs containing aromatic cations and immiscible in phosphonium- and ammonium-based counterparts, thus confirming that the intermolecular hydrogen-bonds between polymers and the acidic hydrogen atoms in the IL cation are crucial features for increasing their mutual miscibility²⁴. Hence, IL/PEG-based ABS are more readily formed when two poorly soluble species are present.

10.4.3. Effect of the Alkyl Chain Length, Number of Alkyl Groups, and Functionalization at the Alkyl Substituent in the Cation of the Ionic Liquid

The family of 1-alkyl-3-methylimidazolium chloride ILs was selected to study the effect of the length of the cationic alkyl substituent (which is one of the major structural features that allows the hydrophobicity of the IL to be tailored) on the PEG/IL/water phase diagrams. Moreover, imidazolium-based ILs with no alkyl chains and only one alkyl group were additionally studied. Specifically, six ILs were investigated: [im]Cl, [mim]Cl, [C₂mim]Cl, [C₄mim]Cl, [C₆mim]Cl, and [C₈mim]Cl. Again, PEG 2000 was used as the common polymer in all experiments. Figure 10.5 illustrates the experimental and correlated binodal curves for the various imidazolium chloride systems.

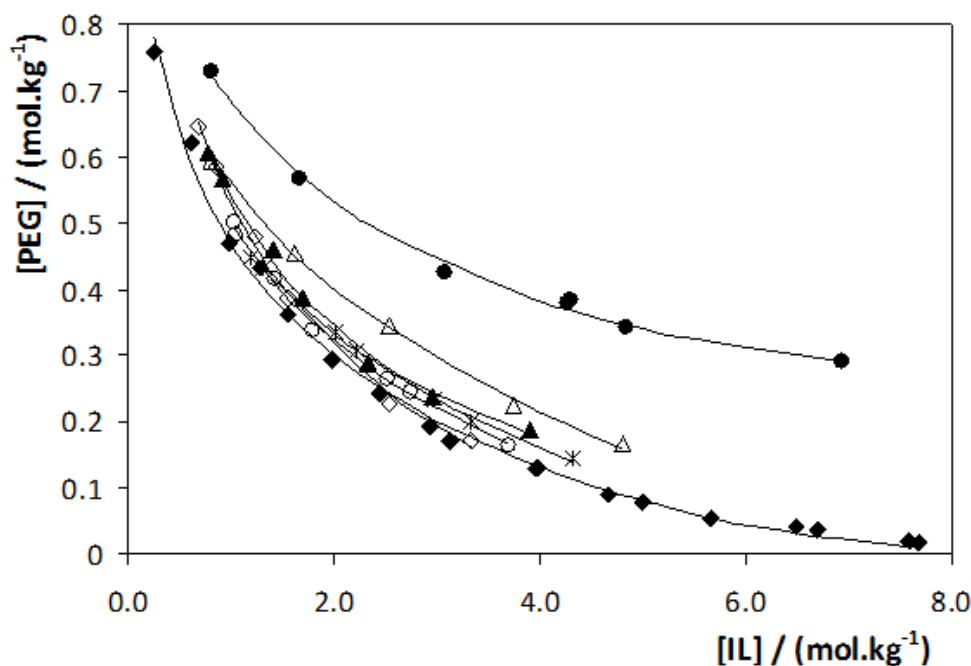


Figure 10.5 Experimental solubility data for PEG/IL ABS, at 298 K to analyze the effect of the length and number of the alkyl substituents in the ionic liquid cation: PEG 2000/[im]Cl (●), PEG 2000/[mim]Cl (△), PEG 2000/[C₁mim]Cl (*), PEG 2000/[C₂mim]Cl (◆), PEG 2000/[C₄mim]Cl (○), PEG 2000/[C₆mim]Cl (▲), and PEG 2000/[C₈mim]Cl (◇). The lines correspond to the respective correlations using Equation 10.1.

The aptitude of the ILs to induce PEG-based ABS decreases on the following order: [C₂mim]Cl ≈ [C₈mim]Cl > [C₄mim]Cl ≈ [C₆mim]Cl ≈ [C₁mim]Cl > [mim]Cl > [im]Cl. It is easy to understand the lower ability of the monosubstituted, unsubstituted, and the 1,3-dimethyl-based imidazolium ILs to promote a biphasic system, given their higher

hydrophilicity (high charge density ILs that resemble inorganic salts) according to the discussion presented above for the cation core. However, for the other bisubstituted imidazolium-based ILs, more complex phenomena take place, and the trends in the phase behavior need to be carefully examined.

Longer alkyl chains enhance the hydrophobic character of the IL and, therefore, decrease their affinity for water while increasing the ABS promoting ability, which was previously observed with ABS of the type K_3PO_4/IL ²⁶. In PEG-based ABS, however, the opposite trend is observed for 1-alkyl-3-methylimidazolium chloride ILs with hexyl or shorter alkyl chains (although the differences are small). This pattern is a direct consequence of the IL that acts, in this case, as the salting-out species.

Instead of the interactions of the solutes with water, the interactions between the PEG polymer and ILs control the phase behavior. As previously reported^{27, 28}, an increase in the alkyl side chain of the cation enhances the solubility between imidazolium-based ILs and PEG polymer. The stronger the cation/anion interaction, the lower the ability of the imidazolium ring hydrogen atoms to hydrogen-bond with PEG polymer²⁹. This trend is in close agreement with the data gathered with $[C_n\text{mim}]\text{Cl}$ (with $n = 2, 4$ and 6). The longer the alkyl side chain of the imidazolium cation, the higher the miscibility/affinity with PEG, thus leading to systems that require more IL to undergo liquid-liquid demixing in aqueous media.

The odd behaviour observed with the system containing $[C_8\text{mim}]\text{Cl}$ implies that other factors besides those discussed above also take place. It should be reminded that this IL, contrary to those members of its homologous family with shorter alkyl substituents, forms micelles in aqueous solution above a critical concentration³⁰, and more complex phenomena are involved. The fact that ILs with long alkyl side chains tend to form phase-separated self-assembled structures corresponds to a decreased ability of $[C_8\text{mim}]\text{Cl}$ to hydrogen bond with PEG polymer. Hence, species that do not show a special affinity between themselves are more easily separated in aqueous solution.

From the gathered results of the effects of the IL cation core and alkyl side chain length, it seems that the formation of PEG/IL-based ABS is not just a direct consequence of the ability of the ions to form hydration complexes, as typically happens for ABS induced by inorganic salts. Instead, a complex interplay of interactions between PEG/water,

IL/water, and PEG/IL takes place. The imidazolium-based cations may form multiple hydrogen bonds by the various ring protons with even weak hydrogen-bond acceptors. Competition for the protons of the imidazolium cation among the anions and PEG molecules is consequently expected. The addition of hydrogen-bond acceptors (*e.g.*, PEG polymers) to an IL system can bring about significant changes in the magnitude³¹. From the results reported herein, it can be concluded that the hydrogen-bonding interactions that occur in IL/PEG pairs of solutes are also driving forces in the formation of the respective ABS.

Figure 10.6 shows the effect of the functionalization of the alkyl substituents in the cation, in particular, the influence of the presence of a double bond or a hydroxyl group in the alkyl side chain of the imidazolium cation. The binodal curves for the systems with [amim]Cl and [HOC₂mim]Cl relative to those with [C₄mim]Cl and [C₂mim]Cl, with PEG 2000 as the common polymer.

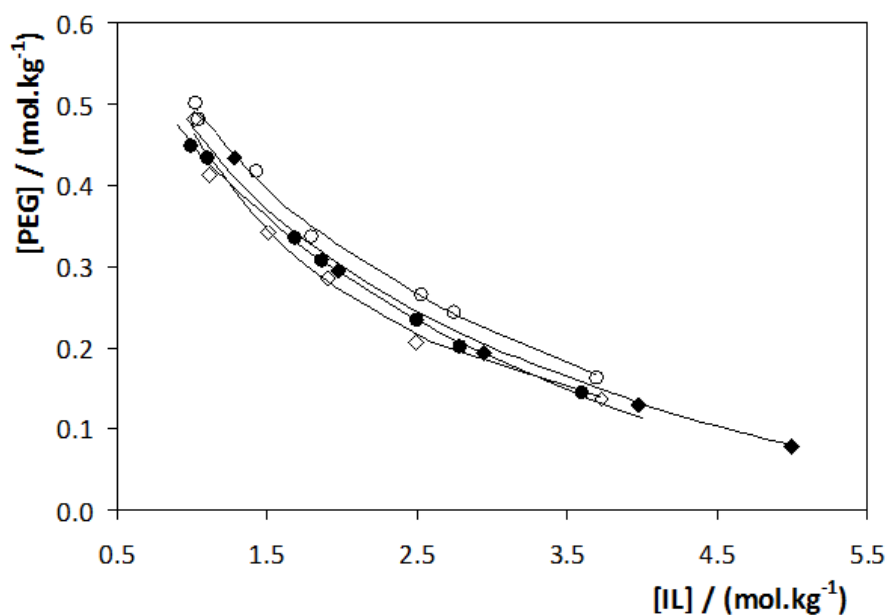


Figure 10.6 Experimental solubility data for PEG/IL ABS at 298 K to analyze the effect of the functionalization of the alkyl substituent in the ionic liquid cation: PEG 2000/[amim]Cl (●), PEG 2000/[HOC₂mim]Cl (◇), PEG 2000/[C₂mim]Cl (◆), and PEG 2000/[C₄mim]Cl (○). The lines correspond to the respective correlations using Equation 10.1.

The ability of the ILs to promote ABS follows the order: [HOC₂mim]Cl > [C₂mim]Cl ≈ [amim]Cl > [C₄mim]Cl. The presence of the hydroxyl group in [HOC₂mim]Cl shifts

the binodal curve to the left, compared to that of [C₂mim]Cl, which means a higher aptitude of the IL to promote the ABS. The presence of the double bond in [amim]Cl also enhances the ABS formation ability, as observed by the comparison with the systems containing [C₂mim]Cl and [C₄mim]Cl. It should be reminded that the [amim]⁺ cation is the equivalent to the [C₃mim]⁺ cation with an additional double bond. As observed before, the trend on the ILs ability to form ABS is the opposite of what was observed in K₃PO₄/IL ABS²⁶. These differences can be explained based on the increased ability of the functionalized IL ions to form hydration complexes, and hence to act as stronger salting-out species.

Regarding the effect of all the structural features related to cation of the IL, a general conclusion can be postulated: for PEG-based ABS containing the chloride-based ILs (an anion that is in the middle rank of the Hofmeister series^{32, 33}), the polymer tends to act as the privileged salting-out agent. Hence, hydrophobic ILs are more readily salted-out from the aqueous media and preferentially form ABS. However, if the increase in the hydrophobicity of the IL corresponds to a higher affinity for the PEG itself, the opposite behavior is observed.

10.4.4. Effect of the Molecular Weight of PEG

The tunable character of the phase behavior of PEG/IL ABS is not exclusively derived from the manipulation of the IL structure. PEG also offers some degree of design by varying the length of its polymeric chains, that is, the average molecular weight. This effect was analyzed by studying ABS formed by the co-dissolution of a given IL (*i.e.*, [C₄mim]Cl) and PEG polymers of different molecular weights. Figure 10.7 depicts the binodal curves for several PEG/[C₄mim]Cl ABS in which the average molecular weight of the PEG was varied from 1000 to 4000 g·mol⁻¹.

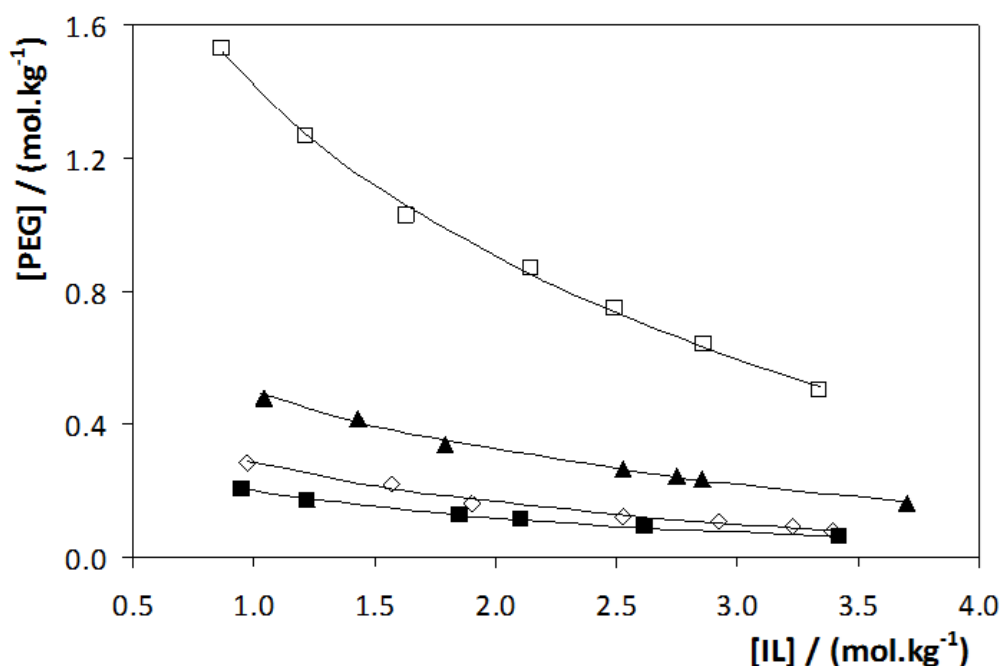


Figure 10.7 Experimental solubility data for PEG/IL ABS at 298 K to analyze the effect of the molecular weight of the PEG: PEG 1000/[C₄mim]Cl (□), PEG 2000/[C₄mim]Cl (▲), PEG 3400/[C₄mim]Cl (◇), and PEG 4000/[C₄mim]Cl (■). The lines correspond to the respective correlations using Equation 10.1.

The influence of the size of the length of the PEG chains on the phase diagrams is notorious, with the PEG ability to induce IL-based ABS that decrease in the following order: PEG 4000 > PEG 3400 > PEG 2000 > PEG 1000. An analogous trend has been observed in conventional polymer/salt ABS³⁴⁻³⁶. Hydrophobicity increases with the increase of the molecular weight of the PEG polymer, thus facilitating the formation of the ABS. Higher-molecular-weight PEG polymers present a lower affinity for water and are preferentially salted-out by the IL.

In the same line of the discussion previously presented, these trends also agree with the affinity/miscibility patterns observed in PEG/IL binary systems²⁷. Rodríguez et al.²⁷ demonstrated that an increase in the molecular weight of the polymer leads to larger immiscibility gaps with chloride-based ILs. Hence, higher-molecular-weight PEGs are less soluble in ILs and are more easily separated from aqueous media.

10.4.5. Effect of the Temperature

To gather information on the effect of temperature on the phase behaviour, additional PEG/IL/water phase diagrams were also determined at 308 and 323 K for two selected

systems, namely PEG 2000/[C₂mim]Cl and PEG 2000/[C₂mim][CH₃CO₂]. The results obtained are presented in Figures 10.8 and 10.9.

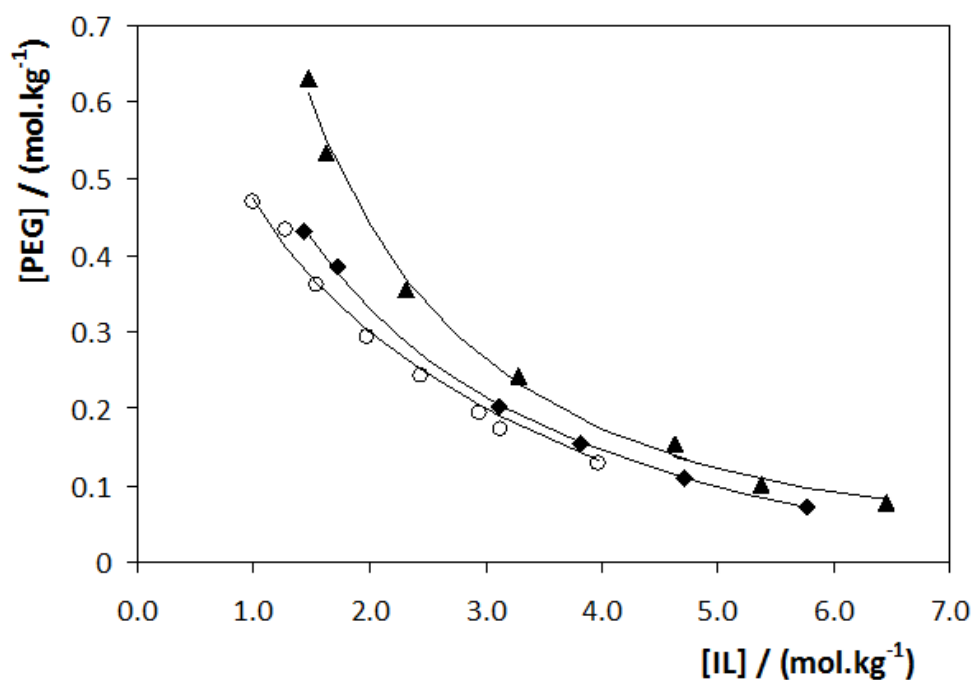


Figure 10.8 Experimental solubility data for PEG 2000/[C₂mim]Cl ABS, at 298 K (○), 308 K (◆), and 323 K (▲). The lines correspond to the respective correlations using Equation 10.1.

The binodal curves show that an increase in temperature decreases the immiscibility region. The pattern observed is in close agreement with that observed in ABS composed of ILs and inorganic salts or constituted by ILs and carbohydrates^{37 38}. Yet, an increase in temperature leads to larger immiscibility regimes in typical PEG/inorganic salt systems, whereas the opposite pattern is verified in polymer-polymer ABS^{39, 40}. Therefore, the dependence on temperature of the phase diagrams behavior for polymer/IL systems resembles that of polymer/polymer systems as a result of the lower charge density of the ILs relative to inorganic salts (and therefore their lower salting-out aptitude). The trends obtained here are, however, a reflection of the hydrophilic nature of the ILs investigated and their capacity to create water/ion complexes. As a result, the pattern obtained in these ternary systems are a consequence of the typical behavior from the upper critical solution temperature behavior observed in binary mixtures composed of ILs and water²³. The larger differences among the binodal curves at various temperatures for the acetate-based system relative to the chloride-based ABS are a

direct result of the higher salting-out aptitude of the acetate anion, which is reproduced in a more pronounced dependence on temperature.

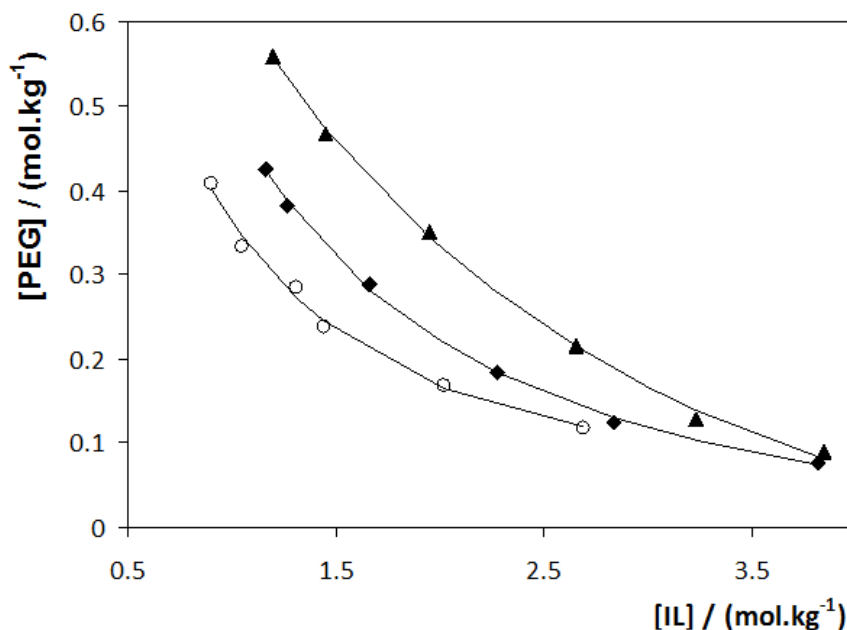


Figure 10.9 Experimental solubility data for PEG 2000/[C₂mim][CH₃CO₂] ABS, at 298 K (○), 308 K (◆), and 323 K (▲). The lines correspond to the respective correlations using Equation 10.1.

In summary, it can be stated that PEG/IL ABS are more complex in their nature and dominating interactions than the IL/inorganic salt ABS previously studied^{30, 38}. For the later, as shown for the K₃PO₄/IL-based ABS^{20, 26}, the phase separation is dominated by the salting-out ability of the inorganic salt, with the less hydrophilic ILs the more prone to undergo ABS formation. In most examples of PEG/IL ABS, the ionic liquid acts instead as the salting-out species and, hence, they are preferentially formed by ILs with enhanced capacity to create IL/water complexes. This trend was verified to be always true when different IL anions are compared; yet, the situation was quite different when evaluating the effect of the cation core of the IL with more hydrophobic ions. The trend observed for the influence of the cation core on ABS formation does not follow the ability of the ions to form hydration complexes. On the contrary, this effect seems to be dominated by the PEG salting-out ability, with the more hydrophobic ILs more able to form ABS, except in the cases where the mutual solubilities of the PEG-IL control the system as observed with the increase of the cation alkyl chain length (verified with the [C_nmim]Cl ILs). In general, for all the structural features evaluated, there is a close

relation to the IL/PEG binary phase behavior. Most inorganic salts are composed of simple and high charge-density ions; yet, when these are substituted by more complex and/or organic ions (as we do in most of the ILs investigated), the organic ion can itself influence the salting-in/-out behavior through specific interactions that are established with the polymer and not just with water. In this context, the interactions that occur between the polymer and the ionic fluid cannot be discarded, and play a crucial role in the phase behavior of PEG/IL-based ABS.

10.5. Conclusions

Novel aqueous biphasic systems of the type polymer/IL have been formed by co-dissolving ILs and PEG polymers in appropriate concentrations in water. It was shown that the phase behaviour of the PEG/IL ABS can be tailored to a relevant extent by a judicious selection of the PEG molecular weight or of the chemical structure of the constitutive ions of the ionic fluid. A detailed understanding of the molecular-level interactions in the binary mixtures composed of ILs and PEGs allowed to show that the phase behaviour in PEG/IL ABS is not only dominated by the ability of the solutes to interact with water. Instead, it is a direct consequence of the favourable (or non-favourable) interactions that occur between the PEG polymer and the IL to a large extent.

ABS composed of PEG polymers and ILs may have great potential in the biotechnology field, in which the use of ILs to substitute the high charge-density ions of inorganic salts can constitute an important improvement towards the extraction of biomolecules. Therefore, the use of these novel systems for extraction purposes is directly envisaged.

10.6. References

1. Lin, D.Q., Wu, Y.T., Mel, L.H., Zhu, Z.Q., and Yao, S.J., Modeling the protein partitioning in aqueous polymer two-phase systems: influence of polymer concentration and molecular weight. *Chemical Engineering Science*, 2003. **58**(13): p. 2963-2972.
2. Pereira, J.F.B., Lima, A.S., Freire, M.G., and Coutinho, J.A.P., Ionic liquids as adjuvants for the tailored extraction of biomolecules in aqueous biphasic systems. *Green Chemistry*, 2010. **12**(9): p. 1661-1669.
3. Qu, J., Blau, P.J., Dai, S., Luo, H.M., Meyer, H.M., and Truhan, J.J., Tribological characteristics of aluminum alloys sliding against steel lubricated by ammonium and imidazolium ionic liquids. *Wear*, 2009. **267**(5-8): p. 1226-1231.
4. Zaslavsky, B.Y., *Aqueous two-phase partitioning, physical chemistry and bioanalytical applications*, 1995, New York: Academic Press.
5. Marcos, J.C., Trindade, I.P., Diogo, M.M., and Prazeres, D.M.F., Purification of plasmid DNA vectors by aqueous two-phase extraction and hydrophobic interaction chromatography. *Journal of Chromatography A*, 2005. **1082**(2): p. 176-184.
6. Aires-Barros, M.R., Azevedo, A.M., Rosa, P.A.J., and Ferreira, I.F., Optimisation of aqueous two-phase extraction of human antibodies. *Journal of Biotechnology*, 2007. **132**(2): p. 209-217.
7. Aires-Barros, M.R., Rosa, P.A.J., and Azevedo, A.M., Application of central composite design to the optimisation of aqueous two-phase extraction of human antibodies. *Journal of Chromatography A*, 2007. **1141**(1): p. 50-60.
8. Aires-Barros, M.R., Rosa, P.A.J., Azevedo, A.M., Sommerfeld, S., Mutter, M., and Backer, W., Application of aqueous two-phase systems to antibody purification: A multi-stage approach. *Journal of Biotechnology*, 2009. **139**(4): p. 306-313.
9. Azevedo, A.M., Ferreira, G.N.M., and Aires-Barros, M.R., Advances in biopartitioning and purification. *Separation and Purification Technology*, 2009. **65**(1): p. 1-2.
10. Hachem, F., Andrews, B.A., and Asenjo, J.A., Hydrophobic partitioning of proteins in aqueous two-phase systems. *Enzyme and Microbial Technology*, 1996. **19**(7): p. 507-517.
11. Ferreira, L.A. and Teixeira, J.A., Salt effect on the (polyethylene glycol 8000+sodium sulfate) aqueous two-phase system: Relative hydrophobicity of the equilibrium phases. *Journal of Chemical Thermodynamics*, 2011. **43**(8): p. 1299-1304.
12. Upfal, J., MacFarlane, D.R., Forsyth, S.A., Solvents for use in the treatment of lignin-containing materials, WO 2005/017252 A1, 2005.
13. Dreyer, S., Kragl, U., Process for the extraction of biomolecules, DE102007001347 A1, 2007.
14. Visak, Z.P., Lopes, J.N.C., and Rebelo, L.P.N., Ionic liquids in polyethylene glycol aqueous solutions: Salting-in and salting-out effects. *Monatshefte Fur Chemie*, 2007. **138**(11): p. 1153-1157.
15. Lopes, J.N.C. and Rebelo, L.P.N., Salting effects in ionic liquid aqueous solutions - From aqueous biphasic system formation to salting agent precipitation. *Chimica Oggi-Chemistry Today*, 2007. **25**(6): p. 37-39.
16. Wang, J.J., Wu, C.Z., Pei, Y.C., Wang, H.Y., and Li, Z.Y., Salting-Out Effect of Ionic Liquids on Poly(propylene glycol) (PPG): Formation of PPG plus Ionic Liquid Aqueous Two-Phase Systems. *Journal of Chemical and Engineering Data*, 2010. **55**(11): p. 5004-5008.
17. Rogers, R.D., Chen, J., Spear, S.K., and Huddleston, J.G., Polyethylene glycol and solutions of polyethylene glycol as green reaction media. *Green Chemistry*, 2005. **7**(2): p. 64-82.
18. Lehn, J.M., Reutenauer, P., Buhler, E., Boul, P.J., and Candau, S.J., Room Temperature Dynamic Polymers Based on Diels-Alder Chemistry. *Chemistry-a European Journal*, 2009. **15**(8): p. 1893-1900.

19. Hatti-Kaul, R., *Aqueous Two-phase Systems: Methods and Protocols*, 2000: Humana Press.
20. Ventura, S.P.M., Neves, C.M.S.S., Freire, M.G., Marrucho, I.M., Oliveira, J., and Coutinho, J.A.P., Evaluation of Anion Influence on the Formation and Extraction Capacity of Ionic-Liquid-Based Aqueous Biphasic Systems. *Journal of Physical Chemistry B*, 2009. **113**(27): p. 9304-9310.
21. Marcus, Y., *Ion Properties*, 1997: Marcel Dekker.
22. Kodama, K., Tsuda, R., Niitsuma, K., Tamura, T., Ueki, T., Kokubo, H., and Watanabe, M., Structural effects of polyethers and ionic liquids in their binary mixtures on lower critical solution temperature liquid-liquid phase separation. *Polymer Journal*, 2011. **43**(3): p. 242-248.
23. Freire, M.G., Neves, C.M.S.S., Carvalho, P.J., Gardas, R.L., Fernandes, A.M., Marrucho, I.M., Santos, L.M.N.B.F., and Coutinho, J.A.P., Mutual Solubilities of water and hydrophobic ionic liquids. *Journal of Physical Chemistry B*, 2007. **111**(45): p. 13082-13089.
24. Bridges, N.J., Gutowski, K.E., and Rogers, R.D., Investigation of aqueous biphasic systems formed from solutions of chaotropic salts with kosmotropic salts (salt-salt ABS). *Green Chemistry*, 2007. **9**(2): p. 177-183.
25. Louros, C.L.S., Claudio, A.F.M., Neves, C.M.S.S., Freire, M.G., Marrucho, I.M., Pauly, J., and Coutinho, J.A.P., Extraction of Biomolecules Using Phosphonium-Based Ionic Liquids + K_3PO_4 Aqueous Biphasic Systems. *International Journal of Molecular Sciences*, 2010. **11**(4): p. 1777-1791.
26. Neves, C.M.S.S., Ventura, S.P.M., Freire, M.G., Marrucho, I.M., and Coutinho, J.A.P., Evaluation of Cation Influence on the Formation and Extraction Capability of Ionic-Liquid-Based Aqueous Biphasic Systems. *Journal of Physical Chemistry B*, 2009. **113**(15): p. 5194-5199.
27. Rodriguez, H., Francisco, M., Rahman, M., Sun, N., and Rogers, R.D., Biphasic liquid mixtures of ionic liquids and polyethylene glycols. *Physical Chemistry Chemical Physics*, 2009. **11**(46): p. 10916-10922.
28. Rodriguez, H. and Rogers, R.D., Liquid mixtures of ionic liquids and polymers as solvent systems. *Fluid Phase Equilibria*, 2010. **294**(1-2): p. 7-14.
29. Fernandes, A.M., Rocha, M.A.A., Freire, M.G., Marrucho, I.M., Coutinho, J.A.P., and Santos, L.M.N.B.F., Evaluation of Cation-Anion Interaction Strength in Ionic Liquids. *Journal of Physical Chemistry B*, 2011. **115**(14): p. 4033-4041.
30. Blesic, M., Marques, M.H., Plechkova, N.V., Seddon, K.R., Rebelo, L.P.N., and Lopes, A., Self-aggregation of ionic liquids: micelle formation in aqueous solution. *Green Chemistry*, 2007. **9**(5): p. 481-490.
31. Singh, T., Rao, K.S., and Kumar, A., Polarity Behaviour and Specific Interactions of Imidazolium-Based Ionic Liquids in Ethylene Glycol. *Chemphyschem*, 2011. **12**(4): p. 836-845.
32. Freire, M.G., Carvalho, P.J., Silva, A.M.S., Santos, L.M.N.B.F., Rebelo, L.P.N., Marrucho, I.M., and Coutinho, J.A.P., Ion Specific Effects on the Mutual Solubilities of Water and Hydrophobic Ionic Liquids. *Journal of Physical Chemistry B*, 2009. **113**(1): p. 202-211.
33. Freire, M.G., Neves, C.M.S.S., Silva, A.M.S., Santos, L.M.N.B.F., Marrucho, I.M., Rebelo, L.P.N., Shah, J.K., Maginn, E.J., and Coutinho, J.A.P., H-1 NMR and Molecular Dynamics Evidence for an Unexpected Interaction on the Origin of Salting-In/Salting-Out Phenomena. *Journal of Physical Chemistry B*, 2010. **114**(5): p. 2004-2014.
34. Rogers, R.D. and Zhang, J.H., Effects of increasing polymer hydrophobicity on distribution ratios of TcO_4^- in polyethylene/poly(propylene glycol)-based aqueous biphasic systems. *Journal of Chromatography B-Biomedical Applications*, 1996. **680**(1-2): p. 231-236.
35. Taboada, M.E., Asenjo, J.A., and Andrews, B.A., Liquid-liquid and liquid-liquid-solid equilibrium in Na_2CO_3 -PEG-H₂O. *Fluid Phase Equilibria*, 2001. **180**(1-2): p. 273-280.
36. Zhi, W.B., Song, J.M., Bi, J.X., and Fan, O.Y., Partial purification of alpha-amylase from culture supernatant of *Bacillus subtilis* in aqueous two-phase systems. *Bioprocess and Biosystems Engineering*, 2004. **27**(1): p. 3-7.

37. Du, Z., Yu, Y.-L., and Wang, J.-H., Extraction of Proteins from Biological Fluids by Use of an Ionic Liquid/Aqueous Two-Phase System. *Chemistry – A European Journal*, 2007. **13**(7): p. 2130-2137.
38. Chen, Y., Meng, Y., Zhang, S., Zhang, Y., Liu, X., and Yang, J., Liquid–Liquid Equilibria of Aqueous Biphasic Systems Composed of 1-Butyl-3-methyl Imidazolium Tetrafluoroborate + Sucrose/Maltose + Water. *Journal of Chemical & Engineering Data*, 2010. **55**(9): p. 3612-3616.
39. Willauer, H.D., Huddleston, J.G., Li, M., and Rogers, R.D., Investigation of aqueous biphasic systems for the separation of lignins from cellulose in the paper pulping process. *Journal of Chromatography B: Biomedical Sciences and Applications*, 2000. **743**(1–2): p. 127-135.
40. Forciniti, D., Hall, C.K., and Kula, M.R., Influence of polymer molecular weight and temperature on phase composition in aqueous two-phase systems. *Fluid Phase Equilibria*, 1991. **61**(3): p. 243-262.

11. PAPER 8

“Washing-out” in Polyethylene Glycol + Ionic Liquid Mixtures to form Aqueous Biphasic Systems

The Journal of Physical Chemistry Letters (2013) (*submitted for publication*).

11.1. Abstract

Albeit all the binary pairs, in ternary phase diagram composed of 1-butyl-3-methylimidazolium chloride ([C₄mim]Cl), polyethylene glycol 1500 (PEG 1500) and water show complete miscibility, a liquid-liquid immiscibility regime exists in the ternary mixture with the formation of aqueous biphasic systems (ABS). The mechanism of formation of these ABS has been eluding the researchers working in this area. To attempt understanding the ABS formation, the complete phase diagram for this ternary system at 323.15 K and 333.15 K is reported for the first time, and identified as a type 0 phase diagram. Molecular dynamics (MD) simulations and density functional theory calculations were used to disclose the molecular level mechanisms which control the phase behavior. They show that in the presence of water, the favorable interactions occurring between the ionic liquid anion and the –OH end groups of the polymer, responsible for their miscibility, are disrupted due to a more favorable solvation of the anion by water, inducing the observed ternary immiscibility, in a phenomenon here named as “washing-out” effect, with the ABS formation.

Keywords: Ionic liquids, polyethylene glycol, aqueous biphasic systems, phase diagrams, molecular dynamics simulations, “washing-out”

11.2. Experimental Section

The polyethylene glycol PEG polymer of average molecular weight 1500 g.mol⁻¹ (abbreviated as PEG 1500) was supplied by Fluka and used as received. The ionic liquid (IL) used was 1-butyl-3-methylimidazolium chloride ([C₄mim]Cl), purchased from Iolitec. The IL was dried under moderate temperature (343 K) and high vacuum conditions (< 0.1 mbar), for a minimum of 48 h, before use. Its purity was additionally checked by ¹H and ¹³C NMR spectroscopy, and found to be > 99 wt%.

The ternary phase diagrams at 323.15 K and 333.15 K were determined according to the protocol established by Ruiz-Angel et al¹. The composition of a ternary system, with the compounds, PEG 1500, [C₄mim]Cl and H₂O, can be represented in three dimensions if the sum of their proportions corresponds to 100%. A ternary phase diagram is a composition map delineating the monophasic, biphasic and multiphase composition regions of the three components. The experimental phase diagrams were determined in weight fraction compositions, and where several binary mixtures of PEG 1500 and

[C₄mim]Cl (*ca.* 1 g) were firstly considered. All the binary mixtures were prepared in closed glass vials and then water was drop wise added. The glass vials were properly stirred and further maintained at the temperature of equilibrium (± 1 K) for at least 12 h. After the equilibration period the resulting solution was visually examined, and if the phases separation was still not observed (clear solution), more water was added until the liquid-liquid demixing appeared (initially observed by turbidity in the system). At this point, the weight of water was measured and the total composition was determined. Then, more water was added to each test tube until another phase change behavior occurred (namely, a clear solution). At this second point, the weight of water added was again determined. The respective mixture compositions correspond to the saturation solubility curve. In summary, the phase diagrams were determined gravimetrically within $\pm 10^{-7}$ kg.

11.3. Computational Methods

The MD calculations were performed both for the TEG + [C₄mim]Cl binary mixture and for different concentrations of the TEG + [C₄mim]Cl + water ternary system. The simulations were carried out using the isothermal-isobaric NpT ($T = 298.15$ K and $p = 1$ bar) ensemble and the GROMACS 4.07 molecular dynamics package². The equations of motion were integrated with the Verlet-Leapfrog algorithm³ and a time step of 2 fs was considered. The Nosé-Hoover thermostat^{4, 5} was used to fix the temperature while the Parrinello-Rahman barostat⁶ was employed to fix the pressure. Starting configurations were generated in cubic boxes with lateral dimensions of 45 Å, and periodic boundary conditions were applied in three dimensions. The systems were prepared by randomly placing all species in the simulation box. For the calculations of the binary systems 90 [C₄mim]Cl ion pairs and 120 TEG molecules were incorporated in each box, while for the ternary solutions, (90/90/90/60/60) [C₄mim]Cl ion pairs, (120/120/120/80/80) TEG molecules and (60/120/180/200/380) water molecules were included, in order to reproduce different concentrations ($H_2O/TEG = 0.0, 0.5, 1.0, 1.5, 2.5, 4.75$), all with the same TEG/IL proportion (1.33). A 10 000 step energy minimization was performed followed by two simulations, the first one with 50 000 steps for equilibration and the final one with 10 000 000 steps (20 ns) for production. Potentials available in the literature⁷⁻⁹ were used for all the species considered in the simulations.

11.4. Introduction, Results and Discussion

The attractive and advantageous properties of both polyethylene glycols (PEGs)^{10, 11} and ionic liquids (ILs)¹²⁻¹⁵ led, in the past few years, to a growing interest in the exploitation of their combinations for a diverse number of industrial and (bio)technological procedures within the framework of *green chemistry*¹⁶⁻²². In this context, very appealing and promising applications have been proposed in the domains of purification and extraction technologies, either as homogeneous solvents, as biphasic solvent systems and, very recently, as novel polymer-IL-based aqueous biphasic systems (ABS)^{17-20, 23-26}. Nevertheless, the improvement and optimization of these applications inherently require a detailed knowledge on the phase behavior of both the IL-PEG binary mixtures and of the corresponding ternary aqueous solutions, as well as of their underlying molecular mechanisms which, due to their more complex nature, are still not completely understood. Rodríguez et al.²³ reported, for the first time, that the liquid-liquid phase behavior of IL + PEG binary mixtures can range from the complete to almost incomplete mutual miscibility if a proper choice of the IL and of the polymer molecular weight is carried out. For instance, the binary pairs composed of 1-butyl-3-methylimidazolium chloride ([C₄mim]Cl) and PEG 1000 or PEG 1500 are totally miscible within the entire range of composition and temperature evaluated whereas systems constituted by [C₄mim]Cl + PEG 2000 or PEG 3400 are not²³. In addition, it has been recently shown that ABS can be formed either with totally or partially miscible IL-polymer pairs²⁰. However, in spite of some novel insights derived from the reported phase behavior^{20, 23}, the molecular-level mechanisms that control the liquid-liquid demixing in polymer/IL and polymer/IL/water systems still remain poorly understood. Unlike for the IL/salt ABS for which it is well established that the phase separation is mainly driven by a salting-out effect²⁷, and thus the two phases domain correlates well with the salting-out ability of the salt²⁸ or with the IL hydrophobicity²⁹, the mechanism driving the phase separation of PEG-IL-based ABS seems to be by far more complex²⁰. Although the major molecular-level mechanisms previously proposed were based on “the PEG hydrophobic nature and the ease with which it is salted-out by charged species”²⁰, a cautious note was added mentioning that “besides the ionic liquid/water and PEG/water interactions that govern the phase behaviour (...) the PEG/ionic liquid interactions could additionally control the phase diagrams”²⁰. In fact, the mechanisms ruling the phase separation of PEG/IL systems in the presence of water, in particular for

those binary systems where complete miscibility is observed, still remains elusive representing a quite challenging scenario. In this context, and trying to better understand the molecular-based phenomena behind the formation of IL-PEG-based ABS, this work addresses the experimental determination of the complete $[C_4mim]Cl + PEG\ 1500 +$ water ternary phase diagram at two distinct temperatures (323.15 K and 333.15 K) with the concomitant use of molecular dynamics (MD) simulations.

The experimental ternary phase diagrams at 323.15 K and 333.15 K, here depicted in Figure 11.1, are shown, for the first time, to be of type 0, characterized by an immiscibility gap in the ternary region while all the binary mixtures are fully miscible. The two-phase regime of IL-PEG-based ABS decreases with increasing temperature. This dependency is similar to that observed before in PEG-IL-based ABS²⁰, and it is the opposite of the solubility behavior presented by PEG-inorganic-salt systems³⁰. Moreover, additional experiments demonstrated that the ternary mixture here studied never displays a complete miscibility even at high temperatures. Instead the immiscibility region starts growing again in an hourglass type diagram.

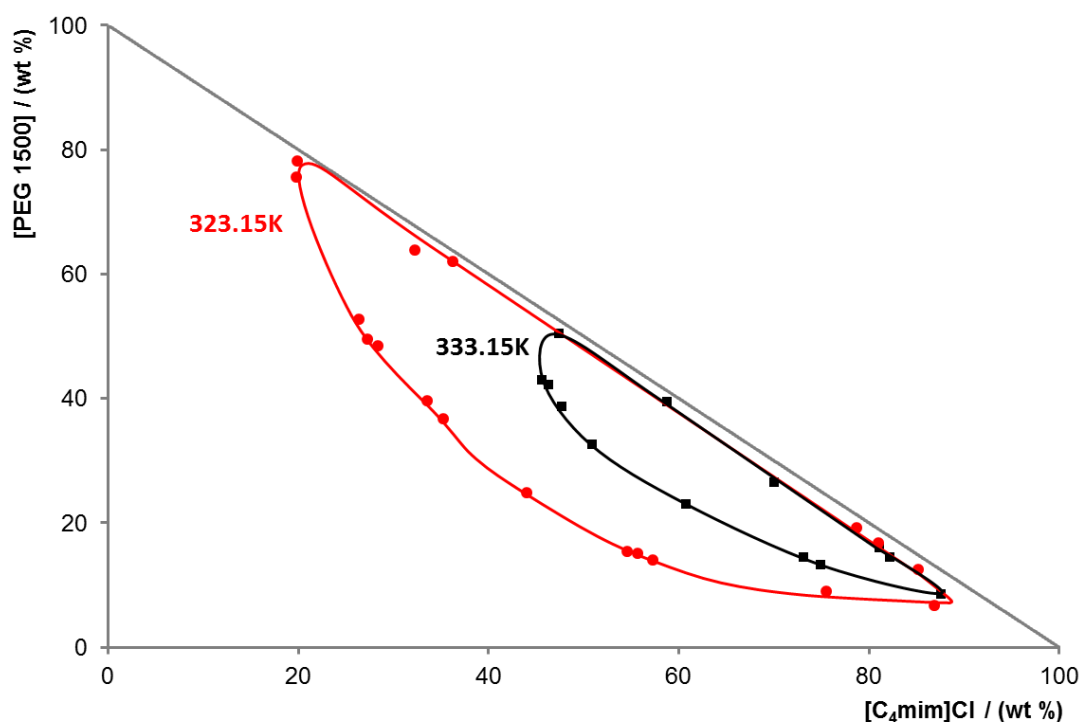


Figure 11.1 Experimental solubility data for the PEG 1500/ $[C_4mim]Cl$ ABS at 323.15 K (red dots) and 333.15 K (black squares).

The complete miscibility reported by Rodríguez et al.²³ for the system composed of [C₄mim]Cl and PEG 1500 was here confirmed. Yet, the phase diagrams here measured suggest that a very small amount of water (\approx 1-3 wt% depending on the binary mixture and temperature) is enough to trigger the liquid-liquid phase separation. The phase behavior observed cannot thus be explained in terms of a salting-out phenomenon induced by the polymer through the IL or of the IL over the polymer, or attributed to an unfavorable miscibility/affinity within the PEG/IL pair.

To foster the understanding of the phase separation observed in aqueous media and reported in Figure 11.1, MD simulations were carried out for mixtures composed of [C₄mim]Cl and tetraethylene glycol (TEG) (taken as a model of polyethylene glycol) with increasing water content. The structure and atom labeling of the studied compounds are presented in Figure 11.2.

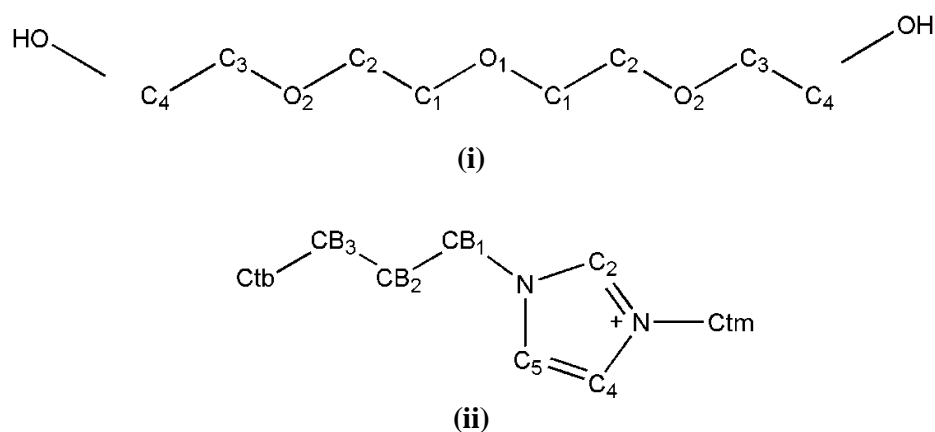
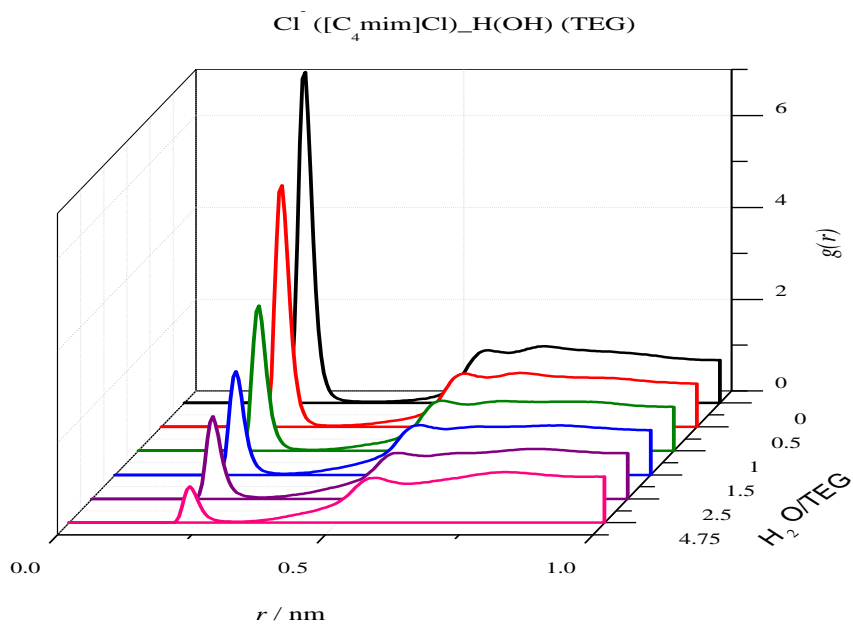
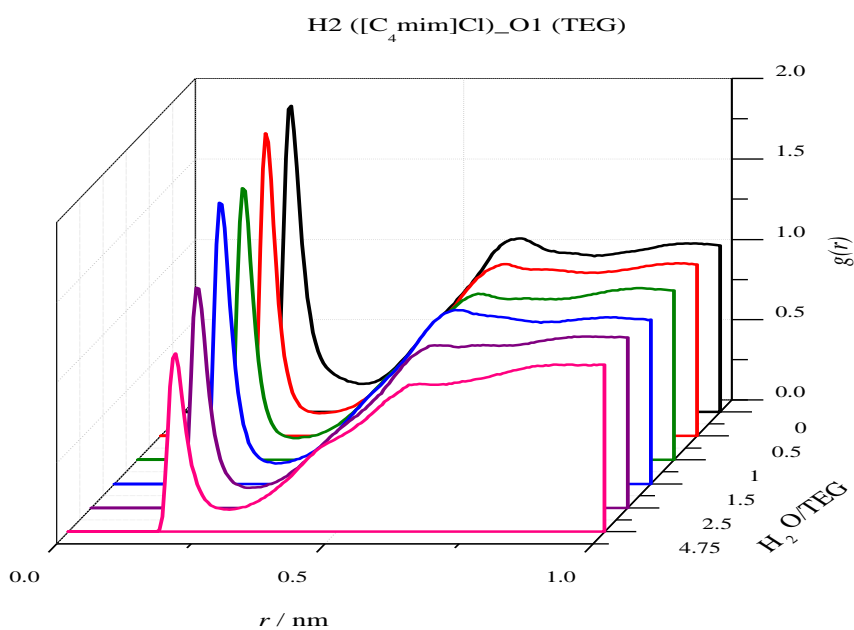


Figure 11.2 Structure and atom labeling of (i) TEG and (ii) [C₄mim]⁺. C_{tb} stands for the terminal carbon atoms of the butyl side chain of the IL cation, while C_{B_x} (x = 1, 2, 3) is used to denote the other carbon atoms of the same alkyl chain. C_{tm} stands for the carbon atom of the methyl side chain of the IL cation. Hydrogen atoms of the molecules, omitted for clarity, are labeled with the number of the carbon atoms to which they are attached to.



(a)



(b)

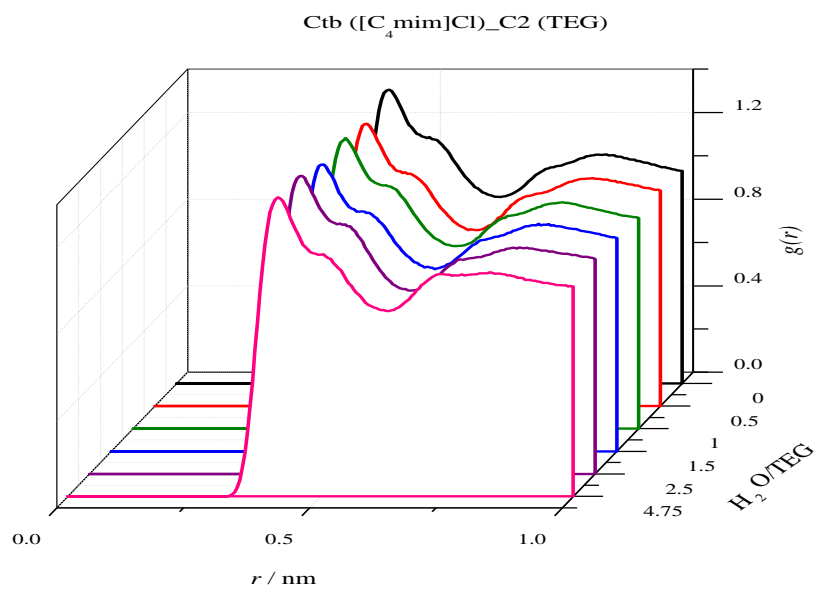
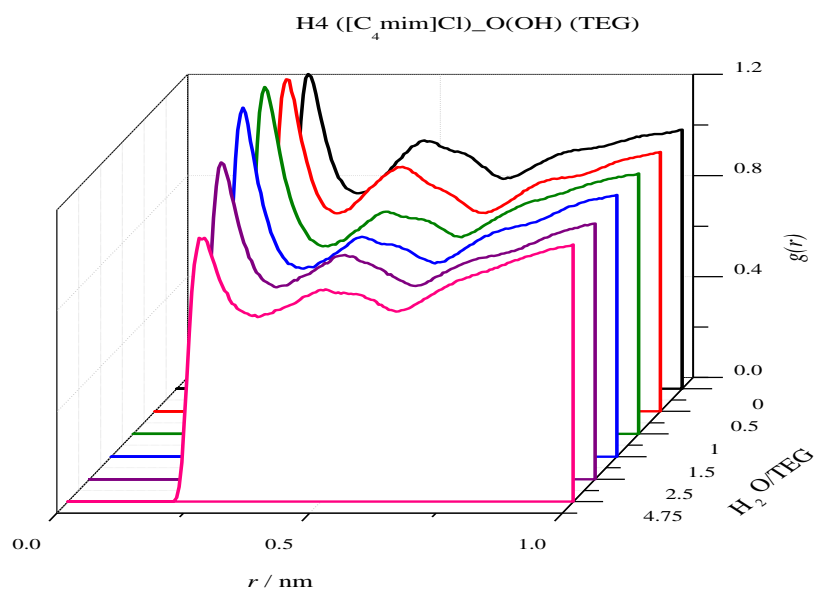


Figure 11.3 Radial distribution functions for the interactions of the (a) IL anion and (b) the H2 atom, (c) the H4 atom and (d) the terminal carbon atom of the alkyl chain of the IL cation with selected atoms of TEG for the ([C₄mim]Cl+water) binary system and for ([C₄mim]Cl + TEG + water) ternary mixtures at different concentrations.

The radial distribution functions (RDFs) for selected interactions are depicted in Figure 11.3(a-d). In agreement with the suggestions previously provided by Rodríguez et al.²³, the H-bonding occurring between the Cl⁻ and the -OH groups of TEG were identified as the main interaction controlling the mutual solubilities of the IL and the polymer in the respective binary system as shown by the strong peak observed in Figure 11.3a. Although of a much weaker intensity, as illustrated in Figures 11.3b and 11.3c, H-bonds are also established between TEG and the IL cation at the level of the hydrogen atoms of the imidazolium ring. Some hydrophobic interactions between the cation alkyl chain and the less polar moieties of the PEG are observed as well - Figure 11.3d. Nevertheless, when water is introduced into the binary system a more complex picture takes place and the intensity of the RDF peaks corresponding to the H(OH)(TEG)⋯Cl⁻ interactions (Figure 11.3a) decreases very quickly along with the water concentration and essentially disappears ($g(r)$ tends to one) when the water content is large enough. Furthermore, as suggested by the RDFs depicted in Figure 11.3b and 11.3c, the association of the hydrogen atoms of the imidazolium ring to the oxygen atoms of TEG is much less affected but also decreases somewhat with the water concentration. In contrast, no significant differences on the interactions between the non-polar moieties of the cation and the polymer are observed with the increasing water content as depicted in Figure 11.3d, indicating that, unlike those of polar nature, they are not significantly affected by the presence of water.

The results here reported show that the chloride anion, being an H-bond acceptor, forms H-bonds with the protons of the terminal hydroxyl groups of the polymer, while the ether oxygen atom of TEG, that is also an H-bond acceptor, establishes H-bonds with the acidic hydrogen atoms of the cation. When water molecules are introduced in the system, which can act either as a (much stronger) H-bond donor or acceptor, the H-bonds formed between water and the IL anion are more favorable and stronger than those occurring between the components of the binary non-aqueous system. Consequently, the H-bonds established between the IL anion and cation with the polymer disappear, as if washed away by the water. The weak hydrophobic interactions between the cation alkyl chain and the less polar moiety of TEG are the only remaining interactions. As a result, both the IL and the PEG become independently solvated by water and two aqueous-rich phases are formed. Given the analogy of this mechanism of

phase separation with the washing process we named this mechanism of ABS formation of “washing-out”.

A support for this molecular scenario can be obtained from the DFT data reported in Tables 11.1 and 11.2 (extended Tables are supplied as Supporting Information). As it can be seen, similar interaction energies are calculated for the interactions between the chloride anion with water or with TEG (Table 11.1), which are visibly larger than the interaction energies for the water-water or water-TEG complexes. The results in Table 11.2 suggest that with the increase of the water content, the interaction energy between the anion and water becomes more important than the interaction between chloride and TEG, i.e., the reaction $[\text{ClTEG}]^- + (\text{H}_2\text{O})_n \rightarrow \text{TEG} + [\text{Cl}(\text{H}_2\text{O})_n]^-$ is thermodynamically favorable for a number of water molecules (n) participating in the hydration shell of the chloride >1 , which results in the washing-out effect. Thus, the driving force for the removal of the IL anion from the vicinity of the polymer is not the binding of water to the OH groups of TEG but instead, the strong(er) water- Cl^- interactions which “wash” the anion away from the TEG, to be solvated into the water bulk. Assuming the most likely $[\text{Cl}-(\text{H}_2\text{O})_6]^{31,32}$ cluster, it is clear that the hydration of the anion is energetically favorable and therefore the latest is removed from the vicinity of TEG by the water molecules as soon as they are introduced into the system. Moreover, studies of the structure and dynamics of $\text{Cl}-(\text{H}_2\text{O})_6$ cluster by MD simulations using nonpolarizable force fields predict that the chloride anion prefers a location on the interior of the cluster³³. It should also be highlighted that the role of the H-bonding in the solvation of cellulose by imidazolium-based ILs has been previously pointed out and the precipitation of monosaccharides, such as glucose, in an aqueous IL medium has been interpreted in terms of an analogous molecular phenomena^{34,35}.

Table 11.1. Interaction energies for some complexes fully optimized at the M06/aug-cc-pVDZ level of theory.^a

System	$\Delta E^0 / \text{kJ mol}^{-1}$
Cl ⁻ - H ₂ O	-89.5; -88.2 ^b
Cl ⁻ - TEG	-98.8; -96.6 ^b
H ₂ O - TEG	-33.5; -30.4 ^b
Cl ⁻ - (H ₂ O) ₂	-112.0 ^c ; -100.0 ^d
Cl ⁻ - (H ₂ O) ₃	-169.7 ^c ; -123.8 ^d
Cl ⁻ - (H ₂ O) ₄	-219.8 ^c ; -136.4 ^d
H ₂ O - H ₂ O ^e	-11.9; -11.1 ^b
H ₂ O - (H ₂ O) ₂	-45.9 ^f ; -33.9 ^g
H ₂ O - (H ₂ O) ₃	-83.4 ^f ; -37.5 ^g

^a ΔE^0 denotes the change in the electronic energies including the zero-point energy corrections. ^b Geometry of the complex optimized with counterpoise corrections. ^c Energy variation corresponding to the reaction $\text{Cl}^- + n \text{H}_2\text{O} \rightarrow [\text{Cl}(\text{H}_2\text{O})_n]^-$. ^d Energy variation corresponding to the reaction $\text{Cl}^- + (\text{H}_2\text{O})_n \rightarrow [\text{Cl}(\text{H}_2\text{O})_n]^-$. ^e High-level computational results range from -12.5 to -13.2 $\text{kJ}\cdot\text{mol}^{-1}$ ³⁶ and benchmark experimental value is $-13.22 \pm 0.12 \text{ kJ}\cdot\text{mol}^{-1}$ ³⁷. ^f Energy variation corresponding to the reaction $\text{H}_2\text{O} + n \text{H}_2\text{O} \rightarrow [\text{H}_2\text{O}(\text{H}_2\text{O})_n]$. ^g Energy variation corresponding to the reaction $\text{H}_2\text{O} + (\text{H}_2\text{O})_n \rightarrow [\text{H}_2\text{O}(\text{H}_2\text{O})_n]$.

Table 2. Energies calculated for the reaction $[\text{ClTEG}]^- + (\text{H}_2\text{O})_n \rightarrow \text{TEG} + [\text{Cl}(\text{H}_2\text{O})_n]^-$ with $n = 1 - 4$.

n	$\Delta E^0 / \text{kJ mol}^{-1}$
1	9.4
2	-1.2
3	-25.0
4	-37.5

It is here reported, for the first time, that ternary PEG-IL-water systems are of type 0 – the mutual miscibility amongst all the binary pairs being always observed with an immiscibility regime appearing in the ternary mixture. Unlike what happens in IL-salt-based ABS, where the phase behavior is dominated by the salt ions ability to form hydration complexes (salting-out inducing effect), and the formation of PEG-IL-based ABS is controlled by the water solvation of the IL anion which leads to the destruction of the H-bonds established between the IL anion and the PEG-OH groups. The ABS formation in PEG/IL systems is thus different than previously anticipated¹¹ and does not result from a salting-out effect of the polymer by the IL or of the IL over the polymer; instead, the PEG-IL-based ABS formation is a result of what is here named a “washing-out” phenomenon.

11.5. References

1. Ruiz-Angel, M.J., Pino, V., Carda-Broch, S., and Berthod, A., Ionic Liquids in separation techniques, *Journal of Chromatography A*, 2007. **1151** (1-2): p. 65-73.
2. Hess, B., Kutzner, C., van der Spoel, D., and Lindahl, E., GROMACS 4: Algorithms for Highly Efficient, Load-Balanced, and Scalable Molecular Simulation. *Journal of Chemical Theory and Computation*, 2008. **4** (3): p. 435-447.
3. Hockney, R.W. and Goel, S.P.J., Quite high resolution models of plasma. *Journal of Computational Physics*, 1974. **14**: p. 148-158.
4. Nosé, S., A molecular dynamics method for simulations in the canonical ensemble. *Molecular Physics*, 1984. **52**(2): p. 255-268.
5. Hoover, W.G., Canonical dynamics: Equilibrium phase-space distributions. *Physical Review A*, 1985. **31**(3): p. 1695-1697.
6. Parrinello, M. and Rahman, A., Polymorphic transitions in single crystals: A new molecular dynamics method. *Journal of Applied Physics*, 1981. **52**(12): p. 7182-7190.
7. Cadena, C. and Maginn, E.J., Molecular Simulation Study of Some Thermophysical and Transport Properties of Triazolium-Based Ionic Liquids. *Journal of Physical Chemistry B*, 2006. **110**(36): p. 18026-18039.
8. Jorgensen, W.L. and Tirado-Rives, J., Potential energy functions for atomic-level simulations of water and organic and biomolecular systems. *Proceedings of the National Academy of Sciences of the United States of America*, 2005. **102**(19): p. 6665-6670.
9. Chandrasekhar, J., Spellmeyer, D.C., and Joergensen, W.L., Energy component analysis for dilute aqueous solutions of lithium(1+), sodium(1+), fluoride(1-), and chloride(1-) ions. *Journal of American Chemical Society*, 1984. **106**(4): p. 903-910.
10. Powell, G.M., *Handbook of Water Soluble Gums and Resins*, ed. R.L. Davidson 1980, New York: McGraw-Hill.
11. Herold, D., Keil, K., and Burns, D.E., Oxidation of polyethylene glycols by alcohol dehydrogenase. *Biochemical Pharmacology*, 1989. **38**: p. 73-76.
12. Wasserscheid, P. and Keim, W., Ionic Liquids—New “Solutions” for Transition Metal Catalysis. *Angewandte Chemie-International Edition*, 2000. **39**(21): p. 3772-3789.
13. Zakrzewska, M.E., Bogel-Lukasik, E., and Bogel-Lukasik, R., Solubility of Carbohydrates in Ionic Liquids. *Energy Fuels*, 2010. **24**: p. 737-745.
14. Domanska, U. and Bogel-Lukasik, R., Physicochemical Properties and Solubility of Alkyl-(2-hydroxyethyl)-dimethyl-ammonium Bromide. *Journal Physical Chemistry B*, 2005. **109**: p. 12124-12132.
15. Seddon, K.R., Ionic liquids for clean technology. *Journal of Chemical Technology and Biotechnology*, 1997. **68**: p. 351-356.
16. Shin, J.-H., Henderson, W.A., and Passerini, S., Ionic liquids to the rescue? Overcoming the ionic conductivity limitations of polymer electrolytes. *Electrochemistry Communications*, 2003. **5**(12): p. 1016-1020.
17. Triolo, A., Russina, O., Keiderling, U., and Kohlbrecher, J., Morphology of Poly(ethylene oxide) Dissolved in a Room Temperature Ionic Liquid: A Small Angle Neutron Scattering Study. *Journal of Physical Chemistry B*, 2006. **110**(4): p. 1513-1515.
18. Sarkar, A., Trivedi, S., and Pandey, S., Unusual solvatochromism within 1-butyl-3-methylimidazolium hexafluorophosphate plus poly(ethylene glycol) mixtures. *Journal Physics Chemistry B*, 2008. **112**(30): p. 9042-9049.
19. Pereira, J.F.B., Lima, A.S., Freire, M.G., and Coutinho, J.A.P., Ionic Liquids as Adjuvants for the Tailored Extraction of Biomolecules in Aqueous Biphasic Systems. *Green Chem.*, 2010. **12**(9): p. 1661-1669.

20. Freire, M.G., Pereira, J.F.B., Francisco, M., Rodríguez, H., Rebelo, L.P.N., Rogers, R.D., and Coutinho, J.A.P., Insight into the Interactions That Control the Phase Behaviour of New Aqueous Biphasic Systems Composed of Polyethylene Glycol Polymers and Ionic Liquids. *Chemistry - A European Journal*, 2012. **18**(6): p. 1831-1839.
21. Li, X., Hou, M., Zhang, Z., Han, B., Yang, G., Wang, X., and Zou, L., Absorption of CO₂ by ionic liquid/polyethylene glycol mixture and the thermodynamic parameters. *Green Chemistry*, 2008. **10**: p. 879-884.
22. Calado, M.S., Ivanis, G.R., Vuksanovic, J.M., Kijevcanin, M.L.J., Serbanovic, S.P., and Visak, Z.P., "Green Meets Green" – Sustainable solutions of imidazolium and phosphonium ionic liquids with poly(ethylene glycol): Solubility and phase behavior. *Fluid Phase Equilibria*, 2013. **344**: p. 6-12.
23. Rodríguez, H., Francisco, M., Rahman, M., Sun, N., and Rogers, R.D., Biphasic liquid mixtures of ionic liquids and polyethylene glycols. *Physical Chemistry Chemical Physics*, 2009. **11**: p. 10916-10922.
24. Visak, Z.P., Lopes, J.N.C., and Rebelo, L.P.N., Ionic liquids in polyethylene glycol aqueous solutions salting-in salting-out effects. *Monatshefte für Chemie*, 2007. **138**: p. 1153-1157.
25. Pereira, J.F.B., Vicente, F., Santos-Ebinuma, V.C., Araújo, J.M., Pessoa, A., Freire, M.G., and Coutinho, J.A.P., Extraction of Tetracycline from Fermentation Broth using Aqueous Two-Phase Systems composed of Polyethylene Glycol and Cholinium-based Salts, *Process Biochemistry*, 2013, doi: 10.1016/j.procbio.2013.02.025.
26. Pereira, J.F.B., Mourão, T., Cojocar, O.A., Gurau, G., Rebelo, L.P.N., Rogers, R.D., Coutinho, J.A.P., and Freire, M.G., *Green Chem.*, 2012. Biocompatible aqueous biphasic systems composed of polyethylene glycols and cholinium-based ionic liquids: towards the understanding of their formation ability. *Chemical Science* (2013) (*submitted for publication*).
27. Gutowski, K.E., Broker, G.A., Willauer, H.D., Huddleston, J.G., Swatoski, R., Holbrey, J., and Rogers, R.D., Controlling the aqueous miscibility of ionic liquids: aqueous biphasic systems of water-miscible ionic liquids and water-structuring salts for recycle, metathesis, and separations. *Journal of American Chemical Society*, 2003. **125**: p. 6632-6633.
28. Shahriari, S., Neves, C.M.S.S., Freire, M.G., and Coutinho, J.A.P., Role of the Hofmeister Series in the Formation of Ionic-Liquid-Based Aqueous Biphasic Systems. *Journal of Physical Chemistry B*, 2012. **116**: p. 7252-7258.
29. Neves, C.M.S.S., Ventura, S.P.M., Freire, M.G., Marrucho, I.M., and Coutinho, J.A.P. Evaluation of Cation Influence on the Formation and Extraction Capability of Ionic-Liquid-Based Aqueous Biphasic Systems. *Journal of Physical Chemistry B*, 2009. **113**: p. 5194-5199.
30. Willauer, H.D., Huddleston, J.G., Li, M., and Rogers, R.D., Investigation of Aqueous Biphasic Systems for the Separations of Lignins from Cellulose in the paper Pulp Process. *Journal of Chromatography B: Biomedical Sciences and Applications*, 2000. **743**(1-2): p. 127-135.
31. Mancinelli, R., Botti, A., Bruni, F., and Ricci, M.A., Hydration of sodium, potassium, and chloride ions in solution and the concept of structure maker/breaker. *The Journal of Physical Chemistry B*, 2007. **111**: p. 13570-13577.
32. Zhao, Z., Rogers, D.M., and Beck, T.L., Polarization and charge transfer in the hydration of chloride ions. *Journal of Chemical Physics*, 2010. **132**(1): p. 14502-14512.
33. Tobias, D.J., Jungwirth, P., and Parrinello, M., Surface solvation of halogen anions in water clusters: an ab initio molecular dynamics study of the Cl-(H₂O)₆ complex. *Journal of Chemical Physics*, 2001. **114**: p. 7036-7044.
34. Liu, H., Sale, K.L., Holmes, B.M., Simmons, B.A., and Singh, S., Understanding the interactions of cellulose with ionic liquids: a molecular dynamics study. *Journal of Physical Chemistry B*, 2010. **114**: p. 4293-4301.
35. Liu, H., Sale, K.L., Holmes, B.M., Simmons, B.A., and Singh, S., Molecular dynamics study of polysaccharides in binary solvent mixtures of an ionic liquid and water. *Journal of Physical Chemistry B*, 2010. **115**: p.10251-10258.

36. Shank, A., Wang, Y., Kaledin, A., Braams, B.J., and Bowman, J.M., Accurate ab initio and "hybrid" potential energy surfaces, intramolecular vibrational energies, and classical IR spectrum of the water dimer. *Journal of Chemical Physics*, 2009. **130**: p.144314-144324.

37. Rocher-Castelline, B.E., Chang, L.C., Mollner, A.K., and Reisler, H.A., Determination of the bond dissociation energy (D_0) of the water dimer, $(\text{H}_2\text{O})_2$ by velocity map imaging. *Journal of Chemical Physics*, 2011. **134**: p.211101-211104.

12. PAPER 9

Combining Ionic Liquids and Polyethylene Glycols to Boost the Hydrophobic-Hydrophilic Range of Aqueous Biphasic Systems

Chemical Communications, (2013) *(submitted for publication)*.

12.1. Abstract

The hydrophobic-hydrophilic range of aqueous biphasic systems is vastly enhanced if ionic liquids and polyethylene glycols are combined. Three probe dyes were used to demonstrate that either the polymer-rich or the ionic-liquid-rich layer can serve as the most hydrophobic phase allowing the tailoring of phase polarities.

12.2. Materials and Experimental Procedure

Chloranilic Acid (CA, > 99 wt% pure) was purchased from Merck, while Indigo Carmine (IC, \geq 98 wt% pure) and Indigo Blue (IB, > 95 wt% pure) were acquired from Sigma-Aldrich. All the ILs were commercially acquired from Iolitec with purities > 98 wt %. All samples were dried for 24 h under vacuum and at a moderate temperature (323 K) before use. PEG of average molecular weight 1500 g.mol⁻¹ (PEG 1500) was supplied by Fluka and used as received. The water used was ultrapure water, double distilled, passed by a reverse osmosis system and finally treated with a Milli-Q plus 185 purification equipment.

The ABS combining PEG 1500 and four different ILs, namely [C₂mim]Cl, [C₄mim]Cl, [C₄mpyrr]Cl and [C₄mpip]Cl were determined by the turbidimetric titration method. A mixture point into biphasic region, approximately 38 wt% of PEG, 52 wt% of IL and 10 wt% of water, was selected and used to evaluate the partitioning of three different dyes, Chloranilic acid (CA), Indigo Carmine (IC) and Indigo Blue (IB), respectively. In each system a small amount of each dye, \approx 0.30 mg, was added to glass tubes containing the ternary compositions with a total mass of 5 g. The ABS were then allowed to equilibrate at 323 K and pressure conditions during 3 h. After that period, the top and bottom phases were carefully separated, and the partition coefficients of each dye were evaluated. The partition coefficient is defined as the concentration of the dye in the IL-rich to that in the PEG-rich phases. The quantification of each dye in both phases was carried out by UV-Vis spectroscopy.

12.3. Introduction, Results and Discussion

Traditional aqueous biphasic systems (ABS) consist of two immiscible aqueous-rich phases based on polymer/polymer, polymer/salt or salt/salt combinations. These systems actually constitute a greener alternative to typical solvent-extraction strategies

which use volatile and hazardous solvents. ABS are constituted by a high water content (*circa* 60-80 % in a weight fraction basis) and are able to maintain the native conformation and biological activity of the most diverse biomolecules. Traditional polymer-based ABS have been largely employed in the separation and purification of proteins, enzymes, blood cells and antibiotics¹⁻⁷. However, and despite their advantages, conventional polymer-based ABS exhibit a limited hydrophobic-hydrophilic range at their coexisting phases which has restricted their application due to limited extraction yields and purification factors. ABS composed of two distinct polymers display coexisting phases of similar polarities whereas polymer-salt ABS present a hydrophobic and an ionic and particularly hydrophilic layer. The limited array of different polarities in these more traditional systems has led the search of alternative strategies, such as the polymer derivatization or use of additives, aiming at improving the extraction yields of a target molecule. Nevertheless, these approaches turn the process more complex and costly⁸⁻¹³.

As alternatives to polymers, ionic liquids (ILs) were proposed as novel phase forming components of ABS^{14, 15}. They exhibit several interesting properties, and one of the most interesting and valuable features in the field of separation approaches is the prospective to tailor their solvent ability by selection of the IL constituting ions¹⁵. ABS composed of ILs have already shown to be enhanced platforms for the extraction of the most diverse biomolecules from aqueous media¹⁶⁻²². Besides the ABS composed of ILs and inorganic/organic salts, it has been recently demonstrated that the IL-based ABS concept can be extend to polymer-IL combinations²³⁻²⁶. Most works address the use of polypropylene glycol (PPG) due to its higher ability to liquid-liquid demixing in the presence of “salting-out” inducing ILs^{27, 28}. Nonetheless, the ABS formed by ILs and polyethylene glycol (PEG), a more hydrophilic polymer than PPG, are by far more interesting and complex²³. It was observed that, despite the hydration capability of the isolated ions in aqueous media, the interactions occurring between the ionic fluid and the polymer play a major role on the formation of these ABS^{23, 29, 30}.

Based on the tailoring aptitude afforded by ILs, as well as on the hydrophilic character of low molecular weight PEG, this work shows the partitioning behavior of three dyes, used as molecular probes of different hydrophobicity, aiming at demonstrating how (IL+PEG)-based ABS can expand the hydrophobic-hydrophilic range of polymer-based ABS overcoming thus one of their major limitations. For that purpose, the ternary phase

diagrams of ABS, composed of different water-miscible chloride-based ILs and PEG 1500, were initially determined at 323 K and atmospheric pressure by the turbidimetric titration method²³. Different ILs were employed, and the experimental binodal curves and respective correlations^{23, 31} are shown in Figure 12.1. The detailed experimental weight fraction data and correlation parameters are given in Supporting Information (Table S12.1).

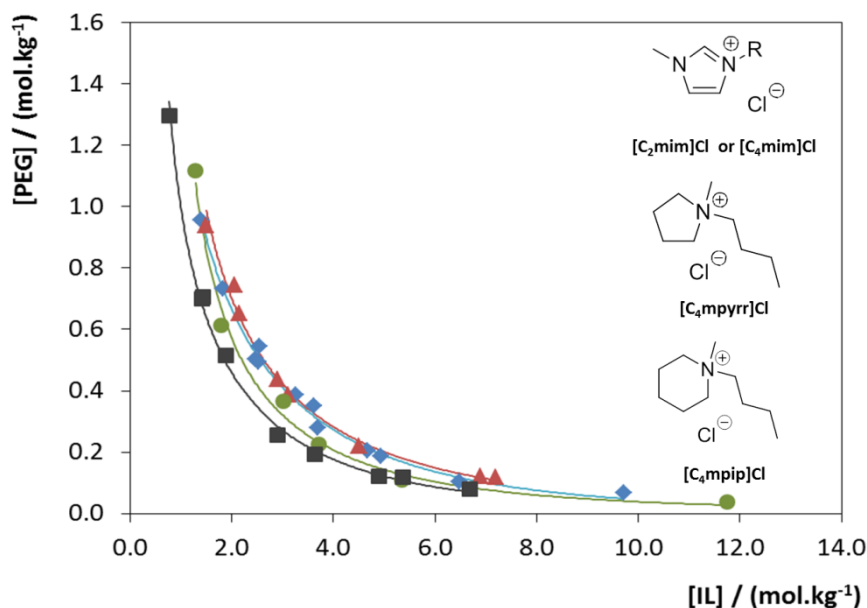


Figure 12.1 Experimental solubility data and correlations for IL/PEG 1500 ABS at 323 K and atmospheric pressure: (■) [C₄mpip]Cl; (●) [C₄mpyrr]Cl; (◆) [C₂mim]Cl; (▲) [C₄mim]Cl. The molecular structures of the ILs are provided as an insert.

The experimental results, shown in molality units (mole of solute *per* kg of solvent), reveal that the ability of the ILs to induce a PEG-1500-based ABS follows the trend: [C₄mpip]Cl > [C₄mpyrr]Cl > [C₂mim]Cl ≈ [C₄mim]Cl. According to the results reported for PPG^{27, 28}, the higher the IL ions ability to create hydration complexes and/or its hydrophilic character the higher it is its salting-out aptitude. However, with PEG, and as observed before²³, the ABS formation phenomenon is more complex. According to this salting-out inducing model the most hydrophobic IL investigated, [C₄mpip]Cl, should be the less effective in promoting the liquid-liquid regime. Instead, this IL is the most proficient in the formation of PEG-based ABS. As detailed elsewhere^{23, 29, 30} the interactions between PEG and ILs and their disruption by water are the driving force behind the ABS formation. Due to the wide polarity range of the ILs

and based on a preferential PEG-IL affinity it is thus conceivable the possibility of tuning the phases' polarities by the adequate selection of the IL.

The partitioning behaviour of three dyes of different hydrophobicity was investigated in the novel determined liquid-liquid systems in order to confirm and macroscopically ascertain on the phases' polarities. For that purpose chloranilic acid (CA, octanol-water partition coefficient – $\log K_{ow} = 1.22^{32}$), Indigo Carmine (IC, $\log K_{ow} = 1.627^{32}$) and Indigo Blue (IB, $\log K_{ow} = 3.188^{32}$) were used. After an equilibration period of 3 h at 323 K, the top and bottom phases were separated and the partition coefficient - defined as the concentration of each dye in the IL-rich to that in the PEG-rich phases, was measured. Additional experimental data, namely phases' compositions and partition coefficient values are provided in Supporting Information (Tables S12.2 and S12.3).

The partition coefficients obtained for CA are depicted in Figure 12.2. At a neutral pH (and charged CA) it is notorious that a wide range of partition coefficients can be obtained with the various PEG-IL ABS. Nevertheless, at these conditions, CA preferentially migrates for the IL-rich phase. This is a consequence of the negative charge of CA at this pH and its preference for the most charged layer driven by electrostatic interactions. CA has pK_a values of 0.58 and 3.18³³. The respective dissociation curves and the pH values of the coexisting phases of each ABS are presented in Supporting Information (Figure S12.1). In aqueous media, at different pH values, CA may exist as a cationic, zwitterionic or anionic species. Therefore, aiming at avoiding the prevalence of electrostatic interactions, further experiments were conducted at a controlled pH (between 3 and 4) to maintain CA as a neutral species. For comparison purposes and to ascertain on the potential of polymer-IL ABS to broaden the hydrophobic-hydrophilic range provided by common systems, the results obtained for typical polymer-salt and polymer-polymer ABS, namely PEG 4000 + Dextran 40000 and PEG 1500 + Na₂SO₄, are also depicted in Figure 12.2.

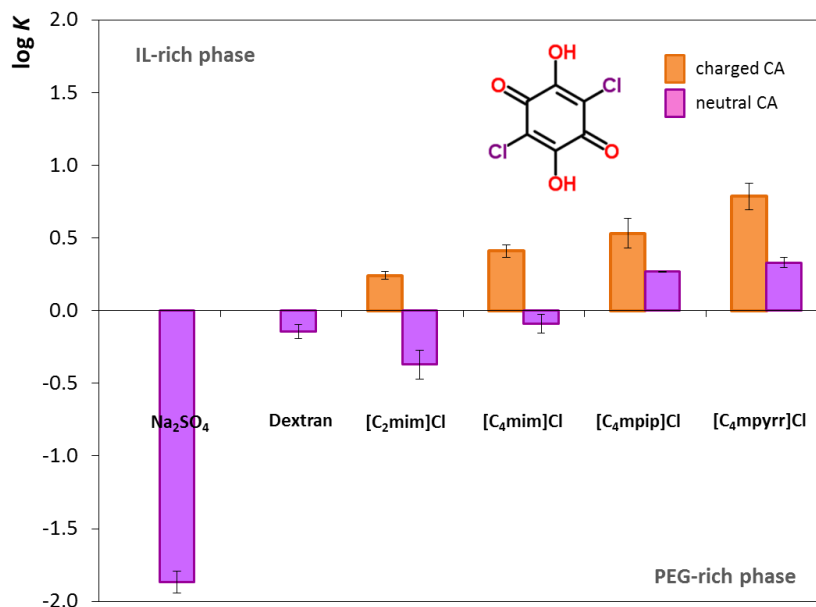


Figure 12.2 Log of the partition coefficients (log K) of CA in several IL-based ABS at 323 K (neutral CA is violet; anionic CA is orange). The molecular structure of CA is provided as an insert.

The partitioning of CA as a neutral molecule is remarkably different from that observed with its charged counterpart. With the traditional systems, CA always migrates for the PEG-rich phase - the most hydrophobic layer in both examples. Now while for the [C₂mim]Cl- and [C₄mim]Cl-based ABS CA still preferentially migrates for the PEG-rich phase an inversion on the migration pattern is observed when using the more hydrophobic ILs, such as [C₄mpip]Cl and [C₄mpyrr]Cl. CA presents a high K_{ow} value which reflects its affinity for more lipophilic solvents. Thus, the partition coefficients here obtained clearly confirm an inversion on the phases' polarities within the PEG-IL-based ABS. They show that it is possible to convert the PEG into the more hydrophilic phase and thus to tailor the preferential migration of a hydrophobic molecule by varying the IL cationic structure. The visual aspect of the systems studied is depicted in Figure 12.3.

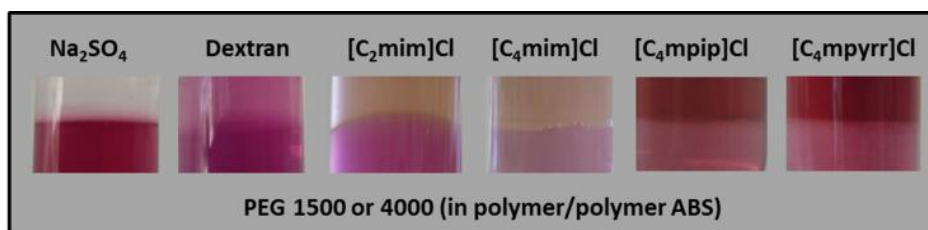


Figure 12.3 Visual aspect of the migration pattern of neutral CA in the studied ABS at 323 K.

Besides the inversion on the migration pattern observed with the neutral CA the effect of the pH towards the partitioning behaviour should be additionally highlighted. In the imidazolium-based systems an overturn on the preferential partitioning of the solute arises as a consequence of the medium pH. An increase in the pH of the aqueous medium leads to a trend shift on the migration of the dye from the polymer- to the IL-rich phase. Visser et al.³⁴ also demonstrated a reversible pH-dependent liquid-liquid partitioning of an indicator dye, thymol blue, but only with water immiscible ILs.

To further support the proposed concept, the partition coefficients of Indigo Blue and Indigo Carmine were also determined in similar ABS. The partition coefficient values and the macroscopic appearance of the migration tendency of the two dyes are depicted in Figures 12.4 and 12.5, respectively. The results obtained with the conventional PEG-1500- Na_2SO_4 ABS are also presented for comparison purposes. The details on the partition coefficient values, pH of the coexisting phases and mixture compositions are shown in Supporting Information (Table S12.3).

The results illustrated in Figures 12.4 and 12.5 were determined at a pH near 7 at which IB is mainly present as a neutral molecule and IC is in a salt form – *cf.* Supporting Information (Figures S12.2 and S12.3) with the respective dissociation curves. While in the conventional system composed of PEG + inorganic salt the favoured partitioning of IB and IC occurs for the PEG-rich phase, as was observed with CA, the IB partitioning pattern demonstrates that it is possible to manipulate and control the dye partition by a judicious choice of the IL employed. The inversion of the phase's polarities is here again confirmed by the reversal on the dyes' preferential partitioning. The partitioning of the IC salt, as previously observed for the charged CA, is different and reveals a preferential migration for the charged IL-rich phase in all systems.

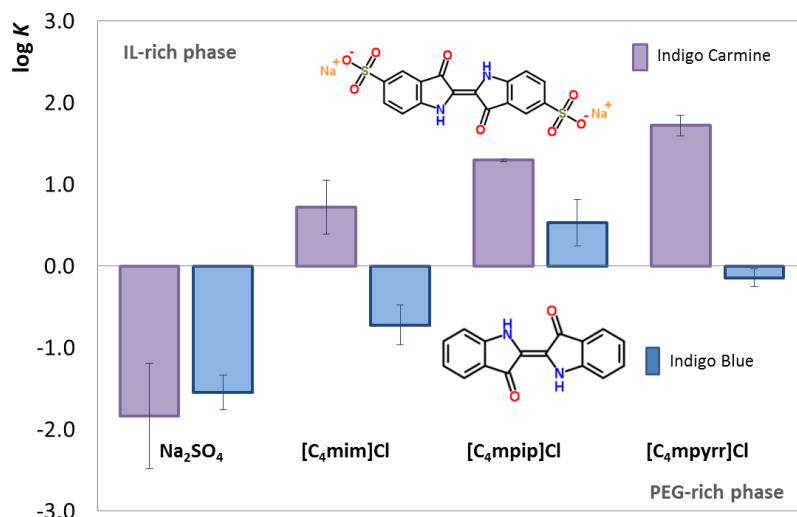


Figure 12.4 Log of the partition coefficients ($\log K$) of neutral IB and charged IC in several IL-based ABS at 323 K and in PEG 1500/Na₂SO₄ ABS. The molecular structures of IB and IC are provided as an insert.

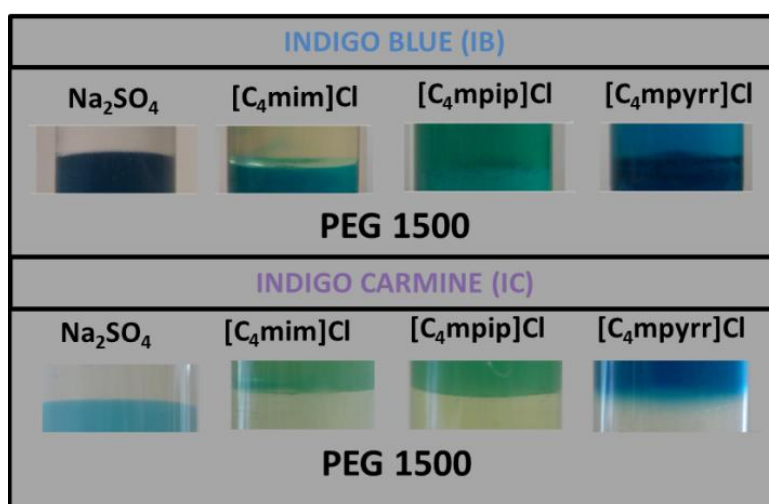


Figure 12.5 Visual aspect of the migration pattern of IB and IC in the studied ABS at 323 K.

In summary, this work shows, for the first time, that IL-PEG-based ABS exhibit a much wider hydrophilic-hydrophobic range than conventional ABS reported to date and that their phases' polarities can be tuned by the choice of an appropriate IL. These features were confirmed with the migration of three probe dyes of different hydrophobicity and making use of their charged and neutral states. The inversion on the phases' polarities was established by an observed trend shift on the dyes' preferential migration, *i.e.*, either for the PEG- or the IL-rich phases. This ample versatility of IL-PEG-based ABS creates thus a new plethora of extraction and purification systems hitherto unknown.

12.4. References

1. Albertsson, P.Å., Partition of cell particles and macromolecules : separation and purification of biomolecules, cell organelles, membranes, and cells in aqueous polymer two-phase systems and their use in biochemical analysis and biotechnology. 3rd ed 1986, New York: Wiley. 346 p.
2. Shanbhag, V.P. and Johansson, G., Specific extraction of human serum albumin by partition in aqueous biphasic systems containing poly(ethylene glycol) bound ligand. *Biochemical and Biophysical Research Communications*, 1974. **61**(4): p. 1141-1146.
3. Johansson, G., Partition of proteins and micro-organisms in aqueous biphasic systems. *Molecular and Cellular Biochemistry*, 1974. **4**(3): p. 169-180.
4. Shanbhag, V.P. and Johansson, G., Interaction of Human Serum Albumin with Fatty Acids. *European Journal of Biochemistry*, 1979. **93**(2): p. 363-367.
5. Walter, H., Brooks, D.E., and Fisher, D., Partitioning in aqueous two-phase systems: theory, methods, uses, and application to biotechnology 1985: Academic Press.
6. Kessel, D., Some determinants of partitioning behavior of lymphoblasts in aqueous biphasic systems. *Biochimica et Biophysica Acta (BBA) - General Subjects*, 1981. **678**(2): p. 245-249.
7. Pereira, J.F.B., Santos, V.C., Johansson, H.-O., Teixeira, J.A.C., and Pessoa Jr, A., A stable liquid-liquid extraction system for clavulanic acid using polymer-based aqueous two-phase systems. *Separation and Purification Technology*, 2012. **98**: p. 441-450.
8. Zalipsky, S., Functionalized Poly(Ethylene Glycol) for Preparation of Biologically Relevant Conjugates. *Bioconjugate Chemistry*, 1995. **6**(2): p. 150-165.
9. Li, J. and Kao, W.J., Synthesis of polyethylene glycol (PEG) derivatives and PEGylated-peptide block copolymer conjugates. *Biomacromolecules*, 2003. **4**(4): p. 1055-1067.
10. Rosa, P.A.J., Azevedo, A.M., Ferreira, I.F., de Vries, J., Korporaal, R., Verhoef, H.J., Visser, T.J., and Aires-Barros, M.R., Affinity partitioning of human antibodies in aqueous two-phase systems. *Journal of Chromatography A*, 2007. **1162**(1): p. 103-113.
11. Jiang, Y.Y., Xia, H.S., Yu, J., Guo, C., and Liu, H.Z., Hydrophobic ionic liquids-assisted polymer recovery during penicillin extraction in aqueous two-phase system. *Chemical Engineering Journal*, 2009. **147**(1): p. 22-26.
12. Wu, C., Peng, J.J., Li, J.Y., Bai, Y., Hu, Y.Q., and Lai, G.Q., Synthesis of poly(ethylene glycol) (PEG) functionalized ionic liquids and the application to hydrosilylation. *Catalysis Communications*, 2008. **10**(2): p. 248-250.
13. Pereira, J.F.B., Lima, A.S., Freire, M.G., and Coutinho, J.A.P., Ionic liquids as adjuvants for the tailored extraction of biomolecules in aqueous biphasic systems. *Green Chemistry*, 2010. **12**(9): p. 1661-1669.
14. Gutowski, K.E., Broker, G.A., Willauer, H.D., Huddleston, J.G., Swatloski, R.P., Holbrey, J.D., and Rogers, R.D., Controlling the aqueous miscibility of ionic liquids: Aqueous biphasic systems of water-miscible ionic liquids and water-structuring salts for recycle, metathesis, and separations. *Journal of the American Chemical Society*, 2003. **125**(22): p. 6632-6633.
15. Freire, M.G., Cláudio, A.F.M., Araújo, J.M.M., Coutinho, J.A.P., Marrucho, I.M., Canongia Lopes, J.N., and Rebelo, L.P.N., Aqueous Biphasic Systems: A boost brought about by using ionic liquids. *Chemical Society Reviews*, 2012. **21**(41): p. 4966-4995.
16. Shahriari, S., Tome, L.C., Araujo, J.M.M., Rebelo, L.P.N., Coutinho, J.A.P., Marrucho, I.M., and Freire, M.G., Aqueous biphasic systems: a benign route using cholinium-based ionic liquids. *RSC Advances*, 2013. **3**(6): p. 1835-1843.
17. Freire, M.G., Louros, C.L.S., Rebelo, L.P.N., and Coutinho, J.A.P., Aqueous biphasic systems composed of a water-stable ionic liquid plus carbohydrates and their applications. *Green Chemistry*, 2011. **13**(6): p. 1536-1545.
18. Freire, M.G., Neves, C.M.S.S., Marrucho, I.M., Lopes, J.N.C., Rebelo, L.P.N., and Coutinho, J.A.P., High-performance extraction of alkaloids using aqueous two-phase systems with ionic liquids. *Green Chemistry*, 2010. **12**(10): p. 1715-1718.

19. Pereira, J.F.B., Vicente, F., Santos-Ebinuma, V.C., Araújo, J.M., Pessoa, A., Freire, M.G., and Coutinho, J.A.P., Extraction of tetracycline from fermentation broth using aqueous two-phase systems composed of polyethylene glycol and cholinium-based salts. *Process Biochemistry*, 2013. doi.org/10.1016/j.procbio.2013.02.025.
20. Passos, H., Sousa, A.C.A., Pastorinho, M.R., Nogueira, A.J.A., Rebelo, L.P.N., Coutinho, J.A.P., and Freire, M.G., Ionic-liquid-based aqueous biphasic systems for improved detection of bisphenol A in human fluids. *Analytical Methods*, 2012. **4**(9): p. 2664-2667.
21. Ventura, S.M., Santos-Ebinuma, V., Pereira, J.B., Teixeira, M.S., Pessoa, A., and Coutinho, J.P., Isolation of natural red colorants from fermented broth using ionic liquid-based aqueous two-phase systems. *Journal of Industrial Microbiology & Biotechnology*, 2013. **40**(5): p. 507-516.
22. Ventura, S.P.M., de Barros, R.L.F., de Pinho Barbosa, J.M., Soares, C.M.F., Lima, A.S., and Coutinho, J.A.P., Production and purification of an extracellular lipolytic enzyme using ionic liquid-based aqueous two-phase systems. *Green Chemistry*, 2012. **14**(3): p. 734-740.
23. Freire, M.G., Pereira, J.F.B., Francisco, M., Rodriguez, H., Rebelo, L.P.N., Rogers, R.D., and Coutinho, J.A.P., Insight into the Interactions That Control the Phase Behaviour of New Aqueous Biphasic Systems Composed of Polyethylene Glycol Polymers and Ionic Liquids. *Chemistry-a European Journal*, 2012. **18**(6): p. 1831-1839.
24. Visak, Z.P., Canongia Lopes, J.N., and Rebelo, L.P.N., Ionic Liquids in Polyethylene Glycol Aqueous Solutions: Salting-in and Salting-out Effects. *Monatshefte für Chemie - Chemical Monthly*, 2007. **138**(11): p. 1153-1157.
25. Visak, Z.P., Lopes, J.N.C., and Rebelo, L.P.N., Ionic liquids in polyethylene glycol aqueous solutions: Salting-in and salting-out effects. *Monatshefte Fur Chemie*, 2007. **138**(11): p. 1153-1157.
26. Rodriguez, H., Francisco, M., Rahman, M., Sun, N., and Rogers, R.D., Biphasic liquid mixtures of ionic liquids and polyethylene glycols. *Physical Chemistry Chemical Physics*, 2009. **11**(46): p. 10916-10922.
27. Wu, C., Wang, J., Pei, Y., Wang, H., and Li, Z., Salting-Out Effect of Ionic Liquids on Poly(propylene glycol) (PPG): Formation of PPG + Ionic Liquid Aqueous Two-Phase Systems. *Journal of Chemical & Engineering Data*, 2010. **55**(11): p. 5004-5008.
28. Zafarani-Moattar, M.T., Hamzehzadeh, S., and Nasiri, S., A new aqueous biphasic system containing polypropylene glycol and a water-miscible ionic liquid. *Biotechnology Progress*, 2012. **28**(1): p. 146-156.
29. Tomé, L.I.N., Freire, M.G., Gomes, J.R.B., and Coutinho, J.A.P., Interactions Between Ionic Liquids and Polyethyleneglycol in Binary Mixtures and Aqueous Biphasic Systems, 2013 (*Submitted for publication*).
30. Tomé, L.I.N., Pereira, J.F.B., Freire, M.G., Gomes, J.R.B., and Coutinho, J.A.P., Watering out Polyethyleneglycol-Ionic Liquid Mixtures to form Aqueous Biphasic Systems. *Journal of Physical Chemistry Letters*, 2013. (*Submitted for publication*).
31. Merchuk, J.C., Andrews, B.A., and Asenjo, J.A., Aqueous two-phase systems for protein separation Studies on phase inversion. *Journal of Chromatography B*, 1998. **711**(1-2): p. 285-293.
32. Chemspider, The free chemical database. Available from: <http://www.chemspider.com>.
33. Andersen, E., The crystal and molecular structure of hydroxyquinones and salts of hydroxyquinones. II. Chloranilic acid dihydrate. *Acta Crystallographica*, 1967. **22**(2): p. 191-196.
34. Visser, A.E., Swatloski, R.P., and Rogers, R.D., pH-dependent partitioning in room temperature ionic liquids provides a link to traditional solvent extraction behavior. *Green Chemistry*, 2000. **2**(1): p. 1-4.

13. PAPER 10

Aqueous Biphasic Systems Composed of Ionic Liquids and Polymers: A Platform for the Purification of Biomolecules

Separation and Purification Technology, 113 (2013) 83-89.

13.1. Abstract

The ability of alternative aqueous biphasic systems (ABS) composed of polyethylene glycol and imidazolium-based ionic liquids (ILs) to selectively separate similar biomolecules was here investigated. The preferential partitioning of three alkaloids (caffeine, xanthine and nicotine) was addressed by means of their partition coefficients and selectivity values. Aiming at optimizing the selectivity of the studied ABS, factors such as the chemical structure of the IL (cation side alkyl chain length, number of aliphatic moieties or their functionalization, and the anion nature) and the temperature of equilibrium were experimentally addressed. In almost all examples it was observed a preferential concentration of caffeine in the polymer-rich phase whereas nicotine and xanthine preferentially migrate to the (opposite) IL-rich phase. In spite of the alkaloids chemical similarities, the studied ABS presented selectivity values of xanthine *vs.* caffeine as large as 19. The gathered results show that polymer-IL-based ABS allow the selective separation of similar structures by an adequate manipulation of the IL' chemical structure and temperature of equilibrium, and can be envisaged as potential platforms to be applied in countercurrent chromatography.

Keywords: Aqueous biphasic system, ionic liquid, polyethylene glycol, alkaloid, selective partition process.

13.2. Introduction

Due to the outstanding properties of ILs, IL-based ABS have led to enhanced performances on separation mainly because of the possibility of tailoring the polarity of both phases by a proper choice of the IL¹⁻³. Polymer-polymer-based ABS usually display two hydrophobic phases and their polarity differences essentially depend on the amount of water in each phase. On the other hand, polymer-salt ABS present a hydrophobic phase mainly constituted by the polymer and a highly hydrophilic (and ionic) phase, typically formed by high charge-density inorganic salts⁴. The limited range of polarity differences between the two phases limits thus the applicability of conventional polymer-based ABS for extraction and separation purposes. However, the substitution of a high charge density inorganic salt and/or a polymer by an IL may provide a precise control of the phases' polarities since they can be adequately chosen taking into account the vast array of their ionic structures (at least 10⁶ simple ILs can be

easily prepared in the laboratory)⁵. Further advantages can be associated to the use of ILs as constituents of ABS when compared with the more conventional high-melting inorganic salts, namely their lower corrosive character⁶, and the possibility of controlling the salt precipitation, since ILs display lower melting temperatures and hydrophilic ILs are usually miscible with water in the complete composition range. Despite the large amount of literature devoted to ABS composed of ILs and inorganic salts⁷, recently some works have further reported the formation of aqueous systems involving polymers and ILs^{6, 8-10}. In those works the influence of the ILs' structure on the phase behaviour and ABS formation was addressed^{6, 8-10}. It was shown that the phase behaviour, as well as the phases polarities, of polymer-IL-based ABS can be properly tailored by a judicious selection of the polymer or IL employed^{6, 8-10}. In particular, a detailed understanding of the molecular-level interactions occurring in ABS composed of ILs and polyethylene glycol (PEG) was carried out by Freire et al.⁶. The liquid-liquid demixing ability in the IL-polymer-based ABS was explained and supported as dominated by the interactions taking place between the polymer and the ionic species and not by the hydration capability of the isolated IL ions⁶.

Despite the reduced number of publications dealing with polymer-IL ABS⁹⁻¹¹, their singular nature and properties makes them promising liquid-liquid separation systems to apply into countercurrent chromatography (CCC) when envisaging large scale applications. The CCC is an emerging low pressure chromatographic technique which can lead to the separation of a large range of molecules on the basis of different partition coefficients obtained between the two immiscible liquid phases¹². In fact, a significant number of works associating the CCC technique with ABS can be found in literature making use of polymer-polymer¹³ or polymer-salt ABS¹⁴⁻¹⁷ being, however, the use of IL-based ABS only limited to one literature study¹⁸. The use of IL-based ABS leads to a density difference that makes the liquid-liquid system easier to retain in a CCC column¹⁸. The use of a new chromatographic strategy for the quantitative determination of several alkaloids was recently reported by Wei et al.¹⁹. The authors applied an IL-based microwave-assisted extraction for a fast and safe quantitative analysis of the active components from pigeon pea leaves¹⁹.

Taking into consideration the wide polarity range displayed by IL-based ABS, in the present work it was investigated the use of some novel PEG-IL-based ABS recently reported⁶ for the selective separation of similar alkaloids, namely xanthine, caffeine and

nicotine. As recently suggested¹, IL-based ABS are an enhanced strategy for concentrating alkaloids from human biological fluids in order to perform doping control analysis. Moreover, several biomass samples and pharmaceutical products present different types of alkaloids. Therefore, their isolated identification and analysis is of foremost importance.

The main objective of this work is to show that, by the application of different ILs as main constituents of ABS, it is possible to manipulate the affinity of different alkaloids for different phases and, consequently, to selectively separate related chemical structures. The studied ABS are composed of polyethylene glycol (with an average molecular weight of 2000 g.mol⁻¹) and different imidazolium-based ILs, so that the effects of the cation alkyl side chain length, the number of alkyl groups at the cation or their functionalization, as well as the anion nature, could be evaluated. The effect of temperature on the selective extraction was also investigated.

13.3. Experimental Section

13.3.1. Materials

The ILs investigated as main constituents of IL-polymer-based ABS were 1-allyl-3-methylimidazolium chloride, [amim]Cl (98.0 wt% pure), 1-(2-hydroxyethyl)-3-methylimidazolium chloride, [OHC₂mim]Cl (99.0 wt% pure), 1-methylimidazolium chloride, [C₁im]Cl (98.0 wt% pure), 1,3-dimethylimidazolium chloride, [C₁mim]Cl (99.0 wt% pure), 1-ethyl-3-methylimidazolium chloride, [C₂mim]Cl (98.0 wt% pure), 1-ethyl-3-methylimidazolium acetate, [C₂mim][CH₃CO₂](98.0 wt% pure), 1-ethyl-3-methylimidazolium methanesulfonate, [C₂mim][CH₃SO₃] (99.0 wt% pure), 1-ethyl-3-methylimidazolium hydrogensulfate, [C₂mim][HSO₄] (99.0 wt% pure) and 1-ethyl-3-methylimidazolium dimethylphosphate, [C₂mim][DMP] (98.0 wt% pure). All ILs were supplied by Iolitec. Their ionic structures are presented in Figure 13.1.

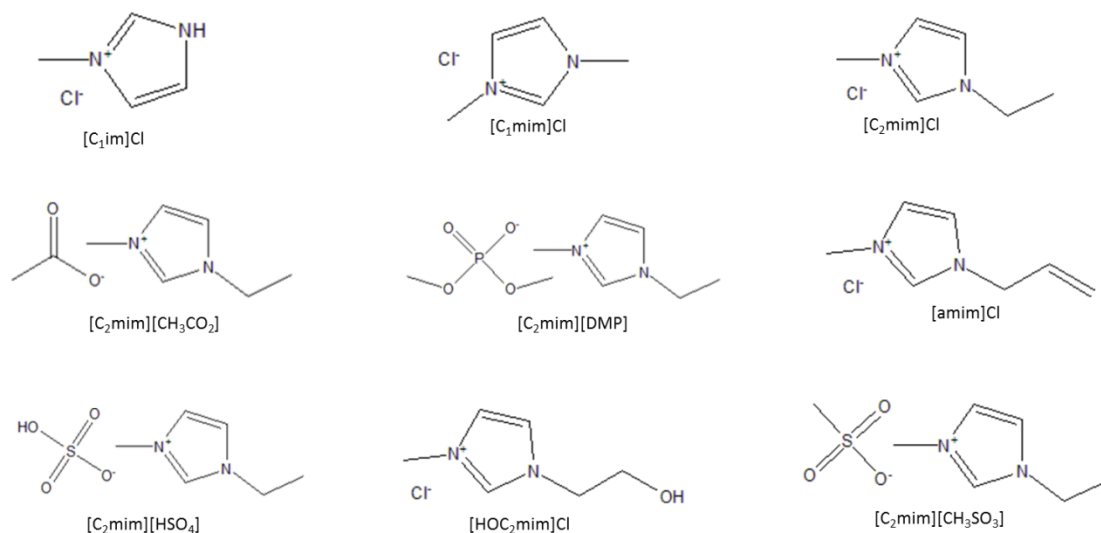


Figure 13.1 Chemical structure and respective abbreviation name of all the ILs investigated.

Before use all ILs were dried under constant stirring, moderate temperature (343 K) and high vacuum conditions (<0.1 mbar) for a minimum of 48 h. The purities of all ILs were additionally confirmed by ¹H and ¹³C NMR and they are according to those given by the supplier. Polyethylene glycol, with an average molecular weight of 2000 g.mol⁻¹ (PEG 2000) was acquired at Sigma-Aldrich and used as received.

The water content of all ILs and polymer was measured by Karl-Fischer titration and was taken into account in the calculation of the global compositions of the PEG 2000 + IL + H₂O mixtures. In general, the water content of IL samples after the drying procedure was found to be <1000 ppm, whereas the water content in the polymer was <10000 ppm. Ultrapure water that was doubly distilled, passed through a reverse-osmosis system, and further treated with a Milli-Q plus water purification apparatus was used.

The alkaloids used as partitioning solutes were xanthine (99.0 wt% pure from Sigma-Aldrich), nicotine (≥97.0 wt% pure from Fluka) and caffeine (≥99.5 wt% pure from José Manuel Vaz Pereira). The molecular structures of the 3 alkaloids are depicted in Figure 13.2.

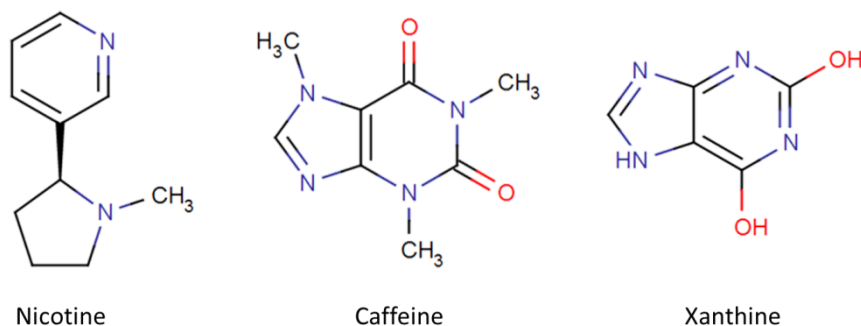


Figure 13.2 Chemical structure of the three alkaloids investigated.

13.3.2. Methods

13.3.2.1. Partitioning Studies and Selectivity of Alkaloids

All the liquid-liquid partitioning systems or ABS were prepared in graduated centrifuge tubes by weighing the appropriate amounts of PEG 2000 (≈ 53 wt%), IL (≈ 27 wt%) and ≈ 20 wt% of an aqueous solutions containing each one of the alkaloids, namely caffeine (15.1 g.L^{-1} , $7.78 \times 10^{-2} \text{ mol.L}^{-1}$), xanthine (0.01 g.L^{-1} , $6.57 \times 10^{-5} \text{ mol.L}^{-1}$) and nicotine (2.0 g.L^{-1} , $1.23 \times 10^{-2} \text{ mol.L}^{-1}$). All the solutions were prepared in order to be guarantee that the alkaloids are at infinite dilution aiming at avoiding solute-solute interactions which could lead to different partitioning behaviors. The different alkaloid concentrations were selected to assure a maximum accuracy within the analytical technique employed. All the biomolecules can be considered as completely solvated in aqueous media avoiding thus specific interactions between them. The selected mixtures form two immiscible aqueous phases as confirmed by the corresponding ternary phase diagrams previously published⁶. All mixtures were gravimetrically prepared within $\pm 10^{-4}$ g. After a complete dissolution of all the components in the mixture by stirring, the mixture was left to equilibrate for 12 h in an air oven and at 323, 333, 343, 353 or 363 (± 1) K, to achieve the complete partitioning of each alkaloid between the aqueous phases. The two phases were then carefully separated and the alkaloids were quantified in both the top and bottom phases by UV-spectroscopy, using a SHIMADZU UV-1700, Pharma-Spec Spectrometer, at the wavelengths of 261 nm (for nicotine), 267 nm (for xanthine) and 274 nm (for caffeine). Calibration curves for the determination of each alkaloid were previously established at the respective maximum absorption peaks. Possible interferences of the polymer or ILs through the quantification of each alkaloid were taken into account and found to be of no concern at the dilutions carried out.

At least three individual ABS for each IL or alkaloid were prepared being the partition coefficient results presented as an average value and being the uncertainty associated to the alkaloids' partition coefficients within $\pm 5\%$.

The alkaloids partition coefficients (K_{alk}) were estimated according to Equation 13.1:

$$K_{alk} = \frac{[alk]_{IL}}{[alk]_{PEG}} \quad \text{Equation 13.1}$$

where $[alk]_{IL}$ and $[alk]_{PEG}$ represent the concentration of each alkaloid in the IL- and PEG-2000-rich phases, respectively.

It should be remarked that the relative densities of the IL- or polymer-rich phases are not constant, *i.e.* the denser phase can be either the polymer- or the IL-phase, depending on the IL which constitutes the ABS - see Table S13.1 in Supporting Information with the detailed information.

The temperature effect in the partitioning process was also evaluated for nicotine and caffeine. The respective thermodynamic parameters of phase transfer, such as the standard molar Gibbs energy ($\Delta_{tr}G_m^0$), the standard molar enthalpy ($\Delta_{tr}H_m^0$), and the standard molar entropy of transfer ($\Delta_{tr}S_m^0$) were determined according to Equations (13.2) to (13.4)^{20, 21},

$$\ln(K_{alk}) = -\frac{\Delta_{tr}H_m^0}{R} \times \frac{1}{T} + \frac{\Delta_{tr}S_m^0}{R} \quad \text{Equation 13.2}$$

$$\Delta_{tr}G_m^0 = \Delta_{tr}H_m^0 - T\Delta_{tr}S_m^0 \quad \text{Equation 13.3}$$

$$\Delta_{tr}G_m^0 = -RT \ln(K_{alk}) \quad \text{Equation 13.4}$$

where K_{alk} is the partition coefficient of the alkaloid, R is the universal gas constant ($8.314 \text{ J}\cdot\text{mol}^{-1}\cdot\text{K}^{-1}$) and T is the temperature (K).

The selectivity on the partition of nicotine ($S_{nic/caf}$) or xanthine ($S_{xant/caf}$) in respect to caffeine was calculated according to Equations (13.5) and (13.6), respectively:

$$S_{nic/caf} = \frac{K_{nic}}{K_{caf}} \quad \text{Equation 13.5}$$

$$S_{xant/caf} = \frac{K_{xant}}{K_{caf}} \quad \text{Equation 13.6}$$

13.2.2. pH Determination

The pH (± 0.02) of the top and bottom phases was measured at 323 (± 1) K using an HI 9321 Microprocessor pH meter (HANNA instruments). The calibration of the pH meter was carried out with two buffers (pH values of 4.00 and 7.00). The compositions adopted at the biphasic region mixture correspond to those used in the partitioning experiments. All mixtures were gravimetrically prepared within $\pm 10^{-4}$ g.

13.4. Results and Discussion

The migration of a target molecule in an ABS depends on the physico-chemical properties of the two phases so that specific extractions or its selectivity can be manipulated. Several conditions can be used to control the molecules partitioning, such as the chemical composition of the system, temperature, pH, and the inclusion of adjuvants, affinity ligands or amphiphilic structures^{8,22}.

In this work, it was first evaluated the effect of the IL which composes the IL-PEG-2000-based ABS on the partitioning of three alkaloids, namely caffeine, nicotine and xanthine at a similar composition (27 wt% of IL + 53 wt% of PEG 2000 + 20 wt% of an aqueous solution containing the alkaloid) and temperature (323 ± 1 K). This first set of results allows the analysis of the impact of the IL on the partition coefficients of the alkaloids, as well as the nature of the solute and its partitioning pattern. Regarding the structural variations at the IL cation, the selected ILs allow the study of the effects of the alkyl side chain length, the aliphatic moiety functionalization and of the number of alkyl groups present at the imidazolium ring. For that study the chloride anion was fixed and was combined with the following cations: [C₁im]⁺, [C₁mim]⁺, [C₂mim]⁺, [amim]⁺ and [OHC₂mim]⁺. The logarithm of the partition coefficients ($\log K_{alk}$) for the three alkaloids at 323 (± 1) K, is depicted in Figure 13.3 (the detailed partition coefficients, and respective standard deviations, and extraction efficiencies are reported in Table S13.2 in Supporting Information). The gathered results indicate that all the alkaloids

preferentially migrate for the IL-rich phase with the exception of caffeine that favorably partitions for the PEG-2000-rich phase in the ABS composed of [C₂mim]Cl, [amim]Cl and [OHC₂mim]Cl.

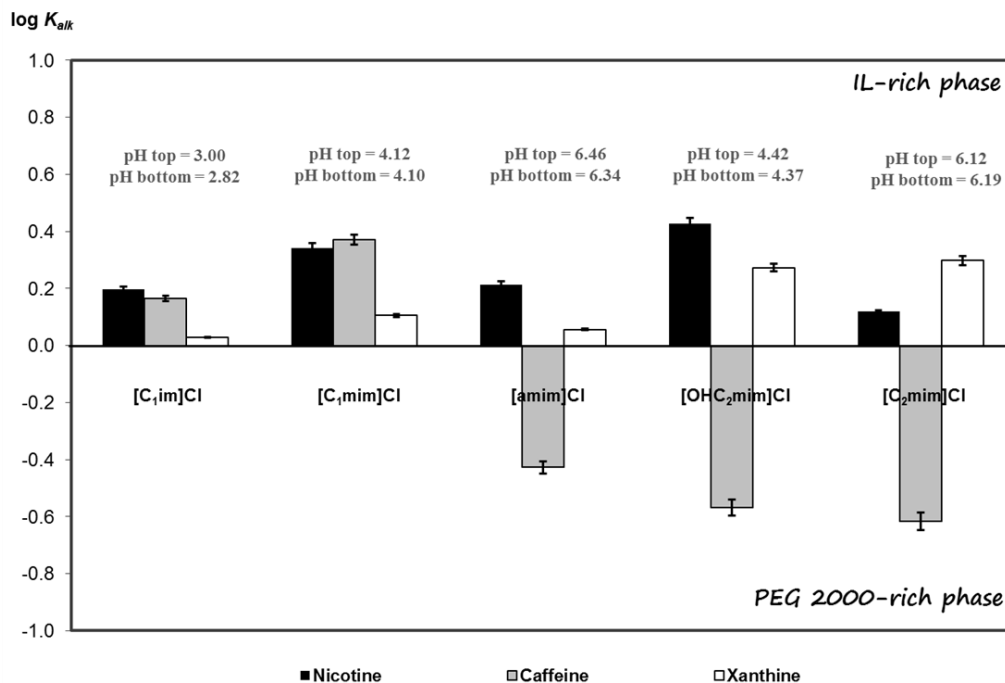


Figure 13.3 Logarithm of the alkaloids partition coefficients ($\log K_{alk}$) in the ABS composed of PEG 2000 (≈ 53 wt%) + chloride-based ILs (≈ 27 wt%) and at 323 K. The pH values of the top and bottom phases are also displayed.

The pH values of the coexisting phases of the systems shown in Figure 13.3 range between 2.8 and 6.5. Taking into account the alkaloids speciation as a function of the pH in the systems investigated (the individual speciation curves are presented in Figures S13.1 to S13.3 in Supporting Information), both xanthine and caffeine are present mainly as neutral molecules, whereas nicotine is present mostly as a positively charged species.

From the three alkaloids studied, nicotine is the one with the lowest affinity for water, as expressed by the higher octanol-water partition coefficient, $K_{ow} = 3.71^{23}$. However, despite this higher affinity for more hydrophobic phases and an expected preferential migration for the polymeric phase, nicotine, being present mostly as a positively charged species in all the investigated systems, preferentially partitions for the most hydrophilic and charged IL-rich phase. In addition, when comparing the trends collected

with the two neutral alkaloids in the systems displayed in Figure 13.3, xanthine always migrates for the IL-rich phase while caffeine shows an inversion to this pattern with more hydrophobic ILs. The K_{ow} values of caffeine and xanthine are 0.23²³ and 0.74²³, respectively, indicating that contrarily to nicotine, caffeine and xanthine display a higher affinity for more hydrophilic and water-rich phases. This preferential affinity of caffeine for hydrophilic phases is reflected in the inversion on its partition coefficients for the polymer-rich phase that occurs when ILs with longer aliphatic moieties (*i.e.* more hydrophobic ILs) are present.

The effect of the IL anion on the partitioning of the three alkaloids was also investigated with the results depicted in Figure 13.4. As observed before with caffeine and the ABS composed of [C₂mim]Cl, for all the systems composed of [C₂mim]-based ILs, caffeine preferentially migrates for the polymer-rich phase, contrarily to what is observed with nicotine and xanthine. At the pH values of the coexisting phases of the systems considered in Figure 13.4 (1.5 < pH < 9.2), xanthine and caffeine are present mainly as neutral species while nicotine is mostly as a positively mono-charged species – *cf.* speciation curves in Supporting Information (Figures S13.1 to S13.3). Therefore, as observed before, nicotine always favourably migrates for the charged IL-rich phase despite the higher affinity of its neutral form for more organic phases. Xanthine, albeit present as a neutral species, partitions in most examples for the most hydrophilic and IL-rich phase due to its inherent hydrophilic nature.

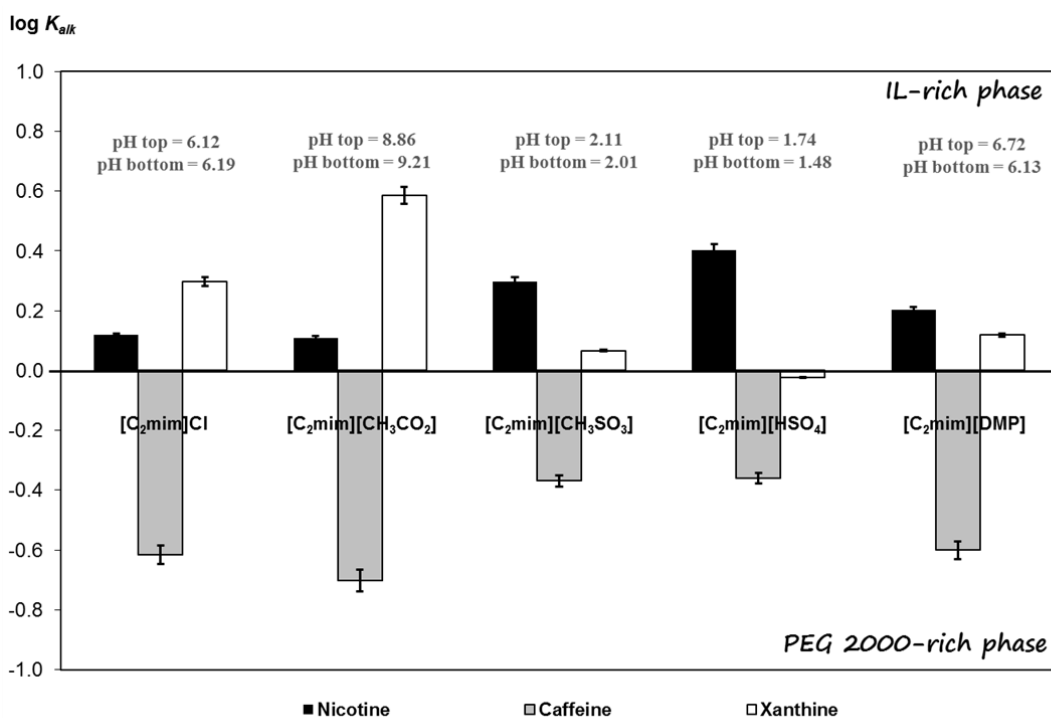


Figure 13.4 Logarithm of the alkaloids partition coefficients ($\log K_{alk}$) in the ABS composed of PEG 2000 (≈ 53 wt%) + [C₂mim]-based ILs (≈ 27 wt%) and at 323 K. The pH values of the top and bottom phases are also displayed.

In summary, both xanthine and nicotine preferentially migrate for the IL-rich phase in practically all the studied ABS whereas the migration of caffeine can be tailored by the choice of the IL which constitutes a given ABS. Therefore, these results suggest that there is an inherent selectivity of the studied ABS for similar chemical structures such as alkaloids. To investigate the selective character of the IL-polymer-ABS studied, the selectivity of nicotine and xanthine in respect to caffeine for the IL-rich phase, $S_{nic/caf}$ and $S_{xant/caf}$, respectively, were further calculated. The corresponding results are presented in Figure 13.5. The data shown in Figure 13.5(A) allow the evaluation of the IL structural influence towards the selectivity at a fixed temperature and mixture composition. The selectivity data indicate that the modification of the IL chemical structure has a huge influence on the selective separation of caffeine from the remaining alkaloids.

Ionic Liquid	Selectivity		Temperature (± 1) K	Selectivity $S_{nic/caf}$
	$S_{xant/caf}$	$S_{nic/caf}$		
[amim]Cl	3.04	4.38	323	5.43
[OHC ₂ mim]Cl	6.94	9.90	333	7.00
[C ₁ im]Cl	0.73	1.07	343	7.34
[C ₁ mim]Cl	0.54	0.93	353	8.45
[C ₂ mim]Cl	8.19	5.43	363	7.94
[C ₂ mim][CH ₃ CO ₂]	19.40	6.49		
[C ₂ mim][CH ₃ SO ₃]	2.73	4.62		
[C ₂ mim][HSO ₄]	2.17	5.79		
[C ₂ mim][DMP]	5.24	6.37		

Figure 13.5 Selectivity parameters for: **A**) xanthine/caffeine ($S_{xant/caf}$) and nicotine/caffeine ($S_{nic/caf}$) pairs considering all PEG 2000-ILs-based ABS tested and **B**) nicotine/caffeine ($S_{nic/caf}$) pair considering the PEG 2000-[C₂mim]Cl-based ABS and different temperatures of extraction.

Despite the molecular structure similarities between caffeine and xanthine, selectivity values up to 19 can be achieved with the ABS composed of [C₂mim][CH₃CO₂]. Indeed, the selectivity values cover a wider range for the caffeine-xanthine binary mixture than for the caffeine-nicotine pair. In addition to these calculations based on the isolated partition coefficients, the experimental investigation on the partitioning behavior of a mixture of alkaloids, namely caffeine and nicotine, was also carried out. For that purpose, a system composed of [OHC₂mim]Cl + PEG 2000 + an aqueous solution containing both nicotine (2.0 g.L⁻¹) and caffeine (2.0 g.L⁻¹) was used – one of the foremost systems leading to high selectivity values.

The UV-Vis spectra of the aqueous solutions of the pure compounds (caffeine and nicotine) and in each IL- or polymer-rich phase are presented in Figure 13.6. The gathered results clearly show that nicotine is preferentially present in the IL-rich phase whereas caffeine is mainly concentrated in the polymer phase. Based on these results, the respective K_{alk} values were calculated and the experimental selectivity parameter was further determined. The respective value is presented in Table 13.1. The results obtained with the real mixture of alkaloids ($S_{nic/caf} = 6.01$) support the high selectivity values obtained with the isolated partition coefficients and validate all the optimization study previously performed. Thus, it is evident that these new IL-PEG-2000-based ABS can be used as viable separation systems of high selectivity for compounds of the same family or with similar structures if a proper selection of the IL is carried out. Since this

is the first time that these polymer-IL-based ABS are applied to the partitioning of alkaloids, the comparison with literature data is difficult. However, several [C₂mim]- and [C₄mim]-based IL-ABS were previously studied in combination with K₃PO₄ as partitioning systems for caffeine and nicotine¹. For these systems much higher partition coefficients were observed, and even complete extractions were verified in the presence of the strong salting-out species, K₃PO₄¹. Nevertheless, if we consider their capability to selectively separate the alkaloids they are by far less efficient than the systems studied in this work ($0.93 < S_{nic/caf}(\text{PEG 2000} + \text{IL}) < 9.90$ and $1.01 < S_{nic/caf}(\text{K}_3\text{PO}_4 + \text{IL}) < 2.02$). The systems here proposed provide a milder extraction but with a more selective character allowing the separation of very similar biomolecules such the caffeine and xanthine.

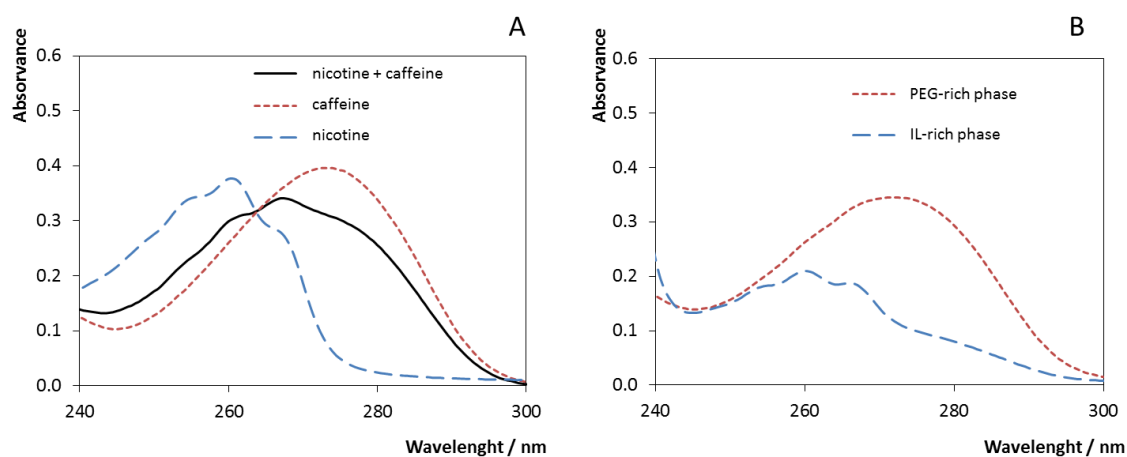


Figure 13.6 **A)** Spectra of the diluted aqueous solutions of nicotine, caffeine and a mixture containing nicotine + caffeine ; **B)** Spectra of the diluted IL- and PEG-rich phases of the ABS composed of PEG 2000 (≈ 53 wt%) + [OHC₂mim]Cl (≈ 27 wt%) containing both alkaloids at (323 ± 1) K.

Table 13.1 Partition coefficients of nicotine (K_{nic}) and caffeine (K_{caf}), and selectivity parameters for the nicotine + caffeine ($S_{nic/caf}$) pair in the ABS composed of PEG 2000 (≈ 53 wt%) + [OHC₂mim]Cl (≈ 27 wt%) at $323 (\pm 1)$ K.

Alkaloid aqueous solution	K_{nic}	K_{caf}	$S_{nic/caf}$
Nicotine	2.67	-	9.90
Caffeine	-	0.27	
Nicotine + Caffeine	1.86	0.31	6.01

The temperature of equilibrium for the alkaloids' separation was also investigated making use of the ABS composed of PEG 2000 + [C₂mim]Cl. With this system the

partition coefficients of both nicotine and caffeine were determined. The detailed partition coefficients are presented in Supporting Information (Table S13.2). The gathered results are depicted in Figure 13.7.

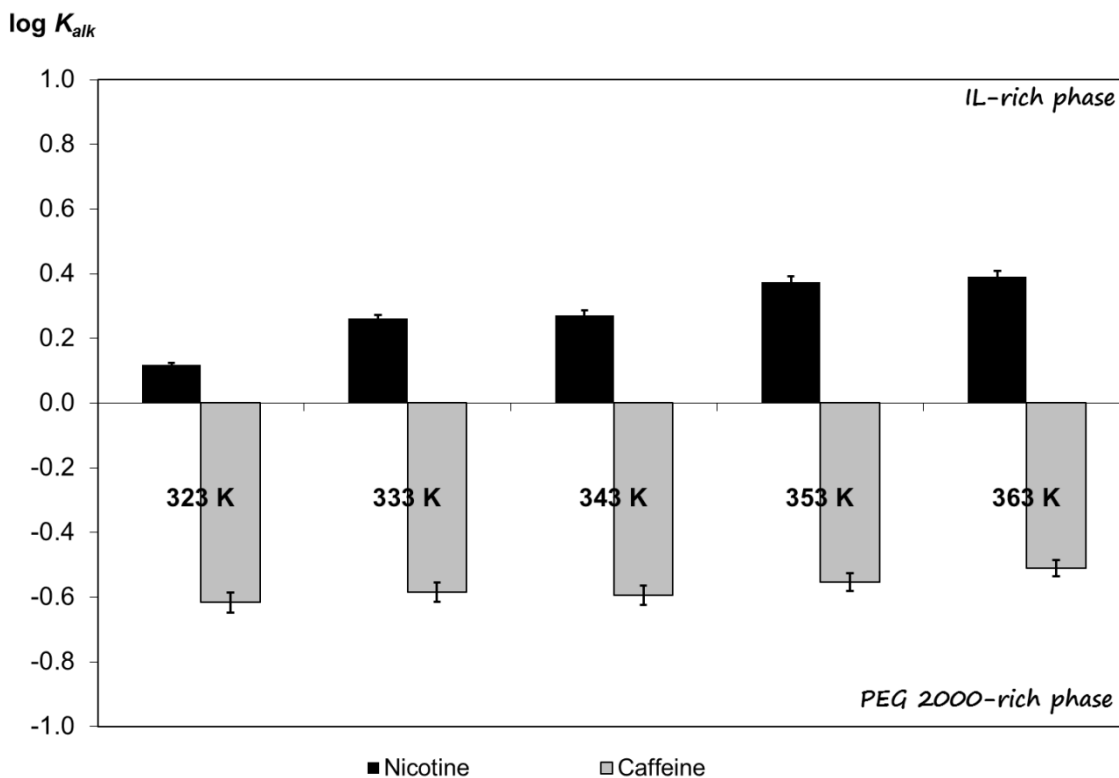


Figure 13.7 Logarithm of the alkaloids partition coefficients ($\log K_{alk}$) in the ABS composed of PEG 2000 (≈ 53 wt%) + $[C_2mim]Cl$ (≈ 27 wt%) and different temperatures.

The data obtained show that an increase in temperature leads to a higher extraction of nicotine for the IL-rich phase and to a decrease on the partition coefficient of caffeine for the polymer-rich phase. Nevertheless, the effect of temperature is more evident in the extraction of nicotine for the IL-rich phase in the 323-363 (± 1) K temperature range.

The preferential partitioning of both alkaloids and their different dependence with temperature has a significant impact in the selectivity values. The selectivity values of nicotine to caffeine as a function of temperature are presented in Figure 13.5(B). The increase in temperature improves the selectivity of the system with a maximum that seems to be achieved at around 353 (± 1) K, meaning that there is an optimal temperature with the highest selectivity.

For a better understanding of the molecular mechanisms responsible for the migration of the alkaloids between the coexisting phases, the thermodynamic parameters of transfer, namely the standard molar Gibbs energy ($\Delta_{tr}G_m^0$), the standard molar enthalpy ($\Delta_{tr}H_m^0$) and the standard molar entropy of transfer ($\Delta_{tr}S_m^0$) were calculated using Equations. 13.2 to 13.4^{20, 21}. The plots of $\ln K_{alk}$ versus $1/T$ are shown in Supporting Information (Figure S13.4). The representation of $\ln K_{alk}$ as a function of $1/T$ is well described by a linear function indicating that the molar enthalpy of transfer for caffeine and nicotine is temperature independent (at least in the temperature range studied in this work).

The thermodynamic parameters of transfer are presented in Table 13.2. The $\Delta_{tr}G_m^0$ of nicotine is negative and reflects the spontaneous and preferential partitioning of this alkaloid for the IL-rich phase with $K_{nic} > 1$. On the other hand, for caffeine, the $\Delta_{tr}G_m^0$ is positive - a result of the preferential migration of caffeine for the polymer-rich phase ($K_{caf} < 1$).

Table 13.2 Standard molar thermodynamic functions of transfer for nicotine and caffeine at 323 K.

Alkaloid	$\Delta_{tr}H_m^0 / \text{kJ.mol}^{-1}$	$\Delta_{tr}S_m^0 / \text{J.mol}^{-1}\text{K}^{-1}$	$\Delta_{tr}G_m^0 / \text{kJ.mol}^{-1}$	$T\Delta_{tr}S_m^0 / \text{kJ.mol}^{-1}$	$\ln K_{alk}$
Caffeine	-5.44	-28.74	3.84	-9.29	-1.43
Nicotine	-14.85	-43.13	-0.91	-13.94	0.34

The $\Delta_{tr}H_m^0$ is negative for both alkaloids, suggesting that the transference of nicotine and caffeine from the polymer- to the IL-rich phase is an exothermic process, *e.g.*, an increase in temperature favours the migration for the IL-rich phase. Although the partitioning of nicotine is an exothermic process it was verified that an increase in temperature seems to contradict this behaviour. Albeit this is a not expected trend, this lower affinity for the PEG-2000-rich phase with an increase in temperature can be related with the lower water content and more “hydrophobic” character of the PEG-rich phase at higher temperatures²⁴. Finally, when comparing the absolute values of $T\Delta_{tr}S_m^0$ and $\Delta_{tr}H_m^0$ for the systems with the two alkaloids it can be seen that the enthalpy of transfer is lower for the caffeine migration and slightly higher when considering the nicotine partitioning. Therefore, the enthalpic effects are of more importance in the systems comprising nicotine.

Taking into account all the gathered results it can be concluded that the IL-polymer-based ABS here studied can be used to selectively separate similar alkaloids. These ABS can be envisaged as potential separation platforms to be applied in CCC techniques.

13.5. Conclusions

In this work, alternative IL-PEG-2000-based ABS were investigated as novel extractive systems aiming at gathering a selective separation of similar solutes. To such an aim it was studied the effect of the IL chemical structure and temperature of equilibrium. The preferential partitioning of three alkaloids (caffeine, xanthine and nicotine) was addressed by means of the measured partition coefficients and calculated selectivity values. In almost all examples it was observed a preferential concentration of caffeine into the PEG-2000-rich phase whereas nicotine and xanthine preferentially migrate to the (opposite) IL-rich phase. Therefore, despite their chemical similarities, the three alkaloids suffer different partitioning trends between the coexisting phases of the studied ABS. Selectivity values of xanthine in respect to caffeine up to 19 were attained with the system composed of $[\text{C}_2\text{mim}][\text{CH}_3\text{CO}_2]$. The promising results here obtained show that polymer-IL-based ABS allow the selective separation of similar structures by a proper manipulation of the ILs chemical structure and temperature of equilibrium, and can be envisaged as potential platforms to be applied in CCC.

13.6. References

1. Freire, M.G., Neves, C.M.S.S., Marrucho, I.M., Canongia Lopes, J.N., Rebelo, L.P.N., and Coutinho, J.A.P., High-performance extraction of alkaloids using aqueous two-phase systems with ionic liquids. *Green Chemistry*, 2010. **12**(10): p. 1715-1718.
2. Shahriari, S., Tome, L.C., Araujo, J.M.M., Rebelo, L.P.N., Coutinho, J.A.P., Marrucho, I.M., and Freire, M.G., Aqueous biphasic systems: a benign route using cholinium-based ionic liquids. *RSC Advances*, 2013. **3**(6): p. 1835-1843.
3. Passos, H., Sousa, A.C.A., Pastorinho, M.R., Nogueira, A.J.A., Rebelo, L.P.N., Coutinho, J.A.P., and Freire, M.G., Ionic-liquid-based aqueous biphasic systems for improved detection of bisphenol A in human fluids. *Analytical Methods*, 2012. **4**(9): p. 2664-2667.
4. Mazzola, P.G., Lopes, A.M., Hasmann, F.A., Jozala, A.F., Penna, T.C.V., Magalhaes, P.O., Rangel-Yagui, C.O., and Pessoa, A., Liquid-liquid extraction of biomolecules: an overview and update of the main techniques. *Journal of Chemical Technology & Biotechnology*, 2008. **83**: p. 143-157.
5. Plechkova, N.V. and Seddon, K.R., Applications of ionic liquids in the chemical industry. *Chemical Society Reviews*, 2008. **37**(1): p. 123-150.
6. Freire, M.G., Pereira, J.F.B., Francisco, M., Rodríguez, H., Rebelo, L.P.N., Rogers, R.D., and Coutinho, J.A.P., Insight into the Interactions That Control the Phase Behaviour of New Aqueous Biphasic Systems Composed of Polyethylene Glycol Polymers and Ionic Liquids. *Chemistry – A European Journal*, 2012. **18**(6): p. 1831-1839.
7. Freire, M.G., Claudio, A.F.M., Araujo, J.M.M., Coutinho, J.A.P., Marrucho, I.M., Lopes, J.N.C., and Rebelo, L.P.N., Aqueous biphasic systems: a boost brought about by using ionic liquids. *Chem. Soc. Rev.*, 2012. **41**(14): p. 4966-4995.
8. Pereira, J.F.B., Lima, A.S., Freire, M.G., and Coutinho, J.A.P., Ionic liquids as adjuvants for the tailored extraction of biomolecules in aqueous biphasic systems. *Green Chemistry*, 2010. **12**(9): p. 1661-1669.
9. Wu, C., Wang, J., Pei, Y., Wang, H., and Li, Z., Salting-Out Effect of Ionic Liquids on Poly(propylene glycol) (PPG): Formation of PPG + Ionic Liquid Aqueous Two-Phase Systems. *Journal of Chemical & Engineering Data*, 2010. **55**(11): p. 5004-5008.
10. Zafarani-Moattar, M.T., Hamzehzadeh, S., and Nasiri, S., A new aqueous biphasic system containing polypropylene glycol and a water-miscible ionic liquid. *Biotechnology Progress*, 2012. **28**(1): p. 146-156.
11. Li, Z., Liu, X., Pei, Y., Wang, J., and He, M., Design of environmentally friendly ionic liquid aqueous two-phase systems for the efficient and high activity extraction of proteins. *Green Chemistry*, 2012. **14**(10): p. 2941-2950.
12. Ito, Y., In *High-speed Countercurrent Chromatography*; Ito, Y., Conway, W.D., Eds.; Wiley Interscience: New York 1996.
13. Shinomiya, K., Kabasawa, Y., Yanagidaira, K., Sasaki, H., Muto, M., Okada, T., and Ito, Y., Protein separation by nonsynchronous coil planet centrifuge with aqueous-aqueous polymer phase systems. *Journal of Chromatography A*, 2003. **1005**(1-2): p. 103-112.
14. Al Marzouqi, I., Levy, M.S., and Lye, G.J., Hydrodynamics of PEG-Phosphate Aqueous Two-Phase Systems in a J-Type Multilayer Countercurrent Chromatograph. *Journal of Liquid Chromatography & Related Technologies*, 2005. **28**(9): p. 1311-1332.
15. Chao, Z., Shibusawa, Y., Shindo, H., and Ito, Y., Countercurrent Chromatographic Purification of Polysaccharides from *Achyranthes bidentata* with an Aqueous Two-Phase System Using a Cross Axis Coil Planet Centrifuge. *Journal of Liquid Chromatography & Related Technologies*, 2003. **26**(12): p. 1895-1903.
16. Shibusawa, Y., Yamaguchi, M., and Ito, Y., Polyethylene Glycol-Potassium Phosphate Aqueous Two-Phase Systems for Countercurrent Chromatography of Proteins. *Journal of Liquid Chromatography & Related Technologies*, 1998. **21**(1-2): p. 121-133.

17. Lee, Y.W., Shibusawa, Y., Chen, F.T., Myers, J., Schooler, J.M., and Ito, Y., Purification of Uridine Phosphorylase from Crude Extracts of *Escherichia Coli* Employing High-Speed Countercurrent Chromatography With an Aqueous Two-Phase Solvent System. *Journal of Liquid Chromatography*, 1992. **15**(15-16): p. 2831-2841.
18. Ruiz-Angel, M.J., Pino, V., Carda-Broch, S., and Berthod, A., Solvent systems for countercurrent chromatography: An aqueous two phase liquid system based on a room temperature ionic liquid. *Journal of Chromatography A*, 2007. **1151**(1-2): p. 65-73.
19. Wei, Z., Zu, Y., Fu, Y., Wang, W., Luo, M., Zhao, C., and Pan, Y., Ionic liquids-based microwave-assisted extraction of active components from pigeon pea leaves for quantitative analysis. *Separation and Purification Technology*, 2013. **102**: p. 75-81.
20. Ahmed, A. and Sandler, S.I., Solvation free energies and hydration structure of N-methyl-p-nitroaniline. *Journal of Chemical Physics*, 2012. **136**(15).
21. Ottiger, C. and Wunderli-Allenspach, H., Immobilized artificial membrane (IAM)-HPLC for partition studies of neutral and ionized acids and bases in comparison with the liposomal partition system. *Pharmaceutical Research*, 1999. **16**(5): p. 643-650.
22. Claudio, A.F.M., Ferreira, A.M., Freire, C.S.R., Silvestre, A.J.D., Freire, M.G., and Coutinho, J.A.P., Optimization of the gallic acid extraction using ionic-liquid-based aqueous two-phase systems. *Separation and Purification Technology*, 2012. **97**: p. 142-149.
23. Chemspider, The free chemical database, <http://www.chemspider.com/>.
24. Fischer, V. and Borchard, W., Thermodynamic properties of poly(ethylene glycol)/water systems. 2. Critical point data. *Journal of Physical Chemistry B*, 2000. **104**(18): p. 4463-4470.

14. PAPER 11

Biocompatible Aqueous Biphasic Systems Composed of Polyethylene Glycol and Cholinium-based Ionic Liquids: Towards the Understanding of Their Formation Ability

Chemical Science (2013) (submitted for publication).

14.1. Abstract

It is here shown, for the first time, that biocompatible ionic liquid (IL)-polymer-based aqueous biphasic systems (ABS) can be formed by combining cholinium-based ionic liquids and polyethylene glycols (PEG) in aqueous solution. The influence of the IL chemical structure, PEG molecular weight and temperature on the ABS formation is investigated. Ternary liquid-liquid phase diagrams, binary water activities, PEG-IL miscibility data, and binary and ternary excess enthalpies estimated using COSMO-RS were used to derive information leading to a molecular-level mechanism for the phase separation. The multiple approaches used concur to demonstrate that the ABS formation on these systems is not the results of a salting-out mechanism but instead indicate that the specific interactions occurring between the IL anion and the PEG hydroxyl groups control the IL-PEG mutual solubilities and the ABS formation.

14.2. Introduction

In the previous chapters we have demonstrated that it is possible to control the phases' polarities by an adequate selection of the IL chemical structure¹⁻³. Nevertheless, only ILs such as imidazolium-, pyrrolidinium-, pyridinium- and piperidinium-based have been investigated¹⁻³. Several of these cations possess some toxicity and are poorly biodegradable, albeit side chain modifications may enhance their primary biodegradability potential and decrease their toxicity⁴⁻⁶. Moreover, if a large-scale application of these systems is envisaged, it is still hampered by the high price of certain ILs. Therefore, the ample versatility of ILs that can be synthesized should permit the creation of new fluids with an acceptable environmental footprint and enhanced biocompatibility, as well as of low cost.

Choline chloride (2-hydroxyethyltrimethylammonium chloride) is a water soluble essential nutrient important for cell membrane structure and for synthesizing folic acid and vitamin B12⁷. Although, choline chloride is a salt with a high melting temperature (302°C)⁸, and recent advances have offered the synthesis of novel cholinium-based ILs ([Ch]-based ILs) conjugated with different anions⁹⁻¹¹. These ILs present outstanding biodegradability^{12, 13} and low toxicity to filamentous fungi and the freshwater crustacean *Daphnia magna*¹¹. Furthermore, a number of works have described novel [Ch]-based ILs in which protein structure and enzyme function can be maintained or

even increased^{9, 10, 14, 15}. Due to these exceptional properties, their interest promptly increased in the past few years, with applications as diverse as crosslinking agents for collagen-based materials¹⁶, in the pre-treatment and dissolution of biomass^{17, 18}, or as co-substrates for microorganisms in the degradation of dyes¹². In addition, this new class of ILs is generally accessible, easy to handle, and cheaper than more common ILs.

Having in mind the plausible application of ABS for the extraction of added-value compounds and their mandatory biocompatibility and biodegradability issues, a new class of aqueous biphasic systems composed of [Ch]-based ILs and an inorganic salt was recently proposed while some authors also reported the possibility to form ABS with polypropylene glycol (PPG) and [Ch]-based ILs¹⁹⁻²¹. It was suggested that the [Ch]-based ILs can either act as the salting-out species of the moderately hydrophobic PPG or being salted-out by a high charge density salt¹⁹⁻²¹. The molecular level mechanism of two-phase formation would be ruled by the formation of hydration complexes and/or the ions affinity for water¹⁹⁻²¹. While the mechanism for ABS formation in PPG + [Ch]-based ILs requires further confirmation, for a more hydrophilic polymer, such as polyethylene glycol (PEG), the molecular phenomenon which governs the formation of an immiscible regime becomes more complex as will be presented and described herein. To this end, the ternary phase diagrams, tie-lines and tie-line lengths of several ABS composed of PEGs and [Ch]-based ILs were determined. A broad range of structurally distinct [Ch]-based ILs, PEGs of different molecular weights, and different temperatures were used to evaluate their impact into ABS formation and to gather evidence that could help to the specific interactions dominating the phase behaviour. Moreover, the binary PEG-IL solubility, their enthalpies of mixing, the water activities of the various compounds and were also used so that the molecular insights on the molecular mechanism of liquid-liquid demixing could be understood.

14.3. Experimental Section

14.3.1. Materials

The following cholinium-based ILs were acquired from Sigma: cholinium chloride, [Ch]Cl, cholinium bicarbonate, [Ch]Bic, cholinium bitartrate, [Ch]Bit, and cholinium dihydrogencitrate, [Ch]DHcit. The cholinium acetate, [Ch]Ac, and cholinium

dihydrogenphosphate, [Ch]DHph, and. Cholinium glycolate, [Ch]Gly, were obtained from Iolitec. Cholinium propanoate, [Ch]Pro, Cholinium butanoate, [Ch]But, and Cholinium Lactate, [Ch]Lac, were synthesized according to standard protocols^{9, 12, 22}. All the ILs were dried under constant agitation and vacuum, at a moderate temperature (323 K), for a minimum of 48h, to reduce the volatile compounds and water contents to negligible values. After this procedure, ¹H and ¹³C NMR was employed to evaluate the purity of each sample. All ILs present a purity level higher than 98 wt%.

PEGs of average molecular weights 400 g.mol⁻¹, 600 g.mol⁻¹ and 1000 g.mol⁻¹ (abbreviated as PEG 400, PEG 600 and PEG 1000, respectively) were supplied by Fluka, and used as received.

The water used was double distilled, passed across a reverse osmosis system and further treated with a Milli-Q plus 185 water purification apparatus.

14.3.2. Methods

14.3.2.1. Phase Diagrams and Tie-lines

Aqueous solutions of each cholinium-based IL (from 40 wt% to 80 wt%) and aqueous solutions of each PEG (from 80 wt% to 100 wt%) were prepared and used for the determination of the binodal curves. The phase diagrams were determined by the cloud point titration method at 298 K and 323 K (± 1 K) and atmospheric pressure, according to literature procedures^{23, 24}. The composition of each system was calculated by the weight quantification of all components added within $\pm 10^{-7}$ kg. The tie-lines (TLs) were also determined and further details are provided in Supporting Information (Table S14.13).

14.3.2.2. Solubility of [Ch]-based ILs in PEG 600

The solubility of each [Ch]-based IL in PEG 600 was determined at 298 K and atmospheric pressure. For that purpose repetitive small amounts of each IL (*ca.* 5 mg) were added to pre-weighed vials containing PEG 600. Then the IL and the PEG binary mixtures were agitated vigorously during 12 h at constant temperature. After this period, the vials were analysed visually, and if the maximum of solubility it was reached the vials were weighed and the respective values of wt% solubilities determined.

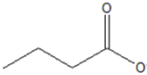
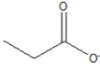
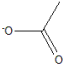
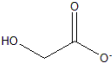
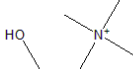
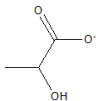
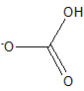
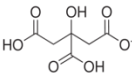
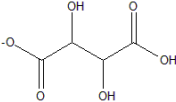
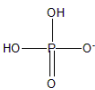
14.3.2.3. COSMO-RS Predictions

The standard procedure for COnductor-like Screening MOdel for Real Solvents (COSMO-RS) modeling consists of two major steps. First, the continuum solvation COSMO calculations of electronic density and molecular geometry of PEG 600, cholinium-based ILs, and water were performed with the TURBOMOLE 6.1 program package on the density functional theory, utilizing the BP functional B88-P86 with a triple- ζ valence polarized basis set (TZVP) and the resolution of identity standard (RI) approximation²⁵. Second, the thermodynamic properties such as activity coefficient, excess enthalpy, and excess free Gibbs energy calculations was performed with the COSMOthermX_2.1 program using the parameter file BP_TZVP_C21_0111 (COSMOlogic GmbH & Co KG, Leverkusen, Germany). In all calculations, the ILs are always treated by means of their isolated ions.

14.3. Results and Discussion

The chemical structures of the studied [Ch]-based ILs or related salts are presented in Table 14.1. We have focused on the subgroup of the cholinium cation ([Ch]⁺) combined with several conjugated bases namely chloride (Cl⁻), bicarbonate (Bic⁻), bitartrate (Bit⁻), acetate (Ac⁻), propanoate (Pro⁻), butanoate (But⁻), dihydrogencitrate (DHcit⁻), glycolate (Gly⁻), lactate (Lac⁻) and dihydrogenphosphate (DHph⁻), to investigate their influence on the ABS formation. PEGs of average molecular weights of 400 g.mol⁻¹, 600 g.mol⁻¹ and 1000 g.mol⁻¹ were used to evaluate the impact of the polymer size on the liquid-liquid immiscibility, and are abbreviated as PEG 400, PEG 600, and PEG 1000, respectively.

Table 14.1 Chemical structure of the studied cholinium-based salts and respective octanol-water partition coefficients (K_{ow})²⁶.

Name	Cation	Anion	$\log K_{ow}$ [#]
Cholinium butanoate ([Ch]But)			N.A.*
Cholinium propanoate ([Ch]Pro)			N.A.*
Cholinium chloride ([Ch]Cl)		Cl ⁻	-3.70
Cholinium acetate ([Ch]Ac)			-4.66
Cholinium glycolate ([Ch]Gly)			-1.20
Cholinium lactate ([Ch]Lac)			-3.70
Cholinium bicarbonate ([Ch]Bic)			-3.70
Cholinium dihydrogen citrate ([Ch]DHcit)			-1.32
Cholinium bitartrate ([Ch]Bit)			-1.43
Cholinium dihydrogen phosphate ([Ch]DHph)			-3.70

[#]The $\log K_{ow}$ values are a measure of the differential solubility of a particular solute between the immiscible liquids octanol and water. *N.A.: not available data.

The phase diagrams of all ABS composed of different PEGs and cholinium-based salts were initially determined at 298 K and atmospheric pressure. The detailed weight fraction experimental data are presented in Supporting Information (Tables S14.1 to Table S14.12). Figure 14.1 depicts the solubility curves of the systems displayed in molality units [mole of PEG *per* kg of (salt + water) *versus* [mole of sal *per* kg of (PEG

+ water)] in order to avoid distortions on the comparisons that could be a direct consequence of the distinct molecular weights of the species involved. An example of the tie-lines of a particular system composed of [Ch]Cl and PEG 600 at 298 K is shown in Figure 14.2. The remaining tie-lines, tie-line lengths and solubility data correlation are shown in Supporting Information (Table S14.13). Figure 14.1 shows the influence of the anion nature of the cholinium-based salts through the phase diagrams behaviour with a common polymer, PEG 600. Although [Ch]Cl, [Ch]Ac, [Ch]Bic, [Ch]Gly, [Ch]Lac, [Ch]Bit, [Ch]DHcit and [Ch]DHph could form ABS with PEG 600, it should be remarked that [Ch]Pro and [Ch]But are not able to undergo liquid-liquid demixing in aqueous media.

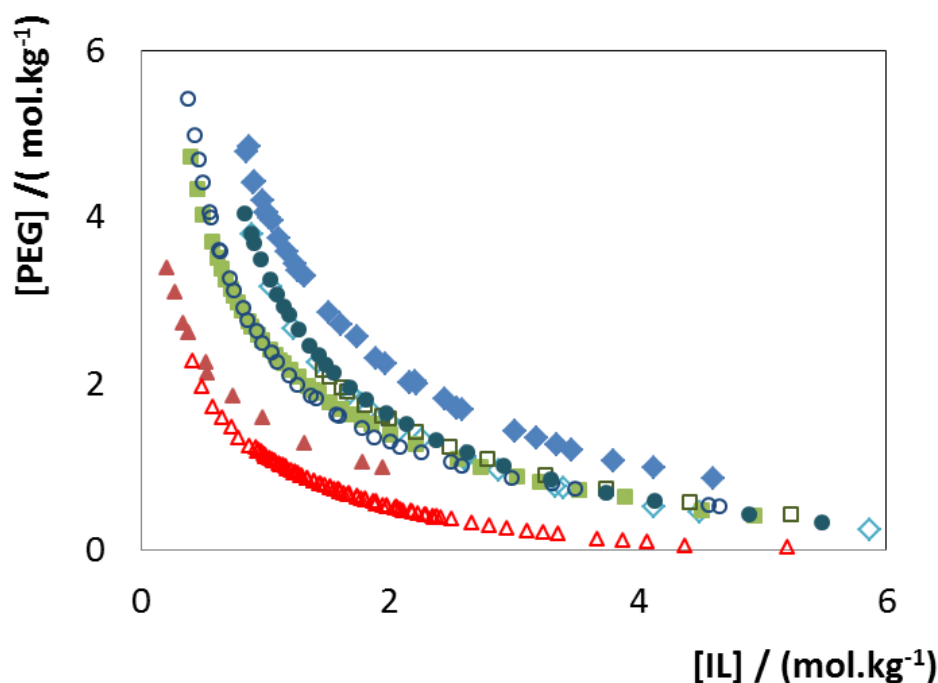


Figure 14.1 Experimental solubility data for ABS composed of PEG 600 + [Ch]-based ILs at 298 K: (Δ) [Ch]DHph; (\blacktriangle) [Ch]Bit; (\blacksquare) [Ch]Bic; (\circ) [Ch]DHcit; (\diamond) [Ch]Lac; (\square) [Ch]Gly; (\bullet) [Ch]Ac; (\blacklozenge) [Ch]Cl.

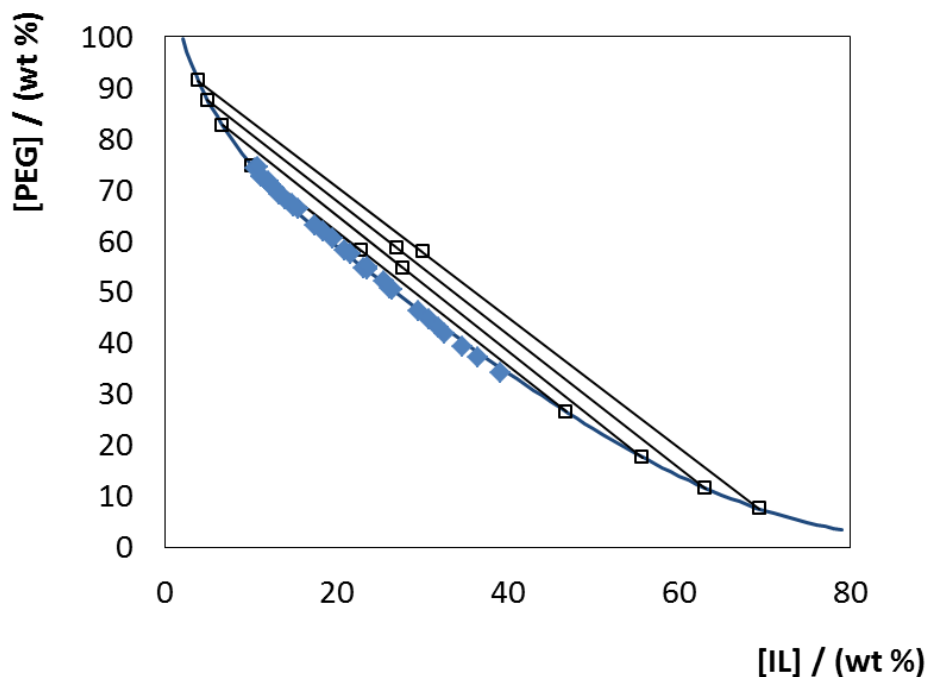


Figure 14.2 Ternary phase diagram of the ABS composed of [Ch]Cl and PEG at 298 K: (◆) binodal curve data; (-) binodal adjusted curve; (□) TL data.

The ability of the [Ch]-based ILs or related salts to promote PEG-based ABS follows the trend: [Ch]DHph > [Ch]Bit > [Ch]DHcit \approx [Ch]Bic > [Ch]Lac \approx [Ch]Gly \approx [Ch]Ac > [Ch]Cl. Even though this trend is only presented here for a common polymer (PEG 600) the data for the remaining PEGs of different molecular weight follows a similar pattern and are presented Supporting Information (Figures S14.1 and S14.2). In the majority of the systems the bottom phase is the cholinium-rich phase whereas the top phase corresponds to the PEG-rich phase. However, particular inversions on the phase densities were observed with [Ch]Cl and [Ch]Ac. A detailed description of the bottom and top phases in each system is provided in Supporting Information (Table S14.14). Since both phases are liquid and non-coloured, the coexisting phases were identified by conductivity measurements at 298 K. The conductivity values are also shown in Supporting Information (Table S14.14).

Albeit in more conventional systems involving aqueous mixtures of ILs and high charge density salts the liquid-liquid demixing has been reported as being the result of a salting-out phenomenon^{23, 27, 28}, *i.e.*, the salt ions are preferentially hydrated and lead to the exclusion of the more “hydrophobic” IL for a second liquid phase, the scenario occurring in ABS composed of ILs and PEG is more complex². Previously, we have

shown that [Ch]-based ILs are also capable of forming salt-salt ABS by a salting-out phenomenon induced by a high charge density salt, K_3PO_4 ²¹. As typically observed with IL-salt ABS the liquid-liquid demixing ability is the result of the enhanced aptitude of the phosphate anion to be hydrated^{23, 24}. When dealing with ABS composed of ILs and a more hydrophobic polymer, such as PPG, the mechanisms of phase separation have been explained as a salting-out effect induced by the IL on the polymer in aqueous media^{19, 20}. Limited or no evidence is, however, available to sustain such hypothesis. When addressing a more hydrophilic polymer, such as PEG, the water hydration capability of the IL ions does not seem to control the phase separation aptitude of PEG-IL-based ABS². Contrarily to IL-salt-based ABS, in all the investigated PEG-based systems the water content is lower than 30 wt%, with the exception of [Ch]DHph with approx. 50 wt% of total water. Thus, in most examples, there is a 1:1:1 volumetric fraction of the [Ch]-based IL, PEG and water, and all the binary specific interactions occurring within the IL-PEG, IL-water and PEG-water cannot be discarded.

The first factor suggesting that the IL affinity for water does not control the ABS phase behaviour is the octanol-water partition coefficient (K_{ow}) of each fluid. The K_{ow} values are a measure of the differential solubility of a particular solute between two immiscible solvents - octanol and water -and are presented in Table 14.1. In more conventional systems of the type IL + salt, and for a common salt, the phases' formation ability is dominated by the ILs affinity for water and clearly correlates with the K_{ow} values²¹. ILs with lower affinity for water, *i.e.* more hydrophobic fluids, are more easily excluded to a second liquid phase. In PEG-[Ch]-based IL systems there is no dependence on the K_{ow} values. This odd behaviour is thus an indication that the formation of ABS composed of [Ch]-based ILs and PEGs are not the result of a salting-out effect of the ionic species over the polymer. Moreover although [Ch]Cl is a weaker salting out agent than most inorganic chloride based salts, it is impossible to generate an ABS with these while this is straightforward with [Ch]Cl, as shown in Figures 14.1 and 14.2, as well as with other Cl-based ionic liquids².

Recently²⁹, the water activity of isolated [Ch]-based ILs has been reported. Figure 14.3 shows a comparison of the water activity at 298 K of the PEG 600 (measured here) and of various ILs here studies as a function of the IL/PEG weight fraction.

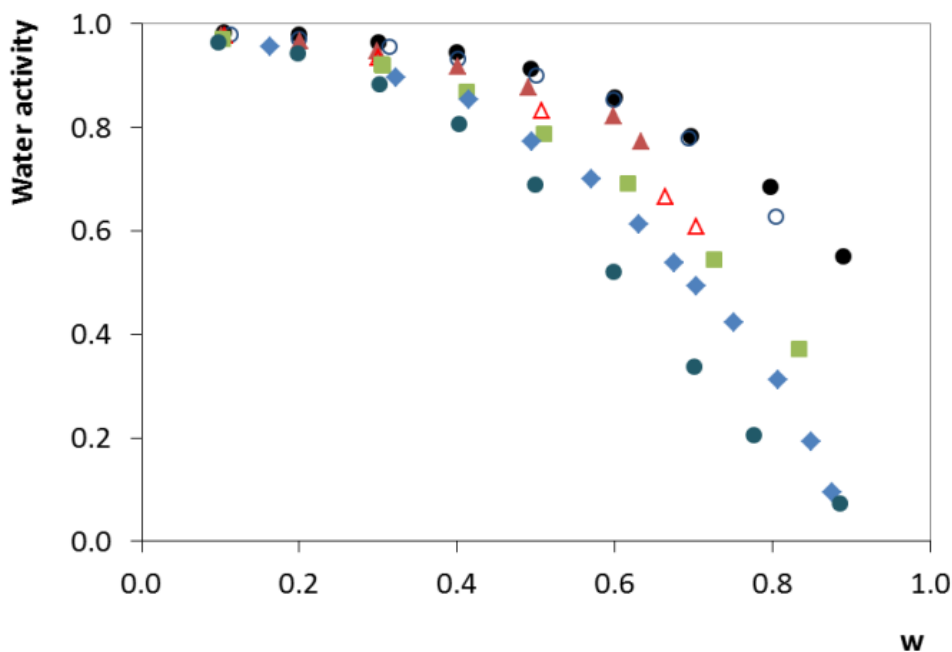


Figure 14.3 Experimental water activities data at 298 K: (●) PEG 600; (○) [Ch]DHcit; (▲) [Ch]Bit; (△) [Ch]DHph; (■) [Ch]Bic; (●) [Ch]Ac; (◆) [Ch]Cl. The data shown for the ILs was adapted from Khan et al²⁹.

The water activity values allow a further evaluation if the water-IL interactions, or the aptitude of the isolated ions to be hydrated, govern the ABS formation. They show that the anions with higher ability to interact with water, such as Cl^- and Ac^- , are those that display a lower capability to promote an ABS with PEG. On the opposite order, the anions Bit^- and DHcit^- are those that present a lower affinity for water, and yet have a stronger phase separation capability. These results clearly show that the ions with higher ability to form hydration complexes are not those with higher capability to induce phase separation, meaning that the formation of PEG-[Ch]-based IL ABS is not driven by a salting-out phenomenon.

In order to gather further insights on the dominant interactions in PEG-[Ch]-based IL ABS, the solubility of each IL in PEG 600 was determined at 298K. The solubility data are presented in Table 14.2. The higher solubility in PEG reveals a higher affinity and the presence of strong favourable interactions with the polymer. As observed in Table 14.2, the [Ch]But and [Ch]Prop are completely soluble with PEG in all the composition range. This behaviour is indicative of strong IL-PEG interactions, and this explains why these compounds are not able to create an ABS with PEG. When evaluating the remaining [Ch]-based ILs capable of forming ABS, it is clear that the compounds

composed of the anions with higher solubilities in the polymer, such as Ac⁻ and Cl⁻ based ILs, display a lower ability to phase separate in aqueous media. However, with the ILs whose solubility is lower than 0.005 mol.kg⁻¹, the phase separation occurs at lower concentrations of these solutes.

Table 14.2 Solubilities of several [Ch]-based ILs in PEG 600 (expressed in molality) at 298 K and atmospheric pressure.

[Ch]-based ILs	Molality / (mol.kg⁻¹)
[Ch]But	completely soluble
[Ch]Pro	completely soluble
[Ch]Ac	4.473
[Ch]Gly	-
[Ch]Lac	-
[Ch]Cl	0.260
[Ch]DHcit	< 0.005
[Ch]Bit	< 0.005

These results provide clear indications that the PEG-IL interactions dominate the ABS formation. Therefore, in order to obtain additional evidence on the molecular mechanisms which rule the two phases formation, we have further employed COSMO-RS, a predictive model based on unimolecular quantum chemistry calculations, to explore the excess enthalpies at 298 K. COSMO-RS was used here to study the interactions on the following binary pairs: PEG-water, IL-water and IL-PEG. The ternary mixture composed of PEG + IL + water was also evaluated. It should be remarked that Khan et al.²⁹ already demonstrated the accuracy of COSMO-RS in predicting the water activity coefficients of cholinium-based ILs supporting the validity of the COSMO-RS predictions obtained here. The liquid-liquid equilibrium description by COSMO-RS (*cf.* Supporting Information, Figures S14.8 and S14.9) demonstrates favourable interactions between the first two binary mixtures, PEG-water and IL-water, as evidenced by the negative excess enthalpies, H^E , and excess free Gibbs energy, G^E , throughout the whole composition range. In all examples, H-bonding is the dominant interaction occurring in these binary mixtures. The ILs [Ch]Cl and [Ch]Ac display the higher energy interactions with water; yet, they present a lower ability to promote the phase separation. On the opposite, the ILs [Ch]Bit and [Ch]DHcit reveal the lower values of total energy interactions with water and are the most effective in creating

ABS. These results again indicate that the hydration aptitude of the IL ions is not ruling the ABS phase behaviour.

The excess enthalpies of mixing of the IL anions with PEG 600 in aqueous media are shown in Figure 14.4. ILs with the Ac^- and Cl^- anions, with lower abilities to promote the ABS phase separation, present stronger interactions with PEG 600 as reflected by the highly negative H^E values. On the other hand, the ILs containing the DHcit^- and DHph^- anions display the less negative H^E values, indicative of weaker binary interactions, and are the more able to induce the liquid-liquid demixing in PEG-based ABS. In this context, ILs with stronger interactions with PEG are more difficult to phase separate and *vice-versa*.

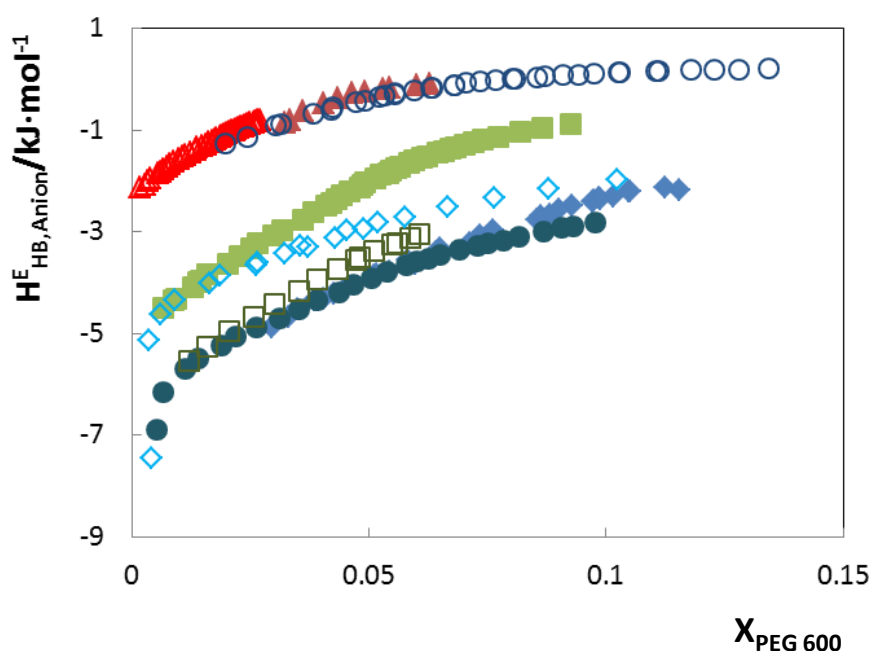


Figure 14.4 Excess enthalpies of mixing between PEG 600 and the IL anion predicted by COSMO-RS as a function of the polymer mole fraction: (Δ) [Ch]DHph; (\blacktriangle) [Ch]Bit; (\circ) [Ch]DHcit; (\blacksquare) [Ch]Bic; (\diamond) [Ch]Lac; (\square) [Ch]Gly; (\bullet) [Ch]Ac; (\blacklozenge) [Ch]Cl.

COSMO-RS was also used to evaluate the molecular phenomena occurring in the ternary mixtures, IL-PEG-water, using the predicted excess enthalpies and taking into account the contribution of each species. The respective results are shown in Supporting Information (Figure S14.10). The liquid-liquid equilibrium predicted by COSMO-RS shows that the favourable interactions that occur in the ABS arises mainly from PEG 600 and the IL anion. The cholinium cation also negatively contributes to the excess enthalpies of the mixture, but its contribution is slightly affected by the concentration of

PEG 600. Meanwhile, the contribution of water to the excess enthalpies was found to be positive, which indicates stronger interactions of water in its pure state rather than in the ternary mixtures.

In summary, Figure 14.4 presents the comparison of excess enthalpies of mixing highlighting the contribution of the IL anion. The favourable PEG-IL interactions can be ranked as follows: $\text{DHph}^- < \text{Bit}^- < \text{DHCit}^- < \text{Bic}^- < \text{Lac}^- < \text{Gly}^- < \text{Ac}^- < \text{Cl}^-$. This sequence closely follows that observed with the IL anion trend to create ABS. In addition, the dominant specific interaction, as expected, is the H-bonding between the terminal hydroxyl groups of PEG and the IL anion. It can thus be concluded that the PEG-IL interactions rule the formation of the respective ABS mediated by an H-bonding network. It should be highlighted that the significance of H-bonding in binary mixtures of PEGs and imidazolium-based ILs was already stated by Rogers and co-workers³⁰ making use of binary liquid-liquid equilibrium data.

The effect of the molecular weight of the polymer through the ABS formation aptitude was also addressed. Figure 14.5 depicts the phase diagrams for ternary systems containing PEG 400 and PEG 1000 combined with fixed cholinium-based salts. The remaining data are shown in Supporting Information (Figures S14.3 to S14.7).

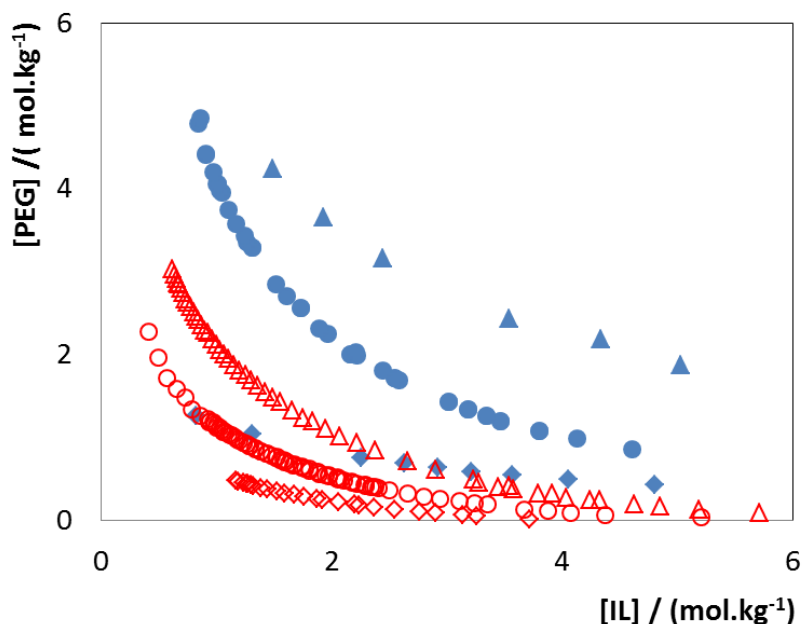


Figure 14.5 Experimental solubility data for ABS composed of PEG + [Ch]-based ILs at 298 K: (◊) PEG 1000/[Ch]DHph; (○) PEG 600/[Ch]DHph; (△) PEG 400/[Ch]DHph; (◈) PEG 1000/[Ch]Cl; (●) PEG 600/[Ch]Cl; (▲) PEG 400/[Ch]Cl.

For all the studied ILs the ability of the polymer for inducing the liquid-liquid demixing follows the order: PEG 1000 > PEG 600 > PEG 400. The higher the molecular weight of PEG the higher the ability of the system to form two macroscopic liquid phases. The same trend has been observed in conventional polymer/salt ABS³¹⁻³³ and, more recently, on PEG/imidazolium-based ILs containing systems². This trend can be related to both an increasing hydrophobic character of PEG with the molecular weight, and thus to a lower affinity for water, and to a decreased miscibility with the ILs. In binary systems of the type PEG-IL it was already reported a decreasing solubility of the IL in the polymer-rich phase with increasing molecular weight of the PEG that was attributed to the lower ratio of terminal -OH groups which limit the sites for the hydrogen bonding of the IL anion³⁰. The predicted H^E values also show to be less negative with the increase of the PEG molecular weight. In this particular example, electrostatic, H-bonding, and van der Waals interactions all contribute to less negative values of enthalpy of mixing. The respective predictions are shown in Supporting Information (Figures S14.11 and S14.12).

To infer about the temperature effect on the ability to liquid-liquid demixing, the ABS of [Ch]-based ILs with the highest and lowest ability to promote the phase separation, [Ch]Cl and [Ch]DHph, respectively, were determined at 298 K and 323 K. The respective phase diagrams are presented in Figure 14.6. The detailed weight fraction data are reported in Supporting Information (Table S14.11).

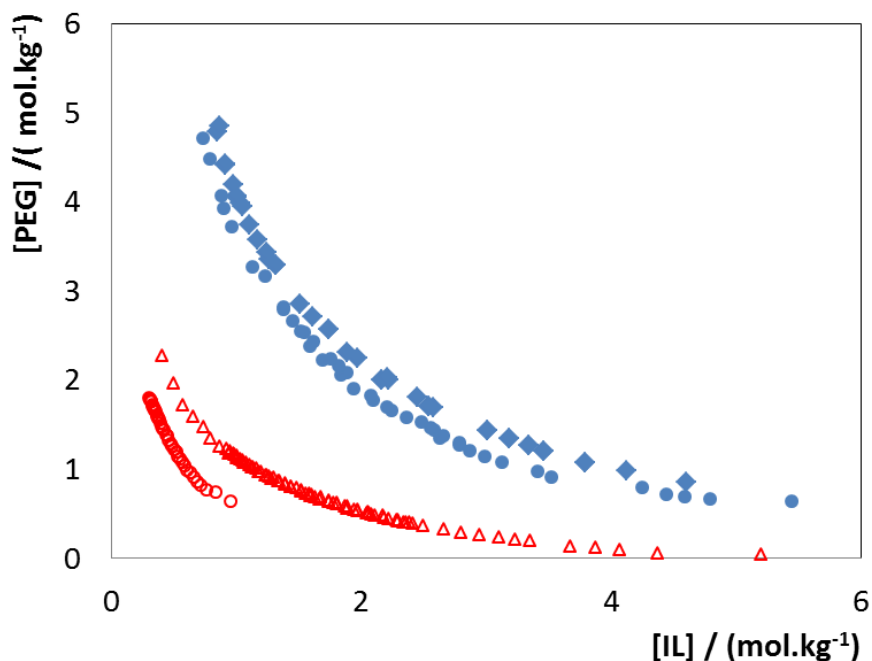


Figure 14.6 Experimental solubility data for ABS composed of PEG 600 + [Ch]-based ILs: (○) PEG 600/[Ch]DHph at 323K; (△) PEG 600/[Ch]DHph at 298K; (◆) PEG 600/[Ch]Cl at 298K; (●) PEG 600/[Ch]Cl at 323K.

The binodal curves show that in both cases an increase in temperature enhances the immiscibility region. This pattern is in close agreement with that observed before for typical PEG/salt systems³⁴ and for PPG/[Ch]-based ABS^{35, 36}. On the other hand, the temperature effect was shown to be the opposite in ABS composed of PEG 2000 and imidazolium-based ILs². In those systems the influence of temperature in the liquid-liquid demixing seems to be dominated by the hydrogen bonding, presenting a lower critical solution temperature-type behaviour as observed for the PEG-water binary mixtures³⁷. For systems dominated by this type of interaction an increase in temperature leads to a decrease on the interactions and consequently to a liquid-liquid demixing. The COSMO-RS H^E values provided in Supporting Information (Figures S14.13) and support this statement.

In summary, based on the ternary phase diagrams, solubility data of each IL in PEG, ILs water activities and excess enthalpies, this work shows that the H-bonding occurring between the IL anion and the terminal -OH groups of the polymer rule the formation aptitude of PEG-IL-based ABS. Contrarily, to more conventional systems composed of ILs and salts, in which the formation of hydration complexes governs the liquid-liquid

demixing by a salting-out mechanism, the PEG-IL-based ABS are by far more complex and are ruled by the interactions occurring between the PEG and the [Ch]-based ILs.

14.5. Conclusions

It was here shown, for the first time, that biocompatible IL-polymer-based ABS can be formed by the combination of cholinium-based salts and PEGs. Using a large array of cholinium-based ILs and polymers it was demonstrated that the specific interactions occurring between the IL anion and the –OH terminal groups of the polymer control the ABS formation.

Albeit favourable interactions are also observed within the IL-water and PEG-water pairs, ILs with strong interactions with the polymer are more difficult to phase separate in aqueous media. An increase of the polymer molecular weight also leads to larger immiscibility regions, thus higher ABS formation ability, due to a decrease on the PEG-IL mutual solubility. Furthermore, an increase in temperature promotes the ability of the systems to phase separate. Higher temperatures weaken the H-bonding interactions occurring in PEG-IL and thereby facilitate the respective separation.

14.6. References

1. Pereira, J.F.B., Vicente, F., Santos-Ebinuma, V.C., Araújo, J.M., Pessoa, A., Freire, M.G., and Coutinho, J.A.P., Extraction of tetracycline from fermentation broth using aqueous two-phase systems composed of polyethylene glycol and cholinium-based salts. *Process Biochemistry*, 2013. doi.org/10.1016/j.procbio.2013.02.025.
2. Freire, M.G., Pereira, J.F.B., Francisco, M., Rodríguez, H., Rebelo, L.P.N., Rogers, R.D., and Coutinho, J.A.P., Insight into the Interactions That Control the Phase Behaviour of New Aqueous Biphasic Systems Composed of Polyethylene Glycol Polymers and Ionic Liquids. *Chemistry – A European Journal*, 2012. **18**(6): p. 1831-1839.
3. Pereira, J.F.B., Rebelo, L.P.N., Rogers, R.D., Coutinho, J.A.P., and Freire, M.G., Combining ionic liquids and polyethylene glycols to boost the hydrophobic-hydrophilic range of aqueous biphasic systems. *Chemical Communications*, 2013. (*submitted for publication*).
4. Gathergood, N., Garcia, M.T., and Scammells, P.J., Biodegradable ionic liquids: Part I. Concept, preliminary targets and evaluation. *Green Chemistry*, 2004. **6**(3): p. 166-175.
5. Harjani, J.R., Singer, R.D., Garciac, M.T., and Scammells, P.J., Biodegradable pyridinium ionic liquids: design, synthesis and evaluation. *Green Chemistry*, 2009. **11**(1): p. 83-90.
6. Petkovic, M., Seddon, K.R., Rebelo, L.P.N., and Pereira, C.S., Ionic liquids: a pathway to environmental acceptability. *Chemical Society Reviews*, 2011. **40**(3): p. 1383-1403.
7. Blusztajn, J.K., Developmental neuroscience - Choline, a vital amine. *Science*, 1998. **281**(5378): p. 794-795.
8. Abbott, A.P., Capper, G., Davies, D.L., Rasheed, R.K., and Tambyrajah, V., Novel solvent properties of choline chloride/urea mixtures. *Chemical Communications*, 2003(1): p. 70-71.
9. Pernak, J., Syguda, A., Mirska, I., Pernak, A., Nawrot, J., Pradzynska, A., Griffin, S.T., and Rogers, R.D., Choline-derivative-based ionic liquids. *Chemistry-a European Journal*, 2007. **13**(24): p. 6817-6827.
10. Weaver, K.D., Kim, H.J., Sun, J.Z., MacFarlane, D.R., and Elliott, G.D., Cyto-toxicity and biocompatibility of a family of choline phosphate ionic liquids designed for pharmaceutical applications. *Green Chemistry*, 2010. **12**(3): p. 507-513.
11. Ventura, S.P.M., Silva, F.A., Gonçalves, A.M.M., Pereira, J.L., Gonçalves, F., Coutinho, J.A.P., Revealing the ecotoxicity of cholinium-based ionic liquids. *Ecotoxicology and Environmental Safety* 2013. (*submitted for publication*)
12. Sekar, S., Surianarayanan, M., Ranganathan, V., MacFarlane, D.R., and Mandal, A.B., Choline-Based Ionic Liquids-Enhanced Biodegradation of Azo Dyes. *Environmental Science & Technology*, 2012. **46**(9): p. 4902-4908.
13. Petkovic, M., Ferguson, J.L., Gunaratne, H.Q.N., Ferreira, R., Leitao, M.C., Seddon, K.R., Rebelo, L.P.N., and Pereira, C.S., Novel biocompatible cholinium-based ionic liquids-toxicity and biodegradability. *Green Chemistry*, 2010. **12**(4): p. 643-649.
14. Fujita, K., MacFarlane, D.R., and Forsyth, M., Protein solubilising and stabilising ionic liquids. *Chemical Communications*, 2005, **38**: p. 4804-4806.
15. Vijayaraghavan, R., Izgorodin, A., Ganesh, V., Surianarayanan, M., and MacFarlane, D.R., Long-Term Structural and Chemical Stability of DNA in Hydrated Ionic Liquids. *Angewandte Chemie-International Edition*, 2010. **49**(9): p. 1631-1633.
16. Vijayaraghavan, R., Thompson, B.C., MacFarlane, D.R., Kumar, R., Surianarayanan, M., Aishwarya, S., and Sehgal, P.K., Biocompatibility of choline salts as crosslinking agents for collagen based biomaterials. *Chemical Communications*, 2010. **46**(2): p. 294-296.
17. Liu, Q.P., Hou, X.D., Li, N., and Zong, M.H., Ionic liquids from renewable biomaterials: synthesis, characterization and application in the pretreatment of biomass. *Green Chemistry*, 2012. **14**(2): p. 304-307.

18. Garcia, H., Ferreira, R., Petkovic, M., Ferguson, J.L., Leitao, M.C., Gunaratne, H.Q.N., Seddon, K.R., Rebelo, L.P.N., and Pereira, C.S., Dissolution of cork biopolymers in biocompatible ionic liquids. *Green Chemistry*, 2010. **12**(3): p. 367-369.
19. Liu, X., Li, Z., Pei, Y., Wang, H., and Wang, J., (Liquid + liquid) equilibria for (cholinium-based ionic liquids + polymers) aqueous two-phase systems. *The Journal of Chemical Thermodynamics*, 2013. **60**: p. 1-8.
20. Li, Z., Liu, X., Pei, Y., Wang, J., and He, M., Design of environmentally friendly ionic liquid aqueous two-phase systems for the efficient and high activity extraction of proteins. *Green Chemistry*, 2012. **14**(10): p. 2941-2950.
21. Shahriari, S., Tomé, L.C., Araújo, J.M.M., Rebelo, L.P.N., Coutinho, J.A.P., Marrucho, I.M., and Freire, M.G., Aqueous Biphasic Systems: A Novel Benign Route using Cholinium-Based Ionic Liquids. *RSC Advances*, 2013. **3**: 1835-1843.
22. Muhammad, N., Hossain, M.I., Man, Z., El-Harbawi, M., Bustam, M.A., Noaman, Y.A., Alitheen, N.B.M., Ng, M.K., Hefter, G., and Yin, C.Y., Synthesis and Physical Properties of Choline Carboxylate Ionic Liquids. *Journal of Chemical and Engineering Data*, 2012. **57**(8): p. 2191-2196.
23. Ventura, S.P.M., Neves, C.M.S.S., Freire, M.G., Marrucho, I.M., Oliveira, J., and Coutinho, J.A.P., Evaluation of Anion Influence on the Formation and Extraction Capacity of Ionic-Liquid-Based Aqueous Biphasic Systems. *Journal of Physical Chemistry B*, 2009. **113**(27): p. 9304-9310.
24. Neves, C.M.S.S., Ventura, S.P.M., Freire, M.G., Marrucho, I.M., and Coutinho, J.A.P., Evaluation of Cation Influence on the Formation and Extraction Capability of Ionic-Liquid-Based Aqueous Biphasic Systems. *Journal of Physical Chemistry B*, 2009. **113**(15): p. 5194-5199.
25. TURBOMOLE V6.1 2009, a.d.o.U.o.K.a.F.K.G., 1989–2007, 25 GmbH, since 2007; available from <http://www.turbomole.com>.
26. Chemspider, The free chemical database. Available from: <http://www.chemspider.com>.
27. Mourão, T., Claudio, A.F.M., Boal-Palheiros, I., Freire, M.G., and Coutinho, J.A.P., Evaluation of the impact of phosphate salts on the formation of ionic-liquid-based aqueous biphasic systems. *Journal of Chemical Thermodynamics*, 2012. **54**: p. 398-405.
28. Neves, C.M.S.S., Freire, M.G., and Coutinho, J.A.P., Improved recovery of ionic liquids from contaminated aqueous streams using aluminium-based salts. *Rsc Advances*, 2012. **2**(29): p. 10882-10890.
29. Khan, I., Kurnia, K.A., Saraiva, J., Pinho, S., and Coutinho, J.A.P., Activity Coefficients of Water Cholinium-based Ionic Liquids and their Modeling by COSMO-RS. 2013. (*in preparation*).
30. Rogers, R.D., Rodriguez, H., Francisco, M., Rahman, M., and Sun, N., Biphasic liquid mixtures of ionic liquids and polyethylene glycols. *Physical Chemistry Chemical Physics*, 2009. **11**(46): p. 10916-10922.
31. Rogers, R.D. and Zhang, J.H., Effects of increasing polymer hydrophobicity on distribution ratios of TcO₄⁻ in polyethylene/poly(propylene glycol)-based aqueous biphasic systems. *Journal of Chromatography B-Biomedical Applications*, 1996. **680**(1-2): p. 231-236.
32. Zhi, W.B., Song, J.M., Bi, J.X., and Fan, O.Y., Partial purification of alpha-amylase from culture supernatant of *Bacillus subtilis* in aqueous two-phase systems. *Bioprocess and Biosystems Engineering*, 2004. **27**(1): p. 3-7.
33. Taboada, M.E., Asenjo, J.A., and Andrews, B.A., Liquid-liquid and liquid-liquid-solid equilibrium in Na₂CO₃-PEG-H₂O. *Fluid Phase Equilibria*, 2001. **180**(1-2): p. 273-280.
34. Willauer, H.D., Huddleston, J.G., Li, M., and Rogers, R.D., Investigation of aqueous biphasic systems for the separation of lignins from cellulose in the paper pulping process. *Journal of Chromatography B*, 2000. **743**(1-2): p. 127-135.
35. Li, Z.Y., Liu, X.X., Pei, Y.C., Wang, J.J., and He, M.Y., Design of environmentally friendly ionic liquid aqueous two-phase systems for the efficient and high activity extraction of proteins. *Green Chemistry*, 2012. **14**(10): p. 2941-2950.

36. Liu, X., Li, Z., Pei, Y., Wang, H., and Wang, J., (Liquid+liquid) equilibria for (cholinium-based ionic liquids + polymers) aqueous two-phase systems. *The Journal of Chemical Thermodynamics*, 2013. **60**: p. 1-8.

37. Fischer, V., Borchard, W., and Karas, M., Thermodynamic Properties of Poly(ethylene glycol)/Water Systems. 1. A Polymer Sample with a Narrow Molar Mass Distribution. *The Journal of Physical Chemistry*, 1996. **100**(39): p. 15992-15999.

15. PAPER 12

Extraction of Tetracycline from Fermentation Broth using Aqueous Two-Phase Systems Composed of Polyethylene Glycol and Cholinium-based Salts

Process Biochemistry, 28(4) (2013) 716-722.

15.1. Abstract

Aiming at developing not only cheaper but also biocompatible and sustainable extraction and purification processes for antibiotics, in this work it was evaluated the ability of aqueous biphasic systems (ABS) composed of polyethylene glycol (PEG) and cholinium-based salts to extract tetracycline from the fermented broth of *Streptomyces aureofaciens*. Conventional polymer/salt and salt/salt ABS were also studied for comparison purposes. The novel systems here proposed are able to extract tetracycline directly from the fermentation broth with extraction efficiencies higher than 80%. A tailored extraction ability of these systems can also be achieved, with preferential extractions either for to the polymer- or salt-rich phases, and which further depend on the cholinium-based salt employed. The gathered results support the applicability of biocompatible ABS in the extraction of antibiotics from complex matrices and can be envisaged as valuable platforms to be applied at the industrial level by pharmaceutical companies.

Keywords: Tetracycline, *Streptomyces aureofaciens*, extraction, aqueous two-phase systems, cholinium-based salts.

15.2. Introduction

The study of alternative techniques for the extraction of antibiotics is the main goal of the second part of this thesis. As described in chapter 8, among the several classes of antibiotics, the Tetracycline (TC) appears as one of the most important and broad spectrum antibiotic class used nowadays. Thus, after the extensive study of novel PEG/IL-based ABS presented in the previous chapters, in this chapter it is shown the separation and extraction of tetracycline produced by *Streptomyces aureofaciens* making use of the novel IL-PEG-based ABS investigated.

As stated on the previous chapters, the main advantages of polymer-salt or polymer-IL ABS, when compared to polymer-polymer systems, relay on their lower viscosities and possibility of changing the polarities of the coexisting phases. Moreover, they usually display a quick phase separation and high extraction efficiencies which can be easily manipulated by a proper selection of the ions composing a given IL or salt¹. Indeed, IL-based ABS have been successfully used in the separation, concentration and purification of proteins, antioxidants, metal ions, alkaloids and antibiotics¹. However, most ILs are

poorly biodegradable and of low biocompatibility. In this context, ILs and salts based on the cholinium cation can be a valuable alternative; yet, poorly studied. These cholinium-based salts, or ionic liquids (ILs) when their melting point is below 100 °C, are constituted by the 2-hydroxyethyl-*N,N,N*-trimethylammonium cation combined with anions as diverse as chloride, bicarbonate, acetate, levulinate, malate, glycolate, among others. Hence, the cholinium-based salts/ILs are a feasible option to be used in the formation of ABS. The possibility of creating aqueous two-phase systems of the type polymer-salt or salt-salt either by the combination of PEG and cholinium-based salts or by the addition of an inorganic salt to mildly hydrophobic cholinium-based ILs was previously demonstrated^{2, 3}. Aiming at exploring the applicability of these novel ABS, this work is focused on the extraction of tetracycline directly from the fermentation broth of *S. aureofaciens*. Systems composed of polyethylene glycol 600 and cholinium-based salts were investigated by means of the partition coefficients and extraction efficiencies obtained for tetracycline. To further ascertain on the enhanced ability of these novel systems to extract tetracycline, further experiments were carried out with conventional polymer/salt and salt/salt ABS for comparison purposes.

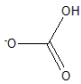
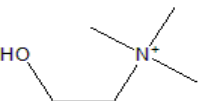
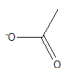
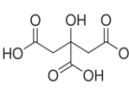
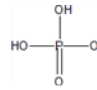
15.3. Materials and Methods

15.3.1. Materials

Polyethylene glycol (PEG) with an average molecular weight of 600 g.mol⁻¹ (abbreviated as PEG 600) and tetracycline (TC), ≥ 98 wt% pure, were supplied by Fluka. The cholinium-based salts were acquired at Sigma-Aldrich: cholinium chloride, [Ch]Cl, cholinium bicarbonate, [Ch]Bic, and cholinium dihydrogencitrate, [Ch]DHcit, with purities of ≥ 98 wt%, 80 wt% (in aqueous solution), and 99 wt%, respectively. The cholinium acetate, [Ch]Ac, and cholinium dihydrogenphosphate, [Ch]DHph, were purchased from Iolitec with purity levels of 98 wt%. These last two cholinium-based salts fall within the category of ILs since they present melting temperatures below 100°C. Nevertheless, to avoid any ambiguity, all these materials will be thereafter referred as cholinium-based salts. The chemical structures of the investigated cholinium-based salts are presented in Table 15.1. ¹H and ¹³C NMR spectra were performed to evaluate the purity of each sample. All samples are of high purity and agree with the purity levels indicated by the suppliers. The inorganic salts K₃PO₄ (≥ 98

wt%) and Na₂SO₄ (> 99.0 wt%) were acquired from Sigma-Aldrich and LabSolve, respectively. All the other reagents are of analytical grade and were used as received.

Table 15.1 Chemical structures of the studied cholinium-based salts.

Cholinium-based salts	Cation	Anion
[Ch]Bic		
[Ch]Cl		Cl ⁻
[Ch]Ac		
[Ch]DHcit		
[Ch]DHph		

15.3.2. Microorganism Maintenance and Fermentation Processes

S. aureofaciens was kindly provided by the Microorganism Collection of the Department of Antibiotics from Federal University of Pernambuco, Recife, PE, Brazil. The frozen microorganism was maintained at -70°C with glycerol in a cryotube. According to the procedure described by Darken et al.⁴, a thick spore suspension contained in the cryotube was transferred to 25 mL of reactivation medium in 250 mL-Erlenmeyer flasks. After an incubation period of 24 h in an orbital shaker at 30 °C and 200 rpm, 5 mL of this suspension were added to 45 mL of the fermentation medium and re-incubated under the same conditions of reactivation during 48 h (at this condition the pH value was 4.50 ± 0.04). For the fermentation processes, 5.0 mL of the resulting cell suspension were added to 45 mL of fermentation medium in 500 mL-Erlenmeyer flasks and incubated during 120 h at the same operational conditions. At the end of the fermentation process, the fermented broth was filtrated through a Whatman N. 4 paper and then centrifuged at 3720 g for 15 min at 5°C. The supernatant obtained from this process presented a final pH of 4.27 ± 0.09 and a TC concentration of 0.175 g.L⁻¹ (quantified as described below). The supernatant was frozen and stored in an ultrafreezer at -70°C and further used in all the partitioning studies.

15.3.3. Media Composition

A modified liquid ISP-2 medium⁵ with a constitution of 4.0 g.L⁻¹ of yeast extract and 10.0 g.L⁻¹ of malt extract was used for reactivation. The medium proposed by Darken et al.⁴ for the preparation of the *Streptomyces aureofaciens* inoculum was used and it is composed as follows (g.L⁻¹ in deionized water): sucrose (30.0), soybean meal (5.0), Na₃C₆H₅O₇·5H₂O (1.0), (NH₄)₂SO₄ (3.3), MgSO₄·7H₂O (0.25), KH₂PO₄ (0.10), K₂HPO₄ (0.10), CaCO₃ (1.0), MnSO₄·4H₂O (0.01), ZnSO₄·7H₂O (0.04), K₂Cr₂O₇ (0.000016) and CH₃COOH (0.40). The fermentation medium was prepared according to the description given by Darken et al.⁴ and it is composed of: H₃C₆H₅O₇·H₂O (12.8), sucrose (40.0), (NH₄)₂SO₄ (6.0), MgSO₄·7H₂O (0.25), KH₂PO₄ (0.15), CaCO₃ (11.0), MnSO₄·4H₂O (0.01), ZnSO₄·7H₂O (0.04) and K₂Cr₂O₇ (0.016.10-3). All media were autoclaved at 121°C for 15 min.

15.3.4. Methods

15.3.4.1. Phase Diagrams and Tie-lines

Phase diagrams for each ternary system composed of PEG 600 + cholinium-based salt + H₂O at 25°C were previously determined³ using the cloud point titration method. Other ABS used for comparison purposes were taken from literature^{2, 6}. The knowledge of these phase diagrams allows the choice of mixture points which correspond to a liquid-liquid two-phase system.

15.3.4.2. Optimization of the TC Partitioning in ABS Composed of PEG and Cholinium-based Salts

In order to optimize the experimental conditions and phase compositions to be applied in the extraction of TC from the fermented broth, several model systems were initially investigated making use of commercial TC of high purity. Three different mixture compositions at the biphasic region, and for each ABS, were selected. Small amounts of commercial TC, 0.25-0.45 mg, were added to glass tubes containing the appropriate weights of PEG, [Ch]-salt and water to form a system with a total mass of 5 g. After the equilibration time, 12 h at 25 (±1)°C, the phases were carefully separated and the quantification of TC in both phases was carried out. The quantification of tetracycline is

described below. All the assays were performed in triplicate and the respective standard deviations were determined.

The partition coefficient of TC, K_{TC} , is the ratio between the antibiotic concentration in the PEG-rich phase ($[TC]_{PEG}$) to that in the cholinium-rich phase ($[TC]_{Ch}$) and as described by Equation 15.1:

$$K_{TC} = \frac{[TC]_{PEG}}{[TC]_{Ch}} \quad \text{Equation 15.1}$$

15.3.4.3. Partitioning of TC in Conventional PEG/Na₂SO₄ and [Ch]Cl/K₃PO₄ ABS

For comparison purposes and to ascertain on the potential of PEG-cholinium-based ABS as improved extraction routes, the K_{TC} data were also determined in two mixture points (biphasic systems) of the PEG 600 + Na₂SO₄+ water system and for three mixture compositions of the [Ch]Cl + K₃PO₄+ water ABS. The partitioning studies were carried out in triplicate and at 25 (±1)°C, and in accordance to the procedure previously described.

The partition coefficient of TC for the PEG-rich phase (K_{TC_PEG}) in the PEG/Na₂SO₄ system and for the cholinium-rich phase (K_{TC_Ch}) in the [Ch]Cl/K₃PO₄ system were determined according to Equations 15.2 and 15.3, respectively:

$$K_{TC_PEG} = \frac{[TC]_{PEG}}{[TC]_{salt}} \quad \text{Equation 15.2}$$

$$K_{TC_Ch} = \frac{[TC]_{Ch}}{[TC]_{salt}} \quad \text{Equation 15.3}$$

where $[TC]_{PEG}$, $[TC]_{salt}$ and $[TC]_{Ch}$ correspond, respectively, to the TC concentration in the PEG-rich, in the inorganic-salt-rich and in the cholinium-rich phase.

15.3.4.4. Recovery of TC from the Fermented Broth

The novel PEG/[Ch]Bic and PEG/[Ch]Cl ABS and the conventional PEG/Na₂SO₄ and [Ch]Cl/K₃PO₄ aqueous systems were also used in the investigation of the recovery/extraction of TC from the fermentation broth of *S. aureofaciens*. The corresponding systems were prepared by choosing the mixture composition for which

the highest partition coefficient was obtained in the optimization step with the model systems previously addressed. The partitioning studies were performed adding directly the liquid supernatant of the fermented broth to known amounts of polymer and cholinium-based salt. The partitioning behavior of TC was quantified in terms of the respective partitioning coefficients in the several ABS, namely K_{TC} (for the PEG 600/[Ch]-based salts ABS), K_{TC_PEG} (for the PEG/Na₂SO₄ ABS) and K_{TC_Ch} (for the [Ch]Cl/K₃PO₄ ABS), as described above.

The percentage extraction efficiency of TC (% EE_{TC}) for a given phase, *e.g.* the phase with higher TC concentration, was also evaluated through Equation 15.4:

$$\%EE_{TC} = \frac{m_{TC\text{-rich phase}}}{m_0} \times 100$$

Equation 15.4

where $m_{TC\text{-rich phase}}$ is the mass of TC in the phase with higher TC concentration and m_0 is the total mass of tetracycline in each system.

15.3.4.5. Quantification of Tetracycline

The TC concentration in each ABS phase was determined using an UV-Vis spectrophotometer (SHIMADZU UV-1700, Pharma-Spect Spectrometer). The UV-Vis spectrum of TC was firstly obtained and calibration curves were properly established at a neutral and alkaline pH since diverse salts can induce different pH values (*cf.* Supporting Information Data, Figures S15.1 to S.15.4). TC shows two distinct wavelengths where maxima in absorbance are observed: (i) at neutral pH the biomolecule has no charge and these maxima occur at 276 nm and 357 nm; (ii) at an alkaline pH, the molecule is negatively charged, and these maxima occur at 269 nm and 381 nm. In the partitioning studies using the fermented broth of *S. aureofaciens* it was not possible to quantify the TC at 276 nm and 269 nm since the proteins present in the broth also contribute to the absorption observed at these wavelengths⁷. Therefore, the TC was measured using the calibration curves established at 357 and 381 nm, for the neutral and alkaline systems, respectively. The validation of the TC quantification using the calibration curves determined at 357 and 381 nm was additionally confirmed taking into account the difference between the total protein concentration ([TP]) present in the fermented broth, which was determined using the bicinchoninic acid method (BCA)⁸, and the protein concentration ([P_{BSA}]) obtained by a calibration curve making use of

Bovine Serum Albumin (BSA) at 280 nm. The difference between the total absorbance and the BSA absorbance at 280 nm gives the TC absorbance. The TC concentration of the fermented broth measured by the second set of calibration curves is similar (within $\pm 5\%$) to that obtained by the measurement of the absorbance in the first maximum wavelength peaks for the UV region (*cf.* Supporting Information, Table S15.1) and validate the experimental procedure adopted.

15.3.4.6. pH and Conductivity Measurements

After the separation of the coexisting phases of each system, the pH values (± 0.02) and conductivity ($\pm 0.01 \text{ mS}\cdot\text{cm}^{-1}$) were measured at $25 (\pm 1)^\circ\text{C}$ using a SevenMulti™ equipment (Mettler Toledo Instruments). The conductivity measurements were used to identify the polymer and the salt-rich phases since they are colorless in most of the cases.

15.4. Results and Discussion

15.4.1. Optimization of the TC Partitioning in ABS Composed of PEG and Cholinium-based Salts

In order to optimize the TC partitioning, different cholinium-based salts were used in combination with PEG 600 to form an ABS. In this study, the cholinium-based salts investigated were [Ch]Cl, [Ch]Bic, [CH]DHcit, [Ch]Ac and [Ch]DHph. The initial mixture compositions were selected so that the liquid-liquid systems could be formed taking into account previous literature data with their phase diagrams³. The initial mixture compositions, the partition coefficients of tetracycline and the pH values of the phases are presented in Table 15.2. Based on the initial mixture compositions and the respective ternary phase diagrams³, the composition of each phase was further determined, and the corresponding tie-lines are presented in Supporting Information, Table S15.2. The tie-line length (TLL) corresponds to the length of each tie-line and indicates the difference in composition of the two phases. The values of the TLLs are presented in Table 15.2.

Table 15.2 Weight fraction composition of the initial mixture, TLL, pH value of each phase and partition coefficient of TC at 25°C.

Ternary System	Weight Fraction		TLL (wt%)	pH _{PEG-rich phase}	pH _{IL-rich phase}	K_{TC}
	Composition (wt%)					
	PEG 600	Salt				
[Ch]Cl	54.94	34.93	115.65	7.12	7.09	0.98±0.03
	54.93	29.98	95.93	7.05	6.72	0.92±0.03
	54.91	24.95	57.58	7.03	6.81	1.02±0.04
[Ch]Bic	49.88	34.93	117.85	11.22	10.65	10.07±1.01
	49.81	29.96	102.38	10.93	10.55	6.72±0.62
	49.87	24.99	73.18	10.83	10.51	5.68±0.96
[Ch]DHcit	45.00	39.92	81.48	5.29	5.25	1.45±0.17
	45.85	37.80	67.52	5.27	5.03	1.30±0.06
	56.89	29.94	95.57	5.39	5.44	1.14±0.05
[Ch]Ac	49.75	39.82	123.64	10.12	10.06	2.69±0.27
	49.55	34.77	109.67	9.44	9.35	2.73±0.40
	49.59	29.81	95.84	8.93	8.90	2.57±0.21
[Ch]DHph	49.90	29.95	111.00	7.65	7.37	2.69±0.43
	40.20	29.91	96.19	6.16	5.97	2.62±0.15
	34.98	29.97	86.35	6.56	5.75	2.60±0.19

It should be remarked that for the systems based on [Ch]Bic, [Ch]DHcit and [Ch]DHph, the bottom phase is the salt-rich phase whereas the top phase corresponds to the PEG-rich phase. However, some inversions on the phases' densities were observed depending on the composition and constituents of the system. Particularly, an inversion on the top and bottom phases was observed with the systems composed of [Ch]Cl and [Ch]Ac. Since both phases are liquid and non-colored, the coexisting phases were identified by conductivity measurements at 25°C (the conductivity values are provided in Supporting Information, Table S15.3).

This first optimization step aimed at understanding the dependence of K_{TC} with the cholinium-based salt and respective TLLs. The values of K_{TC} shown in Table 15.2 suggest that, in most cases, the antibiotic preferentially migrates for the PEG-rich phase. Only one exception was observed with the system composed of [Ch]Cl. In this system the K_{TC} value is always close to unity indicating that TC distributes equally by the two phases. Moreover, the pH values of the phases, which range between 5 and 11, seem to have no significant influence concerning the preferential migration of the antibiotic for

the polymer-rich phase. Albeit tetracycline has preference for more hydrophilic phases, as displayed by its octanol-water partition coefficient ($\log K_{ow} = -1.19$)^{9, 10}, in this study, tetracycline migrates preferentially for the most hydrophobic and polymeric phase. Therefore, this migration pattern could be a consequence of the salting-out effect of the cholinium-based salts over the antibiotic which forces its migration towards the PEG-rich phase.

To facilitate the comparison between the cholinium-salt effect and the composition of the system through the partitioning of TC, the logarithmic function of K_{TC} as a function of the TLL is depicted in Figure 15.1.

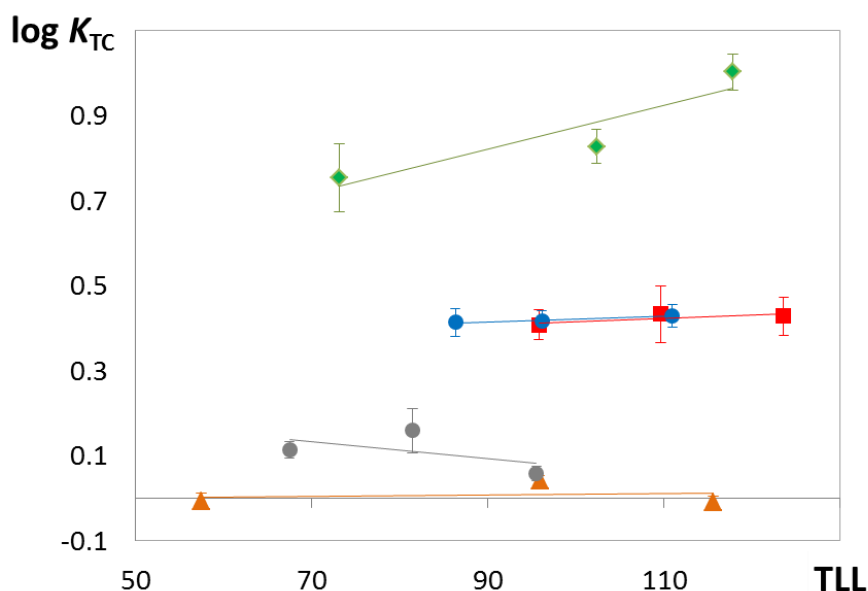


Figure 15.1 Logarithm of K_{TC} versus TLL, at 25°C, for the systems composed of PEG 600 + [Ch]-based salt + water: (◆) [Ch]Bic; (■) [Ch]Ac; (●) [Ch]DHph; (●) [Ch]DHcit; (▲) [Ch]Cl.

An increase in the amount of the [Ch]-based salt or an increase in the polymer content lead to an increase in the TLL, *i.e.* to a higher difference in the composition of the coexisting phases of a particular system. According to Figure 15.1, the most relevant effect of the TLL is observed with the system constituted by [Ch]Bic where an increase in the TLL leads to an increase in the K_{TC} value. In the remaining ABS the K_{TC} values are approximately constant, taking into account the associated standard deviations, and independent of the TLL (in the composition range evaluated).

At a similar TLL, when comparing the different cholinium-based salts, the TC tends to migrate for the PEG-rich phase according to the following tendency: [Ch]Cl < [Ch]DHcit < [Ch]DHph \approx [Ch]Ac < [Ch]Bic. Besides the preferential migration for the PEG-rich phase in most cases, there are differences between the diverse cholinium-based salts which depend on the pH values of the phases.

TCs are amphoteric compounds and show three dissociation constants or pKa values: 3.30, 7.68 and 9.69¹¹. Thus, in aqueous solutions of different pH, TCs can appear in one of the three forms: cationic when $\text{pH} < \text{p}K_{\text{a}1}$ (3.30), zwitterionic when $\text{p}K_{\text{a}1}$ (3.30) < $\text{pH} < \text{p}K_{\text{a}2}$ (7.68) and anionic when $\text{pH} > \text{p}K_{\text{a}2}$ (7.68). The anionic species can be monovalent or divalent when the pH is between the $\text{p}K_{\text{a}2}$ and the $\text{p}K_{\text{a}3}$ (9.68) or when the $\text{pH} > \text{p}K_{\text{a}3}$, respectively¹². The dissociation curves of TC as a function of the pH are shown in Supporting Information, Figure S15.5. Looking at the data in Table 15.2 it can be gauged that in the systems with [Ch]Cl, [Ch]DHcit and [Ch]DHph, TC is mainly in a neutral form ($3.30 < \text{pH} < 7.68$); in the ABS composed of [Ch]Ac and [Ch]Bic, with pH values above the $\text{p}K_{\text{a}2}$ of TC, the antibiotic is in a charged form (anionic); for the systems with 50 wt% of PEG 600 and 40 wt% of [Ch]Ac and all the PEG 600/[Ch]Bic ABS the pH values are above the $\text{p}K_{\text{a}3}$ (9.68) of TC and in these cases TC is present as a divalent anion.

In the PEG/[Ch]Cl ABS there was no preferential affinity of TC for a given phase. This behavior is in close agreement with the weak ability of the chloride anion to induce the salting-out of other species^{13, 14}. Indeed, in a previous work² where a series of cholinium-based salts was evaluated, it was observed that [Ch]Cl was the compound with the weakest ability to form two liquid phases. In addition, in the [Ch]Cl systems with pH values around 7, TC is mainly in its neutral form (with only a small fraction being negatively charged) and has no preference for the highly charged salt-rich phase. When [Ch]DHcit is used to promote the TC partitioning, the antibiotic shows a slight affinity for the polymeric phase. In the [Ch]DHcit system, with pH values between 5 and 6, TC is mainly in its neutral form although some small fraction of positively charged TC is also present. Even though the citrate anion is usually considered a good salting-out agent, according to the Hofmeister series^{13, 14}, the observed biomolecule partitioning for the PEG-rich is not significant possibly due to dissociation effects of the citrate anion. At a pH value around 6 the citrate anion is also dissociated in a divalent species as discussed before by Pereira et al³.

Following the study of different anions in the cholinium-based salts, similar K_{TC} for the PEG 600/[Ch]DHph and PEG 600/[Ch]Ac systems were identified. For the system with [Ch]DHph the antibiotic partitioning for the polymer-rich phase can be a direct consequence of the strong salting-out ability of the salt. On other hand, in the [Ch]Ac-based ABS, despite acetate anion having a lower ability to promote the salting-out of solutes when compared with the other salts, the alkaline pH of both phases seems to favorably induce the partitioning of TC for the PEG-rich phase. This trend is in accordance with the data obtained with the [Ch]Bic-based system where the highest partition coefficients were observed.

Since it was observed that the pH is a relevant feature in the TC partitioning, it was also studied the effect of the pH change within a system. As observed with the systems constituted by PEG 600 and [Ch]Ac or [Ch]Bic the presence of TC in its anionic form leads to higher K_{TC} values. Thus, the effect of increasing the pH value was further studied in the PEG 600/[Ch]Cl system. Here a change of the pH with addition of 0.5 wt% of NaOH from 7 to 12 was achieved. This change leads to an increase in the partition coefficient of tetracycline from 0.98 ± 0.03 to 3.69 ± 0.32 attesting the importance of the pH on the partition of TC on the studied systems.

In summary, the optimization tests using the commercial TC indicate that improved partition coefficients are obtained with ABS composed of [Ch]Bic. Therefore, this cholinium-based salt was chosen, along with the [Ch]Cl salt, to conduct the extractions from the fermented broth described below.

15.4.2. Partitioning of TC in Conventional PEG/Na₂SO₄ and [Ch]Cl/K₃PO₄ ABS

ABS composed of PEG 600, [Ch]-based-salts and water are very recent³. Most of the studies previously published have been dealing with conventional ABS. Hence, two polymer/salt and salt/salt ABS were also studied in the TC extraction in order to compare with the performance of the systems here studied. Two ABS composed of PEG 600 and Na₂SO₄, and K₃PO₄ and [Ch]Cl were also investigated. All assays were prepared in triplicate and the respective weight fraction compositions, K_{TC} , TLL, and the pH of the coexisting phases are presented in Table 15.3. For the PEG600/Na₂SO₄ aqueous system, K_{TC} is the ratio between the TC concentration in the polymer-rich

phase to that in the salt-rich phase whereas for the [Ch]Cl/K₃PO₄ ABS it is the TC concentration ratio between the [Ch]Cl- and K₃PO₄-rich phases.

Table 15.3 Weight fraction composition of the initial mixture, TLL, pH value of each phase and partition coefficient of TC at 25°C in the conventional systems.

Weight Fraction Composition (wt%)				TLL (wt%)	pH _{topphase}	pH _{bottomphase}	K _{TC}
K ₃ PO ₄	[Ch]Cl	PEG 600	Na ₂ SO ₄				
-	-	40.04	7.48	59.22	6.18	5.30	16.61±0.12
-	-	40.02	10.01	65.11	6.25	6.08	13.00±1.08
35.02	20.04	-	-	71.97	14.16	13.66	30.05±1.40
29.97	20.08	-	-	52.67	13.65	13.49	28.75±6.51
27.51	20.10	-	-	35.46	13.51	13.39	22.82±2.21

From the pH values displayed in Table 15.3, it can be anticipated that TC is in different forms in the two conventional ABS: in the PEG 600/Na₂SO₄ system, TC is mainly in its neutral form (5.30 < pH < 6.25) whereas in the [Ch]Cl/K₃PO₄ system it is completely deprotonated (pH of the phases > pK_{a3}). In the polymer/salt system TC is recovered in the top phase (PEG-rich phase) with K_{TC} values higher than 13. In the [Ch]Cl-K₃PO₄ system the antibiotic preferentially migrates for the [Ch]Cl-rich phase (with K_{TC} > 22). Both examples suggest that, independently of the pH, the salt used or the salting-out species employed has a major influence on the partitioning of tetracycline. In the PEG-salt systems it is clear that Na₂SO₄, being a stronger salting-out agent than the cholinium-based salts, enhances the partitioning of TC for the polymer-rich phase. On the other hand, when an inorganic salt is used in combination with [Ch]Cl, TC migrates for the [Ch]Cl-rich phase – a consequence of the strong K₃PO₄ salting-out aptitude^{13, 14}. In summary, the choice of the main constituents of the ABS has a crucial impact in the preferential partitioning of TC. Indeed, according to these results, TC can be recovered in the polymer- or in the cholinium-rich phase depending on the second species added to the medium. Considering that in the PEG/[Ch]Cl ABS at an alkaline pH the TC partitions for the polymeric phase and that in the [Ch]Cl/K₃PO₄ system TC migrates for the [Ch]Cl-rich phase, these two systems can be used sequentially to carry out the back extraction of the antibiotic. Some experiments regarding back extraction procedures were conducted and the results are presented in Supporting Information, Figure S15.6.

The behavior observed with the PEG/Na₂SO₄ system is in close agreement with literature data for other biomolecules such as L-tryptophan, which tends to partition for

the polymer-rich phase in the presence of inorganic salts⁶. Recently, Shahriari et al.² have also applied more hydrophobic cholinium-based salts and K_3PO_4 ABS to separate three antibiotics forms, and among them, TC. The results provided by the authors² showed that the salting-out effect exerted by the phosphate anion is a dominant effect in the partitioning phenomenon.

In summary, although the polymer/cholinium-based ABS here studied exhibit lower TC extraction capabilities as compared with PEG/ Na_2SO_4 and [Ch]Cl/ K_3PO_4 systems, it should be remarked that both the cholinium-based salts and PEG are biocompatible and biodegradable highlighting and supporting their applicability in a fermentation broth to recover an antibiotic for human consumption.

15.4.3. Recovery of TC from the Fermented Broth

Based on the previous results, the PEG 600/[Ch]Cl and PEG 600/[Ch]Bic ABS were selected for the studies on the extraction of TC from the fermented broth of *S. aureofaciens*. The conventional PEG/ Na_2SO_4 and [Ch]Cl/ K_3PO_4 systems were also considered for comparison purposes. All these systems were studied as a pre-purification step capable of concentrating the antibiotic in one aqueous-rich phase while the contaminants would be retained in the other phase. The corresponding systems (at the same concentrations presented in Tables 15.2 and 15.3 with the model systems) were prepared in triplicate, and the values of K_{TC} and respective standard deviations, extraction efficiencies ($\%EE_{TC}$), and pH values of the coexisting phases are presented in Table 15.4.

Table 15.4 pH value of each phase, $\%EE_{TC}$ and partition coefficient of TC from the fermented broth at 25°C.

System	K_{TC}	$\%EE_{TC}$	pH _{topphase}	pH _{bottomphase}
PEG600/[Ch]Cl	0.21 ± 0.03	81.63 ± 5.26	5.03	4.43
PEG600/[Ch]Bic	3.98 ± 0.41	82.54 ± 11.03	9.31	9.48
[PEG600]/ Na_2SO_4	17.78 ± 1.25	54.67 ± 6.55	4.86	4.66
[Ch]Cl/ K_3PO_4	45.95 ± 1.66	92.42 ± 2.84	13.92	13.71

The results obtained are compared in Figure 15.2 where the logarithmic function of K_{TC} and the $\%EE_{TC}$ are presented.

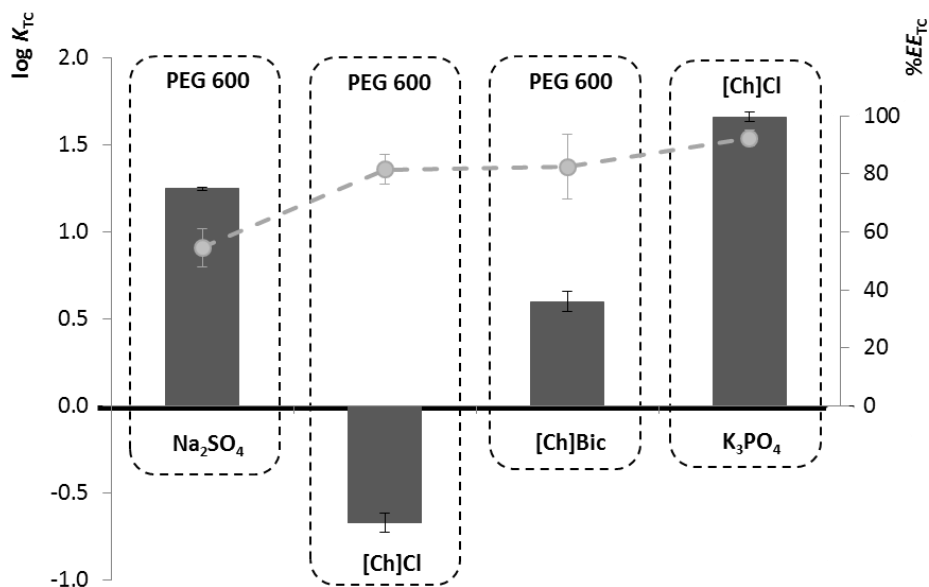


Figure 15.2 Logarithm of K_{TC} (■) and % EE_{TC} (-●-) obtained in several ABS formed with the fermented broth.

The comparison of the K_{TC} values obtained from the fermented broth (Figure 15.2 and Table 15.4) and with the model systems (Table 15.3) shows that the ABS formed by PEG and cholinium-based salts can be applied in real extraction routes. As expected some deviations were observed when compared with the results obtained from the model systems. For the [Ch]Bic-based ABS it was observed a decrease in the K_{TC} values when applying the system directly to the fermented broth (from 10.07 with the commercial TC to 3.98 in the real system). This behavior can be explained by the complexity of the fermented broth that either interferes with the partitioning of TC or changes the pH of the medium. In the real system with [Ch]Bic it was observed a decrease in the pH (from 11.22 to 9.48) which, as previously discussed, changes the TC speciation. On other hand, an interesting result was observed with the PEG/[Ch]Cl system, where the TC was majorly concentrated in cholinium-rich phase ($\log K_{TC} < 0$) – an inverse trend to that observed with the model systems. This inversion of the TC partitioning can be a result of both the system acidification or due to the presence of residuals salts from the fermented medium.

With the conventional systems, namely with the PEG 600 + Na_2SO_4 ABS, it was also observed a lower extraction efficiency. In fact, the extraction efficiency is even lower than that observed for the PEG-cholinium-based ABS. However, with the

[Ch]Cl/K₃PO₄ system almost all TC migrates for the cholinium rich-phase with extraction efficiencies higher than 92 %. With this system it is verified an intensification of the partitioning behavior as observed in other works using IL/salt ABS with complex matrices¹⁵.

Although the [Ch]Cl/K₃PO₄ ABS presents the highest ability to extract TC it should be remarked that other advantages are inherent to ABS composed of cholinium-based salts and PEG. First of all, the ABS composed of PEG and cholinium-based salts are biocompatible and biodegradable and avoid the use of inorganic salts of high ionic strength. Moreover, depending on the salt employed, the extraction of TC can be tailored either for the PEG- or salt-rich phases and with single step extraction efficiencies higher than 80 %. The combination of several PEG-cholinium-based systems can be used as back-extraction approaches for the recovery of TC. The extraction of TC to the polymer-rich phase can be envisaged as an economically viable pre-purification step to remove most part of the fermented broth contaminants, such as proteins, cell-debris and other amphiphilic impurities. This polymeric phase can be further applied in chromatography using fluidized beds processes. Albeit a search on literature data was carried out for comparison purposes, no results concerning the extraction of TC obtained from the *Streptomyces aureofaciens* fermented broth were found. Thus, this work represents a novel contribution regarding the definition of alternative strategies to perform the pre-concentration and pre-purification of TC directly from the fermentation broth.

15.5. Conclusions

The extraction of tetracycline using cheaper and biocompatible ABS as alternative liquid-liquid extraction platforms was evaluated. Both model systems using commercial tetracycline and systems employing the fermentation broth of *S. aureofaciens* were investigated. In general, the cholinium-based salt nature and the pH of the medium largely contribute to the differences observed with the TC partitioning. For the systems composed of PEG 600, cholinium-based salts and the fermented broth, extraction efficiencies of the antibiotic higher than 80% were achieved. Moreover, depending on the cholinium-based salt, the recovery either occurs at the polymer- or at the salt-rich phase. These novel results support a tailoring ability of the cholinium-based ABS which can be further combined and applied as back extraction routes.

15.6. References

1. Freire, M.G., Cláudio, A.F.M., Araújo, J.M.M., Coutinho, J.A.P., Marrucho, I.M., Canongia Lopes, J.N., and Rebelo, L.P.N., Aqueous Biphasic Systems: A boost brought about by using ionic liquids. *Chemical Society Reviews*, 2012.
2. Shahriari, S., Tomé, L.C., Araújo, J.M.M., Rebelo, L.P.N., Coutinho, J.A.P., Marrucho, I.M., and Freire, M.G., Aqueous biphasic systems: A benign route using cholinium-based ionic liquids. *RSC Advances*, 2013. **3**(6): p. 1835-1843.
3. Pereira, J.F.B., Mourão, T., Cojocar, O.A., Gurau, G., Rebelo, L.P.N., Rogers, R.D., Coutinho, J.A.P., and Freire, M.G., Novel biocompatible aqueous biphasic systems composed of polymers and cholinium-based ionic liquids. *Chemical Science*. 2013. (*submitted for publication*).
4. Darken, M.A., Berenson, H., Shirk, R.J., and Sjolander, N.O., Production of tetracycline by *Streptomyces aureofaciens* in synthetic media. *Applied microbiology*, 1960. **8**: p. 46-51.
5. Pridham, T.G., Anderson, P., Folioy, C., Lindenfelser, H.A., Hesseltine, C.W., and Benedict, R.G., A selection of media for maintenance and taxonomic study of *Streptomyces*. *Antibiotics annual*, 1956: p. 947-953.
6. Pereira, J.F.B., Lima, A.S., Freire, M.G., and Coutinho, J.A.P., Ionic liquids as adjuvants for the tailored extraction of biomolecules in aqueous biphasic systems. *Green Chemistry*, 2010. **12**(9): p. 1661-1669.
7. Mester, P., Wagner, M., and Rossmann, P., Biased spectroscopic protein quantification in the presence of ionic liquids. *Analytical Bioanalytical Chemistry*, 2010. **397**(5): p. 1763-6.
8. Pereira, J.F.B., Santos, V.C., Johansson, H.-O., Teixeira, J.A.C., and Pessoa Jr, A., A stable liquid-liquid extraction system for clavulanic acid using polymer-based aqueous two-phase systems. *Separation and Purification Technology*, 2012. **98**: p. 441-450.
9. Caço, A.I., Varanda, F., de Melo, M.J.P., Dias, A.M.A., Dohrn, R., and Marrucho, I.M., Solubility of Antibiotics in Different Solvents. Part II. Non-Hydrochloride Forms of Tetracycline and Ciprofloxacin. *Industrial & Engineering Chemistry Research*, 2008. **47**(21): p. 8083-8089.
10. Varanda, F., de Melo, M.J.P., Caço, A.I., Dohrn, R., Makrydaki, F.A., Voutsas, E., Tassios, D., and Marrucho, I.M., Solubility of antibiotics in different solvents. 1. Hydrochloride forms of tetracycline, moxifloxacin, and ciprofloxacin. *Industrial & Engineering Chemistry Research*, 2006. **45**(18): p. 6368-6374.
11. Qiang, Z. and Adams, C., Potentiometric determination of acid dissociation constants (pKa) for human and veterinary antibiotics. *Water Research*, 2004. **38**(12): p. 2874-2890.
12. Zhao, Y., Gu, X., Gao, S., Geng, J., and Wang, X., Adsorption of tetracycline (TC) onto montmorillonite: Cations and humic acid effects. *Geoderma*, 2012. **183-184**: p. 12-18.
13. Shahriari, S., Neves, C.M.S.S., Freire, M.G., and Coutinho, J.A.P., Role of the Hofmeister Series in the Formation of Ionic-Liquid-Based Aqueous Biphasic Systems. *The Journal of Physical Chemistry B*, 2012. **116**(24): p. 7252-7258.
14. Zhang, Y. and Cremer, P.S., Interactions between macromolecules and ions: the Hofmeister series. *Current Opinion in Chemical Biology*, 2006. **10**(6): p. 658-663.
15. Passos, H., Sousa, A.C.A., Pastorinho, M.R., Nogueira, A.J.A., Rebelo, L.P.N., Coutinho, J.A.P., and Freire, M.G., Ionic-liquid-based aqueous biphasic systems for improved detection of bisphenol A in human fluids. *Analytical Methods*, 2012. **4**(9): p. 2664-2667.

16.CONCLUSIONS AND FUTURE WORK

16.1. Conclusions

In the second part of this thesis novel liquid-liquid extraction systems were developed and characterized aiming at extracting antibiotics from a fermentation broth. Due to the novelty of the IL-PEG-based ABS investigated their phase diagrams and driving mechanisms behind the liquid-liquid demixing were initially addressed. As a first approach it was studied the influence of several ILs on the phase formation of conventional PEG/inorganic ABS. It was observed that the ILs can be used as adjuvants allowing the tailoring of the extraction of model biomolecules, namely L-tryptophan. After this initial study and foreseeing the use of novel ABS on the biotechnological field, the inorganic salt commonly employed were replaced by different ILs in order to form the novel PEG-IL-based ABS. The extensive study performed with several combinations of PEGs and ILs allowed to conclude that the two-phases formation can be tuned by the adequate selection of the ILs cations or anions. In addition, it was also demonstrated that the formation of ABS combining polymers and ILs is not dominated by the ability of the isolated species to be solvated by water; instead, the PEG-IL interactions play a crucial role. Despite these initial assumptions based on experimental data, a more extensive study was carried out with the determination of the complete ternary phase diagram of the system composed of PEG 1500 + [C₄mim]Cl + H₂O at 323.15 K and 333.15 K, and where molecular dynamics (MD) simulations were also employed. It was observed that the miscibility of [C₄mim]Cl/PEG systems results essentially from the H-bonding established between the Cl⁻ and the -OH groups of PEG. The addition of water to the binary PEG-IL system removes the IL from the vicinity of the PEG weakening thus their interactions which further leads to the liquid-liquid demixing – “washing-out” phenomenon.

The main goal of the second part of this thesis concerns the use of the novel ABS for the extraction of biomolecules, in particular antibiotics from aqueous solutions. Then, before the direct use of these systems in more complex media, it was initially proved that these new ABS can enlarge the hydrophobic-hydrophilic range provided by conventional polymer/salt and polymer/polymer ABS. To elucidate this trend it was investigated the liquid-liquid partitioning behavior of three dyes used as molecular probes of different hydrophobicities. The results showed that the IL-PEG-based ABS exhibit a much wider hydrophilic-hydrophobic range than conventional systems reported to date. In fact, the phases' polarities can be properly tuned by an appropriate

choice of the IL chemical structure creating thus a new set of effective ABS to be applied in the biotechnological field. After the evaluation the enhancement of polarities range obtained with these new polymer/IL ABS, it was then tested the ability of the polymer-IL-based ABS for the extraction of three alkaloids of different polarity. It was demonstrated that these systems allow the selective separation of similar compounds by an adequate manipulation of the IL chemical structure and temperature of equilibrium.

Most the ILs previously studied as phase forming components of PEG-IL-based ABS, although of low toxicity, present, however, lower biocompatibility and biodegradability. Thus, having in mind the extraction of antibiotics directly from a fermented broth, the two last chapters of this thesis were focused on the study of a new class of ABS composed of polymers and cholinium-based ILs. It was observed that several cholinium-based ILs are able to promote the phase separation with PEG in aqueous media, being this phenomenon mainly controlled by the PEG-IL specific interactions. Hereafter, it was firstly investigated the extraction of high purity and commercial tetracycline using these PEG-cholinium-based ABS in order to optimize the partitioning conditions. The enhanced PEG-cholinium-based systems identified were then used to recover tetracycline directly from the fermented broth of *Streptomyces aureofaciens*. The results obtained showed that more than 80% of tetracycline can be recovered in a single step procedure. Moreover, the extractions can be tailored either for the PEG- or cholinium-rich phase. Summing up, the results obtained in this work support the applicability and effectiveness of biocompatible ABS in the extraction of antibiotics from complex matrices. In this context, these novel ABS can be envisaged as alternative processes which can be applied in pharmaceutical or biotechnological industries.

16.2. Future Work

The bioprocess described in the part B of this thesis addresses the applicability of PEG-IL-based ABS as a sustainable and alternative extraction technique to the extraction of antibiotics from complex matrices, namely from fermented broths. The studied ABS showed interesting properties to be applied not only to pharmaceutical compounds but also to a wider range of compounds. In addition, they also revealed a high potential to be applied in CCC techniques due to their tailoring ability. Besides all the studies carried out here, some additional investigations should be considered in order to further explore and take advantage of the systems here proposed:

- Extraction of other antibiotics produced from microorganisms, such as clavulanic acid or durhamycin;
- Application of the PEG-IL-based ABS in CCC techniques;
- Optimization of the back-extraction methods for the recovery of the antibiotics from the aqueous phases;
- Studies on the possible recycling of the phase forming components of ABS;
- Combination of ILs and polymers that revealed to be completely miscible to improve the solubility of pharmaceutical compounds in aqueous media.

17. LIST OF PUBLICATIONS

1. Santos, Valéria C.; **Pereira, Jorge F. B.**; Haga, Raquel B.; Rangel-Yagui, Carlota O.; Teixeira, José A.; Converti, A.; Pessoa Jr, Adalberto; “Stability of clavulanic acid under variable pH, ionic strength and temperature conditions. A new kinetic approach”, *Biochemical Engineering Journal*, 2009, 45, 89-93.
2. **Pereira, Jorge F. B.**; Lima, Álvaro S.; Freire, Mara G.; Coutinho, João A. P., “Ionic liquids as adjuvants for the tailored extraction of biomolecules in aqueous biphasic systems”, *Green Chemistry*, 2010, 12, 1661-1669.
3. Freire, Mara G.; **Pereira, Jorge F. B.**; Francisco, Maria; Rodríguez, Hector; Rebelo, Luis Paulo N.; Rogers, Robin D.; Coutinho, João A. P., “Insight into the interactions that control the phase behaviour of new aqueous biphasic systems composed of polyethylene glycol polymers and ionic liquids”, *Chemistry – A European Journal*, 2012, 18, 1831-1839.
4. Gudiña, Eduardo J.; **Pereira, Jorge F. B.**; Rodrigues, Lígia R.; Coutinho, João A. P.; Teixeira, José A., “Isolation and study of microorganisms from oil samples for application in microbial enhanced oil recovery”; *International Biodeterioration & Biodegradation*, 2012, 68, 56-64.
5. Gudiña, Eduardo J.; Rodrigues, Lígia R.; Teixeira, José A.; **Pereira, Jorge F. B.**; Coutinho, João A. P.; Soares, Laura P., “Biosurfactant producing microorganisms and its application to enhance oil recovery at lab scale”; *SPE 154598*, 2012, DOI: 10.2118/154598-MS.
6. **Pereira, Jorge F. B.**; Santos, Valéria C.; Johansson, Hans-Olof; Teixeira, José A.; Pessoa Jr, Adalberto, “A stable liquid-liquid extraction system for clavulanic acid using polymer-based aqueous two-phase systems”, *Separation and Purification Technology*, 2012, 98, 441-450.
7. **Pereira, Jorge F. B.**; Gudiña, Eduardo J.; Dória, M. Luísa; Domingues, M. Rosário; Rodrigues, Lígia R.; Teixeira, José A.; Coutinho, João A.P., “Characterization by electrospray ionization and tandem mass spectrometry of rhamnolipids produced by two *Pseudomonas aeruginosa* strains isolated from Brazilian crude oil”, *European journal of mass spectrometry*, 2012, 18, 399-406.
8. Reis, Igor A. O.; Santos, Samuel B.; Santos, Ludmila A.; Oliveira, Naiana; Freire, Mara G.; **Pereira, Jorge F. B.**, Ventura, Sónia P. M.; Coutinho, João A. P.; Soares, Cleide M. F.; Lima, Álvaro S., “Increased value of food wastes: selective recovery of added-value compounds”, *Food Chemistry*, 2012, 135, 2453-2461.
9. Gudiña, Eduardo J.; Rodrigues, Lígia R.; Teixeira, José A.; **Pereira, Jorge F. B.**; Coutinho, João A. P.; Soares, Laura P.; Ribeiro, Maria T., “Microbial enhanced oil recovery by *Bacillus subtilis* strains under simulated reservoir conditions”; *SPE 161458*, 2012, DOI: 10.2118/161458-MS.
10. Ventura, Sónia S. P.; Santos-Ebinuma, Valéria C.; **Pereira, Jorge F. B.**; Teixeira, Maria F. S.; Pessoa, Adalberto; Coutinho, João A. P., “Isolation of natural red colorants from fermented broth using ionic liquid-based aqueous two-phase systems”, *Journal of Industrial Microbiology and Biotechnology*, 2013, 40, 507-516.
11. **Pereira, Jorge F. B.**; Vicente, Filipa; Santos-Ebinuma, Valéria C.; Araújo, Janete M.; Teixeira, Maria F. S.; Pessoa, Adalberto; Coutinho, João A. P., “Extraction of tetracycline from fermentation broth using aqueous two-phase systems composed of polyethylene glycol and cholinium-based salts”, *Process Biochemistry*, 2013, 48(4), 716-722.

12. **Pereira, Jorge F. B.**; Ventura, Sónia P. M.; Shahriari, Shahla; Freire, Mara G.; Coutinho, João A. P., “Aqueous biphasic systems composed of ionic liquids and polymers: A platform for the purification of biomolecules”, *Separation Purification Technology*, 2013, *113*, 83-89.
13. **Pereira, Jorge F. B.**; Gudiña, Eduardo J.; Costa, Rita; Vitorino, Rui; Teixeira, José A.; Coutinho, João A.P.; Rodrigues, Lígia R., “Optimization and characterization of biosurfactant production by *Bacillus subtilis* isolates towards Microbial Enhanced Oil Recovery applications”, *Fuel*, 2013 doi 10.1016/j.fuel.2013.04.040.
14. Gudiña, Eduardo J.; **Pereira, Jorge F. B.**; Costa, Rita; Coutinho, João A. P.; Teixeira, José A.; Rodrigues, Lígia R., “Biosurfactant-producing and oil-degrading *Bacillus subtilis* strains enhance oil recovery at lab scale”; *Journal of Hazardous Materials*, 2013 (*submitted for publication*).
15. Tomé, Luciana I.N.; **Pereira, Jorge F. B.**; Gomes, José R. B.; Freire, Mara G.; Coutinho, João A. P., ““Washing-out” in polyethylene glycol + ionic liquid mixtures to form aqueous biphasic systems”, *Journal of Physical Chemistry Letters*, 2013 (*submitted for publication*).
16. **Pereira, Jorge F. B.**; Rebelo, Luis P. N.; Rogers, Robin D.; Coutinho, João A. P.; Freire, Mara G.; “Combining ionic liquids and polyethylene glycols to boost the hydrophobic-hydrophilic range of aqueous biphasic systems”, *Chemical Communications*, 2013 (*submitted for publication*).
17. **Pereira, Jorge F. B.**; Kurnia, Kiki A.; Cojocar, O. A.; Gurau, Gabriela; Rebelo, Luis P. N.; Rogers, Robin D.; Freire, Mara G.; Coutinho, João A. P., “Biocompatible aqueous biphasic systems composed of polyethylene glycols and cholinium-based ionic liquids: towards the understanding of their formation ability”, *Chemical Science*, 2013 (*submitted for publication*).
18. Gudiña, Eduardo J.; **Pereira, Jorge F. B.**; Costa, Rita; Evtuguin, Dmitry V.; Coutinho, João A. P.; Teixeira, José A.; Rodrigues, Lígia R., “Characterization of a novel bioemulsifier produced by a *Paenibacillus* strain isolated from crude oil samples”; *Bioresource Technology*, 2013 (*submitted for publication*).

18. SUPPORTING INFORMATION

S3. PAPER 2

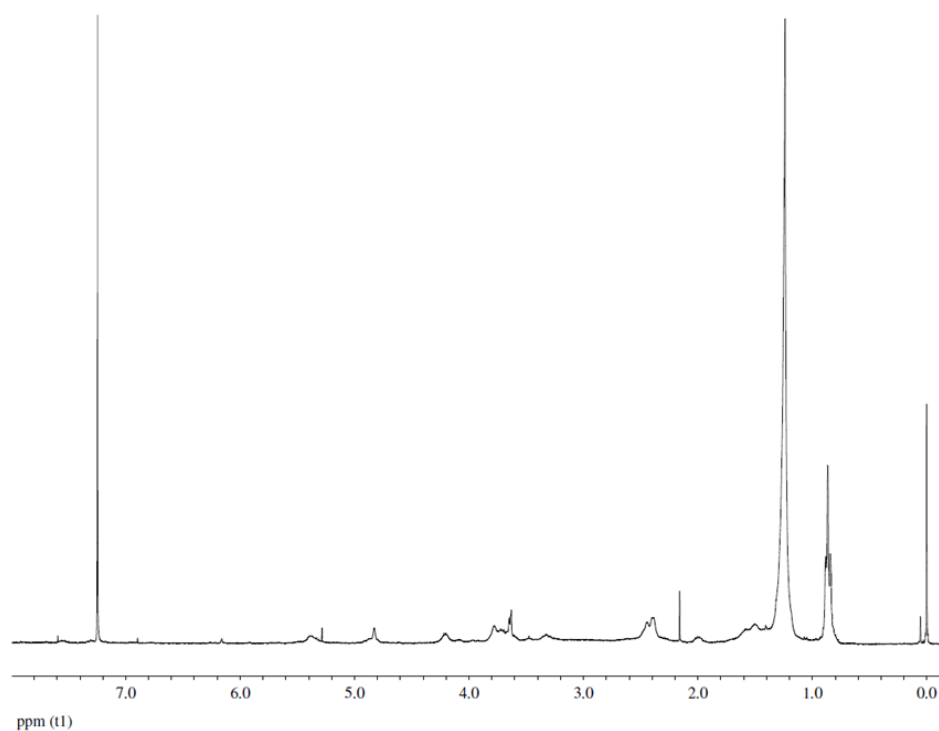


Figure S3.1 ¹H NMR spectrum of the crude biosurfactants obtained from isolate #111.

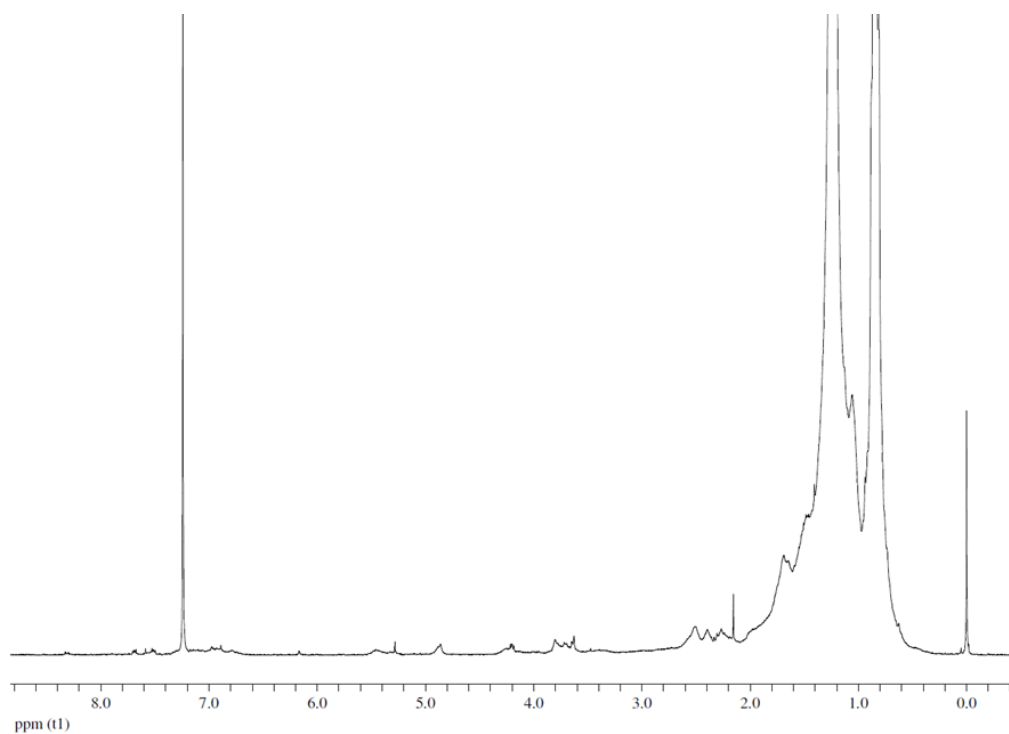


Figure S3.2 ¹H NMR spectrum of the crude biosurfactants obtained from isolate #902.

S9. PAPER 6

Table S9.1 Experimental binodal curve mass fraction data for the system composed of PEG 600 (1) + Na₂SO₄ (2) + H₂O (3) + 5 wt % IL at 298 K

no IL		no IL		[im]Cl	
100 w_1	100 w_2	100 w_1	100 w_2	100 w_1	100 w_2
40.592	2.227	16.459	9.285	45.542	1.681
36.768	2.838	16.336	9.328	42.361	2.399
35.611	3.017	16.224	9.387	40.899	2.708
34.726	3.227	16.050	9.515	39.463	3.088
33.555	3.476	15.922	9.566	37.698	3.451
32.351	3.833	15.812	9.603	36.027	3.758
31.411	4.064	15.639	9.729	34.230	4.059
30.488	4.277	15.418	9.835	32.471	4.533
29.468	4.574	15.229	9.916	31.211	4.959
28.949	4.624	15.053	10.017	29.544	5.563
28.366	4.814	14.960	10.044	28.227	5.823
27.673	5.033	14.817	10.136	27.268	6.162
27.184	5.168	14.663	10.247	26.284	6.457
26.720	5.318	14.544	10.272	25.182	6.820
26.190	5.490	14.396	10.367	23.251	7.549
25.655	5.666	14.007	10.710	22.156	7.997
25.098	5.879	13.829	10.660	21.140	8.363
24.566	6.076	13.703	10.762	19.798	8.944
24.037	6.299	16.551	9.239	19.115	9.191
23.537	6.491	16.459	9.285	17.649	9.872
23.073	6.660	16.336	9.328	16.590	10.350
22.572	6.861	16.224	9.387	15.194	11.008
22.147	7.020	16.050	9.515	13.767	11.678
21.663	7.116	15.922	9.566	12.228	12.408
21.297	7.219	15.812	9.603	11.107	12.958
20.878	7.401	15.639	9.729	10.520	13.259
20.490	7.538	15.418	9.835	9.880	13.595
20.191	7.677	15.229	9.916	9.079	14.007
19.847	7.799	15.053	10.017	8.310	14.461
19.500	7.938	14.960	10.044	7.692	14.812
19.335	8.011	14.817	10.136		
19.083	8.167	14.663	10.247		
18.745	8.307	14.544	10.272		
18.577	8.379	14.396	10.367		
18.308	8.466	14.007	10.710		
18.180	8.522	13.829	10.660		
17.954	8.703	13.703	10.762		
17.764	8.692				
17.543	8.771				
17.329	8.912				
17.089	9.011				
16.978	9.047				
16.670	9.203				
16.551	9.239				

Table S9.2 Experimental binodal curve mass fraction data for the system composed of PEG 600 (1) + Na₂SO₄ (2) + H₂O (3) + 5 wt % IL at 298 K

[C_{1im}]Cl		[C_{2mim}]Cl	
100 w₁	100 w₂	100 w₁	100 w₂
46.741	1.239	47.655	0.841
44.375	1.727	45.434	1.355
41.770	2.263	43.329	1.843
39.577	2.635	40.476	2.544
38.416	2.924	38.071	3.112
36.566	3.320	35.304	3.451
34.897	3.613	33.379	3.705
33.952	3.843	32.073	4.122
32.918	4.135	31.085	4.361
32.254	4.254	29.565	4.732
31.290	4.490	28.138	5.244
30.231	4.770	27.340	5.429
29.459	4.957	26.125	5.839
28.571	5.215	24.436	6.529
27.613	5.502	23.310	6.971
26.554	5.945	22.062	7.484
25.895	6.128	20.583	8.117
24.765	6.576	19.419	8.640
24.104	6.789	18.272	9.157
23.152	7.162	17.628	9.448
22.396	7.435	16.620	9.926
21.774	7.667	15.427	10.508
20.865	8.049	14.355	11.031
19.378	8.638	12.767	11.862
18.518	9.023	12.184	12.149
17.686	9.395	11.114	12.709
16.757	9.832	10.128	13.246
15.972	10.198	8.477	14.188
15.364	10.488		
14.760	10.759		
14.154	11.052		
13.699	11.263		
13.074	11.569		
12.685	11.752		
12.136	12.023		
11.472	12.355		
10.984	12.592		
10.461	12.857		
9.998	13.096		
9.691	13.255		
9.360	13.422		
8.927	13.660		
8.577	13.850		
8.199	14.060		
7.880	14.181		

Table S9.3 Experimental binodal curve mass fraction data for the system composed of PEG 600 (1) + Na₂SO₄ (2) + H₂O (3) + 5 wt % IL at 298 K

[C₄mim]Cl		[C₄mim]Cl		[C₄C₁mim]Cl	
100 w₁	100 w₂	100 w₁	100 w₂	100 w₁	100 w₂
46.807	1.238	13.820	10.076	38.707	1.892
44.357	1.586	13.027	10.516	37.776	2.016
41.813	1.867	12.631	10.730	36.797	2.346
39.905	2.232	12.218	10.974	35.480	2.631
37.828	2.476	11.851	11.178	33.993	2.817
36.338	2.655	11.482	11.390	32.722	3.073
34.825	2.811	11.123	11.602	31.450	3.426
33.473	3.152	10.782	11.801	30.396	3.727
32.638	3.354	10.470	11.950	29.324	3.939
31.958	3.543	10.059	12.198	28.269	4.242
31.043	3.714	9.749	12.377	27.441	4.406
30.669	3.833	9.303	12.646	26.440	4.742
30.287	3.891	8.905	12.898	24.934	5.364
29.851	3.957	8.647	13.056	24.003	5.687
29.174	4.181	8.361	13.234	23.064	6.154
28.624	4.328	7.972	13.495	22.707	6.336
27.886	4.559			22.108	6.544
27.160	4.689			21.146	7.025
26.340	5.009			19.570	7.755
25.874	5.135			18.958	8.073
25.387	5.292			17.991	8.584
24.957	5.407			17.113	9.068
24.323	5.578			15.728	9.866
23.821	5.780				
23.361	5.952				
22.824	6.107				
22.462	6.209				
21.956	6.394				
21.398	6.621				
20.582	6.912				
20.092	7.127				
19.526	7.387				
19.145	7.487				
18.659	7.702				
18.196	7.910				
17.751	8.114				
17.421	8.269				
17.086	8.425				
16.738	8.578				
16.276	8.808				
15.829	9.027				
15.311	9.304				
14.993	9.460				
14.497	9.719				

Table S9.4 Experimental binodal curve mass fraction data for the system composed of PEG 600 (1) + Na₂SO₄ (2) + H₂O (3) + 5 wt % IL at 298 K

[OHC ₂ mim]Cl		[C ₇ H ₇ mim]Cl		[C ₇ H ₇ mim]Cl	
100 w ₁	100 w ₂	100 w ₁	100 w ₂	100 w ₁	100 w ₂
38.646	4.469	48.358	0.574	16.432	8.668
35.800	5.157	46.218	0.969	15.867	8.948
33.389	5.724	44.842	1.189	15.698	9.040
31.752	5.846	43.129	1.464	15.579	9.094
30.488	6.044	41.489	1.763	15.206	9.286
29.237	6.395	39.669	1.964	14.807	9.493
27.932	6.751	38.332	2.216	14.333	9.750
26.922	6.910	37.241	2.303	13.924	9.966
25.997	7.073	36.290	2.504	13.718	10.069
25.281	7.287	35.441	2.639	13.396	10.245
24.607	7.426	34.570	2.717	12.965	10.489
23.908	7.600	33.932	2.839	12.552	10.728
22.989	7.890	32.865	3.026	12.249	10.902
22.399	8.080	32.307	3.139	12.053	11.018
21.461	8.408	31.581	3.358	11.738	11.203
20.607	8.764	31.081	3.513	11.445	11.376
20.025	8.936	30.257	3.692	10.976	11.670
19.135	9.269	29.617	3.882	10.644	11.868
17.930	9.738	29.011	4.067	10.240	12.125
17.356	9.943	28.286	4.208	9.894	12.345
16.417	10.348	27.692	4.378	9.596	12.526
15.467	10.740	27.306	4.474	9.239	12.759
14.727	11.048	26.799	4.642	8.881	12.990
13.418	11.621	26.288	4.773	8.520	13.227
13.030	11.788	25.755	4.943	8.115	13.500
12.416	12.066	25.112	5.129	7.869	13.668
11.910	12.286	24.638	5.326		
11.357	12.549	24.069	5.535		
10.972	12.714	23.809	5.653		
10.322	13.017	23.269	5.844		
9.845	13.247	22.444	6.135		
9.559	13.383	21.949	6.329		
9.078	13.635	21.607	6.441		
8.268	14.065	21.102	6.636		
7.924	14.242	20.746	6.772		
		20.301	6.951		
		19.945	7.084		
		19.441	7.308		
		19.206	7.397		
		18.781	7.573		
		18.401	7.731		
		17.828	8.018		
		17.456	8.185		
		16.937	8.420		

Table S9.5 Experimental binodal curve mass fraction data for the system composed of PEG 600 (1) + Na₂SO₄ (2) + H₂O (3) + 5 wt % IL at 298 K

[amim]Cl		[C₄mim][MeSO₄]		[C₄mim][MeSO₄]	
100 w₁	100 w₂	100 w₁	100 w₂	100 w₁	100 w₂
36.511	3.014	46.968	1.015	10.158	11.939
35.338	3.284	44.026	1.417	9.741	12.202
33.822	3.480	41.366	1.837	9.473	12.353
33.079	3.653	39.412	2.019	9.143	12.546
31.691	3.990	37.911	2.232	8.844	12.703
30.799	4.157	36.438	2.521	8.589	12.849
29.758	4.511	35.165	2.624	8.328	13.002
28.862	4.686	34.479	2.752	8.119	13.127
27.895	4.988	33.513	3.007	7.899	13.259
26.795	5.357	32.619	3.240	7.640	13.418
25.226	5.906	31.773	3.325	7.431	13.540
24.548	6.136	31.091	3.503	7.237	13.660
23.853	6.369	30.287	3.764		
23.063	6.703	29.474	4.025		
22.448	6.903	28.795	4.245		
21.485	7.296	28.165	4.441		
20.232	7.900	26.995	4.551		
19.527	8.223	25.988	4.943		
18.566	8.648	25.202	5.174		
17.379	9.206	24.466	5.444		
16.189	9.819	23.929	5.602		
14.413	10.741	23.524	5.750		
13.481	11.250	23.078	5.879		
12.493	11.807	22.407	6.143		
11.816	12.186	21.760	6.391		
10.935	12.716	21.336	6.508		
9.593	13.512	20.702	6.774		
		19.960	7.116		
		19.313	7.392		
		18.387	7.765		
		17.876	7.977		
		17.320	8.220		
		16.760	8.486		
		16.192	8.773		
		15.424	9.135		
		14.414	9.661		
		13.920	9.908		
		12.780	10.511		
		12.366	10.740		
		12.000	10.918		
		11.586	11.141		
		11.196	11.357		
		10.873	11.529		
		10.445	11.775		

Table S9.6 Experimental binodal curve mass fraction data for the system composed of PEG 600 (1) + Na₂SO₄ (2) + H₂O (3) + 5 wt % IL at 298 K

[C₄mim][CH₃CO₂]		[C₄mim][HSO₄]		[C₄mim][HSO₄]	
100 w₁	100 w₂	100 w₁	100 w₂	100 w₁	100 w₂
39.931	2.213	35.720	3.572	10.108	12.869
38.445	2.289	35.149	3.712	9.415	13.303
37.298	2.517	34.384	3.846	8.964	13.577
36.048	2.663	33.657	3.911	8.382	13.958
35.011	2.819	32.871	4.018	7.762	14.369
34.414	2.925	32.089	4.134		
32.663	3.420	31.325	4.337		
31.947	3.615	30.538	4.519		
31.223	3.838	29.754	4.676		
30.822	3.922	29.070	4.862		
30.440	3.982	28.474	4.958		
29.896	4.131	27.884	5.127		
29.384	4.258	27.390	5.302		
28.609	4.548	26.718	5.405		
28.036	4.701	26.208	5.584		
27.566	4.835	25.802	5.732		
27.087	4.976	25.106	5.928		
26.492	5.166	24.724	6.046		
25.845	5.392	24.371	6.153		
25.413	5.502	23.917	6.333		
24.810	5.754	23.382	6.546		
24.250	5.945	23.053	6.647		
23.742	6.118	22.272	6.928		
23.123	6.352	21.524	7.193		
22.534	6.585	21.232	7.293		
21.994	6.800	20.783	7.480		
21.371	7.055	20.429	7.627		
20.923	7.236	20.088	7.764		
20.364	7.481	19.664	7.944		
19.744	7.725	18.786	8.256		
19.218	7.966	18.127	8.561		
18.567	8.272	17.451	8.889		
18.041	8.527	17.067	9.060		
18.335	8.217	16.520	9.335		
15.938	8.746	15.968	9.617		
15.279	9.130	15.431	9.894		
14.530	9.587	14.966	10.143		
13.743	10.076	14.438	10.430		
12.932	10.584	13.759	10.809		
11.692	11.396	13.076	11.190		
10.426	12.254	12.398	11.566		
9.431	12.936	11.738	11.944		
		11.196	12.253		
		10.426	12.696		

S10. PAPER 7

Table S10.1 Molality correlation parameters used in Equation 10.1 to describe the experimental binodal data and molecular weight of each ionic liquid

M_w	Ionic liquid	A	B	C
PEG 1000 at 298 K				
174.67	[C ₄ mim]Cl	3.8858 ± 0.2691	-1.0033 ± 0.0665	0.0050 ± 0.0021
PEG 2000 at 298 K				
104.54	[im]Cl	1.2494 ± 0.0465	-0.5406 ± 0.0257	-0.0002 ± 0.0001
118.58	[C ₁ im]Cl	1.1347 ± 0.0741	-0.7141 ± 0.0598	0.0036 ± 0.0010
132.59	[C ₁ mim]Cl	1.1796 ± 0.0756	-0.8714 ± 0.0544	0.0040 ± 0.0009
146.62	[C ₂ mim]Cl	1.3066 ± 0.0417	-1.0167 ± 0.0352	0.0042 ± 0.0008
174.67	[C ₄ mim]Cl	1.3734 ± 0.1311	-1.0056 ± 0.0887	0.0035 ± 0.0023
202.72	[C ₆ mim]Cl	1.6001 ± 0.1357	-1.0832 ± 0.0832	0.0007 ± 0.0022
230.78	[C ₈ mim]Cl	1.7136 ± 0.1762	-1.1639 ± 0.1094	-0.0064 ± 0.0041
158.63	[amim]Cl	1.1796 ± 0.0756	-0.9531 ± 0.0595	0.0068 ± 0.0016
162.62	[OHC ₂ mim]Cl	1.7950 ± 0.3770	-1.3452 ± 0.1941	-0.0004 ± 0.0049
185.69	[C ₄ mpy]Cl	1.7531 ± 0.2283	-1.2163 ± 0.1215	0.0013 ± 0.0036
177.72	[C ₄ mpyr]Cl	1.4532 ± 0.1601	-1.1300 ± 0.1064	0.0087 ± 0.0033
191.74	[C ₄ mpip]Cl	1.6999 ± 0.1354	-1.3030 ± 0.0725	0.0010 ± 0.0021
294.88	[P ₄₄₄₄]Cl	1.7820 ± 0.1842	-1.4557 ± 0.1173	-0.0077 ± 0.0069
219.13	[C ₄ mim]Br	1.3975 ± 0.1110	-0.9492 ± 0.0751	0.0028 ± 0.0022
198.27	[C ₄ mim][CH ₃ CO ₂]	1.5861 ± 0.2372	-1.3001 ± 0.1494	0.0017 ± 0.0058
288.29	[C ₄ mim][CF ₃ SO ₃]	1.9465 ± 0.3893	-1.0087 ± 0.1927	-0.0049 ± 0.0091
234.32	[C ₄ mim][CH ₃ SO ₃]	1.3277 ± 0.1852	-1.1068 ± 0.1476	0.0116 ± 0.0094
170.21	[C ₂ mim][CH ₃ CO ₂]	2.8940 ± 0.7139	-2.0847 ± 0.2498	-0.0122 ± 0.0113
206.26	[C ₂ mim][CH ₃ SO ₃]	1.6692 ± 0.3981	-1.4481 ± 0.2432	-0.0003 ± 0.0100
208.26	[C ₂ mim][HSO ₄]	1.4643 ± 0.1536	-1.2088 ± 0.1021	-0.0013 ± 0.0033
236.21	[C ₂ mim][(CH ₃) ₂ PO ₄]	2.0909 ± 0.6677	-1.8760 ± 0.3629	-0.0100 ± 0.0302
PEG 2000 at 308 K				
146.62	[C ₂ mim]Cl	1.9190 ± 0.1912	-1.0167 ± 0.0793	0.0017 ± 0.0008
198.27	[C ₄ mim][CH ₃ CO ₂]	3.3038 ± 0.3930	-1.9009 ± 0.1079	0.0015 ± 0.0026
PEG 2000 at 323 K				
146.62	[C ₂ mim]Cl	4.5566 ± 0.8738	-1.6579 ± 0.1499	-0.0007 ± 0.0012
198.27	[C ₄ mim][CH ₃ CO ₂]	2.4927 ± 0.3980	-1.3441 ± 0.1419	0.0138 ± 0.0033
PEG 3400 at 298 K				
174.67	[C ₄ mim]Cl	0.9176 ± 0.2184	-1.1694 ± 0.2214	0.0068 ± 0.0060
PEG 4000 at 298 K				
174.67	[C ₄ mim]Cl	0.6511 ± 0.0265	-1.1884 ± 0.0385	0.0032 ± 0.0011

Table S10.2 Experimental binodal curve mass fraction (w_i) data for the system composed of PEG (1) + IL (2) + H₂O (3) at 298 K

PEG 2000 + [im]Cl		PEG 2000 + [mim]Cl		PEG 2000 + [C ₁ mim]Cl		PEG 2000 + [C ₂ mim]Cl	
100 w_1	100 w_2	100 w_1	100 w_2	100 w_1	100 w_2	100 w_1	100 w_2
53.21	14.82	54.32	8.699	31.91	28.40	46.46	15.82
45.96	24.33	47.68	16.13	38.11	22.80	37.03	22.48
36.88	42.06	40.80	23.18	22.42	36.37	27.96	30.14
43.41	31.05	30.97	30.78	47.26	13.62	20.70	36.85
43.14	30.84	25.00	36.31	40.15	21.09	13.61	42.28
59.30	7.84			28.63	30.65	6.806	49.53
40.66	33.63			46.41	14.94	55.41	8.339
						3.716	52.64
						3.448	52.97
						20.61	36.77
						25.64	31.49
						60.24	3.617
						48.46	12.68
						41.98	18.50
						32.63	26.37
						15.44	40.64
						9.747	45.36
						7.771	48.78

Table S10.3: Experimental binodal curve mass fraction (w_i) data for the system composed of PEG (1) + IL (2) + H₂O (3) at 298 K

PEG 2000 + [C ₄ mim]Cl		PEG 2000 + [C ₆ mim]Cl		PEG 2000 + [C ₈ mim]Cl		PEG 2000 + [amim]Cl	
100 w_1	100 w_2	100 w_1	100 w_2	100 w_1	100 w_2	100 w_1	100 w_2
34.63	30.62	36.69	32.18	43.60	26.34	31.91	28.40
40.24	23.86	43.68	25.59	25.45	43.45	38.11	22.80
24.57	39.27	27.27	44.20	48.95	22.17	22.42	36.37
45.45	19.99	47.92	22.25	56.33	13.62	47.26	13.62
50.10	15.21	54.80	13.59	31.31	36.90	40.15	21.09
32.79	32.43	32.22	37.46	53.96	16.55	28.63	30.65

49.06	15.39	53.21	15.81	46.41	14.94
32.16	33.25				

Table S10.4: Experimental binodal curve mass fraction (w_i) data for the system composed of PEG (1) + IL (2) + H₂O (3) at 298 K

PEG 2000 + [OHC ₂ mim]Cl		PEG 2000 + [C ₄ mpy]Cl		PEG 2000 + [C ₄ mpyr]Cl		PEG 2000 + [C ₄ mpip]Cl	
100 w_1	100 w_2	100 w_1	100 w_2	100 w_1	100 w_2	100 w_1	100 w_2
30.68	29.96	35.06	31.10	32.29	28.86	32.34	29.82
36.38	23.63	39.94	24.84	39.15	23.13	39.57	23.70
21.45	37.74	24.64	40.49	22.14	36.68	22.79	39.78
49.08	14.22	47.01	20.77	49.35	14.11	40.73	22.33
40.61	19.74	51.52	14.64	41.83	21.16	31.23	30.71
29.31	28.80	32.11	32.02	28.39	32.12	47.76	15.97
45.25	15.29	51.29	15.69	48.82	15.00	44.79	19.30
		43.10	21.73	43.91	17.80	35.81	26.51
		38.84	26.52	22.10	36.03		
		32.01	32.79				

Table S10.5 Experimental binodal curve mass fraction (w_i) data for the system composed of PEG (1) + IL (2) + H₂O (3) at 298 K

PEG 2000 + [P ₄₄₄₄]Cl		PEG 2000 + [C ₄ mim]Br		PEG 2000 + [C ₄ mim][CH ₃ CO ₂]		PEG 2000 + [C ₄ mim][CF ₃ SO ₃]	
100 w_1	100 w_2	100 w_1	100 w_2	100 w_1	100 w_2	100 w_1	100 w_2
43.09	25.84	36.47	36.03	32.05	29.13	54.33	28.00
27.79	44.00	45.309	27.45	38.92	23.66	50.06	36.31
40.43	27.06	27.66	45.03	23.76	38.31	47.19	39.37
53.09	15.52	45.46	24.66	49.15	14.72	54.90	28.58
37.62	31.18	54.40	14.99	41.25	21.06	58.22	23.44
51.03	16.89	35.63	35.97	30.30	30.09	54.40	28.85
49.99	19.32	52.65	17.26	46.91	15.06	51.63	32.88
		47.18	23.46	44.72	18.48		
		40.21	32.41				
		37.30	37.03				

Table S10.6 Experimental binodal curve mass fraction (w_i) data for the system composed of PEG (1) + IL (2) + H₂O (3) at 298 K

PEG 2000 + [C ₄ mim][CH ₃ SO ₃]		PEG 2000 + [C ₂ mim][CH ₃ CO ₂]		PEG 2000 + [C ₂ mim][CH ₃ SO ₃]		PEG 2000 + [C ₂ mim][HSO ₄]	
100 w_1	100 w_2	100 w_1	100 w_2	100 w_1	100 w_2	100 w_1	100 w_2
49.49	15.89	32.24	19.72	37.27	22.70	29.29	34.59
43.46	21.91	19.15	31.42	22.40	37.82	35.97	27.86
33.39	32.89	44.96	13.35	46.52	14.43	24.26	40.70
39.98	25.48	36.30	18.22	38.56	21.39	47.98	16.00
37.96	28.47	25.32	25.61	28.03	30.30	42.20	22.31
34.16	30.88	40.10	15.15	45.76	16.80	29.99	33.15
30.55	34.02					45.68	17.71

Table S10.7 Experimental binodal curve mass fraction (w_i) data for the system composed of PEG (1) + IL (2) + H₂O (3) at 298 K

PEG 2000 + [C ₂ mim][(CH ₃) ₂ PO ₄]		PEG 1000 + [C ₄ mim]Cl		PEG 3400 + [C ₄ mim]Cl		PEG 4000 + [C ₄ mim]Cl	
100 w_1	100 w_2	100 w_1	100 w_2	100 w_1	100 w_2	100 w_1	100 w_2
27.67	27.00	60.51	13.14	49.13	14.53	45.06	14.23
35.48	22.33	55.88	17.54	43.08	21.53	40.83	17.56
18.67	33.89	50.68	22.20	35.69	24.94	33.55	24.45
43.78	15.91	46.51	27.29	29.26	30.61	31.30	26.90
37.72	18.55	42.84	30.35	26.48	33.79	26.65	31.37
26.47	28.48	39.06	33.32	24.32	36.05	20.13	37.41
45.84	14.89	33.40	36.86	21.41	37.24		

Table S10.8 Experimental binodal curve mass fraction (w_i) data for the system composed of PEG (1) + IL (2) + H₂O (3) at 308 K

PEG 2000 + [C ₂ mim]Cl		PEG 2000 + [C ₂ mim][CH ₃ CO ₂]	
100 w_1	100 w_2	100 w_1	100 w_2
46.27	17.31	36.54	22.08
12.73	45.84	43.30	17.76
43.46	20.18	26.98	27.92
28.98	31.36	45.99	16.55
23.50	35.87	19.93	32.55
18.10	40.87	13.32	39.37

Table S10.9 Experimental binodal curve mass fraction (w_i) data for the system composed of PEG (1) + IL (2) + H₂O (3) at 323 K

PEG 2000 + [C ₂ mim] Cl		PEG 2000 + [C ₂ mim][CH ₃ CO ₂]	
100 w_1	100 w_2	100 w_1	100 w_2
55.75	17.73	52.84	16.97
41.56	25.37	41.27	24.94
51.58	19.29	48.30	19.81
32.73	32.47	30.10	31.15
13.50	48.62	20.54	35.48
23.62	40.43	15.22	39.54
16.82	44.07		

S11. PAPER 8

S11.1 DFT calculations

The hybrid meta GGA density functional calculations were performed with the M06 approach¹ as implemented in the Gaussian 09 code². The atomic electronic densities were described by means of the aug-cc-pVDZ basis set^{3, 4}, which incorporates diffuse and polarization functions. Due to the large number of conformational degrees of freedom of TGA, the calculations involving this species followed the computational strategy below: Ten different initial configurations for TGA were taken from the classical MD simulations and then fully optimized at the DFT level using tight criteria (opt=tight and scf=tight keywords in the Gaussian code) but employing a basis set without diffuse functions. Some of the most favorable configurations, were further modified and were also fully optimized. The most favorable configurations retrieved from the previous steps were reoptimized with the larger aug-cc-pVDZ basis set. In the case of the different sized water clusters, the calculations were directly performed on the geometries available at The Cambridge Cluster Database⁵, while the calculations on the chloride-water clusters were based on the geometries reported by Xantheas⁶, by Gora et al.⁷ and by Neogi and Chaudhury⁸. The absence of imaginary vibrational frequencies (M06/aug-cc-pVDZ level of theory) was used to confirm that all the molecular systems studied were true minima on the potential energy surface

Table S11.1. Densities (ρ) for binary mixtures of water (1) + TEG (2) at $T=298.15$ K calculated from the MD simulations.

x_{water}	$\rho / \text{kg m}^3$
0.00	1124.17
0.09	1125.21
0.20	1124.63
0.50	1124.72
0.60	1123.98
0.70	1122.14
0.80	1115.41
0.90	1093.16
1.00	-

Table S11.2. Electronic energies and zero-point energy corrections for the different systems fully optimized at the M06/aug-cc-pVDZ level of theory. All values in atomic units (Hartrees).

System	Energy		Zero-point correction
	without counterpoise	with counterpoise	
Cl ⁻	-460.2647903	—	0.000000
H ₂ O	-76.4067548	—	0.021555
TEG	-691.4265552	—	0.271731
Cl ⁻ - H ₂ O	-536.7076847	-536.7071581	0.023610
Cl ⁻ - TEG	-1151.7273406	-1151.7264232	0.270080
H ₂ O - TEG	-767.8491001	-767.8478427	0.296317
Cl ⁻ - (H ₂ O) ₂	-613.1265463	—	0.048706
Cl ⁻ - (H ₂ O) ₃	-689.5609940	—	0.075965
Cl ⁻ - (H ₂ O) ₄	-765.9910484	—	0.101747
H ₂ O - H ₂ O	-152.8212515	-152.8209500	0.046301
H ₂ O - (H ₂ O) ₂	-229.2463020	—	0.073222
H ₂ O - (H ₂ O) ₃	-305.6710361	—	0.098463

Table S11.3. Interaction energies for some complexes fully optimized at the M06/aug-cc-pVDZ level of theory.^a

System	$\Delta E^e / \text{kJ mol}^{-1}$	$\Delta E^o / \text{kJ mol}^{-1}$
$\text{Cl}^- - \text{H}_2\text{O}$	-94.9; -93.5 ^b	-89.5; -88.2 ^b
$\text{Cl}^- - \text{TEG}$	-94.5; -92.1 ^b	-98.8; -96.6 ^b
$\text{H}_2\text{O} - \text{TEG}$	-41.6; -38.1 ^b	-33.5; -30.4 ^b
$\text{Cl}^- - (\text{H}_2\text{O})_2$	-126.7 ^c ; -106.3 ^d	-112.0 ^c ; -100.0 ^d
$\text{Cl}^- - (\text{H}_2\text{O})_3$	-199.4 ^c ; -131.0 ^d	-169.7 ^c ; -123.8 ^d
$\text{Cl}^- - (\text{H}_2\text{O})_4$	-260.6 ^c ; -144.9 ^d	-219.8 ^c ; -136.4 ^d
$\text{H}_2\text{O} - \text{H}_2\text{O}^e$	-20.3; -19.5 ^b	-11.9; -11.1 ^b
$\text{H}_2\text{O} - (\text{H}_2\text{O})_2$	-68.4 ^f ; -48.0 ^g	-45.9 ^f ; -33.9 ^g
$\text{H}_2\text{O} - (\text{H}_2\text{O})_3$	-115.6 ^f ; -47.2 ^g	-83.4 ^f ; -37.5 ^g

^a ΔE^e and ΔE^o are used to denote electronic energies without and with the zero-point energy corrections, respectively. ^b Geometry of the complex optimized with counterpoise corrections. ^c Energy variation corresponding to the reaction $\text{Cl}^- + n \text{H}_2\text{O} \rightarrow [\text{Cl}(\text{H}_2\text{O})_n]^-$. ^d Energy variation corresponding to the reaction $\text{Cl}^- + (\text{H}_2\text{O})_n \rightarrow [\text{Cl}(\text{H}_2\text{O})_n]^-$. ^e High-level computational results range from -12.5 to -13.2 $\text{kJ}\cdot\text{mol}^{-1}$,⁹ and benchmark experimental value is $-13.22 \pm 0.12 \text{ kJ}\cdot\text{mol}^{-1}$,¹⁰. ^f Energy variation corresponding to the reaction $\text{H}_2\text{O} + n \text{H}_2\text{O} \rightarrow [\text{H}_2\text{O}(\text{H}_2\text{O})_n]$. ^g Energy variation corresponding to the reaction $\text{H}_2\text{O} + (\text{H}_2\text{O})_n \rightarrow [\text{H}_2\text{O}(\text{H}_2\text{O})_n]$.

Table S11.4. Energies calculated for the reaction $[\text{ClTEG}]^- + (\text{H}_2\text{O})_n \rightarrow \text{TEG} + [\text{Cl}(\text{H}_2\text{O})_n]^-$ with $n = 1 - 4$.^a

n	$\Delta E^e / \text{kJ mol}^{-1}$	$\Delta E^o / \text{kJ mol}^{-1}$
1	-0.38	9.4
2	-11.84	-1.2
3	-36.51	-25.0
4	-50.48	-37.5

^a ΔE^e and ΔE^o are used to denote electronic energies without and with the zero-point energy corrections, respectively.

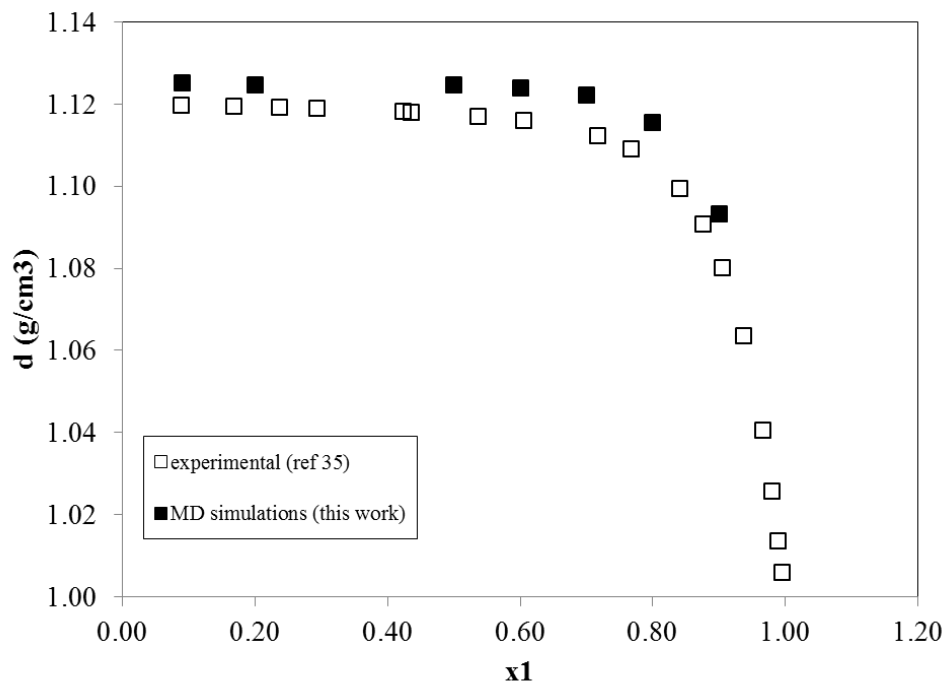
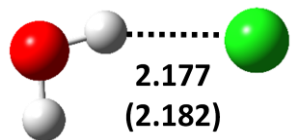
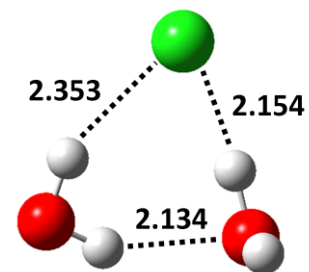


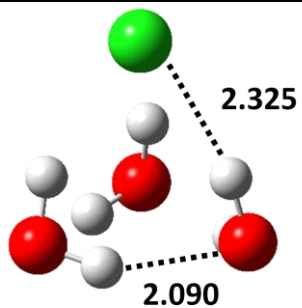
Figure S11.1. Experimental and calculated (this work) densities (ρ) for binary mixtures of water (1) + TEG (2) at $T=298.15$ K.



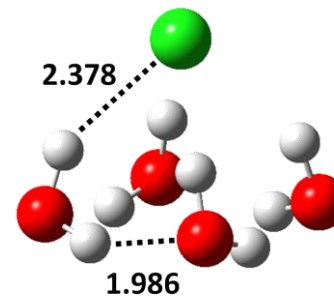
(a)



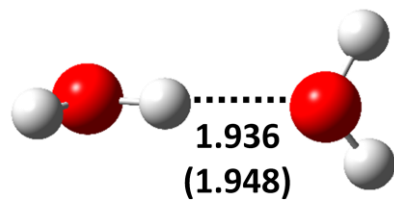
(b)



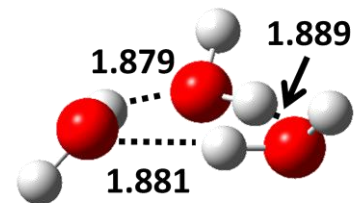
(c)



(d)

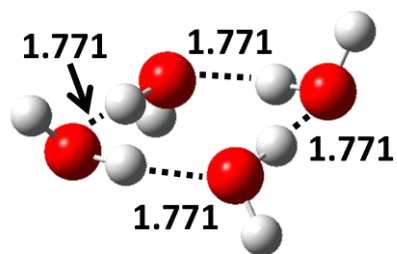


(e)

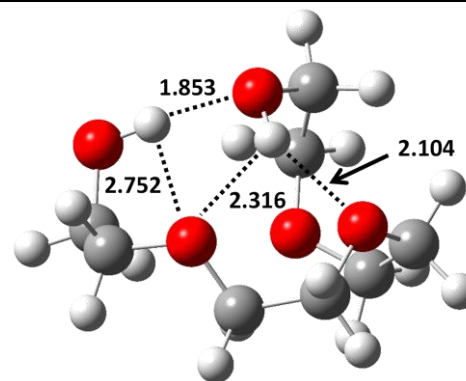


(f)

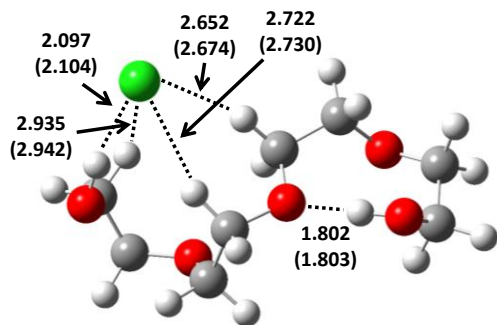
(continues on next page)



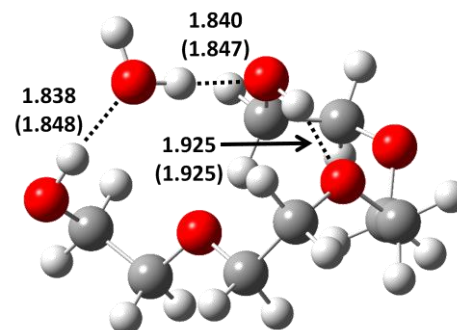
(g)



(h)



(i)



(j)

Figure S11.2. Views of the most stable configurations optimized at the M06/aug-cc-pVDZ level of theory for (a) Cl^- - H_2O , (b) Cl^- - $(\text{H}_2\text{O})_2$, (c) Cl^- - $(\text{H}_2\text{O})_3$, (d) Cl^- - $(\text{H}_2\text{O})_4$, (e) $(\text{H}_2\text{O})_2$, (f) $(\text{H}_2\text{O})_3$, (g) $(\text{H}_2\text{O})_4$, (h) TEG, (i) Cl^- -TEG and (j) H_2O -TEG. Numbers refer to distances in Å and parentheses are used for optimal distances obtained with counterpoise corrections. Color code for spheres is: Green, Cl; red, O; grey, C; white, H.

S12. PAPER 9

Table S12.1 Binodal weight fraction data for the systems composed of PEG 1500 (1) + IL (2) + H₂O (3) at 323 K

[C ₂ mim]Cl		[C ₄ mim]Cl		[C ₄ mpip]Cl		[C ₄ mpyrr]Cl	
100 w ₁	100 w ₂	100 w ₁	100 w ₂	100 w ₁	100 w ₂	100 w ₁	100 w ₂
9.1583	58.7473	14.9858	55.6914	10.60	56.20	5.23	67.60
13.4287	48.6955	15.3017	54.5986	14.96	50.76	13.96	48.78
21.9476	41.9476	24.7752	44.0133	15.30	48.46	25.28	39.77
23.4840	40.6187	36.6849	35.2397	22.49	41.13	35.44	34.93
29.5908	35.0914	39.5797	33.6221	27.62	35.76	47.89	24.07
34.4612	34.7182	49.4692	27.3325	43.56	26.53	62.66	18.64
36.7184	32.3570	52.7198	26.4656	51.19	21.29	62.66	18.64
42.5423	26.9599			51.42	21.50		
42.9489	26.6317			66.03	12.86		
44.9723	27.1613						
52.3509	21.1144						
58.9322	16.9953						

Table S12.2 Weight fraction compositions, partition coefficients (K) of neutral and charged Chloranilic Acid (CA), and pH of the respective top- and bottom-rich phases, for the ABS composed of PEG 1500 + IL, PEG 1500 + Na₂SO₄ and PEG 4000 + Dextran 40000 at 323 K and atmospheric pressure. The results represent the average of three independent experiments \pm associated standard deviation

Ternary System	PEG 1500 / (wt%)	IL/salt/dextran / (wt%)	K	pH_{Top-phase}	pH_{Bottom-phase}
Acidic pH – neutral CA					
Na ₂ SO ₄	16.40 \pm 0.05	22.97 \pm 0.20	0.01 \pm 0.00	3.85 \pm 0.54	3.24 \pm 0.74
Dextran	10.03 \pm 0.07	9.98 \pm 0.01	0.72 \pm 0.08	2.80 \pm 0.22	3.00 \pm 0.80
[C ₂ mim]Cl	39.29 \pm 1.41	51.91 \pm 0.12	0.43 \pm 0.10	3.80 \pm 0.01	3.70 \pm 0.21
[C ₄ mim]Cl	38.54 \pm 0.54	51.65 \pm 0.39	0.82 \pm 0.12	3.23 \pm 0.82	3.09 \pm 0.74
[C ₄ mpip]Cl	38.42 \pm 0.10	51.82 \pm 0.10	1.85 \pm 0.02	3.64 \pm 0.31	4.04 \pm 0.34
[C ₄ mpyrr]Cl	38.54 \pm 0.18	51.88 \pm 0.08	2.15 \pm 0.16	3.53 \pm 0.25	4.17 \pm 0.12
Neutral pH – charged CA					
[C ₂ mim]Cl	40.07 \pm 0.31	49.74 \pm 0.19	1.75 \pm 0.11	5.56 \pm 0.21	5.60 \pm 0.08
[C ₄ mim]Cl	38.50 \pm 0.31	51.80 \pm 0.48	2.58 \pm 0.26	6.21 \pm 0.59	6.25 \pm 0.47
[C ₄ mpip]Cl	38.78 \pm 0.73	51.43 \pm 0.90	3.47 \pm 0.75	5.92 \pm 0.03	5.95 \pm 0.18
[C ₄ mpyrr]Cl	37.26 \pm 1.60	52.98 \pm 1.51	6.19 \pm 1.36	5.70 \pm 0.07	5.66 \pm 0.06

Table S12.3 Weight fraction compositions, partition coefficients (K) of Indigo Blue and Indigo Carmine, and e pH of the respective Top- and Bottom-rich phases, for the ABS composed of PEG 1500 + IL and PEG 1500 + Na₂SO₄ at 323 K and atmospheric pressure. The results represent the average of three independent experiments \pm associated standard deviation

Ternary System	PEG 1500 / (wt%)	IL/Salt / (wt%)	K	pH_{Top-phase}	pH_{Bottom-phase}
Indigo Carmine					
Na ₂ SO ₄	15.94 \pm 0.16	22.45 \pm 0.23	0.02 \pm 0.03	7.02 \pm 0.21	6.51 \pm 0.04
[C ₄ mim]Cl	38.08 \pm 0.50	52.18 \pm 0.83	6.03 \pm 4.20	5.50 \pm 0.06	5.53 \pm 0.11
[C ₄ mpip]Cl	37.83 \pm 0.86	53.34 \pm 0.68	53.74 \pm 15.41	5.90 \pm 0.10	5.82 \pm 0.13
[C ₄ mpyrr]Cl	38.27 \pm 0.14	52.01 \pm 0.28	9.87 \pm 0.98	7.56 \pm 0.24	7.13 \pm 0.58
Indigo Blue					
Na ₂ SO ₄	15.89 \pm 0.10	22.60 \pm 0.21	0.03 \pm 0.01	7.42 \pm 0.10	6.96 \pm 0.02
[C ₄ mim]Cl	37.63 \pm 0.13	52.89 \pm 0.44	0.21 \pm 0.09	6.72 \pm 0.39	6.75 \pm 0.45
[C ₄ mpip]Cl	37.74 \pm 0.22	52.79 \pm 0.15	3.76 \pm 0.98	6.44 \pm 0.76	6.46 \pm 0.90
[C ₄ mpyrr]Cl	38.04 \pm 0.35	52.18 \pm 0.60	0.73 \pm 0.19	7.68 \pm 0.18	7.65 \pm 0.19

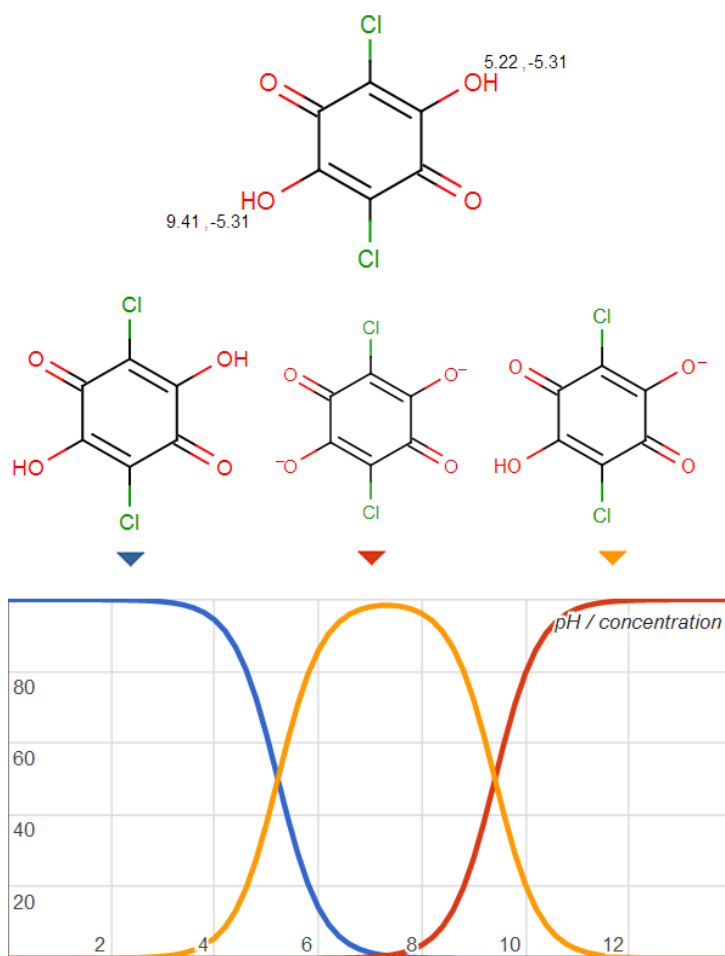


Figure S12.1 Speciation curve of Chloranilic Acid as a function of pH. This content was adapted from the Chemspider chemical database ¹¹.

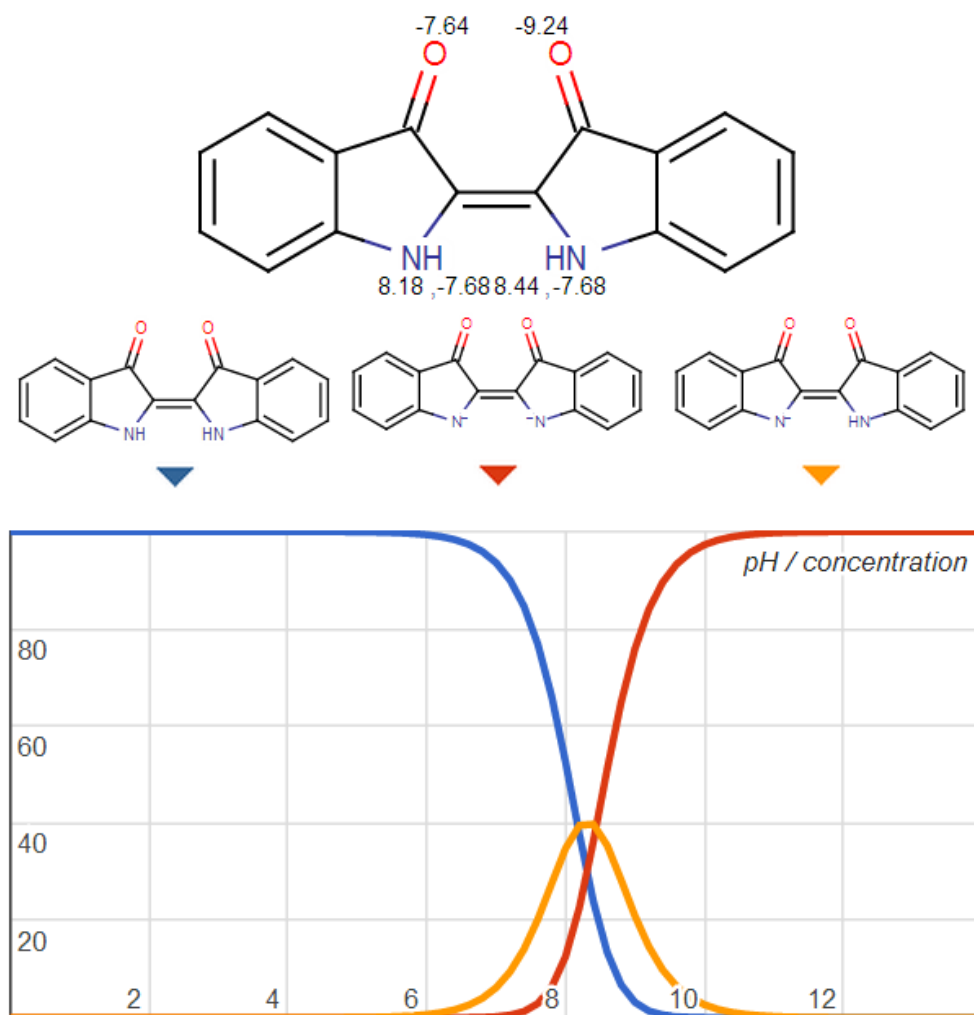


Figure S12.2 Speciation curve of Indigo Blue as a function of pH. This content was adapted from the Chemspider chemical database¹¹.

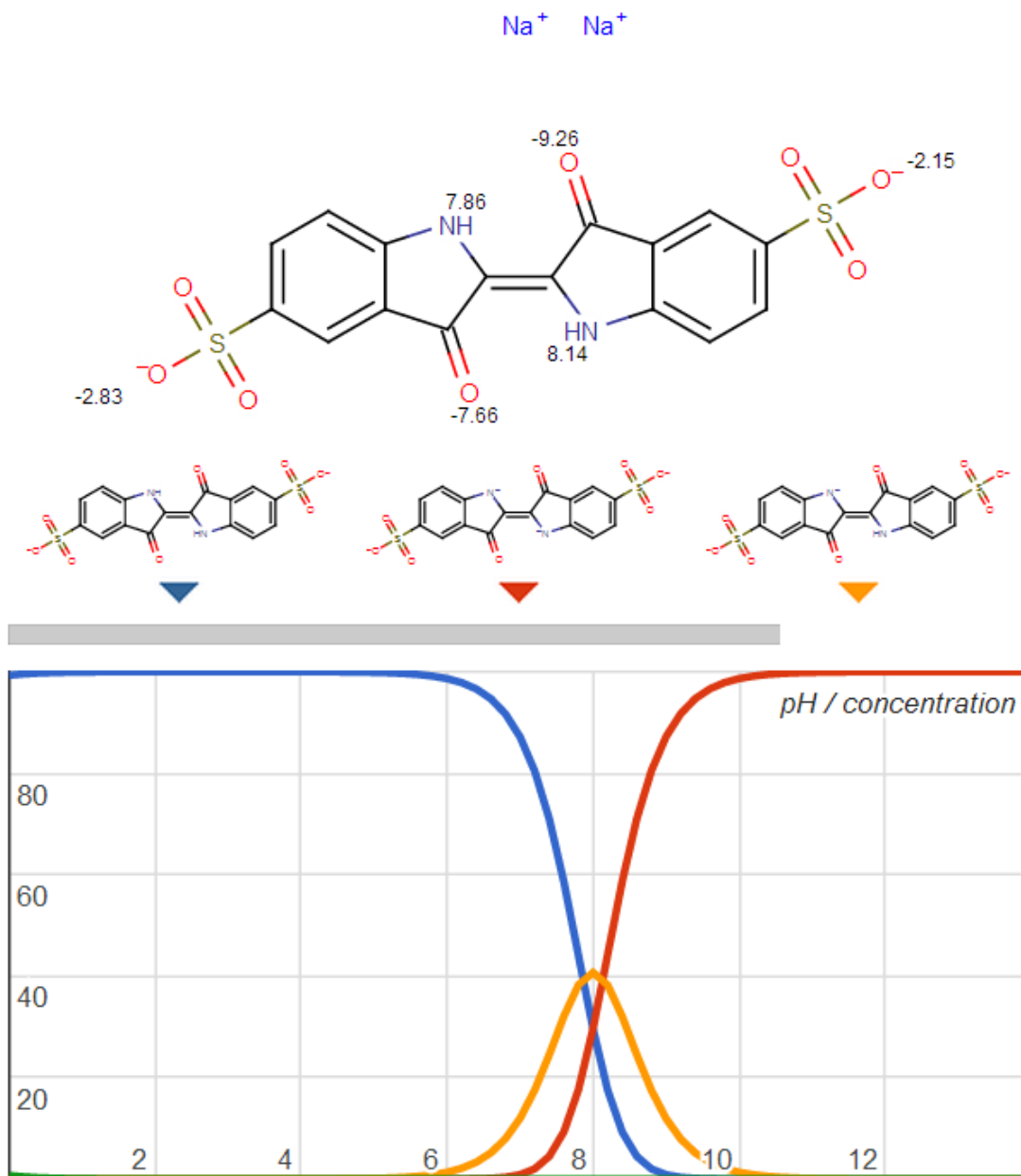


Figure S12.3 Speciation curve of Indigo Carmine as a function of pH. This content was adapted from the Chemspider chemical database¹¹.

S13. PAPER 10

Table S13.1 Identification of each phase for the different ABS composed of PEG 2000 + IL at 323 (± 1) K

Ionic Liquid	Top	Bottom
[amim]Cl	IL	PEG
[OHC ₂ mim]Cl	PEG	IL
[C ₁ im]Cl	PEG	IL
[C ₁ mim]Cl	PEG	IL
[C ₂ mim]Cl	IL	PEG
[C ₂ mim][CH ₃ CO ₂]	IL	PEG
[C ₂ mim][CH ₃ SO ₃]	PEG	IL
[C ₂ mim][HSO ₄]	PEG	IL
[C ₂ mim][DMP]	PEG	IL

Table S13.2 Partition coefficients (K_{alk}) and extraction efficiencies ($EE_{alk} / \%$) for nicotine, caffeine and xanthine in the ABS composed of PEG 2000 (≈ 53 wt%) + IL (≈ 27 wt%), at 323 (± 1) K. The average uncertainty associated to the alkaloids' partition coefficients and extraction efficiencies is within $\pm 5\%$. The percentage extraction efficiency ($EE_{alk} / \%$) of each alkaloid corresponds to the ratio between the weight of the alkaloid in the IL-rich phase to the total an initial weight of alkaloid

Ionic Liquid	K_{nic}	$EE_{nic} / \%$	K_{caf}	$EE_{caf} / \%$	K_{xant}	$EE_{xant} / \%$
[amim]Cl	1.64	52.2	0.37	20.0	1.14	43.1
[OHC ₂ mim]Cl	2.67	62.8	0.27	14.4	1.87	54.2
[C ₁ im]Cl	1.57	31.4	1.46	56.7	1.07	24.0
[C ₁ mim]Cl	2.19	58.2	2.35	61.7	1.28	32.2
[C ₂ mim]Cl	1.31	55.8	0.24	16.1	1.98	62.8
[C ₂ mim][CH ₃ CO ₂]	1.29	51.9	0.20	14.8	3.85	76.5
[C ₂ mim][CH ₃ SO ₃]	1.98	47.0	0.43	15.9	1.17	34.3
[C ₂ mim][HSO ₄]	2.53	56.6	0.44	18.2	0.95	32.9
[C ₂ mim][DMP]	1.60	46.9	0.25	12.7	1.31	42.1

Table S13.3 Partition coefficients (K_{alk}) and extraction efficiencies ($EE_{alk} / \%$) of nicotine and caffeine in the ABS composed of PEG 2000 (≈ 53 wt%) + [C₂mim]Cl (≈ 27 wt%) and at different temperatures (± 1 K). The average uncertainty associated to the alkaloids' partition coefficients and extraction efficiencies is within $\pm 5\%$

Temperature (± 1) / K	K_{nic}	$EE_{nic} / \%$	K_{caf}	$EE_{caf} / \%$
323	1.31	55.8	0.24	16.1
333	1.82	60.7	0.26	18.1
343	1.87	61.4	0.26	17.6
353	2.37	65.9	0.28	19.2
363	2.45	65.4	0.31	20.8

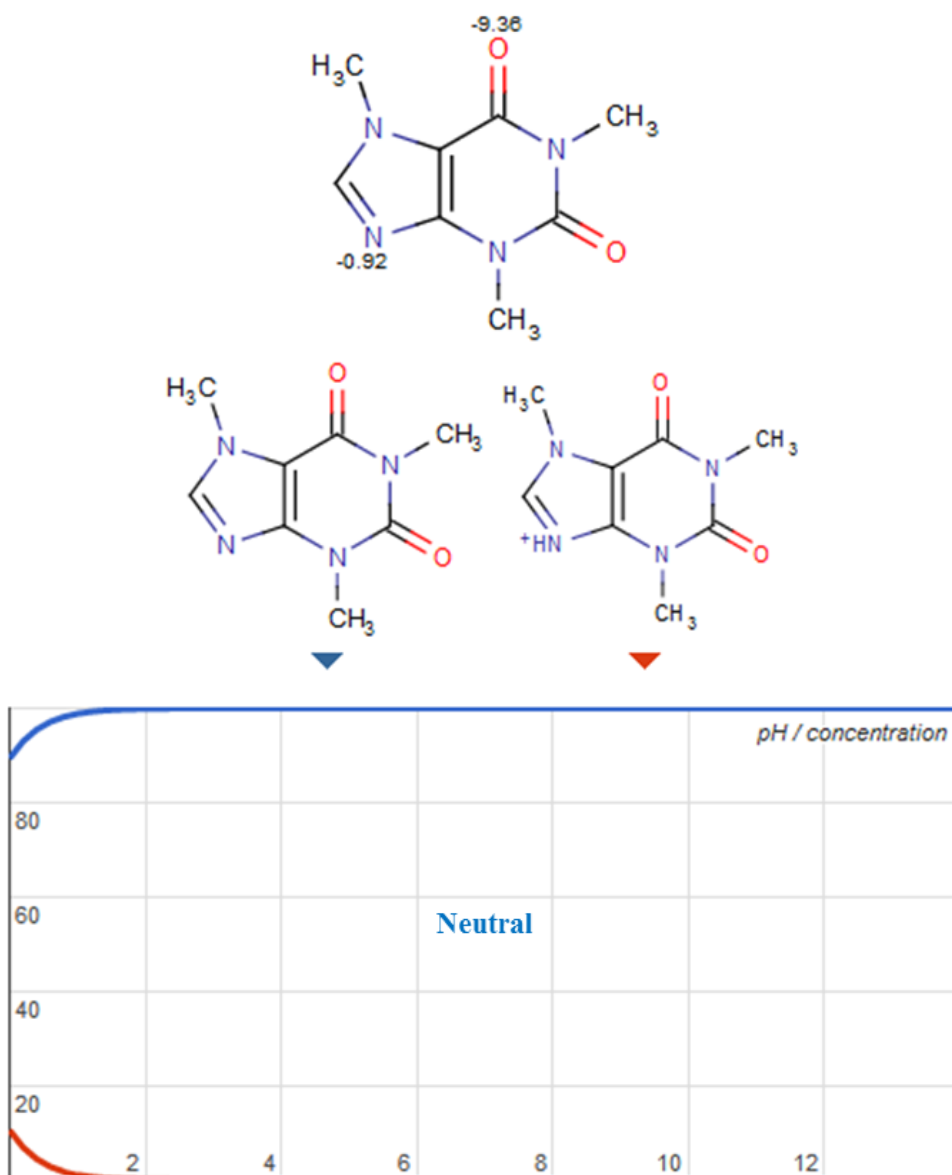


Figure S13.1 Speciation curve of caffeine as a function of pH. This content was adapted from the Chemspider chemical database¹¹.

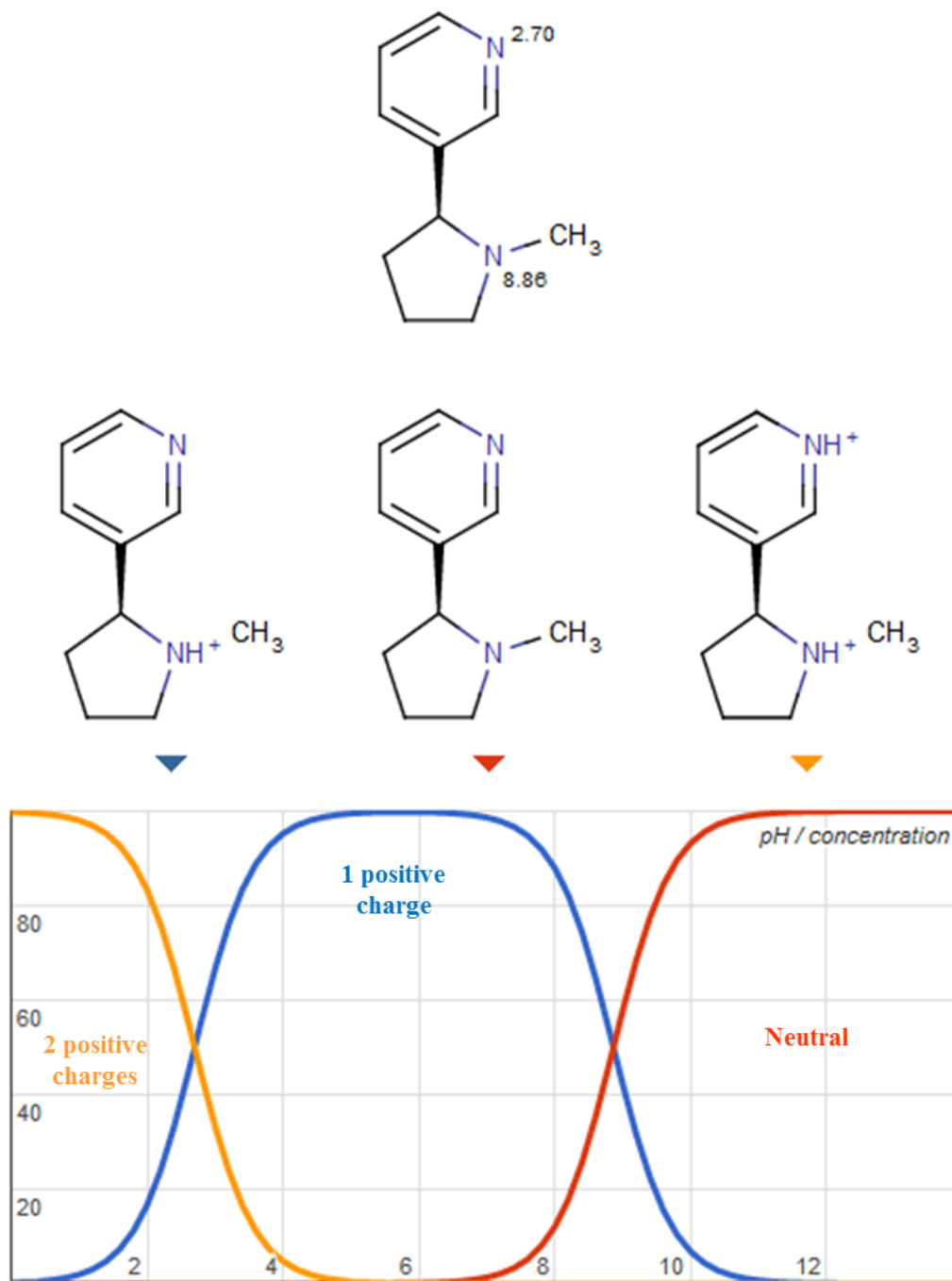


Figure S13.2 Speciation curve of nicotine as a function of pH. This content was adapted from the Chemspider chemical database¹¹.

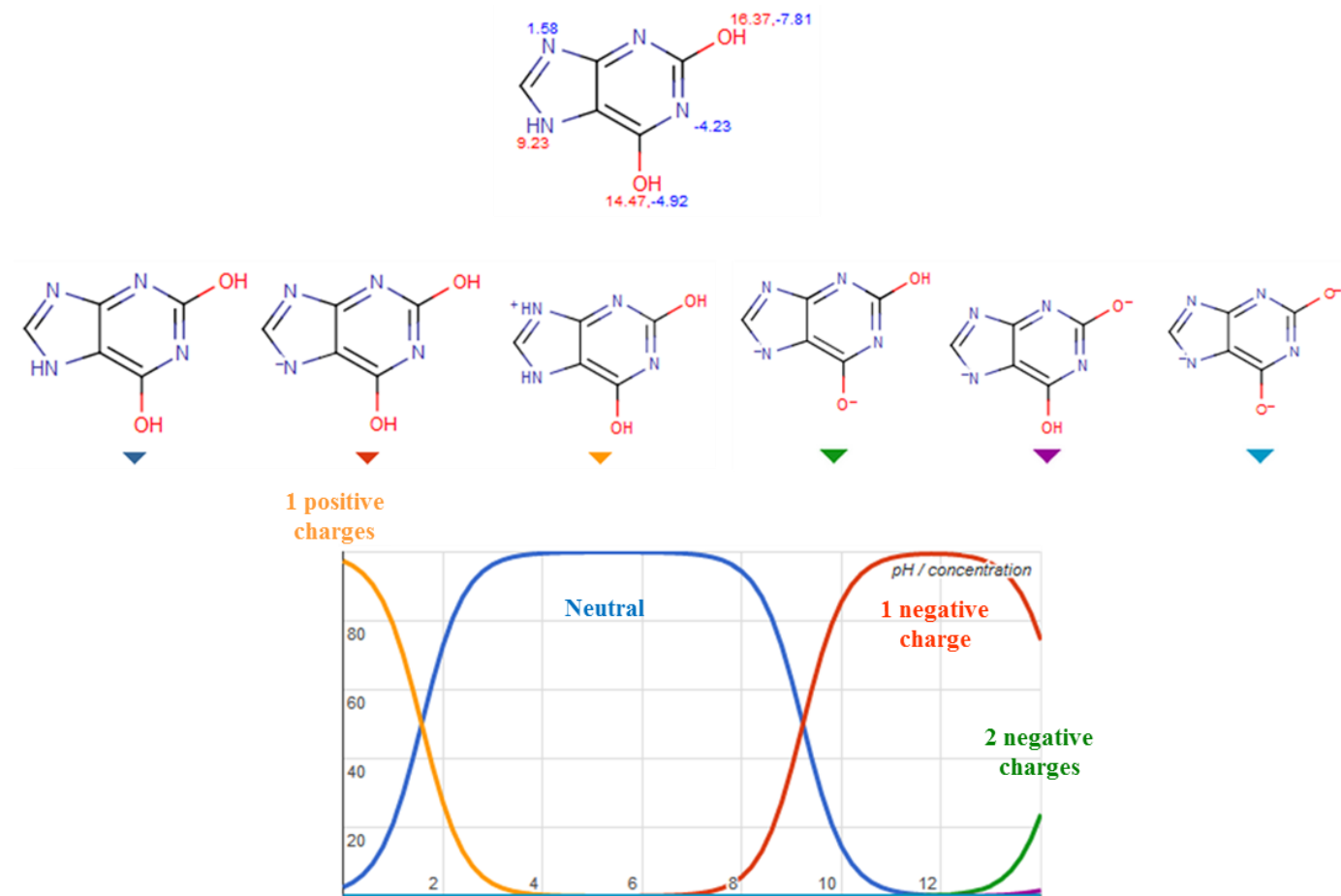


Figure S13.3 Speciation curve of xanthine as a function of pH. This content was adapted from the Chemspider chemical database¹¹.

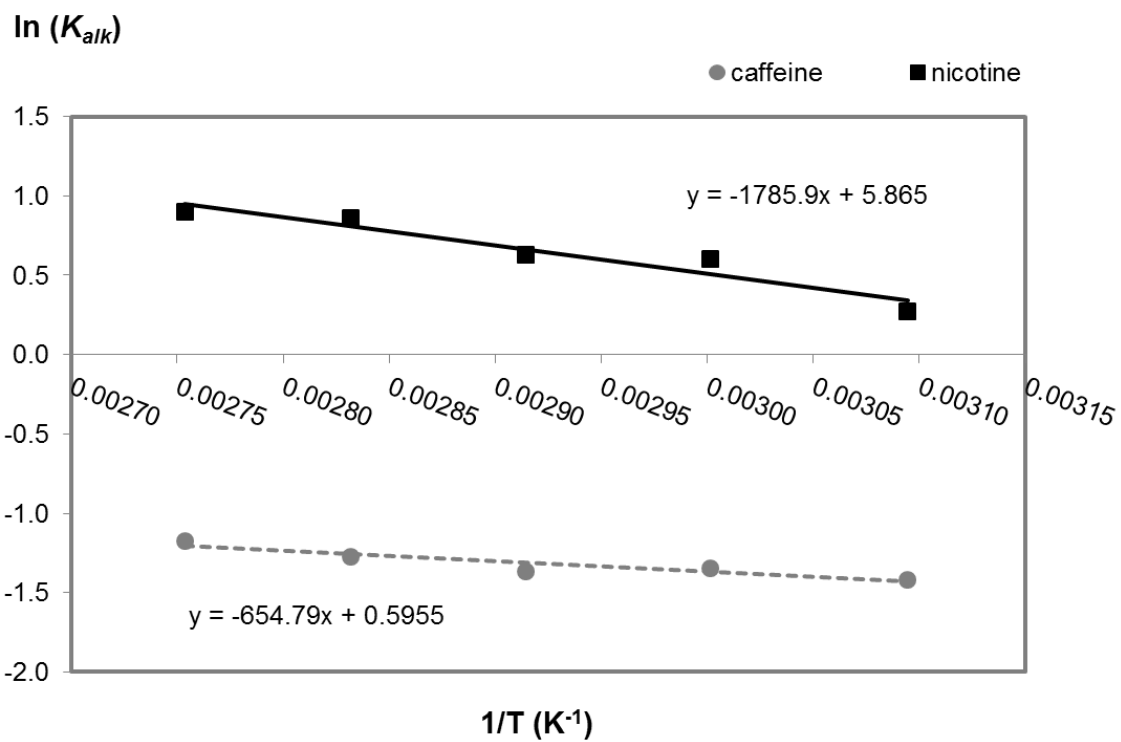


Figure S13.4 Representation of $\ln K_{alk}$ versus $1/T$.

S14. PAPER 11

S14.1. Determination of Tie-lines

The tie-line (TLs) were determined by a gravimetric method as originally described by Merchuck et al.¹². A mixture in the biphasic region was prepared, vigorously stirred and allowed to reach equilibrium by the separation of both phases, for 12 h at 298 K using glass tubes (*ca.* 10 mL). After the equilibration time, the top and bottom phases were carefully separated, recovered and weighed. Each TL was determined by the lever-arm rule according to the relationship between the weight of the PEG-rich phase composition and the overall system composition. For that purpose the experimental binodal curves were firstly correlated using Equation S14.1.¹²

$$[\text{PEG}] = A \times \exp(B \times [\text{IL}]^{0.5} - C \times [\text{IL}]^3) \quad \text{Equation S14.1}$$

where A , B and C are the correlation constants, and $[\text{IL}]$ and $[\text{PEG}]$ are the weight fractions percentages of ionic liquid and PEG, respectively. The tie-line lengths (TLLs) were determined according to standard protocols found in literature.^{13, 14} All the initial mixture compositions and respective TLs and TLLs are reported in Table S13.

S14.2. Conductivity Measurements

After the phase separation, conductivity ($\pm 0.01 \text{ mS.cm}^{-1}$) of both the IL-rich and PEG-rich phases were measured at 298 K ($\pm 1 \text{ K}$) using a SevenMultiTM (Mettler Toledo Instruments) reported in Table S14.13.

Table S14.1 Experimental binodal weight fraction data for the system composed of PEG 600 (1) + cholinium-based salt (2) + H₂O (3) at 298 K

[Ch]Cl		[Ch]Ac		[Ch]Gly	
100 w₁	100 w₂	100 w₁	100 w₂	100 w₁	100 w₂
34.0819	39.1428	7.7463	57.7669	56.4588	20.7596
37.2452	36.5489	10.2532	52.8845	55.4419	21.4341
39.2156	34.6475	16.6263	47.2618	53.9444	22.5325
41.8640	32.5914	20.1027	44.4450	53.3623	22.9262
43.1425	31.8462	25.9081	40.3469	51.0288	24.4749
44.6782	30.7604	29.1567	37.9697	49.1718	25.8242
46.2828	29.6031	33.5656	35.0386	48.4817	26.3869
50.3988	26.4885	37.8865	32.2912	45.7609	28.4222
50.6779	26.2078	41.1845	30.0483	42.5650	30.8665
52.0774	25.4721	44.2316	27.9741	39.4323	33.3652
54.5077	23.6280	47.4464	25.8656	34.8857	36.8404
54.6391	23.1984	49.5218	24.4078	30.8054	40.1912
54.9489	23.5726	51.9556	22.8546	25.6866	44.1907
57.4056	21.5651	53.9060	21.5639	20.4765	48.4258
58.1009	20.8599	56.0332	20.2684	15.8067	52.5080
60.6128	19.5148	57.1339	19.5986		
61.8785	18.3621	58.3577	18.9164		
63.0859	17.4472	59.5557	18.1474		
66.3457	15.4835	61.2758	17.1357		
66.8194	15.0065	62.8528	16.2783		
67.3466	14.7846	63.6795	15.8088		
68.2108	14.0296	64.8256	15.1910		
69.1924	13.3523	66.0323	14.4888		
70.3181	12.7876	67.6526	13.6384		
70.5079	12.5991	68.8174	13.0049		
70.8827	12.2647	69.4803	12.6887		
70.8867	12.3326	70.7682	12.0323		
71.5790	12.0019				
72.5925	11.2409				
72.6452	11.2668				
74.1751	10.5506				
74.4123	10.7863				

Table S14.2 Experimental binodal weight fraction data for the system composed of PEG 600 (1) + cholinium-based salt (2) + H₂O (3) at 298 K

[Ch]Bic		[Ch]Bit			
100 w₁	100 w₂	100 w₁	100 w₂	100 w₁	100 w₂
10.1364	53.3850	64.0030	11.4631	37.4011	33.0364
12.9063	50.8924	64.6590	11.0242	38.9774	31.1285
13.9666	50.0743	65.1924	10.7060	43.6349	24.9897
18.5083	46.4142	66.0494	10.1860	48.7314	19.8116
19.9134	44.9231	66.8701	9.7214	52.5486	15.8215
20.6432	44.3980	67.7031	9.2430	56.1310	11.9558
22.4662	42.7154	68.9080	8.7100	57.5905	11.5956
22.5157	42.7053	70.7096	7.6266	60.9777	8.7913
27.4700	39.1902	72.1638	6.9511	62.0634	7.8021
30.2757	36.8186	73.8744	6.2192	65.0652	6.4409
32.9258	34.7102			67.0270	4.9682
34.4811	33.3278				
37.4937	31.1626				
39.3993	29.6410				
43.3040	26.7841				
45.3727	24.9545				
47.5074	23.5082				
48.4397	22.7086				
49.4359	21.8419				
50.4330	21.0461				
51.6035	20.1329				
53.0482	19.1654				
53.5550	18.6675				
54.0985	18.1978				
55.5111	17.2987				
56.3702	16.5589				
57.2965	16.0009				
57.6738	15.6652				
58.4009	15.1774				
58.9815	14.7285				
60.1266	13.9539				
60.7244	13.5311				
61.6429	12.8892				
62.2029	12.5376				
63.3127	11.8550				

Table S14.3 Experimental binodal weight fraction data for the system composed of PEG 600 (1) + cholinium-based salt (2) + H₂O (3) at 298 K

[Ch]DHph				[Ch]Lac	
100 w_1	100 w_2	100 w_1	100 w_2	100 w_1	100 w_2
3.5450	46.7961	30.4605	24.1434	23.8424	44.3971
5.5537	45.0241	31.4426	23.4425	31.5324	39.1553
6.5756	43.8340	32.0136	22.9432	36.4478	35.7286
7.5547	42.4903	32.6111	22.4686	39.4145	33.4585
10.4529	40.2952	33.4295	21.8383	46.3179	28.6724
11.4670	39.4321	34.2968	21.2053	50.2577	26.1887
12.2377	38.4571	35.1423	20.6526	3.5832	79.9959
13.6488	37.1970	35.6390	20.2979	5.0578	62.7497
14.9396	36.0185	36.0008	19.9463	8.5589	57.2474
16.3723	34.8275	36.6860	19.4659	12.7997	53.1147
18.2424	33.4277	37.6290	18.9087	21.5169	46.5027
19.4753	32.3956	38.0519	18.6007	31.2122	39.6178
20.5612	31.5413	38.5663	18.2132	40.1764	33.4619
22.2142	30.4096	39.1323	17.8482	44.3685	30.4271
23.6806	29.2131	39.7196	17.4718	48.1836	27.8172
24.5360	28.4287	40.0553	17.2073	53.0493	24.5721
25.9339	27.5070	40.7565	16.8094	57.5475	21.6293
27.1792	26.6414	41.0672	16.5481	61.4925	19.2269
28.0101	25.9146	41.4692	16.3546	65.4363	16.8539
29.0850	25.1764	41.8852	16.0180	69.4542	14.6192
30.1346	24.3811	42.4350	15.6749		

Table S14.4 Experimental binodal weight fraction data for the system composed of PEG 600 (1) + cholinium-based salt (2) + H₂O (3) at 298 K

[Ch]Dhcit					
100 w₁	100 w₂	100 w₁	100 w₂	100 w₁	100 w₂
18.3423	64.8204	49.1516	32.0903	68.2303	15.8617
15.4533	66.7641	49.4078	31.7846	68.3316	15.6764
23.8645	57.9325	52.1214	29.4278	70.5148	14.2540
24.5619	57.4332	52.5602	28.7738	70.8166	13.9656
30.4862	50.8230	54.2304	27.1186	72.5303	12.8493
32.4810	49.4946	55.5925	26.0604	73.7325	12.0379
34.0505	46.8840	57.4200	24.4744	74.8951	11.3147
37.7544	43.2658	58.6260	23.7582	76.4397	10.1839
38.7983	42.4853	59.7610	22.3311	79.8048	8.0702
41.1756	39.9710	61.1544	21.5643		
42.6086	38.1728	62.3750	20.2959		
43.8792	37.2230	63.5001	19.6611		
44.7644	35.7307	65.1885	18.1395		
46.6736	34.5025	66.1107	17.5926		

Table S14.5 Experimental binodal weight fraction data for the system composed of PEG 400 (1) + cholinium-based salt (2) + H₂O (3) at 298 K

[Ch]Cl		[Ch]Ac		[Ch]Gly	
100 w₁	100 w₂	100 w₁	100 w₂	100 w₁	100 w₂
14.2673	79.4484	3.20675	76.0150	8.9800	73.0960
23.4290	66.2262	5.16016	71.1452	14.4505	64.3829
34.9210	50.8729	7.86334	65.7875	19.5541	57.2611
42.7682	41.2205	11.7567	61.4120	38.9308	42.4057
46.6534	37.6748	24.3122	51.7457		
49.3497	33.0541	46.8571	34.7135		
55.8806	25.4565				
59.4233	21.2144				
62.9069	17.2346				

Table S14.6 Experimental binodal weight fraction data for the system composed of PEG 400 (1) + cholinium-based salt (2) + H₂O (3) at 298 K

[Ch]Bic		[Ch]Bit			
100 w₁	100 w₂	100 w₁	100 w₂	100 w₁	100 w₂
76.3148	4.6064	15.6340	60.6272	66.6712	13.8823
64.1211	8.3320	18.6920	56.2237	70.1362	11.7189
55.3360	15.6190	24.8828	49.3708	72.6113	10.2361
44.5598	26.7269	28.9362	45.7267	72.9070	9.4832
40.2773	32.0014	31.8304	43.0647	75.9681	7.8011
36.9829	36.4901	34.6342	40.3570		
33.9896	40.6318	37.6425	37.6943		
28.4390	48.0264	38.8954	36.8994		
26.7808	50.5827	42.8230	33.5640		
25.0938	52.9306	46.0316	30.5618		
23.6026	54.9675	47.4200	29.2908		
22.5111	56.6044	50.2153	26.3125		
21.1420	58.5185	52.9587	24.0787		
19.3907	61.2443	53.2156	24.3736		
18.1892	62.8251	55.4117	22.1392		
16.3881	65.7587	57.0553	21.0511		
15.0253	67.9449	58.6358	19.8168		
13.8585	69.7628	60.9821	18.0662		
12.8517	71.5184	62.1231	17.1300		
11.7854	73.3356	66.0368	14.4581		

Table S14.7 Experimental binodal weight fraction data for the system composed of PEG 400 (1) + cholinium-based salt (2) + H₂O (3) at 298 K

[Ch]DHph		[Ch]DHcit			
100 w₁	100 w₂	100 w₁	100 w₂	100 w₁	100 w₂
3.2605	71.0169	45.8533	16.7336	11.8720	78.0665
3.6716	53.4546	46.6915	16.1961	21.8183	63.7696
4.8135	51.0734	47.4843	15.6883	29.6529	55.9746
6.4026	49.3956	47.7704	15.3936	53.5943	33.5173
7.2801	48.1931	48.4656	14.9302	55.5813	31.5365
8.9093	46.5262	49.1764	14.5247	60.6960	26.9756
9.0103	46.0556	49.6188	14.2025	65.2655	22.9814
9.8893	44.7814	50.0597	13.9099	66.9473	21.4908
11.6115	44.0309	50.7538	13.5254	69.0637	19.7794
11.6574	43.2697	51.2901	13.1531	71.8563	17.7629
13.3458	41.8102	51.6791	12.8483	75.1863	15.3116
14.0071	40.9596	52.3539	12.4772	78.3618	13.1806
14.1663	41.5895	52.8065	12.1794	11.8720	78.0665
15.3617	39.7276	53.2681	11.9716	21.8183	63.7696
16.4821	39.4016	53.4129	11.7976	29.6529	55.9746
19.7998	36.8986	53.8357	11.6034	53.5943	33.5173
22.2638	34.8480	54.3215	11.3416	55.5813	31.5365
25.2335	32.3340	54.8049	11.0756	60.6960	26.9756
27.2864	30.8652			65.2655	22.9814
29.0060	29.4020			66.9473	21.4908
30.6375	28.1283			69.0637	19.7794
32.3328	26.9291			71.8563	17.7629
33.2111	26.0991			75.1863	15.3116
34.6032	25.0208			78.3618	13.1806
36.3226	23.8656				
37.1569	23.0901				
38.2859	22.2759				
39.4851	21.4441				
40.3493	20.7602				
41.1913	20.1146				
42.0553	19.4554				
42.7934	18.8797				
43.7738	18.2112				
44.4963	17.7162				
45.1416	17.2364				

Table S14.8 Experimental binodal weight fraction data for the system composed of PEG 1000 (1) + cholinium-based salt (2) + H₂O (3) at 298 K

[Ch]Cl		[Ch]Ac		[Ch]Gly	
100 w₁	100 w₂	100 w₁	100 w₂	100 w₁	100 w₂
8.6214	66.9970	2.6432	78.8540	3.9793	74.8555
30.0426	40.1175	7.3093	54.6305	3.7729	75.8240
33.4080	36.1134	11.7461	48.1524	10.1126	51.8951
35.6205	33.2309	14.1413	44.7570		
37.2033	30.9398				
38.7739	28.9920				
40.6760	26.8315				
42.9799	23.9346				
50.9733	15.4787				
55.9164	10.3159				

Table S14.9 Experimental binodal weight fraction data for the system composed of PEG 1000 (1) + cholinium-based salt (2) + H₂O (3) at 298 K

[Ch]Bic		[Ch]Bit		[Ch]DHcit	
100 w₁	100 w₂	100 w₁	100 w₂	100 w₁	100 w₂
76.2410	3.7279	17.6209	54.4842	11.5142	65.9190
43.1968	17.2464	47.5877	18.7319	20.2953	55.4792
34.5213	28.0776	52.1811	15.6541	24.9578	50.4162
26.5859	38.6946	58.9611	11.3544	30.0832	44.9733
				34.3694	40.6178
				39.6771	35.4297
				65.9776	12.1468

Table S14.10 Experimental binodal weight fraction data for the system composed of PEG 1000 (1) + cholinium-based salt (2) + H₂O (3) at 298 K

[Ch]DHph					
100 w₁	100 w₂	100 w₁	100 w₂	100 w₁	100 w₂
1.4451	71.0387	18.0564	29.3371	30.1286	20.7187
1.7746	42.8039	20.0701	27.8683	30.5535	20.4044
5.1530	39.5994	20.8086	27.3407	30.7845	20.2242
5.9118	38.6642	22.3232	26.1851	31.2736	19.9092
8.3372	36.8751	23.7616	25.1932	32.0671	19.3429
9.5465	35.7104	24.9950	24.2966	32.4456	19.0838
11.9288	33.9082	26.1277	23.4752		
14.1008	32.2892	27.7318	22.4400		
15.6007	31.0811	28.4685	21.8366		
16.1853	30.6909	29.6530	21.0477		

Table S14.11 Experimental binodal weight fraction data for the system composed of PEG 600 (1) + cholinium-based salt (2) + H₂O (3) at 323 K

[Ch]Cl					
100 w₁	100 w₂	100 w₁	100 w₂	100 w₁	100 w₂
27.4636	43.2037	46.7227	26.3233	60.2697	17.7452
28.2913	40.1033	47.7682	25.7388	60.4173	17.5116
29.2787	39.0705	48.6565	24.8002	61.5336	16.8868
30.1001	38.2844	49.8244	23.8900	62.6406	16.1757
32.3096	37.2502	50.4489	23.5896	62.8462	16.1569
35.3568	32.9795	51.5359	22.6979	65.5220	14.6592
36.7088	32.2928	52.2768	22.5276	66.2151	13.6323
39.2230	30.3882	53.2990	21.3104	69.0106	11.8901
40.6534	29.4672	55.2205	20.4676	70.2014	11.1798
41.8976	28.6241	55.5015	20.8819	70.9403	10.9921
43.3273	28.0602	56.3751	20.3168	72.8610	9.9856
43.7878	28.0371	57.1488	19.1507	73.8627	9.3745
44.7675	26.8514	57.3216	19.6921	85.4415	6.2862
45.0558	27.1202	58.8008	18.2194	94.6254	2.2926
46.3820	26.5555	59.2603	18.4464	98.5301	1.1865

Table S14.12 Experimental binodal weight fraction data for the system composed of PEG 600 (1) + cholinium-based salt (2) + H₂O (3) at 323 K

[Ch]DHph					
100 w₁	100 w₂	100 w₁	100 w₂	100 w₁	100 w₂
5.6594	51.10703	15.8156	52.52676	23.5469	50.89493
6.6100	51.14418	16.3048	52.34129	23.8701	50.77896
7.6895	50.98420	17.0688	52.02116	24.1318	50.79141
8.3861	51.24136	17.5074	51.90699	24.2001	50.83366
8.9707	51.18127	17.9930	51.71644	24.4763	50.76389
9.6321	51.13050	18.4118	51.69281	24.6181	50.75666
10.2704	51.13839	19.4970	51.98580	25.0112	50.58326
10.8443	51.13271	19.8359	51.93682	25.1037	50.66240
11.3579	51.16029	20.4429	51.60708	25.5882	50.49637
11.9148	51.12192	21.0640	51.45864	25.9246	50.34239
12.2599	52.42052	21.4203	51.44229	26.2083	50.29351
12.8938	52.10986	22.1092	51.08375	26.4665	50.34134
13.4854	51.88107	22.3789	51.18647	26.7216	50.31928
14.0184	51.72984	22.7849	51.00348	27.0154	50.21379
14.5101	51.65793	22.8493	51.14138		
14.8000	53.04262	23.1523	51.04632		

Table S14.13 Initial mixture compositions and respective TLs and TLLs at 298 K

Weight Fraction Composition / (wt %)							
Ternary System	Initial mixture		PEG-rich phase		IL-rich phase		TLL
	PEG 600	IL	[PEG]	[IL]	[PEG]	[IL]	
[Ch]Cl	57.93	29.93	93.32	3.34	9.20	66.53	105.20
	57.85	26.84	88.12	4.77	16.32	57.41	88.87
	54.69	27.73	82.65	6.65	17.63	55.68	81.44
	57.73	22.88	75.78	9.62	33.07	40.97	52.98
[Ch]Bic	45.78	29.49	85.26	2.22	11.43	53.23	89.73
	39.81	32.01	77.14	4.79	13.74	51.02	78.46
[Ch]Bit	35.97	39.93	64.55	6.45	10.15	70.16	83.78
	35.17	38.73	59.61	9.67	13.36	64.66	71.85
[Ch]Ac	48.52	40.94	96.98	2.71	0.49	78.83	122.90
	50.01	29.97	92.52	3.81	9.15	55.17	97.98
[Ch]DHcit	61.79	28.62	80.38	8.24	3.23	92.82	114.47
	59.61	27.40	76.94	10.05	9.08	78.02	96.05
[Ch]DHph	40.19	30.07	79.86	0.13	0.67	59.90	99.22
[Ch]Gly	30.07	59.92	91.95	2.68	0.47	87.30	124.62

Table S14.14 Initial mixture compositions and conductivities of the coexisting phases at 298 K

Ternary System	Weight Fraction		Conductivity / (mS.cm ⁻¹)		Phase	
	Composition / (wt %)		Top	Bottom	Top	Bottom
	PEG 600	IL				
[Ch]Cl	57.93	29.93	30.50	0.601	IL	PEG
	57.85	26.84	20.70	3.330	IL	PEG
	54.69	27.73	10.98	0.507	IL	PEG
	57.73	22.88	9.810	1.691	IL	PEG
[Ch]Bic	45.78	29.49	0.482	22.00	PEG	IL
	39.81	32.01	0.550	17.70	PEG	IL
[Ch]Bit	35.97	39.93	0.313	4.96	PEG	IL
	35.17	38.73	0.517	4.88	PEG	IL
[Ch]Ac	48.52	40.94	2.690	0.580	IL	PEG
	50.01	29.97	7.760	0.641	IL	PEG
[Ch]DHcit	61.79	28.62	0.208	1.160	PEG	IL
	59.61	27.40	0.364	-	PEG	IL
[Ch]DHph	40.19	30.07	0.092	2.640	PEG	IL
[Ch]Gly	30.07	59.92	0.382	6.670	PEG	IL

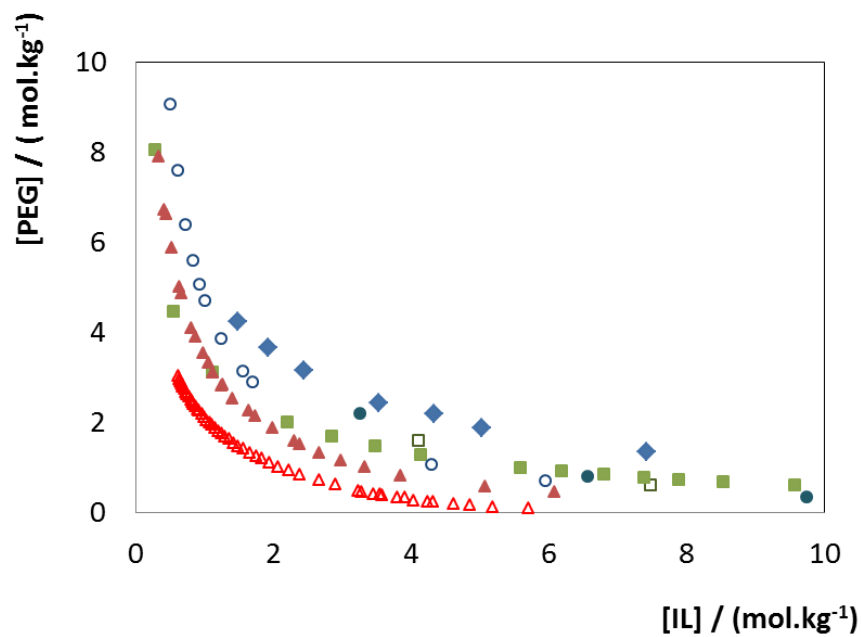


Figure S14.1 Experimental solubility data for ABS composed of PEG 400 and ILs at 298 K: (Δ) [Ch]DHph; (\blacktriangle) [Ch]Bit; (\blacksquare) [Ch]Bic; (\circ) [Ch]DHcit; (\square) [Ch]Gly; (\bullet) [Ch]Ac; (\blacklozenge) [Ch]Cl.

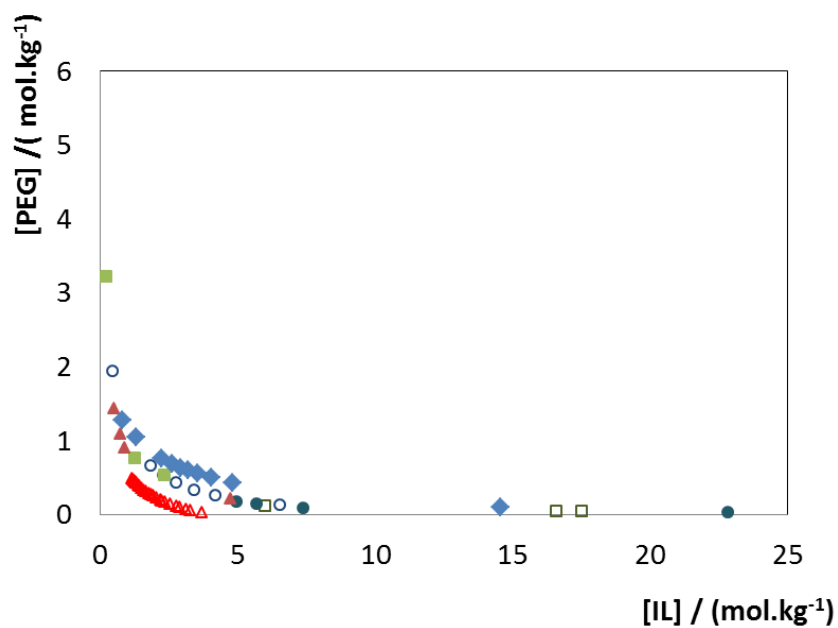


Figure S14.2 Experimental solubility data for ABS composed of PEG 1000 and ILs at 298 K: (Δ) [Ch]DHph; (\blacktriangle) [Ch]Bit; (\blacksquare) [Ch]Bic; (\circ) [Ch]DHcit; (\square) [Ch]Gly; (\bullet) [Ch]Ac; (\blacklozenge) [Ch]Cl.

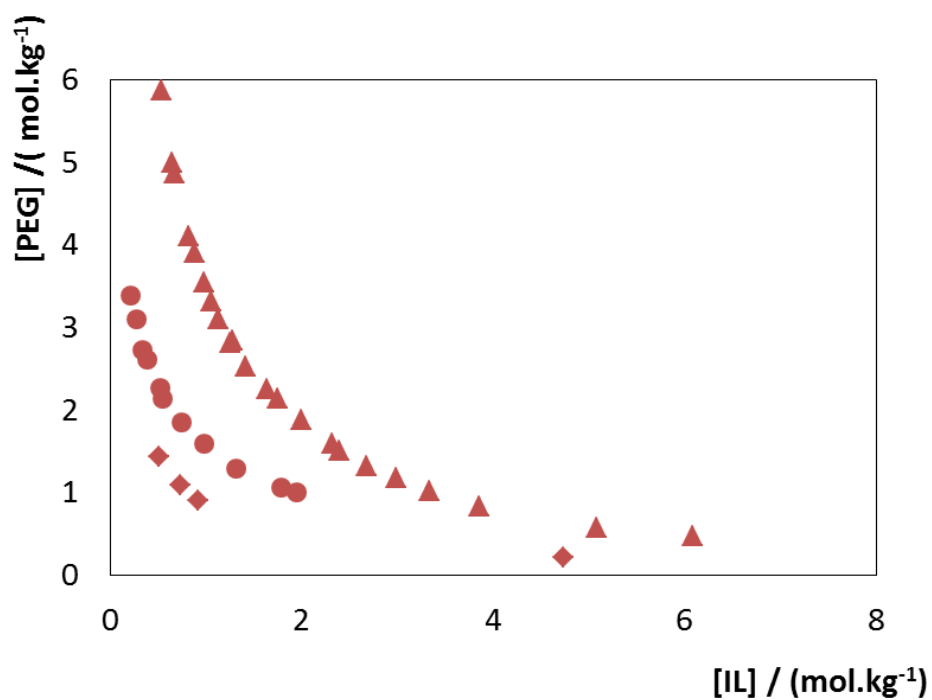


Figure S14.3 Experimental solubility data for ABS composed of [Ch]Bit and different PEGs at 298K: (◆) PEG 1000; (●) PEG 600; (▲) PEG 400.

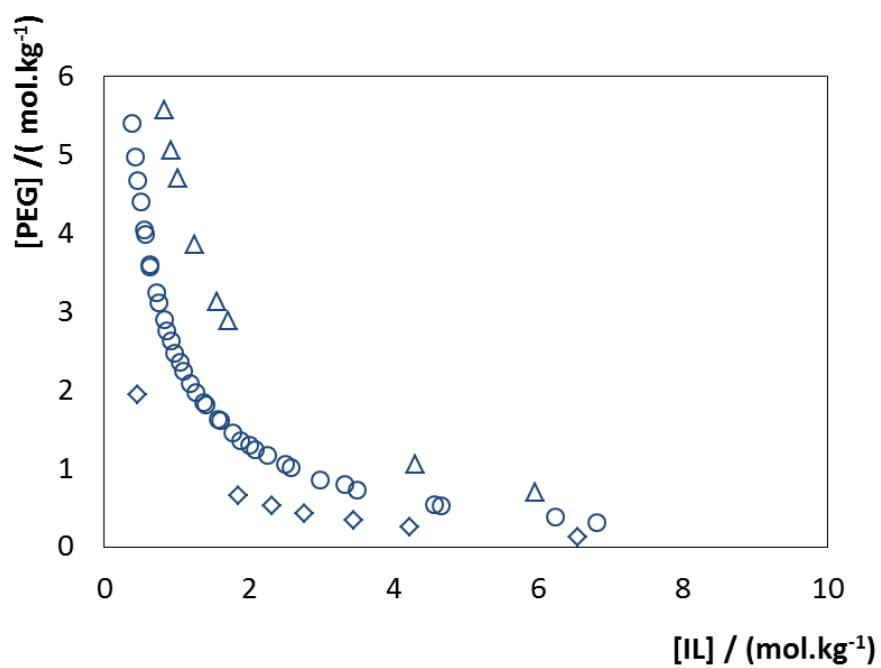


Figure S14.4 Experimental solubility data for ABS composed of [Ch]DHcit and different PEGs at 298 K: (◇) PEG 1000; (○) PEG 600; (△) PEG 400.

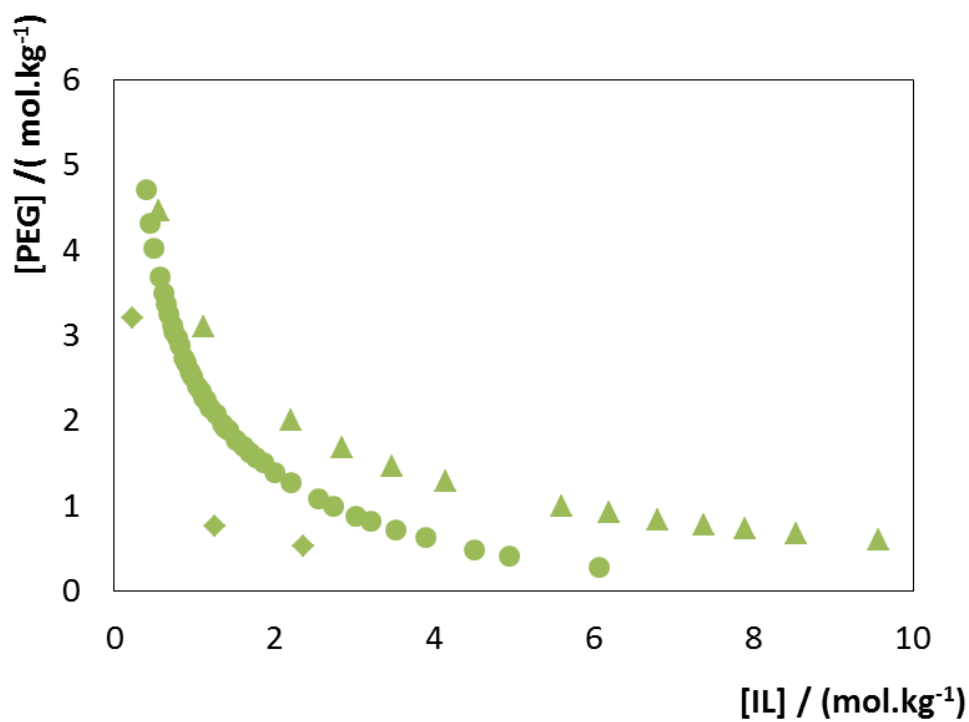


Figure S14.5 Experimental solubility data for ABS composed of [Ch]Bic and different PEGs at 298 K:
 (♦) PEG 1000; (●) PEG 600; (▲) PEG 400.

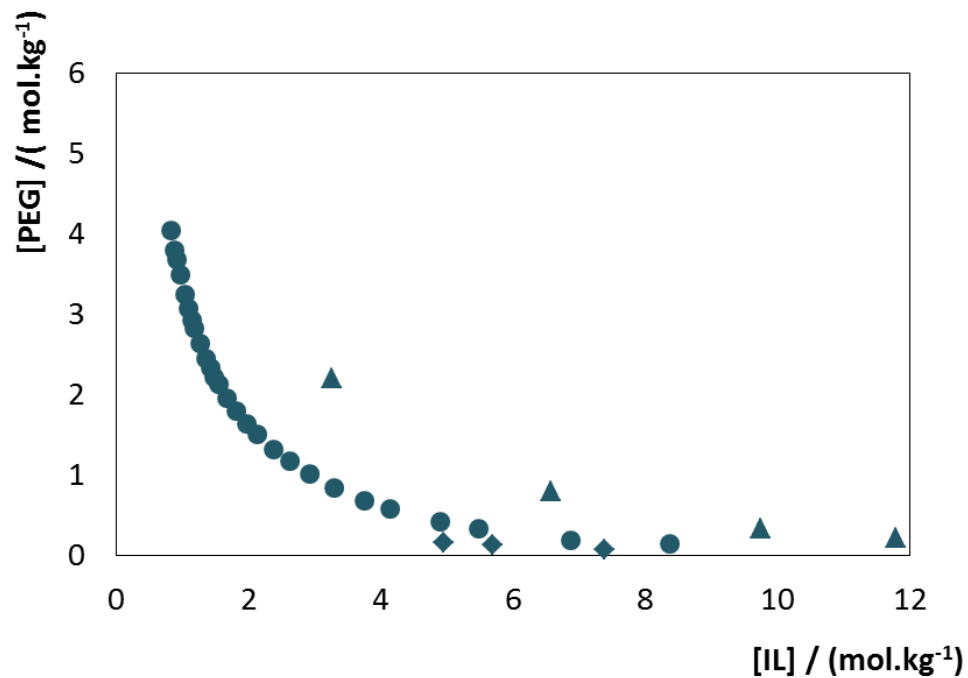


Figure S14.6 Experimental solubility data for ABS composed of [Ch]Ac and different PEGs at 298 K:
 (♦) PEG 1000; (●) PEG 600; (▲) PEG 400.

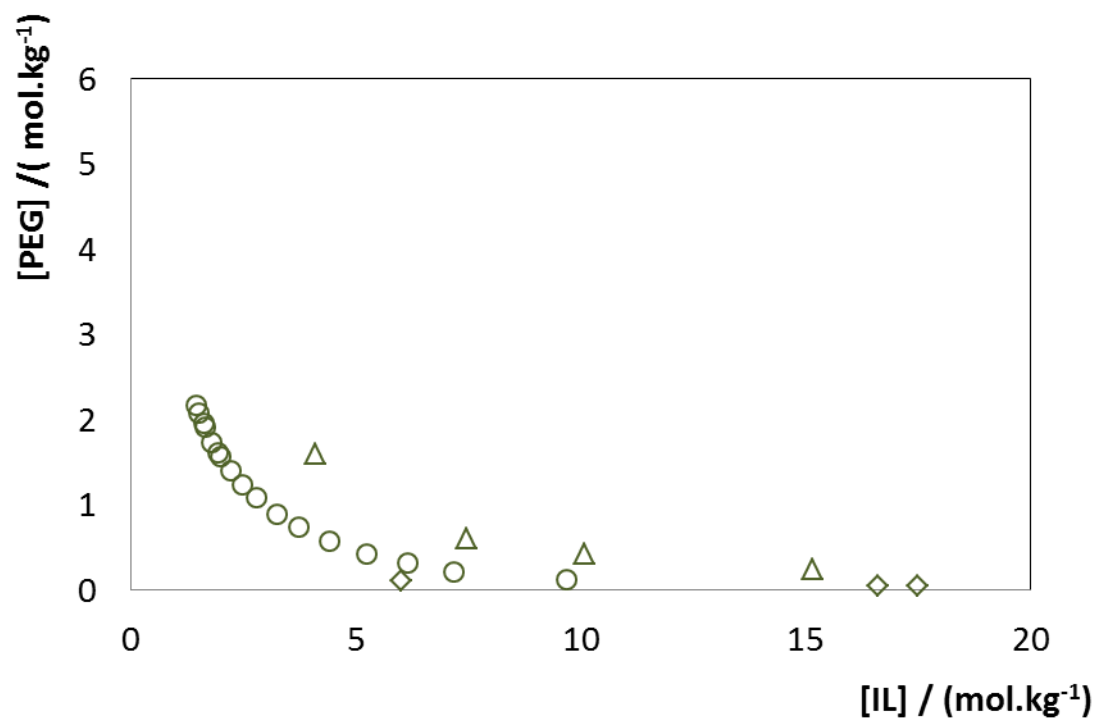


Figure S14.7 Experimental solubility data for ABS composed of [Ch]Gly and different PEGs at 298 K:
 (◇) PEG 1000; (○) PEG 600; (△) PEG 400.

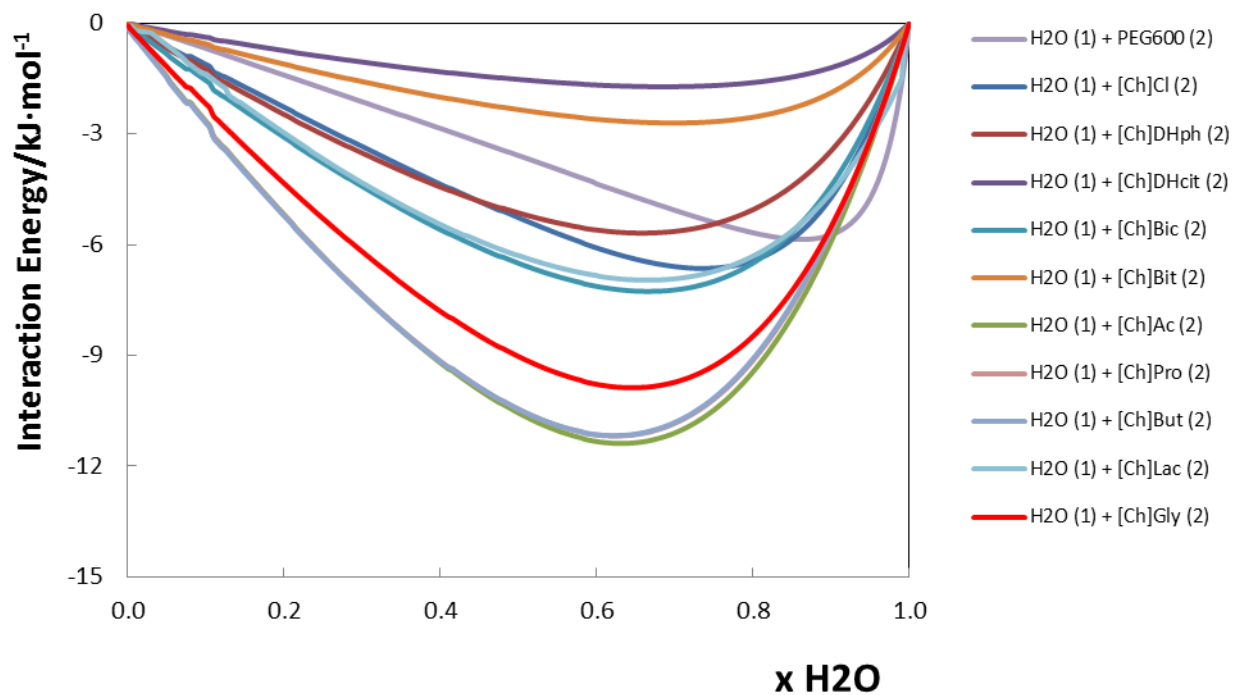


Figure S14.8 Excess enthalpies of mixing between water and the IL or PEG 600 predicted by COSMO-RS as a function of the water mole fraction.

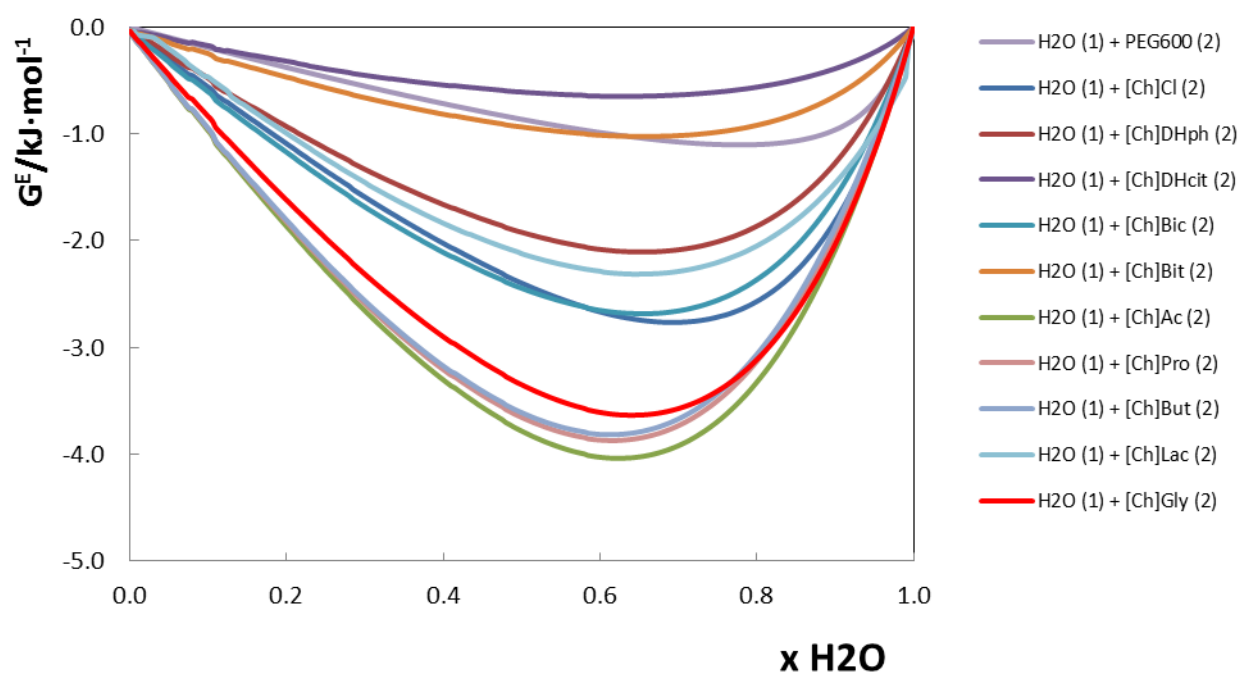


Figure S14.9 Excess free Gibbs energy, G^E , of mixing between water and the IL or PEG 600 predicted by COSMO-RS as a function of the water mole fraction.

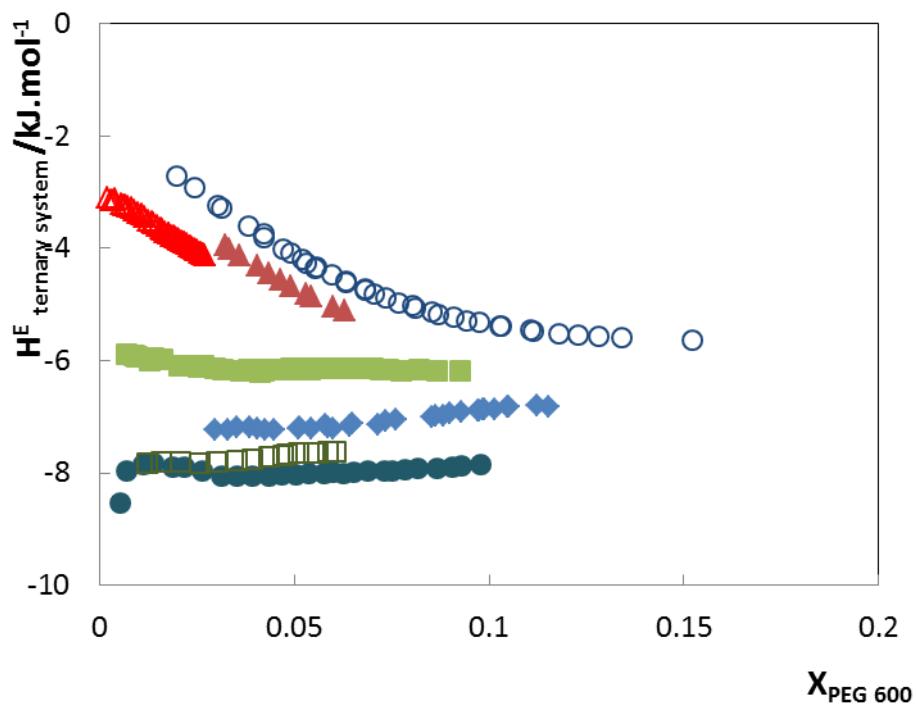


Figure S14.10 Excess enthalpies of mixing between PEG 600 and the IL predicted by COSMO-RS as a function of the polymer mole fraction: (Δ) [Ch]DHph; (\blacktriangle) [Ch]Bit; (\circ) [Ch]DHcit; (\blacksquare) [Ch]Bic; (\square) [Ch]Gly; (\bullet) [Ch]Ac; (\blacklozenge) [Ch]Cl.

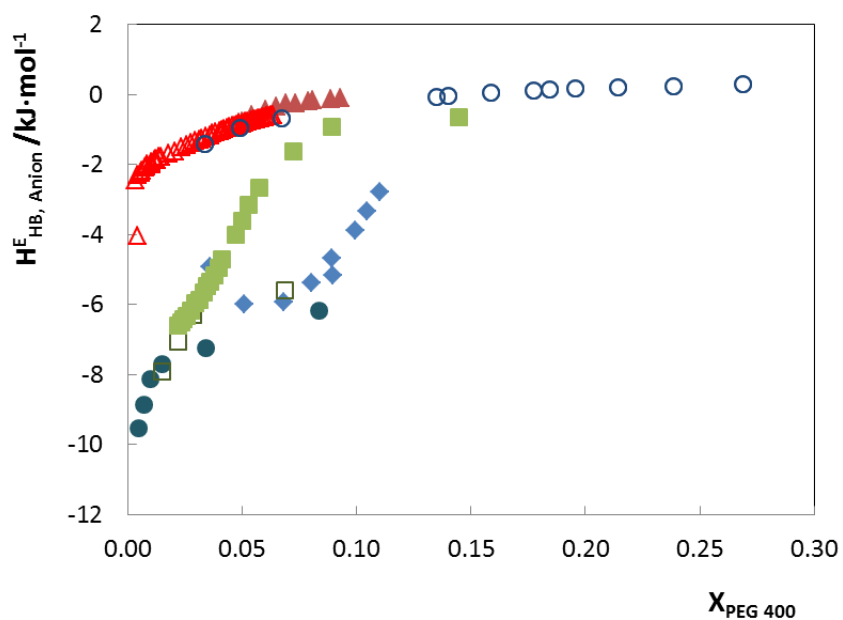


Figure S14.11 Excess enthalpies of mixing between PEG 400 and the IL anion predicted by COSMO-RS as a function of the polymer mole fraction: (Δ) [Ch]DHph; (\blacktriangle) [Ch]Bit; (\circ) [Ch]DHcit; (\blacksquare) [Ch]Bic; (\square) [Ch]Gly; (\bullet) [Ch]Ac; (\blacklozenge) [Ch]Cl.

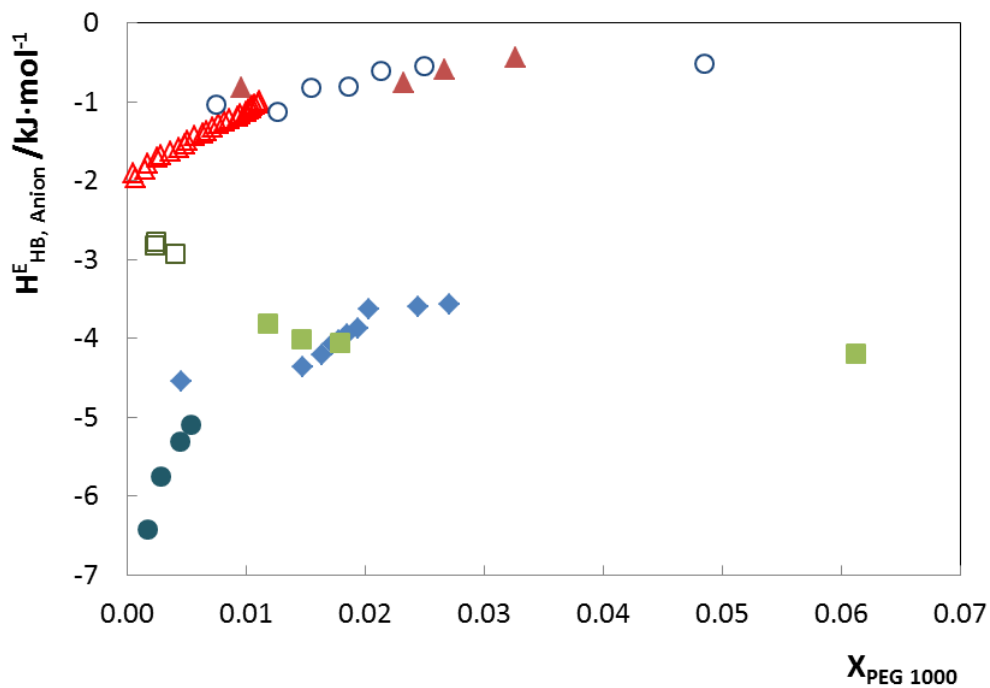


Figure S14.12 Excess enthalpies of mixing between PEG 1000 and the IL anion predicted by COSMO-RS as a function of the polymer mole fraction: (Δ) [Ch]DHph; (\blacktriangle) [Ch]Bit; (\circ) [Ch]DHcit; (\blacksquare) [Ch]Bic; (\square) [Ch]Gly; (\bullet) [Ch]Ac; (\blacklozenge) [Ch]Cl.

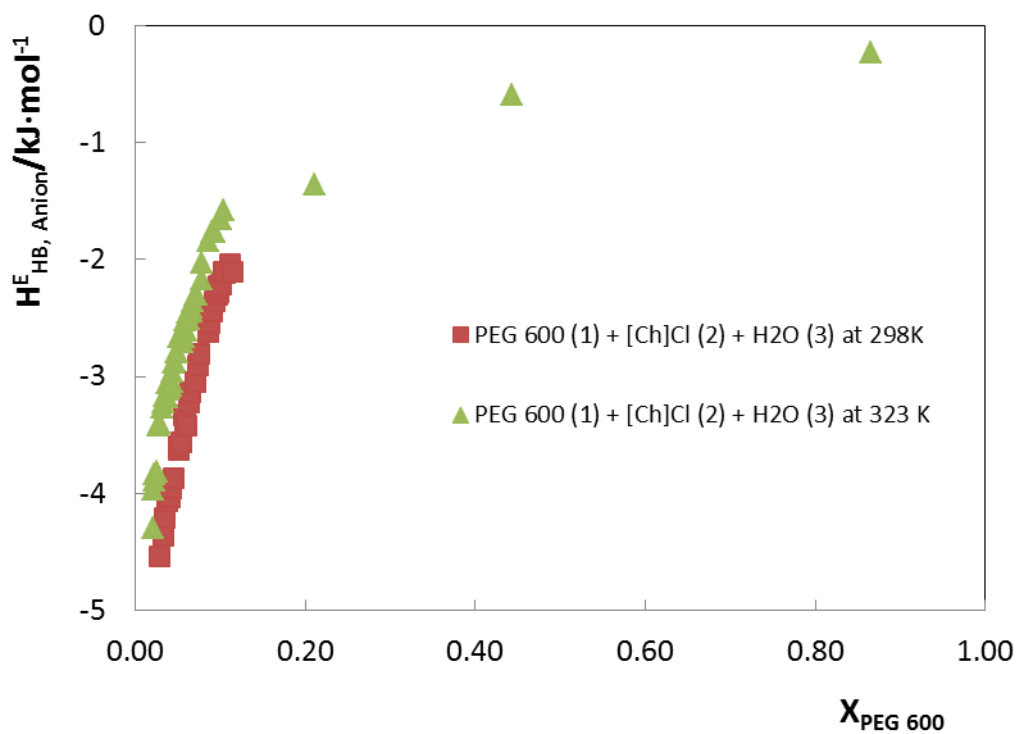


Figure S14.13 Excess enthalpies of mixing between PEG 600 and the [Ch]Cl anion predicted by COSMO-RS as a function of temperature.

S15. PAPER 12

Table S15.1. Validation of the TC quantification.

[Total Protein] / (g.L ⁻¹) ^a	6.187
Dilution Factor	1:10
Absorbance at 280 nm due to the protein content ^b	0.281
Total absorbance at 280 nm	0.816
Absorbance of TC at 280 nm	0.535
[TC] at 280 nm / (g.L ⁻¹) ^c	0.163
[TC] at 357 nm / (g.L ⁻¹) ^d	0.175

^aobtained from the BCA method; ^bobtained by the calibration curve of BSA: **Absorbance=0.4545*[Total Protein]**; ^cobtained from the calibration curve of TC at 280 nm (Fig.A1); ^d obtained from calibration curve of TC at 357 nm (Fig. A2)

Table S15.2 Initial weight fraction compositions, tie-lines and TLLs in the several ABS at 25 °C.

Ternary System	Weigth Fraction Composition (wt %)						α	TLL
	Y_M	X_M	Y_{PEG}	X_{PEG}	Y_{Salt}	X_{Salt}		
[Ch]Cl	54.96	35.01	4.41	76.08	94.17	3.14	0.56	115.66
	55.03	34.93	3.90	77.49	92.84	3.46	0.57	115.72
	54.99	34.90	3.48	78.76	91.52	3.80	0.59	115.63
	54.95	30.01	13.31	60.75	89.82	4.26	0.54	95.10
	55.01	29.93	11.73	62.82	88.14	4.76	0.57	95.96
	54.79	30.04	10.15	65.07	86.23	5.37	0.59	96.71
	55.07	24.91	29.85	43.81	74.82	10.10	0.56	56.20
	54.80	25.00	26.73	46.63	72.75	11.18	0.61	58.09
	54.78	24.95	26.04	47.28	71.95	11.61	0.63	58.14
[Ch]Bic	50.01	34.84	91.17	1.12	1.69	72.74	0.54	114.62
	49.86	35.07	91.26	1.11	1.27	74.93	0.54	116.40
	49.72	35.19	91.63	1.05	1.33	74.60	0.54	116.40
	49.71	30.04	89.89	1.34	5.99	61.27	0.52	103.11
	50.05	29.99	87.37	1.82	4.37	64.47	0.55	103.99
	49.84	29.90	85.38	2.26	3.87	65.64	0.56	103.25
	49.72	25.09	76.74	4.94	11.32	53.72	0.59	81.60
	49.99	25.05	76.05	5.21	9.69	55.72	0.61	83.39
	49.95	25.06	77.77	4.55	11.70	53.27	0.58	82.08
[Ch]DHcit	44.90	39.99	19.51	62.83	79.93	8.47	0.58	81.27
	45.00	39.90	19.22	63.18	79.67	8.60	0.57	81.44
	45.08	39.85	18.82	63.67	79.34	8.77	0.57	81.71
	45.70	37.83	26.30	54.39	77.45	9.77	0.63	67.36
	45.90	37.76	28.14	53.16	79.31	8.78	0.65	67.74
	45.76	37.81	27.28	54.07	77.92	9.25	0.64	67.46
	56.76	29.99	74.79	11.30	7.53	81.01	0.73	96.87
	57.06	29.84	77.05	9.99	9.63	76.96	0.70	95.03
	56.84	30.07	77.28	9.86	9.87	76.54	0.70	94.81
[Ch]Ac	49.93	39.97	0.62	77.42	99.68	2.30	0.50	124.38
	49.31	39.47	0.75	76.16	98.29	2.45	0.50	122.25
	49.92	39.93	0.63	77.32	99.64	2.20	0.50	124.28
	49.84	35.10	0.96	74.61	86.63	5.37	0.57	110.15
	49.79	34.97	0.93	74.80	85.74	5.66	0.58	109.42
	49.96	34.92	0.86	75.34	85.35	5.79	0.58	109.44
	49.84	30.03	5.01	61.47	83.53	6.41	0.57	95.90
	49.93	29.99	5.07	61.36	83.77	6.33	0.57	96.04
	49.94	29.97	4.50	62.48	82.24	6.88	0.58	95.58
[Ch]DHph	49.81	29.92	85.81	0.41	0.09	70.67	0.58	110.84
	50.01	29.99	85.07	0.47	0.06	72.05	0.59	111.14
	49.89	29.95	85.95	0.40	0.08	70.76	0.58	111.01
	40.29	29.78	77.24	1.40	0.77	60.13	0.52	96.42
	40.11	30.00	76.03	1.60	0.63	61.22	0.52	96.12
	40.05	29.95	79.66	1.07	1.04	58.40	0.50	97.32
	35.04	29.89	70.37	2.75	1.67	55.52	0.49	86.63
	35.09	29.99	68.15	3.32	1.26	57.29	0.51	85.95
	34.80	30.04	70.14	2.81	1.65	55.58	0.48	86.46

Y and X are, respectively, the PEG and salt weight percentages, and the subscripts PEG, Salt and M represent the PEG-rich, the Salt-rich and the initial mixture, respectively. The parameter α is the ratio between the weight of the PEG-rich and the total mass of the mixture.

Table S15.3 Initial mixture compositions and respective values of conductivities at 25 °C.

Ternary System	Weight Fraction			Conductivity / (mS.cm ⁻¹)		Phase	
	Composition / (wt %)			Top	Bottom	Top	Bottom
	PEG 600	IL					
[Ch]Cl	54.69	27.73	10.98	0.507	IL	PEG	
[Ch]Bic	45.78	29.49	0.482	22.00	PEG	IL	
[Ch]Ac	50.01	29.97	7.760	0.641	IL	PEG	
[Ch]DHcit	59.61	27.40	0.364	-	PEG	IL	
[Ch]DHph	40.19	30.07	0.092	2.640	PEG	IL	

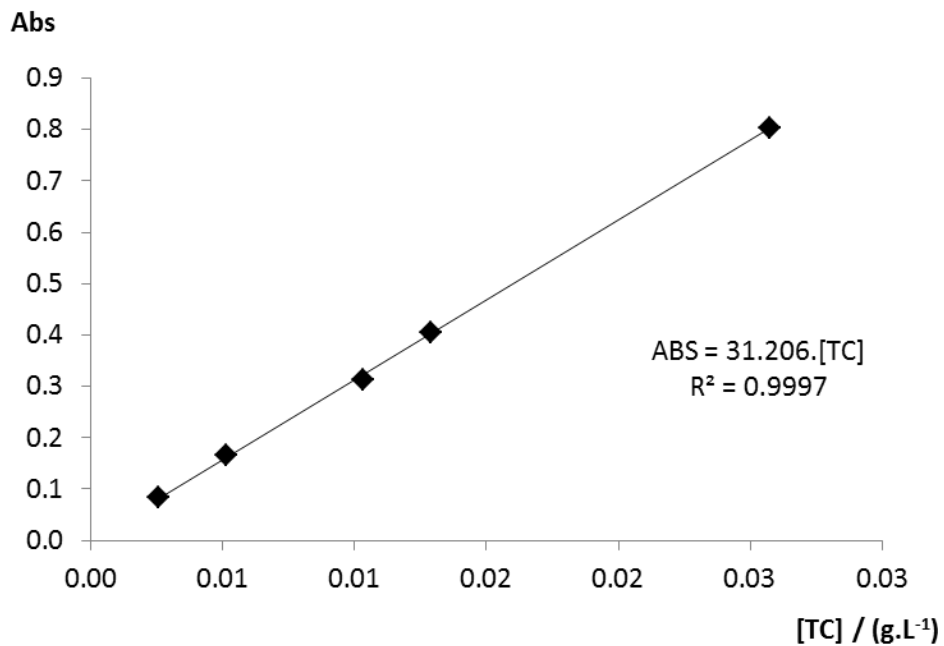


Figure S15.1 Calibration curve of TC at 25 °C, neutral pH and 276 nm, using a stock solution of 0.258 g.L⁻¹ of TC.

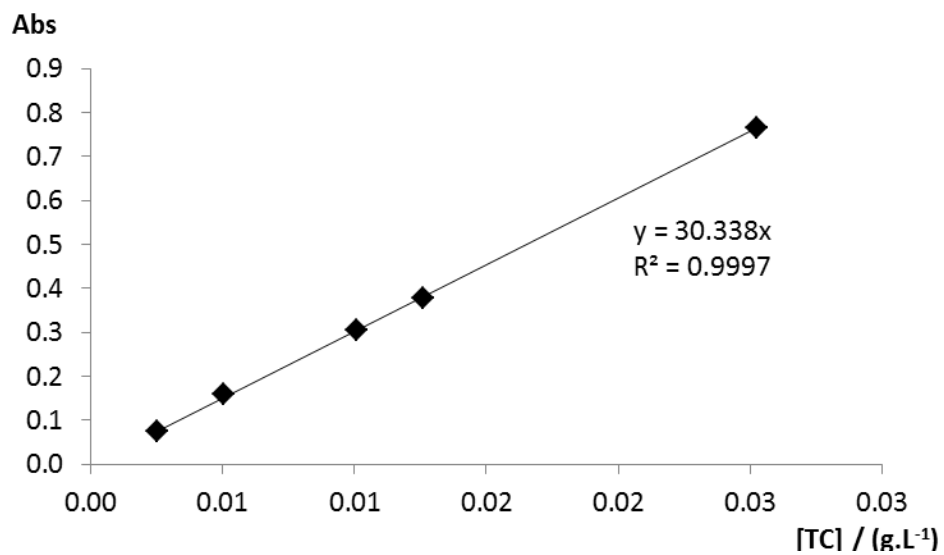


Figure S15.2 Calibration curve of TC at 25 °C, alkaline pH and 276 nm, using a stock solution of 0.253 g.L⁻¹ of TC.

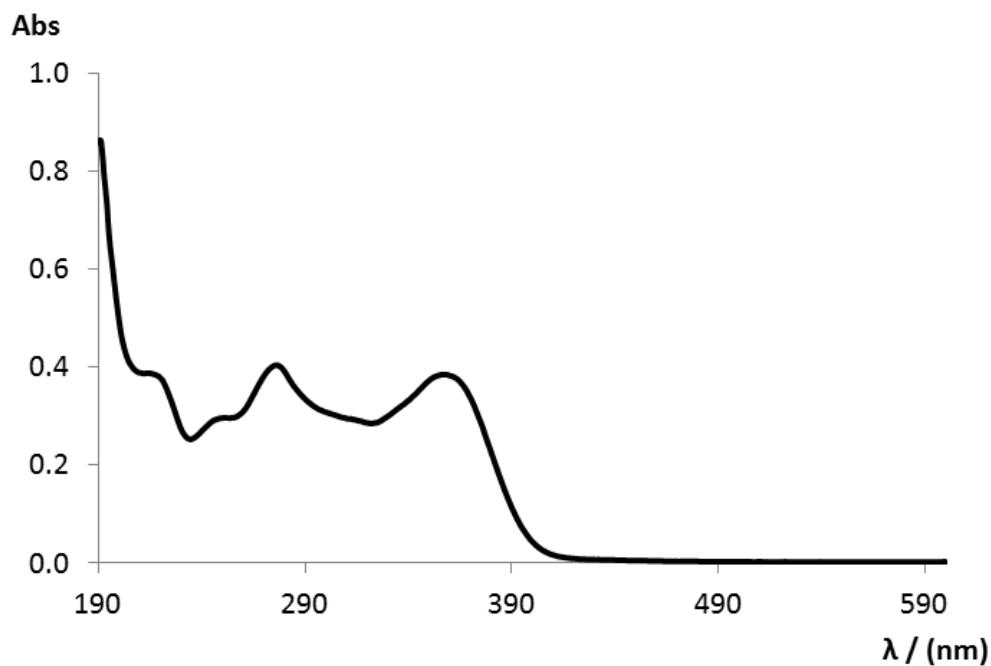


Figure 15.3 Spectrum of TC absorbance in a diluted aqueous solution (v:v, 1:20) from a TC stock solution of 0.258 g.L^{-1} , at $25 \text{ }^\circ\text{C}$ and a neutral pH.

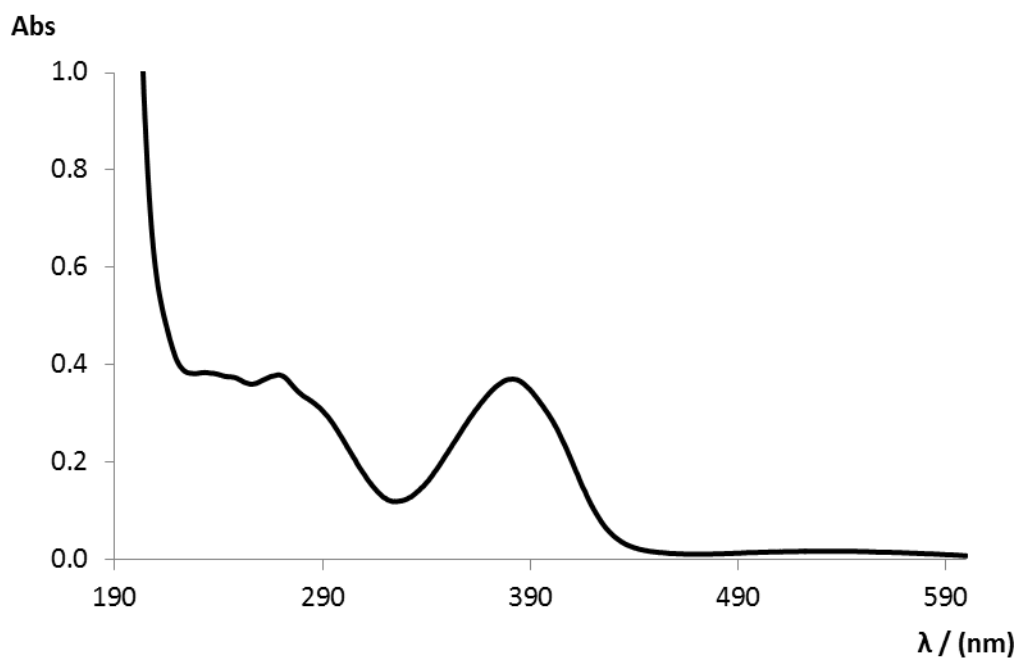


Figure 15.4 Spectrum of TC absorbance in a diluted aqueous solution (v:v, 1:20) from a TC stock solution of 0.253 g.L^{-1} , at $25 \text{ }^\circ\text{C}$ and an alkaline pH.

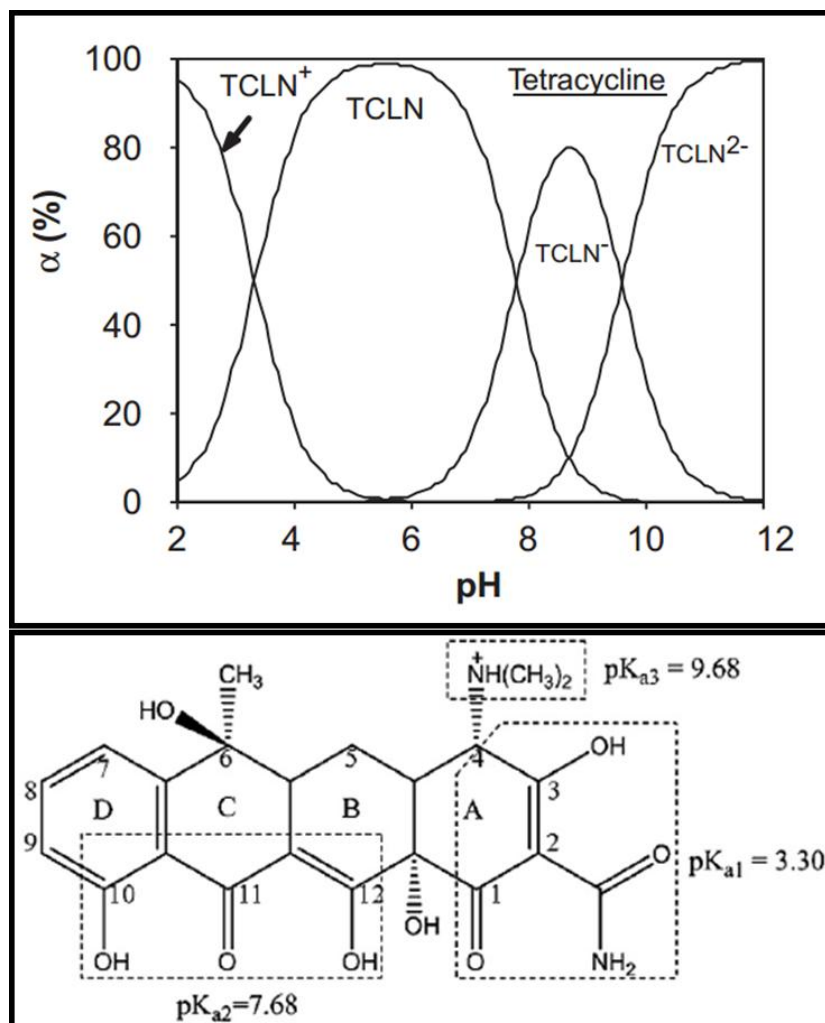


Figure S15.5 Chemical Structure and speciation' curves of tetracycline as a function of the pH (adapted from Qiang, Z. and C. Adams (2004). Potentiometric determination of acid dissociation constants (pK_a) for human and veterinary antibiotics. *Water Research* 38: 2874-2890).

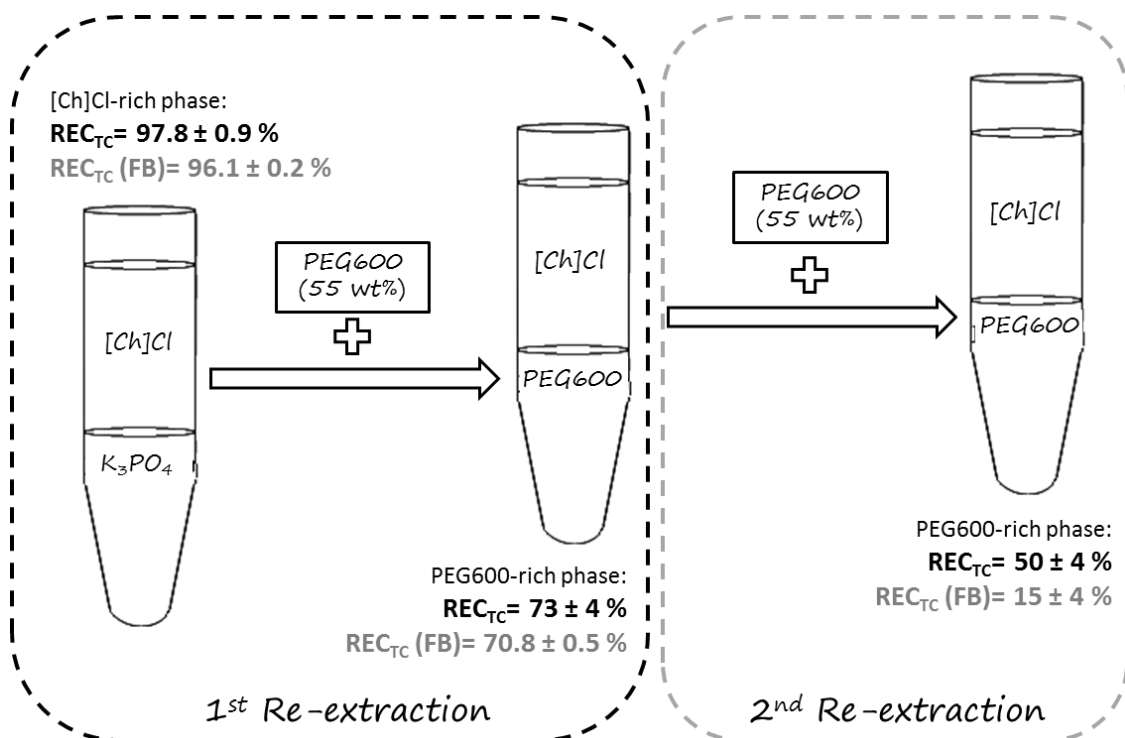


Figure S15.6 Illustrative scheme of the extraction of commercial TC and TC obtained from fermented broth to a [Ch]Cl-rich phase using the [Ch]Cl/ K_3PO_4 ATPS and re-extraction of TC from the previously formed cholinium-rich phase to a PEG600-rich phase using the PEG600/[Ch]Cl ATPS. The TC recovery (REC_{TC}) in the respective PEG- or [Ch]Cl-rich phase is the ratio between the TC concentration in the respective phase to that in the sum of both phases.

18.1. Supporting Information References

1. Zhao, Y.; Truhlar, D. G. The M06 suite of density functionals for main group thermochemistry, thermochemical kinetics, noncovalent interactions, excited states, and transition elements: two new functionals and systematic testing of four M06-class functionals and 12 other functionals. *Theoretical Chemistry Accounts*. 2008, **120**, 215-241.
2. Frisch, M. J.; Trucks, G. W.; Achlegel, H. B.; Scuseria, G. E.; Robb, M. A.; Cheeseman, J. R.; Montgomery, J. A.; Vreven, T.; Kudin, K. N.; Burant, J. C.; Millam, J. M.; Iyengar, S. S.; Tomasi, J.; Barone, V.; Mennucci, B.; Cossi, M.; Scalmani, G.; Rega, N.; Petersson, G. A.; Nakatsuji, H.; Hada, M.; Ehara, M.; Toyota, K.; Fukuda, R.; Hasegawa, J.; Ishida, M.; Nakajima, T.; Honda, Y.; Kitao, O.; Nakai, H.; Klene, M.; Li, X.; Knox, J. E.; Hratchian, H. P.; Cross, J. B.; Bakken, V.; Adamo, C.; Jaramillo, J.; Gomperts, R.; Stratmann, R. E.; Yazyev, O.; Austin, A. J.; Cammi, R.; Pomelli, C.; Ochterski, J. W.; Ayala, P. Y.; Morokuma, K.; Voth, G. A.; Salvador, P.; Dannenberg, J. J.; Zakrzewski, V. G.; Dapprich, S.; Daniels, A. D.; Strain, M. C.; Farkas, O.; Malick, D. K.; Rabuck, A. D.; Raghavachari, K.; Foresman, J. B.; Ortiz, J. V.; Cui, Q.; Baboul, A. G.; Clifford, S.; Cioslowski, J.; Stefanov, B. B.; Liu, G.; Liashenko, A.; Piskorz, P.; Komaromi, I.; Martin, R. L.; Fox, D. J.; Keith, T.; Al-Laham, M. A.; Peng, C. Y.; Nanayakkara, A.; Challacombe, M.; Gill, P. M. W.; Johnson, B.; Chen, W.; Wong, M. V.; Gonzalez, C.; Pople, J. A. Gaussian 03, revision C.01; Gaussian, Inc.: Wallingford CT, 2004.
3. Dunning, J. T. H. Gaussian basis sets for use in correlated molecular calculations. I. The atoms boron through neon and hydrogen. *Journal of Chemical Physics*. 1989, **90**, 1007-1024.
4. Woon, D. E.; Dunning, J. T. H. Gaussian basis sets for use in correlated molecular calculations. III. The atoms aluminum through argon. *Journal of Chemical Physics*. 1993, **98**, 1358-1372.
5. Wales, D. J.; Doye, J. P. K.; Dullweber, A.; Hodges, M. P.; Naumkin, F. Y.; Calvo, F.; Hernández-Rojas, J.; Middleton, T. F. The Cambridge Cluster Database, URL <http://www.wales.ch.cam.ac.uk/CCD.html>.
6. Xantheas, S. S. Quantitative description of hydrogen bonding in chloride-water clusters. *Journal of Chemical Physics*. 1996, **100**, 9703-9713.
7. Gora, R. W.; Roszak, S.; Leszczynski, J. Properties and nature of interactions in Cl-(H₂O)_n n=1,6 clusters: a theoretical study. *Chemical Physics Letters*. 2000, **325**, 7-14.
8. Neogi, S. G.; Chaudhury, P. Structure and spectroscopic aspects of water-halide ion clusters: a study based on a conjunction of stochastic and quantum chemical methods. *Journal of Computational Chemistry*. 2013, **34**, 471-491.
9. Shank, A.; Wang, Y.; Kaledin, A.; Braams, B. J.; Bowman, J. M. Accurate ab initio and "hybrid" potential energy surfaces, intramolecular vibrational energies, and classical IR spectrum of the water dimer. *Journal of Chemical Physics*. 2009, **130**, 144314-144324.
10. Rocher-Casteline, B. E.; Chang, L. C.; Mollner, A. K.; Reisler, H. Determination of the bond dissociation energy (D_0) of the water dimer, (H₂O)₂ by velocity map imaging. *Journal of Chemical Physics*. 2011, **134**, 211101-211104.
11. Chemspider, The free chemical database. [cited 2013 06-05-2013]; Available from: <http://www.chemspider.com/>.
12. Merchuk, J.C., Andrews, B.A., and Asenjo, J.A., Aqueous two-phase systems for protein separation Studies on phase inversion. *Journal of Chromatography B*, 1998. **711**(1-2): p. 285-293.
13. Ventura, S.P.M., Neves, C.M.S.S., Freire, M.G., Marrucho, I.M., Oliveira, J., and Coutinho, J.A.P., Evaluation of Anion Influence on the Formation and Extraction Capacity of Ionic-Liquid-Based Aqueous Biphasic Systems. *Journal of Physical Chemistry B*, 2009. **113**(27): p. 9304-9310.
14. Pereira, J.F.B., Lima, A.S., Freire, M.G., and Coutinho, J.A.P., Ionic liquids as adjuvants for the tailored extraction of biomolecules in aqueous biphasic systems. *Green Chemistry*, 2010. **12**(9): p. 1661-1669.